FLÁVIO ALVES DAMASCENO

COMPOST BEDDED PACK BARNS SYSTEM AND COMPUTATIONAL SIMULATION OF AIRFLOW THROUGH NATURALLY VENTILATED REDUCED MODEL

Thesis presented to the Universidade Federal de Viçosa, as part of the requirements of the Agricultural Engineering's Graduate Program, for the attainment of the title *Doctor Scientiae.*

VIÇOSA
MINAS GERAIS – BRAZIL
2012

Ficha catalográfica preparada pela Seção de Catalogação e Classificação da Biblioteca Central da UFV

T
D155c
2012

Damasceno, Flávio Alves, 1980-
Compost bedded pack barns system and computational simulation of airflow through naturally ventilated reduced model / Flávio Alves Damasceno. – Viçosa, MG, 2012.
xi, 391f. : il. (algumas col.) ; 29cm.

Inclui apêndices.
Orientador: Fernando da Costa Baêta.
Tese (doutorado) - Universidade Federal de Viçosa.
Referências bibliográficas: f. 260-274

1. Construções rurais - Aspectos ambientais. 2. Bovino de leite - Criação - Aspectos ambientais. 3. Bovino de leite - Aspectos climáticos. 4. Bovino de leite - Instalações - Engenharia ambiental. 5. Bovino de leite - Instalações. 6. Construções rurais - Fatores climáticos. 7. Construções rurais - Aquecimento e ventilação - Avaliação. 8. Meio ambiente. 9. Fluidodinâmica computacional. 10. Bactérias aeróbicas - Análise. 11. Bactérias anaeróbicas - Análise I. Universidade Federal de Viçosa. II. Título.

CDD 22. ed. 631.21

FLÁVIO ALVES DAMASCENO

COMPOST BEDDED PACK BARNS SYSTEM AND COMPUTATIONAL SIMULATION OF AIRFLOW THROUGH NATURALLY VENTILATED REDUCED MODEL

Thesis presented to the Universidade Federal de Viçosa, as part of the requirements of the Agricultural Engineering's Graduate Program, for the attainment of the title *Doctor Scientiae*.

APPROVED: August 15, 2012.

Joseph Louis Taraba

Rolf Jentzsch

Ilda de Fátima Ferreira Tinôco
(Co-adviser)

Cecília de Fátima Souza

Fernando da Costa Baêta
(Adviser)

BIOGRAPHY

Flávio Alves Damasceno, son of Abadia Alves Damasceno and José Lincoln de Oliveira Damasceno, was born on August 13, 1980, in Luziânia, Goiás, Brazil. He graduated in Agricultural Engineering at the Universidade Federal de Lavras, Minas Gerais, Brazil, in November, 2006. In February 2007, he began his Master's Degree in Agricultural Engineering at the Universidade Federal de Lavras, obtaining the title of Master in July 2008. In August 2008, he began his Doctor's Degree in Agricultural Engineering at the Universidade Federal de Viçosa, Minas Gerais, Brazil. In August 2010, he began his research as visiting researcher at the University of Kentucky, Lexington, USA. He obtained the title of Doctor in August 2012.

ACKNOWLEDGMENTS

I am ever grateful to God, who has blessed me with this opportunity.

My parents and family who have always supported all of my decisions.

Professor Dr. Fernando da Costa Baêta for his guidance during the Doctors program.

Professors Dr. Joseph L. Taraba, Dr. Rolf Jentzsch, Dr. Ilda de F. Ferreira Tinôco, and Dr. Cecília de Fátima Souza for their wisdom and guidance as my orienting committee.

Professor Dr. Joseph L. Taraba, who contributed with innumerous instructive comments, which allowed me to accomplish this high quality work.

Professor Dr. George Day for his excellent advices and thoughts, which I will carry with me everywhere I go throughout my academic career and life.

Professor Dr. Tadayuki Yanagi Junior was the first person to motivate me to pursue the academic career and I am deeply grateful for all his motivation, help and friendship.

My appreciation goes to Professors Dr. Scott Shearer and Dr. Doug Overhults, who contributed with assistance and support, as well as the entire Biosystems and Agricultural Engineering community, which welcomed me to University of Kentucky.

I would like to express my deep appreciation and gratitude to the following people for helping me complete this work, specially Dr. Cecilia Souza, Dr. Jeffrey Bewley, Ms. Randi Black, Dr. Celia Caruso, Mr. Ígor Lopes, Dr. Jairo Alexander, and Dr. Keller Sullivan.

My friends at the Ambiagro, especially Adriana, Akemi, Alexandre, Cinara, Conceição, Déborah, Diogo, Elohanna, Fábio, Fatinha, Fernanda, Humberto, Irene, Jofran, Keles, Luciano, Luis Gustavo, Maria Clara, Marilú, Maurílio Duarte, Múcio, Neiton, Olga, Roque, Rui, Samuel, and Seu Pedro.

My friends at University of Kentucky, especially Carla, Chance, Christina, Enrique, Ester, Gabriela, Guilherme, Jeniffer, Joe Luck, Lucas Melo, Lucas Revolti, Maíra, Maria, Marina, Paulo, Pedro, Rafael, Rodrigo, Sam Mullins, Santosh, and Tatiana, who helped me in Lexington.

My friends at the Viçosa, especially Anderson, Carlos, Evan, and Wagner.

My friends at the Brasilia, especially Marcelo, Bruno, and Marcos.

Leidimar Brandão, who shared wonderful moments with me, which will eternally remain in my mind and heart.

This work was financed by the Brazilian Organizations (CNPq, FAPEMIG, and CAPES) and University of Kentucky, whose support was greatly appreciated.

TABLE OF CONTENTS

ABSTRACT

DAMASCENO, Flávio Alves, D.Sc., Universidade Federal de Viçosa, August, 2012. C**ompost bedded pack barns system and computational simulation of airflow through naturally ventilated reduced model**. Advisor: Fernando da Costa Baêta. Co-advisers: Ilda de Fátima Ferreira Tinôco and Luiz Fernando Teixeira Albino.

Compost bedded pack (CBP) barns have been receiving increased attention as an alternative housing system for dairy cattle due they consist of a roofed open loose resting area that is bedded with sawdust where compost is actively stirred to aerate in order to maintain an active composting process. Thus systematic investigation of the main management practices of dairy operations utilizing green or kiln dried sawdust in compost CBP barns at Kentucky state (USA) has proven to be of environmental and economic relevance. The present work has as main objectives: a) Summarization of compost bed data, barn dimension data and determination of the major interactive factors in the success of bed composting from qualitative and quantitative methods; b) Summarization of moisture contents and water holding capacities of the compost bed to determine the influence of moisture on successful compost bed operation; c) Development of predictive equations for thermal properties of compost as a function of various combinations of moisture content, compaction, and particle size; and d) Development of a three-dimensional computational fluid dynamic (CFD) model of compost barn with alternate ridge designs and visual demonstration of its impact on air flow through structure. Data for this study was collected from 42 CBP barns, distributed throughout the state of Kentucky (USA) between October 2010 to March 2011. These data were used to describe the building layouts and dimensions, identify barn management practices, and characterize the compost bedding material concerning moisture content, WHC, particle size, thermal properties, and others parameters. The average herd size found in the study was 90 cows and the breeds consisted of Jersey (6.8%), Holstein (72.7%), and mix (20.5%).The average CBP barn dimensions were 49.1 m (length) and 21.9 m (width). Majority of these barns had feed alleys and driveways; overshot ridge with frequent orientation from NE to SW; green sawdust, kiln-dried sawdust, and mixture of both as most common bedding material; bedding process and aeration using mechanical tillage at depths lower than 0.25 m; and loading of fresh material added every one to five weeks, varying by season, weather conditions, barn size, and cow density. Temperatures of bedding compost tended to be

lower on barns which utilized green sawdust. Average bedding moisture content was found to be 59.0% (w.b.) and ranged from 36.2 to 71.8%. The percentage distributions of mass weight in the particle size fractions from the bedding compost materials were very different when compared among them. The average finer index ($p < 0.05$) was the highest weight percent (30.1%) in the samples studied. WHC increased with increasingly fine particle size. The higher bulk density value was 3.6 times that of the lowest bulk density value. In general, the thermal conductivity increased with increasing particle size, while thermal resistivity decreased with increasing particle size. An increasing trend in the thermal conductivity was also observed with the increase in both moisture content and static and dynamic compaction degree for all compost material tested. Whereas, an increasing trend in the thermal resistivity of bed compost was observed with the decrease in both moisture content and static and dynamic compaction degree. Bedding compost always contained bacteria, moreover *Coliforms* count was not present in barns that had a higher compost temperature and *Coliforms*, *E. coli*, *Bacillus* and *Streptococcus* count were higher in the barns that showed lower moisture content. The developed barn ventilation CFD model provided good agreement with experimental measurements and it was able to identify the effect on air flow through structure in a CBP barns with alternative roof ridge type. The CFD models results showed that the best ridge vent and wind direction in the winter weather was observed in the open ridge with chimney (ORC) and West to East, respectively.

RESUMO

DAMASCENO, Flávio Alves, D.Sc., Universidade Federal de Viçosa, Agosto, 2012. G**alpões com sistema de cama com compostagem e simulação computacional do fluxo do ar através de modelo reduzido naturalmente ventilado**. Orientador: Fernando da Costa Baêta. Coorientadores: Ilda de Fátima Ferreira Tinôco e Luiz Fernando Teixeira Albino.

Galpões com sistema cama em compostagem (CBP) têm recebido maior atenção como um sistema de criação alternativo para gado leiteiro por ser constituído de uma área de descanso aberta e coberta utilizada como cama serragem onde o composto é ativado e aerado por agitação a fim de manter um processo de compostagem ativo. Sendo assim, a investigação sistemática das principais práticas de manejo das operações de produção de leite empregando-se serragem verde ou seca nos compostos de instalações do tipo CBP no estado de Kentucky (USA) tem demonstrado ser de grande interesse econômico e ambiental. O presente trabalho teve como objetivos principais: a) Sumarizar os dados do composto da cama, dimensão das instalações e determinar os principais fatores interativos para o sucesso do composto da cama a partir de métodos qualitativos e quantitativos; b) Sumarizar a capacidade de retenção de água do composto da cama (WHC) e comparar dos teores de umidade encontrados com a WHC, a fim de determinar a influência da umidade sobre o composto da cama; c) Desenvolvimento de equações de previsão para propriedades térmicas em composto de cama em função de varias combinações de teor de umidade, compactação e tamanho de partícula; e d) Desenvolvimento de um modelo em três dimensões em dinâmica de fluídos computacional (CFD) de instalações em compostagem com projetos alternativos de cumeeira e demonstração visual do impacto do fluxo do ar sobre a estrutura. Dados para realização deste estudo foram coletados em 42 instalações CBP, distribuídos através do estado de Kentucky, entre outubro de 2010 e março de 2011. Estas informações foram usadas para descrever o esboço e as dimensões das instalações, identificar as práticas de manejo e caracterizar o material de compostagem da cama quanto ao teor de umidade, capacidade de retenção de água (WHC), tamanho da partícula, propriedades térmicas, entre outros parâmetros. A média de tamanho do rebanho encontrado nesse estudo foi de 90 vacas com proporção de 6,8% de Jersey, 72,7% de Holstein e 20,5% de mistura destas raças. A média das dimensões das camas de compostagem foram 49,1 m (comprimento) e 21,9 m (largura). A maioria destas

instalações tinham corredores de alimentação e acesso de veículos, cumeeiras do tipo “overshot” (com um dos lados ultrapassado) e frequência de orientação de NE para SO, serragem verde, seca ou mista como materiais mais comuns da cama, preparo da cama por aeração mecânica a profundidade menores do que 0,25 m e carga de material fresco adicionado a cada uma ou cinco semanas, variando por estação do ano, condições climática, tamanho da instalação e densidade animal. As temperaturas dos compostos das camas tenderam ser menores em instalações que utilizaram serragem verde. A umidade média do material da cama foi de 59,0% (b.u.), variando de 36,3% a 71,8%. A comparação da distribuição percentual do peso (massa) nas fracões de tamanho de partícula revelou que esses materiais de compostagem da cama encontrados nas instalações CBP foi muito diferentes. Assim, a média do índice de finura ($p < 0.05$) foi a porcentagem de peso mais alta (30.1%) nas amostras estudadas. WHC aumentou com o aumento de partículas finas. O maior valor de densidade aparente da cama foi 3,6 vezes maior que o menor valor de densidade aparente encontrado. Em geral, a condutividade térmica aumentou com aumento do tamanho da partícula, enquanto a resistividade térmica diminuiu com o aumento do tamanho da partícula. Uma tendência de aumento na condutividade térmica foi ainda observada com o aumento no conteúdo de umidade e grau de compactação estática e dinâmica para todos os materiais de compostos testados. Por outro lado, uma tendência de aumento na resistividade térmica do composto da cama foi observada com a diminuição do conteúdo de umidade e do grau de compactação estática e dinâmica. Os materiais da cama sempre mostraram presença de bactérias, sendo que as contagens de Coliformes não estavam presentes em instalações que possuíam compostos com temperaturas mais elevadas e as contagens Coliformes, E. coli, Bacilo e Estreptococos foram maiores nas instalações que apresentaram menores teores de umidade. O desenvolvimento do modelo em CFD permitiu uma boa concordância com medições experimentais e foi capaz de identificar os efeitos do fluxo de ar através da estrutura em instalações CBP com diferentes tipos de cumeeiras. Os resultados dos modelos CFD mostraram que a melhor tipo de telhado e direção do vento no durante o periodo de inverno foi observado em cumeeira aberta com chaminé (ORC) e oeste para leste, respectivamente.

1 - INTRODUCTION

1.1 Summary and justification

In the late 1980`s, innovative dairy producers in the state of Virginia introduced a new variation on the loose-housing dairy system generally referred to as a compost bedded pack (CBP) barn. Since then, CBP barns are being used in many states in the United States, especially in the Midwest and Northeast, and in other countries such as Japan, China, Germany, Italy, Netherlands, Israel, and recently in Brazil. The first CBP barns of Kentucky were constructed in 2002. By the end of 2010, CBP barn number had been increased to 58 barns. This significant increase was an indicative that a CBP barn may be a reasonable, economically feasible alternative type of dairy housing facility for Kentucky dairy producers wanting to upgrade or modernize their milking herd facilities. As consequence, factors based on dairy producer experiences such as current design, management recommendations of manure compost packs, animal behavior, herd health, and milk production has been described in some publications (Russelle et al., 2009). Additional field observations have also been reported in several U.S. states (Shane et al., 2010; Barberg et al., 2007; Janni et al., 2007) and specially in Kentucky (Black et al., 2011a; Black et al., 2011b; Bewley and Taraba, 2009).

CBP barn structures generally have a retaining wall that typically surrounds the bed and also separates the feed alley from the composted manure pack. The most commonly employed bedding material in the composting process is green and dry sawdust or kiln dried shavings to maintain a dry bedding surface and to absorb water. However, producers often ask whether green sawdust (high moisture sawdust from sawing green wood) is harmful or beneficial to the composting bed. The primary difference between green and kiln dried sawdust is that green sawdust will not absorb as much water as kiln-dried sawdust. All that this implies is that to achieve the same compost bed moisture content, more green sawdust will be used than kiln dried sawdust.

Compost packs produced by composting are tilled or stirred twice daily to incorporate the manure, provide a fresh, soft surface, and aerate the pack to encourage aerobic microbial activity in the pack (Janni et al., 2007). Compared to windrow composting, CBP has a larger surface area to heat generating volume, thus more heat losses. Since the temperature is one of the most important CBP operational parameters, the understanding of

the thermal properties and heat balance in compost systems is required to design and properly control the composting processes (Ahn et al., 2009; Janni et al., 2007). Additionally, the key to maintaining a good working CBP barn include, a structure designed with an open ridge and high open side walls, enhanced ventilation, frequent bed stirring, optimal moisture in the bedded pack, appropriate biodegradability of the bedding/manure bed mixture, and optimal animal density.

Therefore, the effectiveness of the composting process is dependent upon the environmental conditions as oxygen content, moisture, temperature, amount of organic matter, and the size and activity of microbial populations presents within the CBP (Janni et al., 2005). Composting increases the bedding temperature which reduces pathogenic microbial populations, and decreases bedding moisture by increased drying rate (Black et al., 2011a; Barberg at al., 2007). The large numbers of microorganisms and high microbial activity in the compost bedding are largely a reflection of manure deposition, bedding chemical properties (available C and N), and water contents. Facultative anaerobic bacteria also are more numerous in the surface of CBP material and constitute a larger proportion of the total microbial population in tilled or stirred compost (NRCS, 2010). Some research shows the direct influence of poor environment conditions that could be created within the CBP as one of the factors that predispose the development of respiratory diseases in birds and pigs (Reece et al., 1980; Sainsbury, 1981; Takai et al., 1983; Menegali et al., 2009), but a thorough search of the literature found few studies related to air quality in facilities for cattle.

A more in-depth study is needed to assess and correlate detailed information regarding the building structure, bed management, and compost parameters of these housing systems and to determine the most significant factors that achieve CBP success. Thus, the findings of this research may be used by current and future compost bedded pack barn managers.

1.2 Dissertation objectives

The present work will provide a systematic investigation of the main management practices of dairy operations utilizing green or kiln dried sawdust in their compost bedded pack barns. Four major objectives were established:

1) Summarization of compost bed data, barn dimension data and determination of the major interactive factors in the success of bed composting from qualitative and quantitative methods;

2) Summarization of moisture contents and water holding capacities of the compost bed to determine the influence of moisture on successful compost bed operation;

3) Development of predictive equations for thermal properties of compost as a function of various combinations of moisture content, compaction, and particle size;

4) Development of a three-dimensional computational fluid dynamic (CFD) model of compost barn with alternate ridge designs and visual demonstration of its impact on air flow through structure.

2 - LITERATURE REVIEW

2.1. Compost dairy barn system

For the past several decades, loose housing systems of dairy cattle has given way to freestall barns in light of less labor, cleaner cows and reduced bedding costs when compared to the conventional straw bedded-pack. Nevertheless, loose housing with freestalls can still lead to a high risk of lameness and hock lesion. Since the concrete flooring systems are constantly covered with urine and manure, this type system may cause digital dermatitis and other hoof disorders (Klaas et al., 2010), especially with inadequate positioning of stall hardware, limited area resting space, hard lying surface or insufficient bedding (Weary and Taszkun, 2000; Tucker et al., 2004; Dippel et al., 2009). In view of this, a new concept in loose housing called compost bedded dairy barn system, commonly called compost barns or compost bedded pack barns (CBP), has been gaining attention from dairy producers and the scientific community.

CBP barns are an alternative loose housing system for dairy cows. In CBP barns, cows have more freedom of movement and are able to lie down in a more natural manner. In theory, this should lead to cows spending more time lying down. However, even as cows are standing up, they also spend more time on a softer surface than in concrete alleys within freestall barns. Thus, cow welfare and health are important indications of the compost bed. Bedding quality can also be decreased as the moisture content increase once the cows are directly exposed to the elements constituting of bedding, feces and urine resulting in an increase in the bacterial cells counts of both bedding and teats (Zdanowicz et al., 2004). But, when CBP barns are properly managed, drier bedding material is present and may result in decrease of the milk somatic cell counts (SCC), cleaner cows, increased milk production, and reduced lameness. A published example of this was found in Minnesota where the percentage of mastitis infection rates in CBP barns was 12% lower than in freestall herds (Barberg et al., 2007).

CBP barns are generating a lot of interest among Kentucky dairy producers who are adopting CBP barns as dairy cattle housing at a rapid rate. Kentucky has at least fifty one compost barns in operation and some more under construction. Experience with well-managed CBP barns in Kentucky has generally been positive. Cows are relatively clean, very comfortable, have fewer lameness issues, and in most cases has increased milk

production and lower SCC after moving from tie-stall or freestall barns, or pasture based systems to a compost barn.

However, since this is a new system, many questions still remain regarding best management practices and key factors for their success. More research is needed on these housing systems after assessing the effect of current design and management recommendations based on dairy producer experiences. As result, CBP barn recommendations can be made for proper design, location, and exceptional management. Thus, the keys to maintaining a good working CBP barn should include a structure designed with an open ridge and high open side walls, enhanced ventilation, frequent bed stirring, optimal moisture in the bedded pack, and optimal animal density (Wagner, 2002) in order to provide a healthy, comfortable surface on which cows may be kept to result in with a higher quality of life and milk production.

2.1.1. Facility design

CBP barns are similar in many respects to typical freestall dairy barns (NRAES-76, 1995; MWPS-7, 2000). Both have feed mangers, feed alleys and waterers. One of the key differences is that the freestall and freestall alleys are replaced with a bedded pack area in CBP barns which it is aerated at least twice daily.

CBP barns have a concrete feed alley, a composting bedded pack, a 1.20 m high wall surrounds the pack on three sides and one side that separates the pack from the feed alley. The 1.20 m wall the bedded pack and the feed alley has a fence for safety to prevent cows from walking over the wall (Endres and Janni, 2009). The wall separating the pack and the feed alley has one to four walkways for cows and equipment to access the pack. This wall is typically of poured concrete construction.

A feed alley is located along one long side of the bedded pack. CBP barns can be laid out for drive-by feeding, covered feeding, or drive-through feeding with pens on both sides. They can also be used with outside feed bunks under roof. The recommended feed alley width is 4.25 m because cows eat off one side of the alley and drink from waterers on the other side (Gay, 2009).

The bedded pack area can have a concrete or clay base. The sidewall height for a bedded pack is recommended to be higher than that for a freestall barn to accommodate the sidewall opening lost due to the manure pack walls. A size 0.91 m or more of eave

overhangs is recommended to minimize the chance of roof runoff and rain being blown onto the bedded pack (Janni et al., 2005). Roof gutters will help reduce roof runoff from being blown onto the pack. The ground surrounding a compost barn should be sloped to minimize rain and snow runoff from entering the barn and wetting the bedded pack (Endres and Janni, 2009). Dairy producers in Minnesota have used 4.25 m sidewalls but some producers have used 4.90 m for their next barn to provide better access for bedding trucks. Walkways, at least 3.05 m to 3.65 m wide, are minimum recommended at each end of the wall separating the bedded pack and the feed alley for cow and equipment access to the pack area. Long barns will require additional walkways (Endres and Janni, 2009).

2.1.2. Waterers

Water intake increases during heat stress, and one of the critical factors in managing heat stress is to provide adequate access to water. Economy and ruggedness are two criteria for selection of the waterers. Two choices for materials are concrete or plastic. Concrete is more rugged for the long term but requires more skill and equipment for forming and placing. Plastic can be easy to modify or repaired and economically viable.

Waterers located closer to the feed alley are easier to inspect from the alley and cleaning can be performed more easily. Many CBP barns have the waterers along the retaining wall with access from, the feed alley, usually within an indented space . Waterers are not located in the bedded pack area to minimize wetting of the pack, to keep cleaner waterers, and to avoid having to adjust waterer height as pack depth increases. Ideally, 0.60 meters of tank perimeter should be provided for each 10 to 20 cows (Brouk et al., 2001).

2.1.3. Lighting

Lighting in compost barns is similar to that used in freestall barns (MWPS-7, 2000). Lighting in CBP barns is desired mainly for the convenience of the operator, for inspecting animals and handling dairy cows. Dairy producers, veterinarians, and other animal care workers often report easier and better cow observation and care. Cows move more easily through uniformly lit entrances and exits.

Enhanced lighting for the milking herd is profitable (Dahl et al., 1997). The increased milk production generates a payback of less than one year considering initial, installation,

operating, and replacement costs of the lights, and the increased feed intake (Chastain and Hiatt, 1998).

Light levels are measured in lux. The power and type of the lamp determines the brightness. The height of the lamp above the ground and the lamp spacing determines the uniformity and distribution of light (Winchell et al., 1996). Yard lights should therefore be located over feed alleys and/or waterers.

2.1.4. CBP barn ventilation and location

Determining the best CBP barn ventilation system to employ is one of the biggest facility related decisions to make it. The ventilation in the CBP barns helps in maintaining a healthy and comfortable environment for cows and reduces the effect of environment on the structure of the building. The renewal of the air removes cow heat and moisture as well as the odor, gases, heat and moisture that the composting pack generates. It is necessary to constantly exchange warm, humid air inside the barn for cooler, drier air outside of the barn. This exchange must occur regardless of outside temperature or weather conditions.

A continuous supply of fresh air is necessary whenever animals are closely confined, as in CBP barn, in order to maintain animal health and integrity of the building. Evidence of inadequate ventilation includes condensation or condensation stains on walls, ceilings and structural members, and mainly the presence of foul odors in the barn. Perennial respiratory diseases may be another symptom of poor ventilation. Winter barn temperatures should not exceed 10°C. If this temperature is often exceeded, inadequate ventilation may be the reason (Wells, 2004).

The rate of ventilation is the air volume changed in a given period of time. The ventilation system in dairy barns may be natural or mechanical ventilation (positive or negative), or a combination of both (Teye and Hautala, 2008), as seen in Figure 2.1.

A mechanical ventilating system uses fans to provide air exchange. Both naturally and mechanically ventilated buildings need properly sized openings for fresh air to enter and exhaust air to exit. Ventilating system control can be accomplished either automatically or manually. Mechanical ventilating systems almost always use thermostatic control while natural ventilating systems are commonly adjusted manually (MWPS-7, 2000).

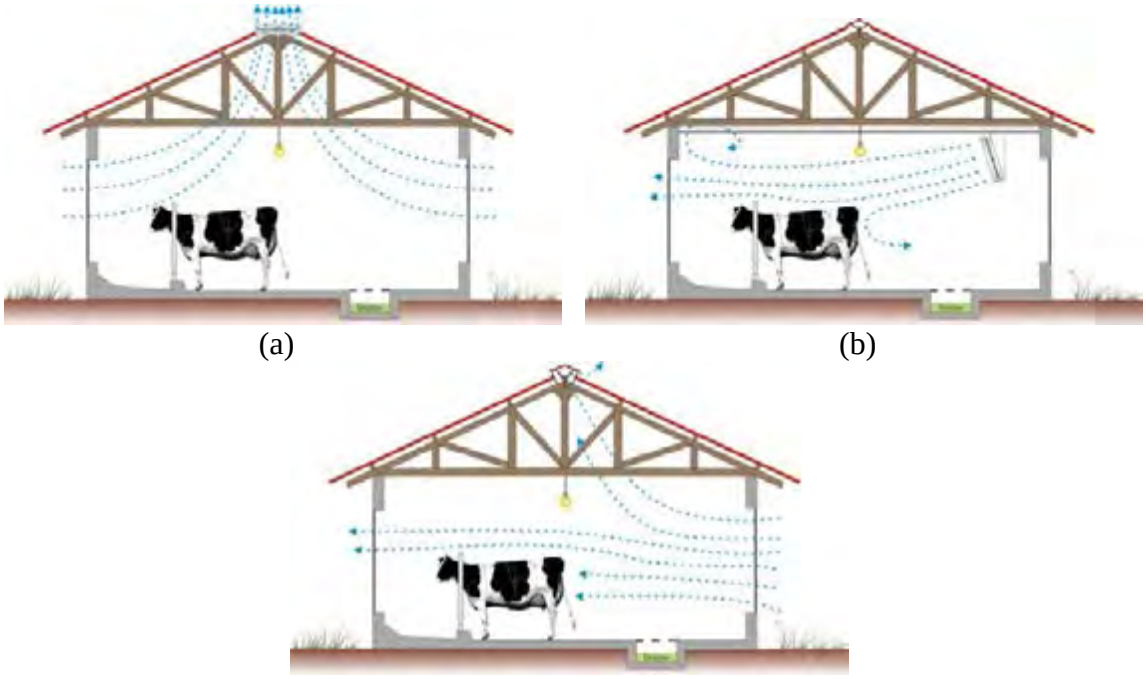

(a) (b)

(c)

Figure 2.1 - Ventilation system in dairy barns: (a) negative pressure, (b) positive and (c) natural (Adapted from Teye, 2008).

2.1.4.1. Natural ventilation in CBP barns

In a natural ventilating system, the wind and the difference between inside and outside temperature moves air through the building. Natural air exchange or building ventilation rates are influenced sidewall opening, eave opening, building width, ridge opening, and wind speed (Brouk et al., 2001).

Wind blowing across the open ridge and sidewall and endwall openings, and indoor/outdoor temperature differences moves air through the building to provide the air exchange. Fresh air enters through eave or sidewall openings, see Figure 2.1c.

Heat, moisture, and air contaminants exits through the open ridge and downwind sidewall opening. Some ventilation occurs even on calm days because warm, moist air rise up causing a chimney effect. Large, adjustable or full sidewall openings allow increased air movement due to wind in summer. Continuous openings help provide good fresh air distribution.

a) Location and Sitting

The most CBP barns are naturally ventilated, which makes location very important. Naturally ventilated barns are located in an open area where summer winds can blow through open sidewalls and the ridge in warm weather (Teye, 2008). Building location is

critical for natural ventilation to work well. Buildings on high ground are located where trees or structures do not disturb airflow around or through the building.

Trees, silos, tall growing crops, and other structures can disrupt airflow for a distance of 5 to 10 times their height downwind. Thus, naturally ventilated buildings should be located at least 25 meters, in any direction, from such obstructions (MWPS-7, 2000).

b) Building Orientation

The first dairy barn design criteria to be considered are the orientation of the structure. Barns with a north-south orientation have a greater internal solar radiation exposure than barns with a east-west orientation (Brouk et al., 2001). Moreover, building orientation affects natural ventilating system performance. Orient naturally ventilated buildings to provide maximum wind exposure, especially for summer winds. Greater and more uniform wind driven air exchange occurs when the wind enters through the continuous sidewall or eave opening rather than through the smaller end wall. Cross ventilation, from side to side, is especially important during warm weather. Orient buildings so prevailing summer winds are perpendicular to the ridge openings (MWPS-7, 2000).

The ideal orientation of the barn allows prevailing summertime winds to intersect the barn perpendicular to the sidewalls. When the farmer builds the barn using this orientation, the air entering the barn though the sidewall travels the shortest distance possible to exit the barn through the opposite sidewall. This improves the rate of air exchange in the barn and consequently enhances the environment of the cows. Since winds change direction, winds striking the sidewall within 45 degrees of the perpendicular will still result in adequate air exchange in most cases. Other factors that can affect barn orientation include future expansion, topography, cow flow, and manure flow. Producers should consider all of these factors when sitting and orientating their barns.

c) Ventilation Openings

The primary types of openings used in a naturally ventilated dairy barn are eave, ridge, and wall openings (sidewall and endwall). Controlling the size of these openings can control the ventilation rate to a great extent. The amount of inlet control needed depends on the season of the year and the climate (Chastain, 2000).

In addition to building width and sidewall height, ridge openings are required. Armstrong et al. (1999) observed greater increases in afternoon respiration rates relative to

morning rates when cows were housed in barns with ridge coverings as compared to opening ridges. A ridge opening of at least 0.15 m (measured horizontally) should be provided for each 9.0 m of building width (Chastain, 2000) and the bedded pack area or other less critical areas should also located under the ridge (Brouk et al., 2001).

The sidewall opening should be at least 2.50 meters high, continuous the entire length of the building. Open sidewalls fully to provide maximum summer ventilation. With large sidewall openings, provide a 0.90 to 1.20 meters overhang at the eave to shade and partially shield the opening from blowing rain and snow piles and drifts. Ventilation through existing buildings can be improved by increasing the amount of open area, but do not compromise the structural integrity of the building. Endwall openings can provide additional ventilation to supplement sidewall openings in the summer (MWPS-7, 2000).

The vertical separation between the eave and ridge openings has a significant impact on the pressure differences generated by the chimney effect (Chastain, 1987). Therefore, the roof slope is an important consideration in the design of a naturally ventilated building (Chastain, 2000). Roof slopes of 4/12 to 6/12 works very well in naturally ventilated dairy barns. Condensation and high interior summer temperatures are more likely with roof slopes less than 4/12 because of reduced air movement. Buildings with roof slopes steeper than 6/12 have greater chimney effect but they are generally not needed. Slopes of 3/12 are acceptable for open front buildings less than 9.0 m wide (MWPS-7, 2000).

Determine ventilation rates in naturally ventilated facilities is a task even more difficult (Albright, 1990; Zhang et al., 2005). The air flow in CBP barn naturally ventilated is irregular and multidirectional, and generally has a very small value to measure accurately. Ventilation is also driven by temperature differences between indoor and outdoor installation. Therefore, to accurately estimate the natural ventilation is very difficult, because the areas of ventilation openings are large and along the entire length of the installation or through the ridge vent. Most CBP barns which has ventilation problems are resulted from poor design, construction or ventilation operational control system (Seedorf et al., 1998).

2.1.4.2. Mechanical ventilation in CBP barns

There are endless approaches to the mechanical ventilation design in dairy farming. For example, the precise number and location of fans required in a building would depend upon factors such as the density, construction, utilization and local climatic conditions (Wells,

2004). However, the components of the ventilation system should accommodate winter and summer conditions, such as:

i) A continuous minimum air exchange: This is certainly required to remove the moisture constantly created by dairy cows, particularly during the colder, sub-freezing months of the year.

ii) Higher air exchange rates and air velocity across the cows during the hotter summer weather to remove excessive heat from the cows.

Mechanical ventilating systems have fans, controls, and air inlets or outlets. A well-designed system provides greater control over barn temperature and air movement than natural ventilation (MWPS-32, 2000). Mechanical ventilation is used to ventilate barns or rooms with flat ceilings and buildings that are blocked from good natural ventilation by existing buildings and obstructions.

Fans are the driving force in providing the required air exchange and it must be combined with properly sized and distributed fresh air inlets in order to work properly. The main criteria for selecting ventilation fans are capacity to provide a good air throw, fan size, drive type, and purchase and operating costs. In barns with tight construction and continuous, fan location has little effect on air distribution. Fans placed in groups or banks at a single location are preferred rather than spacing them out singly at different locations (Wells, 2004). Thus, fans should be selected to provide the required air volume for different weather conditions based on the number of cows in the barn.

The minimum ventilation rates for dairy cows are given in Table 2.1. Recommended ventilation rates depend primarily upon the total weight of livestock housed in the space to be ventilated.

Table 2.1 - Minimum ventilation rates for dairy barns.

Animals	Winter	Mild weather	Summer
	Air flow ($m^3 s^{-1}$) per animal		
Calves (0 - 2 months)	0.007	0.024	0.047
Heifers			
(2 - 12 months)	0.009	0.028	0.061
(12 - 24 months)	0.014	0.038	0.085
Cows	0.024	0.080	0.236

Source: Dairy freestall housing and equipment handbook (MWPS-7, 2000).

A recent innovation for hot weather cooling in CBP barns is the High Volume Low Speed (HVLS) ceiling fan (Figure 2.3). These fan units may be up to 7.2 m in diameter and they are operated by a 1 to 2 hp motor (Clarke and House, 2010). While the units are expensive to purchase, the payback period falls into the 4 to 5 year range, depending on the electricity prices and installation costs at the time. HVLS fans create a higher percentage of floor area with fewer dead or low velocity spaces.

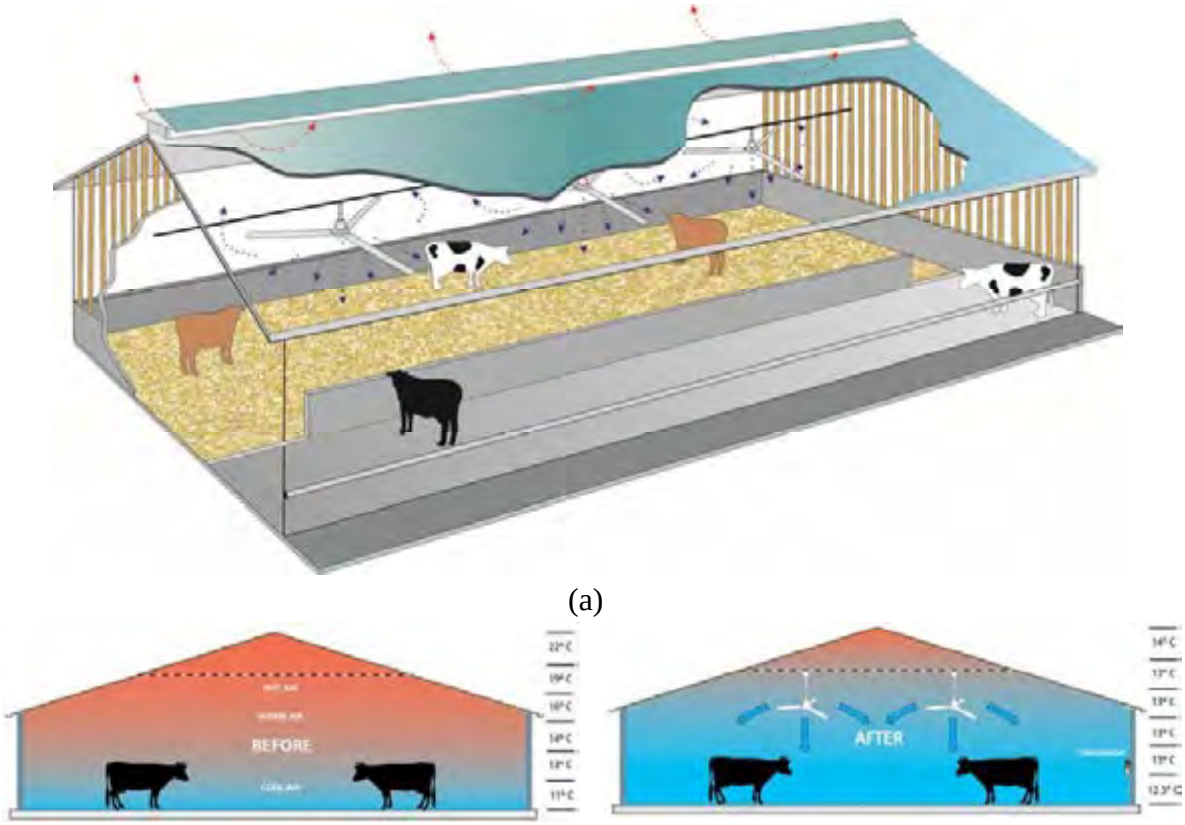

(a)

(b) (c)

Figure 2.2 - High Volume Low Speed (HVLS) ceiling fan (a) and differences before (b) and (c) after the installation HVLS in CBP barns.

The Figure 2.2 illustrates a typical dairy herd enclosure in the height of the summer months without mechanical circulation. Thereby, before ceiling fans (HVLS) are installed (Figure 2.2b), the warm, muggy air sits in the building, which creates uncomfortable conditions for the cattle, creating heat stress for the animals, attracting flies, whilst also creating uncomfortable working conditions for staff. By installing ceiling fans within the enclosure (Figure 2.2c), this provides positive air movement, equalizing the temperature levels within the building during the summer for cattle and workers, with better cooling to minimize heat stress with the constant air circulation.

2.1.5. Economic considerations

Numerous economic factors must be considered before deciding to build a CBP barn. CBP barns have lower capital costs compared to freestall barns because CBP barns require less concrete and stall equipment. In other words, the bedded pack can be built up on clay. Furthermore, there is less investment in manure storage structures because the bedded pack provides storage (Gay, 2009).

Bedding costs and availability of bedding materials was by far the major concern expressed by the producers. Dairies with more than 200 cows may want to consider an alternative bedding to a CBP barn if they plan to use a compost barn for all their cows. A large number of cows will produce enough manure to require a significant amount of bedding material. In CBP barns, approximately three to four times more bedding is used in a CBP barn as in a freestall barn. Alternative bedding options are currently being tested. Preliminary results indicate that sawdust is the best option for these types of barn, but combinations of sawdust with other materials, such as finely ground soybean or flax straw, finely processed corn cobs, or wood chip fines can work relatively well (Endres and Janni, 2009).

The building costs ranged widely depending on the amount of on-farm labor utilized and amenities added. Labor requirements are similar for both types of barns. Properly maintained CBP barns require more daily labor (packs must be stirred twice daily and must have dry bedding added). However, less daily labor is required for manure handling.

Producers should also consider the cost of handling manure. CBP barns reduce the amount of manure storage, but producers may need equipment to handle both liquid and dry manure. Keep in mind that dry manure can be easier to handle and may not have to be applied as frequently (Bewley and Taraba, 2009).

2.2. Compost bedding pack

2.2.1. Bedding source

There are two driving factors behind good bedding choices. One is cow comfort, and the other is farmer comfort. Both of these objectives have some common and diverging areas. Cow comfort is critical because of the importance to both cow and farmer for the cow to spend time to lie down and performing the process of rumination. Therefore bedding must be comfortable to lie on. Nonabrasive bedding promotes both comfort and

injury reduction. A dry bedding surface is critical at all times both for cow comfort, reduction of infection from environmental mastitis organisms and for reduction in pathogen growth. Farmer comfort requires low bedding cost, labor efficiency, and the bedding drain or dry well to keep cows dry and limit growth of pathogens (Hashemi et al., 2001). Besides, drainage of bedding can be considered a negative factor, because regulatory agencies requires protection from groundwater contamination. Thus, operation of the bed should be below the water holding capacity (WHC).

Fine wood shavings or sawdust is most commonly used in CBP barns as a bedding material (Janni et al., 2005). Wood shavings are preferred over sawdust because the small size of sawdust particles can enhance bacterial growth and irritate teat ends. Sawdust should be kiln-dried if used as bedding. However, competition for wood products has stiffened, driving up the price for wood residue. This calls into question the future cost and availability of this bedding. Faced with this uncertainty, producers and researchers have explored alternative materials that could work for bedding in CBP barns (Vokey, 2008). Some experience indicates that green or wet sawdust is not recommended. Other types of bedding may not work satisfactorily, increasing the mastitis risk for dairy cows.

2.2.2. Management of the bedded pack

Management of the composting bedded-pack is critical to the success of compost barns. The minimum space per cow for a CBP barn is recommended to be 6.0 m^2 per animal for Jersey cows and 7.9 m^2 for large breeds (Janni et al., 2007). However, 9.3 m^2 or more per cow is recommended to prevent overcrowding and compaction of the bedding (Gay, 2009). Overcrowding may lead to increased SCC levels, increased bedding needs and potential for increased teat injury. The compost pack area is sized to allow all cows to lie down at the same time and still have space for a cow to get up to go and eat or drink. It is hypothesized that compost pack area per animal depends on the amount of manure and urine added to the pack daily. Moreover, more space per animal will reduce the frequency of bedding addition as a result of water evaporation rate, as affected by weather conditions and bed temperature, that may be comparable to deposition rate from manure and urine. The microbial activity and drying need to balance the amount of manure and urine added daily.

CBP barns have bedding covering the loose housing floor to an initial depth of 0.30 to 0.60 m. Cows deposit manure and urine onto the bedding when utilizing the CBP barn. Sometimes confinement in the barn is continuous between milking sessions. When cows

are in the barn, they have free access to a concrete alley where waterers and the feed bunk are installed. While the cows are being milked (two or three times per day), the bedded pack is tilled or stirred to incorporate the urine and manure that accumulate between milkings and to aerate the bedding material. Tillage is done with a skid steer, small tractor, or even an ATV equipped with a variety of tools (field cultivators, harrows, and rototillers have been employed), to a depth of 0.20 to 0.40 m. It is proposed that aeration is essential to incorporate oxygen for aerobic decomposition and to provide a fresh surface without accumulated manure for cows to lie down on after returning from the milking parlor or feeding. Some producers are aerating the pack deeper using a chisel plow with 0.40 to 0.45 m deep, and have observed a reduction in bedding needs and increased pack temperatures (Janni et al., 2007). Manure handling on a daily basis takes about the same time or less as maintaining a freestall barn.

Fresh bedding is added when there is moisture build up in the bedding and the cows become dirty. Typically this occurs every few weeks. The CBP barn may have increased to a depth of 1.0 to 1.2 m when removed after one year.

2.2.3. Composting process in bedded pack

Composting is the biological decomposition process that occurs under controlled aerobic conditions where microorganisms reduces heterogeneous organic matter into more stable chemical compounds with the release of heat, water vapour, and carbon dioxide. The description of the microorganisms participating in the composting process is complex, because the populations and communities change continuously as a function of the evolution of temperature, nutrient availability, oxygen concentration, water content and pH in the course of composting. The composting processes occur in nature, but systems can be designed and managed to enhance and accelerate the process. The by-product of composting consists of the biomass of dead and living microorganisms, and undegradable raw material besides stable by-products of decomposition (NRCS, 2010).

Compost, in turn, is the nutrient amendment produced by an aerobic composting process as it is viewed in a compost bedded pack which is sufficiently stabilized to minimize or eliminate unpleasant odors, substantially reduce viable pathogens, facilitate storage, and handling without attracting insects and vectors. However, its complete stabilization is not considered practical or desirable because it would consume all the slowly degradable organic matter. The degree of stabilization and pathogen destruction

desired in compost depends on the purpose for composting and intended use of the compost by-product with a low risk of pathogen contamination. Compost is more stable (less microbially degradable), lighter, smaller in volume than raw manure. The finished product will need to meet the customer's or operator's needs (Goyal et al., 2005; Gajalakshmi and Abbasi, 2008).

In addition to the presence of the needed microorganisms, major factors as nutrients, carbon to nitrogen ratio, moisture content, temperature, and aeration are important factors to a successful composting process. Characteristics as appearance, texture, and even maturity may not be an issue if the compost from a bedded pack is used for land application on the farm.

In a CBP barn, the bed depth from surface that is tilled is called an oxic zone and acts like a frequently turned aerobic compost windrow with temperatures rising to the range of 45 to 60°C when good composting conditions occur. The bottom of the CBP is called an anoxic zone and is under an anaerobic decomposition process with little oxygen available. No agitation occurs and it becomes compacted with the added overburden of compost, by cows and tractor wheels. As would be typical for compacted manure piles, temperature rises above ambient, but it is only in the 25 to 40°C range. Figure 2.3 illustrates a CBP zones with possible gas pathways and temperature profile.

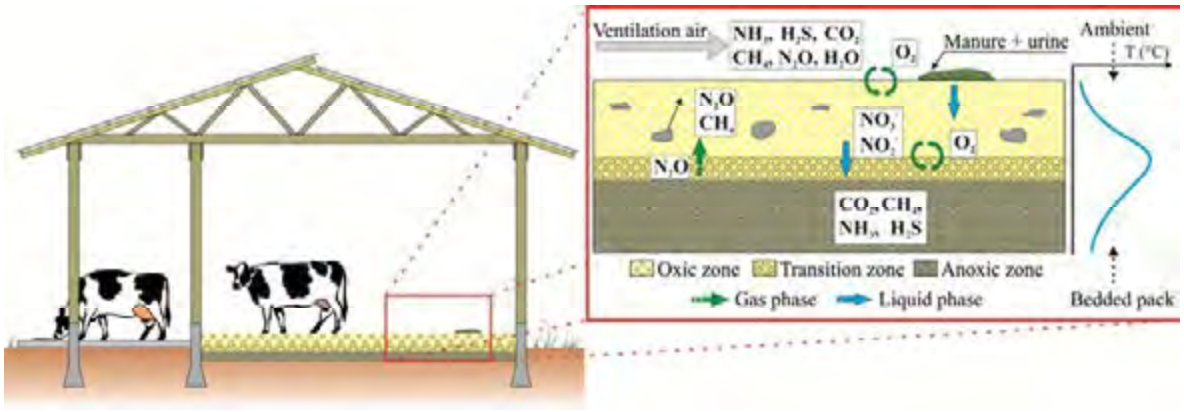

Figure 2.3 - Scheme of CBP zones with possible gas pathways and temperature profile.

As previously mentioned, composting is an aerobic process, meaning it requires large amounts of oxygen for the microorganisms to grow. It can be supplied to the compost bed by diffusion, wind, natural convection or forced aeration. A minimum oxygen concentration of 5% within the pore spaces of the compost is necessary for composting

occurs. If the supply of oxygen is limited, the composting process slows and may turn anaerobic, which is a much slower and odorous process with the potential for large N nutrient losses through denirification. During the initial stages of this aerobic process, oxygen and the easily degradable nutritional components of the raw materials are rapidly consumed by the microorganisms (NRCS, 2010).

Carbon (C), nitrogen (N), phosphorous (P), and potassium (K) are the essential and primary nutrients required by the microorganisms involved in composting. Microorganisms use carbon for both energy and growth, while nitrogen is essential for protein production and reproduction. Thus, an appropriate ratio of carbon to nitrogen (C:N ratio) usually ensures that the others required nutrients for their survival are present in adequate amounts. In this process, the temperature is directly related to the microorganism activity of composting and is a good indicator of how the process is going inside the bed (Goyal et al., 2005; Gajalakshmi and Abbasi, 2008).

Composting process becomes inhibited when the moisture content is below 40%. Water displaces much of the air in the pore spaces of the composting materials when the moisture content is above 65%. This limits air movement and leads to anaerobic conditions. Once moisture, is over 65%, the rate of decomposition in the anaerobic zone is likely not to be high enough to generate mature compost because it is too wet to support rapid bacterial activity. Some activity certainly does occurs, however, the material is not uniformly heated to the extent necessary to be sold commercially as compost and it would not meet USDA Organic Certification requirements for pathogen reduction. In addition, the volume of the pack does not increase much during the summer months, as it does in winter, indicating that composting is reducing the volume of the bedded pack. If the operator wants to market the material as compost after removing it from the barn, it will require further processing (NRCS, 2010).

Oxic zone can be modeled as a semi-continuously stirred tank reactor (CSTR) with moisture and fresh organic matter (manure and urine) added by the confined cows and intermittently stirred with gases continuously exchanged between atmosphere and CBP barn. As the depth of the bed deepens with organic matter, solid material is exiting the base of the oxic zone since tillage or mixing is only in the top 0.20 to 0.40 m. Anoxic layer can be modeled as a batch reactor with organic matter decomposition occurring producing gases that move up to the oxic layer. A transition oxic/anoxic zone lies between these

layers where the oxygen in the gas phase decreases with depth from the bottom of the oxic layer to zero concentration at the anoxic layer. The material in this zone could be mixed during tillage (Goyal et al., 2005; Gajalakshmi and Abbasi, 2008).

2.2.3.1. Microbiological processes in composting bedded pack

In a model system, aeration decreases as depth of CBP bed increases in depth and causes an oxygen concentration gradient between aerobic surface and anaerobic subsurface environments. The CBP system represents a dynamic environment in which spatial distribution of microbes and microbial metabolic processes develops. The composting process results from the breakdown and stabilization of organic matter, with CO_2 evolution and H_2O evaporation. It is impacted by relatively simple management practices such as barn ventilation and circulation and mechanical mixing of the bed.

Manure deposition provides a steady input of unstable C, organic N (protein and urea), and liquid fraction of the animal waste, which starts a cyclical series of microbial transformations over time transforming a fraction of this organic matter into inorganic C or N **(**Warner, 1942; Kristensen, 2000; Karthikeyan and Bhandari, 2001; Beffa, 2002; Megonigal, 2004; Peigne and Girardin, 2004; Goyal, et al., 2005). Figure 2.4 shows a spatial distribution of various microbiological processes in composting bedding.

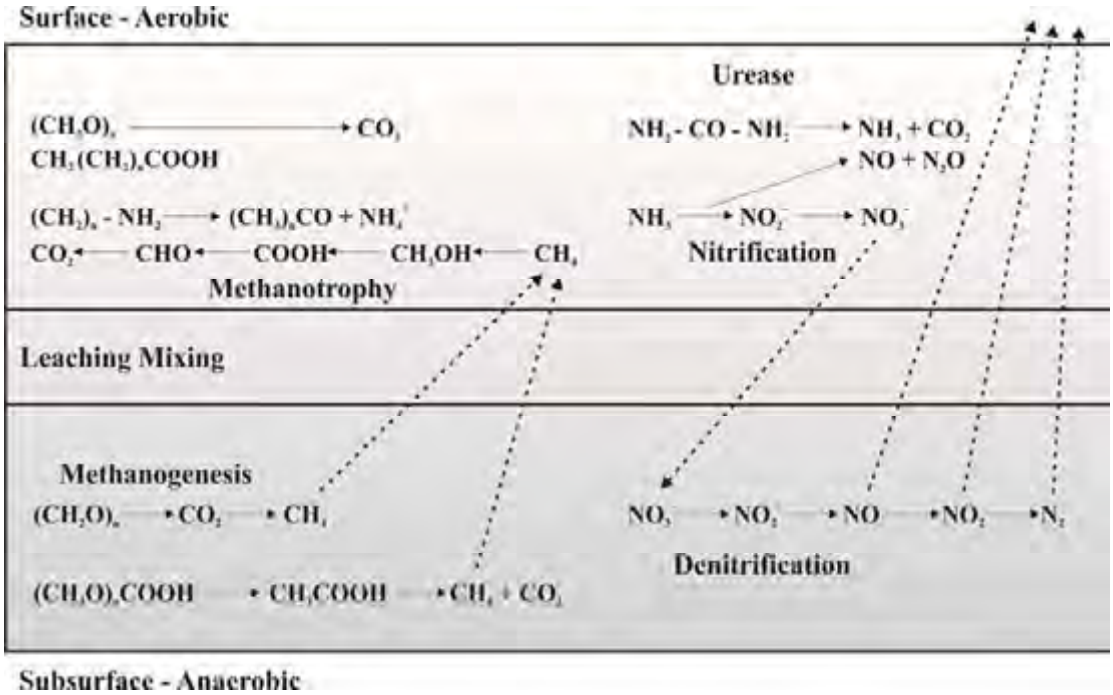

Figure 2.4 - Spatial distribution of various processes in composting bedding that lead to trace gas formation.

a) Oxic zone:

Gaseous emissions from the oxic zone during aerobic composting would contain emissions of ammonia (NH_3) and moisture and greenhouse gas emissions (GHGs): carbon dioxide (CO_2), methane (CH_4), and nitrous oxide (N_2O). In aerobic respiration, bacteria and fungi use molecular oxygen (O_2) to liberate the bulk of the energy (ΔH) from the organic matter that is being decomposed, producing carbon dioxide (CO_2) and water (H_2O) into the CBP oxic zone.

$$C_xH_yO_z + O_2 \Rightarrow CO_2 + H_2O + \Delta H$$

This is the principle fate of mineralized or oxidized organic carbon, occurring first by oxygen (O_2). This process generates more energy, increasing the temperature of the tilled top zone, and consequently inactivates the disease organisms and increases the evaporation of moisture (Warner, 1942; Kristensen, 2000; Karthikeyan and Bhandari, 2001; Beffa, 2002; Megonigal, 2004; Peigne and Girardin, 2004; Goyal, et al., 2005).

In the manure substrate, nitrogen (N) is present in organic matter as protein or in urine in the form of urea ($CO(NH_2)_2$). Aerobically, $CO(NH_2)_2$ undergoes hydrolysis and it is rapidly decomposed to NH_4^+ and CO_2 by the intracellular and extracellular urease enzyme produced by bacteria present in both feces and soil. NH_4^+ and CO_2 is also produced from the hydrolysis of protein in the organic matter. This process is known as ammonification. Controlled by thermodynamic equilibrium, the NH_4^+ form is in equilibrium with NH_3. This equilibrium is pH and temperature dependent. Due to concentration gradients, a fraction of NH_4^+/NH_3 is diffuse in the air-water interface of the manure, and it is partially emitted into the air. However, the dominant part of NH_4^+/NH_3 is either assimilated into microbial matter or nitrified to NO_3^-.

$$\text{Organic-N} \Rightarrow \underset{\Updownarrow}{\underset{NH_4^+}{NH_3}} \Rightarrow NO_2^- (+NO, N_2O) \Rightarrow NO_3^-$$

At the first stage of nitrification, the NH_4^+/NH_3 fraction is oxidized to NO_2^-. In the second stage, NO_2^- is further oxidized to NO_3^-. NO_3^- can subsequently be converted into nitrous oxide (N_2O), nitric oxide (NO) and dinitrogen (N_2) through denitrification (Blackburn, 1988; Robertson et al., 1989; Davidson, 1991; Henry et al., 1999; Maier et al., 2000; Beffa, 2002; Senga, 2002; Megonigal, 2004). The process by which NO_3^- is reduced

to nitrogen gases (N_2 or N_2O) is normally anaerobic but it can also occur in aerobic conditions where anaerobic microzones exist, such as internal spaces of porous organic particles.

b) Anoxic Zone:

The amount of denitrification depends on the availability of NO_3^-, on moisture saturation, on temperature, and on availability of easily decomposable organic matter. Thus, if the bed becomes depleted of O_2, some microorganisms can use the oxygen in NO_3^- as an alternative. During this process, NO_3^- is used as electron acceptor by fermentative microorganisms able to grow without free oxygen. The metabolic processes occurring while NO_3^- is used as electron acceptor to form N_2O and N_2 are equal to those occurring with the presence of O_2. In addition to N_2 formation, N_2O, NO and NO_2 may be produced under not completely anaerobic conditions.

The lower CBP anoxic layer also shows typical anaerobic gaseous emissions as methane (CH_4), CO_2, and other major gaseous emissions such as hydrogen sulfide (H_2S) and NH_3, that *moves upward* or are absorbed in the oxic zone. Anaerobically, carbohydrates and organic acids originating from *protein degradation* are converted by mixed heterotrophic and fermentative bacteria and fungi to acetate (CH_3COO^-/CH_3COOH) and CO_2, which in turn are transformed into CH_4 by two different microbial pathways in a process called methanogenesis.

$$CO_2 + H_2 \Rightarrow CH_4$$

$$CH_3COOH \Rightarrow CH_4 + CO_2$$

Methanogenesis represents a significant portion of the carbon gas flow in the anaerobic zone. CH_4 diffusing upward reaches the anoxic/oxic zone and it is consumed by oxidizing bacteria in a process known as methanotrophy (Megonigal, 2004). Thus, CH_4 is oxidized in the presence of O_2 so that it diffuses upwards to the oxic zone.

$$CH_4 + O_2 \Rightarrow H_2O + CO_2$$

The same microorganisms that oxidize NH_3 can oxidize CH_4. This implies that CH_4 could inhibit NH_3 oxidation and NH_3 could inhibit CH_4 oxidation, depending on the concentrations. Acidity of the CBP can affect this balance (Maier et al., 2000).

c) Oxic/Anoxic Zone:

The oxic/anoxic interface of these two layers becomes a zone where organisms can potentially produce or decompose similar emission gases. Denitrifiers convert NO_3^- to gaseous end products (NO, N_2O, N_2). The final gaseous phase products depend on available C and O_2 supply. Oxygen level is reduced by microbial oxidation of available organic C, which affects the reductive steps controlled by distinct enzymes affected.

$$NO_3^- \Rightarrow NO_2^- \Rightarrow NO \Rightarrow N_2O \Rightarrow N_2$$

N_2O is formed as an intermediate and it is available for release to the atmosphere through diffusion or during tillage (Warner, 1942; Kristensen, 2000; Karthikeyan and Bhandari, 2001; Beffa, 2002; Megonigal, 2004; Peigne and Girardin, 2004; Goyal et al., 2005; Coyne, 2008). Within the oxic/anoxic environment, an alternative route for the conversion and removal of NH_3 is possible for which substantially less information is known - anaerobic oxidation of NH_3 (ANAMOX).

$$NH_3 \Rightarrow NO_2^-$$
$$NH_3 + NO_2^- \Rightarrow N_2$$

This process has been found at the oxic/anoxic interface, both in an aquatic microenvironment (Warner, 1942; Kristensen, 2000; Karthikeyan and Bhandari, 2001; Beffa, 2002; Megonigal, 2004; Peigne, and Girardin, 2004; Goyal, et al., 2005) and in wastewater treatment (Maier et al., 2000). In natural oxic/anoxic interface of aquatic sediment microenvironments where CH_4, NO_2^- and NO_3^- are present, the following anaerobic methane oxidations are found (Raghoebarsing et al., 2006).

$$CH_4 + NO_3^- \Rightarrow N_2 + H_2O + CO_2$$
$$CH_4 + NO_2^- \Rightarrow N_2 + H_2O + CO_2$$

d) Entire Bed:

There are implications that gases, such as H_2S, CO_2, and CH_4 that are formed in the anoxic zone and move upward through the CBP zones, can affect the microbial processes shown above. H_2S emission can block the enzymes of microorganisms that oxidize NH_3 to NO_2^- at the oxic zone and the enzyme that reduces N_2O to N_2 at the oxic/anoxic interface of

both zone (Joye and Hollibaugh, 1995; Kristensen, 2000; Karthikeyan and Bhandari, 2001; Beffa, 2002; Megonigal, 2004; Peigne and Girardin, 2004; Goyal, et al., 2005).

The enzymatic system for anaerobic NH_3 oxidation can also be blocked by H_2S effect. Because of these blockages, the N_2O concentration at the oxic/anoxic interface rises if the organisms producing the needed enzyme for its production are present. The NH_3 concentration also rise. The CH_4 produced in the anoxic zone it infiltrates the oxic zone and compete for the enzyme that oxidizes NH_3. It is because the same microorganisms that oxidize NH_3 can oxidize CH_4 (Peigne and Girardin, 2004; Goyal et al., 2005).

Factors, such as, aeration, moisture, mixing, and substrate supply alter the dynamic equilibrium that exists between all these processes. Aeration can increase methanotrophy and nitrification process. Poor ventilation or moisture saturation can enhance the capacity for menthanogenesis and denitrification. GHG evolution depends in large part on how the systems are managed to generate the starting substrates, the rates of the microbial processes, and the subsequent transfer of by-products formed between aerobic and anaerobic zones (Warner, 1942; Kristensen, 2000; Karthikeyan and Bhandari, 2001; Beffa, 2002; Megonigal, 2004; Peigne and Girardin, 2004; Goyal et al., 2005).

Within the oxic layer, it is still possible to have the formation of anoxic zones where dense clumps exist (Bewley and Taraba, 2009) and the air diffusion is restricted. The tillage sweeps do not produce homogenous aggregates which leads to a second mode by which aerobic and anaerobic microbial processes can produce GHGs. Spatial distribution of aerobic and anaerobic zones is not simply by depth, but also by location within large aggregates that are created in the CBP.

2.2.4. Composting and moisture

Composting requires sufficient moisture for active microbial activity but not so much moisture to hinder aeration. Moisture levels between 50% and 60% are generally recommended for the most of composting materials. Urine, wet manure, and moisture from microbial activity are the moisture sources in a composting bedded-pack. When moisture is too low, the microbes won't have enough water, and the compost will be too cool, resulting in a compost rate that it is too slow. If the moisture level is too high, the pack becomes anaerobic (lacking in oxygen). In another words, the rate of microbial decomposition will be slow and again, composting and heat generation will also be too slow (Bewley and Taraba, 2009).

By stirring the pack, both moisture and manure can be mixed into the composting bedded-pack and will aerate the tilled layer. Good ventilation helps dry the freshly turned bedded-pack surface to retard bacterial growth on the surface and keep cows cleaner since dry bedding does not stick to the teat or leg surfaces. Compost barn owners from Minnesota recommend adding fresh bedding when the bedded pack becomes moist enough to stick to cows (Janni et al., 2005).

A wet bedded pack is more vulnerable to compaction. The compaction may be caused by the machinery that is used for stirring. Lower ground pressure tillage machinery should help reduce media compaction. Compaction in turn reduces air flow and oxygen in the bedded pack and thereby the pack can become anaerobic more rapidly. An anaerobic pack shows lower temperatures which leads to reduced pathogen kill, and more pest and odor problems (Janni et al., 2005; Graves, 1999).

2.2.5. Manure and effluent management

Management of animal manure and effluent is an integral part of a total dairy producer management plan. Changes in agricultural production have led to fewer producers, larger average herd sizes, purchase of feed from distant areas, and a much higher concentration of animals and production facilities on less land. In some areas livestock operations have become concentrated, and non-farm residents have located amongst the farms. These features increase the challenge for implementing good manure management plans (MWPS-7, 2000).

A manure management system includes: collection, transfer, storage, possible treatment, land application, nutrient utilization, and sampling.

Intensive, more specialized, concentrated animal production systems have altered the nutrient cycle and balance between crop production and animal production. Independent of operation size, a proper manure management system and plan are essential. A complete manure management system has the following goals: a) maintain good animal health and milk quality by providing sanitary facilities; b) avoid pollution of soil, groundwater or surface water; c) reduce odors and dust; d) control insect and other pest reproduction; e) and others (SWIM, 2011).

Failure to provide adequate manure collection, handling, and storage facilities in conjunction with adequate land area for proper application and utilization of manure nutrients could adversely affect air, water, and land resources.

CBP barns owners have some strategies for managing the effluent and manure. Some producers have added a little of the composted pack to the feed alley to absorb moisture (Barberg et al., 2007). The concrete feed alley is scraped at least twice a day. The collected manure and bedding is stored in an approved manure storage unit until land applied according to a manure management plan.

Bedded packs should be completely cleaned out each fall and applied to cropland as part of a manure management plan (Gay, 2009). CBP barns owners in Minnesota have been removing a portion of the pack for land application in Spring, and doing a complete cleanout in the Fall. While this works well for manure management, it presents concerns for nutrient management, since manure applied in Fall may lose nitrogen over the winter. The rationale for Fall cleanout is that the CBP barns owners want maximum manure storage over the winter (Barberg et al., 2007). When the material is removed from the barn, it can either be land spread as is, or composted further to produce a product suitable for horticulture, organic agriculture, and home gardens. As it comes out of the barn, the bedded pack material has a high C:N ratio, is high in soluble salts, and has pathogens in it, but it works well for meeting the nutrient requirements of field crops (Petzen et al., 2009). Compost used as a soil conditioner has the potential to result in higher crop yields and reduced erosion (NRAES-54, 1992).

Care must be taken to avoid disturbing the clay base during clean out and pack stirring when the bedded pack is less than 0.30 m deep. Some users recommend starting with 0.45 to 0.60 m of sawdust to avoid problems. The composting bedded pack is typically cleaned out and land applied in the fall after corn silage is harvested. Fall clean out allows time for a new pack to accumulate and begin composting before cold weather sets in. Some operators remove some of the bedded pack in the spring before fields are planted to make sure there is sufficient space for pack accumulation during the summer when cropland is not available for manure application. However, if a compost bed is active, particularly during the non-winter months, bed depth is reduced by microbial activity, but it can also occur due to less bedding used. Going into winter, there may not be a great depth and therefore adequate storage is present to get through winter. CBP barns require equipment to handle manure as both a solid (the pack) and a slurry (the feed alley manure). This increases a producer's investment in equipment (Janni et al., 2007).

2.3. Physical properties of the bedding material

The physical properties of compost bedding materials play an important role in every stage of compost production as well as in the handling and utilization of the end product. From the mixing of various feedstock and process monitoring and maintenance, to the packaging and shipping of the final product, parameters such as porosity, bulk density, particle density, moisture content, water holding capacity and particle size affect the optimum composting environment and the design of machinery used in the system to promote the aeration of the compost bedding material.

Although compost can vary and must be carefully tested to determine their exact nature, numerous laboratory trials with different products have successfully quantified the beneficial effects (CUC, 2003).

2.3.1. Porosity

Transport of mass and heat in a compost layers is significantly affected by the geometry and size distribution of the pores and the composition of the composting material. Therefore it is at least necessary to have information about the spatial distribution of porosity. Porosity can be calculated from dry matter content, true density of dry matter and total bulk density. Dry matter content and true density of dry matter are easily measured in the laboratory (Ginkel et al., 1999).

Porosity is the ratio of the pore space to the total volume occupied by the material and the ideal bed porosity is one that provides the greatest surface area for microbial activity and the least resistance to airflow through the compost layer. It is determined by the particle size, the size gradation of the materials, and the continuity of the air spaces. Larger particles and more uniform particles increase porosity (NRAES-54, 1992).

Porosity greater than 50% causes the compost layer to remain at a low temperature because energy loss exceeds heat produced. Too little porosity leads to anaerobic conditions and odour generation from too little oxygen occupying the reduced void space. The percentage air-filled pore space of composting layer should be in the range of 35% to 50% (Bernal et al., 2009).

2.3.2. Bulk density

The bulk density of compost is a measure of the mass of material within a given volume and it is important in the determination of initial compost mixtures. The bulk

density determines how much material can be placed at a certain site (Agnew et al., 2003). The density of compost also influences the mechanical properties such as strength, porosity, and ease of compaction (Agnew and Leonard, 2003). Therefore, knowing the bulk density of the material throughout the compost layer is important for aeration, handling, and storage requirements.

However, distinction is made between time dependent and independent processes to describe bulk density distribution. The time independent process results from the compressibility of composting material. Compressibility is defined as the reciprocal of the resistance of the material against mechanical deformation, or more precisely, as the ratio between deformation and stress. Due to this property the bulk density is a function of the local pressure and therefore depends on the position within in the compost bed (Ginkel et al., 1999).

The time dependent process is defined as the increase of mechanical deformation as a function of time under constant pressure conditions (Ginkel et al., 1999). When a composting material is spread over the pack area, the initial bulk density distribution is only determined by the compressibility of the composting material. However, during the process, bulk density and porosity are also influenced by the combined effects of subsidence, loss of organic matter due to biological degradation processes and change of water content due to transport processes.

The effect of compaction pressure on bulk density is also studied. It is observed that the effect of compaction pressure on bulk density for larger particles is higher in comparison with smaller particles, because smaller particles are closely packed leaving less space among the particles (Mozammel et al., 2006).

Parameters that influence the bedding material performance are moisture content, bulk density and porosity (Wright and Inglis, 2002). This is relative to green materials that are high in water, which would not be suitable for bedding. Dried straw wood and other forages would be needed. Thus, increasing bulk density, moisture content and depth of the pack can result in decreased permeability, especially for oxygen. If the moisture content in the pack increases, particles get wet resulting in reduced strength of the media (Ahn et al., 2009). This can cause anaerobic condition in the pack which leads to odor, low temperatures and emission of nitrogen compounds as well as methane. Materials that absorb too much water or urine are not suitable such as bedding material as this high

moisture content can rupture the cell walls which results in additional free water. In addition wet bedding also contributes to dirtier cows.

Soybean straw and chipped pallet material worked well in combination with sawdust in the compost bedded pack system. Both materials provided the absorbency and bulk density necessary to meet cow comfort and the porosity required to promote an aerobic compost process (Petzen et al., 2009).

2.3.3. Particle density

The accurate quantification of particle density, as a component of bulk density, is vitally important for gravimetric compost measurements. For other media such as soil, particle density is often assumed to be 2.65 g cm^{-3}, the density of quartz (Brady and Weil, 2002). However, compost particle density is more inconsistent due to variation in source materials.

Concisely stated, the method employs the submersion of a known mass of compost in methanol to determine the volume of the compost solids. While methanol is used because of its low density (0.66 g cm^{-3}), the premise of the method remains valid for many other low density liquids. The use of a low density liquid causes particles that are normally buoyant in water to sink, facilitating an accurate measurement of the compost solids volume (Weindorf and Wittie, 2003).

2.3.4. Moisture content

It is the fraction or percentage of a substance comprised of water. The moisture content on a dry basis is the wet weight minus dry weight divided by the dry weight minus the container weight. To obtain the moisture content in percent, multiply this ratio by 100 (Mukhtar et al., 2004). The general procedure involves weighing the wet sample and then drying the sample for 24 hours at temperatures of 105°C. The moisture content on a wet basis can be calculate using equation 2.1.

$$\text{Moisture content (\%)} = \frac{\text{Wet weight - Dry weight}}{\text{Wet weight - Container weight}} \cdot 100 \qquad (2.1)$$

Methods for determining moisture content on the farm differ in the way that the sample is dried. Three common methods include air drying, conventional oven drying and

microwave oven drying. Although the results produced by these methods are less accurate than laboratory procedures, they are satisfactory for almost all composting situations (NRAES-54, 1992).

The moisture content of compost affects the bulk density. Moisture content is also relevant because it affects compost handling. Compost which is dry can be dusty and irritating to the cows and workers, while compost which is wet can become heavy, making its application more difficult and transport more expensive.

The ideal moisture content for composting must therefore be a compromise between achieving adequate moisture for the microorganisms to survive and adequate oxygen flow to maintain aerobic conditions. The moisture content for composting is generally recommended to be in the range of 40 to 60% (Shane et al., 2010; NRAES-54, 1992), and can be tested accurately using analytical equipment or approximated using a hand-squeeze method. In the hand-squeeze method, a handful of compost material is squeezed firmly several times to form a ball. If the ball crumbles or breaks into fragments, the moisture content is much less than 40%. If it remains intact after being gently bounced 3-4 times, the moisture content is nearly 50%. If the ball texture is slimy water droplets drip from or appear on the surface of squeezed bedding, the pack is too wet, the moisture content is much higher than 60% (Mukhtar et al., 2004). When the pack is working well, the bedding material will appear loose and fluffy, not compacted and chunky (Bewley and Taraba, 2009). Pack moisture content in the top layer should ideally be monitored weekly to decide when clean bedding needs to be added to the pack (Shane et al., 2010) as opposed to when the cows are dirty.

2.3.5. Water Holding Capacity

Water holding capacity (WHC) is the ability of a given volume of compost to hold water under one atmosphere of pressure. In another words, WHC is the ability of compost to retain moisture against drainage due to gravity. Moisture (manure and urine) is held in the spaces, or pores, between compost material particles and thin films around these particles. Organic matter and particle size affect the compost ability to retain moisture. WHC is measured as a percent of dry weight.

The WHC provides information on the amount of water that can be absorbed by the bedding material. High WHC allows the media to absorb water into the bedding. However,

depending on the cell structure of the media, high water content in the cell can sometimes lead to rupture of the cell which results in the media releasing free water (Vokey, 2008). This limits the media's ability to function as a bedding material for longer periods of time. Some research have observed that WHC increased with decrease in the particle size of the compost media (Changirath et al., 2011). For this reason, one of the functions of the bedding material in the CBP barns is to retain moisture. Therefore, if the compost material has a high WHC, the ability of dairy producer to dry in the pack can be lower.

2.3.6. Particle size

Particle size and distribution are critical for balancing the surface area for growth of microorganisms and the maintenance of adequate porosity for aeration. The larger the particle size, the lower the surface area to mass ratio. So, compost with large particles does not decompose adequately because the interior of the particles has difficult accessibility for oxygen for aerobic microorganisms (Bernal et al., 1993). However, particles which are too small can compact the mass, reducing the porosity and airflow within the compost layer will be restricted. A mix of particle sizes creates the most porous layer, see Figure 2.5.

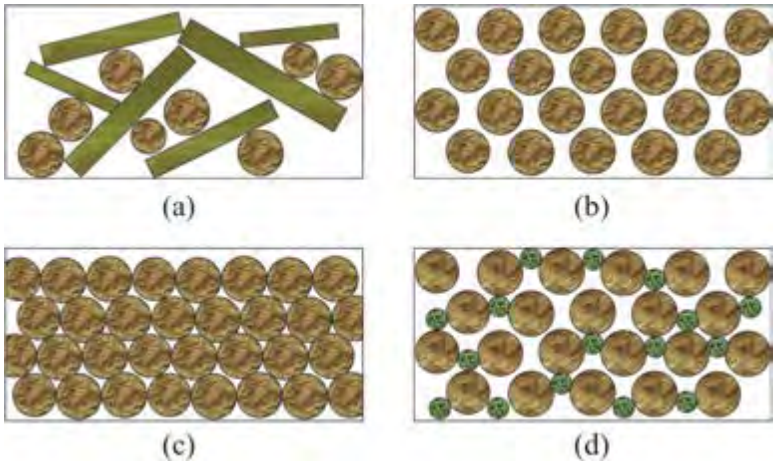

Figure 2.5 - Porosity affecting the aeration: (a) Loosely packed - well structured, (b) Loosely packed - uniform particle size, (c) Tightly packed - uniform particle size, and (d) Tightly packed - mixed particle sizes. (CUC, 2003).

Media particle size distribution is an important factor influencing the bedding moisture content, compaction and bulk density. Sawdust serves as a good carbon source and when fine materials like sawdust are used as a bedding media. They need to be turned frequently in the pack. It has also been suggested that the amount of fine particles in the bedding has

an effect on the bacterial population on the teat ends. Factors such as particle size may be more important than simply bacterial counts in the used bedding (CWMI, 2006). The finer the media, the more time is required to clean the udder before milking.

Microbial activity generally occurs on the surface of the organic particles. Therefore, decreasing particle size, through its effect of increasing surface area, will encourage microbial activity and increase the rate of decomposition. On the other hand, when particles are too small and compact, air circulation through the compost layer is inhibited. This decreases O_2 available to microorganisms within the compost and ultimately decreases the rate of microbial activity (NRAES-54, 1992).

Particle size also affects the availability of carbon and nitrogen. Large wood chips in bedding, for example, provide a good bulking agent that helps to ensure aeration through the compost layer, but they provide less available carbon per mass than they would have in the form of wood shavings or sawdust.

Handreck (1983) studied the particle size and physical properties of compost media and concluded that the fraction smaller than 0.5 mm, and in particular between 0.1 and 0.25 mm, has the highest influence on porosity and water retention.

2.4. Thermal property of the bedding material

Compost thermal properties are required in many areas of agriculture engineering, agronomy, and animal science. In recent years, considerable effort has gone into developing techniques to determine these properties (Abu-Hamdeh, 2003).

Thermal properties of compost bulking materials affect temperature and biodegradation during the composting process. Well determined thermal properties of compost feedstock will therefore contribute to practical thermodynamic approaches (Ahn et al., 2006).

Thermal conductivity, specific heat capacity, and thermal diffusivity are the three important thermal properties regarding heat transfer analysis. These three thermal properties can be measured by several methods (Ahn et al., 2009).

The thermal conductivity is the property that describes the heat transfer capacity within the compost material. The specific heat capacity is the amount of energy required to raise the compost material one degree Celsius. Thermal diffusivity has been used as an indicator for the utility of compost materials as an insulator or heat conductor. In other words, thermal diffusivity is the measure of thermal inertia.

Although thermal properties are very important in composting, information on their values for various compost materials is lacking. In general, it is difficult to determine the thermal properties of moist materials because forced heating during the measurements causes internal liquid and/or gas convection. This often results in overestimating the thermal properties. The thermal probe method is the most attractive method, because it uses relatively simple equipment to determine the thermal properties for moist materials (Iwabuchi et al., 1999).

2.4.1. Thermal conductivity

The thermal conductivity coefficient of a compound medium is often a very complex quantity. It is dependent not only on the components themselves, but also on structure, composition, density, porosity, water content and temperature (Van Ginkel et al., 1999). Certainly in a compost bedding layer, where all these parameters are changing during the compost management and process, the only way to obtain reliable values is to measure this quantity. Thermal conductivity can be measured by the steady and non-steady state (transient heat dissipation) methods (Mohsenin, 1980).

Transient line heat source methods have been used several years to measure thermal conductivity of porous materials, like bedding compost. Typically a probe for this measurement consists of a needle with a heater and temperature sensor inside. A current is passed through the heater and the temperature of the probe is monitored over time. An analysis of the probe temperature is used to determine thermal conductivity. More recently the heater and temperature sensor have been placed in separate needles. In the dual probe the analysis of the temperature versus time relationship for the separated probes yields information on diffusivity and heat capacity as well as conductivity (Bristow et al., 1994).

2.4.2. Specific heat capacity

The specific heat capacity can be defined as the amount of heat energy required raising the temperature by one degree Celsius per unit mass (Incropera and DeWitt, 2001). Several researchers studied the behavior of thermal properties with the variation of water content of various biological materials and observed that there is a relationship in which the increase of water content causes high values of specific heat (Ahn et al., 2009).

Factors influencing specific heat capacity that can be managed externally include moisture content and compost density. Moisture content plays a major role in specific heat

capacity but is the most difficult to manage (Abu-Hamdeh, 2003). Compost management affects specific heat capacity by the machinery that is used for stirring (Janni et al., 2005). Because of this, the bulk density increases and the porosity of a compost bedding decreases. This in turn have a significant effect on specific heat capacity.

2.4.3. Thermal diffusivity

Several studies have reported two of the thermal properties and obtained the thermal diffusivity using the following relationship (Haug, 1980; Briaud and Chaouch, 1997; Bristow, 1998; Abu-Hamdeh, 2001):

$$\alpha = \frac{k}{\rho \cdot C_p} \tag{2.2}$$

where: α is the thermal diffusivity (m^2/s), k is the thermal conductivity (W/m °C), ρ is the bulk density (kg m^{-3}) and C_P is the specific heat capacity (J/kg °C).

Thermal diffusivity, like thermal conductivity, is a property of the substance. The term $k \cdot \rho^{-1} \cdot C_p^{-1}$ appears in many heat conduction problems and is related to the diffusion coefficient used in mass transfer analysis or modeling.

2.5. Chemical properties of bedding material

Since a variety of organic materials can be used to make bedding composts (i.e., rice husks, coffee husks, bagasse, paper, peanut shell), it becomes very important to know their chemical characteristics, in order to obtain the required chemical characteristics for growth media (Zoes et al., 2001).

Carbon (C), nitrogen (N), phosphorus (P) and potassium (K) are the primary nutrients required by the microorganisms involved in composting. Nitrogen, phosphorus, and potassium are also the primary nutrients for plants; so their concentrations also influence the value of the compost.

Many organic materials, including manures and organic materials, contain ample quantities of nutrients (Table 2.2). Composts that are derived primarily from wood by-products have high carbon to nitrogen ratios unless additional nitrogen is added during the composting process. Excessive or insufficient carbon or nitrogen is most likely to affect the

composting process. Microorganisms use carbon for both energy and growth while nitrogen is essential for essential protein production to the metabolism and reproduction. In general, biological organisms need about 25 times more carbon than nitrogen (NRAES-54, 1992). Therefore, it is important to provide carbon and nitrogen in appropriate proportions. The ratio of carbon to nitrogen is referred to as the C:N ratio.

Table 2.2 - Common feedstock and their characteristics

Feedstock	Moisture content (%)	C:N	Bulk density
High in Carbon			
Hay	8 - 10	15 - 30	-
Corn stalks	12	60 - 70	32
Straw	5 - 20	40 - 150	50 - 400
Sawdust	20 - 60	200 - 700	350 - 450
Wood chips	-	100 - 500	-
High in Nitrogen			
Dairy manure	80	5 - 25	1400
Grass clippings	-	15 - 25	

Source: Adapted from NRAES-54 (1992).

A balanced C:N ratio usually ensures that the other required nutrients are present in adequate amounts. To calculate the carbon content given C:N and percent nitrogen, solve:

$$C(\%) = N(\%) \cdot C{:}N \tag{2.3}$$

Raw materials blended to provide a C:N ratio of 25:1 to 30:1 are ideal for active composting, although initial C:N ratios from 20:l up to 40:1 consistently give good composting results. For many applications, C:N ratios of even 50:1 and higher are acceptable. With C:N ratios below 20:1 the available carbon is fully utilized without stabilizing all of the nitrogen. The excess nitrogen may then be lost to the atmosphere as ammonia or nitrous oxide and odor can become a problem. Mixes of materials with C:N ratios higher than 40:1 require longer composting times for the microorganisms to use the excess carbon (NRAES-54, 1992).

Compost bedded pack manure is an excellent nutrient source to use with zone-till and no-till cropping systems. This is because more of the nitrogen is in its stable organic form, compared to liquid or fresh (Petzen et al., 2009).

2.6. Biological properties of compost bedding material

One of the aspects of composting that makes it an attractive alternative to the direct application of untreated manure is the high degree of pathogen destruction that is possible with a well-managed composting operation. The pathogen content of the compost is important because improperly treated compost can be a source of pathogens to the environment and, as such, a threat to humans and animals.

2.6.1. Predominant groups

Pathogenic microorganisms that may be in compost include bacteria, viruses, fungi, and parasites. Although parasites and viruses cannot reproduce apart from their host, they can often survive for extended periods. If they are not killed during the composting process, they can survive until the compost is land applied. At that time, they may infect a new host (NRCS, 2010). In the compost process, these species will thrive or fail according to their abilities to find a niche in the compost ecosystem (Sales, 2008). Typical species are shown in Table 2.3.

Table 2.3 - Some species of microorganisms found in composting.

Actinomycetes	**Algae**
Actinoplanes sp.	Chlorococcum humicola
M. vulgaris	Dactylococcus (bicandatus)
Micromonospora parva	Euglena mutabilis
Nocardia brasiliensis	Hormidium (nitens)
Pseudomocardia	Kentrosphoera sp.
S. recius	Microcoleus vaginatus
Bacteria	**Fungi**
Aerobacter (aerogenes)	Abridia (ramosa)
B. cereus	Aspergillus flavus
B. mycoides	Geotrichum candidum
B. stearothermophilus	Hanisenuia sp.
Bacillus megatherium	Mucor pusillus
Cellumonas folio	Mucor racemosus
Chondrococcus exiguus	Penicillium digitatum
Protozoans	
Cercomonas (crassicauda)	
Chilomonas (paramecium)	
Cyathomonas (truncate)	
Lycogala epidendrum	

Adapted from Epstein (1997).

2.6.2. Bacteria

Bacteria are the smallest living organisms and the most numerous in compost. They make up 80 to 90% of the billions of microorganisms typically found in a gram of compost. Bacteria are responsible for most of the decomposition and heat generation in compost. They are the most nutritionally diverse group of compost organisms, using a broad range of enzymes to chemically break down a variety of organic materials (CWMI, 2006).

Among the bacteria, the actinomycetes, and the bacteria (gram negative and positive) are most important in the context of composting (Table 2.4), the former as allergens and opportunistic pathogens, and the latter as indicators of an insufficient thermohygienization (fecal coliforms) and as producers of endotoxins (Beffa, 2002).

Table 2.4 - The following groups of human and animal pathogens as having the most importance in composting environments.

Bacteria	Fungi	Viruses
Coliform	Aspergillus fumigatus	Coxsackie-B-Virus
Enterobacteraceae	Penicillium	Echo-Virus
E. coli		
Pseudomonas		
Staphylococci		
Streptococci		
Staphylococcal species		
Streptococcal species		

Source: Beffa (2002).

Bacterial growth over time can be graphed as cell number versus time. This is called a growth curve. The cell number is plotted as the log of the cell number, since it is an exponential function. Regardless of the generation time, in a growing culture, the plot of the log of cell number versus time gives a characteristic curve (MBS, 1999). This curve typically has four distinct phases: lag phase, exponential phase, stationary phase, and death phase, see Figure 2.6.

Many factors affect the generation time of the organism: temperature, pH, oxygen, salt concentration and nutrients are some of the common factors that may change in the normal environment of bacteria. Due to difficulties in tracking and quantifying the relationships between physical factors and bacterial populations, it has not been possible to fully understand the ecological processes important in composting. Identifying these

relationships has been complicated by the presence of an uncontrolled bacterial inoculum that varies between operations due to variations in material handling, air conditioning, and substrate composition (Schloss et al., 2003). Several previous composting studies, though, have attempted to quantify bacterial populations using different techniques (Nakasaki et al., 1985; Strom, 1985).

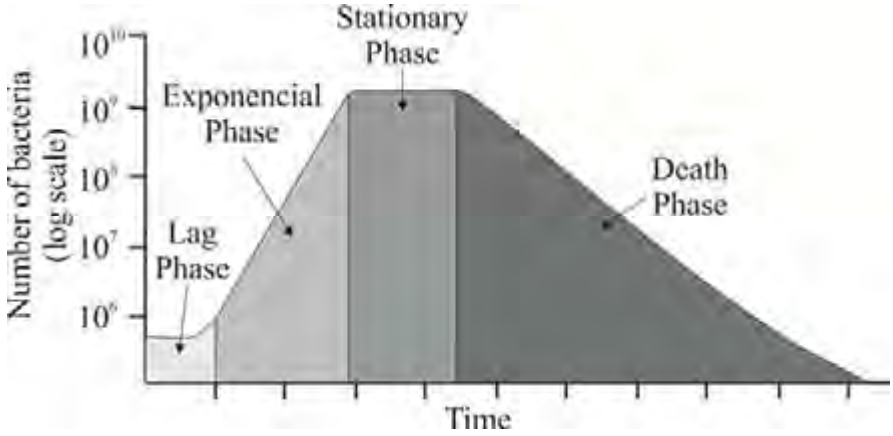

Figure 2.6 - Bacterial growth curve and the four phases of growth versus time (Adapted from MBS, 1999).

2.7. Mathematical modeling

Mathematical modeling is a method of research that investigates, through mathematical problems, phenomena or situations from different areas such as physics, chemistry, biology, engineering, and others, consisting in an area of research that is essentially interdisciplinary, to make predictions about the situation or problem investigated. This set of relations is called a mathematical model of the problem studied. The dynamic process used to create and validate such models is called mathematical modeling (Bassanezzi, 2002).

Mathematical modeling has a role to evaluate the interaction between several factors allowing a more detailed study in order to predict the processes of interest, and the ideal is to formulate a model capable of describing the original study, without the difficulties encountered in observations and measurements made during examination of the problem. Moreover, the mathematical model is a simplification of the system being studied, and cannot predict all the variables present. The resulting prediction may not be accurate or reliable. When using f mathematical models, it is necessary to determine the parameters

through empirical experimentation implying the need for several samples (Pereira and Machado, 1987).

Over many years agricultural buildings, such as dairy barns, have become tailored for specialized production The need to maintain control over the indoor climate has become ever more important so that the requirements of the production system can be continuously met. In essence it is necessary to understand the interaction of all climatic variables, alongside their contribution to the occupants heat exchange with its surroundings in order to predict the micro-climate (Norton et al., 2007).

Therefore, the thermal environment of a agricultural building is intricately linked with ambient conditions. Optimizing and controlling ventilation systems are not elementary problems and may require extensive experimentation (Boulard et al., 2002a; Zhang et al., 2000). Sophisticated techniques that allow efficient and accurate description of the dominant phenomena are often required. The mathematical modeling of the interaction between the indoor production system, the ventilation system and the outdoor environment is thus a necessary requirement. The clear advantages of developing mathematical models for agricultural buildings are as follows (Schauberger et al., 2000):

a) They can quantify the essential needs of the occupant in all parts of ventilated buildings and consequently contribute to the development of optimization strategies aimed at increasing production performance.

b) They can be incorporated as part of indoor climate control, as well as to check the design values of the ventilation system.

c) They can combine the spatial and temporal dependent parameters that affect release of all pollutants within the building to efficiently calculate time-varying concentrations within, and emissions from production systems.

d) They can quantify different housing systems with alternative manure management techniques to achieve a fully integrated control of pollution.

Therefore, agricultural production systems, which are amenable to description through the physical laws of fluid motion, heat and mass transfer processes, can be effectively modeled so that the benefits of pre-design evaluation, design and optimization strategies can be realized (Norton et al., 2007).

The modeling of ventilation flow in agriculture building can be can be performed using the Navier-Stokes equations (Norton et al., 2007). The Navier–Stokes equations

represent the dynamic behavior of a flow regime, both spatially and temporally. These equations constitute a micro-model of fluid motion, and require time consuming iterative techniques to solve them. Thus, the efficient quantification of ventilation in agricultural buildings can be carried with a macro-model based on Bernoulli's equation. This requires some qualifying assumptions so that the model matches the spatial domain of interest, such as the flow is not viscous; steady, not rotational; with hydro-static and gravity as the only acting external force (Roy et al., 2002). Consequently, much information on the flow is lost, including details on the spatial distribution of the airflow patterns, which can lead to inaccuracies in the calculated airflow variables (Boulard et al., 2002b).

According to Mueller and Krause (2007), when sizing ventilation systems there are different methods which may be used to obtain an overall view of the heat transfer and mass transport phenomena inside the animal production facility, including numerical simulation of flow, physical models and measurements on a real scale.

a) Numerical simulation of flow: from this simulation it is possible to study the behavior of fluids in motion. Therefore, it has become very interesting to study these phenomena with the advance of faster computer processors and more efficient software. Fluid mechanics include, for example, study of either laminar or turbulent fluid and gas flow in animal installations. This type of study may present important practical applications in the diverse areas of engineering.

b) Physical models: investigations with physical models offer greater support to the numerical simulation of mass flux. The ventilation system as well as the flux of air volume may be altered by a simple formula, i.e., the reconstruction of entire elements may be performed quite simply in such models.

c) Another form of evaluating the dispersion behavior of gases coming from animal installations is by the utilization of the wind tunnel boundary limit, where in many cases these are equipped with air velocity sensors and gas analyzers to measure the variation in concentration.

d) Real scale measurements: are necessary to confirm the numerical and physical models in real conditions. A specific problem is the determination of volumetric air flux in naturally ventilated animal installations (Mueller and Krause, 2007).

Various studies involving mathematical modeling and computational simulations have been developed during experimentation to improve understanding of the processes involved in the transfer of heat and mass between animals and their thermal environment.

2.8. Computational Fluid Dynamics (CFD)

Computational fluid dynamics (CFD) can be defined as a numerical resolution based on computational loops and the equations of mass, momentum and energy conservation for physical systems (Miranda, 2009). The method works by solving the equations of transporting mass and energy and momentum through a process number called difference numerical methods. Figure 2.7 illustrates the initial work of the numerical method, which is discretize the domain in a number of non-coincident sub-domains forming a grid of small elements (or volume control) to which a discrete solution can be obtained. For this, some transformations are performed in differential transport equations, defined continuously in the domain, in a system of algebraic equations for the discretized Domain (Maliska, 1995).

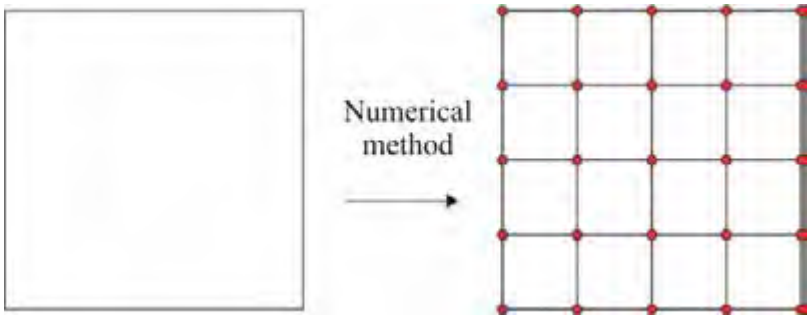

Figure 2.7 - The initial work of the numerical method: discretize the continuous domain (Maliska, 1995).

The CFD methodology was initially and widely used in aerospace industry, automotive, naval, and nuclear. Recently it has been applied in agricultural engineering. The availability of high-performance, low cost computers and with the emergence of CFD programs with friendly interfaces, has allowed great advances in the use of this technique since the 90's. Moreover, the versatility and generality of the numerical methods for simulation of engineering problems, and the relative simplicity of application of these techniques are other factors motivating the use of CFD.

This technique provides precise solutions as well as visualizations of velocity, pressures, temperature, turbulence and gas concentrations in the entire space of the animal

installation without various physical scale test models. Results allow that engineers and operators to develop new ventilation strategies to meet the standards for air quality (Lee and Short, 2000).

Modeling in CFD is important to predict mass transport in different types of animal structures, especially when field measurement of the variables related to the model is difficult. In the case of modeling gas emission that eliminate from inside the installations, for example NH_3, the computational models are based on the NH_3 transport process and the transport mechanism to the atmosphere (Bjerg et al., 2002).

Currently, sophisticated commercial CFD programs like CFX (ANSYS CFX 13.0, 2011), can run on personal computers in the workplace and even at home. Also the costs of the required equipment acquisition are getting smaller. Thus, it becomes easier to use numerical techniques for solving engineering problems.,

Undertaking a CFD study demands the use of four predefined environments within the software, with each environment representing an equally important section of the modeling process. The following provides an introduction to the different modules comprising a CFD software package: a) generating geometry and mesh; b) pre-processor; c) solver manager; and d) post-processor.

a) Geometry and mesh generator:

It consist of insertion of problem into CFD code. The embedded information involves:

i) Definition of geometry and solution domain: This step can be performed in a secondary program; CAD (Computer Assisted Drawing) as SOLIDWORKS® or Rhinoceros® and then imported by the CFD code, operation commonly performed when working with CFX.

ii) Meshing: consists of discretization of a continuous domain into a set of discrete sub-domains, usually called elements.

Approximately 50% of the time used in a CFD project is to define the geometry and mesh generation (Malalasekera and Versteeg, 1995). In CFX, DESIGNMODELER module is used to generate or import geometry and *CFX-Mesh* is used to generate the mesh.

b) Pre-processing:

The pre-processor of CFD software holds all the mathematical statements attributable to the potential success of a modeling exercise and therefore embodies the most important

phase of model definition. The main tasks facing a user in the pre-processing environment include problem consideration, geometry creation or import, mesh development, physical property set-up, and the implementation of solving techniques and parameters.

c) Solver manager:

The solver environment, within all commercial CFD software packages, organizes the mathematical input from the pre-processor into numerical arrays and solves them by iterative methods (Norton et al., 2007). Iterative methods are commonly used to solve a whole set of discretized equations so that they may be applied to a single dependent variable. Segregated solving techniques, such as Semi-Implicit Method for Pressure-Linked Equations (SIMPLE) used by most commercial CFD software packages, determine the pressure field indirectly by closing the discretized momentum equations with the continuity equations in a sequential manner (Patankar and Spalding, 1972). However, as the number of cells increase the elliptic nature of the pressure field becomes more profound and the convergence rate is inhibited. This has led to the development of multigrid techniques that compute velocity and pressure corrections in a simultaneous fashion, thus enhancing convergence rates (Ferry, 2002).

d) Post-processor:

The post-processing environment allows the user to visualize and investigates the resulting field solution. Contour, vector and line plots enhance interpretation of results and are being progressively fortified in commercial software packages. Some packages also allow the export of field data to external modeling programs so that it can be processed further (Norton et al., 2007). In CFX, the CFX-POST module is used for post-processing.

Thus, the complete analysis in CFD is composed of pre-processing, processing and post-processing, which includes the procedures and phenomena to adequately analyze the configuration of the problem with the solution, monitoring and analysis of results at the end of simulation (Rocha, 2012).

2.8.1. ANSYS

ANSYS is a set of commercial software for numerical solutions in fluid dynamics modeling and other physical phenomena with a multidisciplinary approach and the possibility of integration with other types of physical simulation technologies, which the

main tools for simulation and analysis of fluids are known by FLUENT and CFX (Xia and Sun, 2002).

2.8.2. Governing equations

The governing equations of fluid flow and heat transfer can be considered as mathematical formulations of the laws of conservation which regulate all fluid flows, heat transfer and associated phenomena. These laws of conservation describe the rate of variation of a desired fluid property as a function of external forces.

a) Conservation of mass:

The law of conservation of mass states that mass can neither be created or destroyed. This is the basis for the continuity equation. It can be represented in Cartesian coordinates by the following equation (Rocha, 2012; Hirsch, 2007).

$$\frac{\partial \rho}{\partial t} = \frac{\partial(\rho \cdot u_x)}{\partial_x} + \frac{\partial(\rho \cdot u_y)}{\partial_y} + \frac{\partial(\rho \cdot u_z)}{\partial_z} = 0 \tag{2.4}$$

where,

t is the time (s);

ρ is the density (kg m^{-3});

x, y, z are the coordinate direction;

u_x, u_y, u_z are the velocity in the directions x, y, z respectively.

b) Conservation of momentum:

The sum of the external forces acting on the fluid particle is equal to its rate of change of linear momentum (Rocha, 2012).

$$\underbrace{\frac{\partial u}{\partial t}}_{\text{Unsteady acceleration}} + \underbrace{u_i \cdot \frac{\partial u}{\partial_i} + u_j \cdot \frac{\partial u}{\partial_j}}_{\text{Convective acceleration}} = \underbrace{-\frac{1}{\rho} \cdot \frac{\partial P}{\partial_i}}_{\text{Pressure gradient}} + \underbrace{\nu \cdot \frac{\partial^2 u}{\partial i^2} + \nu \cdot \frac{\partial^2 u}{\partial j^2}}_{\text{Diffusion}} \tag{2.5}$$

where,

ν is the kinematic viscosity (m^2 s^{-1});

P is the pressure (Pa).

The equation for the moment can be described by the following expression.

$$\underbrace{\rho \cdot u_i \frac{\partial u}{\partial_i} + \rho \cdot u_j \frac{\partial u}{\partial_j}}_{\text{Inertia}} = \underbrace{-\frac{1}{\rho} \cdot \frac{\partial P}{\partial_i}}_{\text{Pressure}} + \underbrace{\mu \left(\frac{\partial^2 u}{\partial i^2} + \nu \cdot \frac{\partial^2 u}{\partial j^2} \right)}_{\text{Friction}} \quad (2.6)$$

c) Conservation of energy:

The equation for the conservation of the energy is derived from considerations of the first law of thermodynamics. The rate of change of energy of a fluid particle is equal to the heat addition and the work done on the particle (Rocha, 2012).

$$\underbrace{u_i \frac{\partial T}{\partial_i} + u_j \frac{\partial T}{\partial_j}}_{\text{Advection}} = \underbrace{\alpha \left(\frac{\partial^2 T}{\partial i^2} + \nu \cdot \frac{\partial^2 T}{\partial j^2} \right)}_{\text{Diffusion}} + \Psi \quad (2.7)$$

where,

T is the temperature (K);

Ψ is the viscous dissipation (K s^{-1});

α is the thermal diffusivity (m^2 s^{-1}).

2.8.3. Method solution

Two methodologies are used to solve the system of equations: segregated solver solution and coupled solution. The method employs a numerical strategy solution, where the equations of conservation of momentum are solved with a estimated pressure, and then a correction equation for the pressure is applied. Because of the nature of this methodology of correction estimation, a large number of iterations, and a very careful selection of the significant parameters affecting the convergence of a numerical parameters are necessary, in the case of steady state (Santos, 2008).

The coupled method, used by CFX, solves the hydrodynamic equations as a single system. Figure 2.8 illustrates the general procedure of solution. The solution of equations for each set consists of two intensive numerical operations, for each step in time.

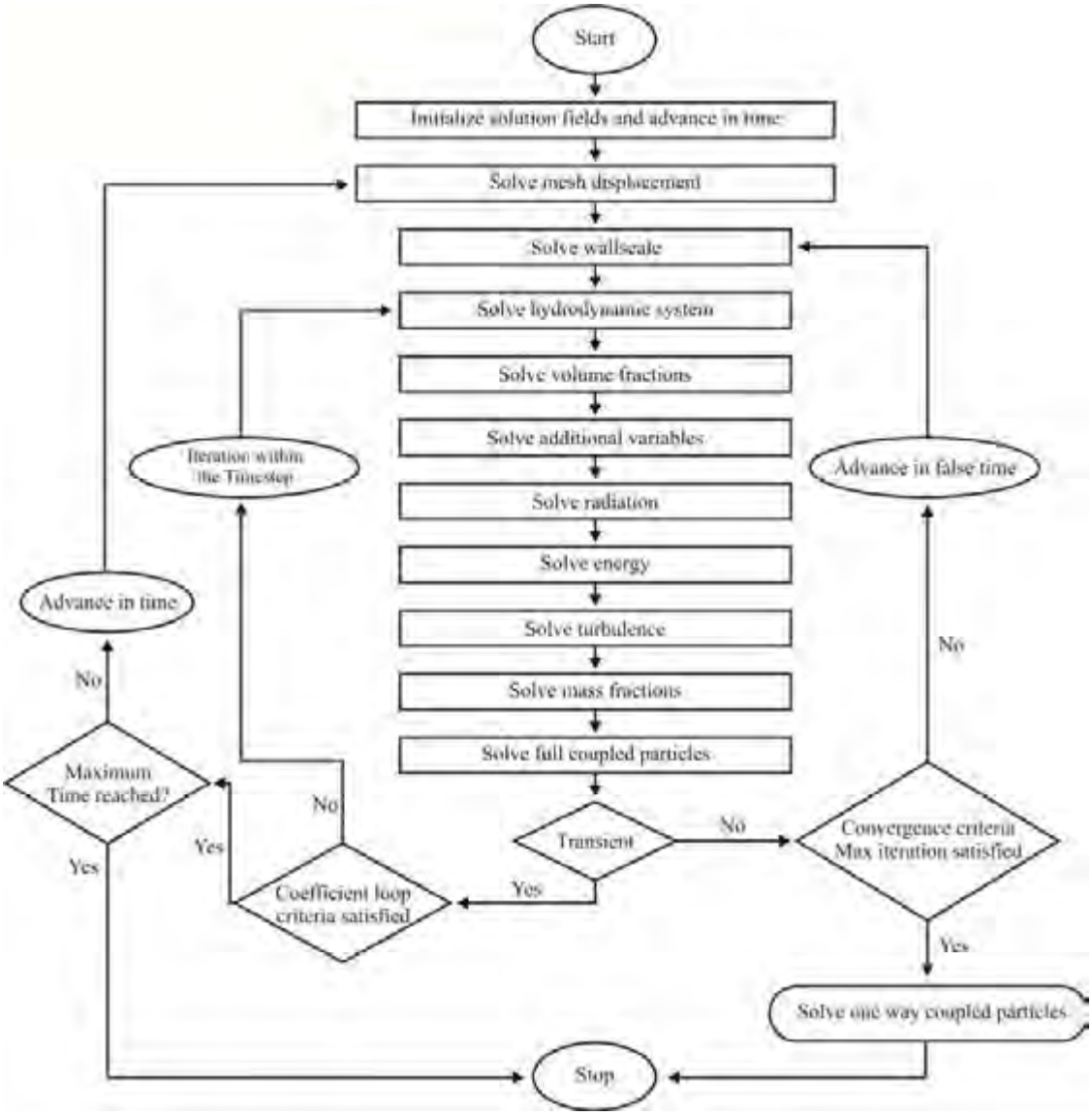

Figure 2.8 - Overall solution strategy of CFX (ANSYS CFX 13.0, 2011).

The iteration time is controlled by a step of physical time, global, or a false time step, locally configured to advance the solution for a simulation time in continuous operation. If the model is steady state, there is only one interaction of linearization step of virtual time.

The solution's performance is improved with the use of a technique called *Multigrid* (Brandt, 1977), a process to increase the size of the mesh elements for later iterations. This results in a reduction of virtual quality of the spacing of the mesh during the iteration, and return to the original mesh obtaining an accurate solution. The use of this technique significantly improves the convergence rate.

The CFX uses a particular implementation of the algebraic *Multigrid* called correction additive (Hutchinson and Raithby, 1986). This approach is ideally suited to the ANSYS

CFX-Solver implementation, because it takes advantage of the fact that the discrete equations are representative of the balance of conserved quantities over a control volume. The coarse mesh equations can be created by merging the original control volumes to create larger ones as shown in Figure 2.9. Figure 2.9 shows the merged coarse control volume meshes to be regular, but in general their shape becomes very irregular.

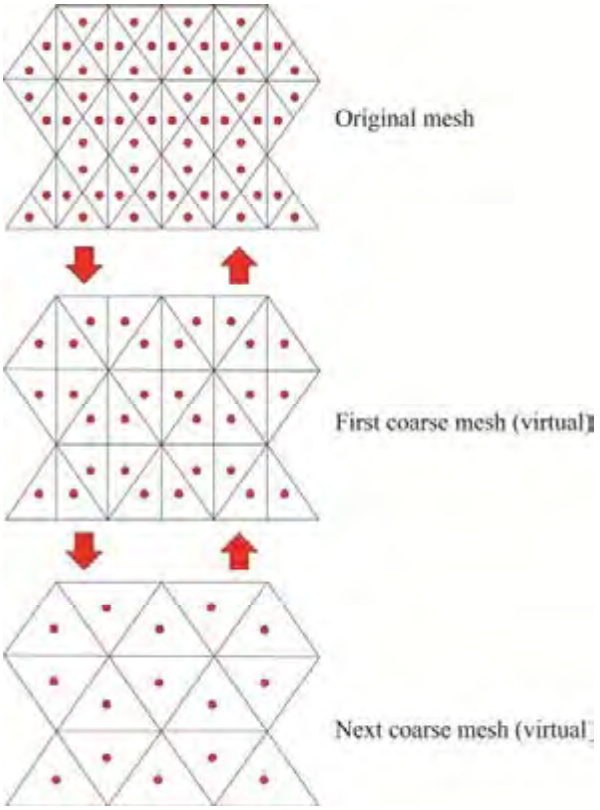

Figure 2.9 - Scheme of an algebraic *Multigrid* method.

2.8.4. Simulation in CFD for animal facilities

The first studies using livestock installations in CFD were performed by Choi et al. (1988), in which a simple geometry was used to represent the animal installation, but results showed little precision. Small advances in the development of real solutions were made in the next year. Hoff et al. (1992) utilized CFD to model air flow in a rectangular shaped installation, in which heat transfer was modeled using a heated floor. Harral and Boon (1997) later simulated isothermal flow patterns in a 3D geometric representation of a cattle confinement. In following years, more studies were developed for validation of animal installations with a focus on the creation of more precise CFD models (Zhang et al., 2000). Only in recent years have CFD models used for simulation of heat and mass transfer

in a geometric representation become reliable in animal production installations (Van Wagenberg et al., 2004). Therefore, more detailed conditions are provided of all phenomena that occur when CFD is employed, and dynamic models, together with estimates, are provided.

a) Birds:

Among environmental factors, thermal factors represented by air temperature, relative humidity, thermal radiation, and air movement are those which most directly affect the bird since they are warm-blooded animals. These environmental variables may have either positive of negative effects on bird production. High temperature and high relative humidities inside aviculture installations are factors which limit the achievement of optimal productivity (Damasceno et al., 2010a). Therefore, the need to maintain the thermal environment within an optimal production scale is evident. However, there are few studies with CFD which utilize a mass balance and heat transfer inside aviculture facilities.

Worley and Manbeck (1995) utilized a CFD model to analyze the distribution of contaminants in a highly turbulent flow inside an aviculture installation under different roofing configurations, whose objective was to obtain a better configuration of air circulation to eliminate particulate material.

Pawar et al. (2007) analyzed the distribution of virus particles which generate diseases in aviculture installations, and for this considered an analogy between the diffusion of ammonia gas (NH_3) and dispersion of virus particles.

Damasceno et al. (2010b) developed and validated a CFD model to analyze the temperature and air velocity distribution inside a common commercial heater used in Brazilian poultry production. These authors concluded that the CFD models may be used for real time prediction of thermal behavior and velocity distribution (inside the combustion chamber for heating), aiding in project improvements.

Tinôco et al. (2010) used CFD to simulate an aviculture installation with mechanical ventilation associated with an evaporative cooling system. In this study the authors developed a CFD model to obtain a better understanding of the temperature and air velocity distribution inside the aviculture installation. The obtained results showed a good statistical correlation with experimental data, which permits its use to address future modifications to the installation.

b) Cattle:

The air quality conditions in a cattle confinement are dynamic and change continuously. Pollutant gases and excesses of humidity, microorganisms and particulates are produced from various sources, such as the floors, walls, feeds, water and air which infiltrates the installation. Therefore gas emissions directly depend on atmospheric influences which permanently change the conditions.

Various approaches to solve this problem have been studied. The quantification of carbon dioxide as well as mass and heat balances were performed by Van Ouwerkerk and Pedersen (1994) according to a method for calculating the concentration difference between interior and exterior air to determine the concentration levels.

Gebremedhin and Wu (2003) utilized predictions based on CFD simulations to aid in modeling of the thermal environment in dairy cattle installations. In their study, the Fortran computational program was used to calculate all models which were necessary for determination of heat and mass transfer on the body of these animals. These authors thus used this method together with CFD simulations for heat and mass transfer between animals and the environment.

Gebremedhin and Wu (2005) studied the utilization of CFD simulations for air flux in a simple geometric cattle installation with forced ventilation to investigate the heat and mass transfer phenomena. They discovered that the total heat loss of an animal is highly dependent on its position and orientation for the flow field. For example, a cow positioned near the air entrance may lose a total of 710 W in heat, while an animal positioned at the other extremity of the installation may lose only 214 W of heat. Figure 2.10 illustrates a CFD predicted flow field around cows in a ventilated room.

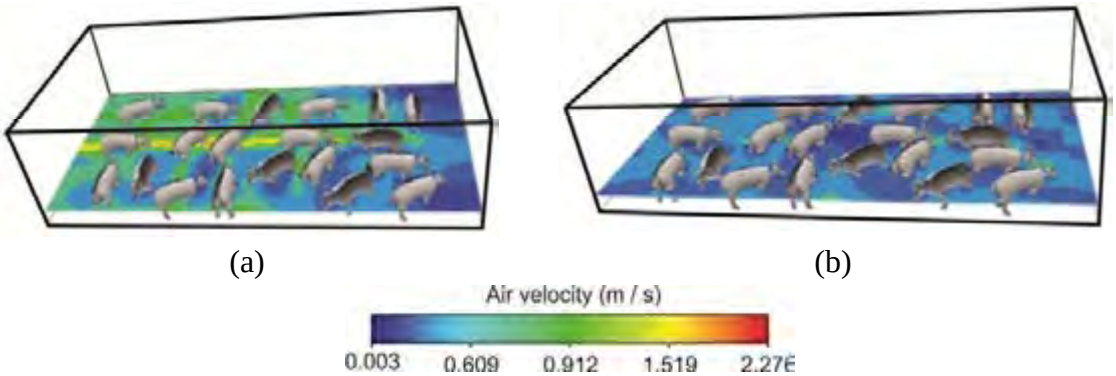

Figure 2.10 - Difference in the air velocity around cows in a ventilated room. (Gebremedhin and Wu, 2005).

Norton et al. (2010a) used a CFD model to provide insight into the air mixing characteristics in a calf building during wind-driven and wind and buoyancy-influenced ventilation. This study found the porosity of the eave opening cladding system heavily influenced the mixing of indoor air during wind-driven ventilation, with the low porosity cladding significantly enhancing the building's ventilation efficiency. Figure 2.11 shows the simulated air distribution patterns in the calves building.

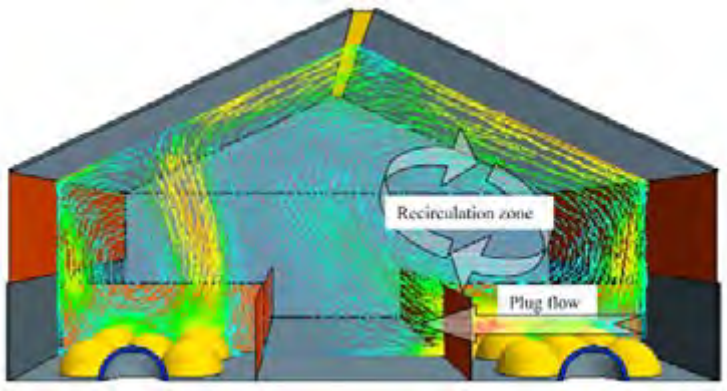

Figure 2.11 - The predicted flow patterns on a vertical plane in the calves building with a wind speed of 0.5 m s^{-1} (Norton et al., 2010a).

c) Swine:

Production and reproductive performance of swine depend on the employed management system, which involves the selected system of breeding, nutrition, and the installations themselves. These installations, which demand a large initial investment, are constructed in function of the costs and facilities of the caretaker, often neglecting the comfort of the animals. Thus, many times the application of CFD models on the environment of these animals are directed towards the optimization of environmental conditions (Bjerg et al., 2000; Sun et al., 2002; Sun, 2004). These studies may be efficiently grouped for modeling of pollutant dispersion and the thermal environment inside swine production installations.

Sun (2004), utilizing CFD models for two and three dimensions, obtained good results for the determination of ammonia concentration distributions during summer and winter conditions in a commercial High-Rise™ Hog Building (HRHB).

2.9. Reduced models

The use of reduced models is a widely used tool in engineering, but its use requires a clear understanding of the principles governing the relationship between the model and prototype. For the behavior of a prototype can be derived from a model is necessary that both behave in a qualitatively similar and that a quantitative relationship can be established among them (Jentzsch, 2002).

Reduced models, when examined with certain criteria of similarity, can be substitutes for valid systems that, for some reason cannot be studied in full-size prototypes. The scale utilization of physical phenomena can be advantageous for four reasons (Schuring, 1977):

a) When the problem is treated as very complex or unfamiliar, and empirical information is necessary for an analytical approach;

b) Reduced models allow the reduction ratio of the system to facilitate the handling;

c) Allows a reduction in time required to perform the research; and

d) Provides a greater understanding of the phenomenon investigated.

The similarity theory is developed by dimensional analysis. Objectives establish the necessary relations for the behavior of a prototype and can be determined from observations in a model and the relationships between the variables involved in the phenomenon, so that the data can be systematized safely (Költzsch and Walden, 1990).

The high cost involved in building a structure for agricultural research of new technologies, such as dairy housing, often do not include the execution of a study due to limited resources. In this way, the use of reduced models to study various types of roof ridge and effects on natural ventilation in a dairy housing can contribute significantly to reducing the cost of research, and allows testing various settings by changing the model at a lower cost than in a full-scale prototype.

The use of reduced building models for animal production are mainly limited by the difficulty of performing the tests under production conditions, thus simulating the heat and moisture dissipation by the animals must be added to the system.

The use of scale models to study the behavior of physical phenomena of a system, expanded with the development of the theory of similarity from the 19th century. This development was due to the need to understand the behavior of physical phenomena involved in new technologies generated mainly in the aerospace industry and shipbuilding.

In this way, several models have been proposed to solve field problems and to facilitate the understanding of various physical processes, such as air-flow characteristics of a scale model chamber (Weller et al., 1970), reduced model to study of alternative ventilation systems for a broiler house (Wilson and Bishop, 1974), ridge vent and wind direction effects on ventilation characteristics of a model livestock building (Egan and Hellickson, 1977), algorithm for determining opening effectiveness in natural ventilation by wind (Nääs et al., 1998), and others.

An important factor in making reduced models is the relationship between cost and accuracy or quality. If the cost increases with the requirement of accuracy of the model, it is necessary to establish the standard that meets the proposed objectives, see Figure 2.12.

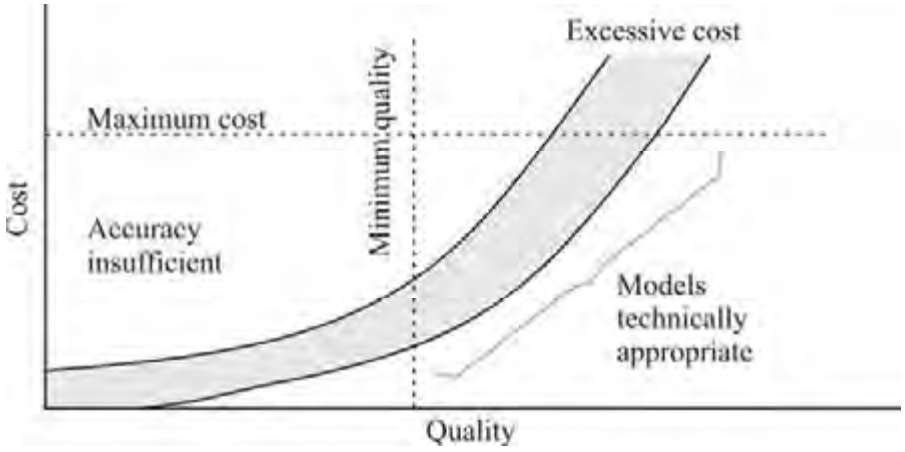

Figure 2.12 - Relationship between cost and accuracy of the model. Adapted from Költzsch and Walden (1990).

2.9.1. Similitude theory

Many problems in practical engineering, involving heat and mass transport over time, can be modeled using solved equations and procedures to describe processes. But a large number of problems can be solved only if the mathematical models are related to the experimental data (Rocha, 2012).

A mathematical model describes the behavior of a real-life system in terms of mathematical equations. These equations represent the relations between the relevant properties of the system under consideration. Parameters that can be influenced by the observer are referred to as adjustable. The other parameters act as constants in the model. For example, in atmospheric models used in weather forecasting, one is interested in properties like temperature and humidity (the dependent variables) as functions of position

and time (the independent variables). Important parameters are then the gravity field and the rotational speed of the earth, and these clearly belong to the class of nonadjustable parameters. The solution of a mathematical model is known if we can determine the relations between dependent and independent variables. Since the solution depends on the values of the adjustable parameters, mathematical models are a powerful tool with which to determine which values of the adjustable parameters yields specific required behavior.

The basic considerations of dimensional analysis and similarity theory are also used to assist the engineer to understand and correlate the data that were obtained in their study or by other researchers. One objective of experimental research is to analyze the systems to make them applicable. Thus, the concept of similarity is often used (Vekariya et al., 2011).

In the process of construction of scientific knowledge, the models have been used as the link between research and theory. In this way, it means that the model productions and physical reproductions of the processes, structures, and objects can be accomplished using the homology and analogy. In homology, the original and model have the same basic physical qualities, and the difference between them is mainly quantitative (Jentzsch, 2002).

The use of homology results in physically similar models. However, in analogy, the original and model have different basic physical qualities, but have in common structural and functional characteristics. The use of models results in similar physical analogy (Murphy,1950).

So the prototype and the model are similar when all quantities homologous features present a constant relationship between them, in other words, similarity between them are constants (Jentzsch, 2002). These constants of similarity (cs) can be set for all magnitudes a basic measurement system, such as length, mass, time, temperature (index M = model and P = prototype):

$$\text{Length} \rightarrow \text{cs}_\text{l} = \frac{\text{l}_\text{M}}{\text{l}_\text{P}} \tag{2.8}$$

$$\text{Mass} \rightarrow \text{cs}_\text{m} = \frac{\text{m}_\text{M}}{\text{m}_\text{P}} \tag{2.9}$$

$$\text{Time} \rightarrow \text{cs}_\text{t} = \frac{\text{t}_\text{M}}{\text{t}_\text{P}} \tag{2.10}$$

$$\text{Temperature} \rightarrow \text{cs}_\theta = \frac{\theta_\text{M}}{\theta_\text{P}} \tag{2.11}$$

By combining these constants of similarity, one can obtain a variety of products, such as widely used dimensionless physical quantities (terms Pi), the Reynolds, Grashof, and Prandtl numbers (Jentzsch, 2002).

2.9.2. Buckingham Pi -Theorem

The Buckingham theorem provides a method for computing sets of dimensionless parameters from the given variables, even if the form of the equation is still unknown. Thereby, according Murphy (1950), consider a system with variables x_1, x_2, x_3,. . . , x_n and a function between them:

$$f(x_1, x_2, x_3, \dots, x_n) = 0 \tag{2.12}$$

If k is the number of fundamental dimensions required to describe the n variables, then there will be k primary variables and the remaining s = k – n variables can be expressed as n – k dimensionless and independent quantities or Pi groups. Thus, the function f can be replaced by the function:

$$f(\pi_1, \pi_2, \pi_3, \dots, \pi_s) = 0 \tag{2.13}$$

The previous function can be determined if the term π_1 had a intended dependent variable, then:

$$\pi_1 = f(\pi_2, \pi_3, \dots, \pi_s) \tag{2.14}$$

Thus, Equation 2.14 is general and can be applied to any other system that is a function of these variables, and consequently a particular system called model (index M).

$$\pi_{1M} = f(\pi_{2M}, \pi_{3M}, \dots, \pi_{sM}) \tag{2.15}$$

Thus, can one can obtain a prediction equation for π_1 from π_{1M} through division Equation 2.14 by Equation 2.15.

$$\frac{\pi_1}{\pi_{1M}} = \frac{f\left(\pi_2, \pi_3, ..., \pi_s\right)}{f\left(\pi_{2M}, \pi_{3M}, ..., \pi_{sM}\right)} \quad (2.16)$$

If the model is designed and operated as follows below:

$$\pi_{2M} = \pi_2 \quad (2.17)$$
$$\pi_{3M} = \pi_3$$
$$\pi_{sM} = \pi_s$$

Then,

$$f(\pi_2, \pi_3, \ldots, \pi_s) = f(\pi_{2M}, \pi_{3M}, \ldots, \pi_{sM}) \quad (2.18)$$

And consequently:

$$\pi_{1M} = \pi_1 \quad (2.19)$$

Equation 2.19 is the prediction equation, which will be valid only if the operating conditions and project demands are fulfilled (Murphy, 1950).

On the other hand, if it is not found that all design criteria and operating conditions affecting the prediction equation are not met, then this may change the behavior of the model, (Timmons et al, 1978). Thus, the correction of the prediction equation can be made by determining predictive factor δ, so (Murphy, 1950):

$$\pi_1 = \delta\pi_{1M} \quad (2.20)$$

2.9.3. Models versus prototype

Performing scale analysis is mathematically straightforward. However, there are several issues to consider (Bahrami, 2012):

a) List of variables that are involved in the phenomenon under investigation: Selection of important variables is not a trivial task and requires considerable judgment and experience.

b) Reynolds number: generally the prototype has a very large Reynolds number (Re), in which case slight variation in Re causes little effect on the behavior of the problem. Unfortunately, models are sometimes so small and the Reynolds numbers are large and the viscous effects take effect. This situation should be avoided to achieve correct results. Solutions to this problem would be to increase the size of the model, or more difficult, to change the fluid (change the viscosity of the fluid) to reduce the Re.

c) After selecting important parameters and determining Pi groups, one should seek to achieve similarity between the model tested and the prototype to be designed. In general, flow conditions for a model test are completely similar if all relevant dimensionless parameters have the same corresponding values for the model and the prototype. Therefore, three particular types of similarity can be determined.

i) Geometric similarity: concerns the length dimension (L) and it must be ensured before any model testing can proceed. In general geometrical similarity is established when a model and prototype are geometrically similar when all body dimensions in all 3 coordinates have the same linear scale ratio.

Figure 2.13 is showing a general example of geometric similarity in model testing.

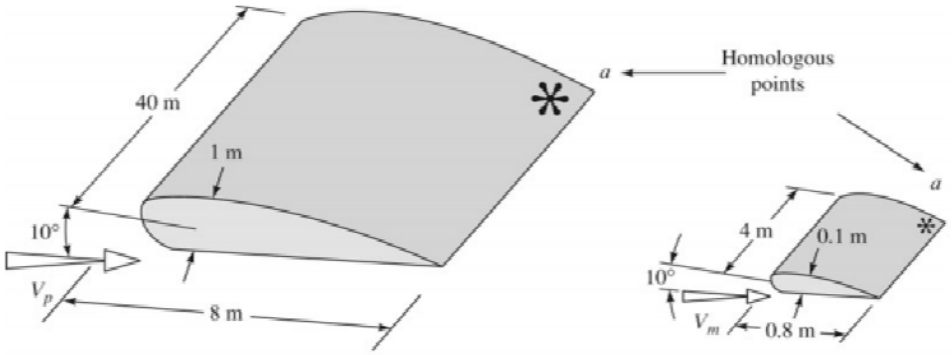

Figure 2.13 - Geometric similarity in model testing (Bahrami, 2012).

ii) Kinematic similarity: requires that the model and prototype have the same length scale ratio and the same time scale ratio; thus the velocity scale ratio will be the same for both.

Length scale equivalence simply implies geometric similarity, but time scale equivalence may require additional dynamic considerations such as equivalence of the Reynolds and Mach numbers.

iii) Dynamic similarity: exists when the model and the prototype have the same length scale ratio, time scale ratio, and the force scale (mass scale) ratio.

Dynamic similarity exists, simultaneously with kinematic similarity, if the model and prototype force and pressure coefficients are identical. This is established if:

- For compressible flow: the model and prototype Reynolds number and Mach number and specific heat ratio are correspondingly equal.

- For incompressible flow:

With no free surface: model and prototype Reynolds numbers are equal;

With a free surface: model and prototype Reynolds number, Froude number, and (if necessary) Weber number and cavitation number are correspondingly equal.

2.10. Wind tunnel

Roberts (2001) describes hydrodynamics as the study of how fluids and gases move around an object. He further states that the study of hydrodynamics is important in that fluid movements help determine the shape and function of many vehicles and building structures.

Konstantin Tsiolkovsky conducted experiments in the study of fluid movement in 1892. He developed prototypes of wind tunnels to study and measure aerodynamic concepts. His contributions helped lead to the understanding of aerodynamics employed by race car drivers, pilots and engineers today (Fitzgerald, 2005). Although CFD have added another dimension in testing recently, wind tunnels are still used to familiarize and appreciate aerodynamic forces at work. It is essential to recognize fluid properties and changes that affect the accuracy throughout the test section (Husainie and Qamar, 2012).

In general, Agriculture Engineers have used wind tunnels to study mockups and prototypes of animal building and food storage structures. They collect data so they can design a better structure. They may use a wind tunnel to study the ventilation characteristics of a mockup before spending money on a prototype building. They also investigate the characteristics of the building, how the control surfaces react at various air velocity and drag characteristics.

Wind tunnels represent a useful tool to investigate various flow phenomena (Lindgren and Johansson, 2002). In another words, the wind tunnel is an installation producing a regular and controlled air stream to determine experimentally the conditions of flow and to measure distribution of pressures, monitoring the temperature, and other relevant aspects of

the study (Gorecki, 1988). With various features provided by wind tunnels, these results can be classified according to the position of construction (vertical or horizontal), the type of camera (open or closed) and the fluid velocity (from subsonic to hypersonic).

Concerning buildings, horizontal models are the most used, due to convenience and lower cost of construction. The use of an open or closed chamber will depend on the type of study to be performed, as well as the fluid velocity and body size needed to meet the test objectives (Barlow et al., 1999).

There are two basic types of wind tunnels and two basic test-section configurations (Rae and Pope, 1984):

1) Open circuit tunnel: In this type of tunnel the air follows along a straight path from the entrance through a contraction to the test section, followed by a diffuser, a fan section, and an exhaust of the air. The tunnel may have a test section with or without solid boundaries, see Figure 2.14.

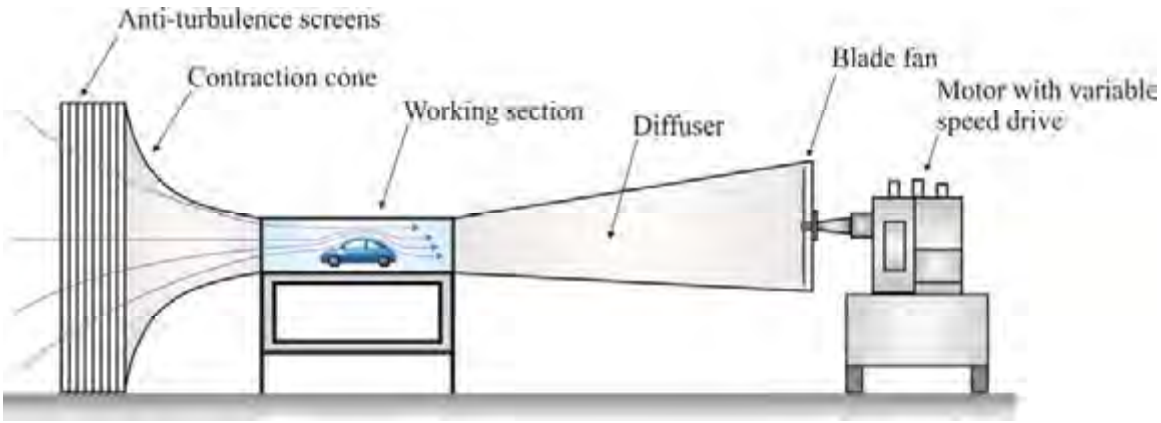

Figure 2.14 - Schematic of open return tunnel (Adapted from Mueller, 1989).

An open circuit tunnel has the following advantages and disadvantages (Rae and Pope, 1984).

a) Advantages:

i) Construction cost is less;

ii) If one intends to run internal combustion engines or if there is flow visualization via smoke, there is no purging problem if both inlet and exhaust are open to the atmosphere.

b) Disadvantages:

i) If located in a room, depending on the size of the tunnel to the room size, it may require extensive screening at the inlet to get high-quality flow. The same may be true if

the inlet and/or exhaust is open to the atmosphere, when wind and cold weather can affect operation;

ii) For a given size and speed the tunnel will require more energy to run. This is usually a factor only if used for developmental testing where the tunnel has a high utilization rate;

iii) In general, a tunnel is nosy. For larger tunnels noise may cause environmental problems and limits on hours of operations.

Because of the low initial cost, an open circuit is often ideal for schools and universities where a tunnel is required for classroom work and research and high utilization is not required.

2) Closed return wind tunnel: This tunnel has a continuous path for the air. The great majority of the closed circuit tunnels have a single return (Figure 2.16), although tunnels with both double and annular returns have been built. Again, the closed circuit tunnel may have either a closed or open test section, and some have been built where it can be run with either an open or closed test section.

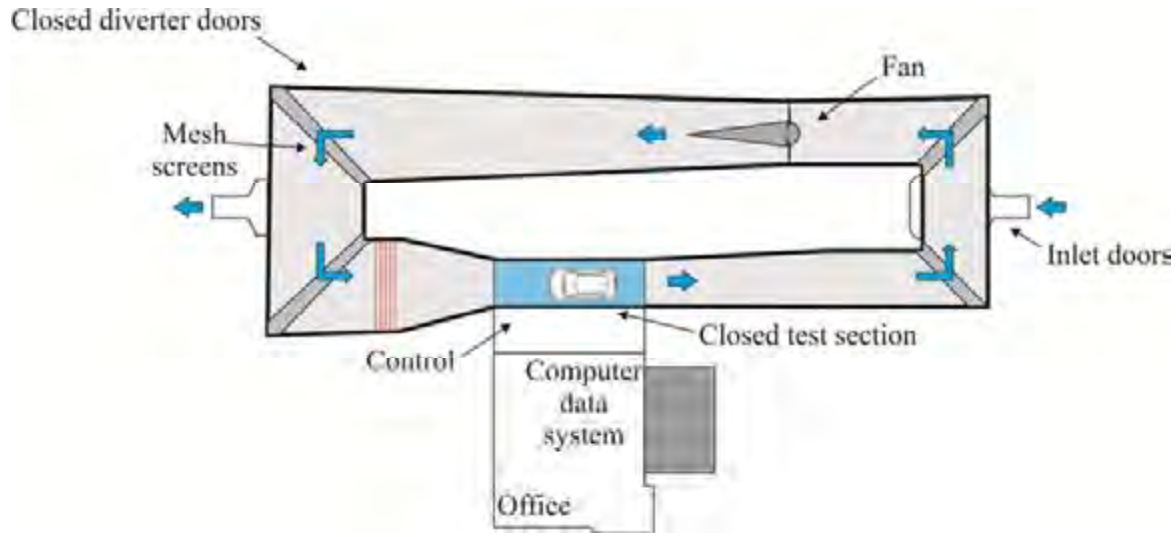

Figure 2.15 - Schematic of closed return wind tunnel (Adapted from Tatman, 2006).

A closed return tunnel has the following advantages and disadvantages (Rae and Pope, 1984).

a) Advantages:

i) Through the use of corner turning vanes and possibly screens, the quality of the flow can be easily controlled;

ii) Less energy is required for a given test-section size and velocity;

iii) Less noise when operating.

b) Disadvantages:

i) Higher initial cost due to return ducts and corner vanes;

ii) If used extensively for smoke tests or running of internal combustion engines, there must be a way to purge tunnel;

iii) If tunnel has high utilization, it will be necessary to install an air exchanger or some other method of cooling during hot summer months.

The Reynolds number is the basis for the behavior of real systems when using reduced physical models (Fox and McDonald, 1998). A common example is the wind tunnel that is used to measure aerodynamic forces in models of wings of airplanes, automobiles, and buildings. Thereby, in the ideal case, the model should be tested at the same Reynolds number as the full-scale vehicle or building. Typically, for experimental values, the flow is laminar when $Re < 2100$, and it is turbulent when $Re > 4000$ (Fox and McDonald, 1998; Incropera and Dewitt, 2001).

In most wind tunnels, air at atmospheric pressure is used as the fluid. The gases are compressible and density varies with temperature and pressure. But in many cases the density of air can be considered constant, to assist engineer in calculating accurate results (Barlow et al., 1999).

2.10.1. Wind tunnel design

Wind tunnel design is a complex field involving many fluid mechanics and engineering aspects and it is impossible to cover them all in just a few pages. Some books and articles have been written about this topic and some references are useful references when designing and constructing low-speed wind-tunnels (Bradshaw and Pankhurst, 1964; Rae and Pope, 1984).

There are many types of wind-tunnels and they can be classified by flow speed dividing them into four groups (Lindgren and Johansson, 2002): a) Subsonic or low-speed wind-tunnels; b) Transonic wind-tunnels; c) Supersonic wind-tunnels; d) Hypersonic wind-tunnels.

There are special-purpose subsonic tunnels, such as spin tunnels, icing tunnels, meteorological tunnels, and tunnels designed for the testing of buildings. In this study, a subsonic tunnel was built for the evaluation of the air flow in reduced models of CBP barns.

There are some large wind-tunnels used in the auto and aircraft industries. These tunnels have test sections that can accommodate full scale vehicles and small aircraft (Lindgren and Johansson, 2002). In the medium size tunnels with a test-section area around 9.3 m^2, large amounts of both research and aircraft developmental testing is accomplished. In a smaller size test section, the tunnels are used for research and instructional purposes. The size of smaller tunnels is usually determined in the final analysis by the size of the room that will house the tunnel. Ideally, the size of a tunnel is determined by its purpose (Rae and Pope, 1984).

a) Test section:

This is the starting point in the design of a wind tunnel. The purpose of a wind tunnel is to provide a uniform and controllable air flow in the test section that passes over the model (Rae and Pope, 1984). The test section is the chamber in which measurements and observations are made and its shape and size are largely determined by the testing requirements.

The test section should be long enough that flow disturbances resulting from a contraction or screens are sufficiently damped before the reaching the test object. However, care should be taken not to make this section too long as this will lead to detrimental boundary layer growth which can separate when it enters the exit diffuser and create a power loss. This can be prevented by slightly enlarging the tunnel or by partially obstructing the exit end of the tunnel to create an overpressure which allows the use of small vents to control boundary layer growth (Tatman, 2006).

b) Diffuser:

Diffusers are chambers that slowly expand along their length, allowing fluid pressure to increase with decreasing fluid velocity. Angles slightly larger than 5 degrees do increase pressure recovery, but can also lead to boundary layer separation and thus flow unsteadiness. Exit diffusers are located downstream of the test section and are used to

recover pressure from kinetic motion of the fluid thereby reduced the power required to drive the tunnel (Tatman, 2006).

Wide angle diffusers are located between the fan and the settling chamber and are necessary in order to facilitate the use of a beneficial contraction section, but the wide angle leads to boundary layer separation which must be controlled with the use of screens.

c) Contractions sections:

Contractions sections are located between the settling chamber and the test sections and serve to both increase mean velocities at the test section inlet and moderate inconsistencies in the uniformity of the flow. Large contraction ratios and short contraction lengths are generally more desirable as they reduce the power loss across the screens and the thickness of boundary layers. Small tunnels typically have contraction ratios between 6 and 9.

d) Fan section:

Axial fans are popular in open return tunnels, and are almost always found in closed return tunnels. In larger tunnels, pre-rotation vanes called stators are commonly positioned upstream of the fan, substantially decreasing swirl in the exit flow. Axial fans have a relatively limited effective operating range as the reduction it pressure increase through the fan as the blades approach stall speeds is far more abrupt than in centrifugal blowers. Care must also be given to choosing the proper blade size, shape and spacing in order to prevent shock wave production, stalling, and backflow (Wallis, 1983).

Centrifugal blowers are most often in blower type open return tunnels, though they can be used in closed return tunnels if mounted in a corner. Centrifugal blowers have a much larger operating range than axial fans with acceptable levels of unsteadiness (Johnson and Hancock, 1997).

e) Settling chamber:

The settling chamber is located between the fan or wide angle diffuser and the contraction and contains the honeycombs and screens used to moderate longitudinal variations in the flow. Screens in the chamber should be spaced at 0.2 chamber diameters apart so that flow disturbed by the first screen can settle before it encounters the second (Tatman, 2006). Turbulence in the test section is reduced by the installation of honeycombs and screens upstream of the contraction.

Screens reduce the axial turbulence more than lateral turbulence. Screens have a relatively large pressure drop in the flow direction, which reduces the higher velocities more than the lower, and thus promote a more uniform axial velocity (Rae and Pope, 1984).

Honeycombs have a small pressure drops and thus have less effect on axial velocities, but owing to their length, they reduce the lateral velocities. The minimum length of a honeycomb should be 6 - 8 times the diameter of the hole (Rae and Pope, 1984).

Both screens and honeycombs reduce lateral and axial turbulence, probably due to an exchange in energy along the axis as the turbulence tends toward isotropic turbulence downstream.

2.10.2. Flow visualization

In this field of hydrodynamics science, the flow visualization has been a nebulous observation simply because air is invisible. Flow visualization has led to the discovery of flow phenomena and has helped in the development of mathematical models for complex flow problems. It is also useful in the verification of existing theories, and has been an important tool in the development of complicated engineering systems (Mueller, 1989).

The use of saw dust, tufts, fluorescent dye in oil with black light, and laser beam, are some of the methods and materials used to attempt flow visualization. The use of saw dust increases the difficulty of maintenance in the wind tunnel and its associated equipment. The tuft and oil methods show flow on the surface of the model. The laser beam has not yet been perfected as a usable tool for this purpose (Shindo and Brask, 1969).

Mitchell and Ross (1977), and Ogilvie and Boyd (1984) used a water flume to visualize the airflow patterns in naturally ventilated barns while Aynsley et al. (1977) and Simango and Schulte (1983) used a neutral buoyancy bubble technique in a wind tunnel. Whatever the method used, the substance introduced into the tunnel should be non-corrosive, non-toxic, and the equipment must be safe to handle. Because of their high initial costs, neither of these two techniques was used in this study. Rather, a simple wind tunnel with smoke was used to allow qualitative determination of air patterns.

The smoke tunnel was an important research tool since 1959. The system consists of a low-turbulence wind tunnel, smoke-generation and injection apparatuses, and lighting and photographic equipment. The arrangement and use of these system components must be coordinated to obtain good results (Mueller, 1989).

3 - MATERIAL AND METHODS

3.1. Introduction

This chapter is divided into four main sections based upon the chronology of the investigation: i) Summarize compost bed data, barn dimension data and determine from qualitative and quantitative methods major interactive factors in the success of bed composting; ii) Summarize bed compost water holding capacities (WHC) and compare moisture contents found with water holding capacity to determine the influence of moisture on bed compost; iii) Develop predictive equations for thermal properties of compost as a function of at various combinations of moisture content, pressure, and particle size; and iv) Develop 3-D CFD model of compost barn with alternate ridge designs and visually demonstrate effect on air flow through structure.

3.2. Characterization and description of CBP barns

3.2.1. Barn facilities measurements

Data to realization of this study were collected from different CBP barns, distributed throughout the state of Kentucky - U.S. (Figure 3.1), between October 2010 to March 2011. In this way, if a farmer described the barn as a compost bedded pack barn but the pack was rarely or never stirred, the barn was not included in any data analysis. Thus, forty-two farms participated in the study.

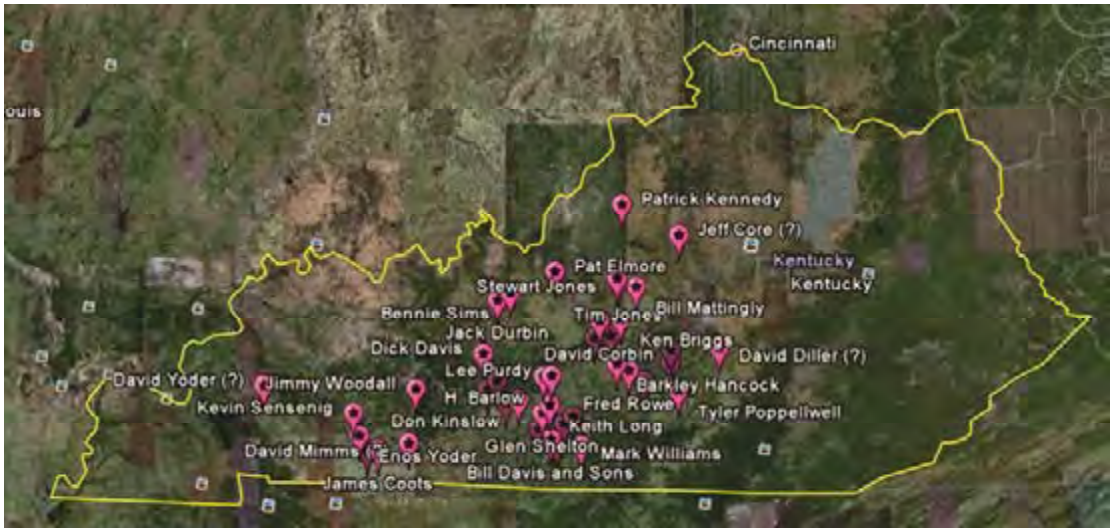

Figure 3.1 - CBP barns utilized of this study in Kentucky State.

The barn dimensions were measured using a steel tape measure, surveyor`s tape, level rod, and a measuring wheel (Figure 3.2). Roof pitch was determined using a level and framing square placed directly on the roof. Two fiberglass ladders were used to allow access to roof structures and ventilation fans (Figure 3.3). Digital photography was used extensively to document interior and exterior structures and systems to assist in accurate creation of the database of barn structure, layout and ventilation details. All information was recorded in a notebook.

(a)

(b)

Figure 3.2 - Equipments used to measure CBP barn dimension: (a) surveyor`s tape and (b) measuring wheel.

(a)

(b)

Figure 3.3 - Equipments used to measured roof pitch and fans dimension: (a) Level and framing square and (b) fiberglass ladders.

3.2.2. Environmental measurements

Air temperature, relative humidity, and air velocity and wind direction were measured inside and outside of each barn. At nine locations within a barn, measurements were taken

in the compost pack area at two different heights (0.05 and 1.2 m) one time on the day of the site visit (Figure 3.4). Air temperature and relative humidity were measured using a weather meter (accuracy of ±1°C; Kestrel®, model 4000, Sylvan Lake, MI, USA). Air velocity was measured using a hot wire anemometer (accuracy of ±0.01 m s^{-1}; Testo®, model 425, Sparta, NJ, USA). The air direction was measurement with a weather vane. Sampling points (A1 to A9) represent the approximate center of nine grid spaces within the manure pack. The grids were established based on post spacing along the pack and generally along the center of the pack (Figure 3.5).

(a) (b)

Figure 3.4 - Equipments used to measured environment: (a) hot wire anemometer and (b) weather meter.

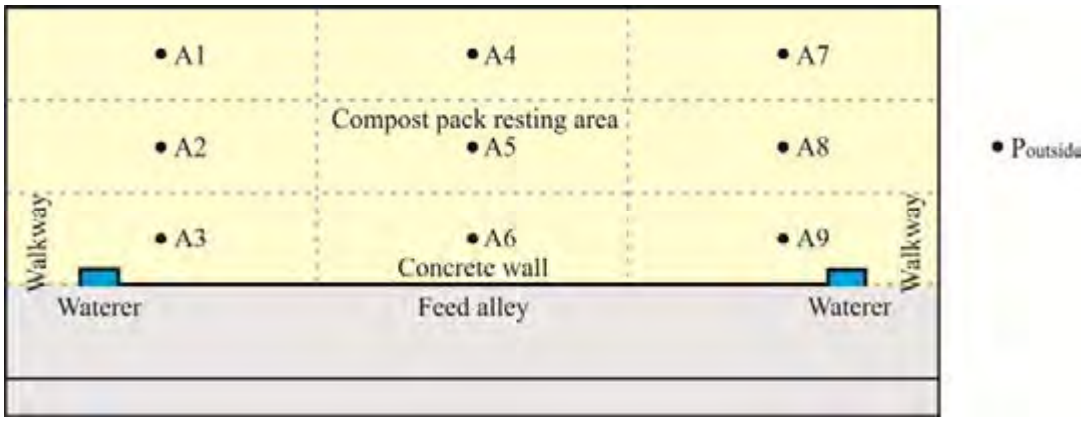

Figure 3.5 - Nine grid spaces (A1 - A9) and one outside point ($P_{outside}$) of environmental measurements and samples collections inside of the barns.

3.2.3. Bedding temperature measurements

Bedding temperature was measured at nine locations as previously described (Figure 3.5) across each pack at the surface and at two different depths (0.10 and 0.20 m). Bedding

surface temperature was measured using two types of sensors. An infrared thermometer (accuracy of ± 1°C; Fluke®, model 62, Everett, WA, USA) and a compact thermal camera (accuracy of ± 0.1°C; Extech®, Flir i5, Waltham, MA, USA) were used (Figure 3.6). Bedding temperature was measured using a thermocouple-based thermometer (0.22 m length, accuracy of ± 2.2°C; Fluke Inc., model 87, Everett, WA, USA), see Figure 3.7.

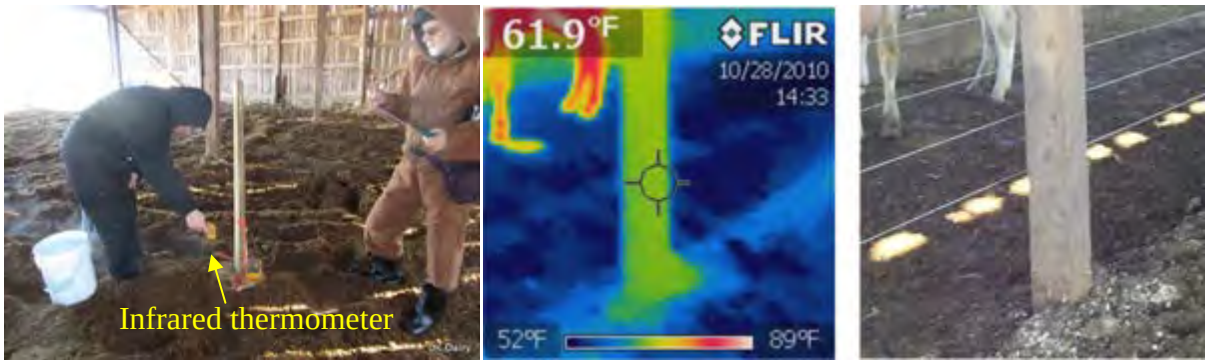

(a) (b)

Figure 3.6 - Equipments used to measured bedding surface temperature: (a) infrared thermometer and (b) a picture of compact thermal camera.

(a) (b)

Figure 3.7 - Thermocouple-based thermometer used to measure bedding temperature.

3.2.4. Bedding moisture analysis

Samples of pack bedding were collected from a mixture of compost of the top (0.10 m) in nine different locations inside the barns using plastic bags (Ziploc®, Double Zipper, Racine, WI, USA). Samples were collected using an iron hoe with a wooden handle and a soil auger (Figure 3.8). The bedding samples were cool on ice upon collection and refrigerated when returned to lab at 1.0 ºC.

(a) (b)

Figure 3.8 - Equipments used to collect the bedding sample: iron hoe (a) and (b) storage in plastic bags.

Bedding compost moisture contents throughout this study were measured by drying at 105°C for approximately 24 h (Figure 4.9). Moisture content (dry-basis) of bedding compost was defined by Equation 4.1 (Sales, 2008; Melo, 2011).

$$MC_{dry-basis} = \left(\frac{m_w - m_d}{m_d}\right) \cdot 100\% \quad (4.1)$$

Where: m_w is the mass of wet material (g) and m_d is the mass of dry material (g) determined by placement of the sample in a convective oven at 105°C for 24 hours. $MC_{dry-basis}$ is expressed as a percentage.

(a) (b) (c)

Figure 3.9 - Determination of moisture content in compost material: (a) wet weight of sample, (b) samples inside the oven, and (c) dry weight of sample.

3.3. Physical, chemical, bacterial and thermal properties of compost materials

3.3.1. Sample preparation and characteristics of materials

Fresh compost bulking materials were collected from 42 CBP barns in Kentucky (Figure 3.1). The bedding compost samples were collected during farms visits between mid-October 2010 and early-February 2011.

Samples of bedding compost were collected from the surface layer (0.10 m deep) in nine different locations in the resting area of a CBP barn (Figure 3.5). Each location is the center of a rectangular area of a 3 x 3 m grid that divides the CBP resting area into 9 equal areas. Samples were collected using iron hoe and soil auger (Figure 3.8). A 20 liters container was filled with incremental quantities of bedding collected from the nine location. The bedding compost samples were immediately refrigerated upon return to the lab at 1.0 ºC, see Figure 3.10.

(a) (b)

Figure 3.10 - The bedding compost samples refrigerated in container upon collection.

3.3.2. Physical properties of compost materials

Physical analyses including particle size distribution, bulk density, particle density, porosity, water holding capacity were performed to characterize the compost materials.

3.3.2.1. Particle size distribution

As-received compost was allowed to air-dry for 48 hours before the determination of the particle size distribution (Figure 3.11a). Dried compost was poured in graduated volume cylinders sieved in a sieve shaker (Ro-Tap Model B, W. S. Tyler, Inc., Mentor,

OH, USA) with sieves vertically aligned in series in a decreasing mesh screen opening order: 25.00 mm, 8.00 mm, 5.60 mm, 4.75 mm, 2.00 mm and a pan of the bottom (Figure 3.11b). Compost bedding material was sieved in the shaker for 3 minutes. The amount of compost retained by each screen was poured in a beaker and its weight determined.

(a) (b)

Figure 3.11 - As-received compost drying (a) and (b) shaker and sieves used to characterize particle size ranges.

The total compost bedding sample weight (W_{total}) can be assumed as the sum of all sieved particle ranges plus bottom pan (Maia, 2010). So, W_{total} is given by Equation 3.2:

$$W_{total} = W_{coarse} + W_{R2} + W_{R3} + W_{R4} + W_{R5} + W_{fines} \quad (3.2)$$

Where, W_{course}, W_{R2}, W_{R3}, W_{R4}, $W_{R5,}$ and W_{fines} represent weights of course material, R2, R3, R4, R5 and fines (pan), respectively.

Particle weight fractions for ranges 2, 3, 4, and 5 ($F_{W_{R2}}$, $F_{W_{R3}}$, $F_{W_{R4}}$, and $F_{W_{R5}}$ respectively) were determined by Equation 3.3:

$$F_{W_{R\#}}(\%) = \left(\frac{W_{R\#}}{W_{total}}\right) \times 100 \quad (3.3)$$

Where, $W_{R\#}$ represents the weight for particles sizes of the three ranges.

Compost weight fraction of fines on the pan, $F_{W_{pan}}(\%)$, were calculated as in Eq. 3.4.

$$F_{W_{pan}}(\%) = \left(\frac{W_{fines}}{W_{total}}\right) \times 100 \quad (3.4)$$

Finally, weight particle fractions were estimated as in Equation 3.5.

$$F_{W_{total}}(\%) = F_{W_{coarse}}(\%) + F_{W_{R2}}(\%) + F_{W_{R3}}(\%) + F_{W_{R4}}(\%) + F_{W_{R5}}(\%) + F_{W_{fines}}(\%) \quad (3.5)$$

3.3.2.2. Bulk density, particle density, and porosity

Compost bulk density was measured by adding 1.6 liters of air-dried compost into a 2.0 liters graduated volume cylinder (0.05 m height and 0.20 m diameter). The container was filled with bedding compost material, and then the material was slightly compacted to ensure absence of large void spaces and, then the material was vibrated using a vibrating Jigsaw (Black & Deck, Model JS515, MD, USA) for 30 seconds (Figure 3.12). The bulk density can be calculated by dividing the weight of the material by the compost filled volume of the cylinder (Ahn et al., 2009; Sales, 2008).

Figure 3.12 - Cylinder with compost bulking material vibrating.

Compost particle density was determined by pouring 20 g of as-received compost into five graduated cylinders and adding a portion of 0.10 liter of methanol (90%) to each cylinder up to fill to the 0.10 liter mark (Figure 3.13). The remaining unused methanol volume represented the volume of particles in the compost filled cylinder (Sales, 2008).

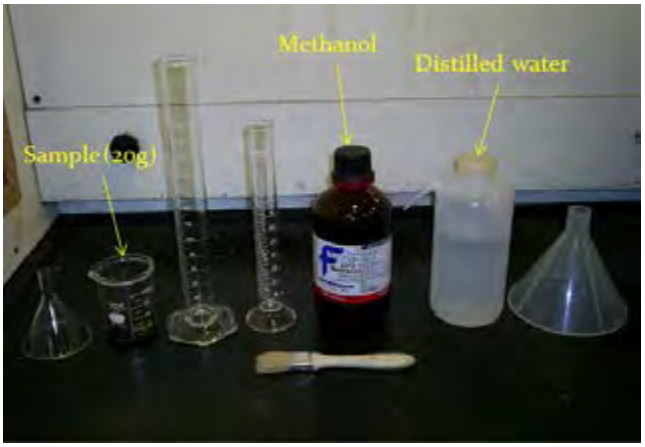

Figure 3.13 - The methanol and other equipments used to determinate particle density.

Porosity was determined for each collected CBP bedding compost from the results of bulk and particle density by using Equation 3.6:

$$\varepsilon = \left(1 - \frac{\rho_b}{\rho_p}\right) \tag{3.6}$$

where: ε is the overall porosity (%), ρ_b is the bulk density (g cm^{-3}) and ρ_p is the particle density (g cm^{-3}).

3.3.2.3. Water holding capacity (WHC)

The WHC was determined using 30 grams of the as-received compost that was saturated with deionized water in a beaker, stirred for 3 minutes and left to rest for 7 minutes to absorb water. Saturated compost was poured into three Buchner funnels on top of Erlenmeyer flasks to drain excess water (Whatman #41 filter paper), covered with parafilm, and taken to an environmental chamber at 25ºC and 58% RH, where they drained for 12 hours (Figure 3.14). Drained compost was weighed (W_i) and dried (W_s) in a convection oven for 24 hours at 105ºC. The water holding capacity (g water/g dry material) is calculated as (Ahn et al., 2009):

$$WHC = \frac{\left\{\left(W_i - W_s\right) + MC_i \cdot M\right\}}{\left\{\left(1 - MC_i\right) \cdot W_i\right\}} \tag{3.7}$$

where: MC_i is the initial moisture content of sample and M is the mass of the wet sample.

(a) (b) (c)

Figure 3.14 - As-received compost saturated with deionized water (a), environmental chamber (b) controlled for temperature and relative humidity and (c) interior of the unit with the six compost samples.

3.3.3. Thermal property measurement

Thermal properties were determined with transient heat dissipation device (KD2, Decagon, Pullman, WA, USA). The thermal properties, thermal conductivity (k, W/m K) and thermal resistivity (rho, °C cm/W), were measured for varying particle size ranges (0.00mm < Finer < 2.00mm < PS2 < 4.75 mm < PS3 < 5.60 mm < PS4 < 8.00 mm < Coarser < 25.00 mm), water content (30, 45 and 60%), and different static (fluffy material, 0.0, 0.1, 0.2, 0.3, and 0.4 MPa) and dynamic compaction degree (0.1, 0.2, 0.3, and 0.4 MPa).

The thermal properties was measured using a handheld device. It consists of a handheld controller and sensors made from thin-wall stainless steel tubing with 2.4 mm diameter x 100 mm long (see KD2 Pro® Operator`s manual, 2008). This probe was inserted into the bedding compost medium.

First, thermal conductivity and thermal resistivity were measured for all samples in different particle size ranges (0.00mm < Finer < 2.00mm < PS2 < 4.75 mm < PS3 < 5.60 mm < PS4 < 8.00 mm < Coarser < 25.00 mm), as described earlier (Figure 3.15).

Wet sample of compost bulking material with different moisture content (30%, 45% and 60%) was produced in a concrete mixer that mixed the bedding material with the added water for 3 minutes (Figure 3.16a). The desired moisture contents (30%, 45%, and 60% w.b.) was achieved by adding a known water amount for each particle size range's initial moisture contents (Table 3.1). If the initial moisture contents was higher than the selected MC, a 50 g of compost was weighed and left to air dry until reaching the target MC.

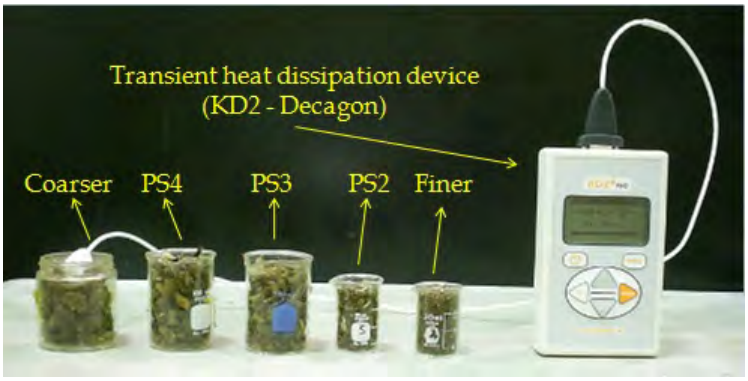

Figure 3.15 - Thermal properties sensor used to determinate the thermal conductivity and thermal resistivity in different particle size.

Table 3.1 - Amount of water added to each particle size range to reach 30%, 45%, and 60% (w. b.) moisture contents. Sample amount = 30g. Number of samples = 3.

Barn number	Initial Moisture (%)			Water added or removed (g) to again		
	Average		S. deviation	30%	45%	60%
1	37.5	±	11.8	-5.3	6.9	28.2
2	49.0	±	7.3	-13.6	-3.7	13.7
3	49.1	±	5.8	-13.7	-3.8	13.6
4	36.2	±	6.3	-4.4	8.0	29.8
5	52.2	±	5.6	-15.9	-6.6	9.7
6	39.6	±	9.6	-6.8	4.9	25.5
7	46.0	±	3.2	-11.4	-0.9	17.5
8	61.6	±	2.5	-22.6	-15.1	-2.0
9	41.9	±	6.6	-8.5	2.9	22.7
10	51.7	±	7.3	-15.5	-6.1	10.4
11	61.2	±	2.4	-22.3	-14.8	-1.6
12	60.4	±	2.8	-21.7	-14.0	-0.5
13	57.3	±	4.3	-19.5	-11.1	3.4
14	57.5	±	4.2	-19.7	-11.4	3.1
15	54.7	±	2.7	-17.6	-8.8	6.6
16	66.5	±	2.2	-26.1	-19.6	-8.2
17	56.0	±	4.3	-18.6	-10.0	5.0
18	64.8	±	0.8	-24.9	-18.0	-6.1
19	68.4	±	1.9	-27.5	-21.3	-10.5
20	60.3	±	3.3	-21.7	-14.0	-0.4
21	58.8	±	3.3	-20.6	-12.6	1.5
22	64.0	±	1.6	-24.3	-17.3	-5.0
23	67.3	±	1.3	-26.7	-20.3	-9.2
24	52.0	±	4.4	-15.7	-6.3	10.1
25	66.4	±	1.3	-26.0	-19.5	-8.1
26	61.7	±	3.7	-22.6	-15.2	-2.1

Continue...

Table 3.1 - Amount of water added to each particle size range to reach 30%, 45%, and 60% (w. b.) moisture contents. Sample amount = 30g. Number of samples = 3.

Barn number	Initial Moisture (%)			Water added or removed (g) to again		
	Average		S. deviation	30%	45%	60%
27	64.6	±	2.8	-24.7	-17.9	-5.8
28	47.4	±	2.6	-12.4	-2.2	15.7
29	67.8	±	1.3	-27.0	-20.7	-9.7
30	61.2	±	2.3	-22.3	-14.7	-1.5
31	61.1	±	2.1	-22.2	-14.6	-1.4
32	57.3	±	2.8	-19.5	-11.2	3.4
33	62.6	±	5.6	-23.3	-16.0	-3.2
34	68.9	±	2.0	-27.8	-21.7	-11.1
35	69.5	±	0.9	-28.2	-22.3	-11.8
36	71.8	±	0.8	-29.9	-24.4	-14.7
37	64.3	±	3.5	-24.5	-17.6	-5.4
38	61.7	±	6.4	-22.7	-15.2	-2.2
39	66.5	±	1.0	-26.1	-19.6	-8.1
40	64.6	±	1.7	-24.7	-17.9	-5.8
41	70.1	±	2.7	-28.7	-22.9	-12.7
42	69.1	±	1.2	-27.9	-21.9	-11.4

Different methods used to determined particle density and the amount of water added to the compost to reach 30, 45, and 60% (w.b%) moisture content are described in Liberty (2002) and Sales (2008).

A fluffy bedding material was weighed and the PVC cylinder (detailed cylinder apparatus description in the following paragraphs) was filled. The PVC cylinder was then vibrated using vibrating Jigsaw (Black & Deck, Model JS515, MD, USA) for 60 seconds and resulting volumes were measured (Figure 3.16b).

(a) (b)

Figure 3.16 - Concrete mixer (a) used to mix the compost bulking material and (b) PVC cylinder vibrated by a vibrating Jigsaw.

For study of different degrees of compaction, a mechanical pressing device was designed and constructed at the shop of the Biosystems and Agricultural Engineering at Department of the University of Kentucky. The press device was assembled and located in the Agricultural Air Quality Laboratory of the same Department (Figure 3.17).

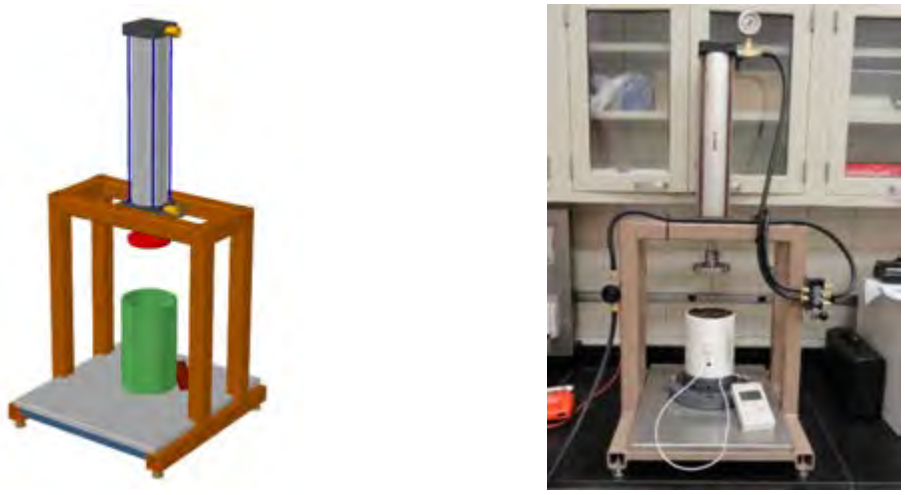

(a) (b)

Figure 3.17 - Mechanical pressing device designed (a) and (b) constructed to provide different degrees of static and dynamic compaction.

Material compaction was achieved by a mechanical pressing device that was developed to pack the sample down in the PVC container. The PVC cylinder had 0.27 m height and diameter of 0.15 m. This PVC cylinder had a series of three equally spaced (0.075, 0.150, and 0.225 m) holes through the entire height. Pipe flange was used to hold the PVC cylinder on the base frame assembly using knurled hold down knobs (see Appendix C - Figure 1). The compaction level inside of a PVC cylinder was adjusted using a valve and manometer that controlled the air pressure inside of steel cylinder chamber that moved the steel piston (Figure 3.18). A Moisture drain valve prevented water condensation in the line of air pressure. The pressures applied (0.0, 0.1, 0.2, 0.3, and 0.4 MPa) were based on studies conducted by van der Tol et al. (2003) and van der Tol et al. (2002).

The Decagon KD2-Pro (Decagon Devices Inc.) was used to evaluate the thermal properties (thermal conductivity and thermal resistivity) associated with type pressure applied (static and dynamic pressure). This sensor uses a metal probe (0.0024 m diameter x 0.100 m long) that heats up the material and then reads the temperature decay as the material dissipates the heat to calculate its thermal properties. The probe was used with the entire length of the needle embedded inside the compost. Measurements were made by

placing the sensor probe into the three holes over cylinder and recording the measurement after one minute, which was the recommended procedure for this sensor. Dynamic pressure was applied when varying the opening and closing the air in the valve control (Figure 3.18b), during 12 times per minute. This range of moisture content (30%, 45%, and 60%) was selected to simulate the conditions of the bedded compost found in the field. The Decagon KD2-Pro sensor was calibrated by factory and performance verification standards were observed during this study.

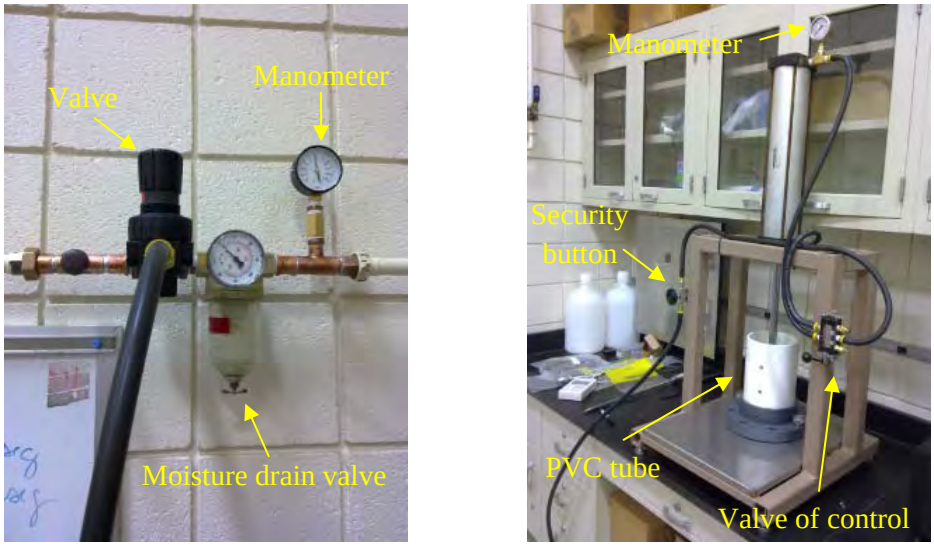

(a) (b)

Figure 3.18 - Valve and manometer (a) and (b) mechanical pressing device components used to compress the bedding compost samples.

3.3.4. Chemical properties of the compost bedding material

Each compost barn pack was subdivided in three equal areas within each of the nine spots (Figure 3.5) from which 0.4 liters bedding sample were collected during the visiting. The bedding samples were collected from the surface and kept cooled upon collection at 0°C till it was placed in a -40°C freezer and held for chemical analyses. Sub-samples were ground as-is before analysis for Carbon (C), nitrogen (N), phosphorus (P), potassium (K), calcium (Ca), magnesium (Mg), zinc (Zn), Copper (Cu), manganese (Mn), and iron (Fe). The analysis was performed at the Division of Regulatory Services at the University of Kentucky. The solid compost was dried in an oven at 75°C for 24 hours, ground to pass a 2 mm screen, and stored at room temperature prior to analysis. Nitrogen (%) and Carbon (%) were determined via combustion. Macro nutrients (P, K, Ca, Mg) and micro nutrients (Zn,

Cu, Mn, and Fe) were extracted by digestion using a combination of HCl and H_2SO_4 acids. The digestate was assayed by Inductively Coupled Plasma Spectrometer for concentration determination. The P, K, Ca, Mg and Zn are reported in a weight percent basis and Zn, Cu, and Fe in ppm.

The following section summarizes information collected by a collaborator (Black, 2012). It is included to give a more details about chemical analysis.

3.3.5. Bedding bacterial of the compost bedding material

Compost samples were collected from nine equally spaced locations throughout the barn described previously (Figure 3.5). Half of a cup was collected from each location, thoroughly mixed together, and stored in a -57°C freezer to later be thawed for analysis of bacterial content. The samples were sent to three different laboratories for analysis. University of Kentucky in Laboratory of Soil analyzed the CBP bedding and fresh bedding material for the following pathogens on a wet weight basis: *Coliform, E. Coli, Staphylococcal species, Streptococcal species, and Bacillus.*

The samples were thawed in a refrigerator. Fifty cubic centimeters (cc) of bedding material was measured using a sterile placed into a plastic bag (Ziploc®, Johnson & Son, Racine, WI, USA). Two-hundred fifty cc of sterile distilled water was added to the bedding material which was mixed and allowed to stand for 10 minutes. The sample was mixed again, a liquid sample was removed by pipette and serial 10-fold dilutions were made in sterile Brain Heart Infusion broth. Sample dilutions were plated (200 μL) on colistin naladixic acid (CNA) agar (BBL, Sparks, Md.), MacConkey agar (BBL, Sparks, Md.), and thallium sulfate-crystal violet-B toxin blood (TKT) agar medium. Colony counts were determined for each sample after 24 hours of incubation at 37°C. Bacterial groups were identified as coliforms (lactose-positive colonies on MacConkey's agar, which include Klebsiella by visual identification), streptococcus species (growth on TKT agar), Bacillus species (growth on CNA agar and gram-positive) and coagulase negative staphylococci (growth on the CNA agar and catalase activity). Bacteria counts are expressed as colony forming units (cfu) / mL of bedding sample.

The following section summarizes information collected by a collaborator (Black, 2012). It is included to give a more details about bacterial analysis.

3.4. Study of natural ventilation in reduced model of CBP barn

3.4.1. Wind tunnel

A wind tunnel was built to evaluate the effect of air flow through reduced structure model (1:16) of CBP barn with alternate ridge designs. The purpose of this wind tunnel was to provide a uniform and controllable air flow in the test section that passes over this reduced model. This wind tunnel was composed of an air intake, flow straightening section, test section, and fan section. All studies were carried out in the wind tunnel of Biosystems and Agricultural Engineering at Department of the University of Kentucky.

The wind tunnel was a low speed open circuit type with dimensions of 3.25 m wide, 8.85 m length, and a height of 3.15 m (Figure 3.19). The internal dimensions were 3.15 m x 8.75 m x 3.05 m comprising a total volume of 84.0 m^3. Concrete blocks were used on the base of the wind tunnel. Two by six wood boards were used to build the framing and sheets of plywood were installed on the internal side of the framing members on the top, bottom and both of side walls. Two metal doors were used for access to internal sections of the wind tunnel.

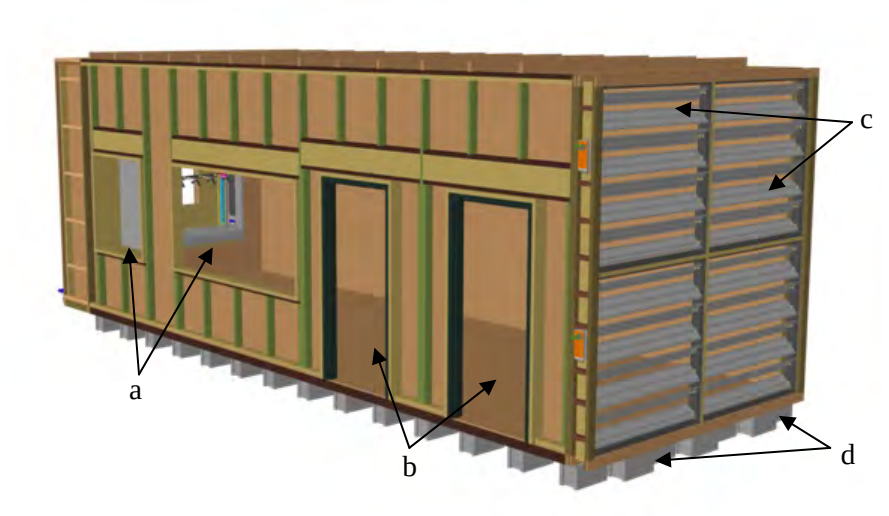

Figure 3.19 - Wind tunnel 3D model design is showing placements of (a) windows, (b) doors, (c) dampers, and (d) concrete blocks.

The axial fan diameter was approximately 1.22 m and was capable of producing 2.33 $m^3\ s^{-1}$ of airflow at a maximum 380 rpm and against a 10.0 Pa pressure increase. The fan section can be easily altered to accommodate smaller fan sizes. Given the 9.60 m^2 cross-section of the wind tunnel, this allows for a maximum mean wind speed of 2.0 m s^{-1}. The fan had three cambered blades, also made from sheet metal, and full power requirement for fan operation was 0.746 kW (1.0 hp). The fan was set in a custom welded

steel frame that was mounted on a fiber glass box. This fiber glass box was attached to a sheet of plywood. Thereafter sixteen metallic clamps pressure were used to hold whole structure (fan and fiber glass box) in the end wall (Figure 3.20).

Figure 3.20 - View of the fan mounted on the wind tunnel.

This wind tunnel was equipped with four metal dampers (1.52 m x 1.52 m) to control the wind speed. The dampers were assembled at air intake of the wind tunnel and were controlled by a handle on the outside. The room controls were located adjacent to the test section. The dampers were made with stainless steel and were fitted with actuators which has a rotation speed of 15s for 0 - 90 degree pivot.

Turbulence in test section was dampened by the installation of a plastic honeycomb plates. This honeycomb plate was placed at 1.77 m down flow from the dampers to promote a laminar flow of air. For optimum benefit, the length of honeycomb was 6 times of the diameter of the hole (Rae and Pope, 1984). The honeycombs were supported by metal frame. This frame was made from aluminum channel to hold and seal the edges of the honeycomb. The channels were secured to one another with rivets. The honeycombs slid snuggly into the settling chamber and were attached to the walls on each side.

This wind tunnel had two clear viewing windows (test section) with different sizes . These windows were covered by 2.40 x 1.20 m and 1.10 x 1.20 m, respectively, of Plexiglas with 0.003 m thickness. Those windows were placed at 3.60 m and 6.65 m, respectively, from the upwind edge of the window. The Plexiglas windows were secured in the wind tunnel with screws and silicone to seal and to prevent air infiltration. Care was taken to drill holes through the Plexiglas for the screws to prevent cracking. Smoke was used to attempted to fix air infiltration problems which arose. The length of the test section

was chosen to be around 2.0 m to be able to get a high enough Reynolds number (Re < 2100) on a flat plate for anticipated wind tunnel uses.

Smoke was used primarily for flow visualization and photographs and videos were the primary method of data recording. Airflow patterns were visualized using a fog machine (power 1190 W, Rosco®, model 1700, CT, USA) which vaporized Glycerin for a smoke source. The smoke tracer was introduced from the generator with a funnel on an end of a duct and allowed to entrain smoke with the air using the negative pressure of the wind tunnel as draw. Three light boxes, with 300 W incandescent lamps, focused light at three different points along the length of the wind tunnel. The bright light combined with the black inner surfaces allowed for photographing of air movement by both camera and camcorder.

Airflow patterns were assessed using both air flow visualization and by measuring the airspeed along the length of the test section. Airflow visualization allowed for a qualitative image of the airflow patterns.

The final step in constructing of wind tunnel was sealing air leaks using foam sealant. Figure 3.21 illustrates the metal dampers, plastic honeycombs, and fog machine used in the wind tunnel.

Further information regarding constructions and calibration of the wind tunnel and others details used in this study can be seen in Lopes (2012).

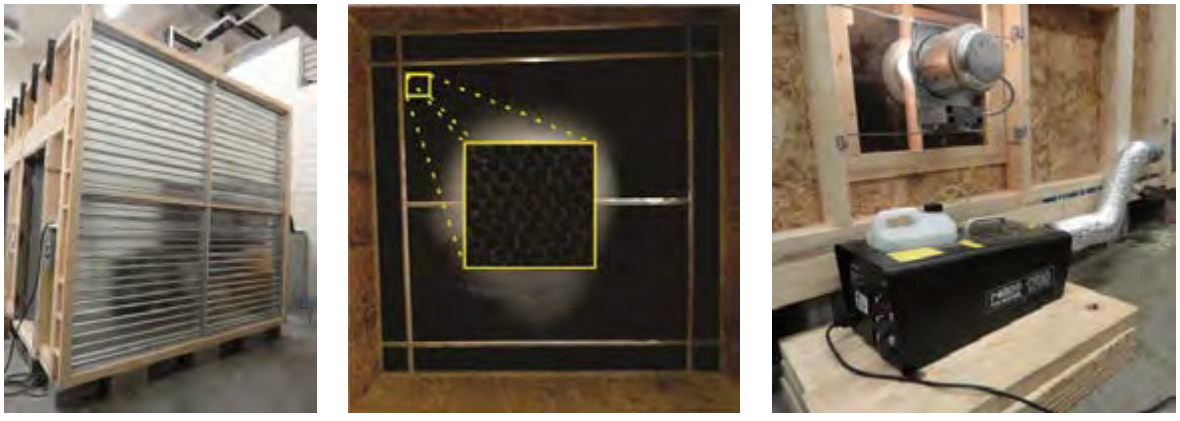

(a) (b) (c)

Figure 3.21 - Details of (a) metal dampers, (b) plastic honeycombs, and (c) fog machine.

3.5. Reduced model

3.5.1. Determination of pertinent variables

Airflow through the roof ridge opening of a building acts essentially as fluid flow through an orifice. The flow is governed by viscous forces, inertia forces, gravitational forces, buoyancy forces and geometric relationships. Heat transfer from the buildings is controlled by fluid flow, fluid properties and building geometry and characteristics. Assuming that the same phenomenon governs performance in the reduced model, a list of pertinent variables affecting the ventilation characteristics were compiled (Table 3.2) and reduced to the basic dimensions of length (L), mass (M), temperature (θ), and time (T). The selection of pertinent variables was based on the assumptions that fluid flow is incompressible, the building atmosphere will be without manure gases and added moisture, and there will be significant internal heat source present (heat of compost pack).

Table 3.2 - Variables affecting ventilation characteristics.

Variable n◦	Description	Units (S.I)	Symbols	Dimensional symbol
1	Building length	m	l	L
2	Building width	m	w	L
3	Building height	m	h	L
4	Gravitational acceleration	$m\ s^{-2}$	g	$L\ T^{-2}$
5	Coefficient of heat transfer	$kg\ s^{-3}\ K^{-1}$	h_c	$M\ T^{-3}\ \theta^{-1}$
6	Heat	$kg\ m^2\ s^{-2}$	Q	$M\ L^2\ T^{-2}$
7	Wind velocity	$m\ s^{-1}$	v_w	$L\ T^{-1}$
8	Temperature of air	K	T_a	θ
9	Density of air	$kg\ m^{-3}$	ρ	$M\ L^{-3}$
10	Specific heat of air	$m^2\ s^{-2}\ K^{-1}$	c_p	$L^2\ T^{-2}\ \theta^{-1}$
11	Heat transfer coefficient	$kg\ s^{-3}\ K^{-1}$	U	$M\ T^{-3}\ \theta^{-1}$
12	Dynamic viscosity of air	$kg\ m^{-1}\ s^{-1}$	μ	$M\ L^{-1}\ T^{-1}$
13	Thermal conductivity of air	$kg\ m\ s^{-3}\ K^{-1}$	k	$M\ L\ T^{-3}\ \theta^{-1}$
14	Coefficient of thermal expansion	βe	k^{-1}	θ^{-1}

According Buckingham Pi Theorem, a group of ten (14 variables minus 4 dimensions) independent pi terms (Table 3.3) was derived with the details of the determination shown in Appendix D. The relationship among the pi terms for fluid flow and heat transfer can be expressed as:

Table 3.3 - List of pi terms.

Term nº	Pi term
1	$\pi_1 = w \cdot l^{-1}$
2	$\pi_2 = h \cdot l^{-1}$
3	$\pi_3 = g \cdot l^{-1} \cdot \rho^{-1}$
4	$\pi_4 = {v_w}^{-3} \cdot {T_a}^{1} \cdot \rho^{-1} \cdot {h_c}^{1}$
5	$\pi_5 = Q \cdot l^{-3} \cdot {v_w}^{-2} \cdot \rho^{-1}$
6	$\pi_6 = c_p \cdot {v_w}^{-2} \cdot T_a$
7	$\pi_7 = U \cdot {v_w}^{-3} \cdot {T_a}^{1} \cdot \rho^{-1}$
8	$\pi_8 = \mu \cdot l^{-1} \cdot {v_w}^{-1} \cdot \rho^{-1}$
9	$\pi_9 = k \cdot l^{-1} \cdot {v_w}^{-3} \cdot {T_a}^{1} \cdot \rho^{-1}$
10	$\pi_{10} = \beta_e \cdot T_a$

Thus, the function represented by equation 2.13 is:

$$f(\pi_1, \pi_2, \pi_3, \pi_4, \pi_5, \pi_6, \pi_7, \pi_8, \pi_9, \pi_{10}) = 0 \quad (3.8)$$

The terms π_6 and π_9 have the dependent variables necessary to predict heat transfer and fluid flow, respectively. According the equations 2.14 and 2.15 showed previously, can be determination that (Murphy, 1950; Klin, 1966; Jentzsch, 2002):

$$\pi_6 = f(\pi_1, \pi_2, \pi_3, \pi_4, \pi_5) \quad (3.9)$$

$$\pi_9 = f(\pi_1, \pi_2, \pi_3, \pi_4, \pi_5, \pi_7, \pi_8, \pi_{10}) \quad (3.10)$$

According Similitude theory, the equations 3.9 and 3.10 can apply to another system (using index M) and the function needs to use the same variables and be submitted to the same conditions of operation.

$$\pi_{6M} = f(\pi_{1M}, \pi_{2M}, \pi_{3M}, \pi_{4M}, \pi_{5M}) \quad (3.11)$$

$$\pi_{9M} = f(\pi_{1M}, \pi_{2M}, \pi_{3M}, \pi_{4M}, \pi_{5M}, \pi_{7M}, \pi_{8M}, \pi_{10M}) \quad (3.12)$$

So, the prediction of equation to π_6 and π_9 from π_{6M} and π_{9M} can be calculated using the division of equation 3.9 by equation 3.11 and equation 3.10 by equation 3.12, respectively:

$$\frac{\pi_6}{\pi_{6M}} = \frac{f(\pi_1, \pi_2, \pi_3, \pi_4, \pi_5)}{f(\pi_{1M}, \pi_{2M}, \pi_{3M}, \pi_{4M}, \pi_{5M})} \quad (3.13)$$

$$\frac{\pi_9}{\pi_{9M}} = \frac{f(\pi_1, \pi_2, \pi_3, \pi_4, \pi_5, \pi_7, \pi_8, \pi_{10})}{f(\pi_{1M}, \pi_{2M}, \pi_{3M}, \pi_{4M}, \pi_{5M}, \pi_{7M}, \pi_{8M}, \pi_{10M})} \quad (3.14)$$

Therefore, the model is designed and operated to:

$$\pi_1 = \pi_{1M} \quad (3.15)$$
$$\pi_2 = \pi_{2M}$$
$$\pi_3 = \pi_{3M}$$
$$\pi_4 = \pi_{4M}$$
$$\pi_5 = \pi_{5M}$$
$$\pi_7 = \pi_{7M}$$
$$\pi_8 = \pi_{8M}$$
$$\pi_{10} = \pi_{10M}$$

Thus,

$$f(\pi_1, \pi_2, \pi_3, \pi_4, \pi_5, \pi_7, \pi_8, \pi_{10}) = f(\pi_{1M}, \pi_{2M}, \pi_{3M}, \pi_{4M}, \pi_{5M}, \pi_{7M}, \pi_{8M}, \pi_{10M}) \quad (3.16)$$

As a result,

$$\pi_6 = \pi_{6M} \quad (3.17)$$
$$\pi_9 = \pi_{9M} \quad (3.18)$$

Equations 3.17 and 3.18 predict of the behavior of heat transfer and fluid flow, respectively. Those equations are valid if the criteria of the design and operation conditions are acceptable, as showing in Appendix D, according Murphy (1950).

The design conditions (Table 3.3) must be met if the reduced model is to accurately predict conditions quantitatively in prototypes. Design conditions 1 through 5 require the model geometric dimensions to be 1 : n (n = 16, the geometric length scale) times the prototype geometric dimensions. Design condition 6 through 10 establishes the ratio of prototype wind velocity to model wind velocity. Using the same fluid in both the reduced model and prototype systems requires the model wind velocity to be n times the prototype wind velocity. Details about design conditions can be seen in Appendix D.

The tests were performed with the airflow in the reduced model geometrically and dynamically similar to a full-scale CBP barn. To ensure that similarity of the characteristics

of the air flow in the reduced model and real scale CBP barn, the flow regime, expressed by the Reynolds number must be equal in both cases. Therefore:

$$[\mathrm{Re}]_{\mathrm{Model}} = [\mathrm{Re}]_{\mathrm{Full}} \tag{3.19}$$

$$\left(\frac{\rho \cdot v \cdot L}{\mu}\right)_{\mathrm{Model}} = \left(\frac{\rho \cdot v \cdot L}{\mu}\right)_{\mathrm{Full}} \tag{3.20}$$

where, Re is the Reynolds number (dimensionless), L is the characteristic length describing the geometry of the flow field (m), ρ is the specific mass of the air ($kg \cdot m^{-3}$); v is the velocity of the air ($m \cdot s^{-1}$), and μ is the viscosity of the air ($N \cdot m^{-2} \cdot s^{-1}$).

While the CFD simulated the real CBP barn and the reduced model, the equations (3.20) were used for the similarity of the air speed results. More details in Appendix D.

3.5.2. Reduced model procedure

One of the conditions of scaling is geometric uniformity which requires that all dimensions of the real object should be equally scaled. In this study all dimensions of the CBP barn were proportionally reduced with exception of the thickness of the roof. Reducing the thickness of the roof would result in a deformation in the shape of the roof and hence would change the speed and behavior of the airflow.

The scale of the model depends on:

a) The height and width of the test section in the wind tunnel. A model that is too large could block the airflow in the tunnel and would be subject to wall effects.

b) The thickness of the boundary layer. Thereby under natural conditions the CBP barn is situated in the boundary layer, the reduced model should also be placed in the boundary layer in the wind tunnel.

3.5.2.1. Experimental reduced model

A reduced model was constructed in accordance with the design conditions and has a geometric length scale of 16 for testing. The five ridge vents studies (Appendix E - Figure 1) were constructed with a 0.057 m ridge outlet corresponding to a 0.913 m opening in the prototype. The four wind directions investigated (North, South, East, and West) were to represent wind directions found in the field by rotating the model in the wind tunnel.

The reduced model was built using balsa wood and wood glue was used to join pieces. Two aluminum plates were used as the roof cover this model. This reduced model had an overall width of 1.20 m, length of 1.33 m, high at the ridge of 0.50 m, and the slope of the roof was 4:12, so that the scale factor is 1:16. The reduced model is a copy of a CBP barn 24 (Appendix B - Figures 43 and 44) with 36 dairy cows situated in Kentucky (USA). The ventilation openings in the reduced model consisted of a 1.20 m wide ridge opening and eave openings of 0.30 m in height. The top of front wall and end wall under the gable were made of Plexiglas to accommodate airflow visualization. This reduced model was built on a wood table equipped with four wheels. The table has an opening of 0.93 m x 1.33 m and aluminum perforated plate was used to covered this opening. This opening was occupying 80.9% of the floor area that represent the compost pack area. Figure 3.22 is showing the 3D model design used in this study.

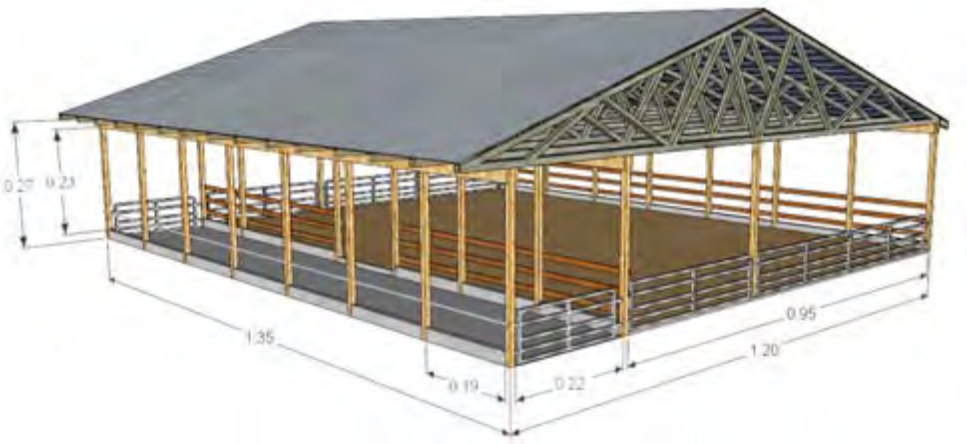

Figure 3.22 - 3D model design used in this study. Dimensions in meters (m).

3.5.2.2. Heating system

Eighteen incandescent lights of 40 W each were installed as electrical heaters under the perforated plate to simulate the sensible heat of microbial activity in the compost bedding. The maximum power flux was ≈ 560 W m^{-2} and was controlled by dimmer varying the intensity of the lights. Thus, it was varied to maintain the floor (compost area) at 45°C. The reduced model floor was maintained at a constant temperature to simulate the heat gains from the compost bedding in the occupied zone.

An insulated box was built below and around the sides of the opening to promote the heat transmission only through the perforated plate. The perforated plate was cover with

aluminum sheet and 2.5 kg of sawdust was spread out over the surface. The heating system and the reduced model with perforated plate, that was used in this study, see Figure 3.23.

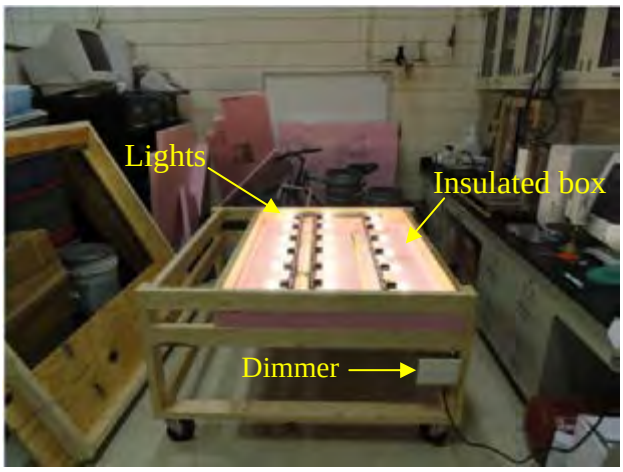

(a)

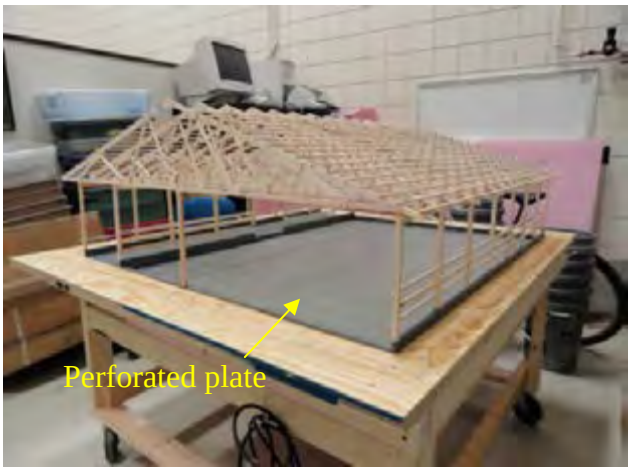

(b)

Figure 3.23 - The heating system (a) and (b) reduced model without roof used in this study.

3.5.2.3. Static pressure, airspeed and temperature measurements

Static pressure was read using two hoses connected with the static pressure sensor (Setra Systems Model 265, series 0811) shown in Figure 3.24, which measure static pressure from 0 to 62 Pa, with an advertized accuracy of 1%. One hose goes inside the wind tunnel, while the other goes outside the wind tunnel. In this way, the sensor could provide the difference in pressures from outside and inside the wind tunnel during the tests. The tests were run with the static pressure range 0 to 10 Pa.

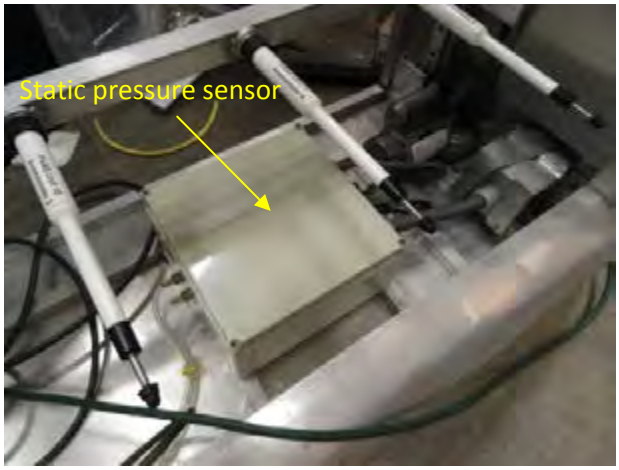

(a)

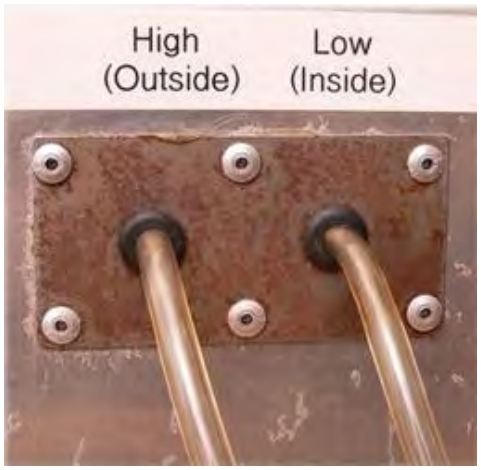

(b)

Figure 3.24 - Static pressure sensor (a) and (b) hoses on the sensor for static pressure measurement.

Airspeed and air temperature were measured using two hot-wire anemometer (accuracy of ±0.01 m/s; Testo®, model 425, Sparta, NJ, USA). One sensor was placed at the beginning of the working section at 1.00 m height above the floor of the wind tunnel and another sensor was placed inside the reduced model using a non-uniform measured grid. This non-uniform grid ranged from 0.10 m to 1.20 m horizontally at 0.55 m intervals and from the floor to ceiling vertically ranged from 0.02 m to 0.20 m at 0.09 m intervals. The locations of the measurement positions used in the experimental analysis are illustrated in Figure 3.25. The hot-wire anemometer inside the building was mounted on a frame, which allowed the anemometer to be manually moved to each measurement position (see Figure 3.25) once measurements at each location were complete. The values measured were replicated three times. The sampling period was fixed at 10 minutes per collection point.

The experiments were carried out with two reference airspeeds: 0.1 m s^{-1} (low wind speed) and 1.0 m s^{-1} (high wind speed). Those airspeeds were selected based on the tunnel capacity and the wall opening area of the reduced model in order to achieve the desired Reynolds numbers ($Re < 2100$) for laminar airflow around and through the model.

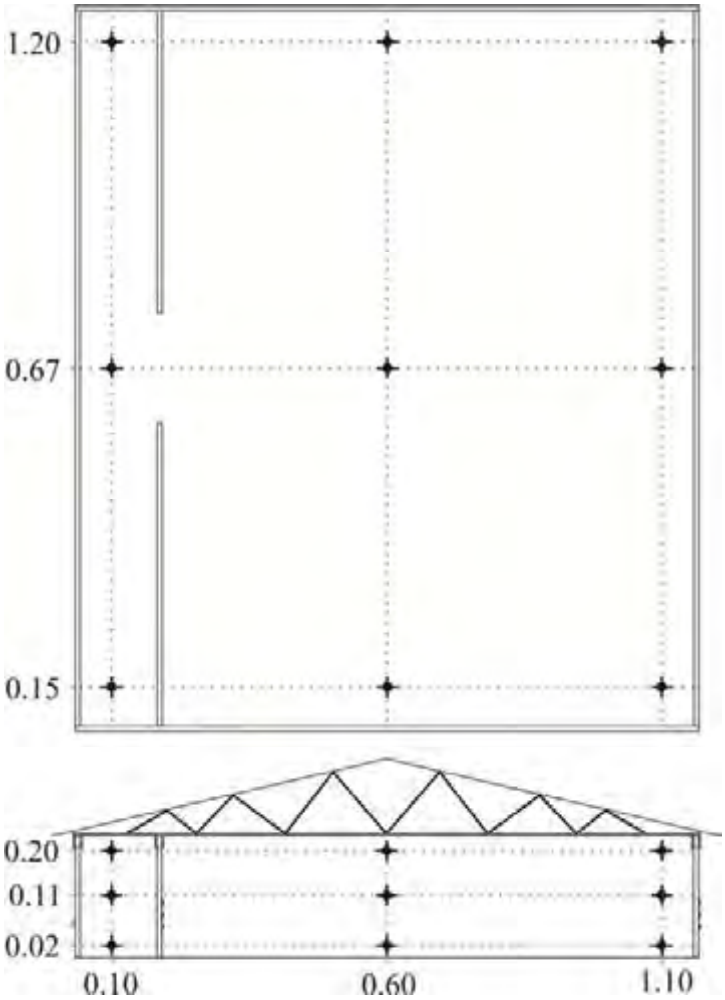

Figure 3.25 - The plan and elevation showing the distribution of measurement points throughout the reduced model.

3.6. The CFD model

3.6.1. CFD representation of the reduced model geometry

In order to validate the CFD model, a 3D Rhinoceros® design of the experimental reduced model was developed and imported into the CFD package. The dimensions of the computational model were: length (Y direction) 1.35 m, width (X direction) 1.20 m, eave height (Z direction) 0.27 m, and the ridge height 0.48 m. The computational model had a total volume of 0.64 m^3. With 78.1% of the total compost pack space provided for animal occupation and bearing in mind the minimum specification for dairy cows housing at 9.3 m^2/cow (Barberg et al., 2007; Janni et al., 2007). The effect of confined dairy cows on airflow was not considered in this CFD model.

In this study, five different ridge vents were built, subdivided into: (a) Closed ridge - CLR, (b) Open ridge - OPR, (c) Open ridge with chimney - ORC, (d) Elevated ridge -

ELR, and (e) Overshot ridge - OVR. The dimensions of the ridge opening were 1.35 m in length and 0.057 m wide. The eave openings were also 1.35 m in length and were 0.23 m in height (0.31 m^2). The total compost pack surface area of the building was 0.877 m^2 and total area of the side wall openings was 0.077 m^2. The modifications in ridge vents were adjusted in simulations that examined the influence of different types of the ridge design on the ventilation performance.

The measured values obtained experimentally for an open reduced model of CBP barn and subjected to natural ventilation were used to assign the boundary conditions of the model (Figure 3.26 and Table 3.4). Two cases (shown in Table 3.4) were tested using four building orientation (North, South, West, and East).

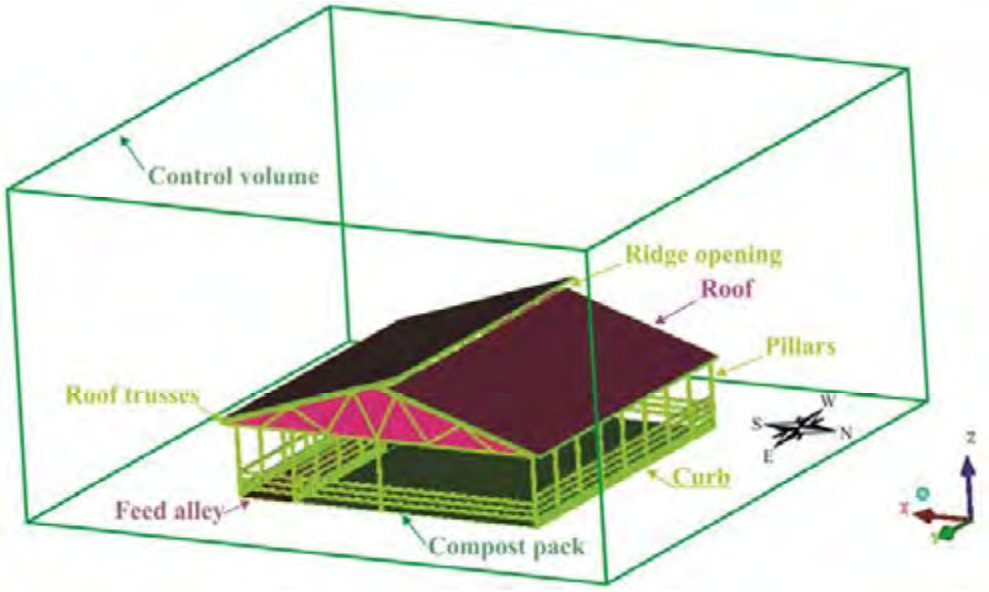

Figure 3.26 - Diagram of the modeled and simulated reduced model of CBP barn.

Table 3.4 – Boundary conditions utilized in the CFD model

Case	Location	Boundary condition	Value
1	Inlet	Average air speed	0.1 m s^{-1}
		Air temperature	22.0 °C
	Outlet	Atmospheric pressure	0.0 Pa
	Floor	Temperature of surface compost	45.0 °C
2	Inlet	Average air speed	1.0 m s^{-1}
		Air temperature	22.0 °C
	Outlet	Atmospheric pressure	0.0 Pa
	Floor	Temperature of surface compost	45.0 °C

3.6.2. Computational modeling

To improve the CFD accuracy, the study exerted much effort to find the appropriate mesh quality and density, and optimum setting condition of wind velocity. The mesh quality is very important to get accurate data and computational convergence. Thus, due to the geometric complexity of the reduced model of CBP barn, it was opted to utilize the ANSYS ICEM CFD® software for construction of a tetrahedral computational mesh which allows for obtaining results with fewer errors (Lee et al., 2007). This software has been specifically designed to fulfill the task of automatically generating high quality tetrahedral meshes, which are suitable for scientific computing using numerical methods such as finite volume methods.

The tetrahedral volume element is very useful to maintain the high quality of the mesh to a region using different forms of complex geometry to be modeled in the region of interest. But, it requires more nodes than the mesh elements and results in a hexametrical file size and computational time increased (Lee et al., 2007; Katz and Sankaran, 2011).

When the reduced model and CFD computed results were compared with each other, the reduced model and CFD computed airflow distribution at a cross-section plane of the reduced model were mainly comparable with each other.

3.6.3. Boundary conditions

The results obtained by simulation using CFD were compared with the corresponding data obtained experimentally in the wind tunnel. In this study, the CFD boundary condition was specified as the same as the wind tunnel boundary condition of test section.

The measured values obtained experimentally in the wind tunnel were used to assign the boundary conditions of the model. Thus, it is necessary to provide the initial values of variables such as air temperature and velocity, calculate the terms of air temperature and velocity for each condition and solve the equations of conservation of energy, mass and momentum

Air flow rates are associated with turbulent flows and, combined with heat transfer rates, generate a complex system of coupled equations difficult to resolve. Therefore, the CFD technique was utilized to solve the average Navier-Stokes and energy equations, determining velocity, temperature and pressure by the finite volumes technique. The model for non-isothermal fluid flow is described by equation of mass, continuity, energy and species, simplified as follows (Kin et al., 2008).

$$\frac{\partial \rho}{\partial t} + \nabla \cdot (\rho U) = 0 \quad (3.21)$$

$$\frac{\partial (\rho U)}{\partial t} + \nabla \cdot (\rho U) = 0 \quad (3.22)$$

$$\frac{\partial \rho}{\partial t} + \nabla \cdot (\rho UU) = \nabla p + [\mu_\tau (\nabla U + \nabla U^T] \quad (3.23)$$

$$\frac{\partial (C_p T)}{\partial t} + \nabla \cdot \left(-k \nabla T + \rho C_p TU\right) = 0 \quad (3.24)$$

$$\frac{\partial C_A}{\partial t} + \vec{m} \cdot \nabla C_A = \nabla \cdot (D \nabla C_A) \quad (3.23)$$

where, ρ is the specific mass ($kg \cdot m^{-3}$); t is the time (s); U is the velocity vector; p is the pressure ($N \cdot m^{-2}$); μ_τ is the dynamic viscosity of the fluid ($kg \cdot m^{-1} \cdot s^{-1}$); T is the temperature (K); C_p is the specific heat ($W \cdot kg^{-1} \cdot K^{-1}$); k is the thermal conductivity ($W \cdot m^{-1} \cdot K^{-1}$); $\vec{m}$ is the velocity component ($m \cdot s^{-1}$); C_A is the concentration of specie A ($g \cdot m^{-3}$); and D is the diffusion coefficient ($m^2 \cdot s^{-1}$).

The Reynolds tensor was modeled using standard k-ε model, which evaluates viscosity (μ_τ) from the ratio between turbulent kinetic energy (k) and dissipation of the turbulent kinetic energy (ε). The ANSYS CFX® software belongs to the Department of Agricultural and Environmental Engineering of the Federal University of Viçosa, and was employed to program and simulate the proposed method. The following considerations were assumed: (a) steady state, (b) incompressible flow, and (c) turbulent flow.

Two computational meshes were generated with different refinement levels using the CFX Mesh computational program, with the objective of verifying effect of refinement on local concentration gradients at the spatial levels.

3.6.4. Statistical analysis methods

a) Barns measurements, compost management practices, and herd characteristics

Descriptive statistics (mean, standard deviation, minimum, maximum, and quartiles) were used to describe individual barn measurements, compost management practices, and herd characteristics (Microsoft Excel, Microsoft Corp., Redmond, WA).

b) WHC, moisture content and bacterial analysis of composts

The data were statistically analysed using Analysis of Variance and Correlation by using computer software SigmaPlot®, version 11.0, Systat Software®, Inc (Wass, 2009) on a Personal Computer.

c) Thermal properties as a function of particle size, moisture content, and compaction degree

Statistical calculations were performed using Sisvar 4.6 (Ferreira, 2003) which is developed by the Federal University of Lavras, Minas Gerais, Brazil. Average values for thermal properties in each particle size, moisture content, and compaction degree ranges were generally used for statistical analyses by ANOVA. For each ANOVA, a particle size, moisture content, and compaction degree ranges consisted of a treatment. Differences between groups were tested by Tukey`s test at significance levels of 5%.

d) Validation of the computational model

The statistical parameter used to evaluate measured (reduced model) versus simulated (CFD model) air velocity and temperature were coefficient of determination (r^2) and Student's t-test. The r^2 values indicate how consistently measured versus predicted values follow a best fit line and can range from zero (no correlation) to 1.0 (perfect correlation). The data were evaluated in the computer software SigmaPlot®, version 11.0, Systat Software®, Inc (Wass, 2009) for statistical analysis and data representation. The p-value was fixed at 5% ($\alpha < 0.05$).

4 - RESULTS AND DISCUSSION

4.1. Introduction

Results are presented in four main sections:

a) Characterization and description of CBP barns (section 4.2): building layout and dimensions, bedding pack characteristic, manure management practices, environmental characteristics, cow characteristics, and producers responses;

b) Evaluate and determine the physical, bacterial, chemical, and thermal properties of compost bulking materials (section 4.3): compost particle size distribution, particle density, bulk density, porosity, water holding capacity, chemical properties of composts, bacterial analysis of composts, and thermal properties of composts;

c) Development of predictive equations for thermal properties of compost as a function of various combinations of moisture content, pressure, and particle size (section 4.3):

d) Develop computational fluid dynamics (CFD) model of compost barn with alternate ridge designs and visually demonstrate impact on air flow through structure (section 4.4):

4.2. Characterization and description of CBP barns

4.2.1. Barn structure and layout

The compost dairy barn measurement and layout information collected included: barn and pack dimensions, feed alley dimensions, waterer location and size, fan and light description, stock density, sidewall height, as well as other barn specifications. General barn characteristics for 42 CBP in Kentucky are shown in Appendix A (Table A.1).

Type and orientation of ridge, roof structure and type, roof pitch are showing in Appendix A (Table A.2).

Ventilation system, cooling fan number, power, size, number of luminaries, and illumination type are listed in Appendix A (Table A.3).

In general, the first CBP barn was constructed in Kentucky in 2002 and the CBP barn number has increased to 58 by the end of 2010. The type of barn construction varied, including barn dimensions, type of ridge, ridge orientation, ventilation system, etc.

CBP barns are a low capital-cost alternative to freestall barns. However, the lower initial investment for bedded-pack barns may be offset by higher annual operating costs.

Barn building costs ranged from $8.000,00 to $400.000,00. Barberg et al. (2007) reported that the building costs ranged widely depending on the amount of on-farm labor utilized and amenities added.

Barn ventilation rates are influenced building dimensions, orientation of ridge, sidewall opening, eave opening, ridge opening, and wind speed. The average compost bedding pack barn dimensions and were 49.1 m (length) and 21.9 m (width). The most frequent barn length was between 25 to 50 m (45.2%), 33.3% was between 50 to 75 m, 11.9% was higher than 75 m, and 9.5% was less than 15 m. The most of frequent barn width was between 15 to 30 m (61.9%), 19.0% was less than 15 m, 16.7% was 30 to 45 m, 2.4% was higher than 75 m. The majority of compost bedded pack barn had areas between 500 to 1000 m (33.3%). The frequency distribution of compost bedding pack barn area is illustrated in Figure 4.1.

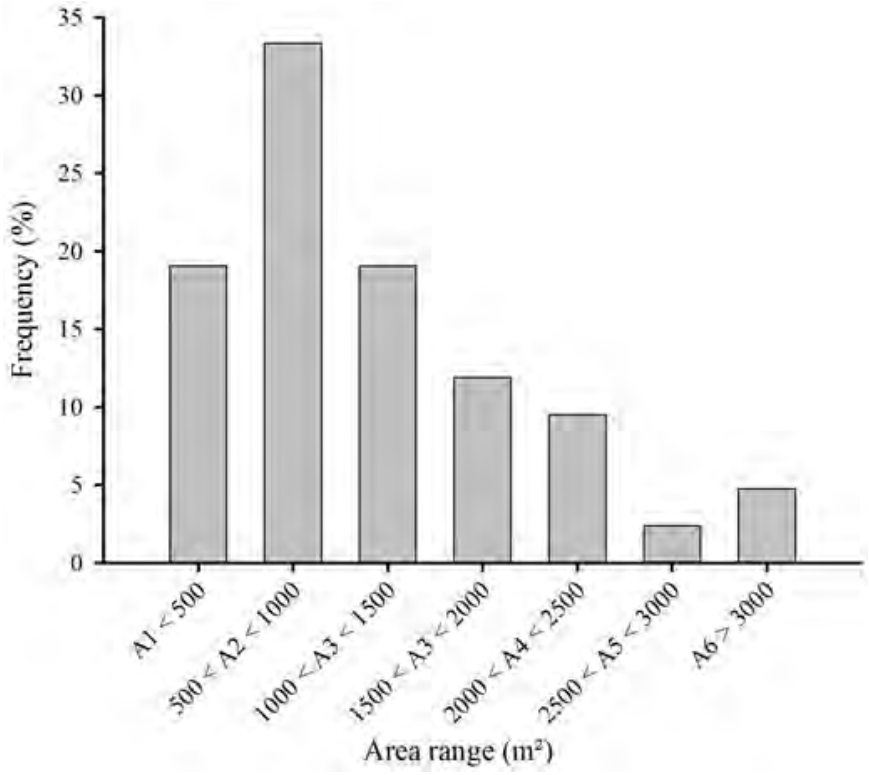

Figure 4.1 - The frequency distribution of compost bedding pack barns area.

Majority of these barns had feed alleys and driveways. Only 26.2% of the barns, the cows had free access to pasture, 9.5% was equipped with cow brush. A feed store and anaerobic lagoon was present around these barns in 52.3%. Headlocks was found in 19% of the CBP barns.

Cow water intake has a critical effect on her milk productivity and reproductive performance since it regulates dry matter intake. A cow must have access to water when needed to satisfy this need. Only 19.0% meet recommendations of 0.10 to 0.15 m per cow (McFarland et al., 2007). In addition, cows did not have access to water at the barn in 24% of the compost bedded pack barns. Cows in over 76.0% of the barns were critically short of waterer space which would limit their milk production.

The recommended feedbunk (stock density) space per cow is 0.03 to 0.06 m / cow (Smith and Harner, 2001). It was found that 29% of the compost bedded pack barns met this recommendation with an additional 12% exceeding it. Only 31% of the compost bedded pack barns had no feedbunks, although most of these had concrete alleyways leading to nearby feedbunks. Inadequate bunk space was found at 25% of the compost bedded pack barns. Overstocking at the feed bunk increases competition among cows and may limit milk production.

Barn orientation will determine the intensity of solar radiation falling on the walls, bedded and feed alley, and roof of the building. Barns oriented are generally an E-W orientation in Kentucky, though the recommended orientation is site-specific based upon natural wind flows. The typical prevailing winds in Kentucky come from the SW in the summer and from the NW in the winter which would suggest the East-West ridge orientation as the most effective. The frequency distribution of ridge orientation is listed in Figure 4.2. Results show that the most frequent orientation is NE-SW (50.0%) with the next highest being NW-SE (45.2%).

The vertical separation between the eave and ridge openings has a significant impact on the pressure differences generated by the chimney effect (Chastain, 2000). Therefore, the roof slope is an important consideration in the design of a naturally ventilated building. All barns with a gable design are best ventilated with a roof pitch of 3:12 or 4:12 (Smith and Harner, 2001). There are 42 measurements since 2 barns were found to have different pitches on each side of the ridge and 2 barns were using hoop structure. Most of barns had roof pitch of 4:12 (54.8%) and 14.3% had roof pitch of 3:12. Barns with roof pitches higher than 4:12 or lower than 3:12 (MWPS-7, 2000), can limit the natural ventilation rate per cow.

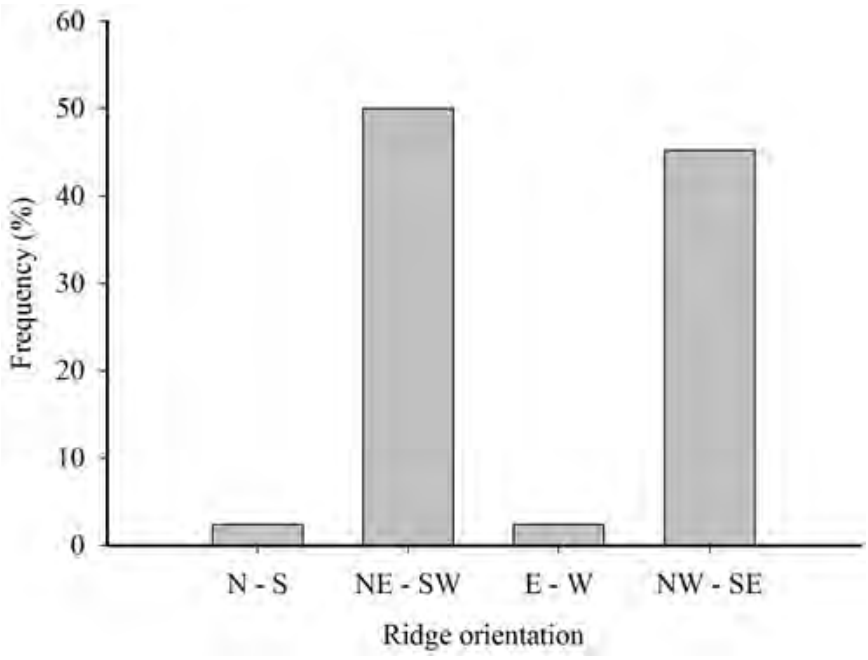

Figure 4.2 - Frequency distribution of ridge orientation.

Sidewall opening height and eave height are provided to protect the cows from sun, rain, and wind, thus helping to maintain proper ventilation and animal comfort. A 3.5m sidewall opening is recommended for barns less than 12.2 m wide while a 4.2 m opening height is recommended for barns wider than 12.2 m (Graves and Brugger, 1994). Frequency distribution of sidewall opening height and eave height for the barns in this study are presented in Figure 4.3. Results show that the most frequent sidewall height is between 2.0 to 4.0 m (66.7%). In 66.7% of barns, the eave height had more than 4.0 m. Some of these barns had low walls on outside perimeter to contain the compost and would reduce the effectiveness of the measured eave height.

A proper eave overhang minimizes the entry of sun, snow, and rain through open sidewalls. Gay (2009) recommend eave overhang with 1/3 of the sidewall height. Majority of barns (54.8%) had eave overhand less than 1.0 m. In 35.7% of barns had eave overhang between 1.0 m and 2.0 m and only 9.5% of barns had eave overhang with 2.0 m or more. Figure 4.4 is showing the frequency distribution of eave overhang.

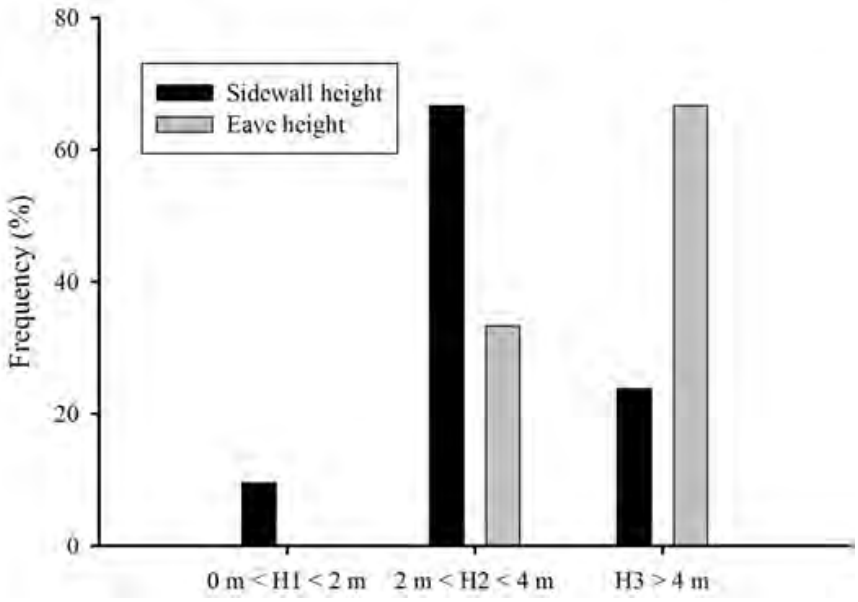

Figure 4.3 - Frequency distribution of sidewall opening and eave height for the barns.

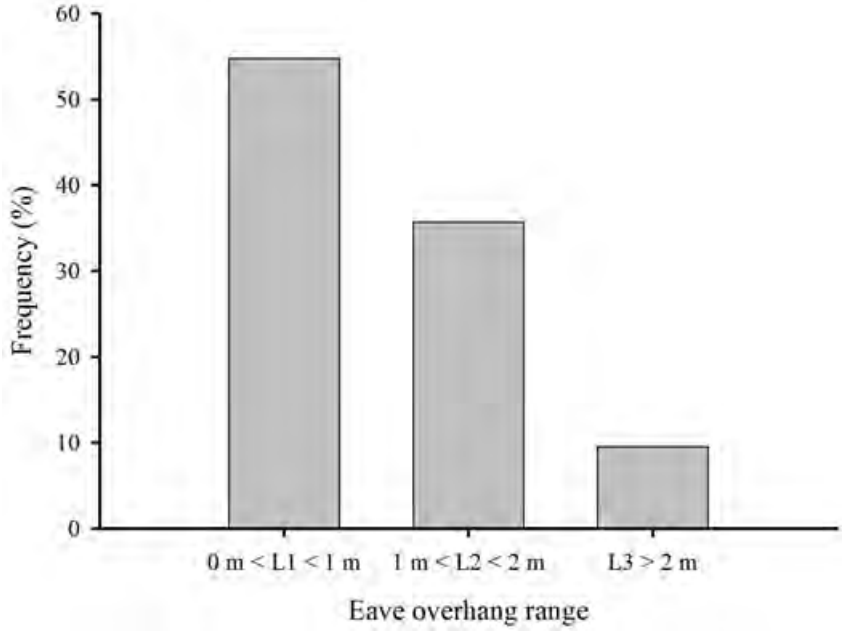

Figure 4.4 - Frequency distribution of eave overhang in barns.

Ridge design affects air movement by removing warm/hot moist air that collects under the roof. The design of the ridge can help or inhibit barn ventilation depending on the wind velocity and direction relative to the ridge line. Characteristics of the CBP barn ridge are showed in Figure 4.5. The primary types of barn ridge found in the compost bedded pack barn study were overshot ridges (59%), open ridge with cover (19%), capped ridge (12%), open ridge without cover (5%), and hoop structure (5%).

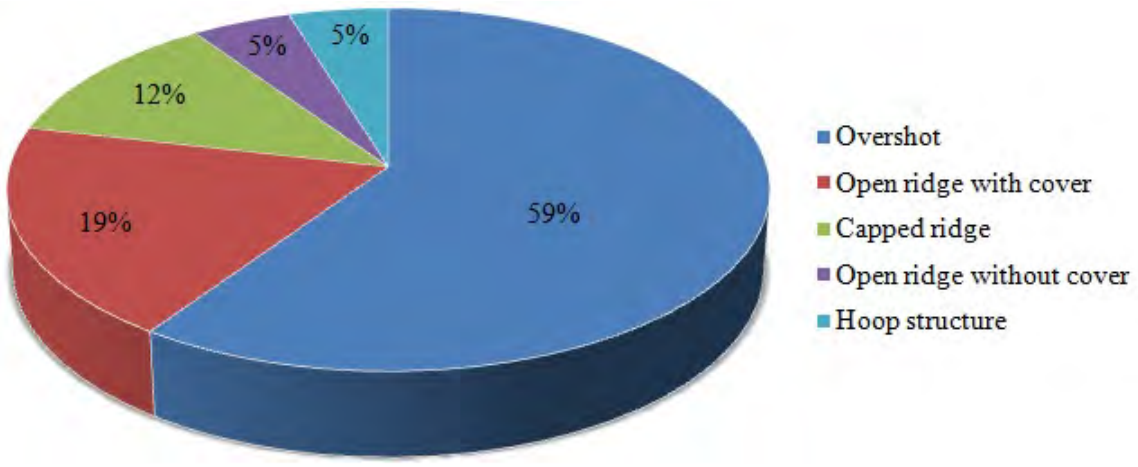

Figure 4.5 - Frequency distribution of the CBP barn ridge in Kentucky.

The width of the continuous ridge opening controls air exhausting from the barn. As the width of a barn increases, the ridge opening should also increase. Figure 4.6 summarizes the ratio of ridge opening to barn width on the compost bedded pack barns visited in Kentucky. Figure 4.6 notes the present recommended ridge opening width of 0.07 m / 3.05 m of barn width with a minimum width requirement of 0.30 m for barns of less than 12.20 m width. There are two ridge opening values shown in Figure 4.6: a) apparent ridge opening (0.02 meters / 3.05 meters of building width) and b) effective ridge opening (0.02 meters / 3.05 meters of building width). The apparent opening is the ridge opening width as seen from inside the barn. The effective opening is the smallest width through which air flows to the outside of the barn at the ridge.

Figure 4.6 indicates the compost barn ridge measurements as a ratio of the ridge opening to barn width (meters / 3.05 meters). There were 17% of the barns with no ridge opening. Based on the apparent ridge opening, 18% had inadequate ridge opening (< 2.5 0.02 meters / 3.05 meters), while 17% had marginal ridge openings (2.5 to < 0.07 meters / 3.05 meters), and 48% equaled or exceeded the recommended ridge opening. However, based on the effective ridge opening, 53% had inadequate ridge opening, while 20% had marginal ridge openings, and only 11% equaled or exceeded the recommended ridge opening. The large majority of barns had ridge opening restrictions that could cause inadequate natural ventilation that can significantly affect cows, particularly under heat stress conditions.

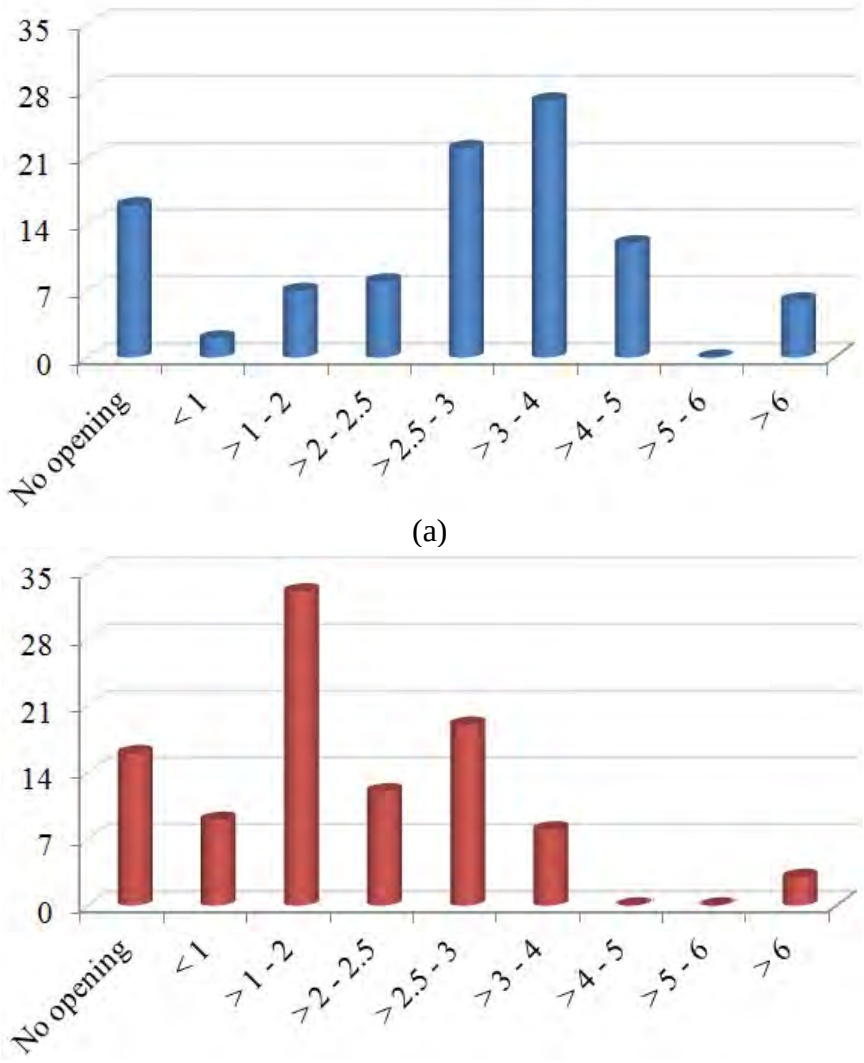

Figure 4.6 - Ridge opening to barn width ratio for compost bedded pack barns: (a) Apparent Ridge Opening Compost Barns - 0.02 meters / 3.05 meters width and (b) Effective Ridge Opening Compost Barns - 0.02 meters / 3.05 meters width.

The majority of compost bedded pack barns were equipped with box fans (42.8%) for circulation, 30.9% using natural ventilation, 23.8% using High Volume Low Speed Fans (HVLS) for circulation, and 2.5% Tunnel ventilation (hoop structures). Buildings that will use tunnel ventilation require more elaborate ridge openings with some type of closure system. In this case, it is recommended to consult a competent designer (Agricultural Engineer) who has experience with cattle shelter ventilation for special situations. Most of HVLS fans used had diameter of 7.32 m. The average diameter of box fans was 0.98 m, ranged from 0.46 m to 1.32 m.

Lighting in compost bedded pack barns was noted at each dairy visited. It was found that 41% of compost bedded pack barns didn't have lights. High Intensity Discharge (HID) was the most frequent form of light producers used. This was followed by Fluorescent (14%), Compact fluorescent (12%), and Incandescent (10%). Total lighting wattage is also noted. The light average power used in a barn was 124 W, ranged from 13 to 192 W.

4.2.2. Description of structure and layout in each barn

Barn 1 was built in October 2010 and cost $60,000 (Appendix A - Table A.1). The dimensions of the barn were 51.2 m x 15.2 m, and a 1.48 m high wood sidewall surrounding the pack. Waterers was outside of the pack area and the dimensions were 2.4 m x 0.8 m. Sidewall was built using seven wood board of 0.05 m x 0.20 m and sidewall opening of 3.4 m. The feed alley was away from this barn, and the animals were feed in separate of the building. There were no headlocks, see Figure 4.7. Geographic position of the Barn 1 were 37° 13' 53" N of latitude and 86° 20' 20" W of longitude (Appendix A - Table A.2) and ridge orientation of 249° East (E). Wood structure was used to build this barn and metal roof was used to covered. The eave height was 4.87 m and eave overhang was 1.22 m. The ridge type used was open ridge with cover. Roof pitch measured was 4:12 and ridge cap had dimensions of 0.51 m x 0.51 m, height of 0.51 m and ridge opening of 0.38 m. Drawings about Barn 1 can be seen in Appendix B (Figures 1 and 2). Forced ventilation system was used with eight box fans (Appendix A - Table A.3). Lamps and cow brush were not present this barn. One anaerobic lagoon was used close to the barn.

(a) (b)

Figure 4.7 - The main constructive characteristic of CBP barn 1.

Barn 2 was built in March 2008 and cost was $80,000 and including fans was $110,000. The dimensions of the barn were 76.3 m x 30.3 m, see Appendix A (Table A.1).

Concrete wall with 0.6 meter high was used around of the perimeter of the barn 2 and wire cables were above the wall to prevent cows from falling or jumping out of this building (Figure 4.8). The feed alley and waterers were in other building, away from barn 2, but the animals had free access. This barn had sidewall opening of 3.48 m. Waterers was located along the feed alley. There were no headlocks. A drive-by feed manager was located in another building close to Barn 2. Geographic position of the Barn 2 were 36° 54' 32" N latitude and 86° 16' 42" W longitude (Appendix A - Table A.2) and ridge orientation of 241° Northeast (NE). Type of construction in Barn 2 was steel-framed pole sheds and stainless steel wire. The eave height was 3.67 m and eave overhang had dimension of 1.47 m. Metal roof was used to covered and the roof pitch was 4:12. The ridge type used was open ridge with cover. Ridge cap had dimensions of 0.51 m x 0.51 m, height of 1.01 m and ridge opening of 0.61 m. The Barn 2 was equipped with three High Volume Low Speed (HVLS) Fans above the pack (Appendix A - Table A.3). Lighting utilized in barn 2 was three high intensity discharge, with power of 175 watts each. Cow brush was present this barn. An anaerobic lagoon was located close to the barn. See Appendix A (Figures 3 and 4) for more details about CBP barn 2.

(a) (b)

Figure 4.8 - The main constructive characteristic of CBP barn 2.

There was no information about date of construction in Barn 3. The cost of this barn was approximately $175,000. The barn dimensions were 87.8 m x 16.7 m (Appendix A - Table A.1). Concrete feed alley and waterers were separated from the pack by low concrete walls. Concrete wall was used around of the perimeter of this barn and wire cables were above the wall to prevent cows from falling or jumping onto feed alley. This barn had open sidewalls without curtains of 2.25 m. Waterers were located adjacent to the concrete wall separating the pack area and the feed alley (Figure 4.9). In this barn , there were no

headlocks. Geographic position in Barn 3 were 36° 25' 56" N of latitude and 86° 44' 9" W of longitude, and ridge orientation of 36° Southwest (SW), as can be seen in Appendix A (Table A.2). Steel-framed pole sheds and stainless steel wire were used to built this barn and metal roof was used to covered. The eave height was 3.18 m and eave overhang was 2.35 m. The ridge type used was overshot, roof pitch measured was 4:12, overlap of the ridge of 0.9 m, and ridge opening of 0.76 m. Drawings of Barn 3 can be seen in Appendix B (Figures 5 and 6). The Barn 3 was equipped with seventeen box fans (Appendix A - Table A.3). Lighting utilized was two high intensity discharge. Cow brush was and anaerobic lagoon were not present around this barn.

(a) (b)

Figure 4.9 - The main constructive characteristic of CBP barn 3.

Barn 4 was built October 2010 and the total cost was $10,900, is detailed in Appendix A (Table A.1). The dimensions of the barn were 51.5 m x 9.1 m. Waterers had dimensions with of 2.4 m x 0.8 m. The feed alley was away from facility, and the animals were feed in separate of the building (Figure 4.10). In this barn, the sidewall opening had 1.22 m. The ridge orientation of the Barn 4 was 80° Southwest (SW) and the geographic position were 36° 42' 10" N latitude and 86° 40' 34" W longitude (Appendix A - Table A.2). Thirty treated wood posts were used to build this barn. Posts had dimensions of 0.15 m x 0.15 m and spaced of 1.83 m from each other. Two treated boards (0.05 m x 0.15 m) were used in each sidewall. Tubular steel arches fastened to the tops and sides of the posts to form a hooped roof were used and white poly vinyl tarp used to covered. The eave height was 4.57 m. Left-side eave overhang of this barn had width of 1.37 m and eave overhang over feed area had width of 4.82 m. Only natural tunnel ventilation was used in Barn 4. Lightings and

cow brush were not present this barn (Appendix A - Table A.3). Anaerobic lagoon was not present around this barn. Drawings of Barn 4 can be seen in Appendix B (Figures 7 and 8).

(a) (b)

Figure 4.10 - The main constructive characteristic of CBP barn 4.

Barn 5 was built in 2003 and there was no information about costs of construction (Appendix A - Table A.1). The dimensions of the barn were 48.7 m x 15.2 m. There were no information about waterers. The dimensions of feed alley of 3.41 m x 48.7 m and one concrete curb was separating the pack and the feed alley. This concrete wall had a height of 0.3 m and a wood fence was installed above this concrete wall to prevent cows from jumping onto feed alley. A drive-by feed manger was located on the left side of the barn. Five wood boards (0.05 m x 0.10 m) were used in sidewall (Figure 4.11). Barn 5 had a sidewall opening of 3.53 m. Geographic position founded in Barn 5 were 37° 44' 25" N latitude and 85° 44' 55" W longitude and ridge orientation of 31° Southwest (SW) is detailed in Appendix A (Table A.2). Wood pole and stainless steel plate were used to built this barn and metal roof was used to covered. The eave height was 3.66 m. This barn had two different widths in the eave overhang of 1.06 m and 0.76 m. The ridge type used was overshot, roof pitch measured was 4:12, overlap of the ridge of 1.11 m, and ridge opening of 0.76 m. Barn 5 was used natural ventilation system (Appendix A - Table A.3). There were no information about type of lighting. Headlocks and cow brush were not present in this barn. An anaerobic lagoon was not present around this barn. Drawings about Barn 5 can be seen in Appendix B (Figures 9 and 10).

(a)

(b)

Figure 4.11 - The main constructive characteristic of CBP barn 5.

Barn 6 was built in June 2010 and there was no information about costs of construction (Appendix A - Table A.1). The dimensions of the barn 6-A were 30.5 m x 16.4 m and barn 6-B were 33.0 m x 26.2 m. This barn had a wood fence wall separating the pack and feed alley (Figure 4.12). Two concrete waterers were used on the pack area. Sidewall were open during winter. The sidewall opening had 2.73 m. Geographic position of the Barn 6 were 37° 2' 27" N of latitude and 85° 11' 2" W of longitude (Appendix A - Table A.2). The ridge orientation of this barn was 145° Northwest (NW). Wood structure was used to build this barn and metal roof was used to covered. The eave height of barn 6-A and 6-B were 3.18 m and 4.27 m, respectively. The eave overhang was 0.61 m. The roof pitch measured was 4:12. This barn had two different ridge type: capped ridge (Barn 6-A) and overshot (Barn 6-B). The ridge opening in barn 6-B was 0.35 m, and overlap of the ridge of 0.83 m. Twelve box fans were used in ventilation system (Appendix A - Table A.3). Five incandescent lightings were used to illumination. Cow brush was not present in this barn. Anaerobic lagoon was not present around this barn. Drawings of Barn 6 can be seen in Appendix B (Figures 11 and 12).

(a)

(b)

Figure 4.12 - The main constructive characteristic of CBP barn 6.

Barn 7 was built in November 2008 and cost $50,000 (Appendix A - Table A.1). The barn dimensions were 36.6 m x 16.3 m. Waterers was around of this barn and had dimensions of 2.0 m x 0.6 m. This building had sixty headlocks along a covered drive-by feed manger. Sidewall opening had 3.65 m. The cows had a free access to pasture. A tubular steel gates were used to access to another building (Figure 4.13). Geographic position of the Barn 7 were 37° 46' 27" N of latitude and 84° 38' 52" W of longitude and the ridge orientation of this barn was 40° South-west (SW), as can be seen in Appendix A (Table A.2). Wood structure was used to build this barn and metal roof was used to covered. The eave height was 3.65 m and eave overhang was 0.91 m. The ridge type used was overshot and the roof pitch measured was 4:12. The ridge opening of 0.45 m and overlap of the ridge of 0.64 m. Metal roof was used to covered and the roof pitch measured was 4:12. Barn 7 was equipped with two High Volume Low Speed (HVLS) fans with 7.32 m of diameter and power of 1491.4 watts (Appendix A - Table A.3). Six High Intensity Discharge (HID) lamps with 175 watts each were used to illumination. Cow brush was not present in this barn. Anaerobic lagoon was not present around this barn. Details about Barn 7 can be seen in Appendix B (Figures 13 and 14).

(a) (b)

Figure 4.13 - The main constructive characteristic of CPB barn 7.

Barn 8 was built in January 2011 and cost to built without concrete was $60,000. The building dimensions of this barn were 65.8 m x 29.2 m, as can be seen in Appendix A (Table A.1). A covered drive-by feed manger was located on the center of the barn (Figure 4.14). This barn had an indoor concrete feed alley and 0.91 m high concrete wall around of the barn. The sidewall opening had 2.7 m. This barn had installed guardrail fence above the concrete wall to prevent cows from jumping onto feed alley or outside of the barn. The two plastic waterers were outside of pack area. Geographic position in Barn 8 (Appendix A -

Table A.2) were 36° 54' 55" N of latitude and 86° 15' 1" W of longitude and ridge orientation of 210° Northwest (NW). Galvanized steel H-beam columns were used and metal roof was used to covered of this barn. The eave height was 3.65 m. The ridge type used was open ridge with cover and the roof pitch was 4:12. Ridge cap had dimensions of 0.48 m x 0.48 m, height of 0.61 m and ridge opening of 0.61 m. The Barn 8 was equipped with 4 box fans over pack area (Appendix A - Table A.3). Lamps were not present in this barn. One tractor was used to stirring the bedding compost using cultivators on skid loader. Headlocks and cow brush were present this barn. One anaerobic lagoon was present around this barn. See Appendix B (Figures 15 and 16) for more details about CBP barn 8.

(a) (b)

Figure 4.14 - The main constructive characteristic of CBP barn 8.

Barn 9 was built in September 2010 and cost of construction was $120,000 (Appendix A - Table A.1). The building dimensions of this barn were 76.3 m x 27.6 m. This barn had three waterers on the concrete scrape alley and dimensions of 3.1 m x 0.6 m, 2.1 m x 0.6 m, and 1.2 x 0.6 m, respectively. A concrete wall separating the pack and the feed alley had three walkways for cows to access the pack (Figure 4.15). Geographic position of the Barn 9 were 36° 54' 55" N latitude and 86° 40' 34" W longitude and the ridge orientation was 75° Northwest (NW), as can be seen in Appendix A (Table A.2). This barn was built using wood pole. The eave height was 4.57 m. The eave overhang had two different width of 0.30 m and 0.61 m. The ridge type used was overshot. Roof pitch measured was 4:12, overlap of the ridge of 0.50 m and ridge opening of 0.46 m. Barn 9 equipped with twenty eight box fans with 735.5 W each (Appendix A - Table A.3). Thirty high intensity discharge (HID) lamps were used with 175 w each. Headlock was present in this barn. This barn was not equipped with cow brush. Anaerobic lagoon was present around this barn. Details about CBP barn 9 can be seen in Appendix B (Figures 17 and 18).

(a)

(b)

Figure 4.15 - The main constructive characteristic of CBP barn 9.

Barn 10 was built in Fall 2009 and cost $120,000 including fans and lamps (Appendix A - Table A.1). The building and pack dimension of this barn were 61.0 m x 30.5 m. Waterers was not present in this barn. A tubular steel gates were used to access to another building (see Figure 4.16). The sidewall was built using three guardrail. In this barn, the sidewall opening had 3.7 m. Geographic position were 36° 54' 55" N latitude and 86° 15' 01" W longitude (Appendix A - Table A.2). The ridge orientation was 349° Southeast (SE). This barn was built using wood board. The eave height was 4.87 m and eave overhang was 0.76 m. The ridge type used was overshot and metal roof was used to covered this barn. This barn had two different roof pitch of 3:12 and 2 1/2 :12. The ridge opening of 0.61 m, and overlap of the ridge of 0.91 m. Five high intensity discharge (HID) lamps were used with 70 watts each. Headlocks and cow brush were not present in this barn. Anaerobic lagoon was around this barn. Barn 10 was equipped with fifteen box fans with 735.5 watts each (Appendix A - Table A.3). Drawings of Barn 10 can be seen in Appendix B (Figures 19 and 20).

(a)

(b)

Figure 4.16 - The main constructive characteristic of CBP barn 10.

Barns 11 and 12 were built in the same time, using the same constructive characteristics and costs of construction. These barns were built in February 2010 and cost $150,000 each with fans and labor. The building dimension of this barn were 91.5 m x 39.0 m, as can be seen in Appendix A (Table A.1). Two different plastic waterers were present in pack area with dimensions of 1.8 m x 0.6 m and 3.6 m x 0.5 m. The waterers were located adjacent to the concrete wall separating the pack area and the feed alley. A covered drive-by feed manger had dimension of 2.74 m. The wall separating the pack and the feed alley had five walkways for cows to access the pack. This wall was built with concrete and had 1.10 m high and one steel fence was installed on this wall to prevent cows from jumping onto the feed alley (Figure 4.17). These barn had open sidewalls without curtains with 3.75 m. One elevated walkway has been installed in the middle of each barn to help the handling of cows. Tubular steel gates were used to access to another building.

Geographic positions of these barn were 37° 44'58" N latitude and 84° 25' 53" W longitude and the ridge orientation was 23° Southwest (SW), as can be seen in Appendix A (Table A.2). The type of these barns construction was wood and steel-framed pole. The ridge type used was overshot with metal roof used to covered in each barn. These barns had a different roof pitch configuration of 3:12 and 2 1/2 :12, overlap of the ridge of 0.61 m and ridge opening of 0.46 m. Details about barn 11 and barn 12 can be seen in Appendix B (Figures 21 and 22).

Five High Volume Low Speed (HVLS) fans with different diameter (three fans of 6.10 m and two fans of 7.32 m) were used under of pack area (Appendix A - Table A.3). Each barn was equipped with six fluorescent (FLL) lamps of 192 watts. Headlocks and cow brush were not present in this barn. Anaerobic lagoon was not present around this barn.

(a) (b)

Figure 4.17 - The main constructive characteristic of CBP barns 11 and 12.

Barns 13 and 14 were built in the same time, using the same constructive characteristics and costs of construction. These barns were built in October 2010 and cost $85,000 each barn, $140,000 for concrete, and total $400,000 without fans (Appendix A - Table A.1). The barns dimensions were 61.0 m x 40.8 m. Barn 13 was 12.2 m away from Barn 14. Eight plastic waterers were present in each barn and had dimensions of 1.8 m x 0.6 m. The waterers were located adjacent to the concrete wall separating the pack area and the feed alley. The drive-by feed manger was located in the middle of the barn (Figure 4.18). The driveway had 4.87 m width. The concrete wall separating the pack and the feed alley had five walkways for cows to access the pack. These barn had open sidewalls without curtains with 2.96 m. Tubular steel gates were used to access to another building.

Geographic positions of these barns were 36° 59' 57" N latitude and 85° 42' 38" W longitude (Appendix A - Table A.2). The ridge orientation was 329° Southeast (SE). These barns were built using concrete floor and wood board. The eave height was 3.96 m and eave overhang was 1.22 m. The ridge type used was open ridge without cover. The ridge opening and height were 0.91 m. Metal roof was used to covered in each barn and the roof pitch measured was 3:12. Barn 13 and 14 utilized natural ventilation (Appendix A - Table A.3). Each barn was equipped with ten compact fluorescent lamps of 32 watts. Headlocks was present in these barns. Anaerobic lagoon was present around these barns. Drawings of CBP barns 13 and Barn 14 can be seen in Appendix B (Figures 23 and 24).

(a)

(b)

Figure 4.18 - The main constructive characteristic of CBP barns 13 and 14.

Barn 15 was built in April 2010 and there were no information about costs of construction (Appendix A - Table A.1). The barns and pack dimensions were 18.3 m x 18.3 m. The waterers was outside of the pack area and the dimensions were 3.6 m x 0.5 m (Figure 4.19). Feed alley was located on the outside of the barn on the Northwest side.

This barns had a 0.58 m high wall surrounding the pack. This barn had open sidewalls without curtains with 3.96 m. The cows had free access to pasture. Geographic positions of Barn 15 was 38° 10' 18" N latitude and 85° 13' 43" W longitude (Appendix A - Table A.2). The ridge orientation was 334° Southwest (SW). These barns were built using concrete floor, wood, and steel plate. The ridge type used was Capped ridge and metal roof was used to covered. The end wall had a opening on the top. The eave height was 3.96 m and the roof pitch of 4:12. More details see Appendix B (Figures 25 and 26). Barn 15 was equipped with one High Volume Low Speed (HVLS) fans under of pack area (Appendix A - Table A.3). These barns were not equipped with Lights. Headlocks and cow brush were not present in this barn. An anaerobic lagoon was present around this barn.

(a) (b)

Figure 4.19 - The main constructive characteristic of CBP barn 15.

There was no information about date and costs of construction of Barn 16. This barn had dimensions of 14.6 m x 13.9 m, as can be seen in Appendix A (Table A.1). One rectangular concrete waterers, 2.4 m x 0.6 m, was outside of pack area, adjacent to drive-by feed manger (Figure 4.20). Opens sidewalls (2.22 m) without curtains were present in this barn. Barn 16 had a concrete sidewall surrounds the pack and a wall separating the pack from feed alley of 0.3 m high. Geographic positions of Barn 16 was 37° 8' 39" N latitude and 85° 18' 14" W longitude (Appendix A - Table A.2). The ridge orientation was 243° Northeast (NE). The type of these barns construction was concrete wall and wood in the structure. The eave height was 3.50 m. This barn had a eave overhang of 1.65 m and eave overhang over feed area of 1.83 m. The ridge type used was capped ridge and metal roof was used to covered. This barn had a roof pitch of 5:28. Drawings of Barn 16 can be seen in Appendix B (Figures 27 and 28). Barn 16 was equipped with three box fans under of pack area and one box fan under feed alley (Appendix A - Table A.3). This barns was

equipped with six incandescent lights of 100 watts each. Headlocks and cow brush were not present in this barn. An anaerobic lagoon was present around this barn.


(a)


(b)

Figure 4.20 - The main constructive characteristic of CBP barn 16.

There was no information about date of construction of Barn 17. The cost of construction was $22,000 without fans (Appendix A - Table A.1). The barn dimensions were 37.8 m x 13.7 m. Sidewalls were open (3.76 m) without curtain and two horizontal stainless steel fence were used around this barn. Two plastic waterers were around this barn and dimensions were 1.5 m each. Two tubular steel gates were used to access to another building (Figure 4.21). Geographic position were 37° 1' 23" N latitude and 85° 9' 29" W longitude (Appendix A - Table A.2). The ridge orientation was 240° Southeast (SE). These barns were built using concrete floor and wood pole. The eave height was 4.92 m and eave overhang was 1.32 m. The ridge type used was overshot and metal roof was used to covered in each barn. The roof pitch measured was 4:12, ridge opening of 0.34 m, and overlap of the ridge of 0.91 m. Details about barn 17 can be seen in Appendix B (Figures 29 and 30). Barn 17 was equipped with six box fans along of pack (Appendix A - Table A.3). Eight incandescent lights of 100 watts each were used. Headlocks were present in this barn. An anaerobic lagoon was present around this barn.


(a)


(b)

Figure 4.21 - The main constructive characteristic of CBP barn 17.

Barn 18 was built in November 2008 and cost $90,000 (Appendix A - Table A.1). The barn dimensions were 61.0 m x 24.4 m. The concrete driveway was outside of barn and had width of 3.95 m. This barn had a small concrete curb and tubular steel gates was above this curb, separating the pack and the feed alley (Figure 4.22). One waterers was outside of the pack with dimension of 3.7 m x 0.6 m. This barn had two feed alley with dimensions of 30.6 m x 5.33 m and 61.0 m x 3.95 m. Sidewall was built using seven wood board of 0.05 m x 0.30 m. Geographic positions of this barn were 37° 29' 23" N of latitude and 86° 51' 58" W of longitude and ridge orientation of 90° South-west (SW), as can be seen in Appendix A (Table A.2). This barn was built using wood posts, wood boards, and metal roof was used to covered. The eave height was 4.9 m and eave overhang was 1.06 m. The ridge type used was overshot, roof pitch measured was 3 1/2 : 12, overlap of the ridge of 0.23 m and ridge opening of 0.16 m. The barn 18 was equipped with twenty box fans and eight fluorescents lamps of 192 W (Appendix A - Table A.3). Cow brush and headlock were not present this barn. One anaerobic lagoon was used close to the barn. Drawings of Barn 18 can be seen in Appendix B (Figures 31 and 32).

(a) (b)

Figure 4.22 - The main constructive characteristic of CBP barn 18.

Barn 19 was built in October 2006 and costs of construction was approximately $8,000 (Appendix A - Table A.1). This barn had dimension of 21.3 m x 14.0 m. The waterers and feed alley were outside of this barn (see Figure 4.23). The cows had free access to pasture. This building had not sidewall opening. Geographic positions of Barn 19 was 37° 34' 15" N latitude and 86° 08' 36" W longitude (Appendix A - Table A.2). The ridge orientation was 28° Northwest (NW). This barns was built using wood board and metal plate. The ridge type used was Capped ridge and metal roof was used to covered. The end wall had one

opening on the top. The eave height was 4.26 m, eave overhang was 0.30 m, and roof pitch of 3 1/2 : 12. Drawings of Barn 19 can be seen in Appendix B (Figures 33 and 34). Barn 19 was equipped with four box fans of 0.91 m (diameter). Two compact fluorescent lamps of 32 watts were used (Appendix A - Table A.3). Cow brush were not present this barn. One anaerobic lagoon was used close to the barn.

(a) (b)

Figure 4.23 - The main constructive characteristic of CBP barn 19.

Barn 20 was built in 2003. There was no information about cost of construction (Appendix A - Table A.1). The dimensions of this barn were 21.9 m x 18.0 m. Two waterers, 0.70 m x 0.64 m, were on the pack area (Figure 4.24). One short concrete curb and two steel pole were separating the pack area and the feed alley. This barn had a covered feed alley width of 3.66 m and one closed sidewall with metal panels was used.

Geographic position were 37° 46' 25" N latitude and 85° 21' 52" W longitude and the ridge orientation was 15° Southwest (SW), as can be seen in Appendix A (Table A.2). This barn was built using wood pole, metal plate, and galvanized steel H-beam was used under the roof metal. The eave height was 4.11 m and eave overhang of 0.23 m. The ridge type used was overshot, roof pitch measured was 1 1/2 : 12 and 2 : 12, overlap of the ridge of 0.33 m and ridge opening of 0.23 m.

Barn 20 was equipped with six box fans of 0.91 m diameter and four box fans of 1.22 m diameter (Appendix A - Table A.3). Lamps, headlock and cow brush were not present this barn. Anaerobic lagoon was not present around this barn. Details about barn 20 can be seen in Appendix B (Figures 35 and 36).

(a)

(b)

Figure 4.24 - The main constructive characteristic of CBP barn 20.

Barn 21 was built in June 2006 and costs of construction was $30,000 with fans. The barn dimensions were 36.6 m x 15.2 m. Sidewalls were open without curtain (Figure 4.25). Eleven wood post were uses on each side and spaced of 3.66 m from each other. Plastic waterers was situated in another barn and the cows had a free access to the building. This barn was equipped with two tubular steel gates. This building had sidewall opening of 4.57 m. Geographic position were 37° 20' 49" N latitude and 85° 21' 41" W longitude (Appendix A - Table A.2). The ridge orientation was 233° Northeast (NE). This barn was built using concrete sidewall curb, wood pole, and metal roof was used to covered. The eave height was 4.57 m and eave overhang was 1.67 m. The ridge type used was overshot, roof pitch measured was 4:12, ridge opening of 0.91 m, and overlap of the ridge of 0.91 m. Drawings of Barn 21 can be seen in Appendix B (Figures 37 and 38). Barn 21 was equipped with six box fans along of pack of 0.91 m diameter and two box fans of 1.22 m diameter above of pack area, as can be seen in Appendix A (Table A.3). This barn was equipped with three high intensity discharge (HID) lamps of 175 watts. Headlocks and cow brush were not present in this barn. Anaerobic lagoon was not present around this barn.

(a)

(b)

Figure 4.25 - The main constructive characteristic of CBP barn 21.

Barn 22 was built in 2002 and costs of construction was $40,000 (Appendix A - Table A.1). The barns dimensions were 60.9 m x 18.9 m. The waterers was outside of pack area, but located adjacent in the endwall. The waterers dimensions were with 1.8 m x 0.6 m. This barn had the same feed alley that the barn 23 and the cows had a free access (Figure 4.26). This feed alley had width of 5.48 m. This barns had a 0.35 m high concrete wall both side of the pack. Sidewalls were open without curtain and hot wires were used above the sidewall curb height. Geographic positions of Barn 22 was 37° 03' 58" N latitude and 86° 18' 33" W longitude (Appendix A - Table A.2). The ridge orientation was 35° Northwest (NW). This barn was built using concrete floor, wood, and steel plate. Two zinc gutter were used on both side and two PVC pipe were carry the rainwater to a concrete box. The eave height was 4.33 m and eave overhang was 0.60 m. The ridge type used was Capped ridge, roof pitch of 4:12, and metal roof was used to covered. Natural ventilation system was used in the Barn 22 (Appendix A - Table A.3). Twelve high intensity discharge lamps (150 watts each) were used above the pack area. Headlocks and cow brush were not present in this barn. Anaerobic lagoon was not present around this barn. Drawings of Barn 22 can be seen in Appendix B (Figures 39 and 40).

(a) (b)

Figure 4.26 - The main constructive characteristic of CBP barn 22.

Barn 23 was built in 2007 and costs of construction was $85,000 (Appendix A - Table A.1). The barns dimensions were 60.9 m x 15.2 m. A plastic waterers of 3.6 m x 0.6 m was outside of pack area (Figure 4.27). Sidewalls were open without curtain and three wood boards were used above the sidewall curb. The sidewall curb height of 0.35 m. Geographic positions of Barn 23 was 37° 03' 58" N latitude and 86° 18' 34" W longitude (Appendix A - Table A.2). The ridge orientation was 305° Southeast (SE). This barn was built using concrete floor, wood, and metal plate. Two zinc gutter were used on both side and PVC

pipe were carry the rainwater to a concrete box. The eave height was 4.33 m and eave overhang was 0.60 m. The ridge type used was Capped ridge, roof pitch of 4:12, and metal roof was used to covered. Details about barn 23 can be seen in Appendix B (Figures 41 and 42). Barn 23 was natural ventilation system (Appendix A - Table A.3). Six high intensity discharge lamps (150 watts each) were used on this barn. Headlocks and cow brush were not present in this barn. Anaerobic lagoon was not present around this barn.

(a) (b)

Figure 4.27 - The main constructive characteristic of CPB barn 23.

Barn 24 was built in 2009 and costs of construction was $35,000 (Appendix A - Table A.1). The barns dimensions were 30.5 m x 18.9 m. Plastic waterers had dimensions of 1.8 m x 0.6 m and was outside of pack area. Curtain was used in one sidewalls during the winter, see Figure 4.28. This barn had sidewall curb height of 0.35 m. Geographic positions of Barn 24 was 37° 03' 58" N latitude and 86° 18' 33" W longitude (Appendix A - Table A.2). The ridge orientation was 286° Southeast (SE). This barn was built using concrete floor, wood, and metal plate. Two zinc gutter were used on both side. The eave height was 3.05 m and eave overhang was 0.60 m. The ridge type used was Capped ridge, roof pitch of 4:12, and metal roof was used to covered. Barn 24 was using natural ventilation system (Appendix A - Table A.3). This barn was not equipped lamps. Headlocks and cow brush were not present in this barn. Anaerobic lagoon was not present around this barn. See Appendix B (Figures 43 and 44) for more details about CBP barn 24.

(a) (b)

Figure 4.28 - The main constructive characteristic of CBP barn 24.

Barn 25 was built in February 2009 and cost of building was $204,000. The dimensions of this barn were 51.2 m x 38.4 m (Appendix A - Table A.1). Concrete wall (0.6 meter high) and three wood board were used around of the perimeter of this barn (Figure 4.29). Concrete feed alley and waterers were separated from the pack by low concrete wall. The feed alley had width of 3.35 m. A drive-by feed manager was located outside of this building. Geographic positions of the Barn 25 were 37° 36' 44" N latitude and 85° 15' 25" W longitude (Appendix A - Table A.2) and ridge orientation of 291° Southeast (SE). This barn was built using concrete floor and wood posts and board. The eave height was 4.87 m. The ridge type used was open ridge with cover, metal roof was used to covered and the roof pitch was 3:12. Ridge cap had dimensions of 1.12 m x 1.12 m, height of 0.32 m and ridge opening of 1.58 m. Details about barn 25 can be seen in Appendix B (Figures 45 and 46). The Barn 25 was equipped with three HVLS fans above the pack area (Appendix A - Table A.3). Twenty four high intensity discharge, 175 watts each, were used in this barn. Cow brush was not present in this barn. This barn was equipped with headlocks along of the feed alley. Anaerobic lagoon was not around of the building.

(a) (b)

Figure 4.29 - The main constructive characteristic of CBP barn 25.

Barn 26 was built in June 2008 and cost of construction was $85,000, as can be seen in Appendix A (Table A.1). This barn had dimensions of 60.9 m x 24.1 m. This barn had three waterers on the pack area and dimensions of 0.61 m x 0.46 m, 1.12 m x 0.46 m, and 0.76 m x 0.46 m. The feed alley had width of 4.26 m and a steel cable and hot wires was used above the sidewall curb height (Figure 4.30). Concrete wall was separating the pack and the feed alley in three walkways. Curtains were used in one sidewall of the building. Geographic position of the Barn 26 were 37° 00' 05" N latitude and 87° 55' 58" W longitude and the ridge orientation was 265° Southeast (SE), as can be seen in Appendix A (Table A.2). This barn was built using concrete floor, wood, and metal plate. The eave height was 4.06 m. The eave overhang of this barn had width of 1.22 m. The ridge type used was overshot, roof pitch measured was 3 1/2:12, overlap of the ridge of 1.60 m, and ridge opening of 0.91 m. Metal roof was used to covered this building and insulation was placed under this metal roof. Drawings of Barn 26 can be seen in Appendix B (Figures 47 and 48). Barn 26 was equipped with three High Volume Low Speed (HVLS) fans of 7.32 m and 1493.2 watts. (Appendix A - Table A.3). Two high intensity discharge lamps of 150 watts each were used. This barn has equipped with headlock, but cow brush was not present. Anaerobic lagoon was present around this barn.

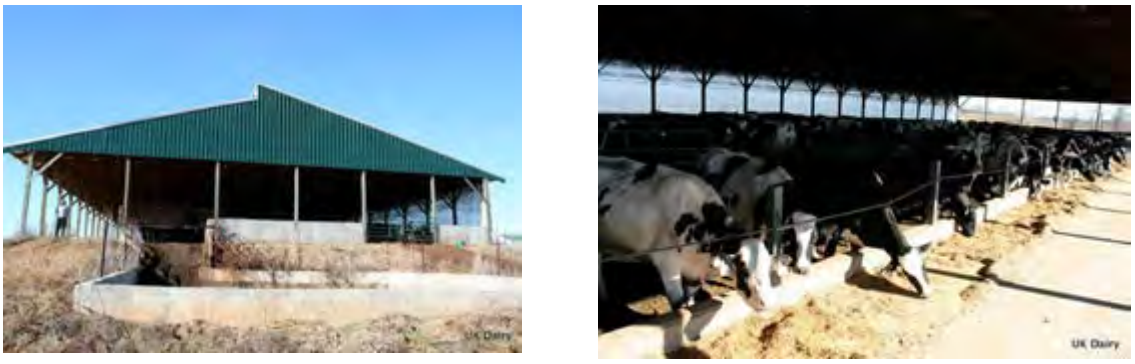

(a) (b)

Figure 4.30 - The main constructive characteristic of CBP barn 26.

Barn 27 was built in September 2010 and cost of construction was $65,000 (Appendix A - Table A.1). The barn dimensions were 36.6 m x 18.0 m. This barn had a concrete feed alley width of 1.73 m. Small concrete wall and wire mesh was separating the pack area and the feed alley (Figure 4.31). Two plastic waterers had dimensions of 2.44 m x 0.38 m. The feed alley width of 3.66 m. Sidewall was built using concrete curb and wire mesh. Curtains were used during the winter and the endwall was closed using metal plate. Two zinc gutter

were used on both side. Geographic positions of the Barn 27 were 36° 54' 23" N of latitude and 87° 20' 34" W of longitude and ridge orientation of 330° Southeast (SE), as can be seen in Appendix A (Table A.2). This barn was built using concrete floor, wood, and metal plate. The eave height was 2.61 m and eave overhang was 0.91 m. The ridge type used was overshot. Roof pitch measured was 4:12, overlap of the ridge of 0.96 m and ridge opening of 0.40 m. Barn 27 was used natural ventilation system. Eight compact fluorescents lamps were used of 13 watts each (Appendix A - Table A.3). Headlock and cow brush were not present this barn. Anaerobic lagoon was not present around this barn. Drawings of Barn 27 can be seen in Appendix B (Figures 49 and 50).

(a)

(b)

Figure 4.31 - The main constructive characteristic of CBP barn 27.

Barn 28 was built in August 2007 and costs of construction was $50,000 (Appendix A - Table A.1). The barn dimensions were 36.6 m x 15.2 m. One sidewall was closed with curtain (Figure 4.32). One plastic waterers was situated in another building and the cows had a free access. This barn was closed to the labor. Two zinc gutter were used on both side. Geographic position were 37° 00' 49" N latitude and 87° 22' 14" W longitude (Appendix A - Table A.2). The ridge orientation was 37° Southwest (SW). This barn was built using concrete floor, wood pole, metal panels, and metal roof was used to covered. The eave height was 3.86 m and eave overhang was 0.81 m. The ridge type used was overshot, roof pitch measured was 4:12, ridge opening of 0.35 m, and overlap of the ridge of 0.60 m. Details about barn 28 can be seen in Appendix B (Figures 51 and 52). Barn 28 was equipped with six box fans along of pack of 1.22 m diameter and 1118.5 watts power, as can be seen in Appendix A (Table A.3). Fourteen compact fluorescent lamps of 13 watts were used. Headlocks and cow brush were not present in this barn. Anaerobic lagoon was present around this barn.

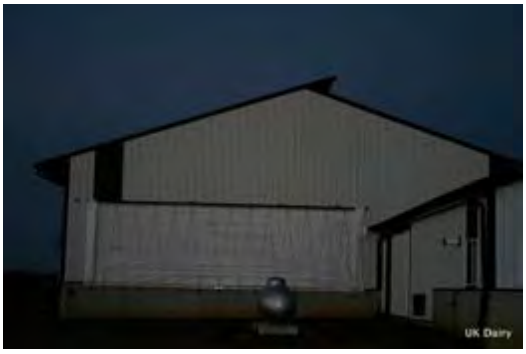

(a)

(b)

Figure 4.32 - The main constructive characteristic of CBP barn 28.

Barns 29 was built in February 2006 and cost of $105,000 with concrete. The building dimension of this barn were 60.9 m x 23.7 m, as can be seen in Appendix A (Table A.1). Three plastic waterers of 3.66 m x 0.56 m were outside of the pack area. The waterers were located adjacent to the concrete wall separating the pack area and the feed alley. This barn had width of feed alley of 4.26 m. The concrete curb was separating the pack and the feed alley had three walkways for cows to access the pack area (Figure 4.33). Geographic positions of Barn 29 were 36° 35' 37" N latitude and 87° 09' 20" W longitude (Appendix A - Table A.2). The ridge orientation was 284° Southeast (SE). This barn was built using concrete floor, wood pole, metal panels, and metal roof was used to covered. The eave height was 4.11 m and eave overhang was 1.22 m. The ridge type used was overshot, roof pitch measured was 3:12, ridge opening of 0.91 m, and overlap of the ridge of 1.52 m. Drawings of Barn 29 can be seen in Appendix B (Figures 53 and 54). Barn 29 was equipped with three HVLS fans (7.32 m) with 2237.1 watts each (Appendix A - Table A.3). This barn was not using lamps. Headlocks was not present in this barn. This barn was equipped with cow brush. Anaerobic lagoon was not present around this barn.

(a)

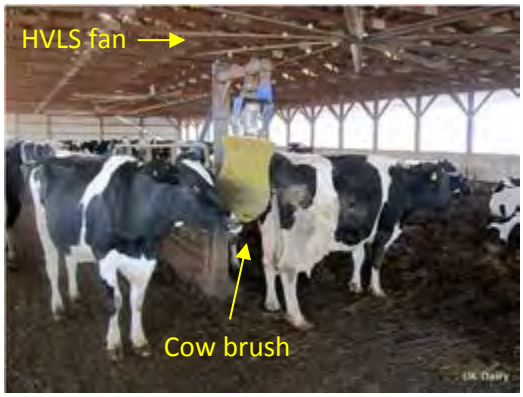

(b)

Figure 4.33 - The main constructive characteristic of CBP barn 29.

Barn 30 was built in December 2009 and cost of construction was $35,000 for building and $120,000 for filling (Appendix A - Table A.1). This barn had dimensions of 45.7 m x 23.4 m. This barn had two waterers on the pack area and dimensions of 3.05 m x 0.56 m. The feed alley had width of 3.05 m (Figure 4.34). Concrete wall was separating the pack and the feed alley in two walkways. Geographic position of the Barn 30 were 36° 38' 53" N latitude and 87° 09' 35" W longitude and the ridge orientation was 253° Northeast (NE), see Appendix A (Table A.2). This barn was built using concrete floor, wood, and metal plate. The eave height was 4.70 m and eave overhang of 1.22 m. The ridge type used was overshot, roof pitch measured was 3 1/2:12, overlap of the ridge of 1.22 m, and ridge opening of 0.61 m. Metal roof was used to covered this building and insulation was placed under this metal roof. Details about barn 30, see Appendix B (Figures 55 and 56). Barn 30 was equipped with two HVLS fans of 7.32 m with 1493.2 watts each. This barn was not equipped with lamps (Appendix A - Table A.3). This barn has equipped with cow brush, but headlock was not present. Anaerobic lagoon was present around this barn.

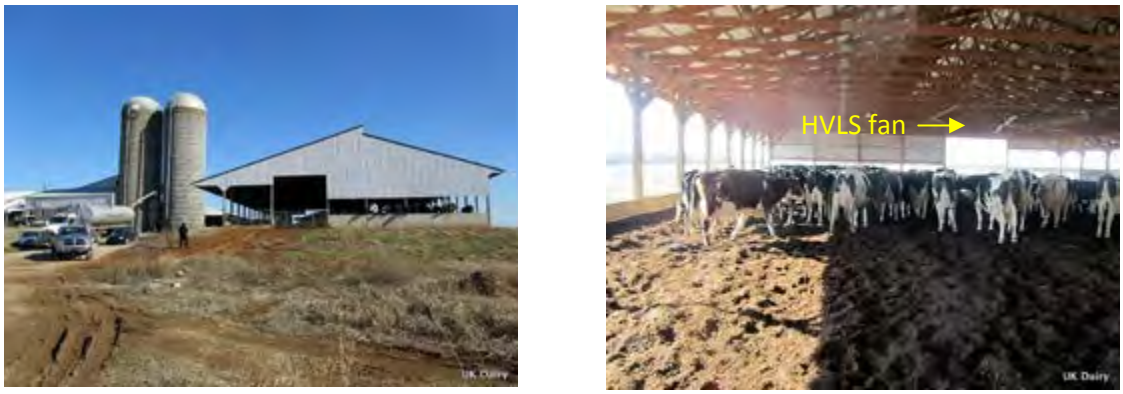

(a) (b)

Figure 4.34 - The main constructive characteristic of CBP barn 30.

Barn 31 was built in November 2009 and cost of building was $207,000. The building dimensions of were 45.7 m x 43.0 m (Appendix A - Table A.1). Concrete curb of 0.2 m high was used around of the perimeter of this building and one wire cable was used above this wall (Figure 4.35). Concrete feed alley was separated from the pack area by low concrete wall. The width of feed alley was 3.35 m. A drive-by feed manager was located outside of this barn. This barn was away another building of 7.31 m. Two zinc gutter were used on both side. Geographic positions of the Barn 31 were 36° 40' 52" N latitude and 86° 52' 37" W longitude (Appendix A - Table A.2) and ridge orientation of 345° Southeast

(SE). This barn was built using concrete floor, galvanized steel H-beam columns, and metal roof was used to covered of this barn. The eave height was 2.81 m and eave overhang had dimension of 1.83 m. The ridge type used was open ridge with cover, metal roof was used to covered and the roof pitch was 4:12. Ridge cap had dimensions of 0.23 m x 0.23 m, height of 0.20 m and ridge opening of 0.40 m. Drawings of barn 31 can be seen in Appendix B (Figures 57 and 58). The Barn 31 was using natural ventilation system (Appendix A - Table A.3). This barn was not equipped with lamps. Cow brush and headlocks were not present in this barn. Anaerobic lagoon was around of the building.

(a) (b)

Figure 4.35 - The main constructive characteristic of CBP barn 31.

Barn 32 was built in December 2007 and cost of construction was $30,000. This barn dimensions were 30.5 m x 18.3 m. The waterers had dimensions of 3.66 m x 0.56 m and was outside of the pack area (Appendix A - Table A.1). The feed alley was another building. Concrete wall was used around of the perimeter of this building and curtains were used above this concrete wall during the winter (Figure 4.36). This barn had one gate on each endwall. Geographic position of the Barn 32 were 36° 54' 22" N latitude and 87° 06' 26" W longitude and the ridge orientation was 90° Southwest (SW), see Appendix A (Table A.2). This barn was built using concrete floor, wood, metal panels were used in the endwall, and metal roof was used to covered this building. The eave height was 4.14 m. The eave overhang of this barn had width of 1.22 m. The ridge type used was overshot, roof pitch measured was 4:12, overlap of the ridge of 1.22 m, and ridge opening of 0.76 m. Barn 32 was equipped with two HVLS fans of 7.32 m with 1493.2 watts each. Three fluorescent lamps of 96.0 watts were used in this building (Appendix A - Table A.3). Cow brush and headlock were not present in this barn. Anaerobic lagoon was present around this barn. Drawings about CBP barn 32 can be seen in Appendix B (Figures 59 and 60).

(a)

(b)

Figure 4.36 - The main constructive characteristic of CBP barn 32.

Barn 33 was built in November 2010 and cost of construction was $86,000 (Appendix A - Table A.1). This barn had dimensions of 60.9 m x 24.1 m. This barn had two waterers of 3.66 m x 0.61 m on the pack area. The concrete feed alley had width of 2.43 m. This concrete feed alley was separated from the pack area by three guardrail fence. Concrete wall was separating the pack and the feed alley in two walkways of 4.88 m each. Geographic position of the Barn 33 were 36° 54' 24" N latitude and 86° 13' 38" W longitude and the ridge orientation was 74° Southwest (SW), see Appendix A (Table A.2). This barn was built using concrete floor, wood board, and metal panels were used in the endwall (Figure 4.37). The eave height was 4.14 m and eave overhang of 2.43 m. The ridge type used was overshot, roof pitch measured was 3 1/2:12, overlap of the ridge of 0.91 m, ridge opening of 0.91 m, and metal roof was used to covered. Drawings of Barn 33 can be seen in Appendix B (Figures 61 and 62). The Barn 33 was using natural ventilation system (Appendix A - Table A.3). This barn was not equipped with lamps. Cow brush and headlocks were not present in this barn. Anaerobic lagoon was around of the building.

(a)

(b)

Figure 4.37 - The main constructive characteristic of CBP barn 33.

Barn 34 was built in October 2010. First of all, this barn was converted tobacco barn and then added a new building. The cost for renovation this building was $6,000 and cost for built a new part was $20,000 (Appendix A - Table A.1). The barns dimensions were 51.2 m x 19.5 m. The waterers was not present in the pack area. Four guardrail fence were used in the sidewall. The labor was close to this building, as can be seen in Figure 4.38. Geographic positions of Barn 34 were 36° 51' 04" N latitude and 85° 54' 25" W longitude (Appendix A - Table A.2). The ridge orientation was 112° Northwest (NW). This barn was built using wood boards, metal panels, metal roof was used to covered this building and insulation was placed under this metal roof. The eave height was 5.90 m and eave overhang was 2.75 m. The roof pitch of measured was 3.2:12. This barn had two ridge type configuration. The tobacco barn had five chimneys, opening of chimneys was 0.43 m and height of chimney was 0.23 m. The ridge type used was overshot in the new building, overlap of this ridge of 1.17 m, and ridge opening of 0.61 m. Drawings of Barn 34 can be seen in Appendix B (Figures 63 and 64). Barn 34 was using natural ventilation system (Appendix A - Table A.3). This barn was not equipped lamps. Headlocks and cow brush were not present in this barn. Anaerobic lagoon was not present around this barn.

(a) (b)

Figure 4.38 - The main constructive characteristic of CPB barn 34.

Barn 35 was built in the Fall of 2006 and cost of building was $60,000. The dimensions of this barn were 36.5 m x 12.1 m (Appendix A - Table A.1). This barn had a concrete wall of 0.3 m high (Figure 4.39). Concrete feed alley and waterers were separated from the pack by low concrete wall and three steel pole. The concrete feed alley had width of 2.35 m. A drive-by feed manager was located outside of this building. This barn had two metal waterers of 3.0 m x 0.4 m on the pack area. Geographic positions of the Barn 35 were 36° 59' 08" N latitude and 86° 57' 12" W longitude (Appendix A - Table A.2) and ridge

orientation of 117° Northwest (NW). This barn was built using concrete floor, metal panels, and galvanized steel H-beam columns. The eave height was 4.72 m and eave overhang had dimension of 1.52 m. The ridge type used was open ridge with cover, metal roof was used to covered and the roof pitch was 4:12. Ridge cap had dimensions of 0.76 m x 0.76 m, height of 0.58 m and ridge opening of 1.12 m. Drawings of Barn 35 can be seen in Appendix B (Figures 65 and 66). Barn 35 was equipped with two HVLS fans of 7.32 m and 1493.2 watts (Appendix A - Table A.3). Four incandescent (INC) lamps of 100.0 watts were used above the pack area. Cow brush and headlocks were not present in this barn. Anaerobic lagoon was around of the building.

(a) (b)

Figure 4.39 - The main constructive characteristic of CBP barn 35.

Barn 36 was built in April 2004. There was no information about the cost of construction (Appendix A - Table A.1). This barn dimensions were 43.9 m x 14.6 m, respectively. The waterers was outside of this barn. The concrete feed alley has width of 3.6 m. Wood board fence was used around of the pack area, see Figure 4.40. Geographic position of the Barn 36 were 37° 12' 19" N latitude and 84° 59' 29" W longitude and the ridge orientation was 335° Southwest (SW), as can be seen in Appendix A (Table A.2). This barn was built using concrete floor, wood boards, and metal panels. The eave height was 4.6 m and metal roof was used to covered this barn. The eave overhang of this barn had width of 1.22 m. This barn had different ridge configuration. The ridge type used was overshot and closed ridge, details are showing in Appendix B (Figures 67 and 68). The roof pitch measured was 4:12, overlap of the ridge of 0.74 m, and ridge opening of 0.43 m. Barn 36 was equipped with eight box fans along of pack of different diameters (Appendix A - Table A.3). This barn was not equipped with lamps. Cow brush and headlock were not present in this barn. Anaerobic lagoon was present around this barn.

(a)

(b)

Figure 4.40 - The main constructive characteristic of CBP barn 36.

Barn 37 was built 2007 and the total cost, $17,000 (Appendix A - Table A.1). The dimensions of the barn were 45.7 m x 10.6 m. This barn was built close to the barn 38. Waterers was outside of this barn and had dimensions with of 0.7 m x 0.3 m (Figure 4.41). The feed alley was away from facility, and the animals were feed in separate of the building. The geographic position of the Barn 37 were 37° 12' 19" N latitude and 84° 59' 29" W longitude and the ridge orientation was 224° Northeast (NE), details are showing in Appendix A (Table A.2). Thirty treated wood posts were used to build this barn. Drawings are showing in Appendix B (Figures 69 and 70). Three treated wood boards, were used in each sidewall. Tubular steel arches fastened to the tops and sides of the posts to form a hooped roof were used and white poly vinyl tarp used to covered. The eave height of this barn was 4.88 m. Only natural tunnel ventilation was used in Barn 37. Lamps and cow brush were not present this barn (Appendix A - Table A.3). Anaerobic lagoon was not present around this barn.

(a)

(b)

Figure 4.41 - The main constructive characteristic of CBP barn 37.

Barn 38 was built in Summer of the 2011. The costs of construction was $25,000 and $30,000 with feed alley. The building dimension were 36.6 m x 21.6 m (Appendix A -

Table A.1). This barn was built close to the barn 37 (Figure 4.42). Sidewalls were open without curtain. Plastic waterers was situated in another barn and the cows had a free access to this building. This barn was built using concrete sidewall curb, wood pole, and metal roof was used to covered. Sixteen wood post were uses on each side and spaced of 2.28 m from each other. Geographic position of the Barn 38 were 37° 20' 49" N latitude and 85° 21' 41" W longitude (Appendix A - Table A.2). The ridge orientation was 233° Northeast (NE). One hot wires were used between Barn 37 and Barn 38 to prevent cows have access of this barn. One opening was on top of each endwall. The eave height was 4.9 m and eave overhang was 0.61 m. Drawings are showing in Appendix B (Figures 71 and 72). The ridge type used was overshot, roof pitch measured was 4:12, ridge opening of 0.44 m, and overlap of the ridge of 0.45 m. Only natural tunnel ventilation was used in Barn 38, as can be seen in Appendix A (Table A.3). This barn was not equipped with lamps. Cow brush were not present this barn (Appendix A - Table A.3). Anaerobic lagoon was not present around this barn.

(a) (b)

Figure 4.42 - The main constructive characteristic of Barn 38.

Barns 39 and Barn 40 were built in the same time, using the same constructive characteristics and costs of construction. These barns were built in July 2010 and the costs of constructions were $80,000 for both barn including fans and concrete (Appendix A - Table A.1). The barns dimensions were 48.7 m x 21.9 m. Two waterers were on the pack area and had dimensions of 1.8 m x 0.6 m. The concrete feed alley width was 3.60 m. This concrete feed alley was separated from the pack area by two guardrail fence, as can be seen in Figure 4.43. Concrete curb wall was used above around this barn and two guardrail fence was used above of this concrete curb wall. Curtains were used on the sidewall during the winter. Geographic position of these barns were 36° 58' 10" N latitude and 85° 38' 36"

W longitude and the ridge orientation was 17° Southwest (SW), as can be seen in Appendix A (Table A.2). These barn were built using concrete floor, wood posts, and metal panels. The eave height was 4.84 m and metal roof was used to covered these barns. These barns had eave overhang of 0.81 m. The ridge type used was overshot. The roof pitch measured was 5:12, overlap of the ridge of 0.91 m, and ridge opening of 0.61 m. Drawings are showing in Appendix B (Figures 73 and 74). Barn 39 and Barn 40 were equipped eight box fans above of pack area, details can be seen in Appendix A (Table A.3). Five fluorescent lamps of 192 watts were used in each barn. Cow brush and headlock were not present in this barn. Anaerobic lagoon was present around this barn.

(a) (b)

Figure 4.43 - The main constructive characteristic of CBP barns 39 and Barn 40.

Barn 41 was built in 2001 and cost of building was $14,000 (Appendix A - Table A.1). The dimensions of this barn were 30.5 m x 15.2 m. The feed alley and waterers were outside of this barn. The waterers had diameter of 1.5 m. Two opening were on the top and the bottom of the sidewall around the perimeter of this barn (Figure 4.44). Geographic positions of the Barn 41 were 36° 39' 54" N latitude and 85° 42' 58" W longitude (Appendix A - Table A.2) and ridge orientation of 102° Northwest (NW). This barn was built using metal panels and wood columns. The eave height was 3.5 m and eave overhang of 0.3 m. The ridge type used was open ridge with cover, metal roof was used to covered and the roof pitch was 4:12. Ridge cap had dimensions of 0.54 m x 0.54 m, height of 0.27 m and ridge opening of 1.0 m. Barn 41 was equipped with eight box fans of 0.61 m and 246.0 watts (Appendix A - Table A.3). Lamps, headlocks and cow brush were not present in this barn. Anaerobic lagoon was around of the building. More details are showing in Appendix B (Figures 75 and 76).

(a)

(b)

Figure 4.44 - The main constructive characteristic of CBP barn 41.

Barn 42 was built in June 2010 and costs of construction was $25,000. The building dimension of this barn were 36.6 m x 15.2 m (Appendix A - Table A.1). One sidewalls was closed with metal panels, but this sidewall had two openings on the top and bottom. Four wood boards were used around of this barn (Figure 4.45). Twenty three wood posts were used on each side and spaced of 1.66 m from each other. Waterers was situated outside of the barn and the cows had a free access to another building. Two tubular steel gates were used to access to another building. Geographic positions of the Barn 42 were 36° 41' 06" N latitude and 85° 42' 15" W longitude (Appendix A - Table A.2). The ridge orientation was 204° Northeast (NE). This barn was built using wood posts, metal panels, and metal roof was used to covered. The eave height was 3.8 m and eave overhang was 0.6 m. The ridge type used was overshot. The roof pitch measured was 4:12, ridge opening of 0.35 m, and overlap of the ridge of 0.57 m. Barn 42 was equipped with eight box fans along of pack of 1.32 m diameter, see Appendix A (Table A.3). Six incandescent lamps were used above the pack area. Headlocks and cow brush were not present in this barn. Anaerobic lagoon was present around this barn. Drawings are showing in Appendix B (Figures 77 and 78).

(a)

(b)

Figure 4.45 - The main constructive characteristic of CBP barn 42.

4.2.3. Compost bedding pack management

The highest percentage (45.2%) of barns are bedded with kiln dried wood shavings or sawdust, followed by the green sawdust (42.9%) and the blend of both materials (11.9%). Fine, dry wood shavings or sawdust is the ideal material for bedding (Endres, 2009). Most of the barns in Kentucky had their compost tilled and aerated to a depth of 0.11 to 0.23 m twice a day in the summer and winter time, while cows were at the milking parlor. The most often used stirring tool was a chisel plow on a small tractor.

A large number of farmers cleaned out the pack entirely once a year. In this case, a load of clean material (shavings or sawdust) was added after removal of the used bedding to a depth 0.30 m in order to start the new pack. Typically, a load of fresh material was added every one to five weeks, varying by season, weather conditions, barn size, and cow density. Some farmers left about 0.15 m of old material in barn to help initiate microbial activity. There were a small number of dairies adding a thin layer of fresh bedding when the bedded pack became moist enough for it to stick to the cows body after they rise from lying down on the bedded pack.

The average pack dimensions for the 42 compost barns we studied were 47.7 m (±19.1) and 16.1 m (±5.9). The average stock density in this study was 8.9 m^2 per cow, ranging from 0.8 to 25.8 m^2 per cow. The suggested minimum space per cow in these building is 7.4 m^2 per cow (Janni et al., 2007). According to Endres (2009), some producers in Minnesota provided 9.4 m^2 per cow.

Temperatures of bedding compost tended to be lower on barns 16, 22, 23, 24, 29, 35, 36, and 38 which utilized green sawdust rather than kiln dried wood shavings or sawdust for bedding (t test, $P > 0.05$). The temperatures were greater in the areas of the pack that were fluffier, that were not heavily soiled or packed by the cows. This observation is consistent with the need for oxygen for microbial activity that promotes composting.

Average bedding moisture content in the top (20 cm) was 59.0% (± 9.0) wet basis ranged from 36.2 to 71.8%. Details can be seen in Appendix A (Table A.4). Moisture content between 40.0% and 65.0% is generally recommended for composting most materials (NRAES-54, 1992). Excessive moisture addition needs to be avoided. The moisture content can vary owing to the addition of fresh bedding, weather, and cow density in the sampling area (Barbeg et al.. 2007). More details about compost bedding pack management in each barn can be seen below.

4.2.3.1. Management practices in each barn

Barn 1 was bedded with green sawdust (Figure 4.46a). The pack was aerated twice a day in the summer and the winter time using a chisel plow (Figure 4.46b), while the cows were milked. The pack was aerated to a depth of 0.28 m, which is the recommended depth of 0.25 to 0.30 m (Janni et al., 2007). This barn was not cleaned out during the year, the pack had dimensions of 41.5 m x 15.3 m. The stock density was 10.0 m^2 per cow (Appendix A - Table A.1).

The average bedding temperatures at surface and 0.10 m and 0.20 m depths were 17.1°C (±1.3), 31.9°C (±10.2), and 35.2°C (±9.4), respectively. Paired t-test statistical analysis indicated that the averages for the two depths were different ($P < 0.05$). Details can be seen in Appendix A (Table A.4).

The average bedding moisture was 44.5% (±8.0). The minimum bedding moisture was 30.7% and the maximum was 56.7% (Appendix A - Table A.5). The first and third quartiles were 40.4% and 49.8%, respectively.

(a) (b)

Figure 4.46 - Green sawdust (a) and (b) chisel plow used to aeration used in barn 1.

Barn 2 was using green sawdust to bed the pack (Figure 4.47a). This barn used a chisel plow on a small tractor (Figure 4.47b) to till the pack twice a day in the summer and the winter time, while the cows were milked. The pack was aerated to a depth of 0.40 m. The pack dimensions were 53.4 m x 30.3 m and the stock density was 9.3 m^2 per cow (Appendix A - Table A.1). This barn was cleaned out once a year.

The average of the pack temperature in the depth 0.1 m [41.5°C (±10.6)] was less than the average of the depth 0.2 m [53.4°C (±4.6)], as can been see in Appendix A (Table A.4).

Paired t-test statistical analysis indicated that at the 0.05 significance level, the averages for the two depths were different. The surface pack temperature measured was 16.5°C (±3.6).

The average bedding moisture was 49.0% (±7.3), ranging from 38.3% to 61.5% (Appendix A - Table A.5). The first and third quartiles were 45.7% and 52.0%, respectively. The moisture content in the bedding compost varied upon time since last addition of fresh bedding, weather, and stock density in the sampling area.

(a) (b)

Figure 4.47 - Green sawdust (a) and (b) the chisel plow used in barn 2.

Barn 3 was bedded with kiln dried wood shavings or sawdust. According Changirath et al. (2011), the cows prefer lying on drier and loose bedding (Figure 4.48). The bedded pack was stirred twice a day in the summer and winter time, while the cows were being milked. Moreover, a small tractor was pulling a chisel plow to promote the aeration. The bedding compost was removed from this barn three a year and spread directly in the fields when necessary. The pack area had dimensions of 87.8 m x 12.2 m and the stock density was 7.4 m^2 per cow (Appendix A - Table A.1). This barn was cleaned out three times per year.

Averages bedding temperatures at surface, 0.1 m and 0.2 m depths were 16.3°C (±3.8), 36.2°C (±9.5), and 52.1°C (±4.6), respectively (Appendix A - Table A.4). Paired t-test statistical analysis indicated that the averages for the two depths were different ($P < 0.05$).

The average bedding moisture was 49.1% (±5.8), which is the moisture content, needed for composting (NRAES-54, 1992). The minimum and maximum bedding moisture was between 43.4% and 58.7%. The first and third quartiles were 46.1% and 54.1%, respectively. Details about bedding moisture content as seen in Appendix A (Table A.5).

(a)

(b)

Figure 4.48 - Cows lying on the bedding compost of the Barn 3.

Barn 4 was bedded with mix material (sawdust mixed with other material as available). Tilling was performed once a day in the summer and winter time, using a chisel plow with 0.45 m shovels (Figure 4.49a). The chisel plow tills to a depth of 0.25 m – 0.38 m. This keeps the bedded pack fairly loose, well aerated, and the surface dry. In fact, this bedded pack was the driest at surface to 0.25 m depth. During cultivation water vapor was visible, indicating a higher temperature of the compost in comparison to the air (Figure 4.49b). This barn was not cleaned out during the year. The pack dimensions were 51.5 m x 9.2 m and the stock density (5.1 m^2 per cow). Details can be seen in Appendix A (Table A.1).

The average surface temperature measured was 15.5°C (±3.5). The average of the pack temperature in the depth 0.1 m and 0.2 m were 41.1°C (±18.7) and 52.4°C (±7.6), respectively (Appendix A - Table A.4). Paired t-test statistical analysis indicated that these two averages were not different ($P < 0.05$).

The average bedding moisture was 36.2% (±6.3). as can be seen in Appendix A (Table A.5). The minimum bedding moisture was 27.8% and the maximum was 44.9%. The first and third quartiles were 30.5% and 40.0%, respectively.

(a)

(b)

Figure 4.49 - Chisel plow used the bedding compost in Barn 4.

Barn 5 was using kiln dried wood shavings or sawdust in the pack (Figure 4.50). This bedding material has been widely used in compost dairy barn throughout Minnesota with different success (Barberg et al., 2007; Janni et al., 2007; Janni et al., 2005). Aeration was performed once a day in the summer time and three times a day in the winter time, using a tractor to pull a chisel plow. The pack was aerated to a depth of 0.23 m. The pack dimensions were 42.7 m x 10.7 m. This barn was cleaned out twice a year. The stock density (5.3 m^2 per cow) was less than suggested minimum (7.4 m^2 per cow) by Janni et al. (2007). Details can be seen in Appendix A (Table A.1).

The average bedding temperatures at surface and two depths (0.1 m and 0.2 m) were 22.2°C (±1.3), 26.0°C (±6.1), and 27.2°C (±6.6), respectively, as can been see in Appendix A (Table A.4). Paired t-test statistical analysis indicated that the averages for the two depths were not different ($P < 0.05$).

The average bedding moisture was 52.2% (±5.6). The minimum bedding moisture was 43.7% and the maximum was 61.7%. The first and third quartiles were 47.5% and 55.2%, respectively. More details about moisture content of bedding see Appendix A (Table A.5).

(a) (b)

Figure 4.50 - Barn 5 was using kiln dried wood shavings or sawdust in the pack.

Barn 6 was bedded with kiln dried wood shavings or sawdust (Figure 4.51a). The loosest and driest compost was found in this barn with a fluffy consistency. The pack was aerated once a day in the summer time and twice a day in the winter time, while the cows were milked, using rotary tiller on a tractor (Figure 4.51b). This barn was not cleaned out. The bedded pack had dimensions of 24.4 m x 12.2 m and the stock density was 4.0 m^2 per cow. Details can be seen in Appendix A (Table A.1).

The surface pack temperature measured was 16.2°C (±3.1). The average of the pack temperature in the depth 0.1 m [34.5°C (±15.0)] was high than the average of the depth 0.2 m [34.0°C (±10.1)], as can been see in Appendix A (Table A.4). Paired t-test statistical analysis indicated that these two averages were not different ($P < 0.05$).

The average bedding moisture was 39.6% (±9.6), which is less than recommended by NRAES-54 (1992). The minimum and maximum bedding moisture was between 22.9% and 51.8%. The first and third quartiles were 32.0% and 47.1%, respectively. Details about bedding moisture content can be seen in Appendix A (Table A.5).

(a) (b)

Figure 4.51 - Rotary tiller used to till the bedding compost in barn 6.

Barn 7 was bedded with kiln dried wood shavings. The pack was mixed twice a day in the summer and winter time, using a rotary tiller (Figure 4.52). This barn was cleaned out once a year and the pack was aerated to a depth of 0.20 m. This barn had pack dimensions of 36.6 m x 12.5 m and the stock density was 11.7 m^2 per cow (Appendix A - Table A.1).

The average bedding temperatures at surface and two depths (0.1 m and 0.2 m) were 13.3°C (±4.7), 38.3°C (±6.0), and 42.2°C (±8.6), respectively (Appendix A - Table A.4). Paired t-test statistical analysis indicated that the averages for the two depths were not different ($P < 0.05$).

The average bedding moisture was 46.0% (±3.2). The minimum bedding moisture was 40.8% and the maximum was 49.7% (Appendix A - Table A.5). The first and third quartiles were 44.4% and 48.9%, respectively.

(a)

(b)

Figure 4.52 – Rotary tiller (was used to till the bedding compost of barn 7.

Barn 8 was bedded using kiln dried wood shavings or sawdust. This barn was not cleaned out a year. The pack was aerated once a day in the summer and winter time using a chisel plow (Figure 4.53). The pack was aerated to a depth of 0.25 m. The compost appeared relatively wet and did stick to the boots when walking on the surface and small lumps of bedding pack material did not smell when broken and rubbed against the palms of our hands. According Klaas et al. (2010), this process can indicate absence of anaerobic processes. The pack dimensions were 65.9 m x 7.9 m and the stock density was 11.0 m^2 per cow. Details can be seen in Appendix A (Table A.1).

Average bedding temperatures at surface and two depths (0.1 m and 0.2 m) were 17.8°C (±4.1). 24.1°C (±4.8), and 24.4°C (±3.5), respectively (Appendix A - Table A.4). Paired t-test statistical analysis indicated that the averages for the two depths were not different ($P < 0.05$).

The average bedding moisture was 61.6% (±2.5). The minimum bedding moisture was 58.2% and the maximum was 65.9% (Appendix A - Table A.5). The first and third quartiles were 59.5% and 63.5%, respectively.

(a)

(b)

Figure 4.53 – Barn 8 was aerated using a chisel plow.

Barn 9 was using sawdust mixed with other material as available. The pack was aerated once a day in the summer time and twice a day in the winter time. A tractor was aerating the pack using a rotary tiller and a chisel plow (Figure 4.54). This barn was cleaned out once a year. The compost pack appeared to be compacted and chunks were seen after stirring. Compaction is expected to reduce aeration and microbial activity compared to the fluffy loose packs (Janni et al., 2007). The pack dimensions were 76.3 m x 18.5 m and the stock density was 13.5 m^2 per cow (Appendix A - Table A.1).

The surface pack temperature measured was 22.3°C (±11.7). The average of the pack temperature in the depth 0.1 m [38.6°C (±13.2)] was less than the average of the depth 0.2 m [42.5°C (±14.8)], as can been see in Appendix A (Table A.4). Paired t-test statistical analysis indicated that these two averages were different ($P < 0.05$).

The average bedding moisture was 41.9% (±6.6). The minimum bedding moisture was 33.6% and the maximum was 53.9% (Appendix A - Table A.5). The first and third quartiles were 37.5% and 45.7%, respectively.

(a) (b)

Figure 4.54 – Barn 9 was aerated using a chisel plow.

Barn 10 was bedded with kiln dried wood shavings or sawdust (Figure 4.55a). The bedded pack was stirred twice a day in the summer and winter time, using a chisel plow (Figure 4.55b), while the cows were being milked. The stirring mixes manure and urine on the surface into the bedded pack to provide a fresh surface for cows to lie down on the pack after milked (Janni et al., 2007). This barn was cleaned out twice a year. The pack dimensions were 61.0 m x 30.5 m. Approximately 184 cows were kept in the bedded pack that provided a stock density of 10.1 m^2 per cow (Appendix A - Table A.1).

The averages bedding temperatures at surface and 0.1 m and 0.2 m depths were 17.3°C (±5.6), 35.6°C (±8.6), and 41.4°C (±11.4), respectively. Paired t-test statistical analysis indicated that the averages for the two depths were different ($P < 0.05$). Details can be seen in Appendix A (Table A.4).

The average bedding moisture was 51.7% (±7.3). The minimum and maximum bedding moisture was between 38.3% and 64.0%, respectively. The first and third quartiles were 48.7% and 54.5%, respectively. The average moisture content of bedding in Barn 10 is given in Appendix A (Table A.5).

(a) (b)

Figure 4.55 - Barn 10 was aerated using a chisel plow.

Barns 11 and 12 were bedded using sawdust mixed with other material as available. The wet compost was found in these barns, with mainly slurry consistency and did stick to the boots when walking on the surface. The bedding materials were aerated to a depth of 0.23 m, once a day in the summer and winter time while cows are being milked. A tractor was pulling a chisel plow to promote the aeration (Figure 4.56). The bedded packs had the same dimensions in both barns of 91.5 m x 15.3 m and the stock density were 9.3 m^2 per cow (Appendix A - Table A.1). These barns were cleaned out twice a year.

The average surface temperature measured in CBP barns 11 and 12 were 15.2°C (±2.5) and 18.5°C (±12.5), respectively (Appendix A - Table A.4). Paired t-test statistical analysis indicated that there were not significant ($P < 0.05$) differences in average temperatures for the two depths in Barn 11, but there were significant ($P < 0.05$) differences in average temperatures for the two depths in Barn 12.

The average bedding moisture in Barns 11 and 12 were 61.2% (±2.4) and 60.4% (±2.8), respectively. Details can be seen in Appendix A (Table A.5).

(a)

(b)

Figure 4.56 - Barns 11 and 12 were bedded using sawdust.

Barns 13 and 14 were bedded using kiln dried wood shavings or sawdust (Figure 4.57a). The compost packs were aerated twice a day in the summer and winter time, using rotary tiller (Figure 4.57b). Water vapor was visible during aeration, indicating a higher temperature of the compost in comparison to the air. These barns were not cleaned out during the year. These barns had the same pack dimensions of 61.0 m x 13.7 m and the same stock density of 8.8 m^2 per cow (Appendix A - Table A.1).

The average surface temperatures measured in Barns 13 and 14 were 11.7°C (±5.3) and 8.9°C (±1.6), respectively. Details about bedding temperature can be seen in Appendix A (Table A.4). Paired t-test statistical analysis indicated that in both barns the averages temperatures for the two depths of were not different ($P < 0.05$).

The average bedding moisture in Barn 13 was less [36.2% (±6.3)] than Barn 14 [57.3% (±4.3)], ranged from 50.6% to 63.4% in Barn 13 and ranged from 49.8% to 64.0% in Barn 14 (Appendix A - Table A.5).

(a)

(b)

Figure 4.57 - Rotary tiller was used to aerated the bedding compost in barns 13 and 14.

Barn 15 was bedded using kiln dried wood shavings or sawdust (Figure 4.58). The compost pack was aerated twice a day (summer and winter time), using chisel plow. The bedding materials were aerated to a depth of 0.18 m. The bedding compost was cleaned out once a year and the bedding compost was spread directly in the fields when necessary. This bedding compost was appearing with fluffy consistency. The pack had dimensions of 18.3 m x 18.3 m and the stock density was 9.3 m^2 per cow (Appendix A - Table A.1).

The average surface temperature measured was 17.2°C (±10.2). The average bedding temperatures across 0.1 m and 0.2 m depths were 52.3°C (±7.5) and 58.0°C (±10.3), respectively. Paired t-test statistical analysis indicated that these two averages were different ($P < 0.05$). Temperature is directly proportional to the biological activity within the composting bedded-pack. Maintaining a temperature of 52°C or more for 3 to 4 days favors the destruction of fly larvae and keeping the pack surface dry (Janni et al., 2005).

Average bedding moisture was 54.7% (±2.7), ranging from 51.0 to 58.6% (Appendix A - Table A.5). The first and third quartiles were 53.0% and 56.2%, respectively.

(a) (b)

Figure 4.58 - The bedding compost in Barn 15 was appearing with fluffy consistency.

Barn 16 was bedded with green sawdust. The wet compost was found in this barn, with mainly slurry consistency. The pack was aerated once a day in the summer and winter time. A tractor was pushing a chisel plow (Figure 4.59). The bedding materials were aerated to a depth of 0.20 m, which is less than minimum recommended depth of 0.25 m to 0.30 m (Janni et al., 2007). This barn was cleaned out twice a year. The pack had dimensions of 14.6 m x 10.1 m and the stock density was 7.7 m^2 per cow (Appendix A - Table A1).

The average bedding temperatures at surface and 0.1 m and 0.2 m depths were 8.9°C (±2.9), 23.5°C (±12.6), and 32.1°C (±7.2), respectively. Paired t-test statistical analysis

indicated that at the 0.05 significance level, the averages for the two depths were not different (Appendix A - Table A.4).

The average bedding moisture was 66.5% (±2.2), which is high than the recommended for composting of 45% to 60% moisture (NRAES-54, 1992). The minimum bedding moisture was 64.3% and the maximum was 70.6% (Appendix A - Table A.5). The first and third quartiles were 64.6% and 67.1%, respectively.

(a) (b)

Figure 4.59 - Barn 16 was aerated using chisel plow.

Barn 17 was bedded using kiln dried wood shavings. This barn was cleaned out once a year. The pack was aerated twice a day (summer and winter time), using a chisel plow (Figure 4.60), and the pack was aerated to a depth of 0.30 m. The compost appeared relatively wet and dried fine material was spread out on top of the compost, however, it still sticks to the boots, when one was walking on the surface. The pack had dimensions of 37.8 m x 13.7 m and the stock density was 4.3 m^2 per cow (Appendix A - Table A.1).

The average bedding temperatures at surface and 0.1 m and 0.2 m depths were 11.7°C (±5.0), 37.4°C (±16.6), and 36.6°C (±17.0), respectively (Appendix A - Table A.4). Paired t-test statistical analysis indicated that the averages for the two depths were not different ($P < 0.05$).

The average bedding moisture was 56.0% (±4.3), ranged from 50.2% to 62.4% (Appendix A - Table A.5). The first and third quartiles were 52.7% and 59.1%, respectively.

(a) (b)

Figure 4.60 - Barn 17 was aerated using chisel plow.

Barn 18 was using kiln dried wood shavings or sawdust. This package was very wet, when walking atop it, the boots were sunk in up to ankles in some spots (Figure 4.61a). The bedding material was aerated twice a day in the summer and winter time, using chisel plow (Figure 4.61b) while cows are being milked. The bedded pack had dimensions of 61.0 m x 24.4 m and the stock density was 12.9 m^2 per cow. This value is high than suggested minimum (7.4 m^2 per cow) by Janni et al. (2007). Compost barns will not perform well if the cows are overcrowded. Details can be seen in Appendix A (Table A.1).

The average surface temperature measured was -5.1°C (±3.5). The average of the pack temperature in the depth 0.1 m and 0.2 m were 12.3°C (±9.7) and 20.9°C (±10.9), respectively (Appendix A - Table A.4). Paired t-test statistical analysis indicated that the averages for the two depths were different ($P < 0.05$). An anaerobic pack shows lower temperatures which leads to reduced pathogen kill and odor problems (Graves, 1999).

The average bedding moisture was 64.8% (±0.8), which was above NRAES-54 (1992) recommended level of 50% to 60%. When moisture is too high, the pack becomes anaerobic (lack of oxygen), rate of microbial decomposition will slow, and the composting will again be too slow (Bewley and Taraba, 2009). The minimum bedding moisture was 63.5% and the maximum was 66.0%. The first and third quartiles were 64.2% and 65.6%, respectively (Appendix A - Table A.5).

(a)

(b)

Figure 4.61 - Barn 18 was aerated using chisel plow.

Barn 19 was bedded with Kiln dried wood shavings. This barn was aerated twice a day, using chisel plow and rotary tiller on a tractor. During cultivation water vapor was visible, indicating a higher temperature of the compost in comparison to the air (Figure 4.62). The pack was cleaned out twice a year and had dimensions of 11.6 m x 14.0 m. The stock density was 6.7 m^2 per cow (Appendix A - Table A.1).

The pack surface temperatures [-0.9°C (±3.8)]. The average bedding temperature measured at 0.1 m depth [39.7°C (±5.6)] was less than average bedding temperatures measured at 0.2 m depth [52.8°C (±3.2)]. Paired t-test statistical analysis indicated that the averages for the two depths were different ($P < 0.05$). The average temperature of bedding in this barn is given in Appendix A (Table A.4).

The average bedding moisture was 68.4% (±1.9), as can be seen in Appendix A (Table A.5). The minimum bedding moisture was 64.5% and the maximum was 71.0%. The first and third quartiles were 68.0% and 69.5%, respectively. A wet bedded pack is more vulnerable to compaction.

(a)

(b)

Figure 4.62 - Water vapor was visible during cultivation in Barn 19.

Barn 20 was bedded with kiln dried wood shavings or sawdust (Figure 4.63). New fresh and dried fine material was spread out on top of the compost once a day. The pack was aerated once a day. A tractor was used to pull a chisel plow. The bedding materials were aerated to a depth of 0.18 m. This barn was cleaned out twice a year. The pack dimensions were 22.0 m x 12.0 m and the stock density was 5.3 m^2 / cow (Appendix A - Table A.1).

The averages bedding temperatures at surface and 0.1 m and 0.2 m depths were 23.7°C (±1.2), 44.0°C (±12.4), and 45.0°C (±11.6), respectively. Paired t-test statistical analysis indicated that at the 0.05 significance level, the averages for the two depths were not different (Appendix A - Table A.2).

The average bedding moisture was 60.3% (±3.3). The minimum and maximum bedding moisture was between 53.6% and 63.0%, respectively. The first and third quartiles were 58.3% and 62.7%, respectively. The average moisture content of bedding in Barn 20 is given in Appendix A (Table A.5).

(a) (b)

Figure 4.63 – Dried fine material was spread out on top of the compost in Barn 20.

Barn 21 was bedded with kiln dried wood shavings. The compost appeared relatively wet and fresh and fine material was spread out on top of the pack once a day. The bedding material was aerated to a depth of 0.20 to 0.25 m once a day (summer time) and twice a day (winter time) while cows were away at the parlor, using a chisel plow on a small tractor (Figure 4.64). This barn was cleaned out once a year. The pack had dimensions of 36.6 m x 15.3 m. The stock density was 7.9 m^2 / cow (Appendix A - Table A.1).

The surface pack temperature measured was 4.5°C (±2.4). The average of the pack temperature in the depth 0.1 m [46.1°C (±32.5)] was less than the average of the depth 0.2 m [50.2°C (±14.7)], as can been see in Appendix A (Table A.4). Paired t-test statistical analysis indicated that these two averages were not different ($P < 0.05$).

The average bedding moisture was 58.8% (±3.3). The minimum bedding moisture was 55.0% and the maximum was 64.5% (Appendix A - Table A.5). The first and third quartiles were 56.8% and 59.2%, respectively.

(a)

(b)

Figure 4.64 - Chisel plow was used to aerate the pack compost of barn 21.

Barn 22 was bedded with green sawdust. The loosest and driest compost was found in the pack with a fluffy consistency (Figure 4.65). The pack was aerated once a day while the cows were milked. A tractor was used to pull the chisel plow. This barn was cleaned out twice a year. The bedded pack had dimensions of 61.0 m x 15.3 m and the stock density was 10.2 m^2 per cow (Appendix A - Table A.1).

The surface pack temperature measured was 6.9°C (±2.7). The average of the pack temperature in the depth 0.1 m [28.8°C (±5.4)] was high than the average of the depth 0.2 m [31.6°C (±3.2)], as can been see in Appendix A (Table A.4). Paired t-test statistical analysis indicated that these two averages were different ($P < 0.05$).

The average bedding moisture was 52.0% (±4.4), ranging from 43.9% to 58.3% (Appendix A - Table A.5). The first and third quartiles were 50.0% and 53.9%, respectively.

Figure 4.65 - Bedding compost was fluffy consistency in Barn 22.

Barn 23 was bedded with green sawdust (Figure 4.66). The bedding compost was appearing compacted and wet, with mainly slurry consistency. The pack was aerated once a day while the cows were milked. A tractor was used to pull the chisel plow. This barn had pack dimensions of 61.0 m x 15.3 m and was cleaned out twice a year. The stock density (25.9 m^2 per cow) was high than suggested minimum (7.4 m^2 per cow) by Janni et al. (2007). Compost barns will not perform well if the cows are overcrowded.

The average bedding temperatures at surface was 6.0°C (±2.6). Paired t-test statistical analysis indicated that at the 0.05 significance level, the averages for the two depths were different. When comparing the pack temperature of the two depths, was found that the average of the depth 0.1 m was less than the average of the depth 0.2 m (Appendix A - Table A.4). The bedding temperatures indicated that the bedding material used for this barn was not composting, although the aerated pack was biologically active.

The average bedding moisture was 67.3% (±1.3), which is high than the recommended for composting of 45% to 60% moisture (NRAES-54, 1992). The minimum bedding moisture was 65.9% and the maximum was 69.7% (Appendix A - Table A.5). The first and third quartiles were 66.3% and 68.1%, respectively.

Figure 4.66 - The bedding compost in Barn 23 was appearing compacted and wet.

Barn 24 was bedded using green sawdust (Figure 4.67). The pack had dimensions of 30.5 m x 15.3 m and was cleaned out twice a year. This farmer added some amount of fresh media every week. It is common for farmers to have to add more media in the winter due to the cold weather inhibiting airflow in the barn thus reducing the drying of the surface of the pack (Changirath et al., 2011). The pack was aerated once a day while the cows were milked, using a chisel plow. The stock density of this barn was 12.9 m^2 per cow (Appendix A - Table A.1).

The average bedding temperatures at surface and 0.1 m and 0.2 m depths were 7.2°C (±2.5), 15.3°C (±5.5), and 19.8°C (±4.9), respectively (Appendix A - Table A.4). Paired t-test statistical analysis indicated that the averages for the two depths were different ($P < 0.05$).

The average bedding moisture was 64.0% (±1.6), which is high than the recommended by NRAES-54 (1992). The minimum bedding moisture was 62.5% and the maximum was 67.3% (Appendix A - Table A.5). The first and third quartiles were 62.9% and 64.2%, respectively.

Figure 4.67 - Fresh media was added every week in Barn 24.

Barn 25 was bedded with kiln dried wood shavings or sawdust. Aerating was done twice a day with a chisel plow that turns over the compost 0.20 to 0.25 m below the surface (Figure 4.68). This farmer was trying to minimize the aeration to two or three times per week or less. The reason given was to lower labor and fuel costs with seeming little benefit to the bedded pack through drying or mixing. Fresh media was added to the pack every two days as needed to keep the pack dry. The pack had dimensions of 51.2 m x 29.9 m and was not cleaned out. The stock density was 9.3 m^2 per cow (Appendix A - Table A.1).

The surface pack temperature measured was 7.0°C (±4.2). The average of the pack temperature in the depth 0.1 m [17.1°C (±3.5)] was high than the average of the depth 0.2 m [20.2°C (±2.3)]. as can been see in Appendix A (Table A.4). Paired t-test statistical analysis indicated that these two averages were different ($P < 0.05$).

The average bedding moisture was 61.2% (±2.3). The minimum bedding moisture was 58.9% and the maximum was 64.5% (Appendix A - Table A.5). The first and third quartiles were 59.4% and 63.8%, respectively.

(a)

(b)

Figure 4.68 - Aerating was done with a chisel plow in CBP barn 25.

Barn 26 was bedded with green sawdust. The dimensions of the bedded pack were 61.0 m x 15.6 m. Approximately 135 cows were kept in the bedded pack that provided a stock density of 7.0 m^2 per cow (Appendix A - Table A.1). Aerating was done with a chisel plow (Figure 4.69) twice a day in the summer and winter time. Fresh media was added to the pack once a week in the winter.

The average bedding temperatures at surface and two depths (0.1 m and 0.2 m) were 6.8°C (±4.5), 39.5°C (±11.2), and 39.5°C (±9.8), respectively, as can been see in Appendix A (Table A.4). Paired t-test statistical analysis indicated that the averages for the two depths were not different ($P < 0.05$).

The average bedding moisture was 57.3% (±2.8). The minimum bedding moisture was 54.1% and the maximum was 63.3% (Appendix A - Table A.5). The first and third quartiles were 55.0% and 58.5%, respectively.

(a)

(b)

Figure 4.69 - Aerating was done with a chisel plow in CPB barn 26.

Barn 27 was bedded with kiln dried wood shavings or sawdust (Figure 5.70a). Aerating was done with a chisel plow (Figure 4.70b) twice a day (summer and winter time) when the cows are being milked. The depth of the bedding media layer was approximately 0.15 m to

0.20 m. This barn was not cleaned out during the year. The dimension of the bedded pack was 36.6 m x 12.2 m. The stock density was 8.6 m^2 per cow (Appendix A - Table A.1).

The average surface temperature measured was 18.2°C (±9.1). The average of the pack temperature in the depth 0.1 m and 0.2 m were 39.4°C (±23.3) and 43.3°C (±14.7), respectively. (Appendix A - Table A.4). Paired t-test statistical analysis indicated that these two averages were not different ($P < 0.05$).

The average bedding moisture was 67.8% (±1.3). as can be seen in (Appendix A - Table A.5). The minimum bedding moisture was 66.2% and the maximum was 70.7%. The first and third quartiles were 67.0% and 68.2%, respectively.

(a) (b)

Figure 4.70 - Aerating was done with a chisel plow in CBP barn 27.

Barn 28 was bedded with green sawdust (Figure 4.71a). This barn had pack dimensions of 36.6 m x 15.3 m and was tilling once a day (summer) and twice a day (winter), thereby mixing and aerating the pack using chisel plough (Figure 4.71b). This farmer removed the bedded pack media from this barn one time per year in summer, and then immediately applied it to the fields. The stock density was 7.0 m^2 per cow (Appendix A - Table A.1).

The surface pack temperature measured was 9.0°C (±4.2). The average of the pack temperature in the depth 0.1 m was less than the average of the depth 0.2 m (Appendix A - Table A.4). Paired t-test statistical analysis indicated that these two averages were different ($P < 0.05$).

The average bedding moisture was 57.3% (±2.8), ranging from 54.1% to 63.3%. The first and third quartiles were 55.0% and 58.5%, respectively. Details can be seen in Appendix A (Table A.5).


(a) (b)

Figure 4.71 - Bedded with green sawdust and chisel plough used in CBP barn 28.

Barn 29 was bedded with green sawdust and the bedded pack had dimensions of 61.0 m x 14.6 m (Figure 4.72a). This package was very wet, when walking atop it, the boots were sunk in up to ankles in some spots. Tilling was performed once daily (summer and winter) using a chisel plow with 0.25 m shovels (Figure 4.72b). The pack appeared to be compacted and chunks were seen after stirring. The stock density was 10.0 m^2 per cow (Appendix A - Table A.1).

The average surface temperature measured was 5.4°C (±3.4). The average of the pack temperature in the depth 0.1 m and 0.2 m were 15.5°C (±6.7) and 18.0°C (±5.6), respectively. (Appendix A - Table A.4). Paired t-test statistical analysis indicated that the averages for the two depths were different ($P < 0.05$). Details can be seen in Appendix A (Table A.4).

The average bedding moisture was 61.1% (±2.1). The minimum bedding moisture was 58.2% and the maximum was 64.5%. The first and third quartiles were 59.2% and 62.4%, respectively. The average moisture content of bedding is given in Appendix A (Table A.5).


(a) (b)

Figure 4.72 - Barn 29 was bedded with green sawdust.

Barn 30 was bedded with green sawdust. This barn was not cleaned out during the year. Aerating was done with a chisel plow twice a day (summer and winter) when the cows are being milked. The depth of the bedding media layer was approximately 0.40 to 0.45 m. The wet compost was close to the scrape alley (Figure 4.73). This barn had pack dimensions of 45.8 m x 18.8 m and the stock density was 8.8 m^2 per cow (Appendix A - Table A.1).

The average surface temperature measured was 14.2°C (±9.8). The average of the pack temperature in the depth 0.1 m and 0.2 m were 49.2°C (±7.8) and 52.9°C (±4.5), respectively (Appendix A - Table A.4). Paired t-test statistical analysis indicated that the averages for the two depths were different ($P < 0.05$). Details can be seen in Appendix A (Table A.4).

The average bedding moisture was 47.4% (±2.6). The minimum bedding moisture was 43.4% and the maximum was 51.2%. The first and third quartiles were 46.2% and 49.0%, respectively. The average moisture content of bedding is given in Appendix A (Table A.5).

(a) (b)

Figure 4.73 - Barn 30 was bedded with green sawdust.

Barn 31 was using green sawdust and a load of green sawdust was spread in early in the winter. Tilling was done twice a day (summer and winter). A tractor was used to pull a chisel plow (Figure 4.74). The depth of the compost media layer was approximately 0.60 m. The bedded pack had dimensions of 45.8 m x 31.7 m and the stock density was 11.0 m^2 per cow (Appendix A - Table A.1).

The surface pack temperature measured was 11.8°C (±8.4). The average of the pack temperature in the depth 0.1 m [32.8°C (±17.2)] was less than the average of the depth 0.2 m [35.1°C (±13.3)], as can been see in Appendix A (Table A.4). Paired t-test statistical

analysis indicated that at the 0.05 significance level, the averages for the two depths were not different.

The average bedding moisture was 61.7% (±3.7). The minimum bedding moisture was 56.8% and the maximum was 68.7% (Appendix A - Table A.5). The first and third quartiles were 60.6% and 62.3%, respectively.

(a) (b)

Figure 4.74 - Barn 31 was using green sawdust and chisel plow was used to till.

Barn 32 was bedded with green sawdust (Figure 4.75a). Aerating was done twice daily (summer and winter) with a chisel plow that turns over the compost 0.15 m – 0.20 m below the surface (Figure 4.75b). The dimensions of the bedded pack were 30.5 m x 18.3 m. Approximately 47 cows were kept in the bedded pack that provided a stock density of 11.9 m^2 per cow (Appendix A - Table A.1).

The average surface temperature measured was 6.7°C (±4.4). When comparing the pack temperature of the two depths, it was found that the average of the depth 0.1 m was less than the average of the depth 0.2 m (Appendix A - Table A.4). Paired t-test statistical analysis indicated that the averages for the two depths were different ($P < 0.05$).

The average bedding moisture was 66.4% (±1.3), which was above NRAES-54 (1992), recommended level of 45% to 60%. The minimum bedding moisture was 64.8% and the maximum was 68.3%. The first and third quartiles were 65.6% and 67.3%, respectively. The average moisture content of bedding in this barn is given in Appendix A (Table A.5).

(a)

(b)

Figure 4.75 - Chisel plow was used to aeration the bedding compost in CBP barn 32.

Barn 33 was using kiln dried wood shavings or sawdust (Figure 4.76a). The pack was aerated twice a day (summer and winter) using chisel plow (Figure 4.76b). The pack was not cleaned out. The compost pack appeared to be compacted and chunks were seen after stirring. The compost appeared relatively wet and did stick to the boots when walking on the surface. The bedded pack had dimensions of 61.0 m x 15.6 m and the stock density was 10.8 m^2 per cow (Appendix A - Table A.1).

The surface pack temperature measured was -1.5°C (±16.1). The average of the pack temperature in the depth 0.1 m [33.0°C (±27.0)] was less than the average of the depth 0.2 m [37.4°C (±25.4)], as can been see in Appendix A (Table A.4). Paired t-test statistical analysis indicated that these two averages were different ($P < 0.05$).

The average bedding moisture was 69.5% (±0.9). The minimum bedding moisture was 68.2% and the maximum was 70.5% (Appendix A - Table A.5). The first and third quartiles were 68.7% and 70.4%, respectively.

(a)

(b)

Figure 4.76 - Chisel plow was used to aeration the pack compost in CBP barn 33.

Barn 34 owner was using kiln dried wood shavings or sawdust for bedding (Figure 4.77). This barn was stirred at least two time each day (summer and winter) when the cows

are being milked. The pack was aerated 0.35 m depth, however experienced compost barn operators suggest that the pack should be stirred to a depth 0.25 m to 0.30 m twice a day (Janni et al., 2007). Bedded pack stirring was done using a cultivator attached to the back of a tractor. The bedded pack had dimensions of 29.3 m x 11.0 m and the stock density was 3.0 m^2 per cow (Appendix A - Table A.1).

The average bedding temperatures at surface and 0.1 m and 0.2 m depths were -0.8°C (±3.7), 27.6°C (±29.3), and 23.3°C (±3.9), respectively. Paired t-test statistical analysis indicated that the averages for the two depths were not different ($P < 0.05$). The average temperature of bedding in this barn is given in Appendix A (Table A.4).

The average bedding moisture was 68.9% (±2.0), which is high than the recommended for composting of 45% to 60% moisture (NRAES-54, 1992). The minimum bedding moisture was 66.2% and the maximum was 71.9% (Appendix A - Table A.5). The first and third quartiles were 67.3% and 70.3%, respectively.

(a) (b)

Figure 4.77 - Barn 34 was using kiln dried wood shavings or sawdust for bedding.

Barn 35 was bedded with green sawdust (Figure 4.78a), but it is not recommended to start with the compost dairy barn using green sawdust (Crary et al.. 2005). The bedded pack was aerated once a day using rotary tiller on a tractor. The rotary tiller was mounted in 3 point diggers on the back of a tractor (Figure 4.78b). This farmer initially started with 0.35 m to 0.40 m depth of green sawdust. The bedded pack had dimensions of 36.6 m x 8.5 m and the stock density was 10.3 m^2 per cow. This barn was cleaned out 2.5 times per year.

The surface pack temperature measured was -3.5°C (±2.6). The average of the pack temperature in the depth 0.1 m was less than the average of the depth 0.2 m. as can be seen in Appendix A (Table A.4). Paired t-test statistical analysis indicated that these two averages were different ($P < 0.05$).

The average bedding moisture measured was 62.6% (±5.6), ranging from 48.7% to 69.4% (Appendix A - Table A.5). The first and third quartiles were 62.5% and 64.6%, respectively.

(a)

(b)

Figure 4.78 - Barn 35 was aerated using rotary tiller.

Barn 36 was bedded with green sawdust. Aerating was done twice daily with a chisel plow that turns over the compost 0.15 m – 0.20 m below the surface. The dimensions of the bedded pack were 43.9 m x 14.6 m. The stock density was 6.9 m^2 per cow (Appendix A - Table A.1). The wet compost was found in this pack, with mainly slurry consistency (Figure 5.79). This barn was cleaned out three times per year. Addition of fresh material is recommended when the bedded pack becomes moist enough for it to stick to the cows.

Average bedding temperatures at surface and 0.1 m and 0.2 m depths were 3.3°C (±2.5), 15.7°C (±6.4), and 18.2°C (±5.8), respectively (Appendix A - Table 4). Paired t-test statistical analysis indicated that the averages for the two depths were different ($P < 0.05$).

The average bedding moisture [71.8% (±0.8)] was the largest that has been found among the farms studied, ranging from 70.8% to 73.3% (Appendix A - Table A.5). The first and third quartiles were 71.3% and 71.9%, respectively. Bedding needs to stay dry for the benefit of keeping cows clean and somatic cell count (SCC) low.

(a)

(b)

Figure 4.79 - Bedded with green sawdust and chisel plow used in CBP barn 36.

Barn 37 was bedded with green sawdust. Tilling was done once a day with a chisel plow that turns over the compost 0.15 m – 0.20 m below the surface. The same chisel plow was used in this barn and Barn 38 (Figure 4.80). A load of green sawdust was added every three weeks. In the winter time, fresh green sawdust was necessary to be added more frequently. This barn was cleaned out twice a year. Care must be taken when removing the bedded pack during clean out, or during pack stirring when the bedded pack is less than 0.30 m deep, to avoid disturbing the base of the barn (Janni et al., 2005). The pack had dimensions of 45.8 m x 10.7 m and the stock density was 10.0 m^2 per cow.

The average surface temperature measured was 4.7°C (±2.9). The average of the pack temperature in the depth 0.1 m and 0.2 m were 20.2°C (±15.3) and 25.3°C (±16.6), respectively. Paired t-test statistical analysis indicated that the averages for the two depths were different ($P < 0.05$). Details can be seen in Appendix A (Table A.4)

The average bedding moisture was 64.3% (±3.5), which was above NRAES-54 (1992) recommended level of 45% to 60%. The minimum bedding moisture was 57.0% and the maximum was 68.7%. The first and third quartiles were 63.4% and 66.5%, respectively. The average moisture content of bedding in this barn is given in Appendix A (Table A.5).

(a) (b)

Figure 4.80 - Bedded with green sawdust and chisel plow used in CBP barn 37.

Barn 38 was bedded with green sawdust (Figure 4.81). The compost appeared relatively loose and dry and did not stick to the boots when walking on the surface. The bedded pack was aerated once a day, at least 0.20 m deep. According to Endres (2009), the bedded pack should be aerated twice daily, at least 0.25 m deep, to keep it aerobic and fluffy, hence biological activity generates heat and helps dry the pack. This barn was cleaned out twice a year and a load of fresh green sawdust was added every three weeks. The pack had dimensions of 36.6 m x 21.7 m and the stock density was 15.9 m^2 per cow.

The average bedding temperatures at surface was 3.8°C (±2.3). Paired t-test statistical analysis indicated that at the 0.05 significance level, the averages for the two depths were different. When comparing the pack temperature of the two depths, was found that the average of the depth 0.1 m was less than the average of the depth 0.2 m (Appendix A - Table A.4).

The average bedding moisture was 61.7% (±6.4). The minimum bedding moisture was 50.5% and the maximum was 67.7% (Appendix A - Table A.5). The first and third quartiles were 56.9% and 66.7%, respectively.

Figure 4.81 - Barn 38 was bedded with green sawdust.

Barns 39 and 40 were bedded using green sawdust (Figure 4.82a). These barns were stirred at least twice a day (summer and winter) when the cows are being milked. The packs were aerated 0.18 m depth. Bedded packs stirring were done using a chisel plow attached to the back of a tractor (Figure 4.82b). These barns had the same bedded pack dimensions of 48.8 m x 22.0 m. The stock density of the barn 39 and 40 were 12.2 m^2 per cow and 12.6 m^2 per cow, respectably. Details can be seen in Appendix A (Table A.1).

The average surface temperature measured in Barns 11 and 12 were -1.7°C (±4.5) and 0.0°C (±8.3), respectively. Paired t-test statistical analysis indicated that there were significant ($P < 0.05$) differences in average temperatures for the two depths in both of barns (Appendix A - Table A.4).

The average bedding moisture in Barns 39 and 40 were 66.5% (±1.0) and 64.6% (±1.7), respectively. Details can be seen in Appendix A (Table A.5).

(a)

(b)

Figure 4.82 - Bedded with green sawdust and chisel plow used in CBP barns 39 and 40.

Barn 41 was bedded with kiln dried wood shavings or sawdust. This farmer used chisel plow (Figure 4.83) to aeration once a day (summer and winter). The pack was aerated 0.15 m depth. According to Endres (2009), some producers in Minnesota are aerating the pack deeper (about 0.35 – 0.40 m) using a chisel plow type of equipment, and they have observed a reduction in bedding needs and increased pack temperatures. Clean bedding was added every time the bedded pack became moist enough for it to adhere to the cows and a load of fresh material was added every three weeks. The pack had dimensions of 30.5 m x 15.3 m and the stock density was 5.2 m^2 per cow (Appendix A - Table A.1).

The surface pack temperature measured was -4.0°C (±2.3). The average of the pack temperature in the depth 0.1 m [25.2°C (±15.1)] was less than the average of the depth 0.2 m [30.0°C (±5.9)], as can been see in Appendix A (Table A.4). Paired t-test statistical analysis indicated that these two averages were different ($P < 0.05$).

The average bedding moisture was 70.1% (±2.7), which is high than the recommended for composting of 45% to 60% moisture (NRAES-54, 1992). The minimum bedding moisture was 65.2% and the maximum was 71.7% (Appendix A - Table A.5). The first and third quartiles were 69.1% and 71.7%, respectively.

(a)

(b)

Figure 4.83 - Kiln dried wood shavings and chisel plow used in CBP barn 41.

Barn 42 was bedded with mix material. Tilling was performed twice a day in the summer and winter time, using a chisel plow with 0.20 m shovels (Figure 4.84). The chisel plow tills to a depth of 0.14 m – 0.18 m. This farmer cleaned out once a year and leave about 0.05 m of old material in the barn to help initiate microbial activity. This pack was cleaned out one time per year. The bedded pack had dimensions of 53.7 m x 14.9 m and the stock density was 8.0 m^2 per cow, as can been see in Appendix A (Table A.1).

The bedding temperatures measured at two depths were 18.2°C (±25.1) and 24.8°C (±5.1) and the pack surface temperatures was 0.9°C (±3.5). Paired t-test statistical analysis indicated that these two averages were different ($P < 0.05$).

The average bedding moisture was 69.1% (±1.2). The minimum bedding moisture was 67.6% and the maximum was 70.7%. The first and third quartiles were 68.3% and 70.2%, respectively. More details about Barn 42 are given in Appendix A (Table A.1).

(a) (b)

Figure 4.84 - Chisel plow was used to aeration in CBP barn 42.

4.2.4. Environment characteristics

The average temperature gradient (taken at 0.05 m and 1.20 m above the pack) was -0.52 °C · m^{-1} (± 1.0), indicating that there was a reduction of the air temperature along the height measurement. Paired t-test statistical analysis indicated that at the 0.05 significance level, the averages air temperatures for the two heights were different. The average surface temperatures on the pack were similar to the average ambient temperature. During the winter, the temperature would be the first indicator of changes in bed performance (Taraba and Bewley, 2010). Air temperatures tended to be lower inside barns which utilized Overshot or Capped ridge, mechanical ventilation system and ridge direction of SW or NW (Table 4.1). Building temperatures must remain above freezing most of the time to prevent frozen manure in the pack. This type of building requires insulation (curtains) and a controlled ventilation system. Most compost packs were warmer than the outdoor air

temperature. This indicates that the packs were heating and microbial activity was occurring.

The average relative humidity gradient in this study was 2.35 % $\cdot$ m^{-1} ($\pm$ 0.5). Thus, the majority of barns tend to increase relative humidity along the height. Paired t-test statistical analysis indicated that the averages relative humidity for the two heights were different ($P < 0.05$). In some barns, sawdust bedding was used to keep cattle comfortable and dry in higher amounts which increases barn operating costs.

The average of air velocity gradient was -0.22 m s^{-1} $\cdot$ m^{-1} ($\pm$ 0.3), indicating that the air velocity decreased along the height. Paired t-test statistical analysis indicated that at the 0.05 significance level, the averages air velocity for the two heights were different. Thus, during the season of fall and winter in Kentucky, the barn orientation was not ideal for air movement since air generally moving along the length meets higher resistance than air moving across the building. Sufficient air exchange is needed in cold weather to remove moisture from the pack and extend the time between bedding addition. Overall, the low sidewalls of the barns promoted high air velocity across the barns. Air movement through the barn should be sufficient to maintain inside temperature only slightly above outside temperature in winter and slightly below outside temperature in summer. A considerable differences between air velocity indoor and outdoor were observed in barns 1, 5, 6, 11, 12, 13, 14, 16, 17, 20, 22, 23, 24, 25, 37, and 38. Buildings and other obstacles (trees, hills, and tractors) around of these barns blocked for airflow and results in more high relative humidity, as can be seen in Table 4.1. On the other hand, high airflow during the winter can reduce the air temperature indoor and the pack temperature. In those conditions, windbreaks become very important. In the winter, side curtains can be an important investment to reduce barn ventilation and winter winds from extracting too much heat from a compost bed (Taraba and Bewley, 2010).

Table 4.1 - Average air temperatures, relative humidity and air velocity inside and outside in 42 CBP barns in Kentucky.

Barn	Air Temperature (°C)						Relative Humidity (%)						Air velocity (m/s)						Outside weather		
	0.05 m			1.2 m			0.05 m			1.2 m			0.05 m			1.2 m			Air temp.	R. H.	Air veloc.
	Aver.		Std Dev	Aver.		Std Dev	Aver.		Std Dev	Aver.		Std Dev	Aver.		Std Dev	Aver.		Std Dev	(°C)	(%)	(m/s)
1	16.7	±	7.1	17.8	±	0.6	79.9	±	2.7	80.7	±	1.2	1.3	±	1.4	2.1	±	2.1	16.7	73.0	0.9
2	20.2	±	0.7	20.9	±	0.5	43.1	±	3.8	34.8	±	3.5	0.7	±	0.6	0.5	±	0.3	24.6	16.5	0.5
3	22.4	±	7.1	21.6	±	1.2	34.0	±	9.3	22.3	±	1.1	0.6	±	0.3	0.8	±	0.8	24.6	16.5	1.7
4	15.4	±	1.0	14.9	±	1.0	59.4	±	3.9	53.6	±	2.3	1.0	±	0.4	1.4	±	1.0	15.0	38.0	2.7
5	24.7	±	1.4	24.8	±	1.4	70.1	±	3.6	66.9	±	5.1	0.7	±	0.4	1.0	±	0.8	26.8	55.7	0.3
6	16.2	±	1.6	15.2	±	0.9	88.4	±	1.1	88.6	±	1.0	0.4	±	0.2	0.5	±	0.3	19.4	84.0	0.3
7	15.9	±	1.2	16.1	±	0.8	48.1	±	4.8	39.7	±	2.6	0.8	±	0.7	1.7	±	1.2	16.2	36.0	2.3
8	19.4	±	3.3	20.3	±	0.5	52.3	±	5.2	43.5	±	1.8	0.5	±	0.2	1.1	±	0.5	21.4	35.5	1.3
9	23.3	±	2.3	23.3	±	1.7	40.8	±	8.4	30.5	±	2.2	0.4	±	0.2	0.7	±	0.7	21.4	35.5	1.3
10	20.0	±	0.5	20.1	±	0.3	49.8	±	5.6	40.9	±	1.9	0.5	±	0.2	0.8	±	0.2	18.8	38.9	0.8
11	14.9	±	1.3	14.0	±	1.1	85.1	±	4.6	84.6	±	5.5	0.4	±	0.2	0.5	±	0.2	9.4	98.0	0.3
12	15.6	±	1.6	15.0	±	3.1	86.1	±	1.7	84.4	±	3.1	0.3	±	0.1	0.4	±	0.3	9.4	98.0	0.3
13	12.8	±	3.0	12.6	±	2.8	81.3	±	2.2	80.9	±	2.4	1.8	±	0.6	2.8	±	1.1	9.3	84.6	1.0
14	10.5	±	1.5	9.8	±	2.1	83.7	±	2.2	82.8	±	1.6	2.8	±	1.5	3.1	±	1.9	9.3	84.6	1.0
15	15.3	±	2.1	14.0	±	2.1	58.7	±	5.6	53.9	±	3.4	0.7	±	0.6	0.9	±	0.7	12.9	52.0	2.2
16	9.7	±	1.2	8.6	±	0.7	92.0	±	1.6	91.9	±	1.7	1.5	±	0.2	1.9	±	0.8	8.9	67.0	1.5
17	10.9	±	1.5	9.2	±	0.6	88.7	±	2.1	89.5	±	1.5	0.6	±	0.5	0.6	±	0.5	6.7	95.0	0.6
18	0.6	±	7.0	-1.9	±	0.7	56.7	±	1.2	55.2	±	1.7	0.5	±	0.5	0.7	±	0.6	0.1	43.8	6.3
19	-0.8	±	4.8	-4.2	±	1.7	57.7	±	6.7	59.9	±	5.3	0.4	±	0.3	0.5	±	0.6	-3.4	63.2	0.5
20	25.7	±	0.9	26.0	±	0.5	42.4	±	13.5	33.4	±	1.0	1.6	±	0.8	2.0	±	1.1	25.9	33	1.4
21	4.3	±	1.5	2.9	±	0.5	62.9	±	6.2	62.3	±	1.6	1.0	±	0.6	1.5	±	0.6	-0.4	50.0	3.2
22	7.9	±	0.4	7.1	±	0.3	80.8	±	2.4	81.3	±	1.6	0.7	±	0.4	0.8	±	0.5	6.9	77.7	0.7
23	8.0	±	0.9	7.6	±	0.7	90.6	±	1.5	91.3	±	1.4	0.5	±	0.5	0.6	±	0.5	6.9	77.7	0.5

Continue...

Table 4.1 - Average air temperatures, relative humidity and air velocity inside and outside in 42 CBP barns in Kentucky.

Barn	Air Temperature (°C)						Relative Humidity (%)						Air velocity (m/s)						Outside weather		
	0.05 m			1.2 m			0.05 m			1.2 m			0.05 m			1.2 m			Air temp.	R. H.	Air veloc.
	Aver.		Std Dev	Aver.		Std Dev	Aver.		Std Dev	Aver.		Std Dev	Aver.		Std Dev	Aver.		Std Dev	(°C)	(%)	(m/s)
24	7.7	±	1.3	7.2	±	1.2	89.2	±	1.8	84.4	±	15.6	0.9	±	0.4	1.0	±	0.4	6.9	77.7	0.7
25	7.3	±	0.7	6.2	±	0.7	86.3	±	2.2	88.8	±	1.3	0.4	±	0.2	0.6	±	0.3	5.7	83.5	0.5
26	5.8	±	1.4	6.5	±	6.4	61.8	±	2.7	58.9	±	5.8	0.6	±	0.2	0.5	±	0.3	3.3	58.6	1.5
27	12.1	±	4.0	10.5	±	3.5	59.6	±	6.8	55.3	±	5.7	0.3	±	0.1	0.2	±	0.1	5.4	42.4	3.4
28	6.9	±	1.4	6.5	±	1.0	56.2	±	4.0	53.0	±	3.6	0.3	±	0.1	0.3	±	0.2	-0.6	55.0	0.9
29	6.1	±	1.3	6.0	±	1.2	58.8	±	3.8	54.0	±	1.9	0.5	±	0.2	0.7	±	0.3	3.8	52.3	2.6
30	9.0	±	4.1	7.3	±	1.0	57.0	±	13.3	54.0	±	1.9	1.1	±	0.7	1.3	±	0.7	8.1	49.9	1.6
31	10.7	±	2.8	9.8	±	1.7	53.1	±	4.1	47.4	±	1.7	0.4	±	0.2	0.6	±	0.4	5.4	42.4	3.4
32	3.1	±	1.5	2.6	±	1.5	67.1	±	2.8	67.5	±	2.3	0.3	±	0.1	0.2	±	0.1	0.4	64.4	1.0
33	0.0	±	1.7	-1.2	±	1.0	64.0	±	4.9	66.3	±	3.9	0.9	±	0.5	1.1	±	0.6	-2.6	61.5	1.4
34	1.4	±	0.9	0.7	±	0.6	66.4	±	3.4	67.6	±	1.5	0.4	±	0.2	0.3	±	0.1	0.4	68.8	3.1
35	2.5	±	4.6	2.4	±	1.9	49.6	±	4.2	50.6	±	3.1	0.3	±	0.2	0.5	±	0.3	0.7	51.7	1.7
36	3.6	±	2.3	3.7	±	0.6	75.9	±	2.5	76.1	±	2.3	0.3	±	0.2	0.2	±	0.1	1.7	71.8	0.5
37	5.3	±	0.9	4.7	±	0.7	80.0	±	1.7	80.0	±	1.1	0.5	±	0.3	0.5	±	0.3	1.1	89.0	0.5
38	5.7	±	0.4	5.3	±	0.6	82.4	±	1.8	82.7	±	1.9	0.4	±	0.2	0.4	±	0.2	1.1	89.0	0.4
39	-2.0	±	1.0	-2.6	±	0.9	70.4	±	1.8	69.7	±	2.3	1.4	±	0.7	3.7	±	6.2	-3.4	65.3	2.5
40	-0.5	±	3.1	-1.6	±	0.9	66.6	±	2.2	64.8	±	2.5	0.8	±	0.4	1.2	±	0.5	-3.4	65.3	2.5
41	-1.4	±	0.6	-2.0	±	1.7	59.6	±	2.8	59.8	±	1.7	0.8	±	0.5	0.6	±	0.3	-2.1	59.2	2.5
42	-0.4	±	1.1	-1.0	±	1.3	64.2	±	3.1	62.7	±	2.6	0.3	±	0.3	0.6	±	0.5	-2.4	54.6	2.5

4.2.5. Herd characteristics

The following section summarizes information collected by a collaborator (Black, 2012). It is included to give a more full picture of the benefits of this type barn.

The cow herd size, as reported by the dairymen, was adjusted for breed size and milk production. The average herd size on the pack in the study was 89.7 cows, ranging from 19 to 184 cows and dry cow numbers ranged from 3 to 75 dry cows with an average of 25.1 dry cows (Figure 4.85). Dry cows were housed on pasture, in a separate or the same area of the compost barn as the lactating cows, or in an alternative housing area. Breeds consisted of Jersey (6.8%), Holstein (72.7%), and mix (20.5%). Average milk production of cows was 27.2 kg per day with a mean fat and protein percentage of 3.85% and 2.35%, respectively.

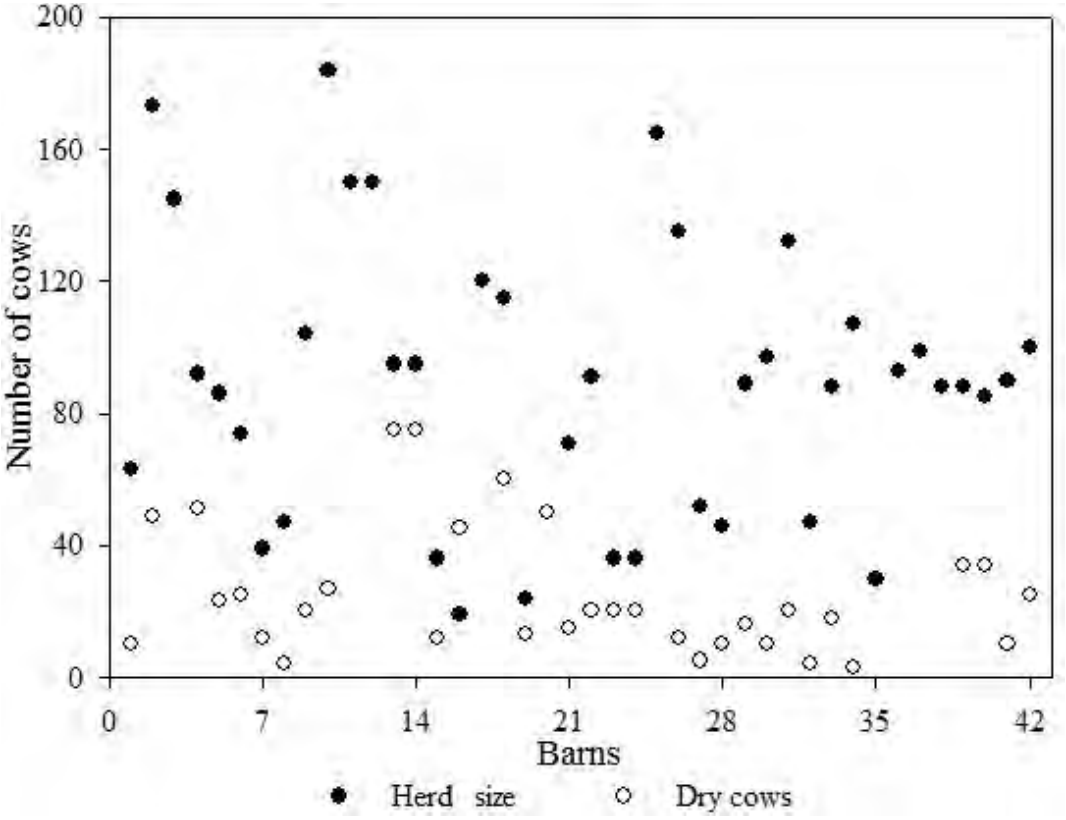

Figure 4.85 - Herd size and dry cows number in 42 CBP barns.

4.2.6. Producer Responses

All producers visited were very satisfied with their compost barns. They observed that cows were more comfortable (24.2%) and that this housing system resulted in increased cow cleanliness (12.1%), see Table 4.2 below for more details.

Table 4.2 - Producer cited benefits of 42 CBP barns.

Benefits	Percent (%)
Improved cow comfort	24.1
Improved cow cleanliness	12.1
Low maintenance	9.5
Good for heifers, lame, fresh, problem, and old cows	8.6
Natural resting position (no stalls)	7.8
Improved feet and legs	6.9
Proximity to parlor (compared to pasture)	6.9
Decreased SCC	5.2
Increased heat detection	5.2
Ease of manure handling	2.6
Increased dry matter intake (compared to pasture)	2.6
Increased production	2.6
Increased longevity	2.6
Fewer leg and teat injuries	1.7
Minimizes time standing on concrete	1.7

However, results of the survey revealed some aspects of the CBP barn producers would change. Their main concern was the size or capacity of the barn (25%). Further, many producers indicated the need for retaining wall (10%) and curtains (8.3%). Other recommended facilities changes are cited in Table 4.3.

Table 4.3 - Recommended facilities changes of CBP barns producers.

Recommended	Percent (%)
Increase size or capacity of the barn	25.0
Higher sidewalls and improved ventilation	20.0
Add a retaining wall	10.0
Add curtains	8.3
More fans	8.3
Larger ridge vent	8.3
No posts in pack	6.7
Change number or location of waterers	6.7
Change location or size of feed bunk	6.7

The majority of producers were concerned about the supply of bedding. Many producers were seeking secure bedding supply (17.7%) and alternative bedding sources that will work in the CBP (9.7%). Producer recommendations also included the importance of maintaining the pack (8.1%), and stirring the pack two times per day or more frequently (14.5%), using kiln-dried shavings (9.7%), avoid the use of straw, wheat straw, corn fodder, or soybean fodder or pine as a bedding material (9.7%), and maintaining the pack by keeping moisture low (8.1%), as can be seen in Table 4.4. Some producers (4.8%) reported that touring other barns was an important influence on their choice of structure. Producers also reported that they spoke with other producers managing a CBP barn, they created their own plans, they reviewed freestall plans and designs, economics, and ease of management. Producers learned that using kiln-dried shavings, keeping the pack stirred, and avoiding the use of straw in the bedding, would help to prevent other mistakes.

Table 4.4 - Producer recommendations and lessons learned of CBP barns producers.

Recommendations and lessons learned	Percent (%)
Secure a bedding supply	17.7
Do not use straw, wheat straw, corn fodder, bean fodder, or pine	9.7
Add bedding frequently	6.5
Tour other barns	4.8
Stir two times per day or more frequently	14.5
Keep pack maintained and moisture low	8.1
Build the barn large	6.5
Add curtains	4.8
Use kiln-dried shavings	9.7
Minimum of 9.3 m2 per cow	8.1
Designated tractor for stirring	4.8
Do not start pack during winter	4.8

4.3. Physical, chemical, and thermal properties of compost materials

4.3.1. Compost particle size distribution

Dried compost was sieved to measure the portion of each particle size range (PS2, PS3, PS4, and PS5) comprising the total amount. Three samples of each particle size range were used to determinate the compost particle size distribution. Particle size distributions on a weight basis (for compost from CBP barns using Green sawdust, Kiln-dried shavings or sawdust, and Mix compost) are presented in Figures 4.86.

A comparison of the particle weight fraction distributions content in Figure 4.86 reveals that these compost materials from the CBP barns using different bedding compost materials are very different. The following percentages and standard deviations were found: in Green sawdust, in the particle size ranges together (PS2 + PS3 + PS4 + PS5) comprised 60.95 ± 10.0% of the total weight, while coarser material represented 3.46 ± 3.4% and finer material, 35.60 ± 11.3%. In Kiln-dried shavings or sawdust, the compost particle size distribution were 25.44 ± 13.1% (finer material), 25.45 ± 8.5% (PS2), 4.12 ± 1.0% (PS3), 10.50 ± 3.0% (PS4), 28.1 ± 14.2% (PS5), and 6.32 ± 8.1% (coarser material). In this plot (Figure 4.85), the distribution values of Mix materials increased in the order of Finer < PS2 < PS5 < PS4 < PS3 < Coarser fractions. In CBP barns using Mix compost material, the lower and higher compost particle size distribution were 14.38% (Coarser > 25.00 mm) and 48.66% (Finer < 2.00 mm), respectively.

The analysis of variance between of compost particle ranges from all CBP barns was obtained and is shown in Figure 4.87 at the significance level of $p < 0.05$. The Tukey test shows that there was a significant difference between average values of compost particle ranges. This results indicate that the distribution of mass weight increased in the order of Coarser = PS3 < PS4 < PS5 = PS2 < PS2 = Finer. The average finer index expressed as weight percent in the samples studied was 30.1%. Details about statistic analysis can be seen in Appendix F (Table 1).

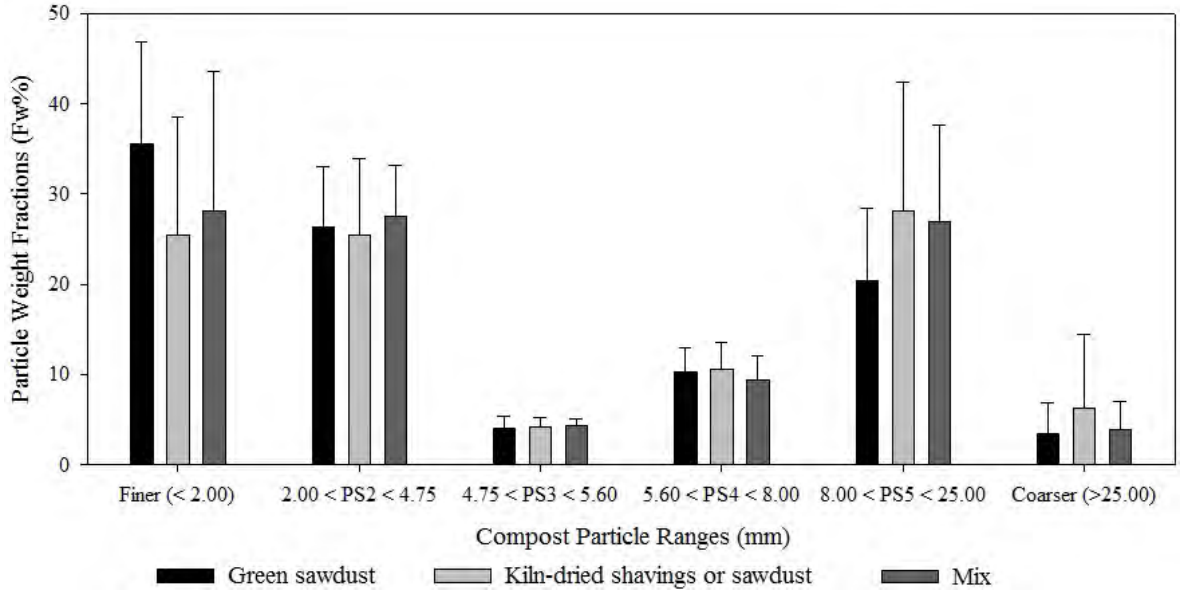

Figure 4.86 - Particle Weight Fractions for compost bedded from CBP barn using Green sawdust, Kiln-dried shavings or sawdust, and Mix compost.

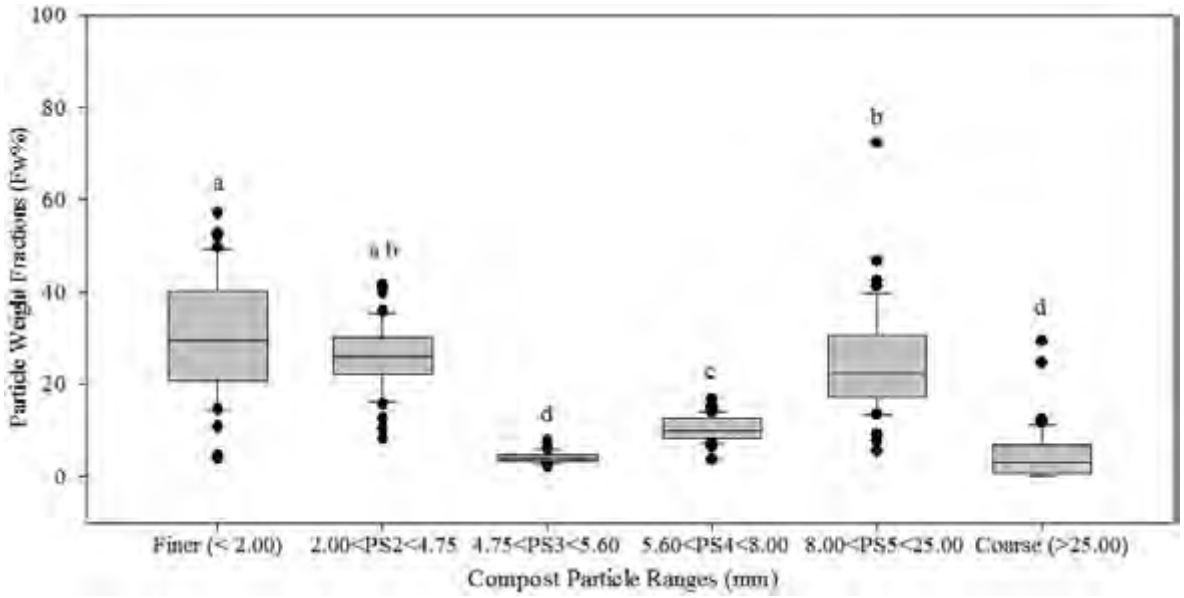

Figure 4.87 - Analysis of variance between compost particle ranges for all bed compost materials. Values followed by different letters are significantly different ($P < 0.05$; Tukey).

4.3.2. Particle density, bulk density, and porosity

Particle density, bulk density, and porosity of 42 compost bulking material results are shown in Table 4.5.

Particle density of all compost material studied ranged from 0.86 to 1.11 g cm^{-3} with an average of 0.98 g cm^{-3} and a standard deviation of 0.02 (Table 4.5). Generally, the compost materials of CBP barns 9, 11, 12, 13, 16, 20, 21, 22, 23, 24, 26, 27, 29, 30, 32, 33, 36, 40,

41, and 42 show high particle density (≥ 1g cm^{-3}) compared with other materials (Table 4.5). It should be noted that the obtained values are somewhat higher than expected, but evaporation of water increase the solids content, particularly with well performing beds or high cow density. Cows that spend time in pasture may return soil to bed.

Results and standard errors of bulk density for compost bed material collected from each barn are shown below (Table 4.5). The average bulk density was 0.37 ± 0.02 g cm^{-3} with a range of 0.15 to 0.54 g cm^{-3}. Higher bulk density suggests that the compost have less pore space and are more compact. The highest bulk density value was 3.6 times that of the lower bulk density value.

The average porosity of the bedding material in all compost barns was 62.65 ± 2.14% with a range of 47.43 to 77.32%. In general, the average porosity increased when the bulk density decreased, significantly higher porosity was found in Barns 41 (77.32%). The variation of average porosity in all compost bulking material was similar to those bulk density in the reverse order due to the inverse relationship between bulk density and porosity (Table 4.5). So, high bulk density and low porosity might cause poor aeration and limiting oxygen concentration uptake by microorganisms and inhibiting microorganisms growth. Previous researchers have reported the optimum and minimum range of porosity for aerobic process in compost systems was 85 to 90%, and 30%, respectively (Schulze, 1962; Rynk, 1992; Nappi and Barberis, 1993).

Table 4.5 - Particle density, bulk density, and porosity in 42 compost-bulking materials, as well as standard deviations (n = 3).

Barn	Particle density (g cm^{-3})			Bulk density (g cm^{-3})			Porosity (%)		
1	0.95	±	0.06	0.50	±	0.06	77.12	±	8.23
2	0.98	±	0.06	0.47	±	0.01	72.30	±	3.30
3	0.92	±	0.04	0.38	±	0.02	65.41	±	2.25
4	0.86	±	0.04	0.31	±	0.01	65.40	±	1.84
5	0.93	±	0.07	0.47	±	0.03	60.53	±	3.26
6	0.91	±	0.05	0.45	±	0.01	60.50	±	3.40
7	0.97	±	0.06	0.37	±	0.01	62.07	±	1.65
8	0.99	±	0.05	0.47	±	0.13	53.63	±	11.28
9	1.04	±	0.05	0.54	±	0.02	47.43	±	3.61
10	0.94	±	0.06	0.45	±	0.01	51.92	±	2.30
11	1.01	±	0.03	0.44	±	0.04	56.52	±	4.34
12	1.05	±	0.07	0.45	±	0.02	56.70	±	4.75

Continue...

Table 4.5 - Particle density, bulk density, and porosity in 42 compost-bulking materials, as well as standard deviations (n = 3).

Barn	Particle density ($g\ cm^{-3}$)			Bulk density ($g\ cm^{-3}$)			Porosity (%)		
13	1.00	±	0.01	0.35	±	0.03	67.37	±	2.18
14	0.99	±	0.03	0.32	±	0.01	65.21	±	2.01
15	0.92	±	0.03	0.28	±	0.05	68.64	±	6.60
16	1.01	±	0.02	0.24	±	0.01	76.72	±	1.57
17	0.98	±	0.04	0.44	±	0.01	55.31	±	2.83
18	0.90	±	0.02	0.40	±	0.02	56.00	±	2.18
19	0.92	±	0.11	0.27	±	0.01	71.99	±	4.26
20	1.06	±	0.01	0.48	±	0.03	54.81	±	2.62
21	1.01	±	0.02	0.24	±	0.01	75.90	±	1.02
22	1.00	±	0.01	0.39	±	0.01	60.94	±	0.96
23	1.02	±	0.06	0.36	±	0.00	64.73	±	2.43
24	0.97	±	0.01	0.28	±	0.01	70.80	±	1.10
25	1.00	±	0.03	0.39	±	0.01	61.11	±	0.41
26	1.11	±	0.01	0.42	±	0.01	62.29	±	0.75
27	0.94	±	0.05	0.34	±	0.02	64.10	±	0.94
28	1.04	±	0.05	0.43	±	0.01	58.88	±	2.64
29	1.06	±	0.04	0.35	±	0.02	66.83	±	1.20
30	0.97	±	0.04	0.37	±	0.00	61.68	±	2.11
31	1.04	±	0.02	0.39	±	0.01	62.58	±	1.81
32	1.00	±	0.00	0.42	±	0.01	57.80	±	0.65
33	0.93	±	0.02	0.33	±	0.02	64.66	±	2.52
34	0.97	±	0.02	0.27	±	0.02	71.80	±	2.12
35	1.01	±	0.01	0.40	±	0.02	59.73	±	1.78
36	0.95	±	0.00	0.41	±	0.01	57.26	±	1.44
37	0.91	±	0.01	0.38	±	0.06	58.34	±	6.60
38	0.87	±	0.04	0.38	±	0.02	56.11	±	4.06
39	1.03	±	0.02	0.40	±	0.02	61.39	±	0.78
40	1.06	±	0.03	0.34	±	0.03	57.50	±	1.87
41	1.05	±	0.00	0.20	±	0.03	77.32	±	2.67
42	1.05	±	0.01	0.32	±	0.04	54.20	±	3.78
Average	0.98	±	0.02	0.38	±	0.02	62.65	±	2.14

4.3.3. Water holding capacity

The water holding capacity (WHC) was evaluated in this study to determine whether the beds operated under moisture conditions that would allow drainage of contaminated water to compost bed base which could infiltrate into groundwater. Since WHC has very important relationship with physical and biological properties of bed compost materials, the moisture levels were set based on the WHC to find the real structure and texture conditions

of compost providing aeration and microbial activity. So, WHC was achieved in the first 12 hours of natural drainage from an initial moisture content greater than the media WHC.

The values of WHC and moisture content in 42 bed compost materials are illustrated in Figure 4.88. The average WHC of all bed compost was at 72.7% on a wet weight basis with a range of 53.6 to 79.8%. WHC was lower for bed compost in CBP barn 1 to the other materials tested and was able to hold water up to 53.6% w.b. moisture content. As expected, the smaller particle size range was able to hold more water (Table 4.5). WHC increases with increasingly fine particle size (decreasingly porosity), as can be seen in Figure 4.88. Coarse particle size of compost have a lower WHC since they are high in large pores subject to free drainage. Fine particle size have a greater occurrence of small pores that hold water against free drainage, resulting in a higher WHC values. Therefore, beds typically operate under MC conditions that would not allow drainage. Good operating range was 40-60% which is below WHC and that groundwater drainage would not occur when bed managed properly.

The present study indicates a positive relationship between WHC and moisture content ($r = 0.383$, $P < 0.05$), see Figure 4.88. Thereby, WHC increased with increasing moisture content. Ahn et al. (2008) reported that WHC increased with increasing moisture content until certain level. They suggested that moisture promotes aggregation of particles, and then decreased porosity. Finally, the lower porosity decreases the WHC.

The WHC method was adequate to estimate the maximum amount of moisture that could be added to the bed compost without the occurrence of adequate drainage or runoff, thus avoiding contamination of the soil or water outside the barn.

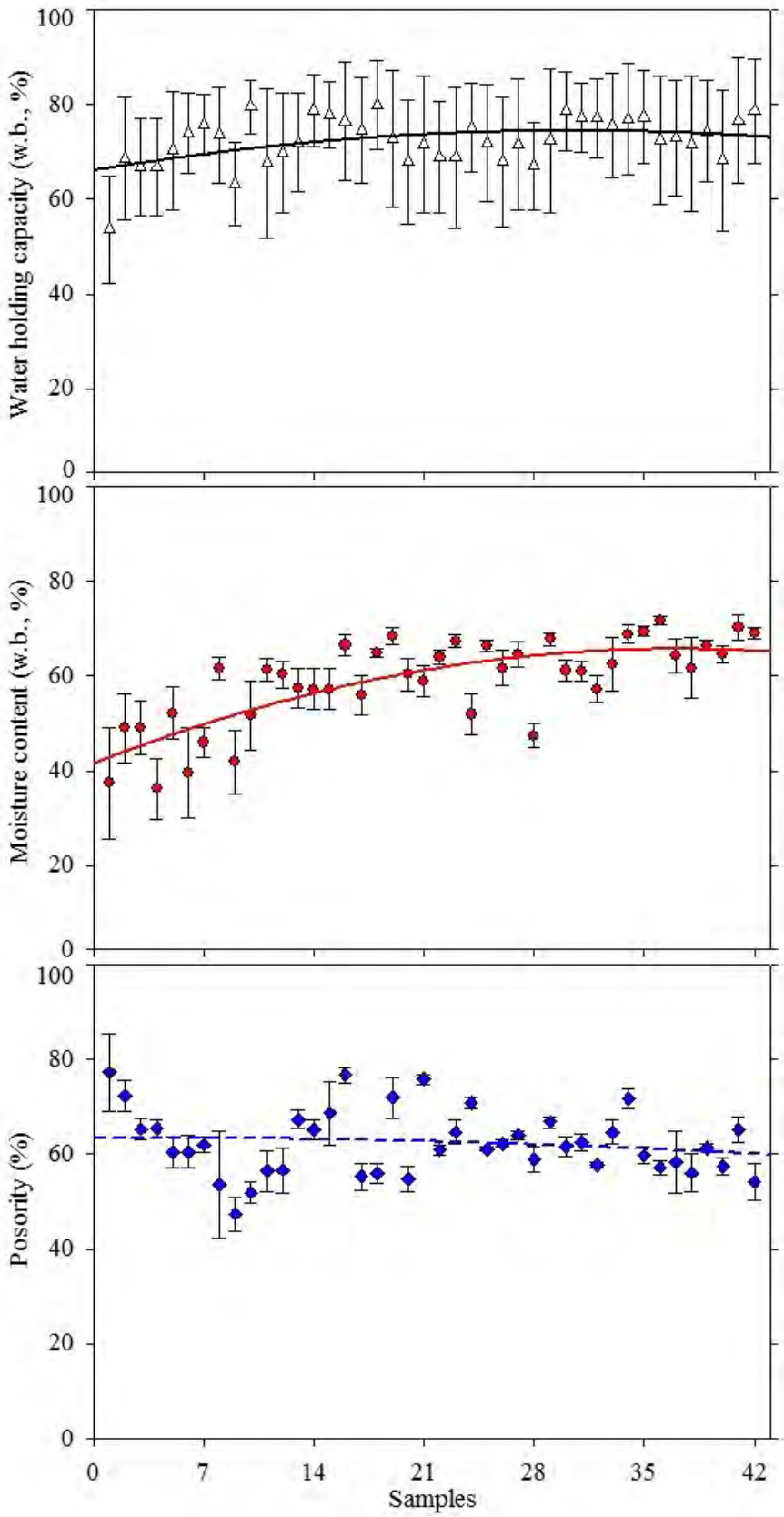

Figure 4.88 - Water holding capacity (w. b., %), initial moisture content (w. b., %), and porosity (%) of 42 bed compost materials.

4.3.4. Chemical properties of composts

Results related to total nitrogen (N), total carbon (C), and carbon-nitrogen ratio (C:N) of each bed compost material are shown in Figure 4.89. Each value is an average of nine samples collected as previously described (Figure 3.5). Further results regarding other chemical compounds are shown in Appendix A (Table 6).

The average total C was 42.7 ± 3.8% with a range of 29.8 to 47.1%. One of the major constituent of the compost, C, was most abundant (47.1%) in CBP barn 19. Only in the barn 9 contain average total C lower than 30.0%. Shane et al. (2010) reported a range total C of 12.7 to 20.1% in six compost barns in Minnesota collected in two different depth. Thus, the bed composts in Kentucky have not stabilized to the extend in this study. In general, many of the beds had not been operating properly, but as a result, the dairy producers learned how to improve beds to operate properly.

The average total N was 1.6% ranged from 0.5 to 2.5%. Shane et al. (2010) reported an average total N of 0.76% with a range of 0.61 to 0.89% during the winter. Barberg et al. (2007) reported an average total N of 2.54% with a range of 0.57 to 4.22%. Russelle et al. (2009) reported average N of 1.12% in eight compost barns in Minnesota. Janni et al. (2007) reported an average total N of 0.99% six compost barns in Minnesota. Overall, the total N from the 42 bed compost materials tested in the study was similar to those reported previously by Barberg et al. (2007) and Shane et al. (2010). Nitrogen level of compost material is an important factor in the determination of C:N ratio of the composted material. Microorganisms for building up their structure of the body require it (Iqbal et al., 2010).

The average C:N ratio was 28.5 ± 8.1. The C:N ratio of barn 10 (15.4) was lowest due to high nitrogen contents as compared to barn 12 (26.2). In barn 20 had the highest C:N ratio (43.9) to the other materials tested. Shane et al. (2010) reported the highest C:N ratio found was 26.0 during winter. Barberg et al. (2007) reported an average of 19.5. Russelle et al. (2009) reported a range of 11.2 to 20.9. Janni et al. (2007) reported an average C:N ratio of 15.5. For effective composting C:N ratio of the compost should be ranged 20 to 25 (Diaz et al., 1993). In another words, a C:N ratio below 25:1 may emit ammonia odor, which may influence the ammonia levels in the compost barns (Rosen et al., 2000). In general, in the present study it was balance enough. However, the barns 1, 3, 6, 9, 10, and 18 will require an additional source of nitrogen to obtain the optimum bedding compost C:N ratio between 20 and 25.

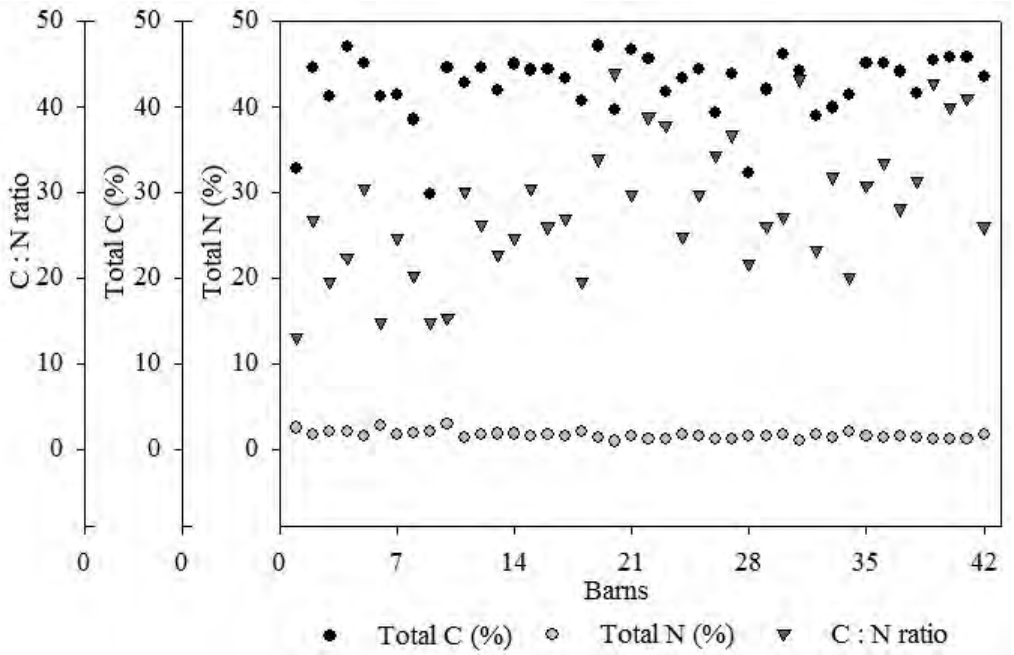

Figure 4.89 - Total Carbon (C), Total Nitrogen (N), and C:N ration presents in 42 bedding compost.

4.3.5. Bacterial analysis of composts

Figure 4.90 shows the pack bacterial count (*Coliform, E. Coli, Staphylococcal, Streptococcal,* and *Bacillus*) and the associated moisture content in the bedding compost material of 42 CBP barns.

Bedding compost always contained bacterial, but the variation was large between different sampling sites and times. However, *Coliforms* were not present in Barn 15 that had a higher compost temperature (Appendix A - Table 4). *Coliforms, E. Coli, Bacillus* and *Streptococcus* count were higher in the barn 4 that showed lower moisture content (36.2%). The average *Coliforms, E. Coli*, *Streptococcus* and *Bacillus* content in the bedding material of barn 4 were 247.5 ± 12.0 cfu/g, 173.0 ± 18.38 cfu/g, 3595.0 ± 148.49 cfu/g, and 1810.0 ± 608.11 cfu/g, respectably. Also, the environmental *Staphylococcus* were highest in the barn 6 that had an average of 2.700 ± 0.00 cfu/g. The present study indicates a inverse relationship between moisture content and bacterial counts (*Coliforms*, $r = 0.377$, $P < 0.05$; *E. Coli*, $r = 0.448$, $P < 0.05$; *Bacillus*, $r = 0.372$, $P < 0.05$). There are no significant relationships between bacterial counts (*Streptococcal and Staphylococcal*) with moisture content ($P > 0.05$).

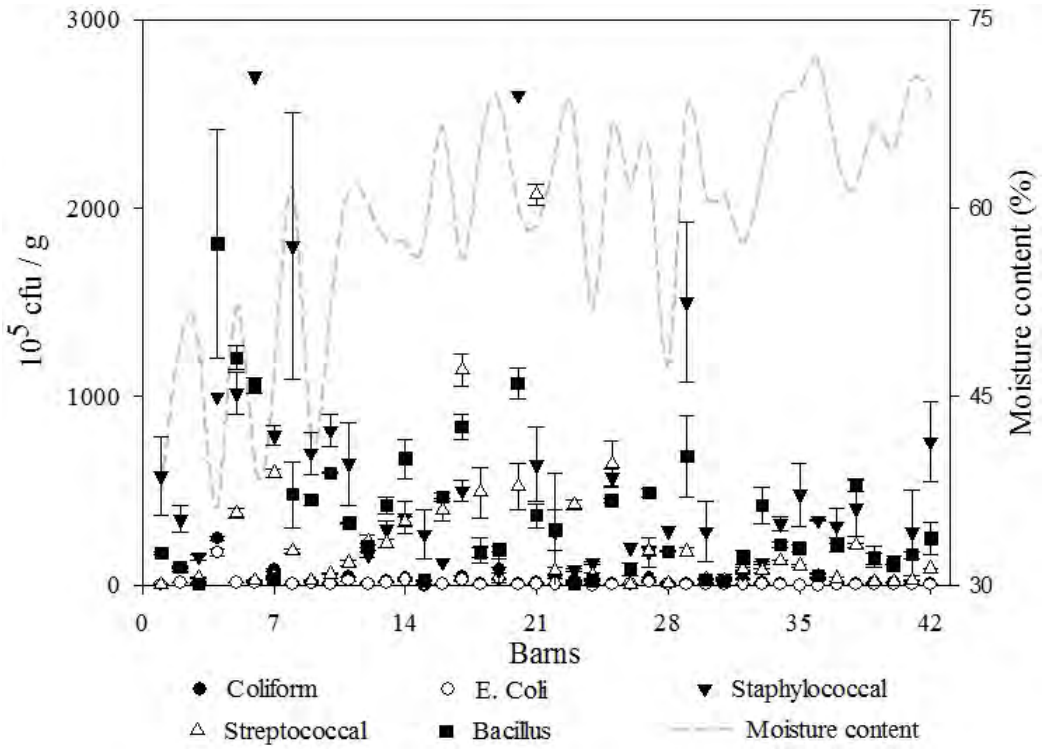

Figure 4.90 - Bacterial analysis of bedding compost samples in 42 CBP barns.

4.3.6. Thermal properties of composts

4.3.6.1. Thermal properties of composts in different moisture content and compaction degree

The thermal conductivity of unsegregated bed compost materials varied from 0.081 to 0.625 W m^{-1} K^{-1} for Green sawdust, 0.071 to 0.618 W m^{-1} K^{-1} for Kiln-dried shavings or sawdust, 0.059 to 0.766W m^{-1} K^{-1} for Mix, and 0.105 to 0.406 W m^{-1} K^{-1} for average of all compost material tested, depending upon the moisture content (30, 45, and 60%) and static compaction degree (fluffy, 0.0, 0.1, 0.2, 0.3, and 0.4 MPa) within the experimental range of the variables. An increasing trend in the thermal conductivity of all compost was also observed with the increase in both moisture content and static compaction degree for all compost material tested (Figure 4.91). The compost with low moisture content exhibited a low thermal conductivity because of the presence of a relatively high fraction of air (a poor conductor). The thermal conductivity increased with compaction due to a reduction in the void space (Chandrakanthi et al., 2005).

a) Thermal Conductivity:

Multiple regressions analysis for compost materials showed that there is also a linear relationship between thermal conductivity (k) and moisture content (MC) and static compaction degree (SC) as follows:

a) Green sawdust:

$$k_{green} = -0.0619 + 0.311 \cdot SC + 0.478 \cdot MC \qquad R^2 = 0.838 \quad (4.1)$$

b) Kiln-dried shavings or sawdust:

$$k_{kiln} = -0.0679 + 0.342 \cdot SC + 0.487 \cdot MC \qquad R^2 = 0.877 \quad (4.2)$$

c) Mix:

$$k_{Mix} = -0.0537 + 0.360 \cdot SC + 0.434 \cdot MC \qquad R^2 = 0.829 \quad (4.3)$$

d) Average of all compost material:

$$k_{Average} = -0.0612 + 0.338 \cdot SC + 0.467 \cdot MC \qquad R^2 = 0.852 \quad (4.4)$$

The response surface presented in Figure 4.91 was almost flat due to the fitted linear model, except at high moisture content and high static compaction degree, which showed an abrupt increase. The analysis of variance (Table 4.6) indicates a greater effect of the static compact degree (high F-value) than that of the moisture content on the thermal conductivity for Green sawdust and Kiln. However, the analysis of variance indicates a greater effect of the moisture content than that of the static compaction degree on the thermal conductivity for Mix. The magnitudes of respective regression coefficients in equations 4.1, 4.2, 4.3, and 4.4 also confirmed the results. The models seem adequately fitted based on the observation of high F-value as well as high coefficient of determination (R^2). The models accounted for 83.8% (Green sawdust), 87.7% (Kiln-dried shavings), 82.9% (Mix), and 85.2% (average of all compost material) variation in the thermal conductivity within the experimental range of input variables.

The maximum differences between measured and estimated values of the thermal conductivity were within ± 0.059 W m^{-1} K^{-1} (Green sawdust), ± 0.060 W m^{-1} K^{-1} (Kiln-dried shavings), ± 0.066 W m^{-1} K^{-1} (Mix), and ± 0.065 W m^{-1} K^{-1} (average of all compost material) in which define desirable levels of accuracy by the thermal sensor for estimating the thermal conductivity (Figure 4.92).

Figure 4.91 revealed that the thermal conductivity of bed compost also increased with increase in moisture content and static compaction degree. The thermal conductivity of leaf

compost increased linearly with increase water content and compaction degree, represented by volume fractions of air (Chandrakanthi et al., 2005). Details about statistic analysis can be seen in Appendix F.

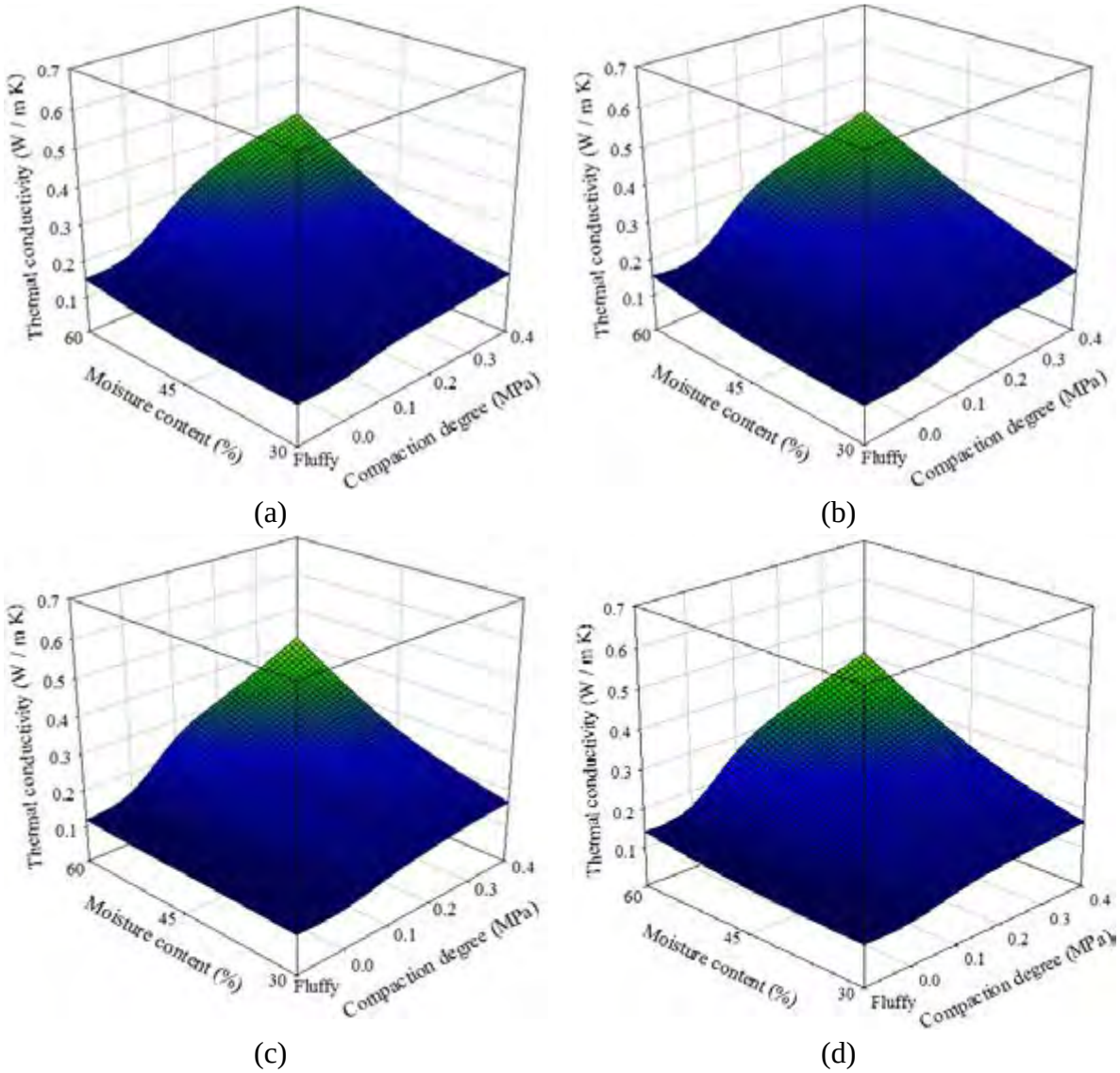

Figure 4.91 - Effect of moisture content and static compaction on thermal conductivity of bed compost materials: (a) Green sawdust, (b) Kiln-dried shavings or sawdust, (c) Mix, and (d) average of all compost material.

Table 4.6 - Analysis of variance for effect of moisture content and static compaction degree on thermal conductivity of bed compost materials.

Source of variation	Sum of squares	Degree of freedom	Mean sum of squares	F_{cal}-value*	Probability
Green sawdust					
Regression	0.1130	2	0.05630	38.863	<0.001
MC	0.0508	1	0.05080	35.030	<0.001
SC	0.0617	1	0.06170	42.551	<0.001
Residual	0.0217	15	0.00145		
Total	0.1340	17	0.00790		
Kiln-dried shavings or sawdust					
Regression	0.1250	2	0.06270	53.561	<0.001
MC	0.0612	1	0.06120	52.307	<0.001
SC	0.0642	1	0.06420	54.871	<0.001
Residual	0.0176	15	0.00117		
Total	0.1430	17	0.00841		
Mix					
Regression	0.1190	2	0.05950	36.375	<0.001
MC	0.0681	1	0.06810	41.524	<0.001
SC	0.0509	1	0.05090	31.036	<0.001
Residual	0.0246	15	0.00164		
Total	0.1440	17	0.00845		
Average of all compost material					
Regression	0.1190	2	0.0593	42.971	<0.001
MC	0.3380	1	0.3380	43.333	<0.001
SC	0.0467	1	0.0467	42.608	<0.001
Residual	0.0207	15	0.0207		
Total	0.1390	17	0.0082		

*Highly significant.

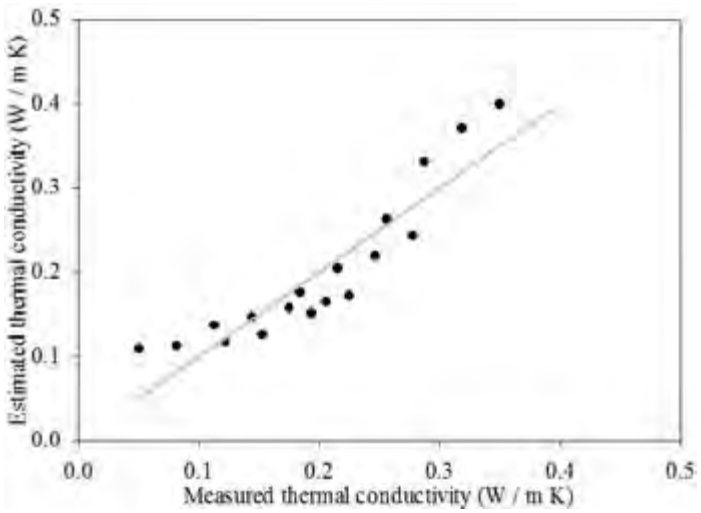

(a)

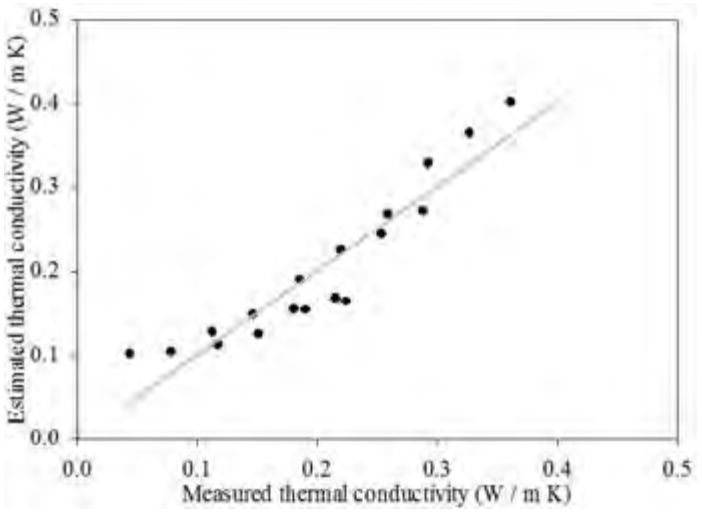

(b)

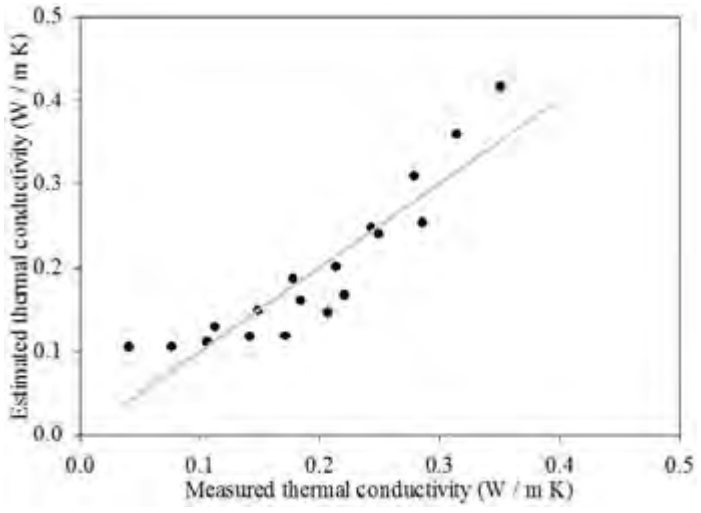

(c)

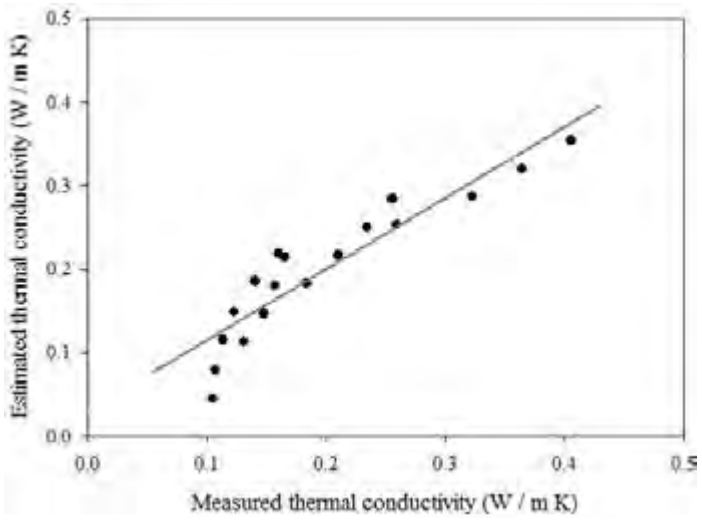

(d)

Figure 4.92 - Estimated thermal conductivity of bed compost materials versus measured values for (a) Green sawdust, (b) Kiln-dried shavings, (c) Mix, and (d) average of all compost material.

Thermal conductivity of bed compost materials as a function of moisture content (30, 45, and 60%) and dynamic compaction degree (0.1, 0.2, 0.3, and 0.4 MPa) are shown in Figure 4.93. Generally, the thermal conductivity increases with increasing moisture content and dynamic compaction. Theoretically, these values can be predictable because compaction over time has an direct effect, because it increases the bulk density of compost by reducing porosity, which increases the thermal conductivity. Thermal conductivity showed highest values at 60% of moisture content and 0.4 MPa of dynamic compaction degree of Green sawdust (0.643 W m^{-1} K^{-1}), Kiln-dried shavings or sawdust (0.626 W m^{-1} K^{-1}), Mix (0.788 W m^{-1} K^{-1}), and average of all compost material (0.244 W m^{-1} K^{-1}).

Multiple regressions analysis for compost materials showed that there is also a linear relationship between thermal conductivity (k) and moisture content (MC) and dynamic compaction degree (DC) as follows:

a) Green sawdust:

$$k_{green} = -0.131 + 0.269 \cdot DC + 0.689 \cdot MC \qquad R^2 = 0.925 \quad (4.5)$$

b) Kiln-dried shavings or sawdust:

$$k_{kiln} = -0.127 + 0.271 \cdot DC + 0.680 \cdot MC \qquad R^2 = 0.956 \quad (4.6)$$

c) Mix:

$$k_{Mix} = -0.122 + 0.193 \cdot DC + 0.623 \cdot MC \qquad R^2 = 0.934 \quad (4.7)$$

d) Average of all compost material:

$$k_{Average} = -0.123 + 0.274 \cdot DC + 0.664 \cdot MC \qquad R^2 = 0.944 \quad (4.8)$$

The analysis of variance indicates a greater effect of the dynamic compact degree (high F-value) than that of the moisture content on the thermal conductivity for all material tested, see Table 4.7. The magnitudes of respective regression coefficients (R^2) in equations 4.5, 4.6, 4.7, and 4.8 also confirmed the results. Thermal conductivity presented an excellent relationship with moisture content and dynamic compaction degree. To fit the curves to the observed data, a linear equation was used (Equations 4.5, 4.6, 4.7, and 4.8). This approach is a functional relationship selected purely by their mathematical flexibility to fit the experimental data points, being the main advantage that it does not require the determination of any additional compost material parameters. Authors in the literature have also used these type of equations to relate the compost moisture content and static compaction degree with different compost properties (Singh et al., 2007; Ahn et al., 2009).

The models seem adequately fitted based on the observation of high F-value as well as high coefficient of determination (R^2). The models accounted for 92.5% (Green sawdust), 95.6% (Kiln-dried shavings or sawdust), 93.4% (Mix), and 94.4% (average of all compost material) variation in the thermal conductivity within the experimental range of input variables. The maximum differences between measured and estimated values of the thermal conductivity were within ± 0.037 W m^{-1} K^{-1} (Green sawdust), ± 0.033 W m^{-1} K^{-1} (Kiln-dried shavings or sawdust), ± 0.045 W m^{-1} K^{-1} (Mix), and ± 0.036 W m^{-1} K^{-1} (average of all compost material), which is desirable accuracy for estimating the thermal conductivity (Figure 4.94). The statistic analysis can be seen in Appendix F.

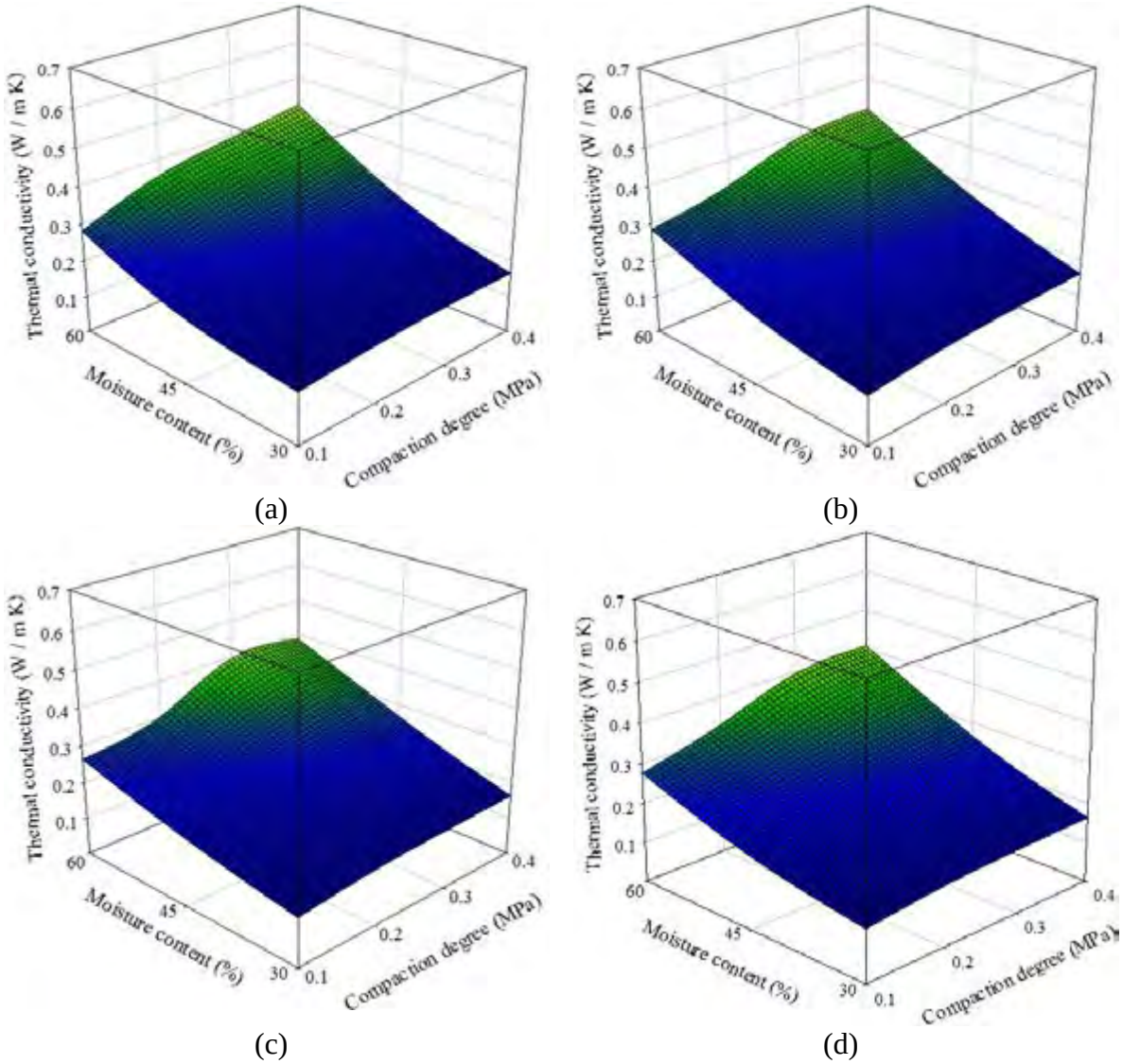

Figure 4.93 - Effect of moisture content and dynamic compaction on thermal conductivity of bed compost materials: (a) Green sawdust, (b) Kiln-dried shavings or sawdust, (c) Mix, and (d) average of all compost material.

Table 4.7 - Analysis of variance for effect of moisture content and dynamic compaction degree on thermal conductivity of bed compost materials.

Source of variation	Sum of squares	Degree of freedom	Mean sum of squares	F_{cal}-value*	Probability
Green sawdust					
Regression	0.09650	2	0.048200	55.323	<0.001
MC	0.01090	1	0.010900	12.500	0.006
DC	0.08560	1	0.085600	98.165	<0.001
Residual	0.00785	9	0.000872		
Total	0.10400	11	0.009480		
Kiln-dried shavings or sawdust					
Regression	0.09430	2	0.047100	98.891	<0.001
MC	0.01100	1	0.011000	23.060	<0.001
DC	0.08330	1	0.083300	174.63	<0.001
Residual	0.00429	9	0.000477		
Total	0.09860	11	0.008960		
Mix					
Regression	0.08160	2	0.04080	63.737	<0.001
MC	0.01180	1	0.01180	18.4375	0.002
DC	0.06980	1	0.06980	109.062	<0.001
Residual	0.00576	9	0.00064		
Total	0.08730	11	0.00794		
Average of all compost material					
Regression	0.09060	2	0.0453	76.520	<0.001
MC	0.01120	1	0.01120	18.918	0.002
DC	0.07940	1	0.07940	134.121	<0.001
Residual	0.00533	9	0.000592		
Total	0.09600	11	0.00872		

*Highly significant.

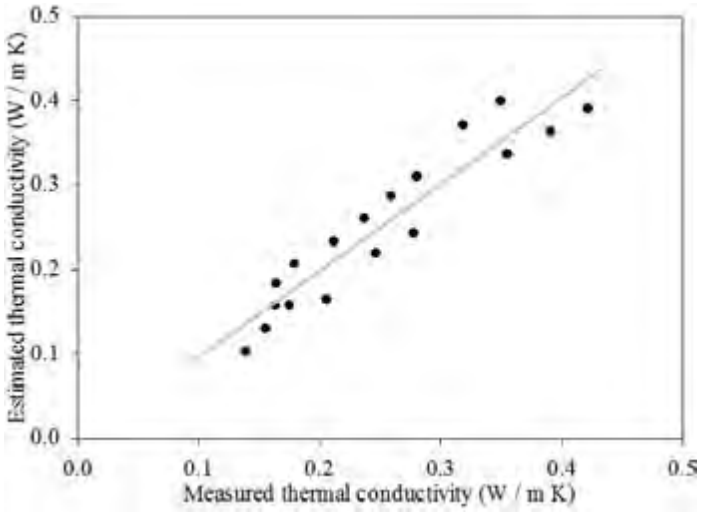

(a)

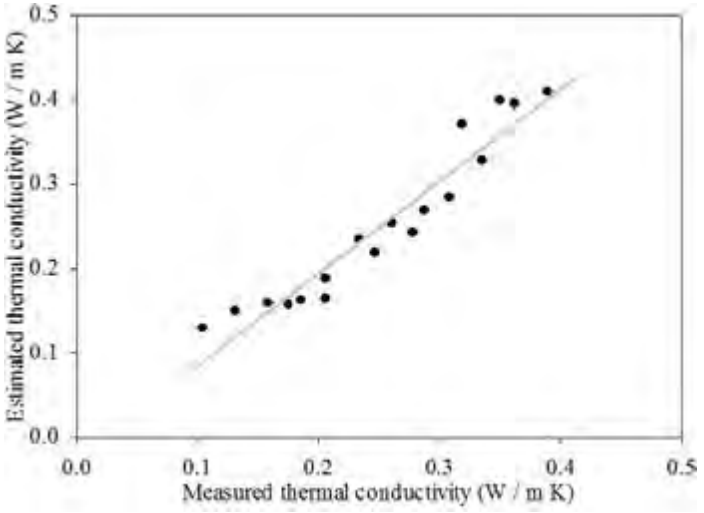

(b)

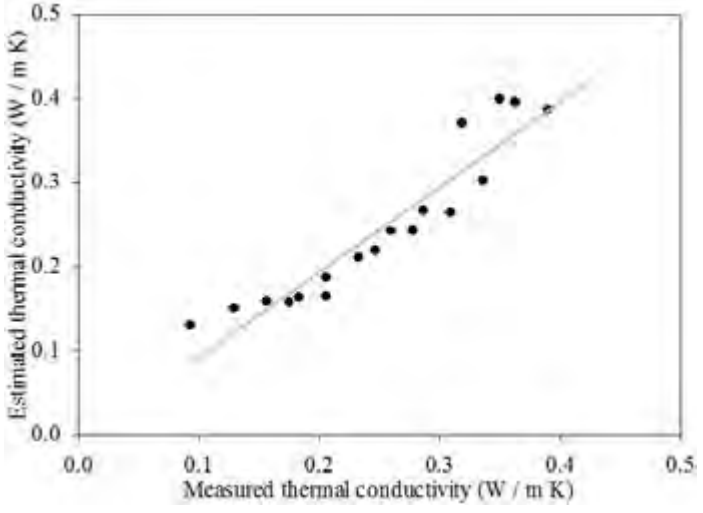

(c)

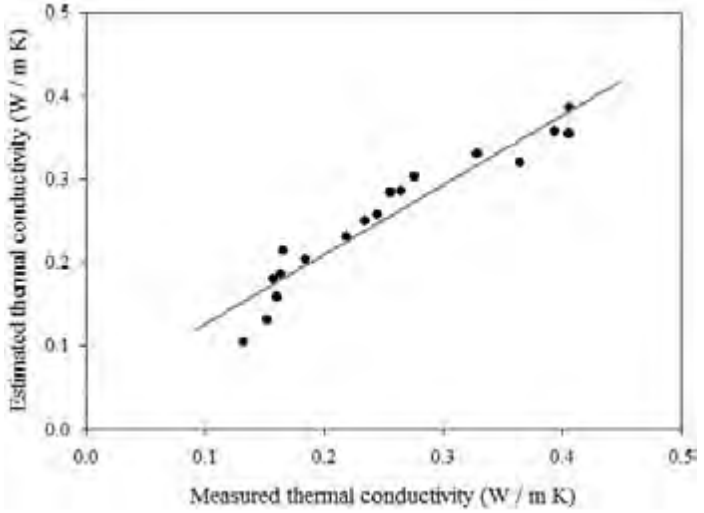

(d)

Figure 4.94 - Estimated thermal conductivity of bed compost materials versus measured values for (a) Green sawdust, (b) Kiln-dried shavings, and (c) Mix.

The analysis of variance between thermal conductivity and moisture content (30, 45, and 60%) and static compaction (fluffy, 0.0, 0.1, 0.2, 0.3, and 0.4 MPa) degree for all bed compost materials were obtained and are show in Figure 4.95 at the significance level of $p < 0.05$. The Tukey test shows that there was a significant difference between average values of moisture content and static compaction degree. These results indicate that the thermal conductivity increased as moisture content decreased in the order of 60% > 45% > 30% and thermal conductivity increased with the static compaction degree in order of 0.4 MPa > 0.3 MPa > 0.2 MPa > 0.1 MPa > 0.0 MPa = fluffy. Details about statistic analysis see Appendix F (Table 16).

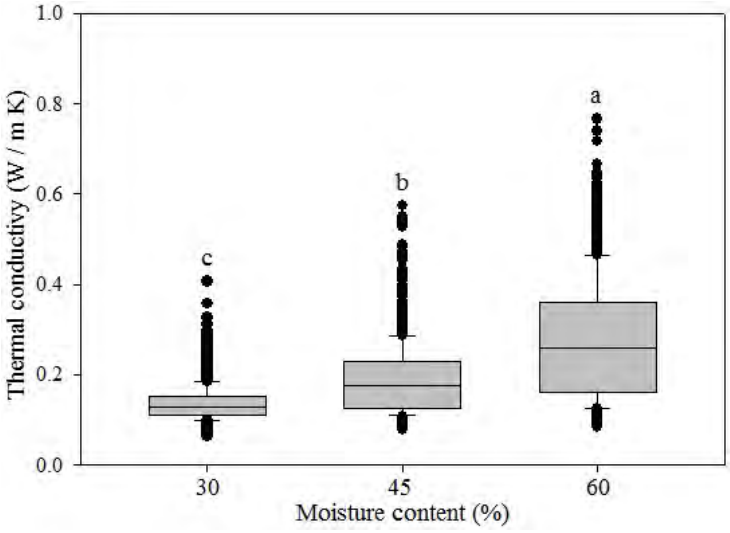

(a)

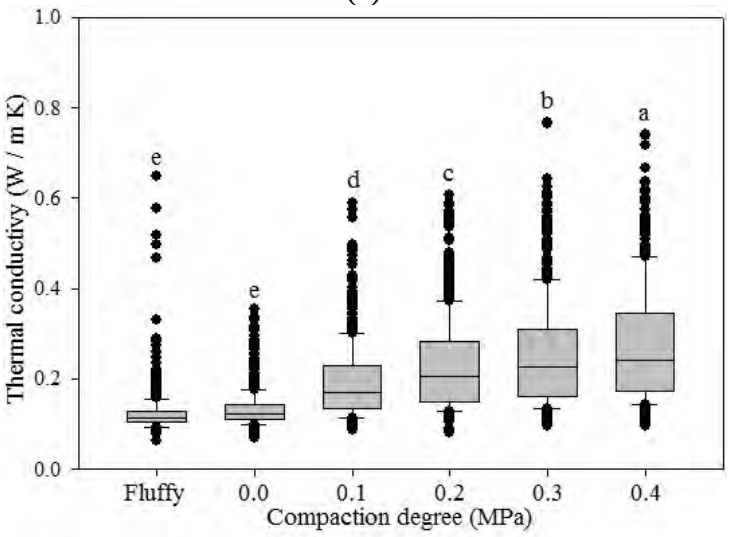

(b)

Figure 4.95 - Analysis of variance between thermal conductivity and moisture content (a) and static compaction degree (b) for all bed compost materials. Values followed by different letters are significantly different ($P < 0.05$; Tukey).

b) Thermal resistivity:

The variations in thermal resistivity of bed compost materials with moisture content (30, 45, and 60%) and static compaction degree (fluffy, 0.0, 0.1, 0.2, 0.3, and 0.4 MPa) are presented in Figure 4.96. The values of thermal resistivity of Green sawdust, Kiln-dried shavings or sawdust, Mix, and average of all compost material varied from 160.0 to 1240.5 °C cm / W, 161.7 to 1384.3 °C cm / W, 130.6 to 1253.3 °C cm / W, 269.5 to 962.6 °C cm / W, respectably, for experimental range of the variables. As depicted in Figure 4.96, an increasing trend in the thermal resistivity of bed compost was observed with the decrease in both moisture content and static compaction degree.

Multiple regression analysis showed that there is a linear relationship between dependent variable of the thermal resistivity (rho) and the independent variables of moisture content (MC) and static compaction degree (SC) as follows:

a) Green sawdust:

$$rho_{green} = 1229.382 - 825.693 \cdot SC - 1099.412 \cdot MC \qquad R^2 = 0.938 \quad (4.9)$$

b) Kiln-dried shavings or sawdust:

$$rho_{kiln} = 1282.485 - 972.177 \cdot SC - 1164.851 \cdot MC \qquad R^2 = 0.929 \quad (4.10)$$

c) Mix:

$$rho_{Mix} = 1229.610 - 987.615 \cdot SC - 948.268 \cdot MC \qquad R^2 = 0.916 \quad (4.11)$$

d) Average of all compost material:

$$rho_{Average} = 1247.159 - 928.495 \cdot SC - 1070.8 \cdot MC \qquad R^2 = 0.932 \quad (4.12)$$

The equations 4.9, 4.10, 4.11, and 4.12 were the first order linear model, so the response surface shown in Figure 4.96 were almost flat.

Analysis of variance (ANOVA) table was constructed to evaluate the individual effect of independent variables on the thermal resistivity (Table 4.8). The high F-values of regression confirmed the adequacy of the linear fitted model which accounted for 93.8% (Green sawdust), 92.9% (Kiln-dried shavings or sawdust), and 91.6% (Mix) variations of the thermal resistivity within the experimental range of the studied input variables. Comparison showed that the maximum differences between measured and estimated values of thermal resistivity were within ± 75.0 °C cm / W, ± 101.3 °C cm / W, ± 111.7 °C cm / W, and ± 87.316 °C cm / W which are desirable accuracy for estimating the thermal resistivity (Figure 4.97). Details about statistic analysis can be seen in Appendix F.

Comparing F-values of the moisture content and static compaction degree showed that the effect of moisture content on the thermal resistivity was higher (high F-value) than the effect of static compaction degree (low F-value), see Table 4.8.

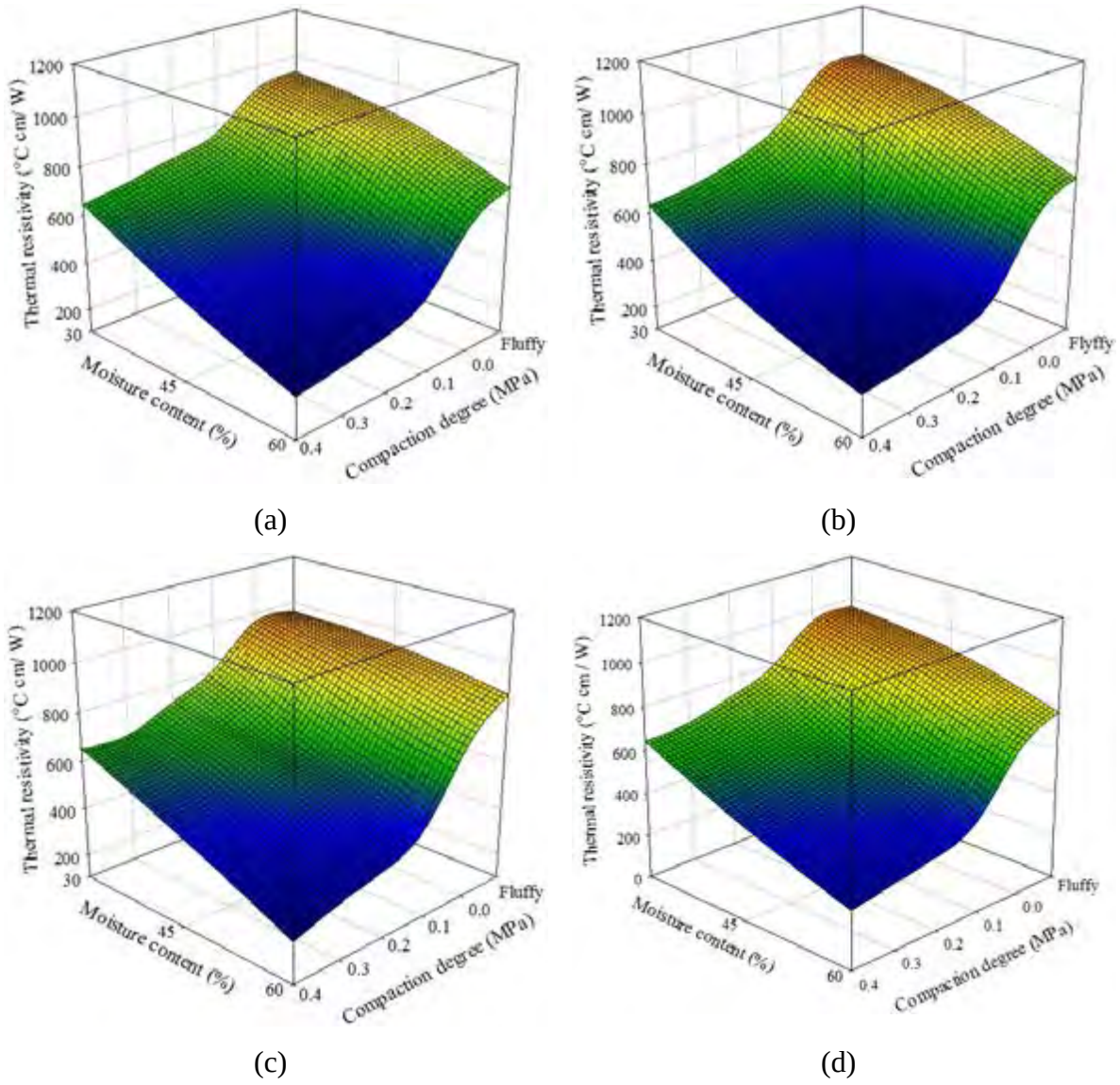

Figure 4.96 - Effect of moisture content and static compaction on thermal resistivity of bed compost materials: (a) Green sawdust, (b) Kiln-dried shavings or sawdust, (c) Mix, and (d) average of all compost material.

Table 4.8 - Analysis of variance for effect of moisture content and static compaction degree on thermal resistivity of bed compost materials.

Source of variation	Sum of squares	Degree of freedom	Mean sum of squares	F_{cal}-value*	Probability
Green sawdust					
Regression	684279.297	2	342139.648	113.361	<0.001
MC	357928.582	1	357928.582	118.592	<0.001
SC	326350.715	1	326350.715	108.129	<0.001
Residual	45272.289	15	3018.153		
Total	729551.586	17	42914.799		
Kiln-dried shavings or sawdust					
Regression	862548.929	2	431274.464	98.276	<0.001
MC	496191.886	1	496191.886	113.069	<0.001
SC	366357.043	1	366357.043	83.483	<0.001
Residual	65826.234	15	4388.416		
Total	928375.163	17	54610.304		
Mix					
Regression	754863.347	2	377431.674	82.195	<0.001
MC	512075.963	1	512075.963	111.517	<0.001
SC	242787.384	1	242787.384	52.873	<0.001
Residual	68878.560	15	4591.904		
Total	823741.907	17	48455.406		
Average of all compost material					
Regression	762214.467	2	381107.233	103.520	<0.001
MC	452603.798	1	452603.798	122.940	<0.001
SC	309610.669	1	309610.669	84.099	<0.001
Residual	55222.387	15	3681.4920		
Total	817436.854	17	48084.521		

*Highly significant.

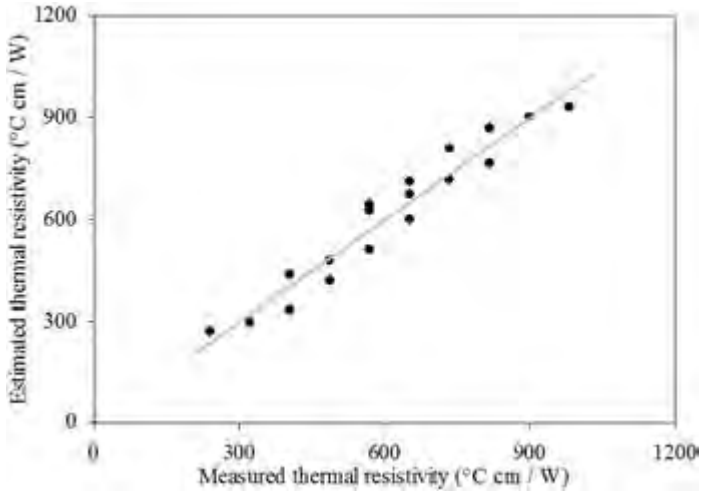

(a)

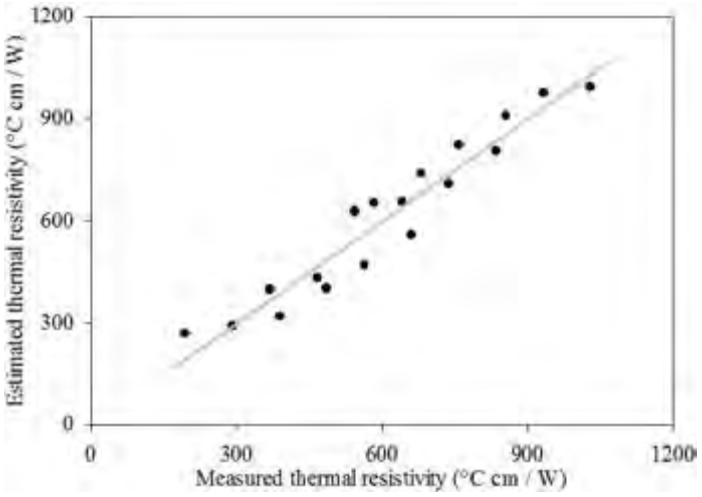

(b)

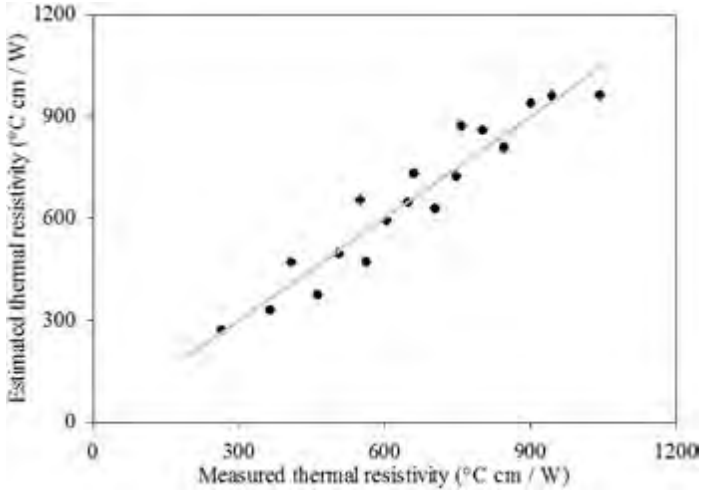

(c)

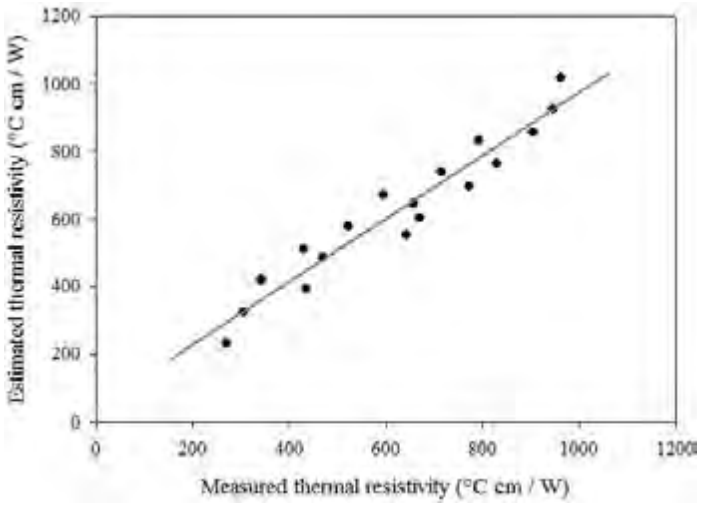

(d)

Figure 4.97 - Estimated thermal resistivity of bed compost materials versus measured values for (a) Green sawdust, (b) Kiln-dried shavings or sawdust, (c) Mix, and (d) average of all compost material.

Figure 4.98 shows the relationship between thermal resistivity as a function of moisture content (30, 45, and 60%) and dynamic compaction (0.1, 0.2, 0.3, and 0.4 MPa) for bed compost materials. The values of thermal resistivity of Green sawdust, Kiln-dried shavings or sawdust, Mix, and average of all compost material varied from 155.5 to 1092.0 °C cm / W, 159.7 to 1097.5 °C cm / W, 126.9 to 1128.6 °C cm / W, and 277.7 to 801.9 °C cm / W respectably, depending upon the moisture content and dynamic compaction degree within the experimental range of the variables.

An decreasing trend in the thermal resistivity of compost materials were also observed with the increase in moisture content and dynamic compaction degree (Figure 4.98). Multiple regression analysis showed that there is also a linear relationship between thermal resistivity (rho) and moisture content (MC) and dynamic compaction degree (DC) as follows:

a) Green sawdust:

$$rho_{green} = 1187.716 - 497.389 \cdot DC - 12.442 \cdot MC \qquad R^2 = 0.987 \quad (4.13)$$

b) Kiln-dried shavings or sawdust:

$$rho_{kiln} = 1211.623 - 532.158 \cdot DC - 12.924 \cdot MC \qquad R^2 = 0.959 \quad (4.14)$$

c) Mix:

$$rho_{Mix} = 1205.911 - 566.171 \cdot DC - 11.412 \cdot MC \qquad R^2 = 0.979 \quad (4.15)$$

d) Average of all compost material:

$$rho_{Average} = 1201.750 - 531.906 \cdot DC - 12.259 \cdot MC \qquad R^2 = 0.985 \quad (4.16)$$

The estimated values were compared with the measured thermal resistivity values. The linear relationship between measured and estimated values (Fig. 4.99) shows high correlation for all the materials. The estimated thermal resistivity from equations 4.13, 4.14, 4.15, and 4.16 depends on the moisture content and dynamic compaction degree of the compost materials. These interdependent relationships between thermal resistivity and the two measured parameters are presented in Figure 4.99. The maximum difference between measured and estimated values of the thermal resistivity were within ±32.1 °C cm / W (Green sawdust), ±68.7 °C cm / W (Kiln-dried shavings or sawdust), ±30.7 °C cm / W (Mix), and ±34.7 °C cm / W (average of all compost material), see Figure 4.99.

The analysis of variance (see Table 4.9) indicates a greater effect of the dynamic compaction degree (high F-value) than that of the moisture content on the thermal resistivity. The magnitudes of respective regression coefficients also confirmed the results (Equations 4.13, 4.14, 4.15, and 4.16). The models showed adequately fitted based on the observation of high F-value as well as high coefficient of determination (R^2). Details about statistic analysis can be seen in Appendix F.

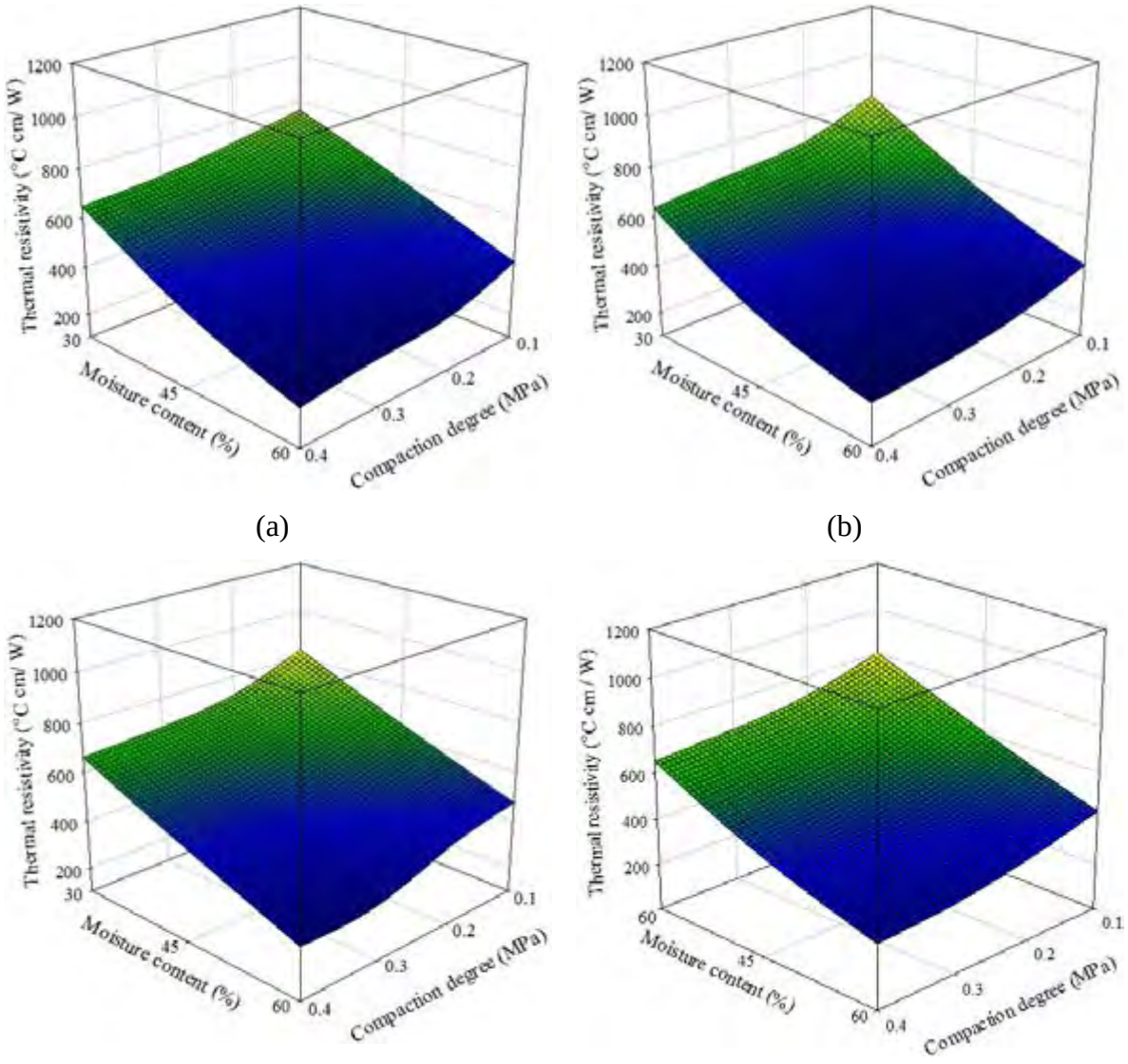

Figure 4.98 - Effect of moisture content and dynamic compaction on thermal resistivity of bed compost materials: (a) Green sawdust, (b) Kiln-dried shavings or sawdust, (c) Mix, and (d) average of all compost material.

Table 4.9 - Analysis of variance for effect of moisture content and dynamic compaction degree on thermal resistivity of bed compost materials.

Source of variation	Sum of squares	Degree of freedom	Mean sum of squares	F_{cal}-value*	Probability
Green sawdust					
Regression	315739.270	2	157869.635	333.989	<0.001
MC	37109.325	1	37109.325	78.508	<0.001
DC	278629.945	1	278629.945	589.469	<0.001
Residual	4254.112	9	472.679		
Total	319993.382	11	29090.307		
Kiln-dried shavings or sawdust					
Regression	343148.017	2	171574.009	128.428	<0.001
MC	42478.822	1	42478.822	31.796	<0.001
DC	300669.195	1	300669.195	225.060	<0.001
Residual	12023.558	9	1335.951		
Total	355171.575	11	32288.325		
Mix					
Regression	282514.235	2	141257.117	262.347	<0.001
MC	48082.414	1	48082.414	89.299	<0.001
DC	234431.821	1	234431.821	435.393	<0.001
Residual	4845.929	9	538.437		
Total	287360.164	11	26123.651		
Average of all compost material					
Regression	312966.440	2	156483.220	296.951	<0.001
MC	42438.574	1	42438.574	80.533	<0.001
DC	270527.865	1	270527.865	513.368	<0.001
Residual	4742.691	9	526.966		
Total	317709.130	11	28882.648		

*Highly significant.

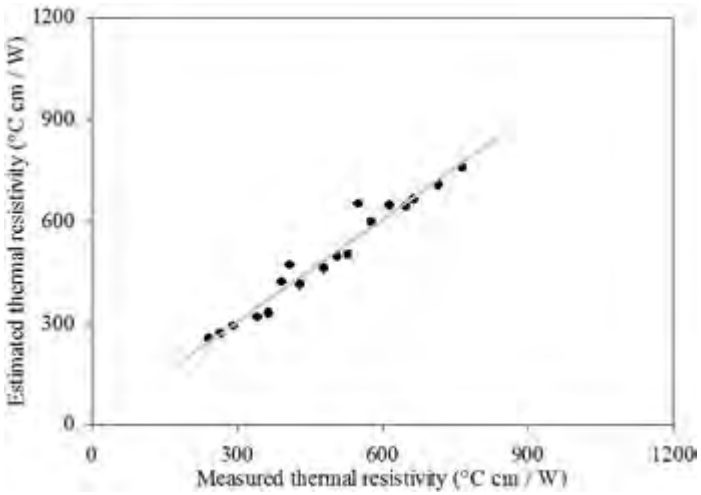

(a)

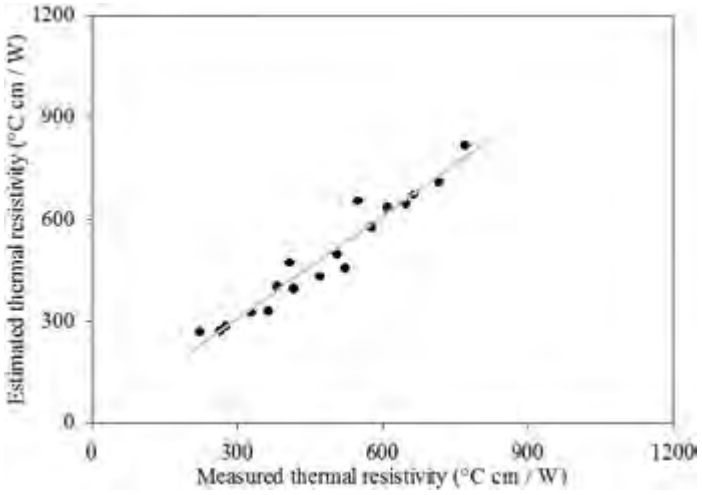

(b)

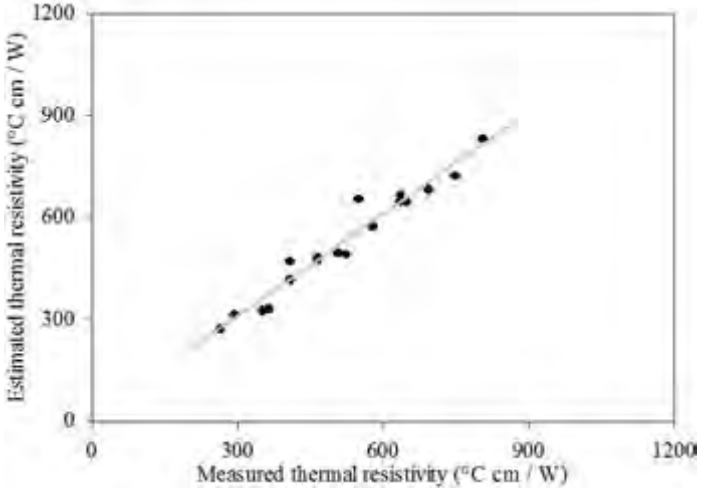

(c)

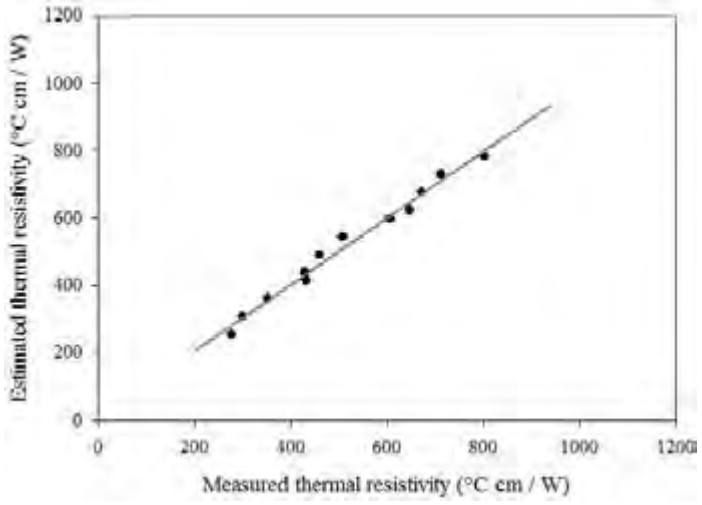

(d)

Figure 4.99 - Estimated thermal resistivity of bed compost materials versus measured values for (a) Green sawdust, (b) Kiln-dried shavings or sawdust, (c) Mix, and (d) average of all compost material.

The analysis of variance between thermal resistivity and moisture content (Figure 4.100a) and static compaction degree (Figure 4.100b) for all bed compost materials were obtained at the significance level of $p < 0.05$. The Tukey test shows that there was a significant difference between average values of thermal resistivity in different moisture content and static compaction degree. This results indicate that the distribution of moisture content decreased in the order of 30% > 45% > 60% and the distribution of static compaction degree decreased in order of fluffy < 0 MPa < 0.1 MPa < 0.2 MPa < 0.3 MPa < 0.4 MPa. Details about statistic analysis can be seen in Appendix F (Table 17).

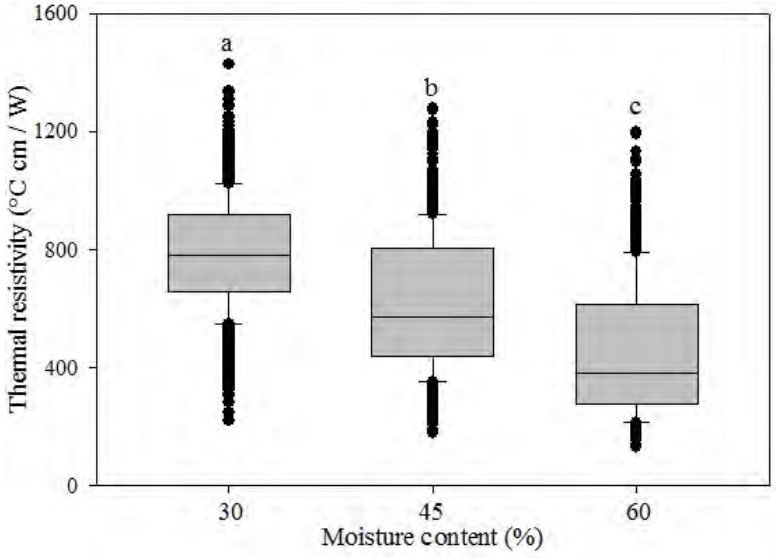

(a)

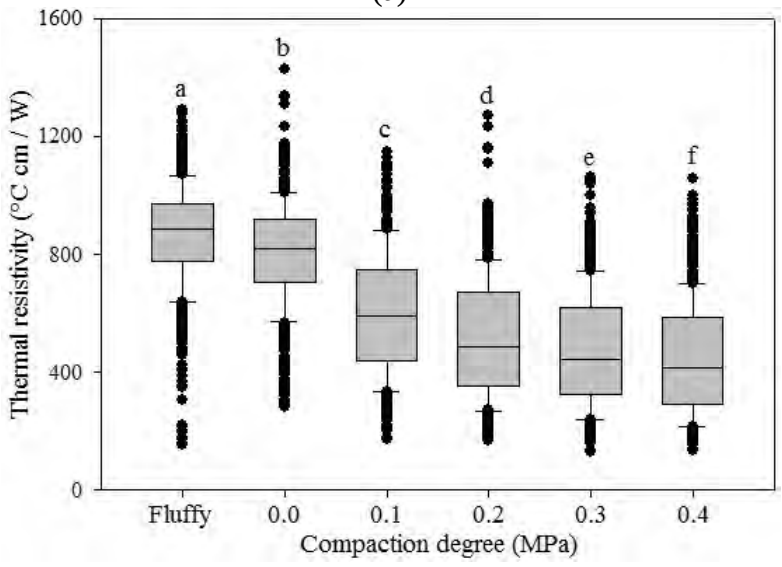

(b)

Figure 4.100 - Analysis of variance between thermal resistivity and moisture content (a) and static compaction degree (b) for all bed compost materials. Values followed by different letters are significantly different ($P < 0.05$; Tukey).

Thermal conductivity relationship to moisture content (30, 45, and 60%) and dynamic compaction (0.1, 0.2, 0.3, and 0.4 MPa) are shown in Figure 4.101. There was significant difference between the thermal conductivity measurements taken on all bed compost materials for different moisture content and dynamic compaction degree ($p < 0.05$). This results indicate that the thermal conductivity increased in the order of 30% < 45% < 60% moisture content and increased in order of 0.1 MPa < 0.2 MPa < 0.3 MPa < 0.4 MPa dynamic compaction degree. Details about statistic analysis can be seen in Appendix F.

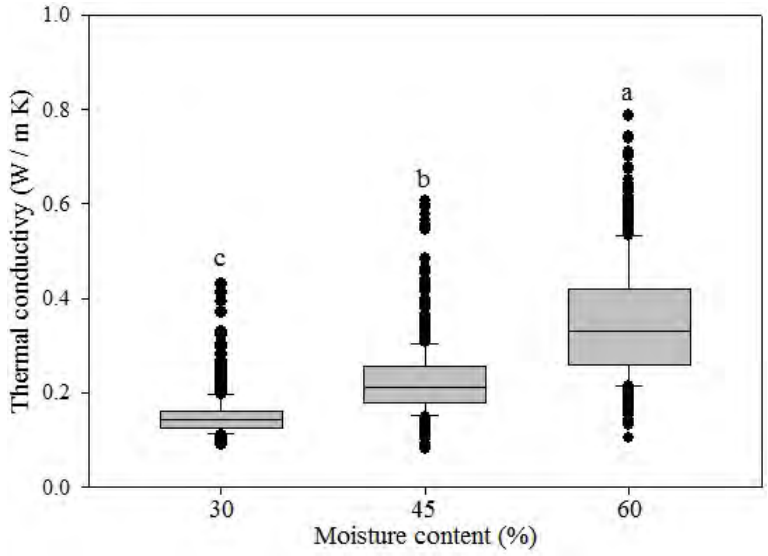

(a)

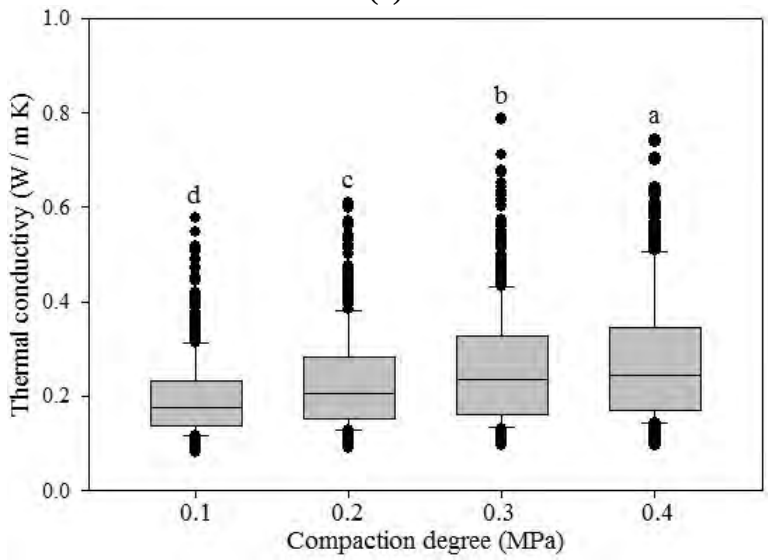

(b)

Figure 4.101 - Analysis of variance between thermal conductivity and moisture content (a) and dynamic compaction degree (b) for all bed compost materials. Values followed by different letters are significantly different ($P < 0.05$; Tukey).

The Tukey test was used to evaluate the moisture content (30, 45, and 60%) and dynamic compaction (0.1, 0.2, 0.3, and 0.4 MPa) on the thermal resistivity each had a significant effect as shown by the ANOVA (Appendix F - Table 19). This results indicate that the thermal resistivity decreased in the order of 30% > 45% > 60% moisture content (Figure 4.102a). and the distribution of decreased in order of 0.1 MPa > 0.2 MPa > 0.3 MPa > 0.4 MPa dynamic compaction degree (Figure 4.102b).

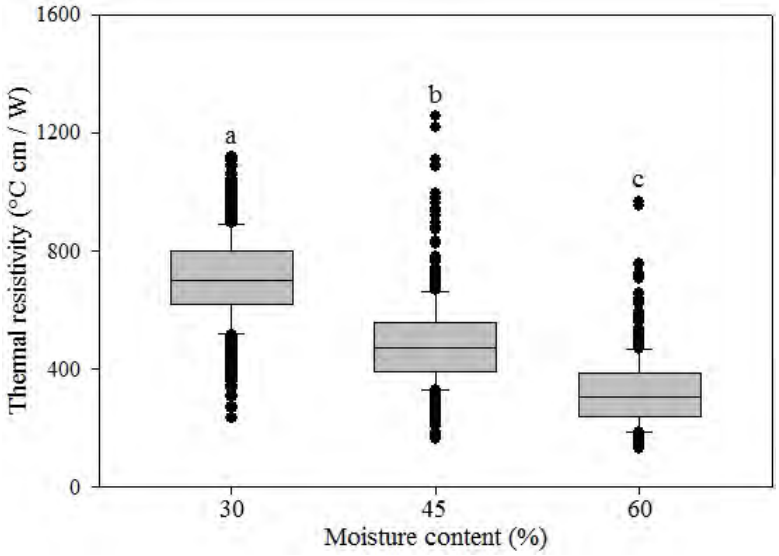

(a)

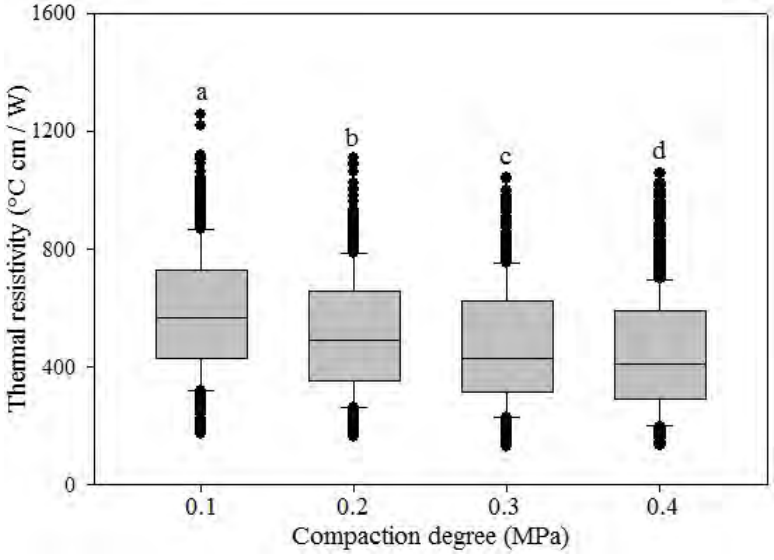

(b)

Figure 4.102 - Analysis of variance between thermal resistivity and moisture content (a) and dynamic compaction degree (b) for all bed compost materials. Values followed by different letters are significantly different (P < 0.05; Tukey).

4.3.6.2. Thermal properties of composts in different particle size

Thermal conductivity and thermal resistivity of granular materials are affected by particle contact quality. The number of contacts per particle depend on the packing density, particle shape and particle size distribution. Their effects on thermal conductivity and thermal resistivity are explored in this section using selected compost materials and the thermal needle probe technique (Decagon KD2-Pro sensor).

Figure 4.103 showed the influence of particle size in the thermal conductivity and thermal resistivity for bed compost samples using Green sawdust, Kiln-dried shavings or sawdust, and Mix. Thermal conductivity and thermal resistivity were plotted versus particle size distribution, just that these two properties were directly observed data. Values of thermal properties and thermal resistivity were not measured in samples of coarser material because it was not possible to insert the probe of sensor into the sample.

The thermal conductivity increases with the decrease of particle size, while thermal resistivity decreases with the increase of particle size. However, as seen in Figure 4.103, the overall thermal conductivity and thermal resistivity varied with each particle size of bed compost materials. In general, the thermal conductivity increased with increasing particle size, while thermal resistivity decreased with increasing particle size what is the exact opposite of what was expected (Yun and Santamarina, 2008; Ahn et al., 2009). This behavior can probably be explained by considering the higher moisture retention of larger particles once compost materials were air dried at the same time. It could possibly have changed the values of the thermal properties. Thus, the effect of particle size on thermal conductivity was more pronounced at higher particle size than at lower particle size. However, the trend of thermal conductivity as a function of particle size, in some barns, was very consistent at particle size below than 4.75 mm. It was also observed that thermal conductivity increased drastically with large particle sizes higher than 8.00 mm.

The effect of particle size on thermal conductivity was more pronounced for the higher particle size than at lower particle size. However, the tendency of lower thermal conductivity as a function of particle size was very consistent at particle sizes below than 4.75 mm. It was also observed that thermal conductivity increased drastically (> 85%) with large particle sizes higher than 8.00 mm. Thermal resistivity shows a decrease as the compost particle size increases after the 4.75 and 5.60 mm range in Mix material (Fig. 4.103c).

The average values and standard deviation of thermal resistivity for all particle sizes were 585.1 ± 117.0°C cm / W (Green sawdust), 600.8 ± 140.8°C cm / W (Kiln-dried shavings or sawdust), and 572.4 ± 109.0°C cm / W (Mix), respectively. In a compost material with smaller particle sizes, a fraction of the particles form a resistivity pathway, which could result in enhanced thermal resistivity.

The analysis of variance between thermal conductivity and compost particle size ranges for all bed compost materials (moisture content ≈ 30%) is shown in Figure 4.104. The Tukey test with a significance level of $p < 0.05$ was applied. There was significant differences between the thermal conductivity and compost particle size. In general, the values of thermal conductivity were higher in compost materials with particle sizes larger than 8.00 mm. Details about statistic analysis can be seen in Appendix F (Table 2).

The thermal conductivity of bed compost materials varied from 0.088 to 0.608 W m^{-1} K^{-1} depending upon the particle size. An increasing trend in the thermal conductivity of bed compost materials was also observed with the increase particle size (Figure 4.104), which is in general agreement with previous findings of some researchers. Investigations of Ahn et al. (2009) showed that the thermal conductivity of 0.03 to 0.05 W m^{-1} K^{-1} to dry sawdust and 0.03 to 0.06 W m^{-1} K^{-1} to dry wood shavings.

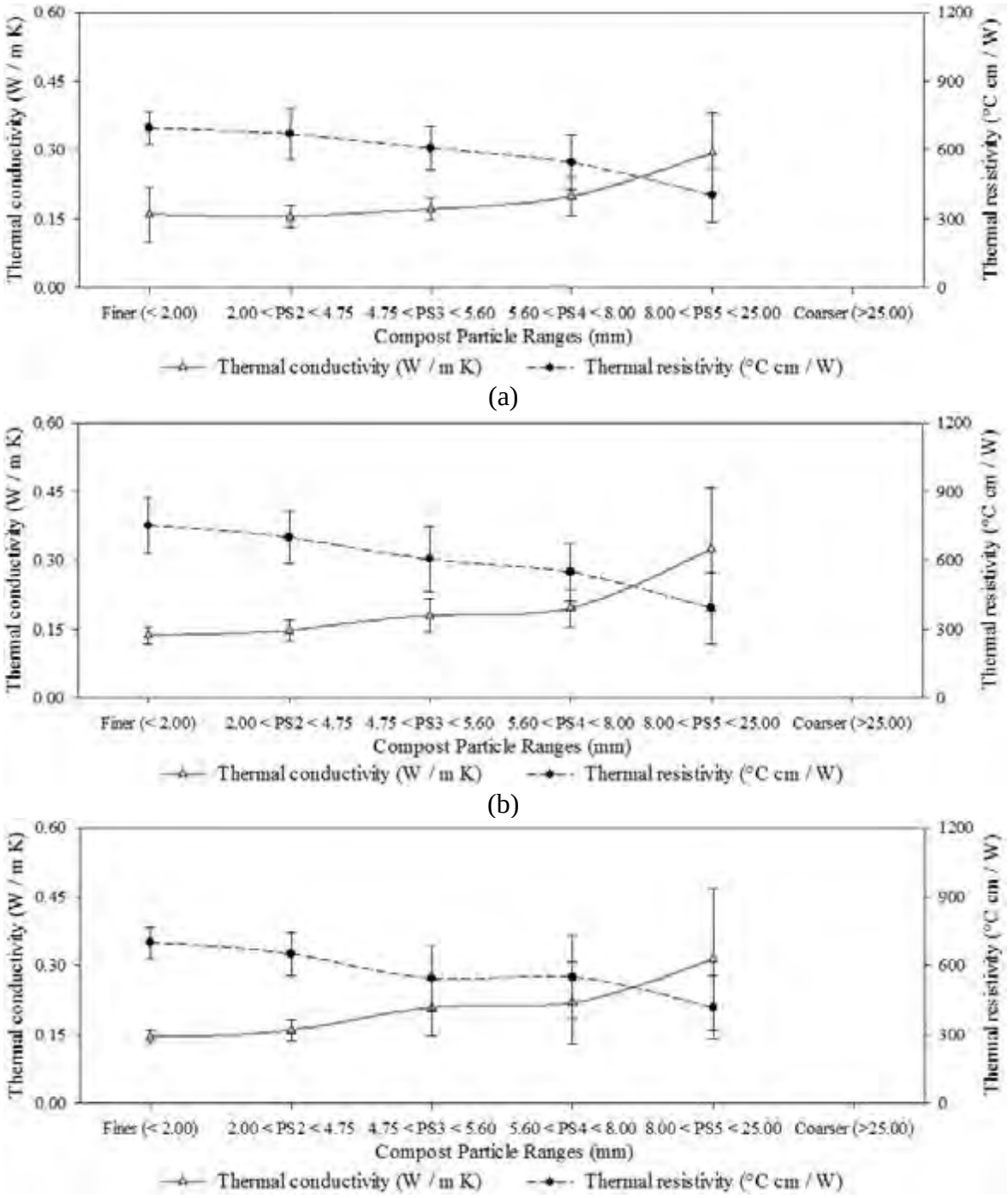

Figure 4.103 - Changes in thermal conductivity (W / m K) and thermal resistivity with different compost particle size of compost materials: (a) Green sawdust, (b) Kiln-dried shavings or sawdust, and (c) Mix.

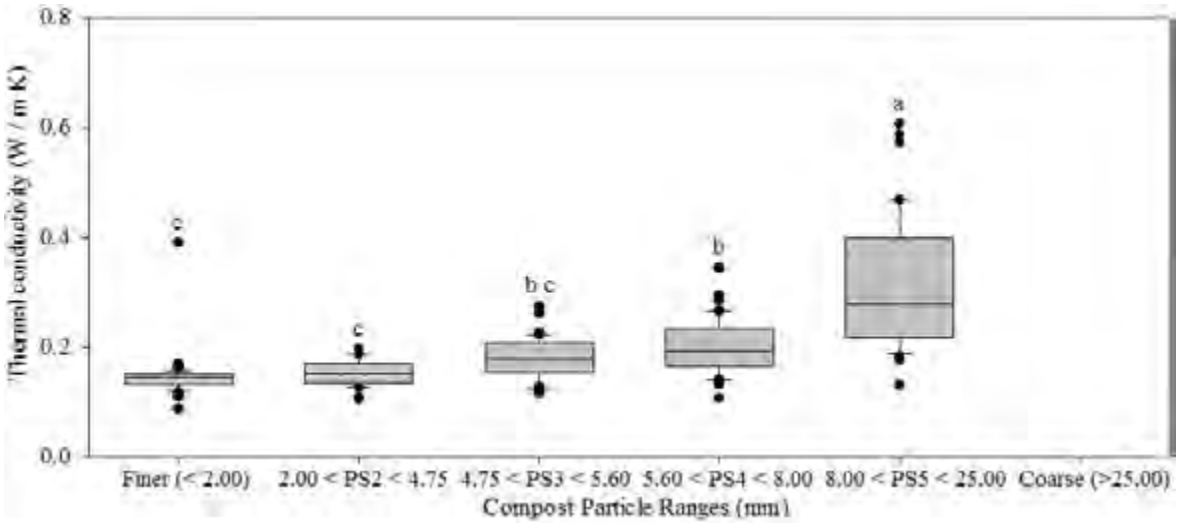

Figure 4.104 - Analysis of variance between thermal conductivity and compost particle ranges (mm) for all bed compost materials. Values followed by different letters are significantly different ($P < 0.05$; Tukey).

Thermal resistivity ranged from 170.2 °C cm / W to 1139.3 °C cm / W with a mean value of 590.7 °C cm / W and associated standard deviation of 163.9 °C cm / W. However, changes in thermal resistivity depending on the weights of each particle in a bed mixture.

The analysis of variance between thermal resistivity and particle size ranges for all bed compost materials was obtained and show in Figure 4.105 at the significance level of $p < 0.05$. The Tukey test shows that there was a significant difference between the values of thermal resistivity and compost particle size. The values of thermal resistivity for all bed compost materials were statistically higher in lower particle size (Finer and PS2). The average values of thermal resistivity in particle size between 4.75 and 8.00 mm (PS3 and PS4) were statistically similar. This results are already expected due to increased particle contact and particle shape effect with the probe of the sensor, thereby increasing the resistance of the heat transfer. More Details about statistic analysis, see Appendix F.

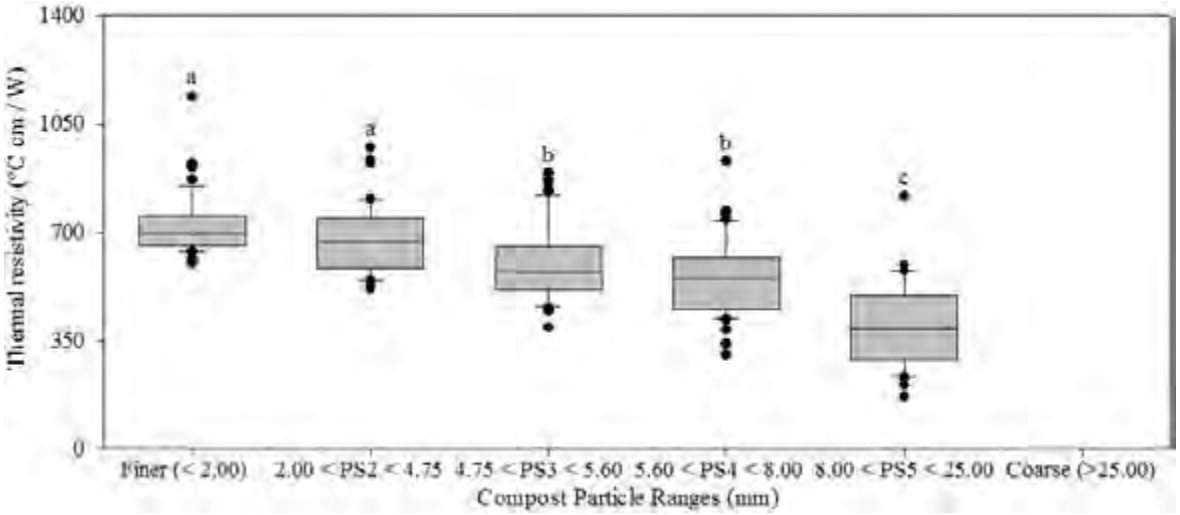

Figure 4.105 - Analysis of variance between thermal resistivity (°C cm / W) and compost particle ranges (mm) for all bed compost materials. Values followed by different letters are significantly different ($P < 0.05$; Tukey).

4.4. Develop computational fluid dynamics (CFD) model of compost barn

4.4.1. Mesh details

The most important aspect of the CFD model, as regards its meshing, was the eave and ridge openings areas which, in order to resolve the small length scale and sharp gradient in the airflow, required a high-resolution mesh. On the other hand, near the top of the computational domain, cells could be relatively large. The mesh type is very important for accurate CFD calculation. The meshes can be mainly composed of hexahedral and tetrahedral volume mesh elements for a 3-D computational domain (Lee et al., 2007). Because of the complicated shapes of the CBP barn, a tetrahedral mesh was built in commercial ANSYS ICEM CFD® and a test of the different meshes was carried out using this software. Various size of tetrahedral meshes were used, and after several levels of previously evaluated refinement, no significant differences ($p < 0.05$) in the air velocity and air temperature were encountered. Thus, the selected mesh was composed of 162,191 nodes and 683,222 elements (Figure 4.106). Such a meshing system was found to conform easily to the exact boundary of the scale model.

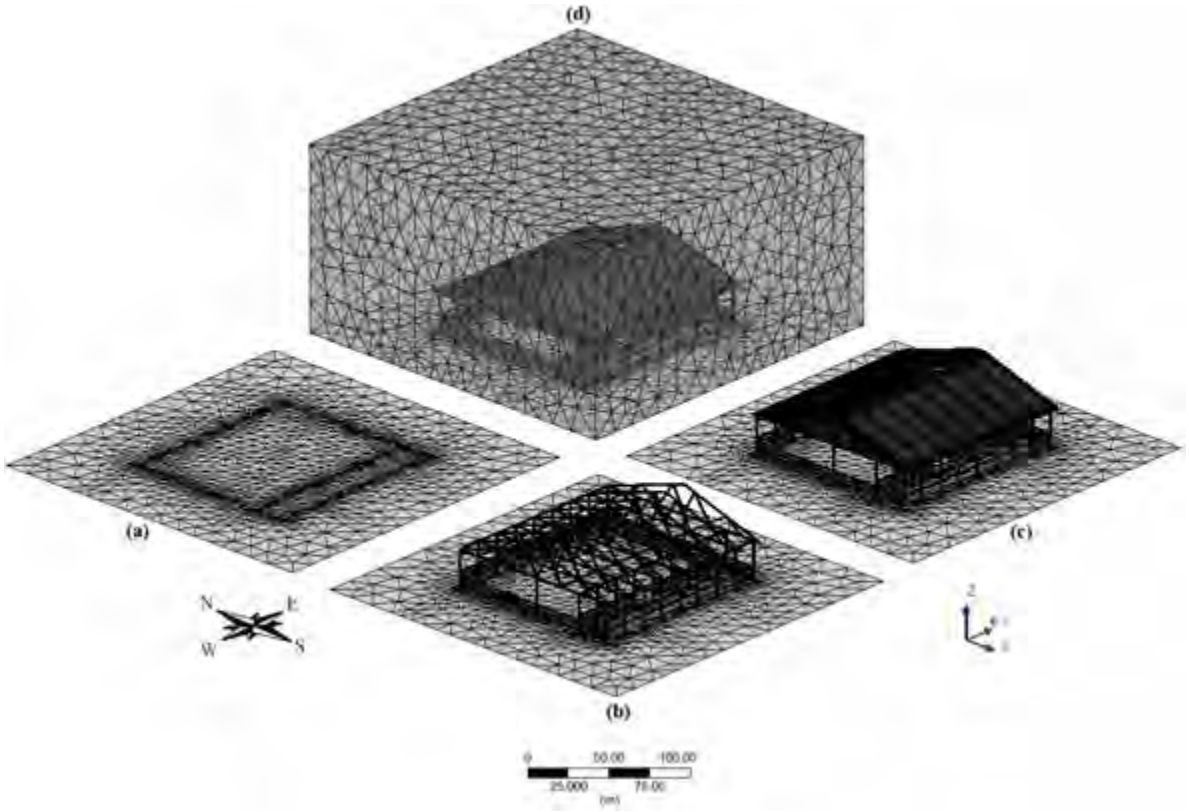

Figure 4.106 - Computational grid mesh detail of the scale model: (a) sidewall and compost pack area, (b) external structure, (c) barn model with roof, and (d) the volume mesh.

Although designing meshes was very time consuming, it was one of the most important procedures to effectively increase the accuracy of CFD results. Unlike the CFD models developed for other engineering fields, the natural ventilation study of agricultural buildings requires a very big computational domain because a vertically and horizontally sufficient area should be secured around the dairy barns. This larger volume needs to be enough to for simulating natural air flow. If the distance between the dairy barn and the boundary walls of the computational domain was not sufficiently secured, the faster airflow stream could be compared with the natural airflow resulting in unreal airflow around the leeward vent opening (Lee et al., 2007). In this study, the size of the CFD domain used during the simulations was chosen in order to ensure that the position of the outer boundaries did not compromise the CFD solution.

The computational domain was 2.40 x 2.40 x 1.20 m and the internal measured barn model area was 1.20 x 1.33 m. The airflow data in the CBP barn is much more important than that of the external area, but the adjacent area of the CBP barn is also very critical to

make a reliable air velocity distribution around the structure. To effectively the total mesh numbers, the dense meshes should be located in the CBP barn model and the mesh size had to be designed gradually bigger as with distance from the CBP barn. The study also found that it was very critical not to make a big and sudden change of mesh size between adjacent meshes. It was assumed that the mesh quality including density and shape around the external surface of the CBP barn model affected the external airflow and air pressure distribution of the CBP barn, which greatly influenced the natural ventilation. Details about refinement of the computational tetrahedral mesh can be seen in Figure 4.107.

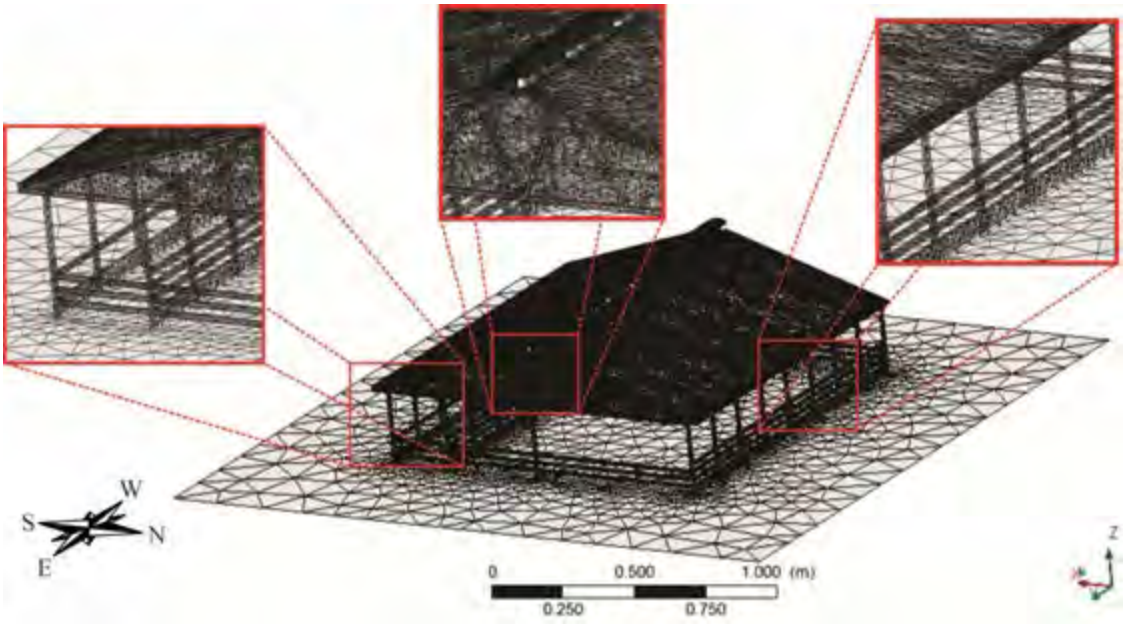

Figure 4.107 - Refinement detail of the computational tetrahedral mesh.

4.4.2. Validation of reduced model and simulations

Figures 4.108 to 4.115 shows the values of the average standard errors for the variables studied (air velocity and temperature) for all treatments tested (Closed ridge - CLR; Open ridge - OPR; Open ridge with chimney - ORC; Elevated ridge - ELR; and Overshot ridge - OVR) in each section and three different heights of data collection.

The simulations were performed to validate the CFD model and showed that the average standard errors between the simulated and measured values for air velocity in all treatments tested, using an air speed of 0.1 m s^{-1}, wind direction south to north, and three different heights, were 0.02 m s^{-1} (± 0.01), 0.02 m s^{-1} (± 0.01), 0.01 m s^{-1} (± 0.01), 0.01 m s^{-1} (± 0.01), and 0.02 m s^{-1} (± 0.01), respectively. Thus, the average standard errors for air

temperature were 0.22°C (± 0.17), 0.65°C (± 0.74), 0.74°C (± 0.54), 0.08°C (± 0.88), and 0.82°C (± 0.91), respectively (see Figure 4.108). However, testing the other condition (air speed of 1.0 m s^{-1}), the highest the average standard errors between the simulated and measured values for air velocity and temperature values were 0.09 m s^{-1} (± 0.12) and 0.93°C (± 0.71), respectively, as can be seen in Figure 4.109.

The highest average standard errors between the simulated and measured values for air velocity (0.02 m s^{-1} ± 0.01) and temperature (0.95°C ± 1.01), using air speed of 0.1 m s^{-1} and wind direction of north to south (perpendicular to ridge) were found in treatment ORC, see Figure 4.110. Thus, using the other air speed (1.0 m s^{-1}), the highest average standard errors between the simulated and measured values for air velocity and temperature were 0.13 m s^{-1} (± 0.10) and 1.17°C (± 1.12), respectively (see Figure 4.111).

The average standard error between simulated and measured air velocity and temperature, using air speed of 0.1 m $s^{-1}$and wind direction of east to west were 0.01 m s^{-1} with a range from 0.00 to 0.03 m s^{-1}, and 1.13°C with a range from 0.05 to 3.35°C, respectively (see Figure 4.112). To other air speed tested (1.0 m s^{-1}), the average standard error between simulated and measured air velocity and temperature were 0.23 m s^{-1} with a range from 0.00 to 0.47 m s^{-1}, and 0.85°C with a range from 0.05 to 3.05°C, respectively (see Figure 4.113).

The highest the average standard errors between simulated and measured values were 0.01 m s^{-1} (± 0.01) for air velocity and 0.72°C (± 0.58) for temperature, using air speed of 0.1 m $s^{-1}$and wind direction of west to east (Figure 4.114). However, using air speed (1.0 m s^{-1}), the highest average standard error between simulated and measured variables studied were 0.18 m s^{-1} (± 0.06) and 0.78°C (± 0.37) for these treatments tested (see Figure 4.115).

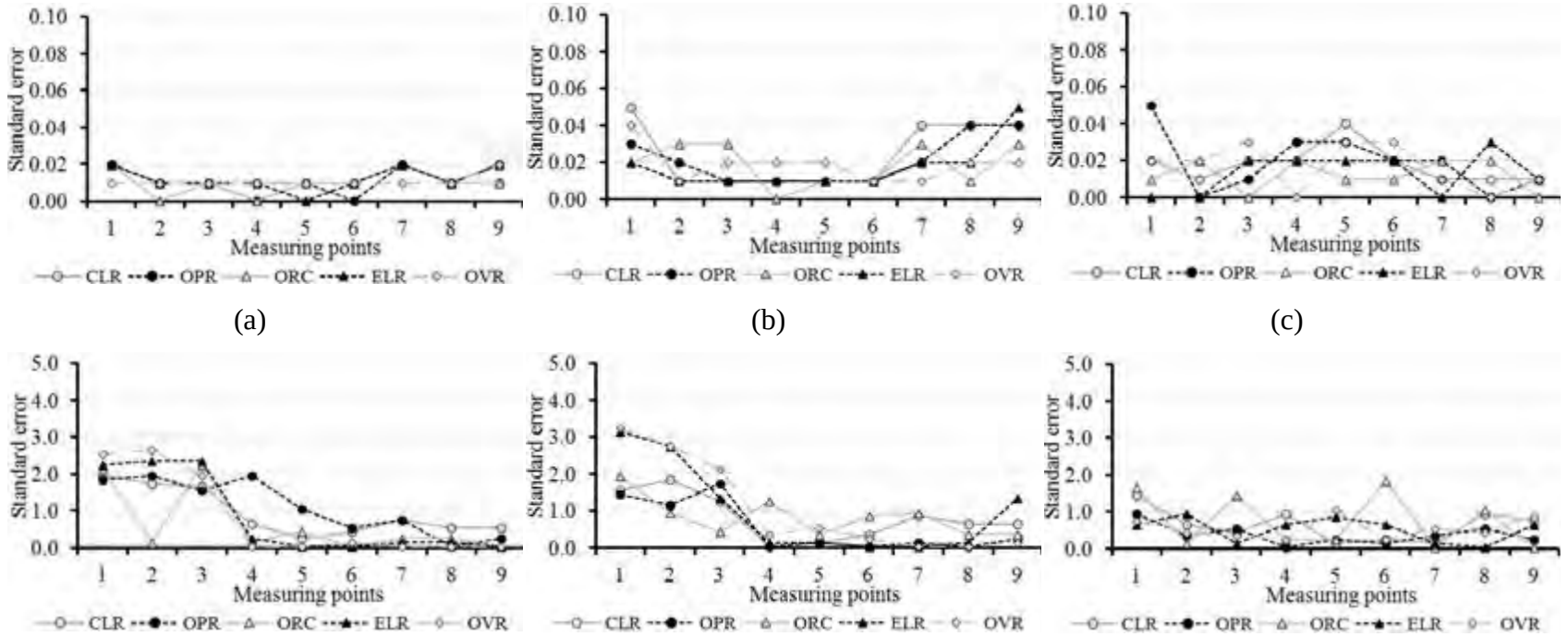

Figure 4.108 - Average air velocity (a, b, and c) and temperature (d, e, and f) standard errors for air speed of 0.1 m s^{-1}, and wind direction of south to north, at nine locations and three different heights: (a and d) 0.02 m, (b and e) 0.11 m, and (c and f) 0.20 m. Types of ridge: Closed ridge (CLR); Open ridge (OPR); Open ridge with chimney (ORC); Elevated ridge (ELR); and Overshot ridge (OVR).

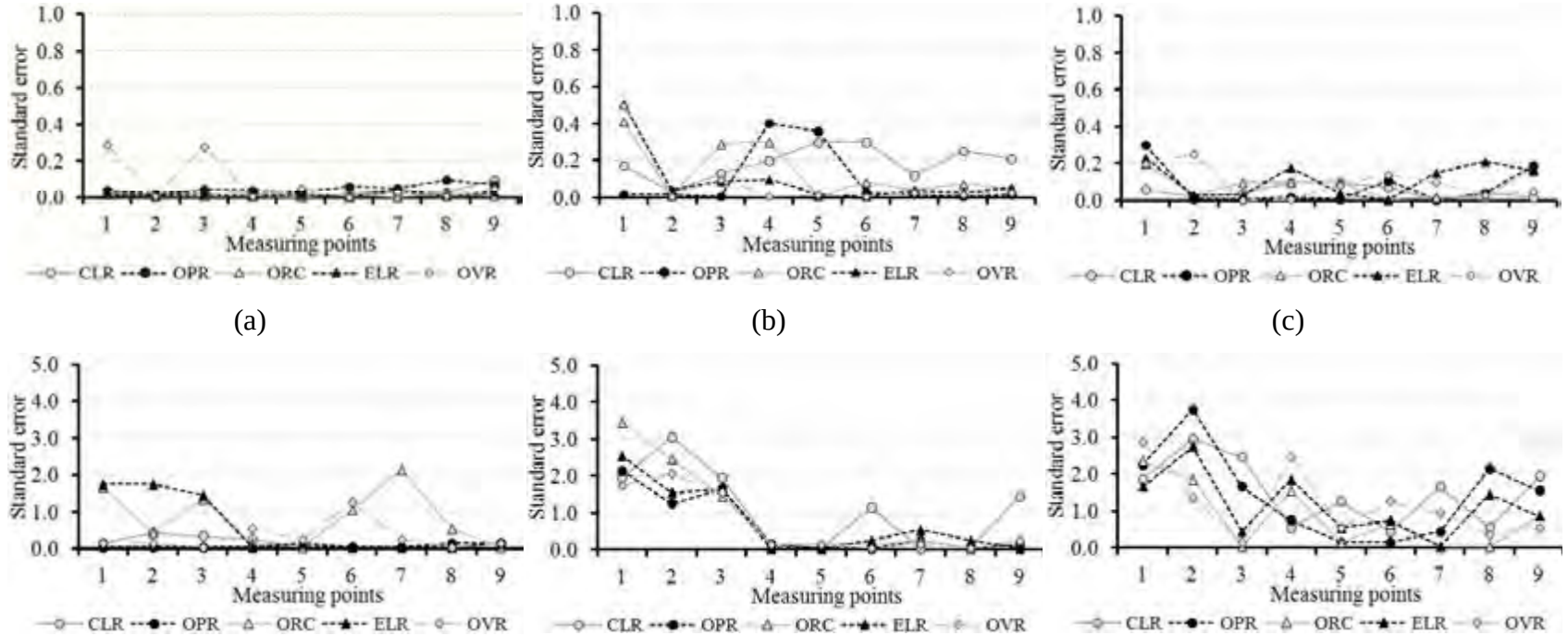

Figure 4.109 - Average air velocity (a, b, and c) and temperature (d, e, and f) standard errors for air speed of 1.0 m s^{-1}, and wind direction of south to north, at nine locations and three different heights: (a and d) 0.02 m, (b and e) 0.11 m, and (c and f) 0.20 m. Types of ridge: Closed ridge (CLR); Open ridge (OPR); Open ridge with chimney (ORC); Elevated ridge (ELR); and Overshot ridge (OVR).

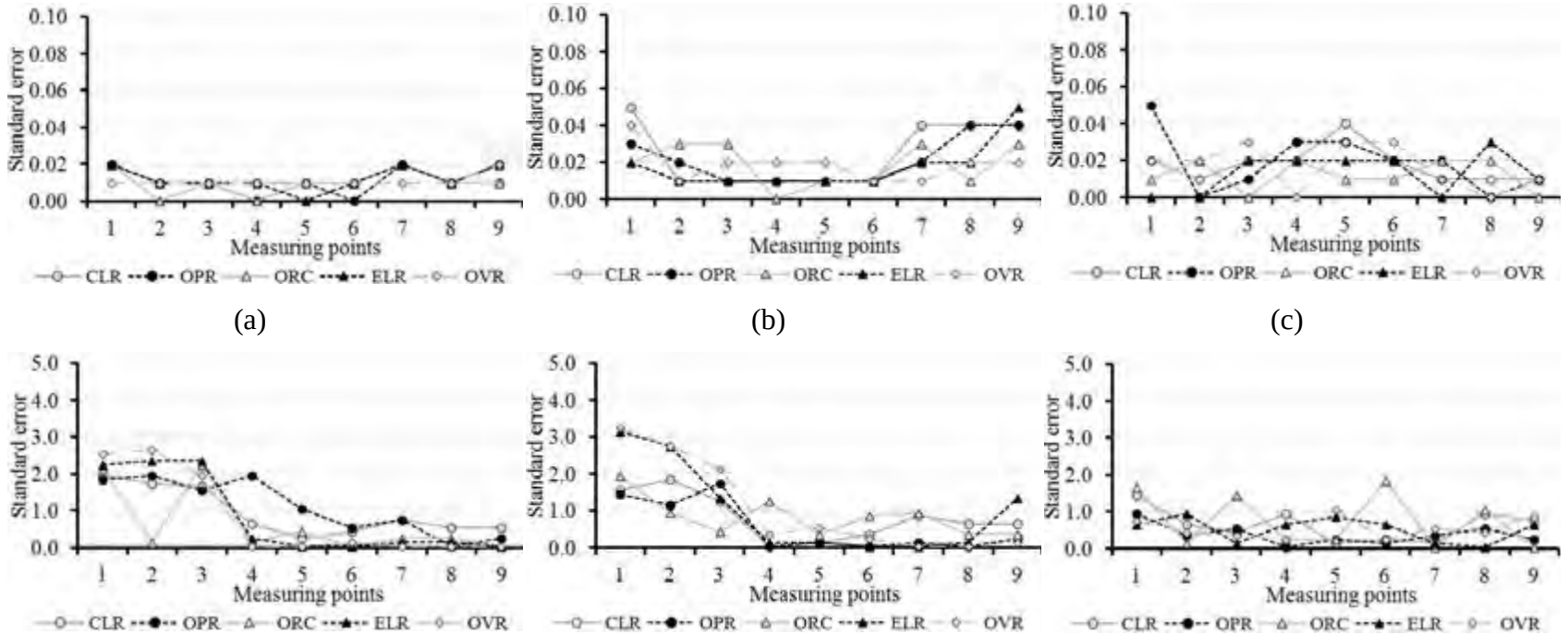

Figure 4.110 - Average air velocity (a, b, and c) and temperature (d, e, and f) standard errors for air speed of 0.1 m s^{-1}, and wind direction of north to south, at nine locations and three different heights: (a and d) 0.02 m, (b and e) 0.11 m, and (c and f) 0.20 m. Types of ridge: Closed ridge (CLR); Open ridge (OPR); Open ridge with chimney (ORC); Elevated ridge (ELR); and Overshot ridge (OVR).

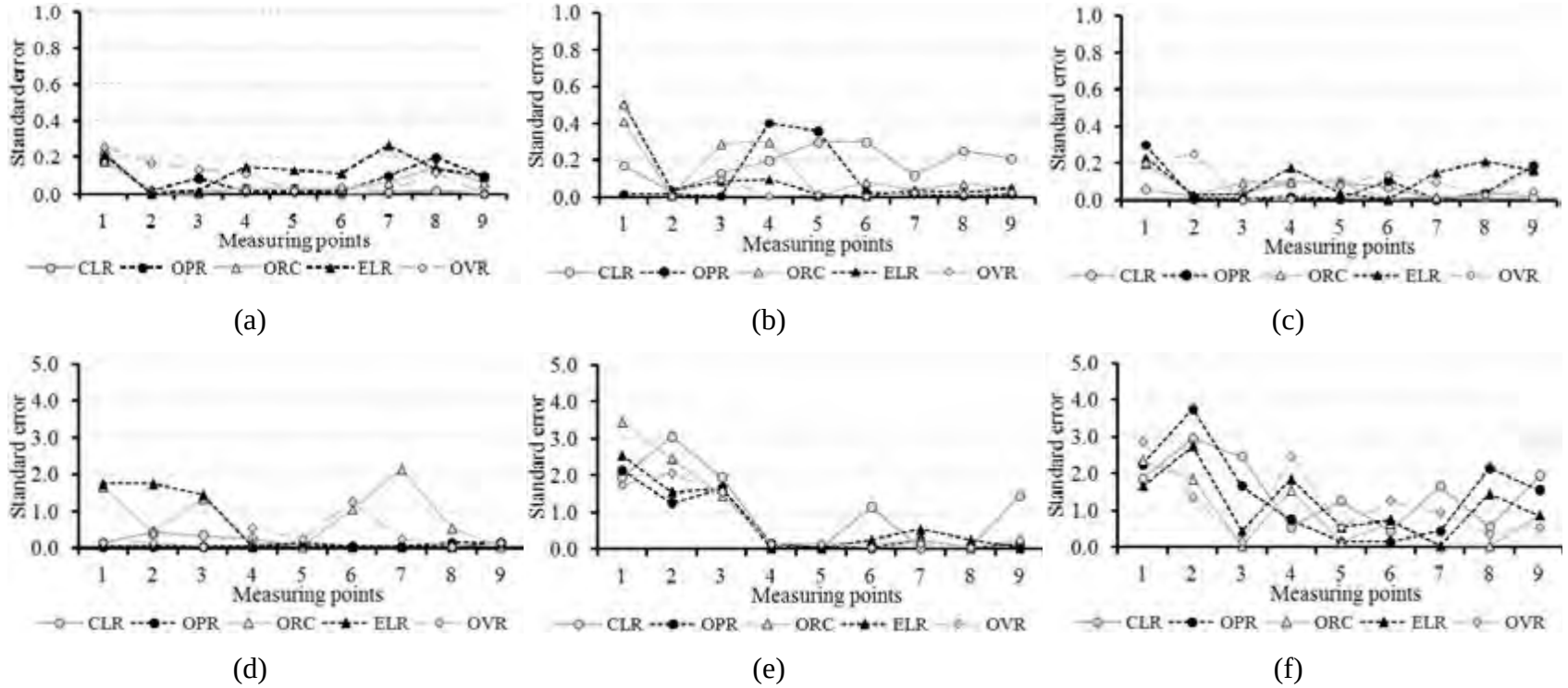

Figure 4.111 - Average air velocity (a, b, and c) and temperature (c, d, and e) standard errors for air speed of 1.0 m s^{-1}, and wind direction of north to south, at nine locations and three different heights: (a and d) 0.02 m, (b and e) 0.11 m, and (c and f) 0.20 m. Types of ridge: Closed ridge (CLR); Open ridge (OPR); Open ridge with chimney (ORC); Elevated ridge (ELR); and Overshot ridge (OVR).

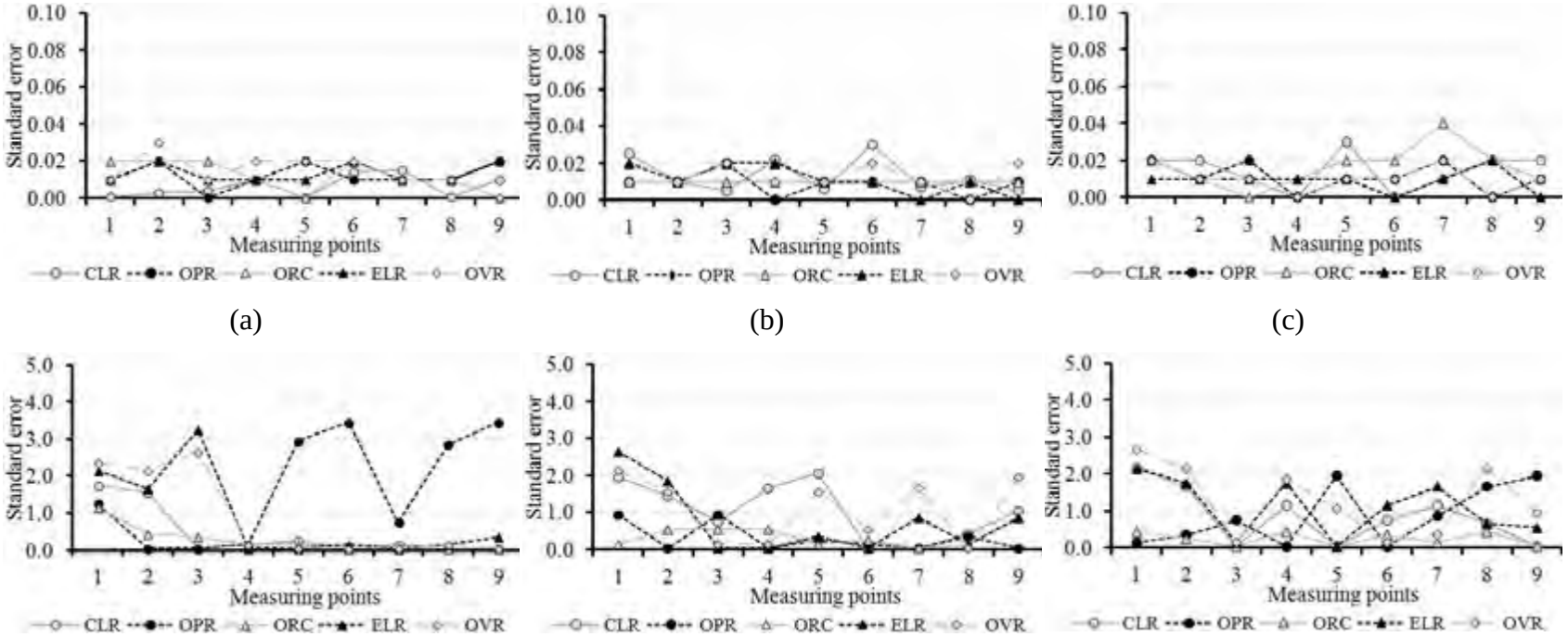

Figure 4.112 - Average air velocity (a, b, and c) and temperature (d, e, and f) standard errors for air speed of 0.1 m s^{-1}, and wind direction of east to west, at nine locations and three different heights: (a and d) 0.02 m, (b and e) 0.11 m, and (c and f) 0.20 m. Types of ridge: Closed ridge (CLR); Open ridge (OPR); Open ridge with chimney (ORC); Elevated ridge (ELR); and Overshot ridge (OVR).

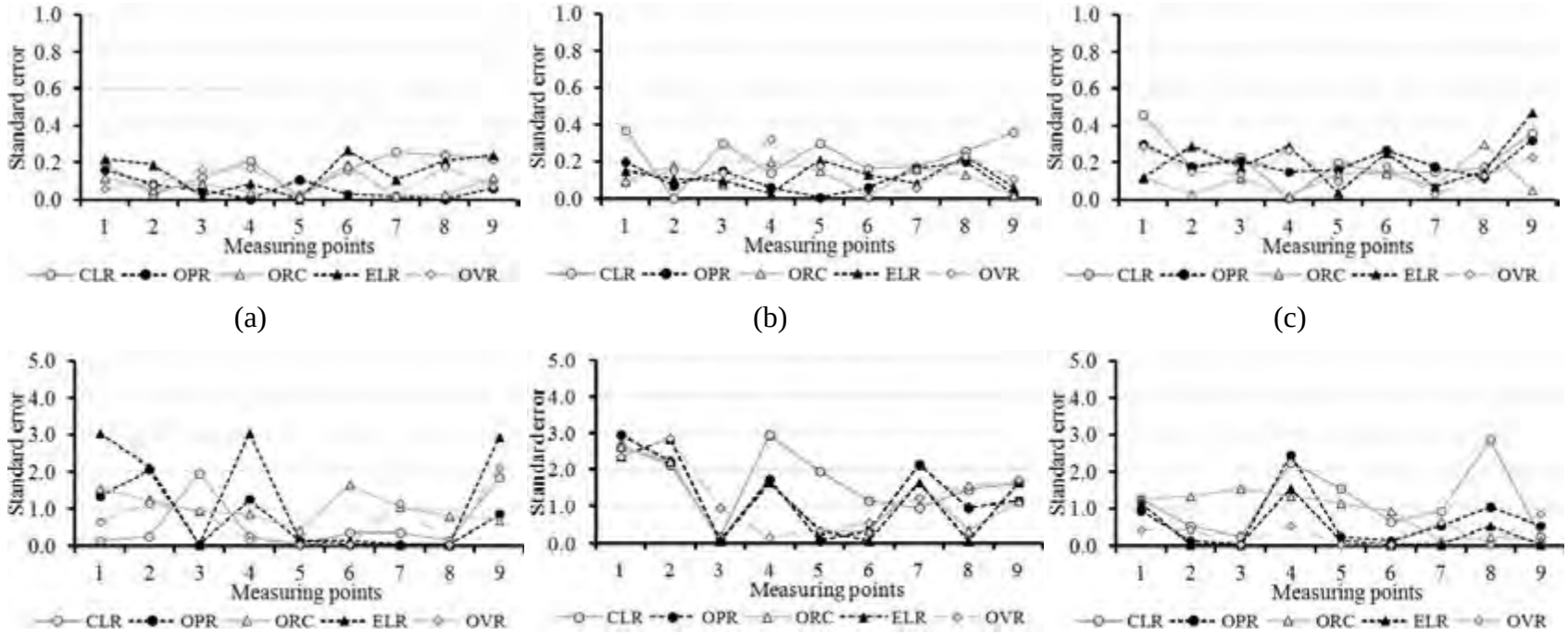

Figure 4.113 - Average air velocity (a, b, and c) and temperature (d, e, and f) standard errors for air speed of 1.0 m s^{-1}, and wind direction of east to west, at nine locations and three different heights: (a and d) 0.02 m, (b and e) 0.11 m, and (c and f) 0.20 m. Types of ridge: Closed ridge (CLR); Open ridge (OPR); Open ridge with chimney (ORC); Elevated ridge (ELR); and Overshot ridge (OVR).

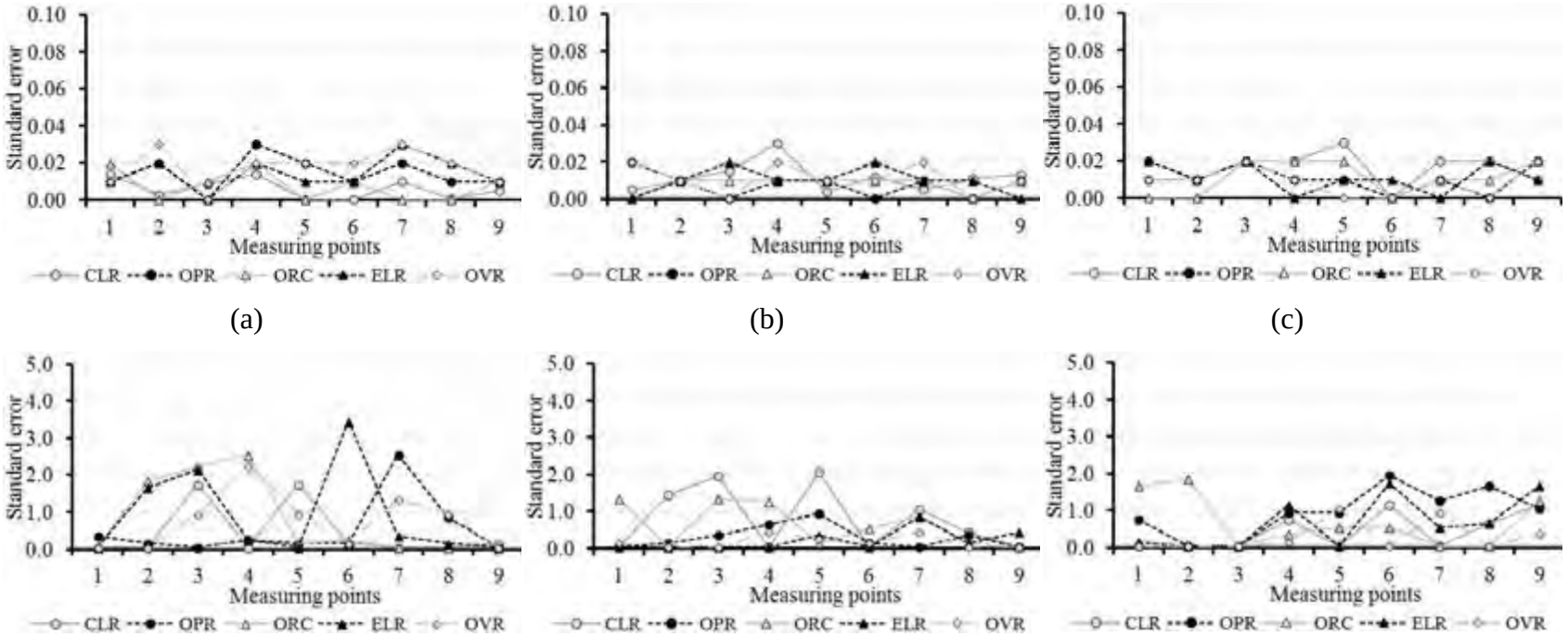

Figure 4.114 - Average air velocity (a, b, and c) and temperature (d, e, and f) standard errors for air speed of 0.1 m s^{-1}, and wind direction of west to east, at nine locations and three different heights: (a and d) 0.02 m, (b and e) 0.11 m, and (c and f) 0.20 m. Types of ridge: Closed ridge (CLR); Open ridge (OPR); Open ridge with chimney (ORC); Elevated ridge (ELR); and Overshot ridge (OVR).

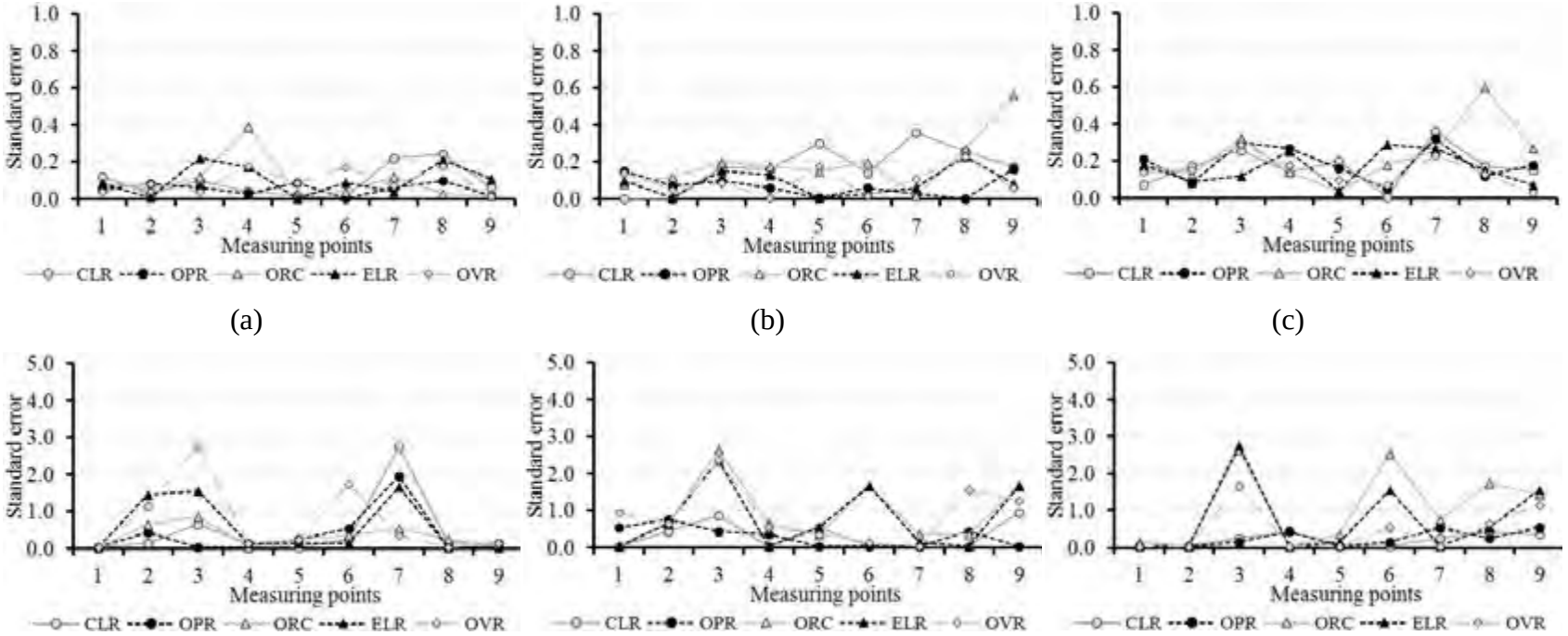

Figure 4.115 - Average air velocity (a, b, and c) and temperature (c, d, and e) standard errors for air speed of 1.0 m s^{-1}, and wind direction of west to east, at nine locations and three different heights: (a and d) 0.02 m, (b and e) 0.11 m, and (c and f) 0.20 m. Types of ridge: Closed ridge (CLR); Open ridge (OPR); Open ridge with chimney (ORC); Elevated ridge (ELR); and Overshot ridge (OVR).

Figures 4.116 to 4.119 shows the regression plots for each variable studied and all treatments tested. The regression equations presented by these figures can be seen in Tables 4.10 to 4.18.

In general, there is a good fit of the model with coefficients of determinations (R^2) of 0.841, 0.671, 0.882, 0.718 and 0.754 (Table 4.10) for air velocity (Figure 4.116a) and 0.986, 0.881, 0.729, 0621, and 0.787 (Table 4.11) for temperature (Figure 4.116b) in CLR, OPR, ORC, ELR and OVR types of ridges, respectively, using air speed of 0.1 m s^{-1} and wind direction of south to north, while, the linear and angular coefficients are significant (t test, $P > 0.05$). The coefficients of determination (R^2) to air speed of 1.0 m s^{-1} were 0.916, 0.894, 0.909, 0.911, and 0.882 for air velocity (Figure 4.116c and Table 4.10) and 0.802, 0.723, 0.676, 0.716, and 0.819 for temperature (Figure 4.116d and Table 4.11) in CLR, OPR, ORC, ELR and OVR types of ridges, respectively.

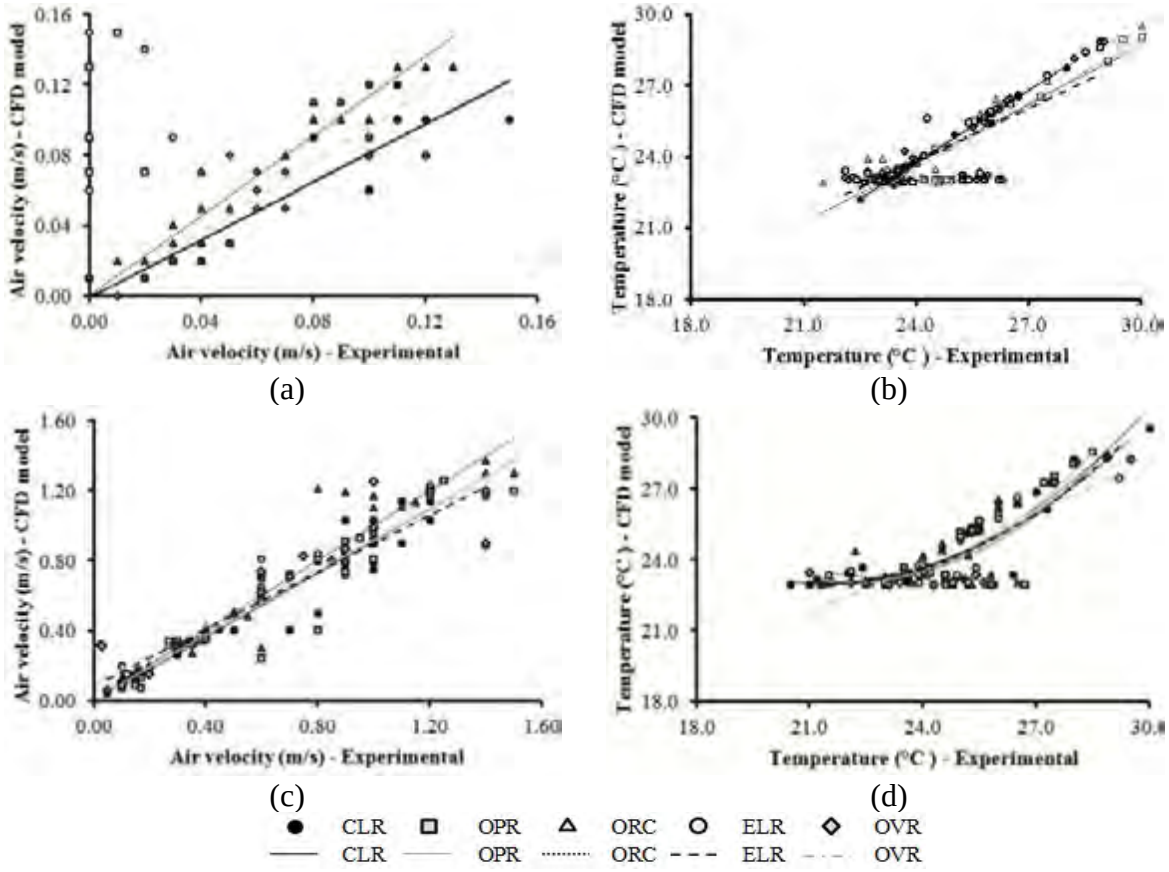

Figure 4.116 - Regression plots for air velocity and temperature in closed ridge (CLR), open ridge (OPR), open ridge with chimney (ORC), elevated ridge (ELR), and overshot ridge (OVR), using air speed of 0.1 m s^{-1} (a and b) and 1.0 m s^{-1} (c and d), and wind direction south to north. Thin lines and curves represent the linear or polynomial regression with the best values of r^2 fitted for each data sets.

Table 4.10 - Adjusted equations between the values of air velocity measured (V_{mes}) and simulated (V_{sim}) using air speed of 0.1 m s^{-1} and 1.0 m s^{-1}, and wind direction south to north.

Ridge type	Equations	R^2
	Air speed of 0.1 m s^{-1}	
CLR	$V_{sim} = 0.8206\ V_{mes} - 0.001$	0.841
OPR	$V_{sim} = 9.2789\ V_{mes} + 0.2068$	0.671
ORC	$V_{sim} = 1.133\ V_{mes} - 0.00006$	0.882
ELR	$V_{sim} = 9.261\ V_{mes} + 0.1776$	0.718
OVR	$V_{sim} = 0.9899\ V_{mes} - 0.0032$	0.754
	Air speed of 1.0 m s^{-1}	
CLR	$V_{sim} = 0.917\ V_{mes} - 0.0094$	0.916
OPR	$V_{sim} = 0.9072\ V_{mes} + 0.0126$	0.894
ORC	$V_{sim} = 0.9961\ V_{mes} + 0.0069$	0.909
ELR	$V_{sim} = 0.8163\ V_{mes} + 0.0785$	0.911
OVR	$V_{sim} = 0.824\ V_{mes} + 0.0974$	0.882

Table 4.11 - Adjusted equations between the values of air temperature measured (T_{mes}) and simulated (T_{sim}) using air speed of 0.1 m s^{-1} and 1.0 m s^{-1}, and wind direction south to north.

Ridge type	Equations	R^2
	Air speed of 0.1 m s^{-1}	
CLR	$T_{sim} = -0.0039\ T_{mes}^2 + 1.2108\ T_{mes} - 3.0157$	0.986
OPR	$T_{sim} = 0.855\ T_{mes} + 3.0072$	0.881
ORC	$T_{sim} = 0.8344\ T_{mes} + 3.6989$	0.729
ELR	$T_{sim} = 0.7427\ T_{mes} + 5.986$	0.621
OVR	$T_{sim} = 0.1668\ T_{mes}^2 - 7.678\ T_{mes} + 111.51$	0.787
	Air speed of 1.0 m s^{-1}	
CLR	$T_{sim} = 0.1002\ T_{mes}^2 - 4.2852\ T_{mes} + 68.81$	0.802
OPR	$T_{sim} = 0.1375\ T_{mes}^2 - 6.0948\ T_{mes} + 90.602$	0.723
ORC	$T_{sim} = 0.1374\ T_{mes}^2 - 6.2277\ T_{mes} + 93.83$	0.676
ELR	$T_{sim} = 0.0952\ T_{mes}^2 - 4.0725\ T_{mes} + 66.549$	0.716
OVR	$T_{sim} = 0.0897\ T_{mes}^2 - 3.8039\ T_{mes} + 63.248$	0.819

The variables studied (air velocity and temperature), using air speed of 0.1 m s^{-1} and wind direction of north to south, gave a fair correlation of measured versus simulated values with r^2 of 0.774, 0.794, 0.915, 0.892, 0.855 (Figure 4.117a) and 0.983, 0.766, 0.729, 0.617, 0.787 (Figure 4.117b), respectively. The slopes values of simulated versus measured air velocities regression for each treatment were 0.8598, 1.1416, 0.9035, 1.0833, and 0.9332, respectively, see Table 4.12. Good correlations were observed between measured and simulated air velocity (R^2 of 0.909, 0.949, 0.905, 0.856, and 0.875) and temperature (R^2 of 0.702, 0.800, 0.701, 0.487, and 0.666) values to air speed of 1.0 m s^{-1}, see Figures 4.117 (c and d), and Table 4.13. In both condition, the linear and angular coefficients are significant (t test, $P > 0.05$).

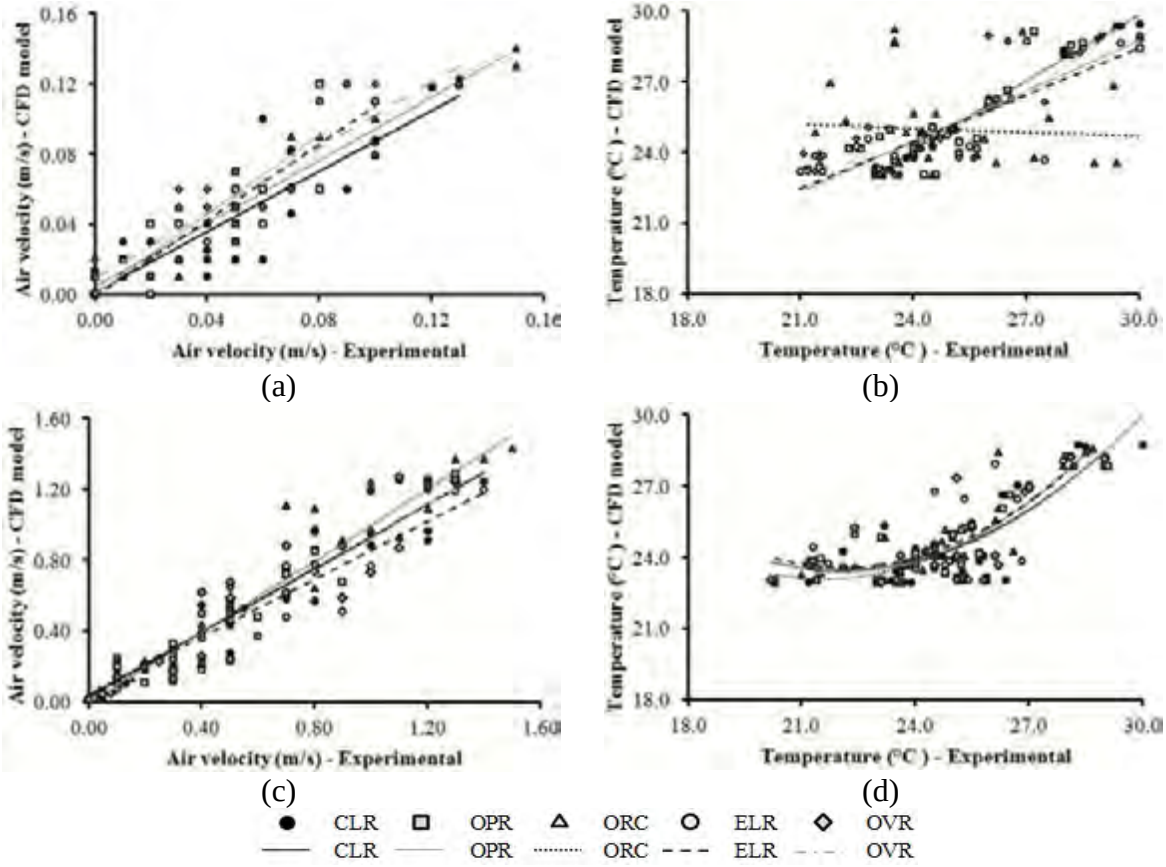

Figure 4.117 - Regression plots for air velocity and temperature in closed ridge (CLR), open ridge (OPR), open ridge with chimney (ORC), elevated ridge (ELR), and overshot ridge (OVR), using air speed of 0.1 m s^{-1} (a and b) and 1.0 m s^{-1} (c and d), and wind direction north to south. Thin lines and curves represent the linear or polynomial regression with the best values of r^2 fitted for each data sets.

Table 4.12 - Adjusted equations between the values of air velocity measured (V_{mes}) and simulated (V_{sim}) using air speed of 0.1 m s^{-1} and 1.0 m s^{-1}, and wind direction north to south.

Ridge type	Equations	R^2
	Air speed of 0.1 m s^{-1}	
CLR	$V_{sim} = 0.8598\ V_{mes} + 0.0013$	0.774
OPR	$V_{sim} = 1.1416\ V_{mes} + 0.00004$	0.794
ORC	$V_{sim} = 0.9035\ V_{mes} + 0.0044$	0.915
ELR	$V_{sim} = 1.0833\ V_{mes} - 0.0011$	0.892
OVR	$V_{sim} = 0.9332\ V_{mes} + 0.0089$	0.855
	Air speed of 1.0 m s^{-1}	
CLR	$V_{sim} = 0.9041\ V_{mes} + 0.0286$	0.909
OPR	$V_{sim} = 0.9905\ V_{mes} - 0.0044$	0.949
ORC	$V_{sim} = 1.0093\ V_{mes} - 0.0093$	0.905
ELR	$V_{sim} = 0.8159\ V_{mes} + 0.0393$	0.856
OVR	$V_{sim} = 0.9329\ V_{mes} - 0.0065$	0.875

Table 4.13 - Adjusted equations between the values of air temperature measured (T_{mes}) and simulated (T_{sim}) using air speed of 0.1 m s^{-1} and 1.0 m s^{-1}, and wind direction north to south.

Ridge type	Equations	R^2
	Air speed of 0.1 m s^{-1}	
CLR	$T_{sim} = -0.0111\ T_{mes}^2 + 1.565\ T_{mes} - 7.1559$	0.983
OPR	$T_{sim} = 0.7181\ T_{mes} + 6.4647$	0.766
ORC	$T_{sim} = 0.8344\ T_{mes} + 3.6989$	0.729
ELR	$T_{sim} = 0.6528\ T_{mes} + 8.1661$	0.617
OVR	$T_{sim} = 0.1668\ T_{mes}^2 - 7.678\ T_{mes} + 111.51$	0.787
	Air speed of 1.0 m s^{-1}	
CLR	$T_{sim} = 0.1067\ T_{mes}^2 - 4.7236\ T_{mes} + 75.701$	0.702
OPR	$T_{sim} = 0.0979\ T_{mes}^2 - 4.2643\ T_{mes} + 69.769$	0.800
ORC	$T_{sim} = 0.1097\ T_{mes}^2 - 4.7301\ T_{mes} + 74.09$	0.701
ELR	$T_{sim} = 0.1159\ T_{mes}^2 - 5.1249\ T_{mes} + 80.221$	0.487
OVR	$T_{sim} = 0.1035\ T_{mes}^2 - 4.5587\ T_{mes} + 73.654$	0.666

For equations of the estimated variables studied, working with air speed of 0.1 m s^{-1} and wind direction of east to west, analysis linear regression and polynomial were performed between the simulated and measured data, where R^2 values were 0.433, 0.704, 0.639, 0.648, and 0.478, respectively, to air velocity (Figure 4.18a) and 0.715, 0.531, 0.815, 0.631, and 0.766, respectively, to air temperature (Figure 4.18b). More details can be seen in Table 4.14 and 4.15. Additionally, using with air speed of 1.0 m s^{-1} and wind direction of east to west, the measurement variable studied were modeled using the linear regression and polynomial and good agreements were observed between the measured and simulated air velocities and temperatures functions, see Figure 4.18c, Figure 4.18d, and Table 4.15.

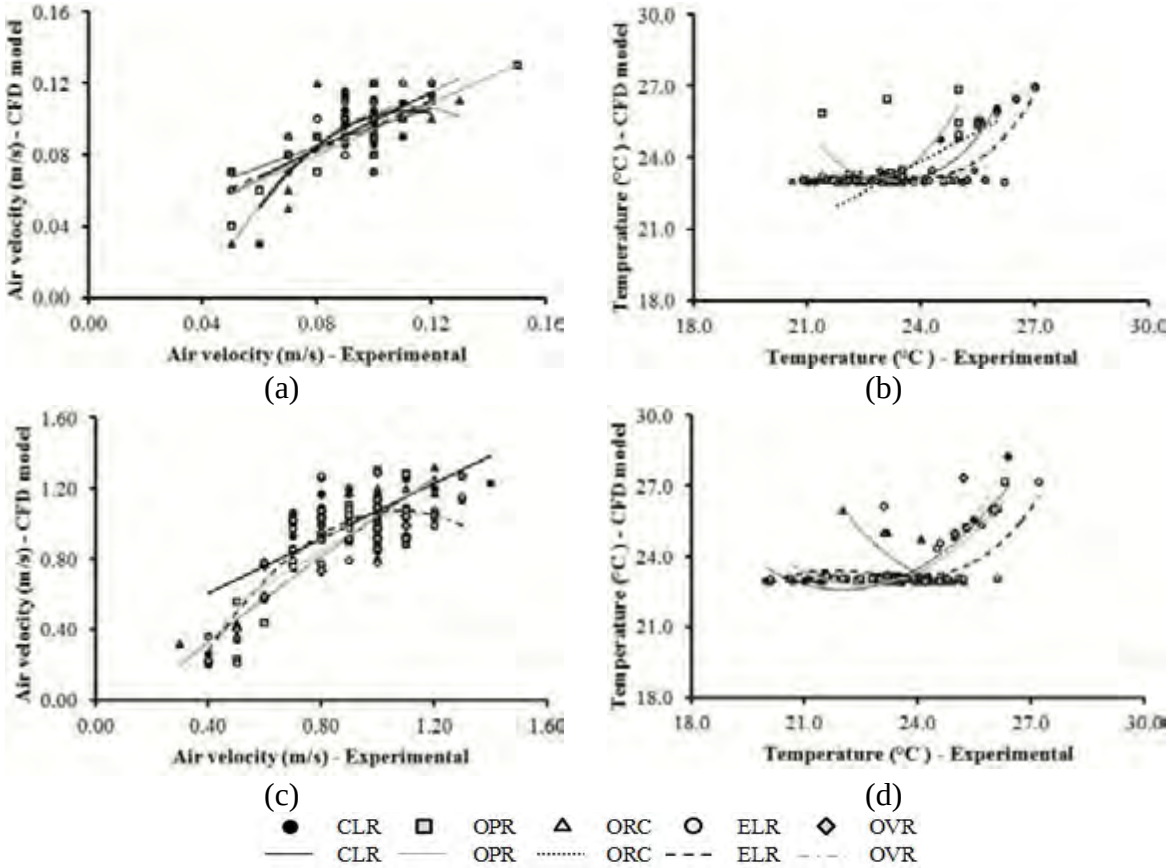

Figure 4.18 - Regression plots for air velocity and temperature in closed ridge (CLR), open ridge (OPR), open ridge with chimney (ORC), elevated ridge (ELR), and overshot ridge (OVR), using air speed of 0.1 m s^{-1} (a and b) and 1.0 m s^{-1} (c and d), and wind direction east to west. Thin lines and curves represent the linear or polynomial regression with the best values of r^2 fitted for each data sets.

Table 4.14 - Adjusted equations between the values of air velocity measured (V_{mes}) and simulated (V_{sim}) using air speed of 0.1 m s^{-1} and 1.0 m s^{-1}, and wind direction east to west.

Ridge type	Equations	r^2
	Air speed of 0.1 m s^{-1}	
CLR	$V_{sim} = -20.274\ V_{mes}^2 + 4.5246\ V_{mes} - 0.1479$	0.433
OPR	$V_{sim} = 0.7207\ V_{mes} + 0.0224$	0.704
ORC	$V_{sim} = -19.65\ V_{mes}^2 + 4.4375x - 0.1438$	0.639
ELR	$V_{sim} = 0.7064\ V_{mes} + 0.0258$	0.648
OVR	$V_{sim} = 0.566\ V_{mes} + 0.0389$	0.478
	Air speed of 1.0 m s^{-1}	
CLR	$V_{sim} = 0.7827\ V_{mes} + 0.2913$	0.479
OPR	$V_{sim} = 1.0003\ V_{mes} + 0.0487$	0.595
ORC	$V_{sim} = -0.1256\ V_{mes}^2 + 1.3607\ V_{mes} - 0.1947$	0.846
ELR	$V_{sim} = -1.7216\ V_{mes}^2 + 3.7201\ V_{mes} - 0.9359$	0.612
OVR	$V_{sim} = -1.4101\ V_{mes}^2 + 3.1535\ V_{mes} - 0.711$	0.666

Table 4.15 - Adjusted equations between the values of air temperature measured (T_{mes}) and simulated (T_{sim}) using air speed of 0.1 m s^{-1} and 1.0 m s^{-1}, and wind direction east to west.

Ridge type	Equations	r^2
	Air speed of 0.1 m s^{-1}	
CLR	$T_{sim} = 0.0861\ T_{mes}^3 - 5.8277\ T_{mes}^2 + 131.4\ T_{mes} - 963.72$	0.715
OPR	$T_{sim} = 0.6551\ T_{mes}^2 - 29.899\ T_{mes} + 364.25$	0.531
ORC	$T_{sim} = 0.8488\ T_{mes} + 3.4548$	0.815
ELR	$T_{sim} = 0.0567\ T_{mes}^3 - 3.8884\ T_{mes}^2 + 88.787\ T_{mes} - 651.8$	0.631
OVR	$T_{sim} = 0.0788\ T_{mes}^3 - 5.4173\ T_{mes}^2 + 123.82\ T_{mes} - 918.22$	0.766
	Air speed of 1.0 m s^{-1}	
CLR	$T_{sim} = 0.2298\ T_{mes}^2 - 10.12\ T_{mes} + 134$	0.870
OPR	$T_{sim} = 0.2583\ T_{mes}^2 - 11.641\ T_{mes} + 153.95$	0.823
ORC	$T_{sim} = 0.3328\ T_{mes}^2 - 16.719\ T_{mes} + 232.84$	0.675
ELR	$T_{sim} = 0.0467\ T_{mes}^3 - 3.192\ T_{mes}^2 + 72.602\ T_{mes} - 525.92$	0.443
OVR	$T_{sim} = 0.5561\ T_{sim}^2 - 25.94\ T_{sim} + 325.46$	0.720

Good relationship was observed in the equations adjusted of variables studied measured and simulated using air speed of 0.1 m s^{-1} and wind direction of west to east (Figure 4.19). The adjusted equations of air velocity and temperature had lowest R^2 of 0.404 and 0.451, respectively. Overall, the models performed similarly with the exception of OVR, which produced the largest values of air velocity measured. In this treatment, there was a positive and linear relationship between the average of measured and simulated air velocity (slope = 0.5333, R^2 = 0.404). Table 4.17 shows models efficiencies for air speed of 1.0 m s^{-1}. The results show a good correlation between measured and simulated air velocity and temperature at five treatment tested. These are demonstrated by the correlation coefficients (R^2). In both conditions, these equations showed the linear and angular coefficients significant (t test, P > 0.05).

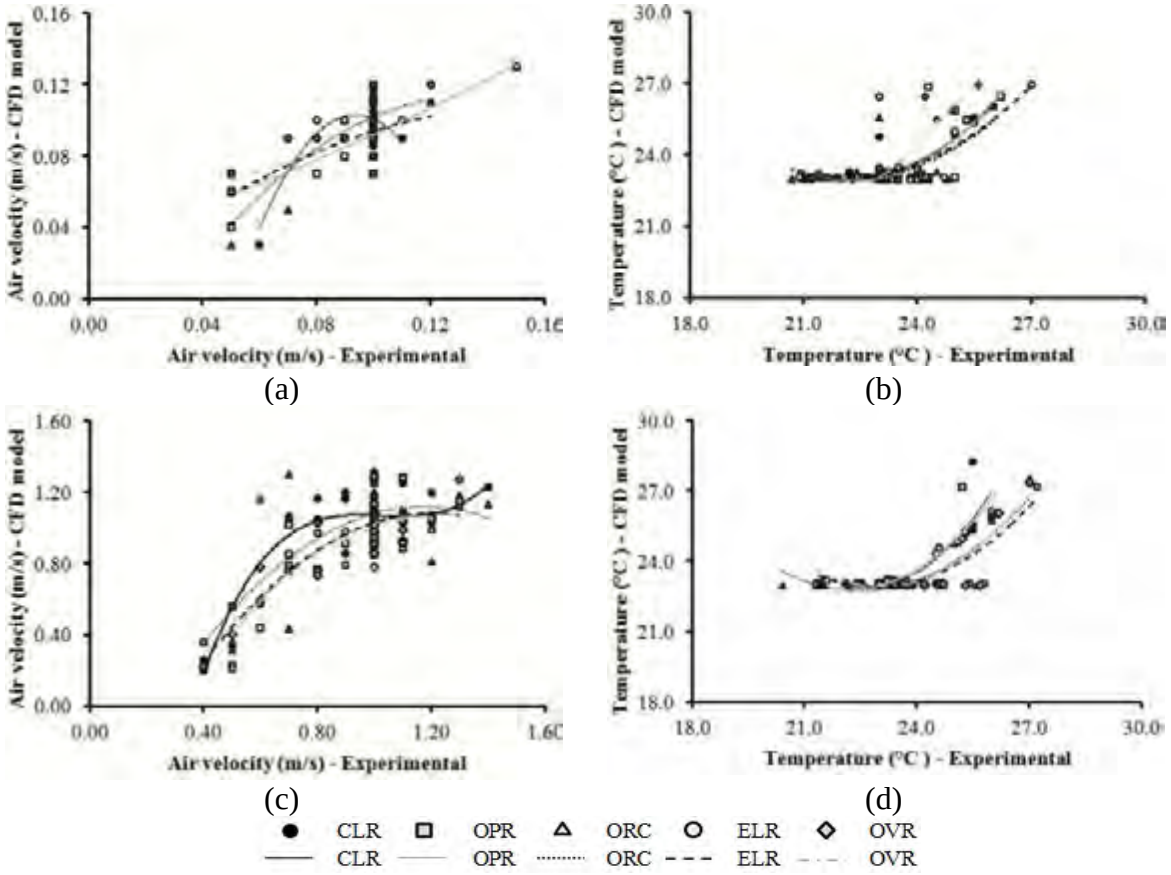

Figure 4.19 - Regression plots for air velocity and temperature in closed ridge (CLR), open ridge (OPR), open ridge with chimney (ORC), elevated ridge (ELR), and overshot ridge (OVR), using air speed of 0.1 m s^{-1} (a and b) and 1.0 m s^{-1} (c and d), and wind direction west to east. Thin lines and curves represent the linear or polynomial regression with the best values of r^2 fitted for each data sets.

Table 4.16 - Adjusted equations between the values of air velocity measured (V_{mes}) and simulated (V_{sim}) using air speed of 0.1 m s^{-1} and 1.0 m s^{-1}, and wind direction west to east.

Ridge type	Equations	r^2
	Air speed of 0.1 m s^{-1}	
CLR	$V_{sim} = -56.112\ V_{mes}^2 + 10.518\ V_{mes} - 0.3899$	0.532
OPR	$V_{sim} = 0.9799\ V_{mes}^2 + 0.5333\ V_{mes} + 0.0289$	0.704
ORC	$V_{sim} = -10.669\ V_{mes}^2 + 2.8147\ V_{mes} - 0.0728$	0.709
ELR	$V_{sim} = -4.2914\ V_{mes}^2 + 1.3652\ V_{mes} + 0.0002$	0.570
OVR	$V_{sim} = 0.5333\ V_{mes} + 0.0396$	0.404
	Air speed of 1.0 m s^{-1}	
CLR	$V_{sim} = 3.8045\ V_{mes}^3 - 11.707\ V_{mes}^2 + 11.943\ V_{mes} - 2.9693$	0.828
OPR	$V_{sim} = -1.6165\ V_{mes}^2 + 3.6835\ V_{mes} - 1.0394$	0.701
ORC	$V_{sim} = -1.2797\ V_{mes}^2 + 3.0085\ V_{mes} - 0.648$	0.524
ELR	$V_{sim} = -1.3077\ V_{mes}^2 + 3.1393\ V_{mes} - 0.8013$	0.724
OVR	$V_{sim} = -1.0585\ V_{mes}^2 + 2.6656\ V_{mes} - 0.6049$	0.725

Table 4.17 - Adjusted equations between the values of air temperature measured (T_{mes}) and simulated (T_{sim}) using air speed of 0.1 m s^{-1} and 1.0 m s^{-1}, and wind direction west to east.

Ridge type	Equations	r^2
	Air speed of 0.1 m s^{-1}	
CLR	$T_{sim} = 0.1986\ T_{mes}^2 - 8.7515\ T_{mes} + 119.33$	0.787
OPR	$T_{sim} = 0.2498\ T_{mes}^2 - 11.159\ T_{mes} + 147.52$	0.544
ORC	$T_{sim} = 0.1744\ T_{mes}^2 - 7.7566\ T_{mes} + 109.19$	0.451
ELR	$T_{sim} = 0.1629\ T_{mes}^2 - 7.2151\ T_{mes} + 102.96$	0.550
OVR	$T_{sim} = -0.1701\ T_{mes}^3 + 12.439\ T_{mes}^2 - 301.37\ T_{mes} + 2444.2$	0.829
	Air speed of 1.0 m s^{-1}	
CLR	$T_{sim} = 0.3824\ T_{mes}^2 - 17.386\ T_{mes} + 220.51$	0.808
OPR	$T_{sim} = 0.2695\ T_{mes}^2 - 11.971\ T_{mes} + 155.71$	0.826
ORC	$T_{sim} = 0.1932\ T_{mes}^2 - 8.6856\ T_{mes} + 120.36$	0.720
ELR	$T_{sim} = 0.2054\ T_{mes}^2 - 9.4132\ T_{mes} + 130.75$	0.676
OVR	$T_{sim} = 0.2539\ T_{mes}^2 - 11.701\ T_{mes} + 157.69$	0.729

In general, the experimental values of air velocity and temperature obtained in the nine points and three high do not significantly differ from those encountered when simulating the model with CFD. This is because the R^2 values were mostly high than 0.700, indicating that the CFD model is capable of predicting real operating conditions of the open scale model of CBP barn with natural ventilation. Thus, the results prove to be promising, given that the simulated system depends on several variables such as geometric characteristics of the reduced model, roughness, temperature of the compost, orientation of the reduced model, type of ridge, others.

The experimental and CFD simulation values of air velocity and temperature obtained in nine locations and three different heights are presented in Figures 4.120 to 4.126.

The mean values and standard deviations of the air velocities measured for each treatment tested using air speed of 0.1 m s^{-1} and wind direction of south to north were 0.07 m s^{-1} (±0.04), 0.04 m s^{-1} (±0.03), 0.06 m s^{-1} (±0.03), 0.04 m s^{-1} (±0.03), 0.05 m s^{-1} (±0.03), respectively. However, the values and standard deviations of the air velocities simulated were 0.06 m s^{-1} (±0.04), 0.05 m s^{-1} (±0.04), 0.07 m s^{-1} (±0.04), 0.05 m s^{-1} (±0.04), 0.05 m s^{-1} (±0.04), respectively, see Figure 4.120. The mean values and standard deviations of the air temperature measured for each treatment tested were 24.39°C (±1.61), 24.93°C (±2.01), 24.72°C (±1.79), 24.70°C (±1.88), and 24.94°C (±1.89), respectively. Moreover, the highest mean values and standard deviations of the air velocities and temperature measured and simulated using air speed of 1.0 m s^{-1} were 0.75 m s^{-1} (±0.37) and 0.73 m s^{-1} (±0.37), respectively, and 24.81°C (±2.44) and 24.74°C (±2.00), respectively, see Figure 4.121.

The highest mean values measured and simulated air velocity, using air speed of 0.1 m $s^{-1}$and wind direction of north to south were 0.06 m s^{-1} with a range from 0.00 to 0.13 m s^{-1} and 0.06 m s^{-1} with a range from 0.00 to 0.14 m s^{-1}, respectively. In the same study, the highest mean values measured and simulated air velocity were 25.26°C with a range from 23.00 to 30.00°C and 25.27°C with a range from 23.05 to 29.15°C, respectively, see Figure 4.122. Thus, analyzing the other air speed tested (1.0 m s^{-1}), the highest mean values measured and simulated air velocity and temperature were 0.68 m s^{-1} (±0.43) and 0.68 m s^{-1} (±0.39), respectively, and 24.98°C (±2.02) and 24.70°C(±1.86) respectively (Figure 4.123).

The highest mean values measured and simulated of air velocity and temperature, using air speed of 0.1 m $s^{-1}$and wind direction of east to west, were 0.10 m s^{-1} (±0.01) and 0.10 m s^{-1} (±0.02), respectively, for air velocity and 23.89°C (±1.57) and 23.55°C (±1.14),

respectively, for temperature (Figure 4.124). However, using air speed of 1.0 m s^{-1}, the highest mean values measured and simulated values of variables studied were 0.96 m s^{-1} (± 0.23) and 0.99 m s^{-1} (±0.28), respectively, and 24.16°C (±0.65) and 23.47°C (±1.27), respectively, for these treatments tested as shown in Figure 4.125.

The mean values and standard deviations of the air velocities simulated and observed, using air speed of 0.1 m s^{-1} and wind direction of west to east, were 0.09 m s^{-1} (±0.02) and 0.09 m s^{-1} (±0.02), respectively, resulting in an average absolute deviation of 0.01 ± 0.01 and an average error of 0.02, respectively (Figure 4.126). The mean values of the air temperature simulated and observed were 23.27°C and 23.47°C, respectively, which resulted in an average absolute deviation of 0.74 ± 0.13 and 0.69 ± 0.10, respectively and an average error of 1.08 and 1.02, respectively. However, the mean values and standard deviations of the air velocities simulated and observed, using air speed of 1.0 m s^{-1} and the same wind direction, were 0.94 m s^{-1} (±0.22) and 0.95 m s^{-1} (±0.22), respectively, proving in an average absolute deviation of 0.01 ± 0.02 and an average error of 0.02, respectively, see Figure 4.127. In the same study, the mean values and standard deviations of the air temperature simulated and observed were 23.67°C (±1.20) and 23.44°C (±1.12), respectively. In this case, the average absolute deviation 0.90 ± 0.27 and 0.73 ± 0.07, respectively.

Given that the absolute average errors calculated between the values of air velocities and temperature measured and simulated are very close to or less than 0.41 m s^{-1} and 2.29°C, respectively, the accuracy values of the anemometer (±0.01 m s^{-1}) and thermometer (±1.0°C) and that the magnitude of these errors would have little influence on the final result for the calculation of the variables studied. Thus, the computer models can be considered suitable for the proposed use.

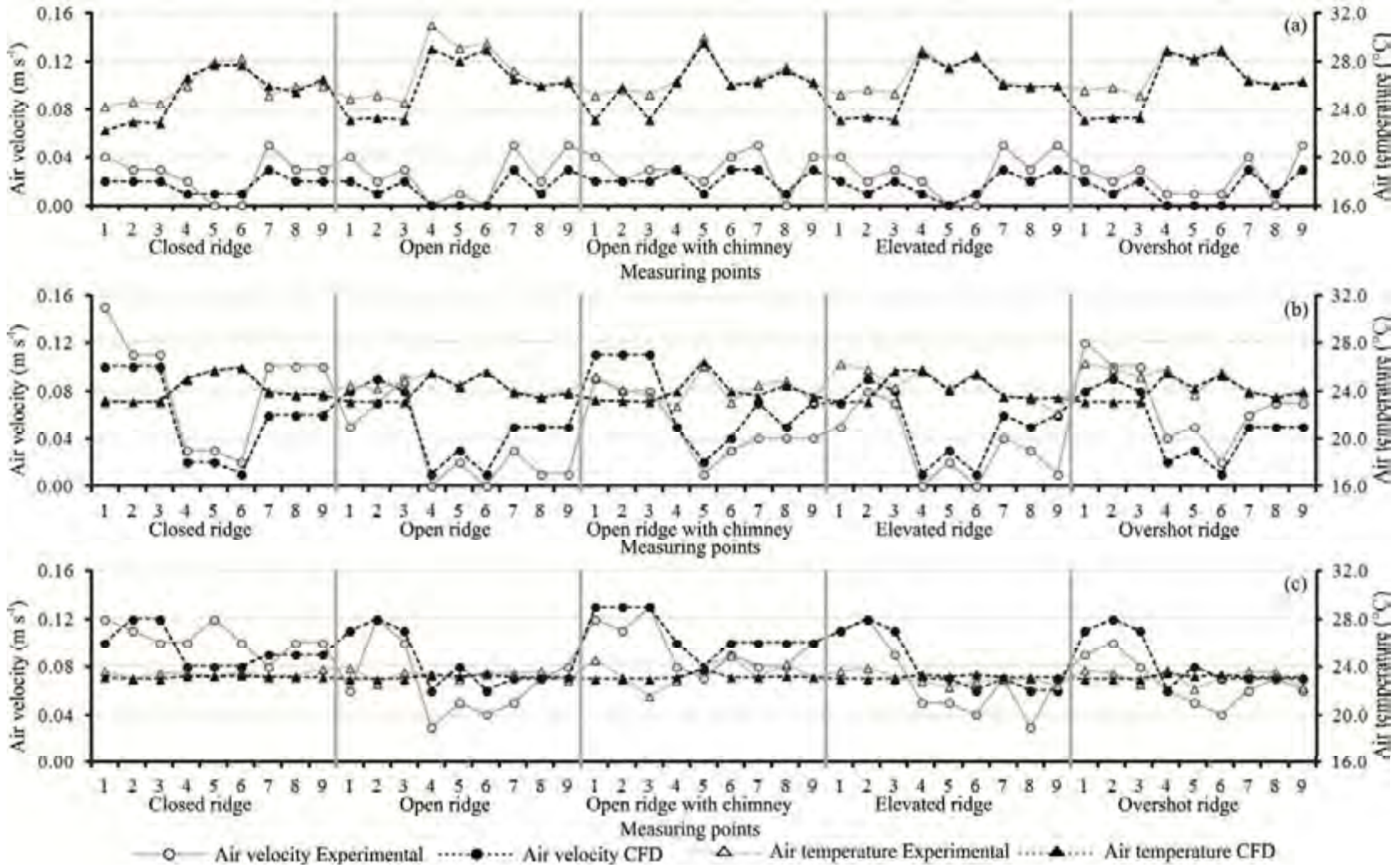

Figure 4.120 - Differences between air velocities and temperature measured experimentally and CFD model, using air speed simulated of 0.10 m s^{-1} and wind direction to north, at 9 locations and 3 different heights: (a) 0.02 m, (b) 0.11 m, and (c) 0.20 m.

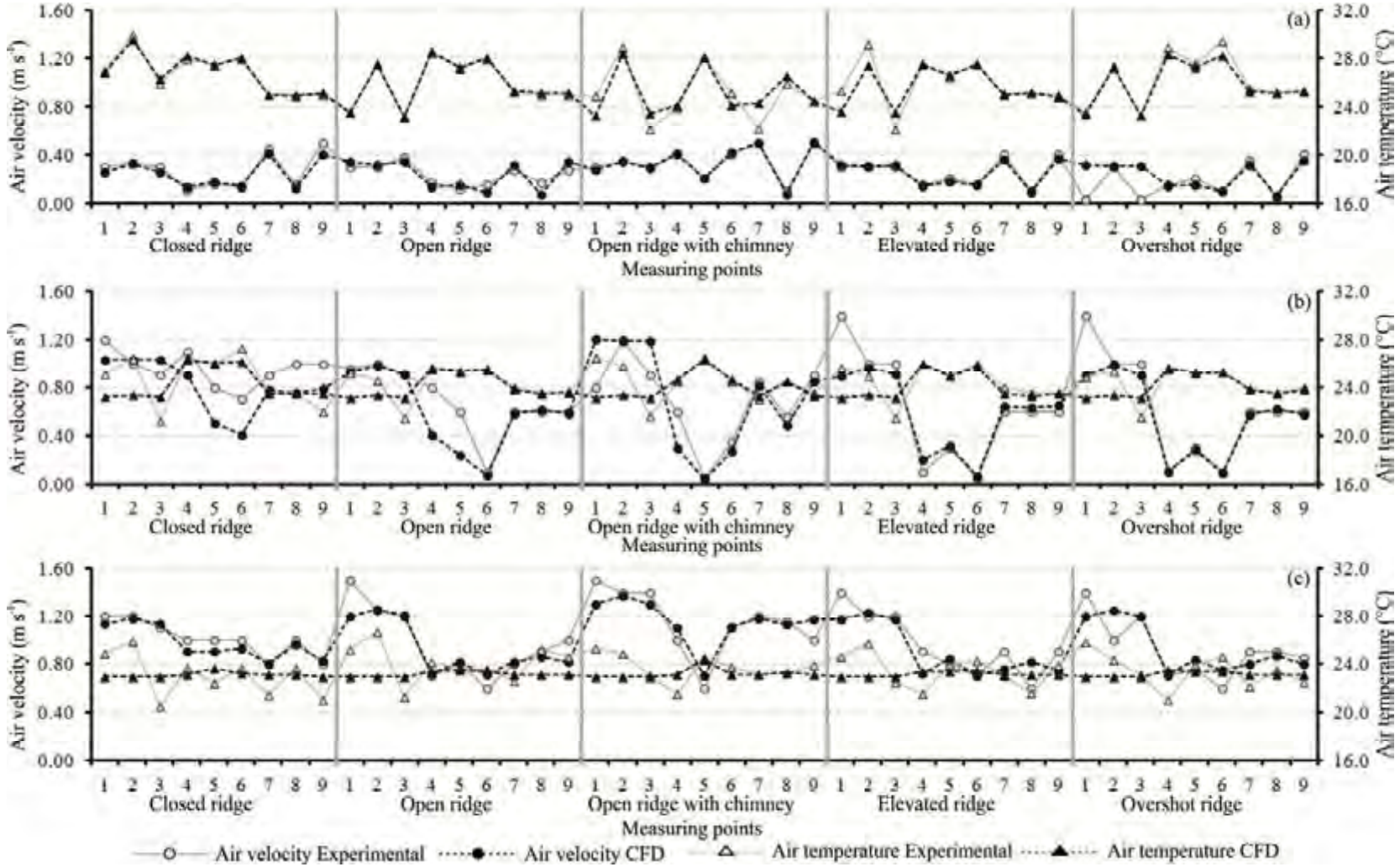

Figure 4.121 - Differences between air velocities and temperature measured experimentally and simulated with CFD, using air velocity of 1.0 m s^{-1} and direction to north, at nine locations and three different heights: (a) 0.02 m, (b) 0.11 m, and (c) 0.20 m.

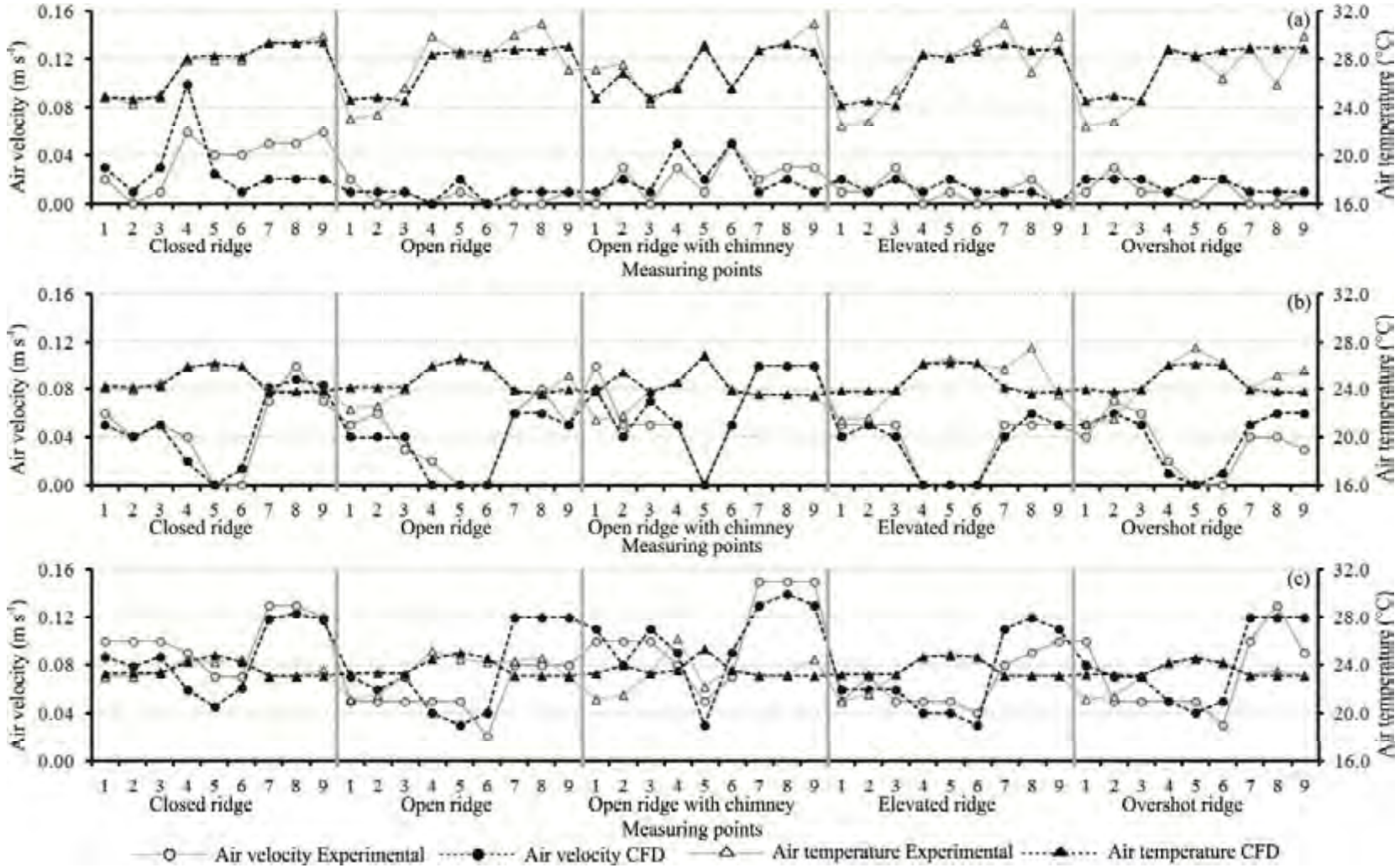

Figure 4.122 - Differences between air velocities and temperature measured experimentally and simulated with CFD, using air velocity of 0.1 m s^{-1} and direction to south, at nine locations and three different heights: (a) 0.02 m, (b) 0.11 m, and (c) 0.20 m.

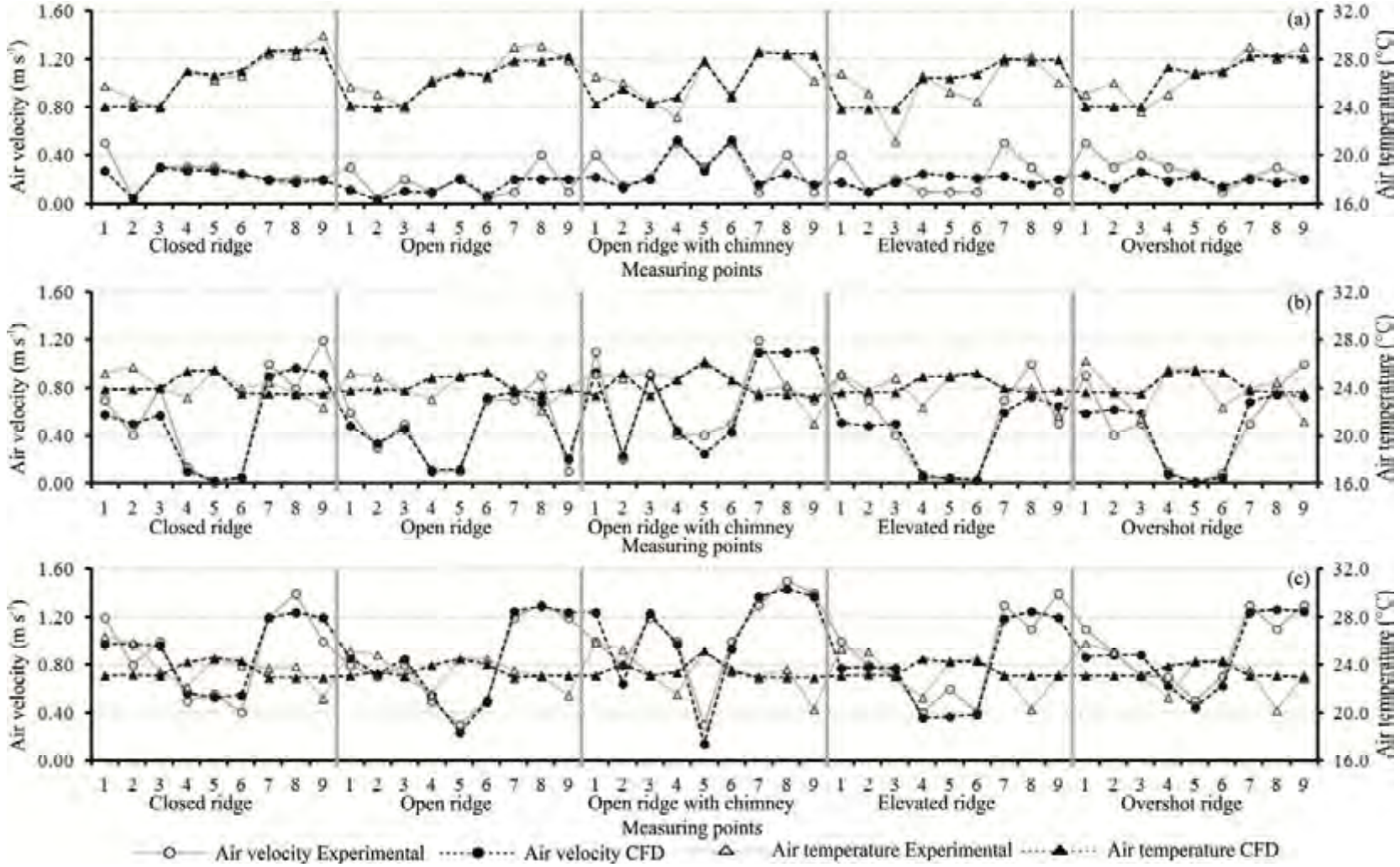

Figure 4.123 - Differences between air velocities and temperature measured experimentally and simulated with CFD, using air velocity of 1.0 m s^{-1} and direction to south, at nine locations and three different heights: (a) 0.02 m, (b) 0.11 m, and (c) 0.20 m.

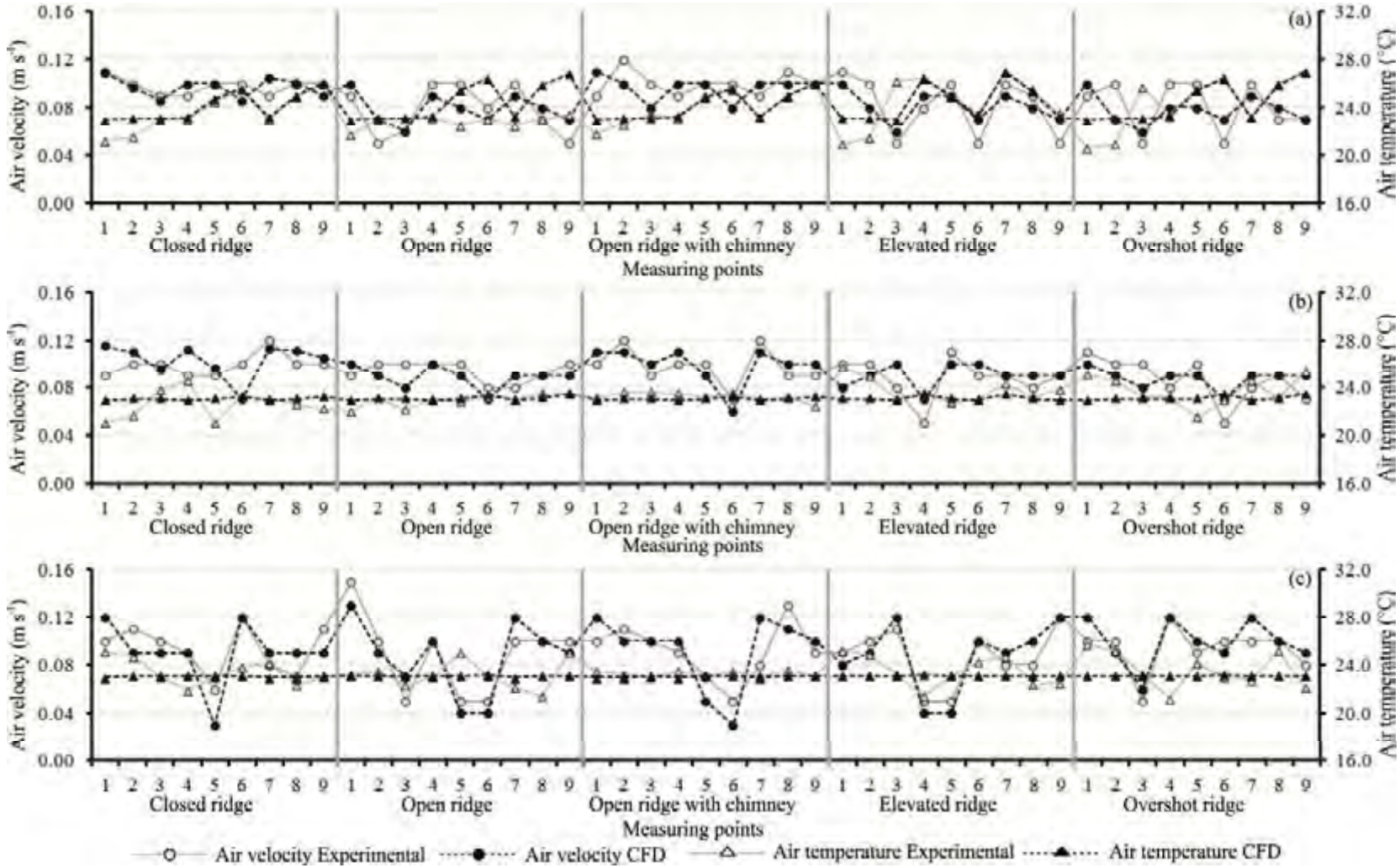

Figure 4.124 - Differences between air velocities and temperature measured experimentally and simulated with CFD, using air velocity of 0.1 m s^{-1} and direction to west, at nine locations and three different heights: (a) 0.02 m, (b) 0.11 m, and (c) 0.20 m.

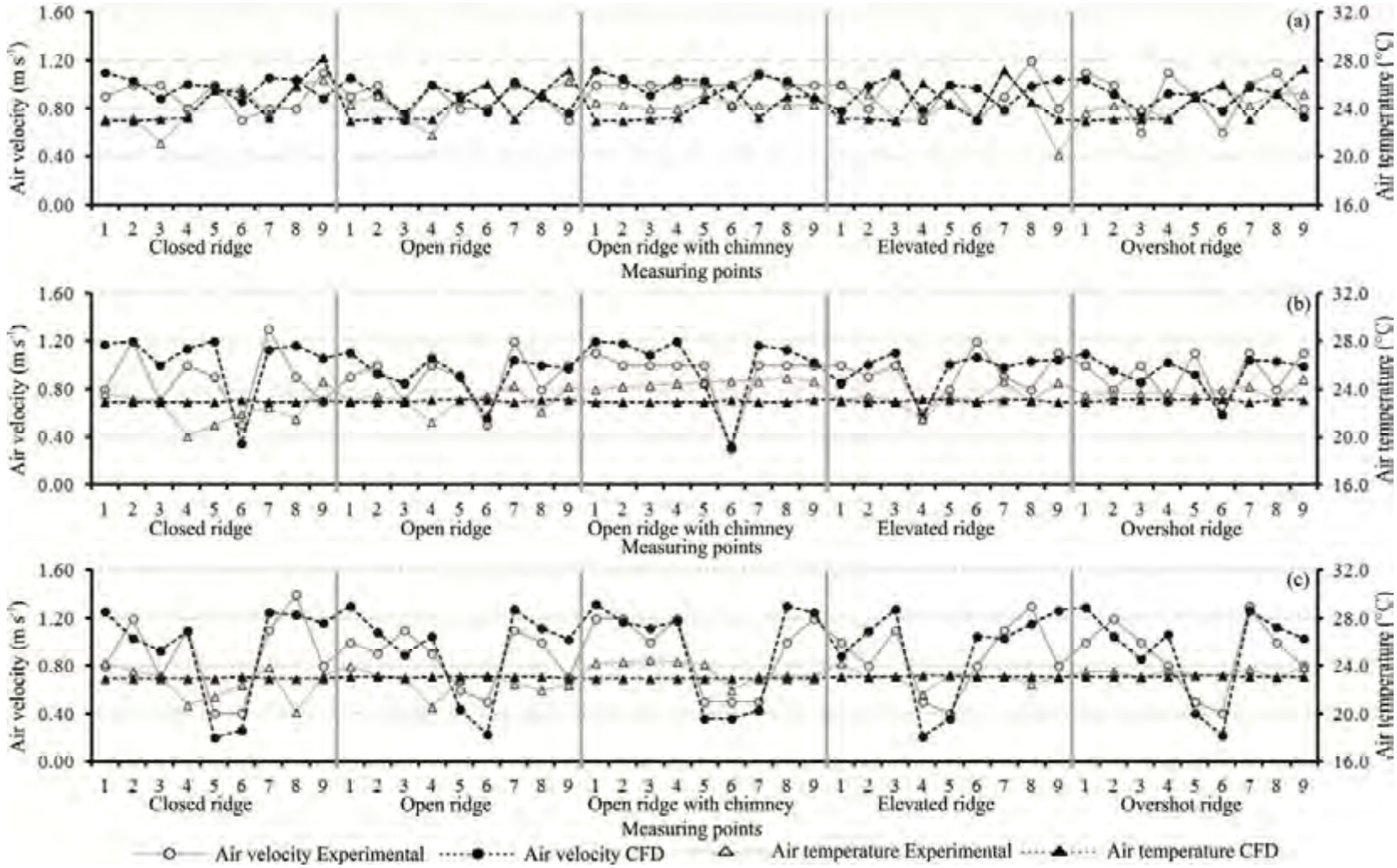

Figure 4.125 - Differences between air velocities and temperature measured experimentally and simulated with CFD, using air velocity of 1.0 m s^{-1} and direction to west, at nine locations and three different heights: (a) 0.02 m, (b) 0.11 m, and (c) 0.20 m.

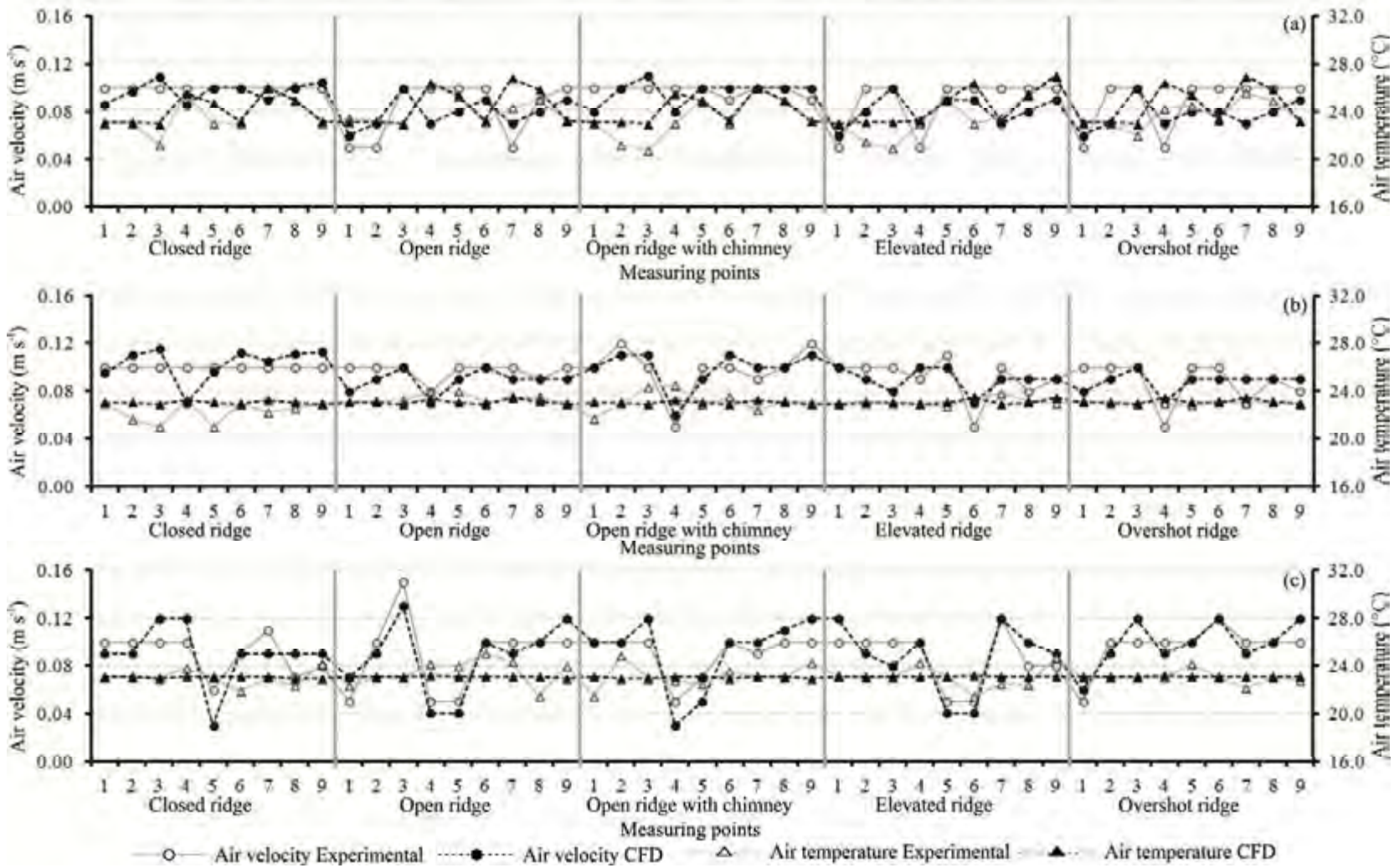

Figure 4.126 - Differences between air velocities and temperature measured experimentally and simulated with CFD, using air velocity of 0.1 m s^{-1} and direction to east, at nine locations and three different heights: (a) 0.02 m, (b) 0.11 m, and (c) 0.20 m.

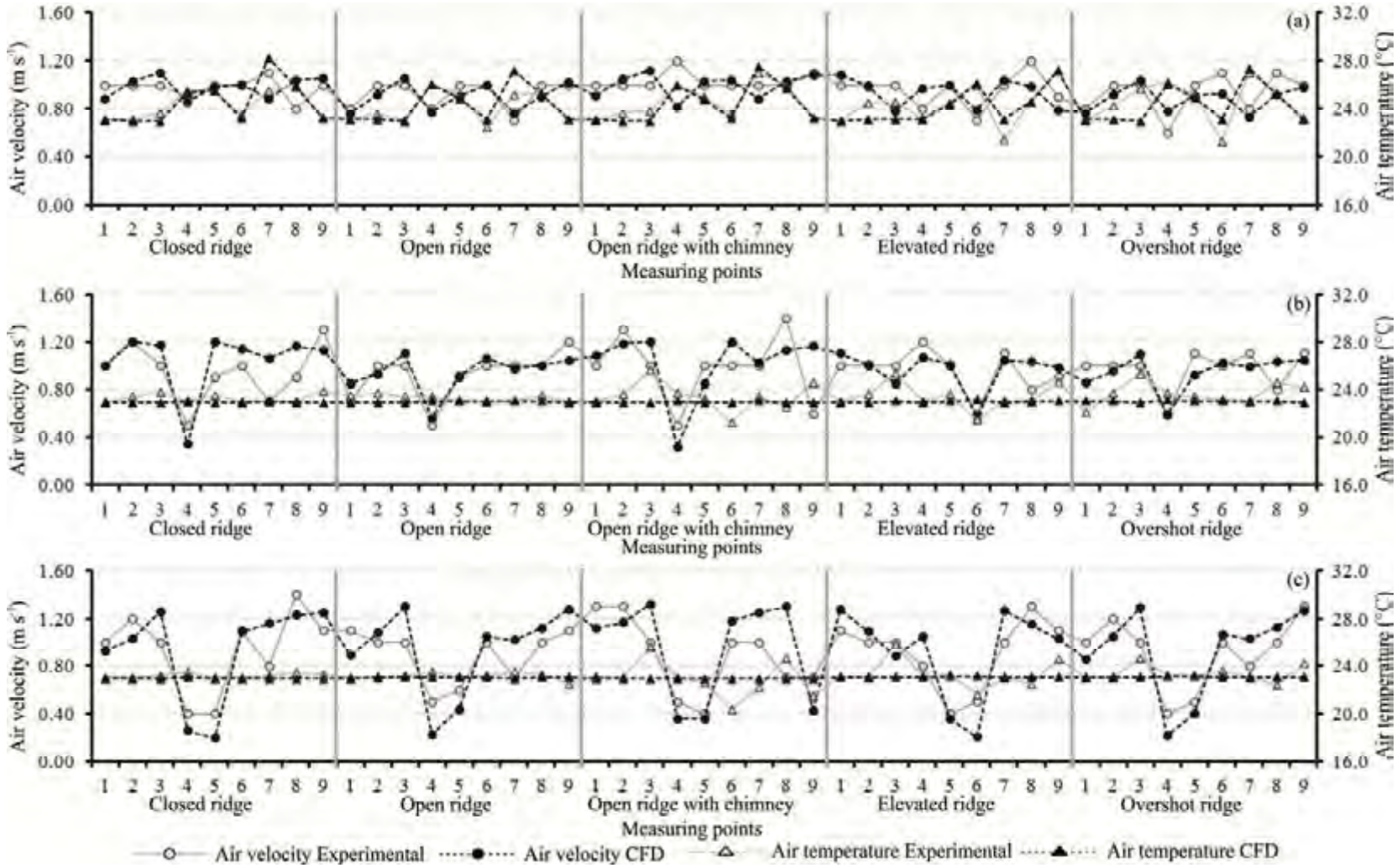

Figure 4.127 - Differences between air velocities and temperature measured experimentally and simulated with CFD, using air velocity of 1.0 m s^{-1} and direction to east, at nine locations and three different heights: (a) 0.02 m, (b) 0.11 m, and (c) 0.20 m.

4.4.3. Airflow patterns

Airflow patterns in the reduced models were analyzed using smoke produced by vaporized Glycerin. These studies were conducted at a wind velocity of 0.1 and 1.0 m s^{-1}. Similar inside airflow distributions were observed in all in simulated and measured five ridge type evaluated when compared with CFD model evaluated with the same wind directions. Small differences in flow patterns inside reduced model and CFD were observed with different ventilation ridge openings. The smoke was visually observed when it was passed through the ridge opening.

4.4.4. Computational simulation

Application of tests with adapted values and calculated variables found in the field were performed to exemplify the application of computational models developed for a CBP barn equipped with five different ridge types and four wind directions.

4.4.4.1. Applying computational simulation of the reduced model

The main conditions used to validate the computational model were used in this study. However, the values (1.35 x 1.20 x 0.27 m) used in these CFD simulations correspond to CBP barn 24, in which the value of air speed and heat flux of the floor (compost area) were 0.04 m s^{-1} and 0.1 W m^{-2} (details about these values calculated can be seen in Appendix E), respectively. The values of air temperature used was 6.9°C (see Table 4.18).

Table 4.18 – Boundary conditions utilized in the CFD model

Case	Location	Boundary condition	Value
1	Inlet	Average air speed	0.04 m s^{-1}
		Air temperature	6.9°C
	Outlet	Atmospheric pressure	0 Pa
	Floor	Heat flux	0.1 W m^{-2}

The results of the simulations performed by the computational models provide visual demonstration of the impact on air flow through structure and information of the effect of the air velocity in cooling an area of the floor (compost area), as can be seen in Figures 4.128 to 4.172.

Such simulations can help engineers and dairy producers in project development and management of the CBP barns. Applying various scenarios and allowing the simulation to aid in the understanding the whole system.

Figures 4.128 to 4.135 shows the simulated air velocity vectors and temperature distribution vertically and on the surface of the floor in CBP barn equipped with closed ridge (CLR).

Figures 4.128a and 4.128b showed that the air entered the CBP barn through the ridge opening at one side, and then exited through the sidewall opening located at the other side. So, the air flow velocity was reduced due to presence of the wall and fences on both side of the barn. It resulted in a internal vortex at the center of the feed alley and compost area.

In the Figure 4.129, one can observe the effect of cooling the compost surface area near the alleyway. From the Figure 4.131, the higher surface temperature in the center of the compost area (after down flow from wall) is due to a reduced air velocity which results in lower cooling in this area. Figures 4.132 to 4.135 shows the simulated results of air velocity and surface temperature on the compost area, when predominant winds enter the installation at east to west and west to east. At the Figures 4.132 and 4.134, it can be seen that there is a considerable variation in the direction of the air velocity vectors. Inside of the trusses structure, it can be seen that the main flow tends to turn opposite the main wind direction.

In Figures 4.133 and 4.135, it can be seen observed that the vortex of the airflow promoted the worst conditions of air circulation and the surfaces temperature of the compost area were higher on the both sides of the barn.

The air velocity distribution in a vertical plan situated in the center of the barn allows us to determine the inside air speed more precisely. Figure 4.136 shows the air velocity distribution in a vertical plan situated in the center of the CBP barn equipped with closed ridge (CLR) in four wind direction. As evidenced in Figure 4.136, the higher air velocity values was observed near to the compost area in east and west winds. However, in the near ridge region, both these winds direction failed to perform well with air velocity values around 0.1 m s^{-1}. Outside air velocity values were higher in south and north wind directions. This aspect coincides with that of other studies performed by Norton et al. (2010b), Majdoubi et al. (2009), Lee et al. (2007), and Koenig et al. (1978).

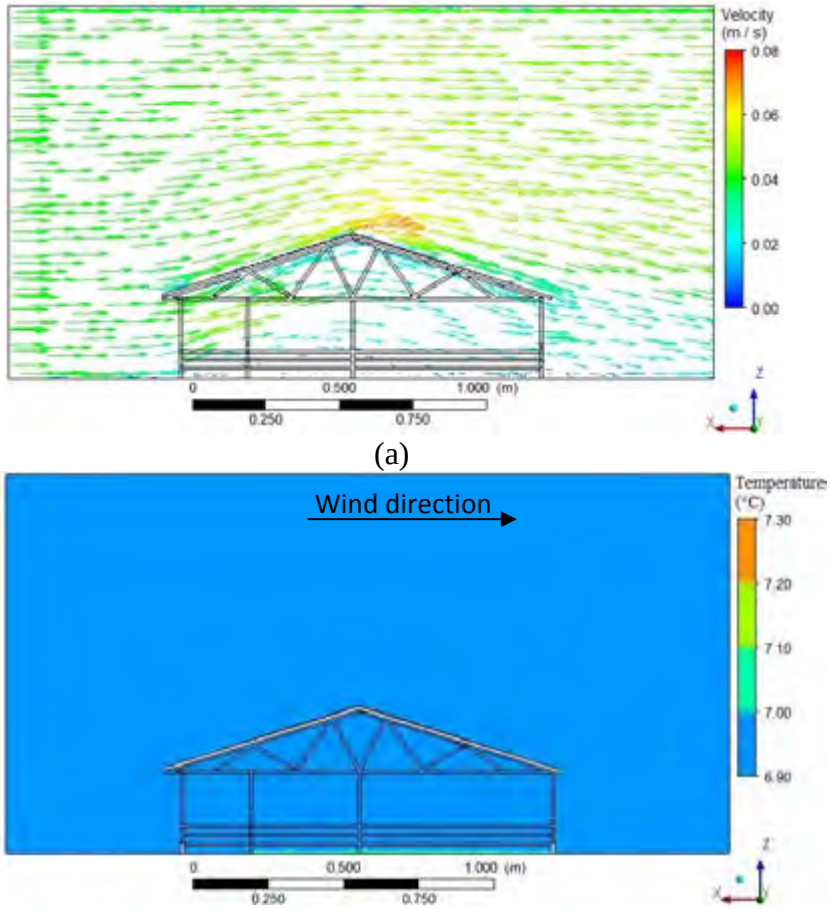

Figure 4.128 - Air velocity (a) and temperature (b) distribution vertically in the CBP barn equipped with closed ridge (CLR) and wind direction of south to north.

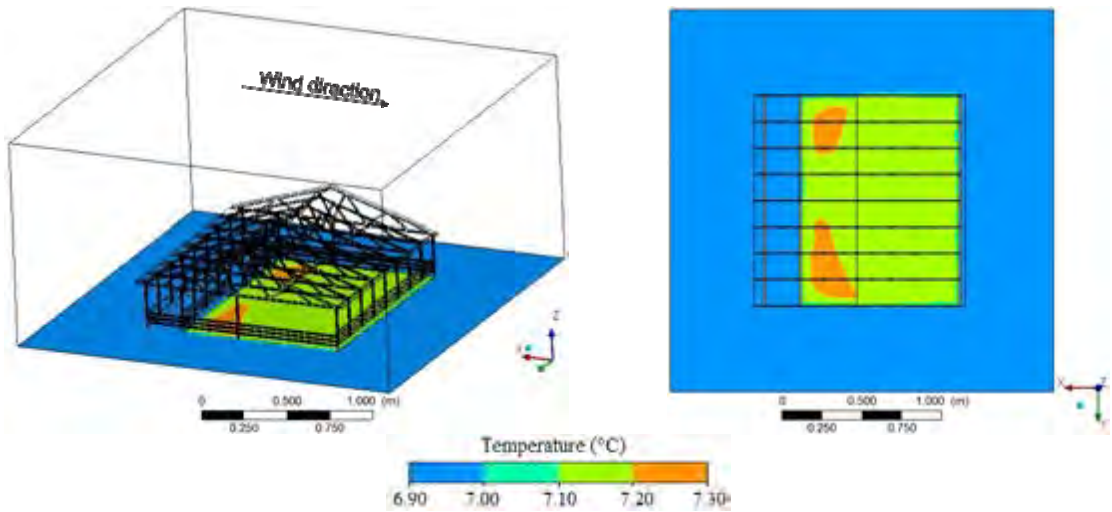

Figure 4.129 - Air temperature distribution on the surface of the floor inside the CBP barn equipped with closed ridge (CLR) and wind direction of south to north.

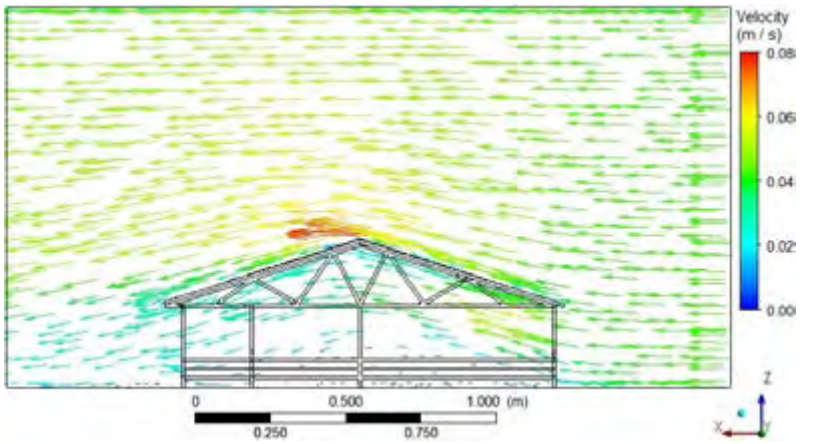

(a)

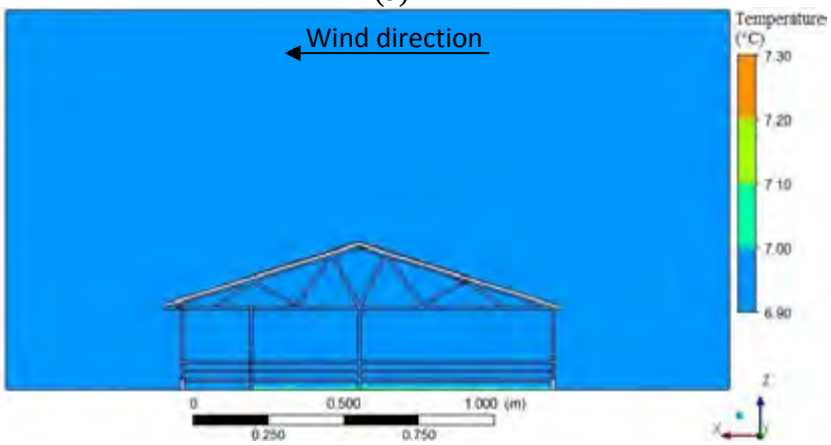

(b)

Figure 4.130 - Air velocity (a) and temperature (b) distribution vertically in the CBP barn equipped with closed ridge (CLR) and wind direction of north to south.

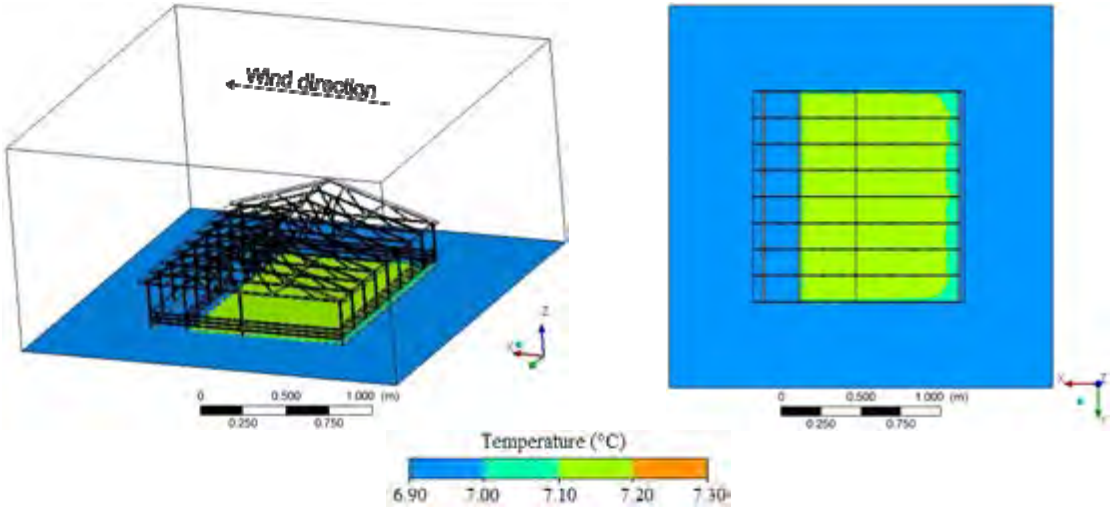

(a) (b)

Figure 4.131 - Air temperature distribution on the surface of the floor inside the CBP barn equipped with closed ridge (CLR) and wind direction of north to south.

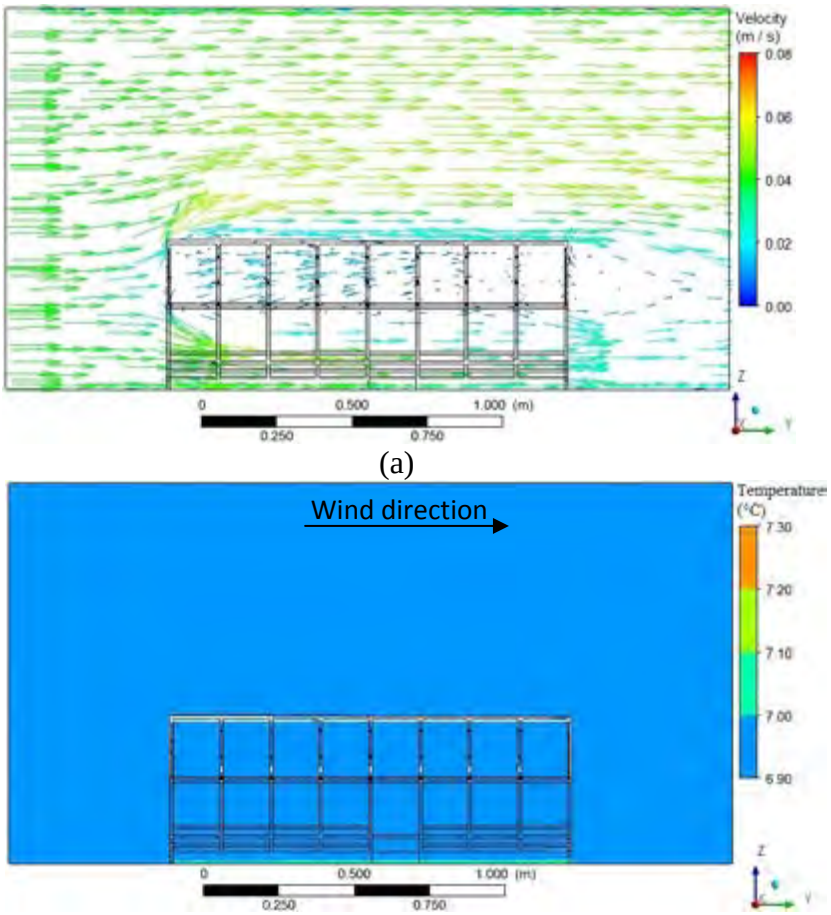

Figure 4.132 - Air velocity (a) and temperature (b) distribution vertically in the CBP barn equipped with closed ridge (CLR) and wind direction of east to west.

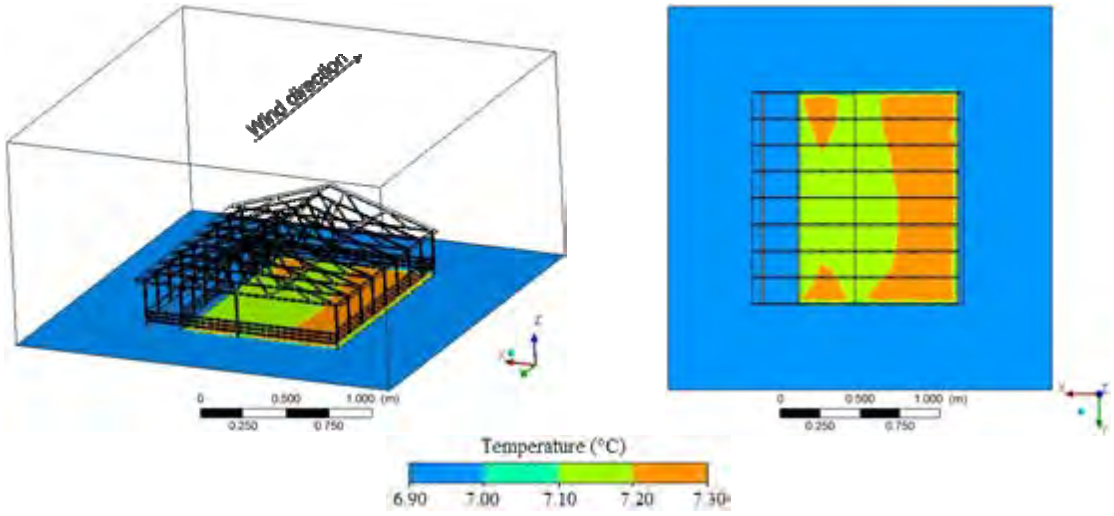

Figure 4.133 - Air temperature distribution on the surface of the floor inside the CBP barn equipped with closed ridge (CLR) and wind direction of east to west.

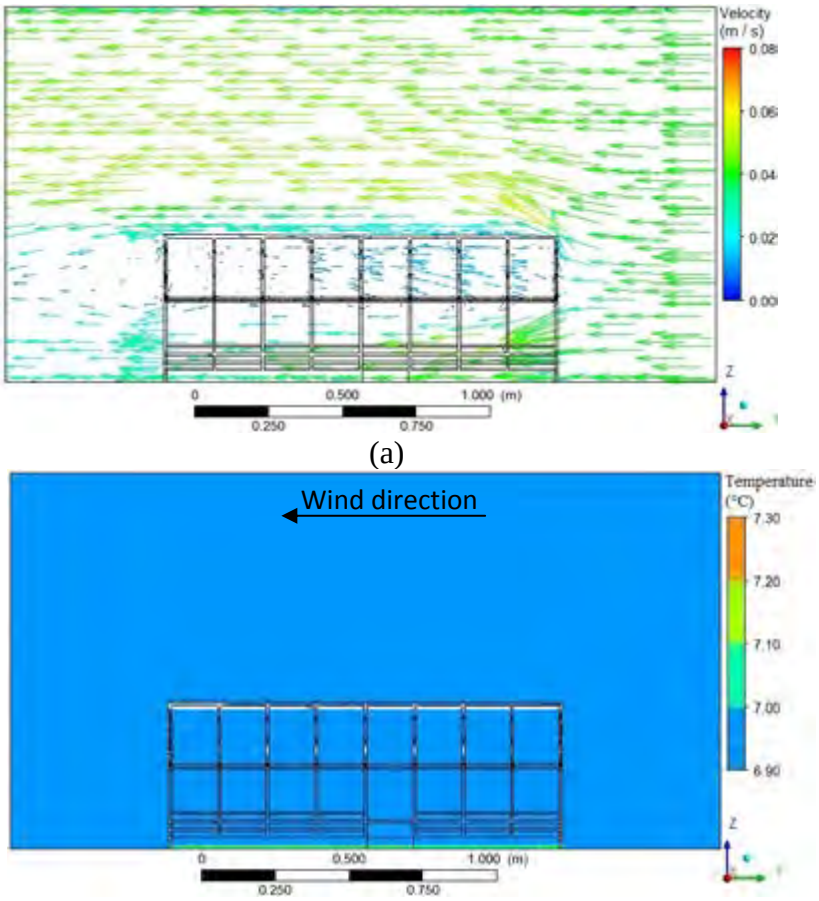

Figure 4.134 - Air velocity (a) and temperature (b) distribution vertically in the CBP barn equipped with closed ridge (CLR) and wind direction of west to east.

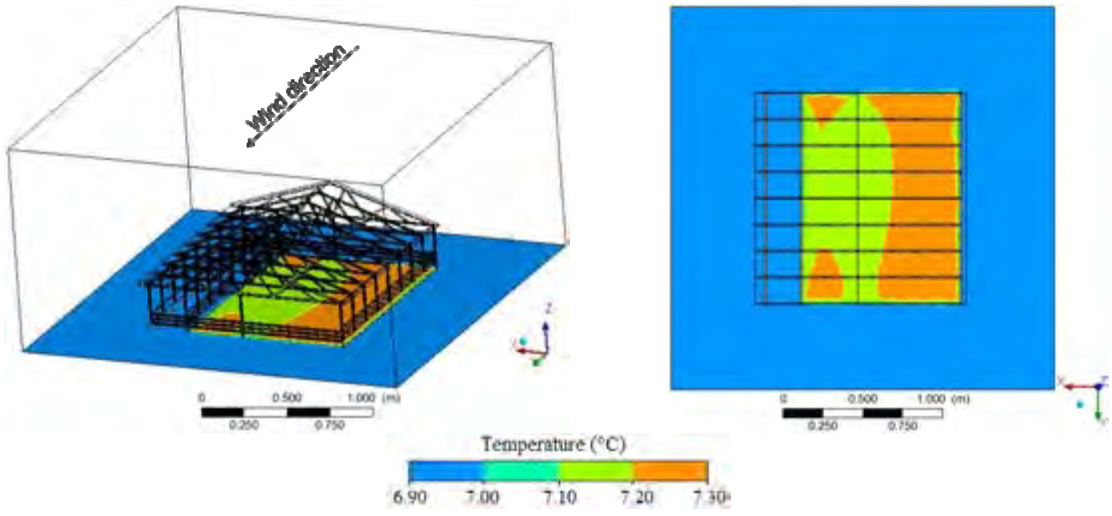

Figure 4.135 - Air temperature distribution on the surface of the floor inside the CBP barn equipped with closed ridge (CLR) and wind direction of west to east.

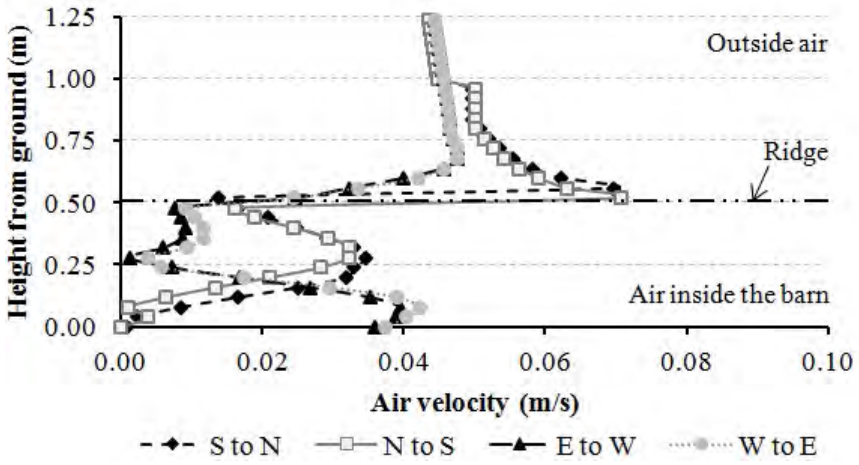

Figure 4.136 - Profile of mean horizontal wind speed in the centre of the CBP barn equipped with closed ridge (CLR) in four wind direction.

Figures 4.137 to 4.145 shows the simulated results of CBP barn equipped with open ridge (OPR) in four wind direction.

According to the Figures 4.137 and 4.139, these barns produced higher ridge vent flows for the south and north wind directions at wind velocities above 0.07 m s^{-1}. Wind direction comparisons indicated that south winds consistently produced the highest ridge vents flows (Figure 137a), however the east and west generated lowest ridge vent flows (Figures 4.141a and 4.143a). Since wind direction had a large influence on ridge vent flow, building orientation with respect to wind direction should be considered in the design of naturally ventilated, open ridge, assuming the reduced model exhibit similar airflow characteristics.

Figures 4.141 and 4.143 shown the reduction of air velocity inside the trusses structure. It can be seen that the main flow tends to turn opposite the main wind direction. Highest values of temperature on the surface of the compost area were observed with wind direction of north (Figure 4.140). By comparison, wind direction of east and west shown the lowest values of surface temperature on the compost area (Figures 4.142 and 4.144, respectively).

Figure 4.145 shows the air velocity distribution in a vertical plan situated in the centre of the CBP barn equipped with open ridge (OPR) in four wind direction. Examination of the air velocity inside the barn above the compost area surface, demonstrates that the values are very close at 0.2 m height from ground. However, one can remark that the air velocity values in south and north winds directions rapid increase at ridge area.

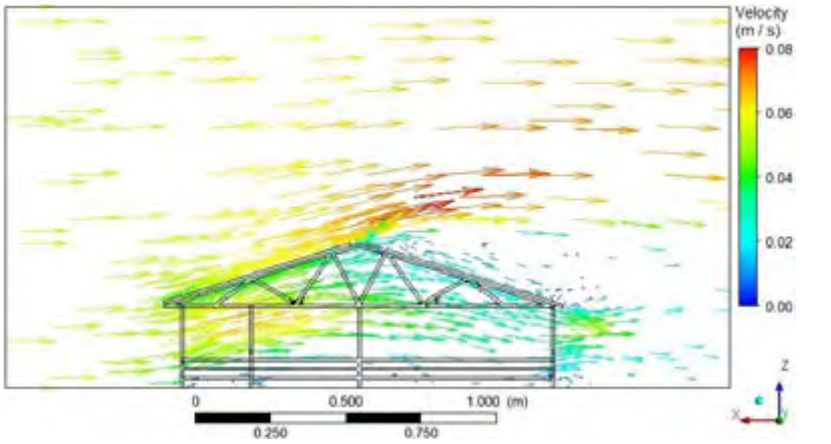

(a)

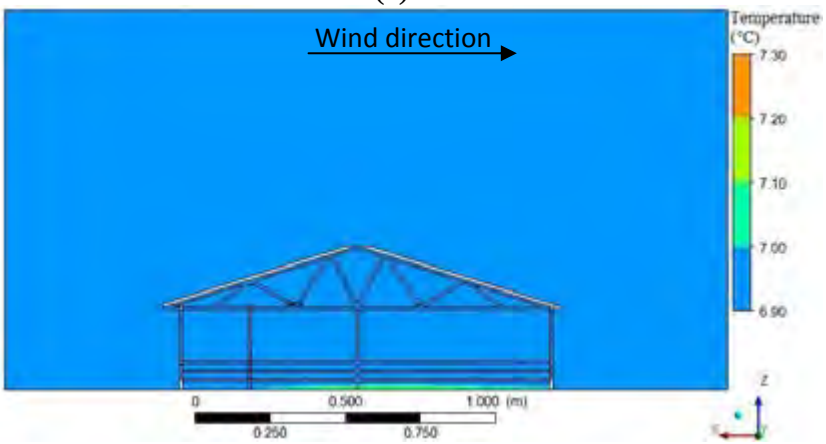

(b)

Figure 4.137 - Air velocity (a) and temperature (b) distribution vertically in the CBP barn equipped with open ridge (OPR) and wind direction of south to north.

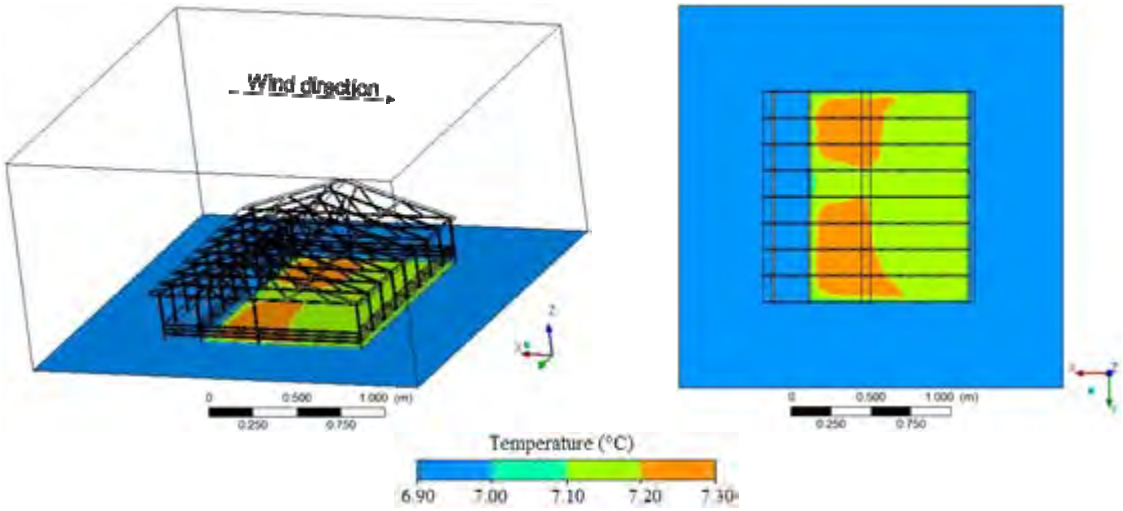

(a) (b)

Figure 4.138 - Air temperature distribution on the surface of the floor inside the CBP barn equipped with open ridge (OPR) and wind direction of south to north.

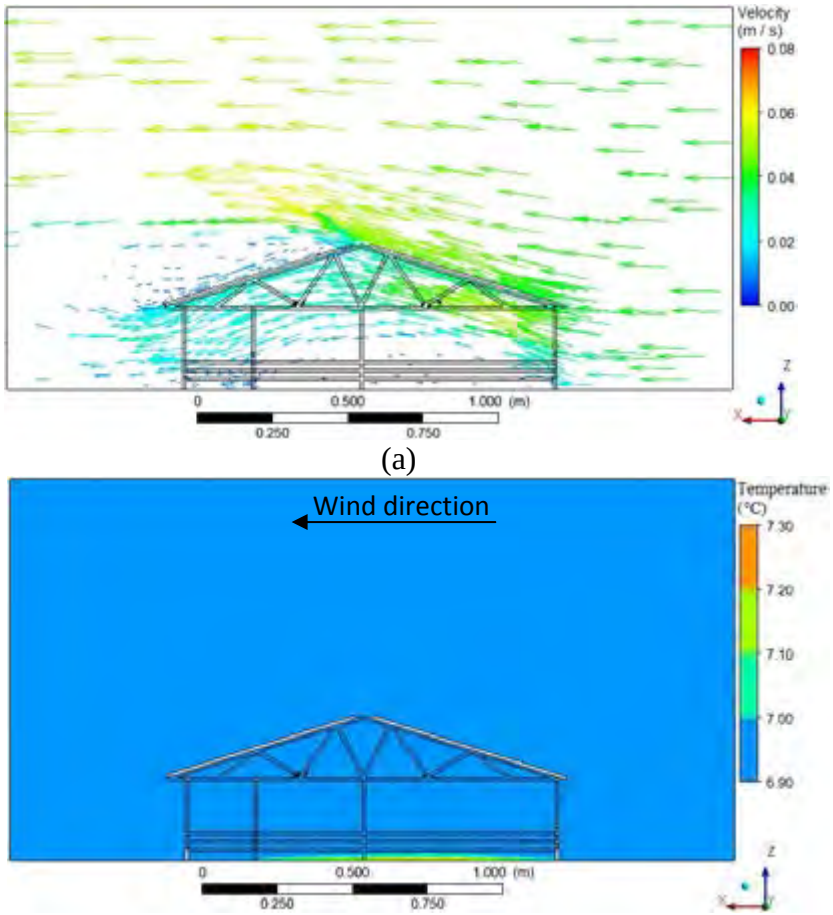

Figure 4.139 - Air velocity (a) and temperature (b) distribution vertically in the CBP barn equipped with open ridge (OPR) and wind direction of north to south.

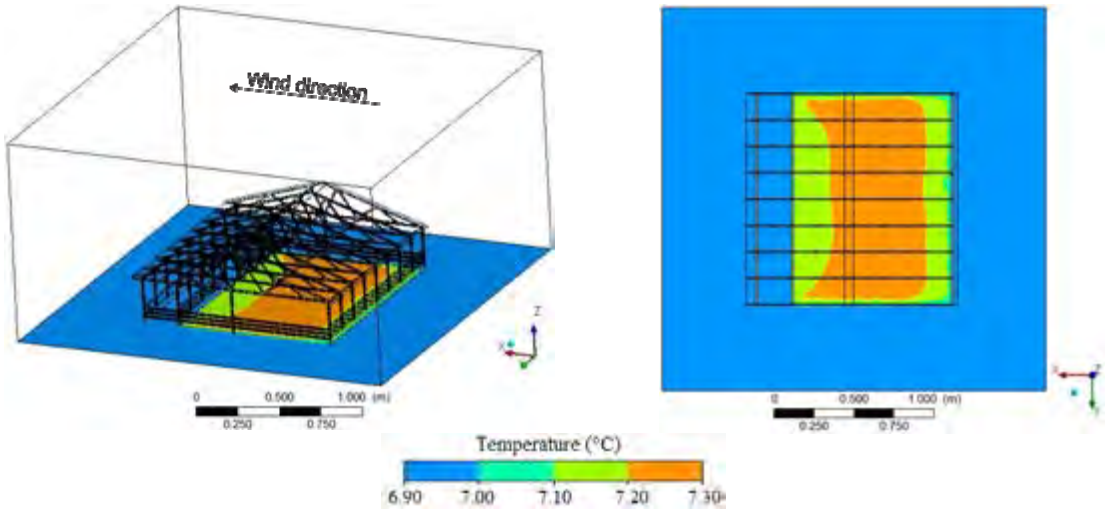

Figure 4.140 - Air temperature distribution on the surface of the floor inside the CBP barn equipped with open ridge (OPR) and wind direction of north to south.

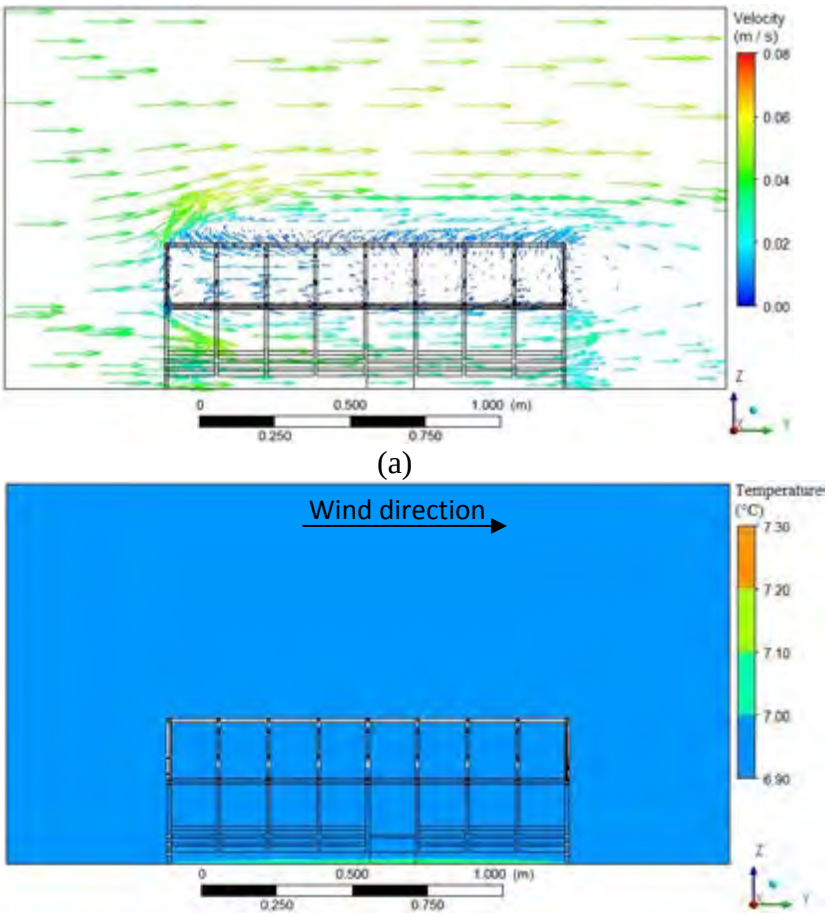

Figure 4.141 - Air velocity (a) and temperature (b) distribution vertically in the CBP barn equipped with open ridge (OPR) and wind direction of east to west.

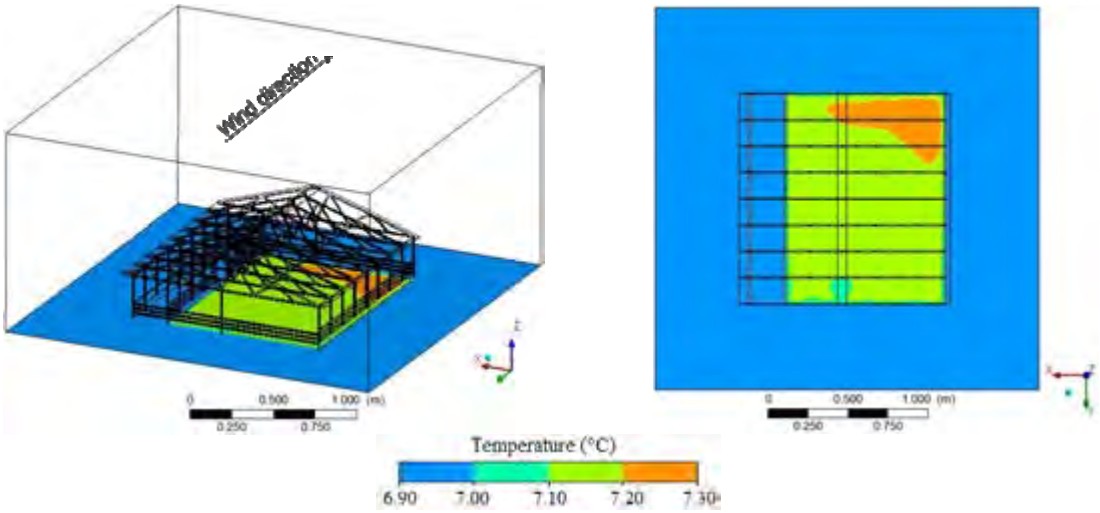

Figure 4.142 - Air temperature distribution on the surface of the floor inside the CBP barn equipped with open ridge (OPR) and wind direction of east to west.

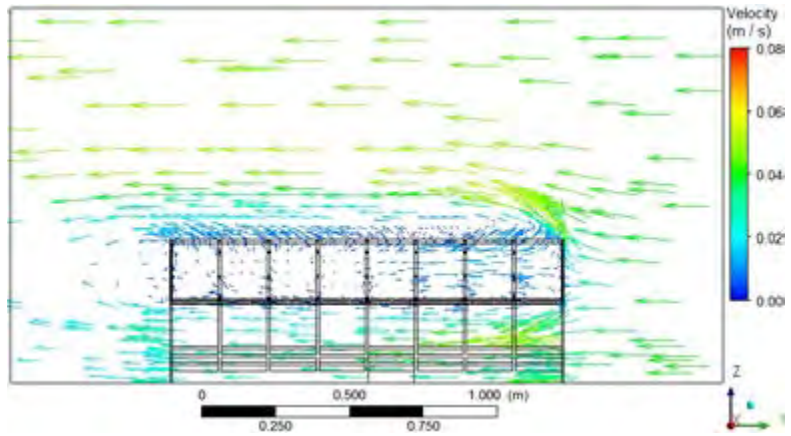

(a)

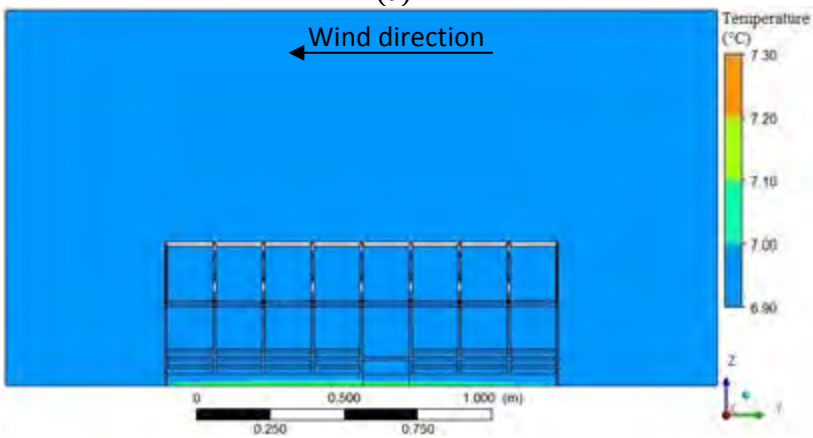

(b)

Figure 4.143 - Air velocity (a) and temperature (b) distribution vertically in the CBP barn equipped with open ridge (OPR) and wind direction of west to east.

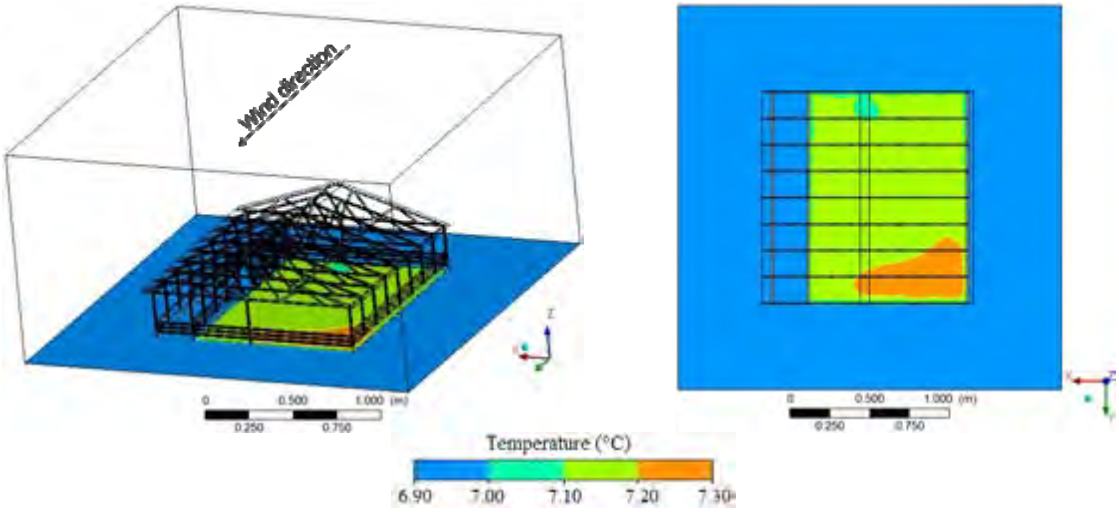

(a) (b)

Figure 4.144 - Air temperature distribution on the surface of the floor inside the CBP barn equipped with open ridge (OPR) and wind direction of west to east.

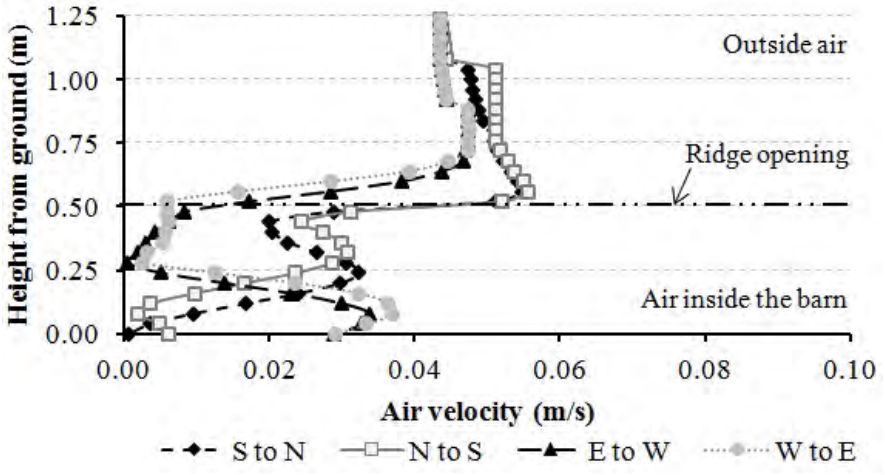

Figure 4.145 - Profile of mean horizontal wind speed in the centre of the CBP barn equipped with open ridge (OPR) in four wind direction.

Figures 4.146 to 4.153 shows the simulated results of CBP barn equipped with open ridge with chimney (ORC) in four wind direction. Figures 4.146 and 4.148 show considerable variation in the direction of the air velocity vectors, and consequently the flow is far from being two-dimensional. Near the ridge opening, it can be seen that center of turbulence is located above the roof in the right (Figure 4.146a) and left (Figure 4146b) side. From the Figure 4.148a, the north wind direction, which produced the highest ridge vent flows, also generated high air velocities inside the structure. So, the contour plot of the value of the vertical component of wind speed which is also shown in Figures 4.146 and 4.148 reveals periodic air circulation loops due to buoyancy forces with horizontal axes which develop perpendicularly to the wind.

Distribution of surface temperature on the compost area are represented in Figures 4.147, 4.149, 4.151, and 4.153. It can be observed that the distribution temperature on the compost area in wind direction north (Figure 4.149) is more uniform than east (Figure 4.151) and west (Figure 4.153). This result can be explained by the fact that the air velocity distribution is almost uniform in near entire compost area. In contrast, when the wind direction were east and west, the air movement tends to stabilize, generating lower air velocity above the compost area. Figure 4.154 shows the air velocity distribution in a vertical plan situated in the center of the CBP barn equipped with open ridge with chimney (ORC) in four wind direction. The air velocity value above the compost area is lower in south and north wind direction due to drag effect of the sidewall and sidewall planks. The air velocity values were lower near ridge opening in east and west wind direction.

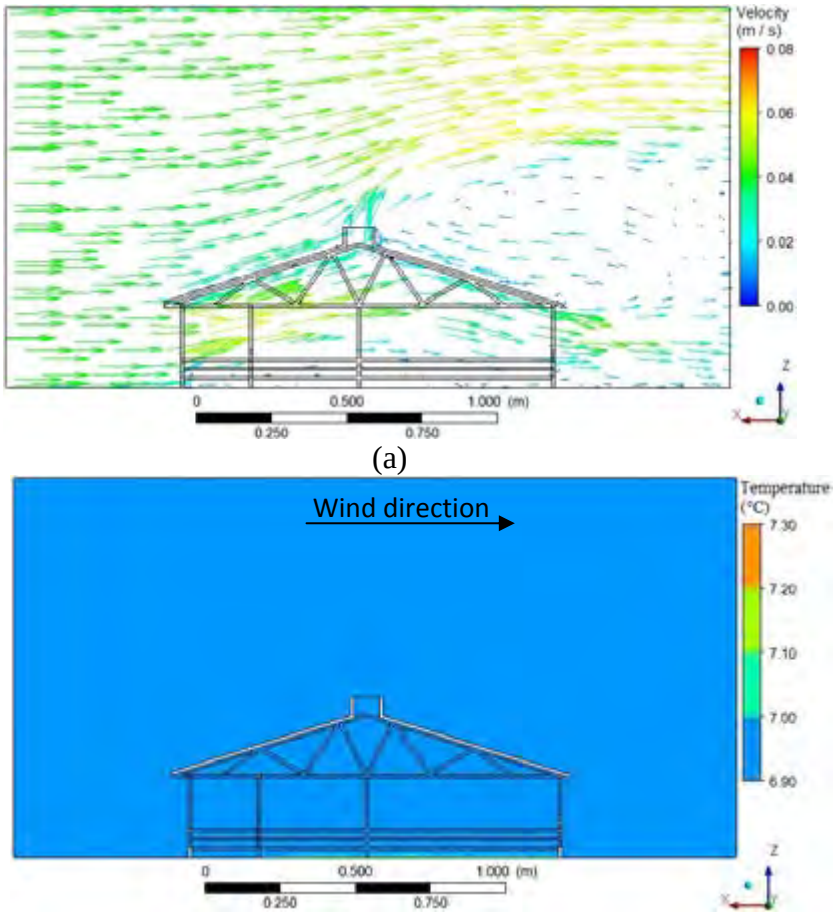

Figure 4.146 - Air velocity (a) and temperature (b) distribution vertically in the CBP barn equipped with open ridge with chimney (ORC) and wind direction of south.

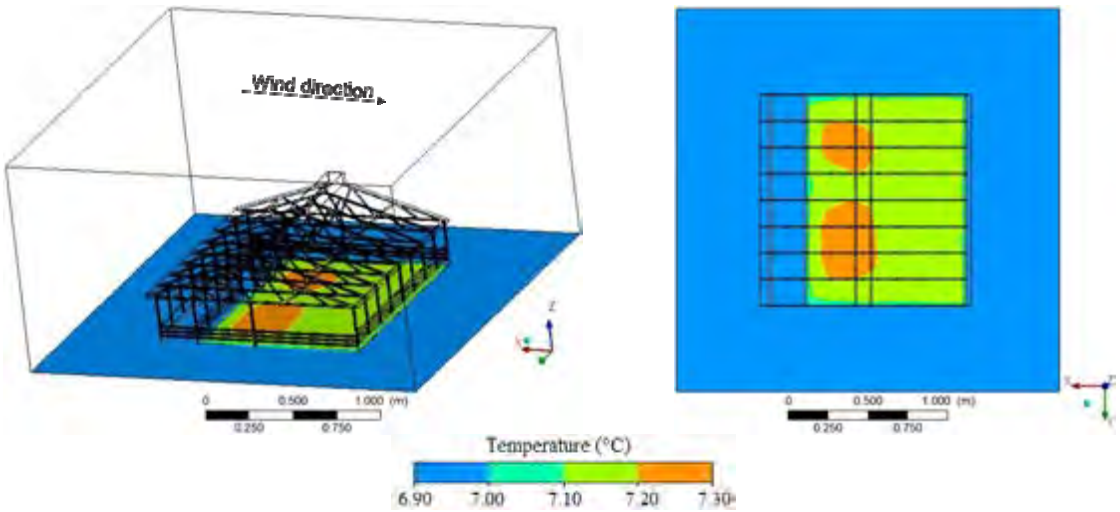

Figure 4.147 - Air temperature distribution on the surface of the floor inside the CBP barn equipped with open ridge with chimney (ORC) and wind direction of south to north.

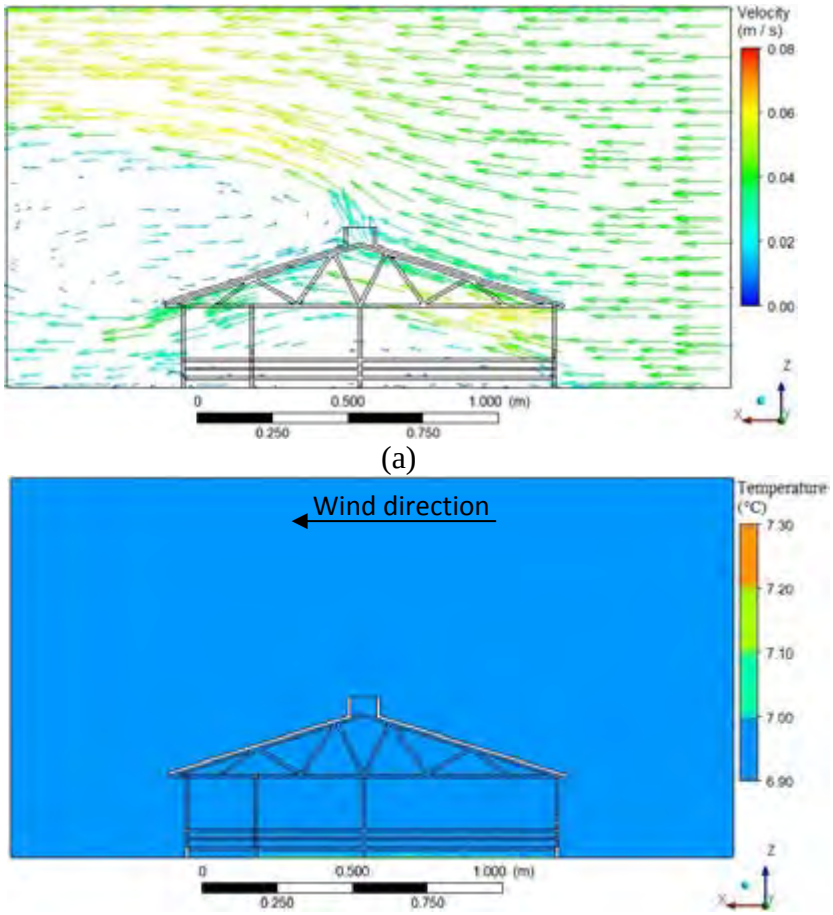

Figure 4.148 - Air velocity (a) and temperature (b) distribution vertically in the CBP barn equipped with open ridge with chimney (ORC) and wind direction of north to south.

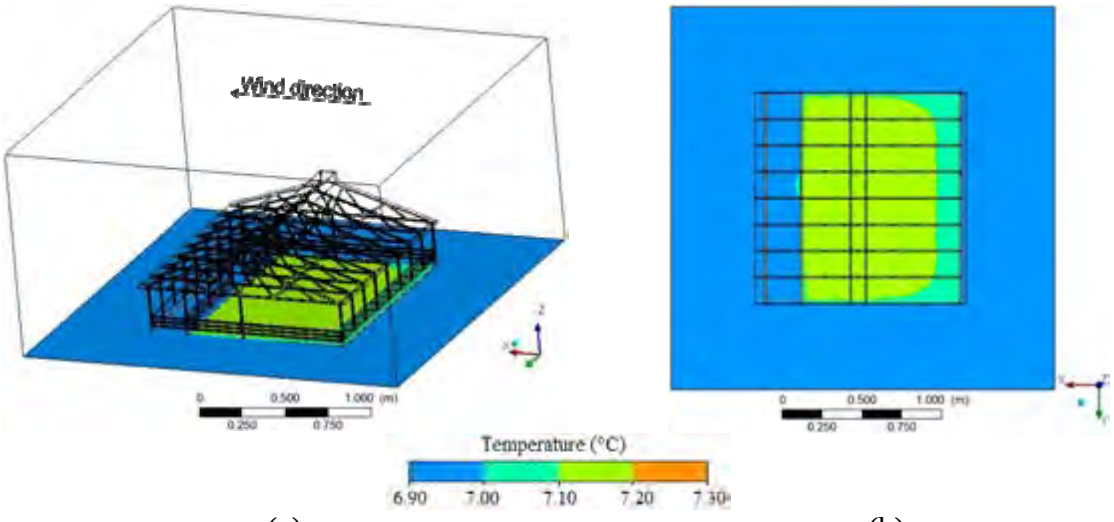

Figure 4.149 - Air temperature distribution on the surface of the floor inside the CBP barn equipped with open ridge with chimney (ORC) and wind direction of north to south.

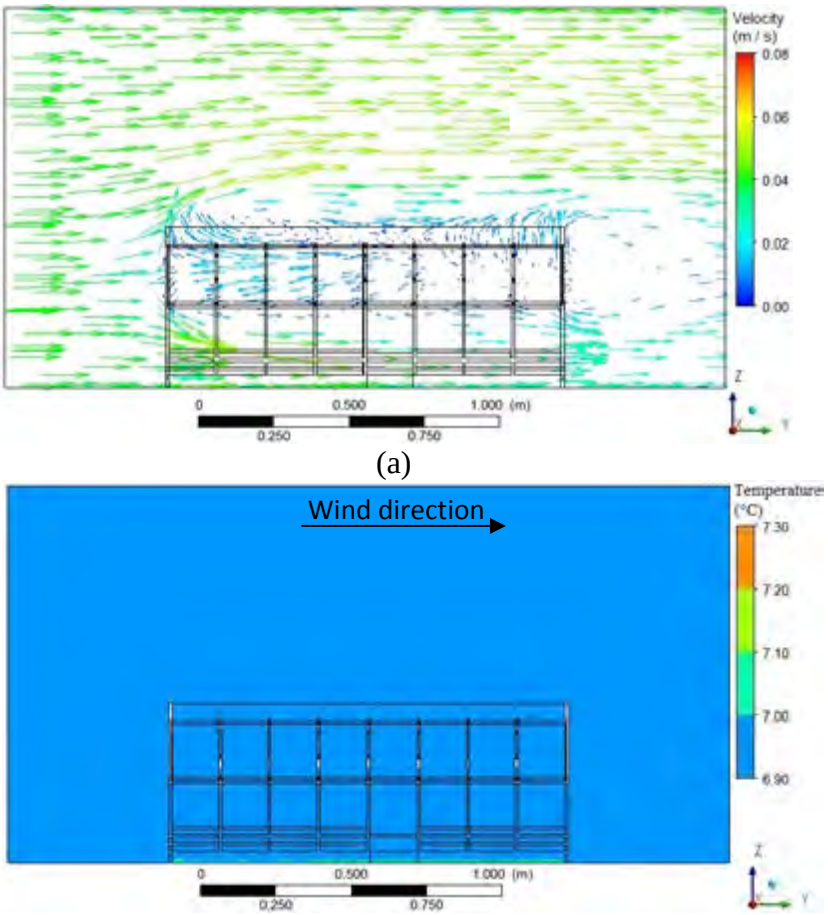

Figure 4.150 - Air velocity (a) and temperature (b) distribution vertically in the CBP barn equipped with open ridge with chimney (ORC) and wind direction of east to west.

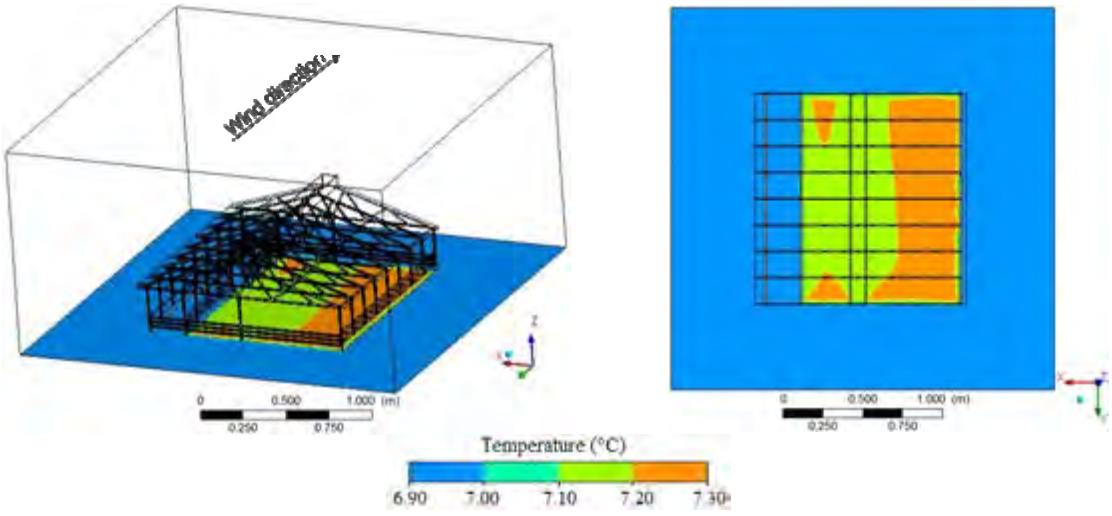

Figure 4.151 - Air temperature distribution on the surface of the floor inside the CBP barn equipped with open ridge with chimney (ORC) and wind direction of east to west.

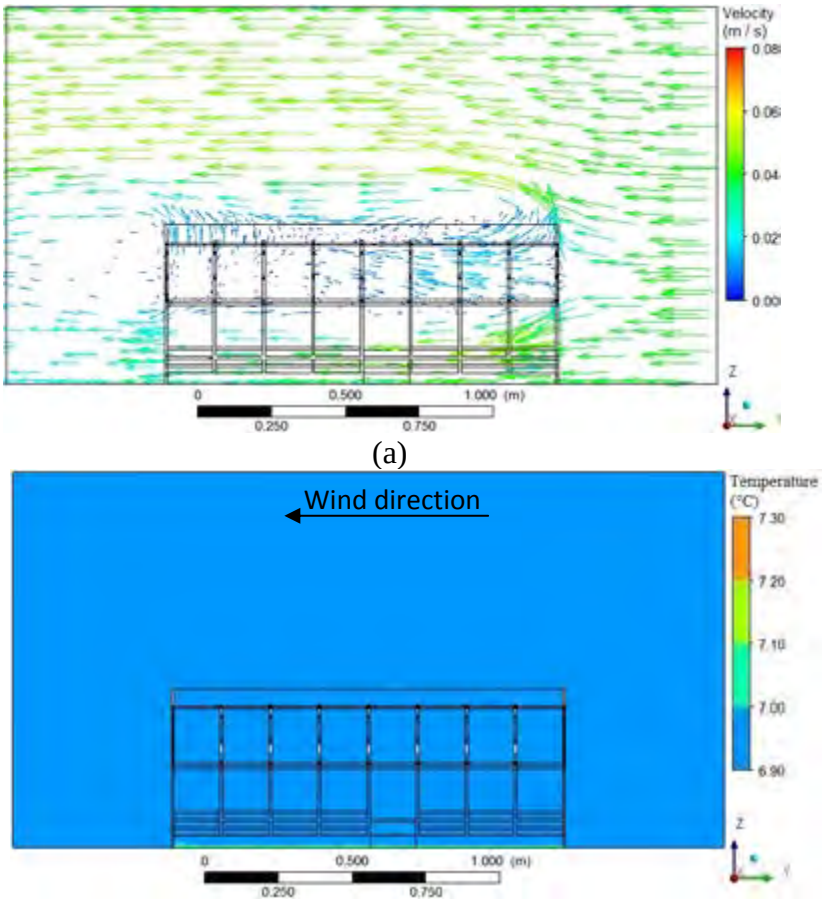

Figure 4.152 - Air velocity (a) and temperature (b) distribution vertically in the CBP barn equipped with open ridge with chimney (ORC) and wind direction of west to east.

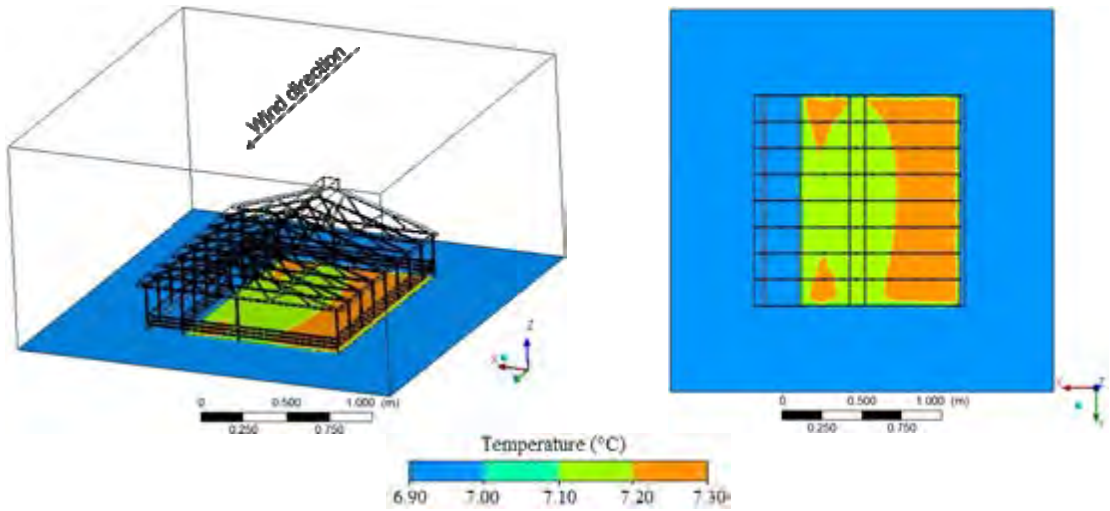

Figure 4.153 - Air temperature distribution on the surface of the floor inside the CBP barn equipped with open ridge with chimney (ORC) and wind direction of west to east.

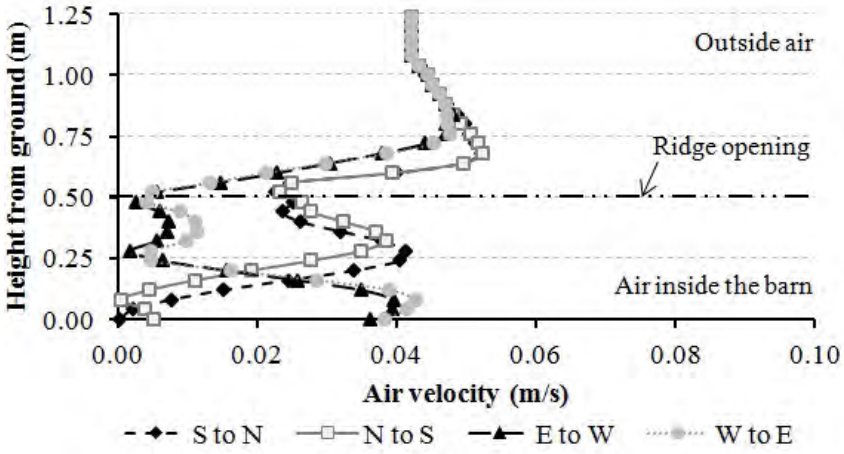

Figure 4.154 - Profile of mean horizontal wind speed in the centre of the CBP barn equipped with open ridge with chimney (ORC) in four wind direction.

Figures 4.155 to 4.162 shows the simulated results of CBP barn equipped with elevated ridge (ELR) in four wind direction. The higher ridge vent outlet flow was visualized in CBP barn equipped with ELR ridge type using east and west winds direction (Figure 4.155a and 4.157a). The wind flows up the windward wall surface and above the roof of the barns with east and west winds (Figures 4.159a and 4.161a) but hits the roof inside the barn with south and north winds (see Figures 4.155a and 4.157a). In addition, a lower pressure area is created above the roof in the east and west winds than above the south and north winds, thereby generating higher ridge opening flows.

Figures 4.155b, 4.157b, 4.159b, and 4.161b represents the air temperature distribution vertically by convection and Figures 4.156, 4.158, 4.160, and 4.162 shown the temperature distribution on the surface of the compost area. The worst uniformity in surface temperature was observed in compost area tested with north wind direction (Figures 4.158) in relation to other winds direction, which may be due to the fact that air flux over the compost area is less uniform.

Figure 4.163 shows the air velocity distribution in a vertical plan situated in the center of the CBP barn equipped with elevated ridge (ELR) in four wind direction. In general, this shows that the average air speed in the space between the top of the compost area and the barn roof is approximately half that of the outside wind, for all wind directions. Air velocity is much lower inside the barn than outside and its flows through ridge opening systematically higher in south and north wind directions.

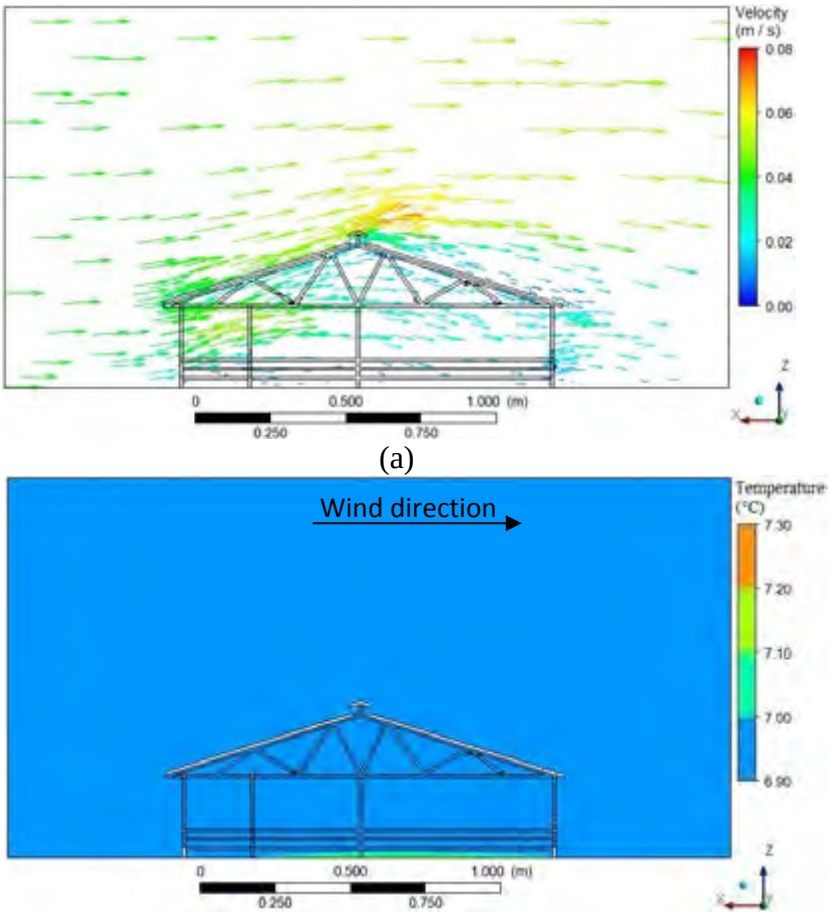

Figure 4.155 - Air velocity (a) and temperature (b) distribution vertically in the CBP barn equipped with elevated ridge (ELR) and wind direction of south to north.

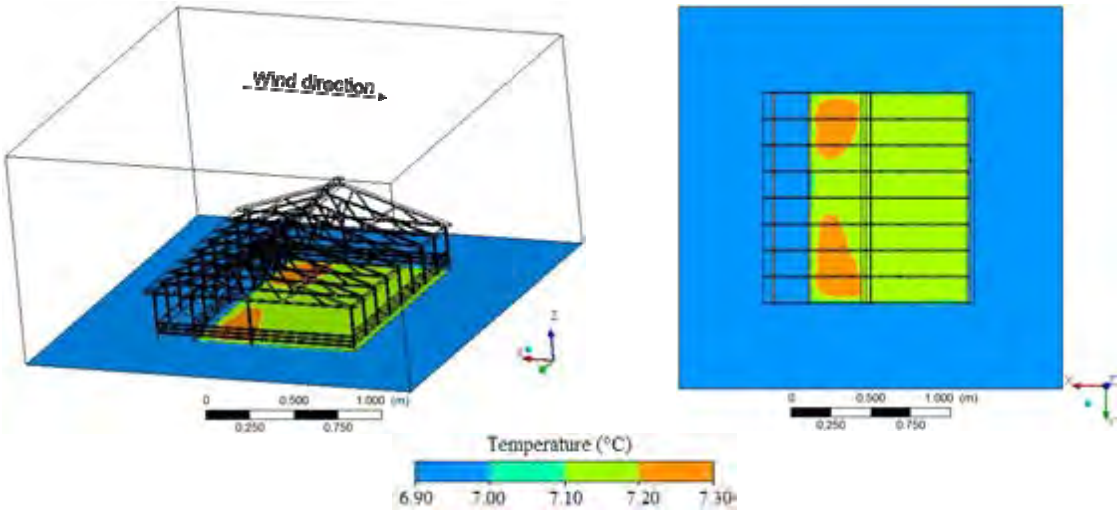

Figure 4.156 - Air temperature distribution on the surface of the floor inside the CBP barn equipped with elevated ridge (ELR) and wind direction of south to north.

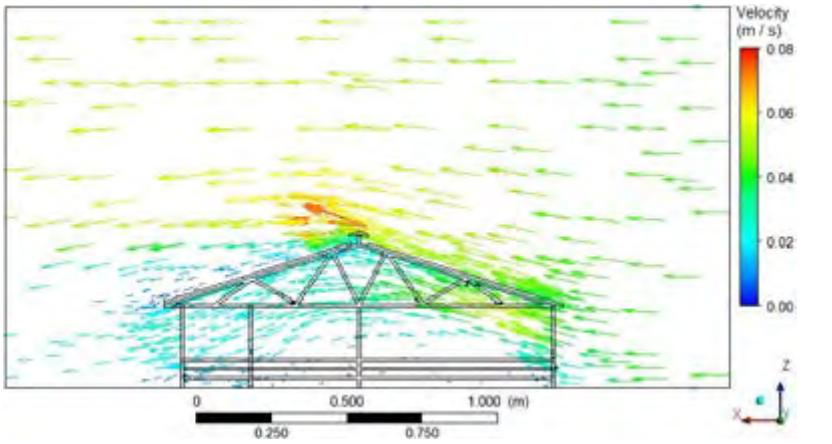

(a)

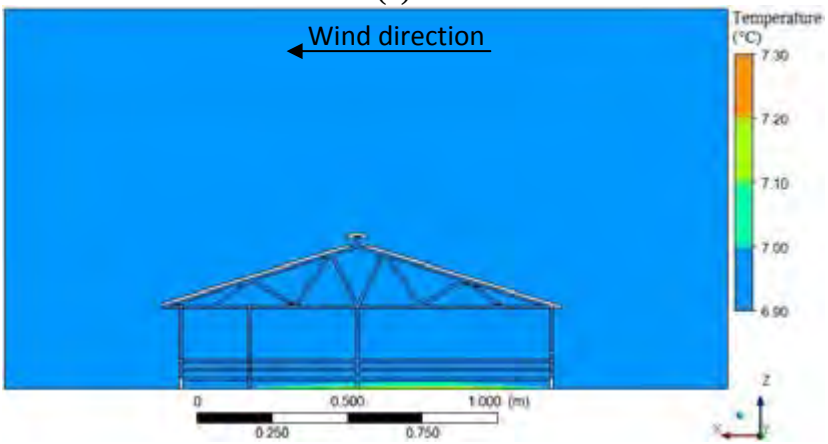

(b)

Figure 4.157 - Air velocity (a) and temperature (b) distribution vertically in the CBP barn equipped with elevated ridge (ELR) and wind direction of north to south.

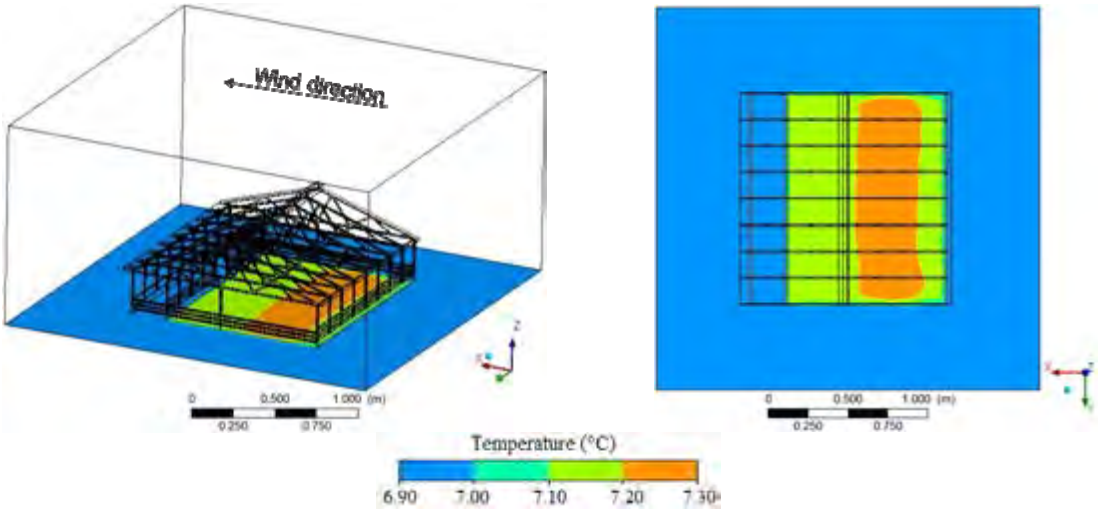

(a) (b)

Figure 4.158 - Air temperature distribution on the surface of the floor inside the CBP barn equipped with elevated ridge (ELR) and wind direction of north to south.

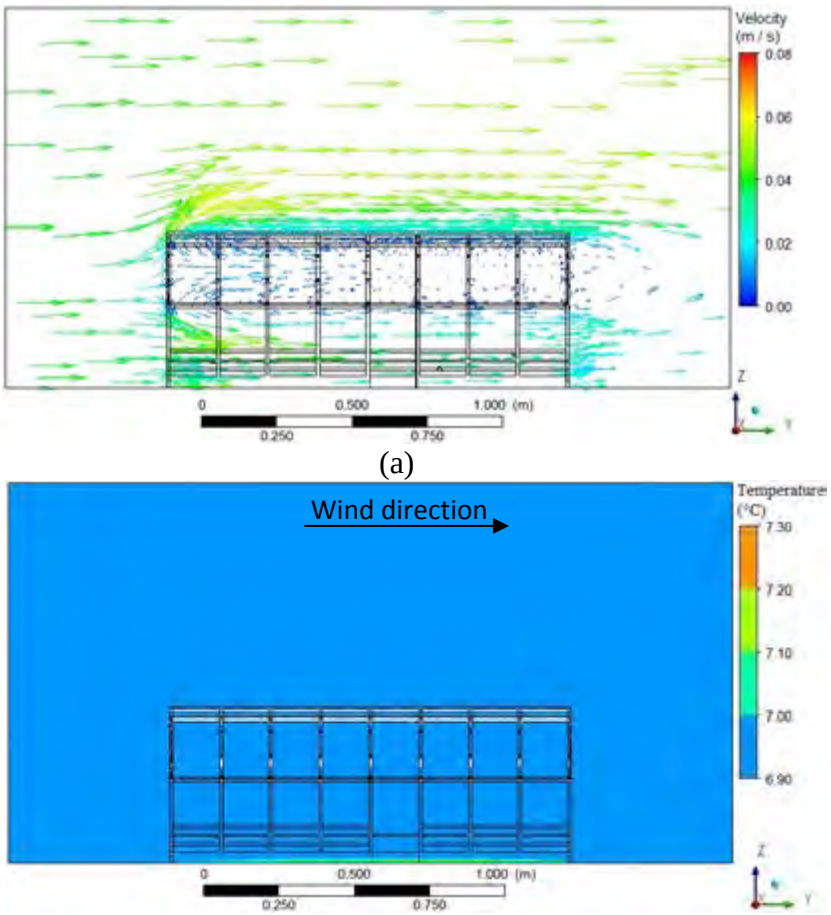

Figure 4.159 - Air velocity (a) and temperature (b) distribution vertically in the CBP barn equipped with elevated ridge (ELR) and wind direction of east to west.

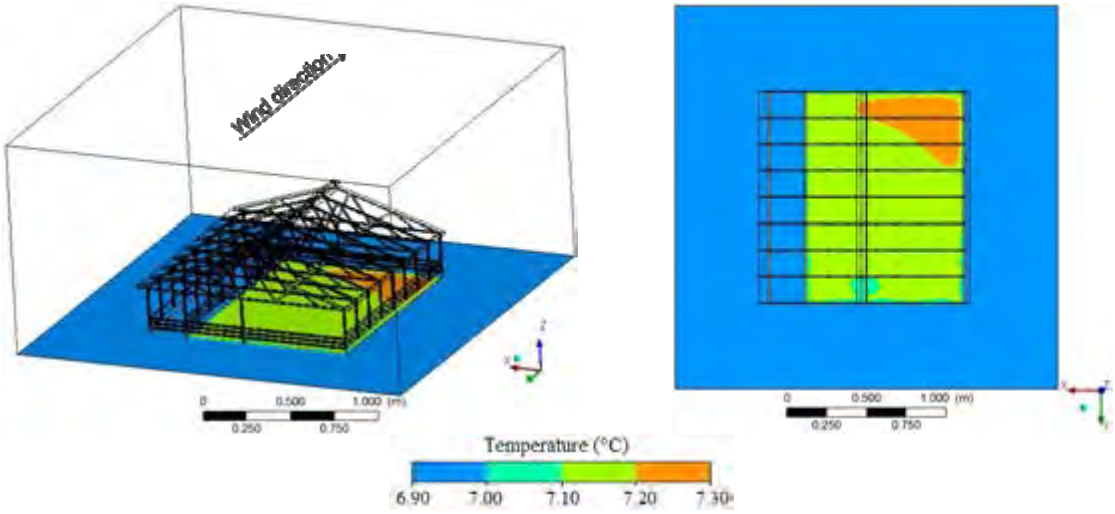

Figure 4.160 - Air temperature distribution on the surface of the floor inside the CBP barn equipped with elevated ridge (ELR) and wind direction of east to west.

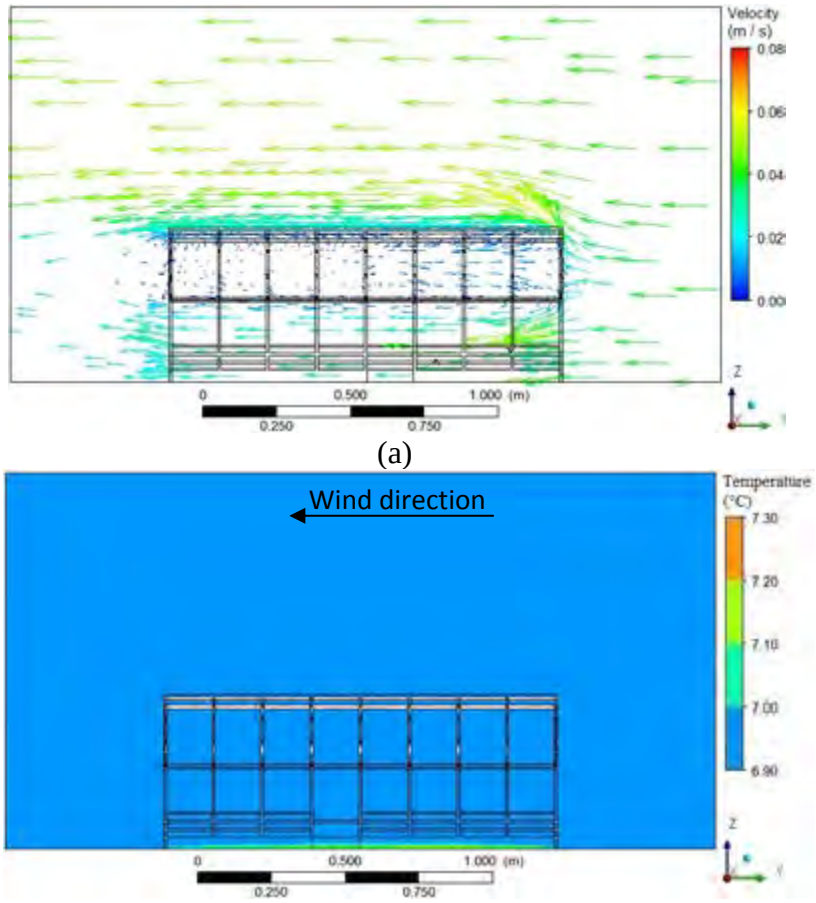

Figure 4.161 - Air velocity (a) and temperature (b) distribution vertically in the CBP barn equipped with elevated ridge (ELR) and wind direction of west to east.

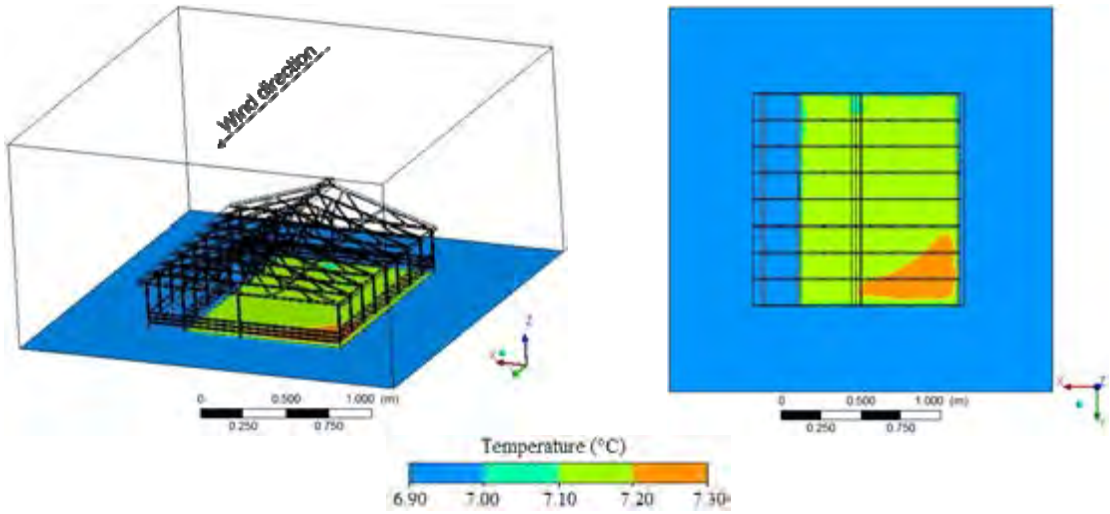

Figure 4.162 - Air temperature distribution on the surface of the floor inside the CBP barn equipped with elevated ridge (ELR) and wind direction of west to east.

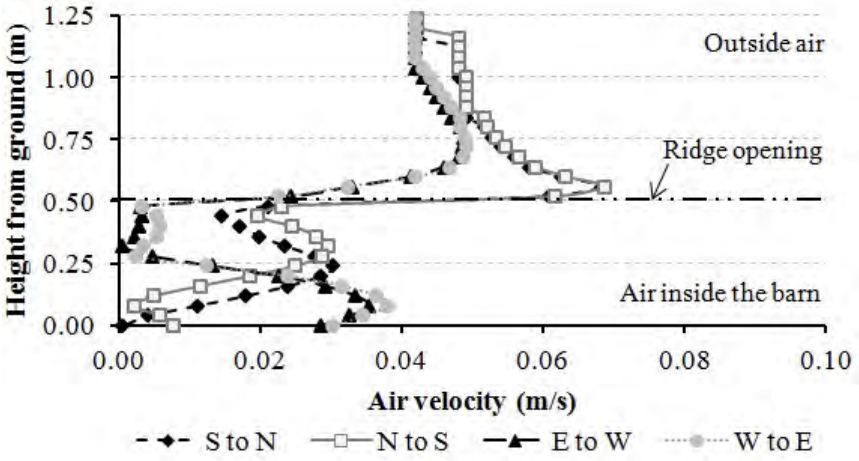

Figure 4.163 - Profile of mean horizontal wind speed in the centre of the CBP barn equipped with open ridge with chimney (ORC) in four wind direction.

Figures 4.164 to 4.171 shows a representation of air velocity vectors, and temperature distribution vertically and on the surface of the floor when overshot ridge (OVR) was equipped in four wind direction, respectably.

The turbulence of the airflow formed above the roof in simulated barn with south winds (Figure 4.164a) is smaller than simulated barn with north winds (Figure 4.166a). Therefore, as can be seen in Figures 4.168a and 4.170a, the turbulence zone was situated after barn at windward gable wall height in simulated barn with east and west winds. The south and north winds direction created the lowest air velocity values differences (Figures 4.164 and 4.166) and east and west winds produced the highest air velocity values differences (Figures 4.168 and 4.170). Airflow enters through both sides the opening wall and owing to density differences between the inside and outside air, immediately drops to the floor. This airflow then travels toward the center of the building, heating up as it passes over the compost area before it eventually rises (see Figures 4.164 and 4.166). A similar observation has already been reported by Norton et al. (2010a).

The highest surface temperature distribution differences on compost area was observed in the east and west winds direction (Figures 4.169 and 4.171). The lowest surface temperature differences on compost area was generally noted south winds (Figure 4.165).

Figure 4.172 shows the air velocity distribution in a vertical plan situated in the center of the CBP barn equipped with overshot ridge (OVR) in four wind direction. The air velocity show approximately the same values at 0.02 m above the compost area for all winds direction tested, but values strongly decreases near the ridge opening in the east and west winds direction, then increases progressively from the ridge opening.

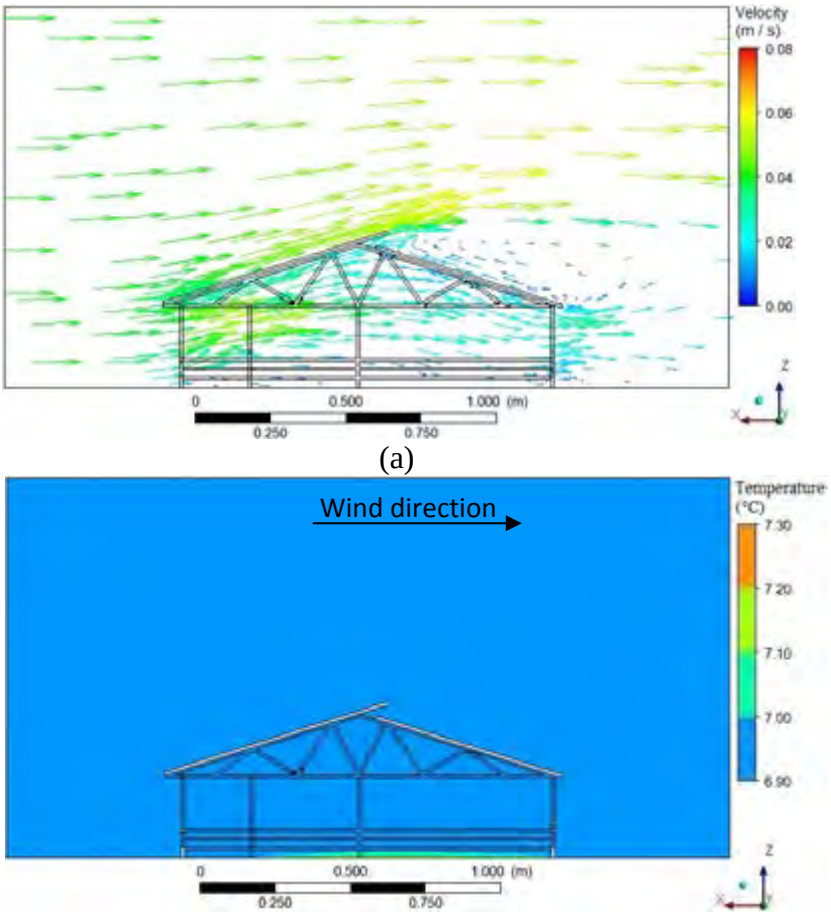

Figure 4.164 - Air velocity (a) and temperature (b) distribution vertically in the CBP barn equipped with overshot ridge (OVR) and wind direction of south to north.

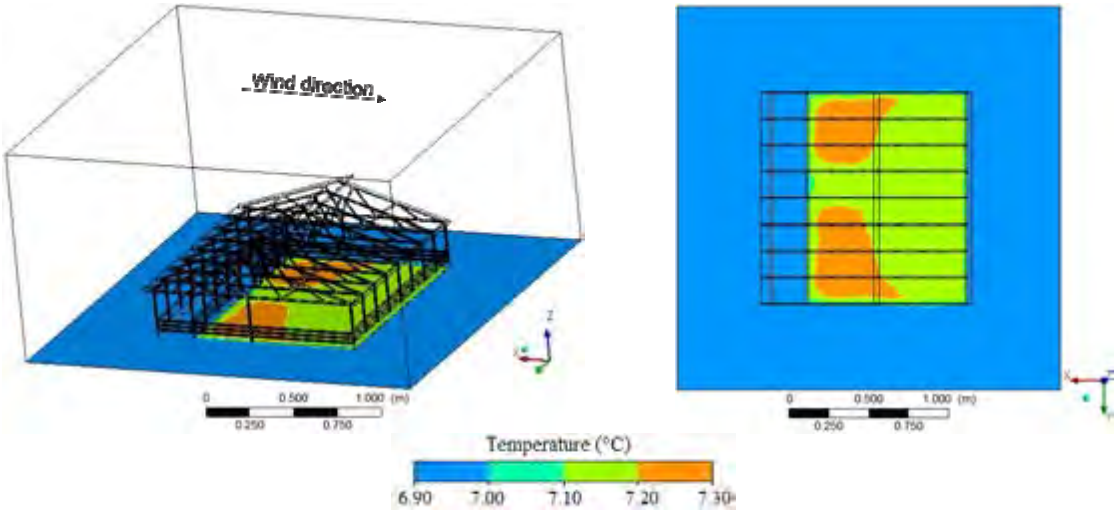

Figure 4.165 - Air temperature distribution on the surface of the floor inside the CBP barn equipped with overshot ridge (OVR) and wind direction of south to north.

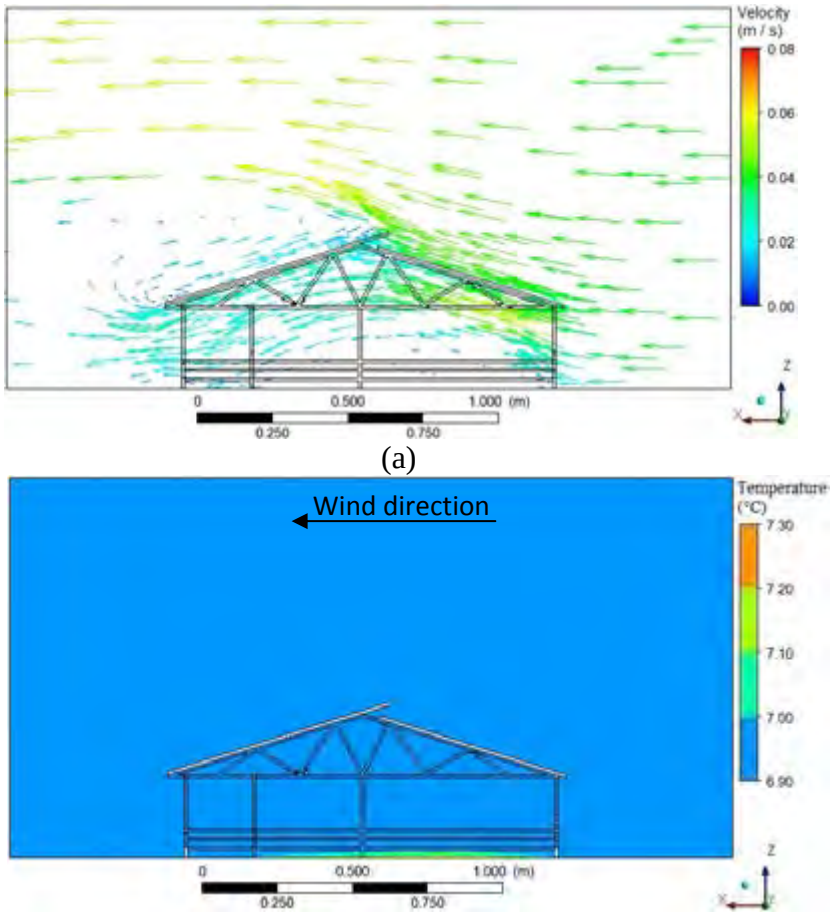

Figure 4.166 - Air velocity (a) and temperature (b) distribution vertically in the CBP barn equipped with overshot ridge (OVR) and wind direction of north to south.

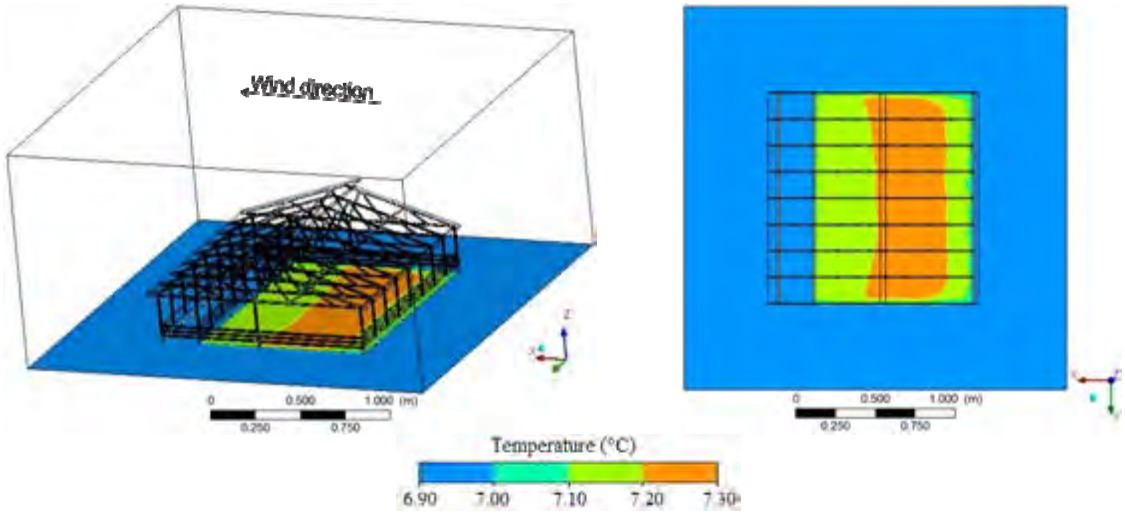

Figure 4.167 - Air temperature distribution on the surface of the floor inside the CBP barn equipped with overshot ridge (OVR) and wind direction of north to south.

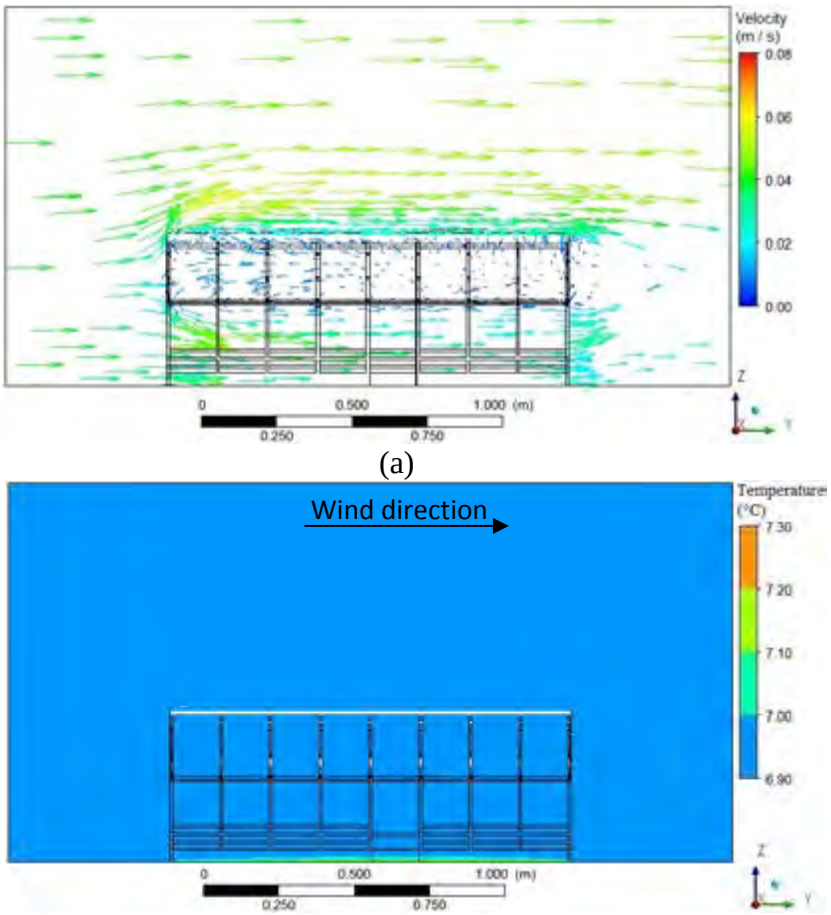

Figure 4.168 - Air velocity (a) and temperature (b) distribution vertically in the CBP barn equipped with overshot ridge (OVR) and wind direction of east to west.

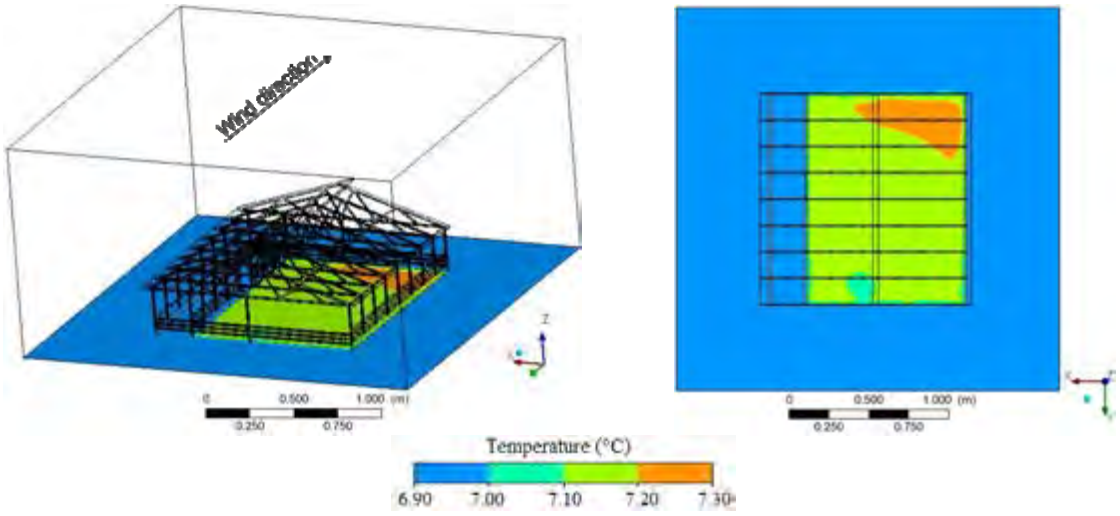

Figure 4.169 - Air temperature distribution on the surface of the floor inside the CBP barn equipped with overshot ridge (OVR) and wind direction of east to west.

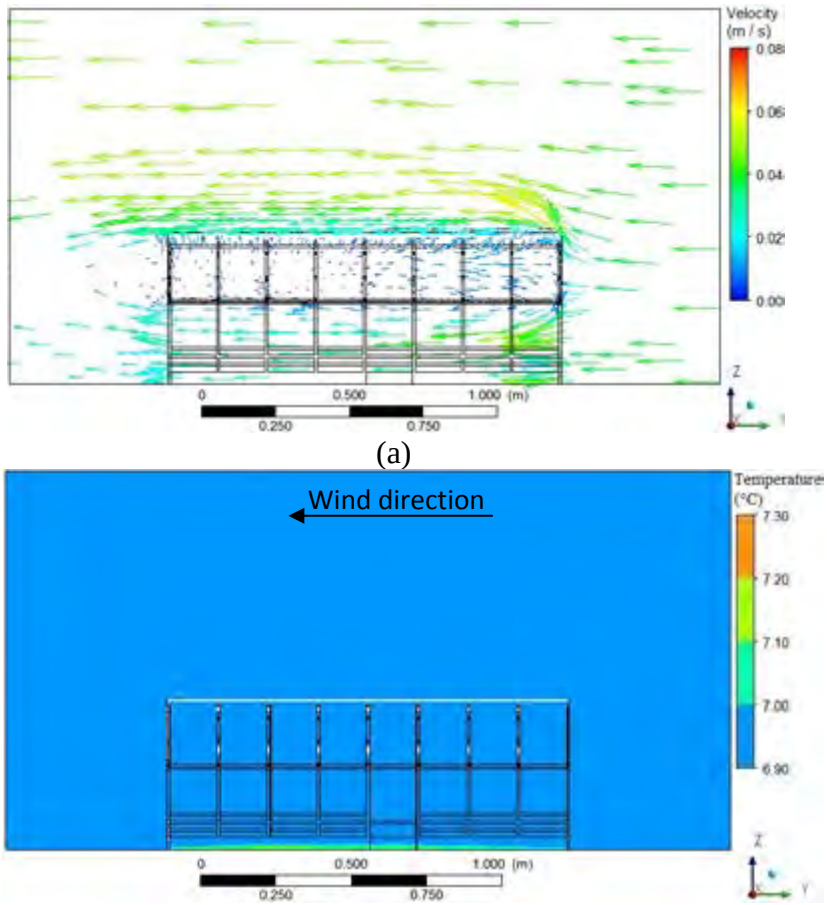

Figure 4.170 - Air velocity (a) and temperature (b) distribution vertically in the CBP barn equipped with overshot ridge (OVR) and wind direction of west to east.

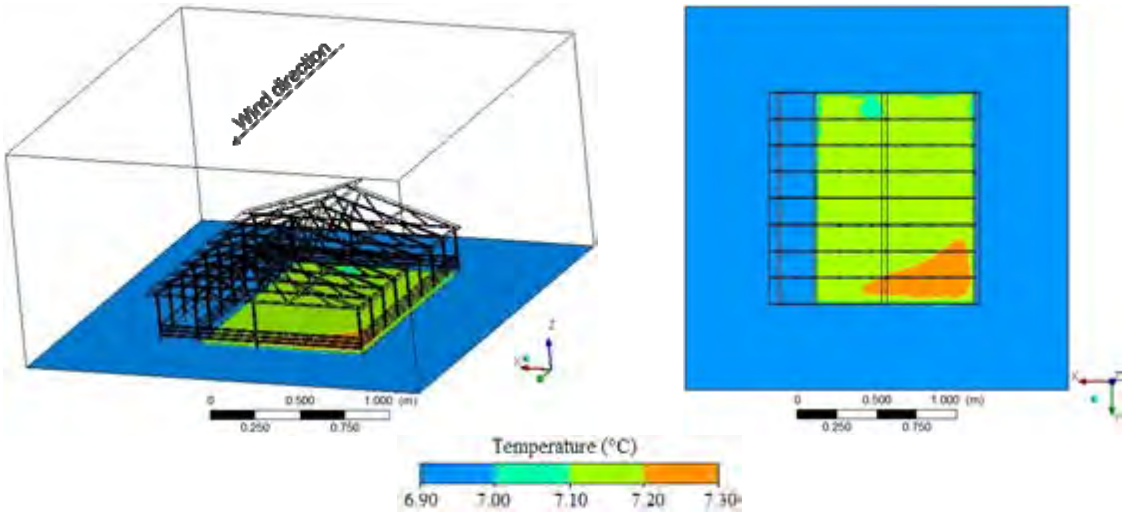

Figure 4.171 - Air temperature distribution on the surface of the floor inside the CBP barn equipped with overshot ridge (OVR) and wind direction of west to east.

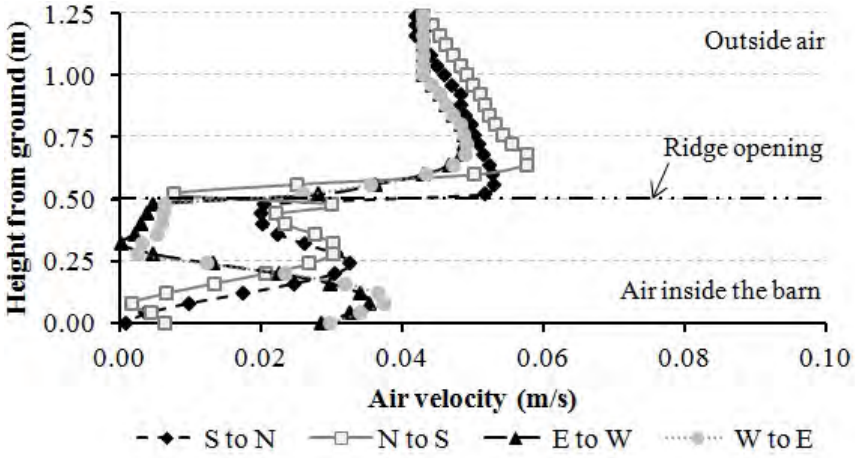

Figure 4.172 - Profile of mean horizontal wind speed in the centre of the CBP barn equipped with overshot ridge (OVR) in four wind direction.

Overall, one can summarise the complex airflow as follows:

a) In general, wind direction indicates that air would approximately move along the length of the barns as opposed to the width or across the barn. The ridge openings noticeably increased the inside air velocities for all the wind directions studied except for the east and west direction. However, in this case, low air velocities were observed inside the trusses structure and near the ridge opening;

b) The airflow patterns were visually higher in all ridge openings tested with wind direction of south and north. With east and west winds higher airflows were observed in the windward ends of the ridge vents than was noted downwind. The airflow patterns for east and west winds also showed that inside the trusses structure the air generally flowed in the opposite direction of the outside winds. With a south and north wind the inside airflow near the trusses structures were generally in the same direction as the outside air. South and north winds produced a swirling action inside the all CFD models with most of the air exiting from the opening wall. This condition was probably due to a slight difference in the outside airflow;

c) CBP barn model geometry effects the surface temperature difference on compost area were visibly significant through the air temperature distribution on the surface of the floor inside the CBP barns in the previous figures for all ridge opening tested and direction of the wind; and

d) Air loops fed by buoyancy forces due to the inside air temperature differences develop perpendicularly between the top of the compost area and bottom of the roof vent openings.

4.4.4.2. Evaluation of the types of ridge vents and wind direction

Maintaining active composting in a compost bedded pack barn is a real challenge during the winter months. It becomes difficult to start or restart a compost bedded pack barn in winter with low bacterial activity since heat losses can easily exceed heat generated. Because of this, to select the best condition of ventilation in the winter weather with reduced cooling of the surface of the bed, the CFD models were evaluated in function of five types of ridge vents (CLR, OPR, ORC, ELR, and OVR) and four wind direction (North, South, East, and West) to promote greater percentage heated surfaces of the floor.

The analyzes of variance for variables five types of ridge vents and four wind direction in function of percentage of heated floor area are showing in Table 4.19. There is not a statistically significant difference ($p > 0.05$) between types of ridge vents ($P = 0.716$) and wind direction ($P = 0.874$).

Table 4.19 - Analysis of variance to heated floor area in different types of ridge vents and wind direction for all CFD models tested.

SV	DF	SS	MS	F_{cal}-Value*	Probability
Ridge	4	1620.038	405.010	0.531	0.716
Direction	3	526.051	175.350	0.230	0.874
Residual	12	9155.593	762.966		
Total	19	11301.682			

Source of Variation (SV), degree of freedom (DF), sum of squares (SS), mean sum of squares (MS), and probability (P).

The mean values of percentage of heated floor area in five types of ridge vents and four wind direction are showing in Table 4.20. Table 4.20 shows that the highest percentage of heated floor of the surface area inside the CFD models were observed in treatments ORC and W to E (Tukey test; $p < 0.05$). Type of ridge vent and wind direction that promoted greater cooling surface of the floor were the treatments ELR and S to N (Tukey test; $p < 0.05$). Details about statistical analysis can be seen in Appendix F (Table 20).

Table 4.20 - Mean values of percentage of heated floor area for different types of ridge vents and wind direction. Values followed by different letters are significantly different (P < 0.05; Tukey).

Treatments	Means values (%)	
	Type ridge design	
ORC	45.292	a
OPR	27.512	b
CLR	24.462	c
OVR	23.497	d
ELR	19.457	e
	Wind direction	
W to E	32.366	a
E to W	32.176	b
N to S	27.922	c
S to N	19.712	d

Once CFD modeling returns results based on temperature variations of the total area in function of the composting area size into barns, highest heating and wind direction percentage can probably be a indicative where the composting process will be occurring with better efficiency or, in other words, what kind of ridge opening will be better to maintain ideal microbiological conditions in terms of aeration and temperature with range of 45 a 60°C, as described early. These results showed that the best ridge vent and wind direction in the winter weather was observed in the open ridge with chimney (ORC) and West to East, respectively. Therefore, open ridge with chimney (ORC) positioned from West to East can possibly be the best barn design with better efficiency among those barns who were studied.

5 - CONCLUSION

The following conclusions were drawn based on the experimental study of 42 compost bedded pack (CBP) barns in Kentucky:

a) Overall, dairies producers visited in Kentucky were very satisfied with their compost barns. They observed that cows were more comfortable and that this housing system resulted in increased cow cleanliness. The compost bedding pack (CBP) barns in Kentucky of this study had a variety of building designs. Majority of these barns had feed alleys and driveways. Most frequent barn orientation was NE to SW. The primary types of barn ridge found in the barns were overshot ridges. Most of barns had roof pitch of 4:12. The majority of barns was equipped with box fans. Air temperatures tended to be lower indoor the barns which utilized overshot or capped ridge, forced ventilation system and ridge direction of SW or NW. The average relative humidity in this study was approximately 65.0%. In general, wind direction was approximately transverse to the barns length direction and the air velocity was 1.0 m s^{-1}. In addition, air quality and possible dust issues in compost dairy barns need to be evaluated.

b) The bedding materials more used in the CBP barns was kild-dried sawdust. However, most dairies producers preferred to use green sawdust rather than the kild-dried sawdust, because this material was harmful or beneficial to the composting bed. Moreover, green sawdust was not absorb as much water as kiln-dried sawdust. Pack temperatures indicated that some of the bedding materials were not able to support microbial activity and produce heat. Average Pack moisture content was 59.0% (± 9.0) wet basis. Our observations indicate moisture content should be between 40-60%. Most of the barns in Kentucky had their compost aerated to a depth below 0.25 m, twice a day in the summer and winter time, while cows were away at the parlor, most often using a chisel plow on a small tractor. Bedding management is critical to encourage microbial activity, minimize pathogen exposure, and maintain cow cleanliness. Further research is necessary regarding the effect of different climatic conditions on the composting processes.

c) A comparison of the particle weight fraction distributions content reveals that these bedding compost materials found in CBP barns are very different. The results indicated that the distribution of mass weight increased in the order of Coarser to Finer. The

average finer index expressed as weight percent in the samples studied was 30.1%, implying excessive water retention and low aeration.

d) Generally, some compost bedding materials showed high particle density ($\geq$ 1g cm^{-3}) compared with other materials. Indeed, these values were higher than expected, but can likely be tied to the presence of carbonates and other inorganic media such as soil particles contained within the compost samples. The higher bulk density value was 3.6 times that of the lower bulk density value. This investigation also showed that porosity is potentially dependent (reverse order) on bulk density although the statistical significance of this relation was high.

e) Water Holding Capacity (WHC) increases with increasingly fine particle size. Coarse particle size of compost have a lower WHC since they are high in large pores subject to free drainage. Fine particle size have a greater occurrence of small pores that hold water against free drainage, resulting in a higher WHC values. In this study, WHC increased with increasing moisture content until certain level. Therefore, compost bedding material with good physical and chemical properties helps to increase the WHC of bedding compost, reduces natural drainage and runoff of the moisture (urine and faeces) through surface of compost, and consequently improves their moisture content. Further research is needed to investigate the influence of moisture content measurement on the determination of WHC.

f) Pack chemical characteristics were almost similar to all bedding materials. Thus, many dairy producers can use the bedding compost to fertilizer their crop fields and avoid over-applying nutrients and reduce water pollution. Bedding compost always contained bacterial, but the variation was large between different sampling sites and times. However, *Coliforms* was not present in barns that had a higher compost temperature. *Coliforms*, *E. Coli*, *Bacillus* and *Streptococcus* count were higher in the barns that showed lower moisture content.

g) Generally, the thermal conductivity increased with increasing particle size, while thermal resistivity decreased with increasing particle size. This behavior can probably be explained by considering the higher moisture retention of larger particles once compost materials were air dried at the same time. It could possibly have changed the

values of the thermal properties. Thus, the tendency thermal conductivity as a function of particle size was very consistent at particle size below than 4.75 mm and thermal resistivity showed an pronounced decrease in compost particle size between 4.75 and 5.60 mm. Thus, results above indicate that the thermal properties are strongly dependent on particle size. However, further studies should be carried out to confirm their positive effects.

h) In the present study, an increasing trend in the thermal conductivity of all compost materials was also observed with the increase in both moisture content and static and dynamic compaction degree for all compost material tested. In contrast, an increasing trend in the thermal resistivity of bed compost was observed with the decrease in both moisture content and static and dynamic compaction degree. The first order regression models developed in this study represent the relationship of degree of moisture content and static and dynamic compaction versus thermal conductivity and thermal resistivity as well. The resulting thermal properties of compost bedding materials can be used to develop heat transfer models for the design of more optimal temperature control in compost bedding pack systems.

i) A 3-D CFD model was established to graphically show the air velocity and temperature distribution in a CBP barns using different ridge vents opening with natural ventilation. The developed model provided good agreement with experimental measurements and it was able to identify the impact on air flow through structure in a CBP barns. To date most published works on CFD simulation for dairy building have been 2-D, and only ventilation has been modeled with 3-D CFD. We hope this developed model can contribute to the optimum design for CBP barn construction. It should also provide guidelines for modifying existing CBP barns towards more uniform and optimum temperature and air movement distribution, thus increasing air quality and cow comfort. Research employing this model or other models with similar characteristics is needed to simulate more accurately the effect on air flow through structure in CBP barns with dairy cows. These results showed that the best ridge vent and wind direction in the winter weather was ORC positioned from West to East can possibly be the best barn design with better efficiency among those barns who were studied.

6 - REFERENCES

ABU-HAMDEH, N. H. Thermal Properties of Soils as affected by Density and Water Content. **Biosystems Engineering**, v. 86, n. 1, p. 97–102, 2003.

ABU-HAMDEH, N. H. Soil and water: measurement of the thermal conductivity of sandy loam and clay loam soils using single and dual probes. **Journal of Agricultural Engineering Research**, v. 80, n. 2, p. 209-216, 2001.

AGNEW, J. M.; LEONARD, J. J.; FEDDES, J.; FENG, Y. A modified air pycnometer for compost air volume and density determination. **Canadian Biosystems Engineering**, v. 25, p. 27-35, 2003.

AGNEW, J. M.; LEONARD, J. J. The physical properties of compost. **Compost Science and Utilization**, v. 11, n. 3, p. 238-264, 2003.

AHN, H.; SAUER, T. J.; RICHARD, T. L.; GLANVILLE, T. D. Determination of thermal properties of composting bulking materials. **Bioresource Technology**, v. 100, p. 3974–3981, 2009.

AHN, H. K.; RICHARD, T. L.; GLANVILLE, T. D. Laboratory determination of compost physical parameters for modeling of airflow characteristics. **Waste Management**, v. 28, p. 660–670, 2008.

AHN, H. K.; SAUER, T. L.; RICHARD, T. L.; GLANVILLE, T. D. Determination of thermal properties of compost bulking materials by using various methods. In **ASABE Annual International Meeting**, Portland, Oregon. 2006.

ALBRIGHT, L. D. **Environmental Control for Animals and Plants.** 4th edition, The American Society of Agricultural Engineers, St. Joseph, MI. 1990.

ANSYS CFX 13.0, "**User manual**", ANSYS Europe Ltd., 2011.

ARMSTRONG, D.V.; HILLMAN, P.E.; MEYER, M.J.; SMITH, J.F.; STOKES, S.R.; HARNER, J.P. Heat stress management in freestall barns in the western U.S. In: **Proceedings…**Western Dairy Management Conference. p. 87-95, 1999.

AYNSLEY, R. M.; MELBOURNE, W. H.; VICKERY, B. J. **Architectural aerodynamics**. Applied Science Publishers Ltd., London, Ont. 250p., 1977.

BAHRAMI, M. 2012. Dimensional Analysis and Similarity Advantages of dimensional analysis. Simon Fraser University. Available at: http://www.sfu.ca. Accessed 26 May 2012.

BARBERG, A. E.; ENDRES, M. I.; SALFER; J. A.; RENEAU, J. K. Performance and welfare of dairy cows in an alternative housing system in Minnesota. **Journal of Dairy Science**, v. 90, p.1575-1583, 2007.

BARLOW, J. B.; RAE W. H.; POPE, A. **Low-Speed Wind Tunnel Testing**, 3rd edition; John Wiley & Sons, 1999.

BASSANEZZI, R. C. **Ensino–aprendizagem com modelagem matemática**. São Paulo: Contexto, 2002.

BEFFA, T. 2002. The composting biotechnology: a microbial aerobic solid substrate fermentation complex process. The composting process and management, Compag Technologies International. Available at: http://www.compag.ch. Accessed 20 May 2012.

BERNAL, M. P.; ALBURQUERQUE, J. A.; MORAL, R. Composting of animal manures and chemical criteria for compost maturity assessment. A review. **Bioresource Technology**, v. 100, p. 5444–5453, 2009.

BERNAL, M. P.; LOPEZ-REAL, J. M.; SCOTT, K. M. Application of natural zeolites for the reduction of ammonia emissions during the composting of organic wastes in a composting simulator. **Bioresource Technology**, v. 43, p. 35–39, 1993.

BEWLEY, J. M.; TARABA, J. L. **Compost Bedded Pack Barns in Kentucky**. Extension Fact Sheet ID-178, 2009.

BJERG, B.; SVIDT, K.; ZHANG, G.; MORSING, S.; JOHNSEN, J. O. Modeling of air inlets in CFD prediction of airflow in ventilated animal houses. **Computers and Electronics in Agriculture**, v. 34, n. 1-3, p. 223-235, 2002.

BJERG, B.; SVIDT, K.; ZHANG, G.; MORSING, S. The effect of pen partitions and thermal pig simulators on airflow in a livestock test room. **Journal of Agricultural Engineering Research**, v. 77 n. 2, p. 317-326, 2000.

BLACK, R. A. **Unpublished data.** 2012. 100p. M.S. Thesis; Animal & Food Sciences, University of Kentucky.

BLACK, R. A.; TARABA, J. L.; DAY, G. B.; DAMASCENO, F. A.; NEWMAN, M. C.; AKERS, K. A.; BEWLEY, J. M. Relationships among temperature, moisture, bacterial counts, and animal hygiene in compost bedded pack barns. In: **American Dairy Science Association (ADSA)**, New Orleans, Louisiana, v. 89. p. 239-239, 2011a.

BLACK. R. A. ; TARABA, J. L. ; DAY, G. B. ; DAMASCENO, F. A. ; BEWLEY, J. M. . An overview of compost bedded pack barn management in Kentucky. In: **American Dairy Science Association (ADSA)**, New Orleans, Louisiana, v. 89. p. 239-239, 2011b.

BLACKBURN, T. H. Benthic mineralization and bacterial production. In: Blackburn T. H., Sorensen J (ed.). **Nitrogen cycling in coastal marine environments**. Wiley, New York. 1988.

BOULARD, T.; WANG, S. Experimental and numerical studies on the heterogeneity of crop transpiration in a plastic tunnel. **Computers and Electronics in Agriculture**, v. 34, n. 1–3, p. 173–190, 2002a.

BOULARD, T.; KITTAS, C.; ROY, J.C.; WANG, S. Convective and ventilation transfers in greenhouses, part 2: determination of the distributed greenhouse climate. **Biosystems Engineering**, v. 83, p. 129–147, 2002b.

BRADSHAW, P.; PANKHURST, R. C. The design of low-speed wind tunnels. **Progress in aeronautical sciences**, v. 6, p. 1-69, 1964.

BRADY, N. C.; WEIL, R. R. **The Nature and Properties of Soils**. 13th ed. Prentice Hall. Upper Saddle River, NJ. 2002.

BRANDT, A. Multilevel adaptive solutions to boundary value problems. **Mathematics of Computation**, v. 31, p. 333-390, 1977.

BRIAUD, J. L.; CHAOUCH, A. Hydrate melting in soil around hot conductor. **Journal of Geotechnical and Geoenvironmental Engineering**, v. 123, n. 7, p.645–653, 1997.

BRISTOW, K. L. Measurement of thermal properties and water content of unsaturated sandy soil using dual-probe heat-pulse probes. **Agricultural and Forest Meteorology**, v. 89, p. 75–84, 1998.

BRISTOW, K. L.; WHITE, R. D.; KLUITENBERG, G. J. Comparison of single and dual probes for measuring soil thermal properties with transient heating. **Australian Journal of Soil Research**, v. 32, p. 447-464, 1994.

BROUK, M. J.; SMITH, J. F.; HARNER, J. P. Fan placement and heat stress abatement in four-row freestall barns. **Kansas Dairy Day Report of Progress**, v. 110, p.1-8, 2001.

BRUIJN, P. J; VAN HANEGHEM, I. A.; SCHENK, J. An improved nonsteady-state probe method for measurements in granular materials. Part 1: Theory. **High Temperatures - High Pressures**, v. 15, p. 359-366, 1983.

CHANDRAKANTHI, M.; MEHROTRA, A. K.; HETTIARATCHI, J. P. A. Thermal conductivity of leaf compost used in biofilters: An experimental and theoretical investigation. **Environmental Pollution**, v. 136, p. 167-174, 2005.

CHANGIRATH, S.; HALBACH, T. R.; DORFF, R. 2011. Media and Media Mix Evaluation for Dairy Barn Compost Bedding Systems. Department of Soil, Water and Climate. Available at: http://www.soils.um.edu/. Accessed 16 May 2012.

CHASTAIN, J.P. Designing and managing natural ventilation systems. In: **Proceedings…** Dairy Housing and Equipment Systems: Managing and planning for profitability. NRAES publication, v. 129, p. 147-163, 2000.

CHASTAIN, J. P.; HIATT, R. S. Supplemental lighting for dairy milk production. **National Food and Energy,** Council, Columbia, MO 65203, p. 20, 1998.

CHASTAIN, J. P. **Pressure gradients and the location of the neutral pressure axis for low rise structures under pure stack conditions**. 1987. M.S. Thesis, Department of Agricultural Engineering, University of Kentucky, Lexington KY.

CHOI, K.; ALBRIGHT, L. D.; TIMMONS, M. B. An application of the k-ε turbulence model to predict air distribution in a slot ventilated enclosure. **Transactions of the ASAE**, v.31, p.1804–1814, 1988.

CLARKE, S.; HOUSE, H. Using Less Energy on Dairy Farms. **Dairy and Beef Housing and Equipment Engineer**, OMAFRA, Clinton. Paper No. 10-067, 2010.

CORNELL WASTE MANAGEMENT INSTITUTE (CWMI, 2006). Using Manure Solids as Bedding. Department of Crop and Soil Sciences. Available at: http://cwmi.css.cornell.edu/bedding.htm. Accessed 15 May 2012.

CORNELL UNIVERSITY COMPOSTING (CUC, 2003). The Science and Engineering of Composting. Available at: http://www.cfe.cornell.edu/compost/science.html. Accessed 16 May 2012.

COYNE, M. S. Biological denitrification. In: Schepers, J.S.; Raun, W. (Eds.). **Nitrogen in agricultural systems**. Agronomy Monograph 49, Madison, WI. p. 197-249, 2008.

DAHL, G. E.; ELSASSER, T. H.; CAPUCO, A. V.; ERDMAN, R. A.; PETERS, R. R. Effects of long day photoperiod on milk yield and circulating insulin-like growth factor-l. **Journal of Dairy Science**, v. 80, p. 2784-2789, 1997.

DAMASCENO, F. A.; YANAGI JUNIOR, T.; LIMA, R. R. ; GOMES, R. C. C. ; MORAES, S. R. P. Avaliação do bem-estar de frangos de corte em dois galpões comerciais climatizados. **Ciência e Agrotecnologia**, v. 34, p. 1031-1038, 2010a.

DAMASCENO, F. A.; AMARAL, A. G.; MARTINS, M. A.; SARAZ, J. A. O.; BAÊTA, F. C. Dinâmica do fluido computacional para simulação da temperatura e velocidade do ar em sistema de aquecimento avícola. In: Congresso Brasileiro de Engenharia Agrícola, 38. 2010b, Vitória. **Anais...** Vitória: Sociedade Brasileira de Engenharia Agrícola.

DAVIDSON, E. A. Fluxes of nitrous oxide and nitric oxide from terrestrial ecosystems. In ROGERS, J.E.; WHITMAN, W.B. (Eds.) **Microbial production and consumption of Greenhouse gases: Methane, nitrogen oxides and halomethanes**. American Society for Microbiology, Washington, DC, p. 219-236, 1991.

DIAZ, L. F.; SAVAGE, G. M.; EGGERTH, L. L.; GOLUEKE, C. G. **Composting and Recycling. Municipal Solid Waste**. Lewis Publishers, USA. v. 33, p. 127-180, 1993.

DIPPEL, S.; DOLEZAL, M.; BRENNINKMEYER, C.; BRINKMANN, J.; MARCH, S.; KNIERIM, U.; WINCKLER, C. Risk factors for lameness in freestall-housed dairy cows across two breeds, farming systems, and countries. **Journal of Dairy Science,** v. 92, p. 5476-5486, 2009.

EGAN, R. K.; HELLICKSON, M. A. Ridge vent and wind direction effects on ventilation characteristics of a model open-front livestock building. **Transactions of the ASAE**, No. 75-4523. ASAE, St. Joseph, Mich. 1977.

ENDRES, M. I.; JANNI, K. A. 2009. Compost Bedded Pack Barns for Dairy Cows. The Cooperative Extension Service. Available at: http://www.bioforsk.no. Accessed 08 May 2012.

ENDRES, M. I. Compost bedded pack barns – Can they work for you?. In: **Proceedings…** Western Canadian Dairy Seminar, Alberta, Canada, p. 271, 2009.

EPSTEIN, E. **The science of composting**. Lancaster, Pennsylvania: Technomic Publishing Company, p. 487, 1997.

FERREIRA, D. F. **SISVAR - Sistema de análise estatística para dados balanceados**. Lavras: UFLA/DEX, 2003.

FERRY, M. New features of the MIGAL solver. In: **Proceedings...** 9th PHOENICS User Conference, Moscow Power Engineering Institute, Moscow, Russia, p. 1–23, 2002.

FITZGERALD, M. **Build a Wind Tunnel**. Tech Directions, p. 6, 2005.

FOX, R. W.; McDONALD, A. T. **Introdução à mecânica dos fluidos**, 4º ed., Rio de Janeiro: LTC, 662p, 1998.

GAJALAKSHMI, S.; ABBASI, S. A. Solid Waste Management by composting: state of the art. **Critical Reviews in Environmental Science and Technology**, v. 38, p. 311-400, 2008.

GAY, S. W. **Bedded-pack Dairy Barns**. Virginia Cooperative Extension, p. 442-124, 2009.

GEBREMEDHIN, K. G.; WU, B. Simulation of flow field of a ventilated and occupied animal space with different inlet and outlet conditions. **Journal of Thermal Biology**, v. 30 n. 5, p. 343-353, 2005.

GEBREMEDHIN, K. G.; WU, B. X. Characterization of flow field in a ventilated space and simulation of heat exchange between cows and their environment. **Journal of Thermal Biology**, v. 28, n. 1, p. 301–319, 2003.

GINKEL, J. T. V.; RAATS, P. A. C.; VAN HANEGHEM, I. A. Bulk density and porosity distributions in a compost pile. **Netherlands Journal of Agricultural Science**, v. 47, p. 105-121, 1999.

GORECKI, J. P. **Túneis aerodinâmicos: passado, presente e futuro**. In: II Encontro Nacional de Ciências Térmicas, Águas de Lindóia, SP, 53p., 1988.

GOYAL, S.; DHULL, S. K.; KAPOOR, K. K. Chemical and biological changes during composting of different organic wastes and assessment of compost maurity. **Bioresource Technology**, v. 96, n. 14, p. 1584-1581, 2005.

GRAVES, R. E. 1999. Dairy Manure Handling. Agricultural and Biological Engineering Extension. Penn State University. Available at http://www.abe.psu.edu. Accessed 14 May 2012.

GRAVES, R. E.; BRUGGER, M. F. Naturally ventilated freestall barns. In: **Proceedings…** Expansion Strategies for Dairy Farms: Facilities and Financial Planning , NRAES-77: Ithaca, NY, p. 409-417, 1994.

HANDRECK, K. A. Particle size and the physical properties of growing media for containers. **Communications Soil Science Plant Analysis**, v. 14, n. 3, p. 209–222, 1983.

HARRAL, B. B.; BOON, C. R. Comparison of predicted and measured air flow patterns in a mechanically ventilated livestock building without animals. **Journal of Agricultural Engineering Research**, v.66, p.221–228, 1997.

HASHEMI, M.; HERBERT, S.; CHICKERING-SEARS, C.; WEIS, S.; GRADIL, C.; PURDY, S.; HUYLER, M.; PROSTAK, R. Bedding Options for Dairy Cows. 2001. UMass Extension Crops, Dairy, Livestock, Equine . Available at: www.umass.edu/cdl. Accessed 08 May 2012.

HAUG, R. T. **Compost Engineering: Principles and Practice**. Technomic Publishing Company, Inc., Lancaster, PA, 655p., 1980.

HENRY, C.; SULLIVAN, D. **The Nitrogen Cycle in Managing Nitrogen from Biosolids**. 1999.

HIRSCH, C. **Numerical Computation of Internal and External Flows**. Butterworth-Heinemann. 2007.

HOFF, S. J.; JANNNI, K. A.; JACOBSON, L. D. Three-dimensional buoyant turbulent flows in a scaled model, slot-ventilated, livestock confinement facility. **Transactions of the ASAE**, v.35, p.671–686, 1992.

HUSAINIE, S. N.; QAMAR, A. 2012. Wind tunnel & airfoil drag analysis. Available at: http://whoknowshowto.com. Accessed 27 May 2012.

HUTCHINSON, B. R.; RAITHBY, G. D. A Multigrid method Based on the Additive Correction Strategy. **Numerical Heat Transfer**, v. 9, p. 511-537, 1986.

INCROPERA, F. P.; DEWITT, D. P. **Fundaments of heat transfer and mass**. 6th Edition, John Wiley and Sons, New York, 2001.

IQBAL, M. K.; SHAFIQ, T.; AHMED, K. Characterization of bulking agents and its effects on physical properties of compost. **Bioresource Technology**, v. 101, p. 1913–1919, 2010.

IWABUCHI, K.; KIMURA, T.; OTTEN, L. Effect of volumetric water content on thermal properties of dairy cattle feces mixed with sawdust. **Bioresource Technology,** v. 70, p. 293–297, 1999.

JANNI, K. A.; ENDRES, M. I.; RENEAU, J. K.; SCHOPER, W. Compost dairy barn layout and management recommendations. **Applied Engineering in Agriculture**, v. 23, p. 97-102, 2007.

JANNI, K.; RENEAU, J.; SCHOPER, W. **Composting Bedded Pack Barns for Dairy Housing**. University of Minnesota, Dairy Extension, Regional Extension Educator-Dairy. 2005.

JENTZSCH, R. **Estudo de modelos reduzidos destinados à predição de parâmetros térmicos ambientais em instalações agrícolas**. 2002. 103p. PhD. Dissertation. Department of Agricultural Engineer, Federal University of Viçosa, Viçosa.

JOHNSON, A. E.; HANCOCK, P. E. Some aspects of centrifugal fan characteristics in blower wind tunnels. **Aero Journal**, Royal Aeronautical Society, v. 101, p. 481, 1997.

JOYE, S. B; HOLLIBAUGH, J. T. Influence of sulfide inhibition of nitrification on nitrogen regeneration in sediments. **Science**, v. 270, p. 623–625, 1995.

KARTHIKEYAN, R.; BHANDARI, A. Anaerobic biotransformation of aromatic and polycyclic aromatic hydrocarbons in soil microcosms: A REVIEW. **Journal of Hazardous Substance Research**, v. 3, n. 1, p. 1-19, 2001.

KATZ, A.; SANKARAN, V. Mesh quality effects on the accuracy of CFD solutions on unstructured meshes. **Journal of Computational Physics**, v. 230, n. 20, p. 7670-7686 2011.

KIM, K.; YOON, J. Y.; KWON, H. J.; HAN, J. H.; EEK SON, J.; NAM, S. W.; GIACOMELLI, G. A.; LEE, E. I. B. 3-D CFD analysis of relative humidity distribution in greenhouse with a fog cooling system and refrigerative dehumidifiers. **Biosystems Engineering**, v. 100, n. 2, p. 245-255, 2008.

KLAAS, I. C.; BJERG, B.; FRIEDMANN, S.; BAR, D. Cultivated barns for dairy cows. **Dansk Veterinærtidsskrift**, v. 9, p. 20-29, 2010.
KLIN, S. J. **Similitude and approximation theory**. New York: McGraw-Hill, 1966.

KOENIG, T. J.; HELLICKSON, M. A.; ROEPKE, W. L. Building geometry and wind effects on model open-front beef building ventilation. **Transactions of the ASAE,** Paper No. 77-4041, 1978.

KÖLTZSCH, P.; WALDEN, F. Ähnlichkeitstheorie und modelltechnik. Heft 1. Freiberg: TU Bergakademie Freiberg, 1990.

KRISTENSEN, E. Organic matter diagenesis at the oxic/anoxic interface in coastal marine sediments, with emphasis on the role of burrowing animals. **Hydrobiologia**, v. 426, p. 1-24, 2000.

LEE, I. B.; SADANOR, S.; SUNG, S. H. Evaluation of CFD accuracy for the ventilation study of a naturally ventilated broiler house. **Japan Agricultural Research Quarterly** (JARQ), v. 41, n. 1, p. 53-64, 2007.

LEE, I. B.; SHORT, T. Two-dimensional numerical simulation of natural ventilation in a multi-span greenhouse. **Transactions of the ASAE**, v.43, n.3, p.745-753, 2000.

LIBERTY, K. R. Yard-Waste Compost Biofilters for Ammonia Adsorption and Biotransformation. 2002. 374p. Ph.D. Dissertation, Biosystems and Agricultural Engineering Department, University of Kentucky.

LINDGREN, B.; JOHANSSON, A. V. **Design and Evaluation of a Low-Speed Wind-Tunnel with Expanding Corners**. Technical Reports, Royal Institute of Technology. Stockholm, Sweden, 2002.

LOPES, I. M. **Evaluation of transitions for testing agricultural ventilation fans with the Fan Assessment Numeration System (FANS)**. 2012. 100p. M.S. Thesis; Biosystems and Agricultural Engineering, University of Kentucky.

MAGNUSSON, M.; CHRISTIANSSON, A.; SVENSSON, B. Bacillus cereus spores during housing of dairy cows: Factors affecting contamination of raw milk. **Journal of Dairy Science**, v. 90, n. 6, p. 2745-2754, 2007.

MAIA, G. D. N. **Ammonia Biofiltration and Nitrous Oxide Generation as Affected by Media Moisture Content**. 2010. 269p. PhD. Dissertation. Biosystems and Agricultural Engineering, University of Kentucky. Kentucky.

MAIER, R. M.; PEPPER, I. L.; GERBA, C. P. **Environmental Microbiology**. Academic Press, San Diego CA, 2000.

MAINTENANCE OF BACTERIAL STRAINS (MBS). Science In The Real World. **Microbes In Action**, p. 1-3, 1999.

MAJDOUBI, H.; BOULARD, T.; FATNASSI, H.; BOUIRDEN, L. Airflow and microclimate patterns in a one-hectare Canary type greenhouse: An experimental and CFD assisted study. **Agricultural and Forest Meteorology**, v. 149, p. 1050-1062, 2009.

MALALASEKERA, W.; VERSTEEG, H. K. **An introduction to computational fluid dynamics – The finite volume method**. 1st Ed., Pearson Education Limited, Essex, England, 1995.

MALISKA, C. R. **Transferência de Calor e Mecânica do Fluidos Computacional**. LTC, Rio de Janeiro, 1995.

MCFARLAND, D. F.; GRAVES, R. E.; TYSON, J. T.; WILSON, T. H. **Ridge openings for naturally ventilated dairy shelters**. Cooperative Extension, Penn State, 2007.

MEGONIGAL, J. P.; HINES, M. E.; VISSCHER, P. T. **Anaerobic Metabolism: Linkages to Trace Gases and Aerobic Processes in Schlesinger**. Elsevier-Pergamon, Oxford, UK. 2004.

MELO, L. D. **Moisture control methodology for gas phase compost biofilters**. 2011. 182p. M.S. Thesis; Biosystems and Agricultural Engineering, University of Kentucky.

MENEGALI, I. ; TINOCO, I. F. F. ; BAETA, F. C. ; CECON, P. R. ; GUIMARAES, M. C. C. ; CORDEIRO, M. B. Ambiente térmico e concentrações de gases em instalações para frangos de corte no período de aquecimento. **Revista Brasileira de Engenharia Agrícola e Ambiental**, v. 13, p. 984-990, 2009.

MIDWEST PLAN SERVICE (MWPS-32). **Mechanical ventilating systems for livestock housing**. 7th edition, Midwest Plan Service, Agricultural and Biosystems Engineering Department, Iowa State University, 2000.

MIDWEST PLAN SERVICE (MWPS-7). **Dairy Freestall Housing and Equipment**. 7th edition, Midwest Plan Service, Agricultural and Biosystems Engineering Department, Iowa State University, 2000.

MIRANDA, R. C. **Simulação de tanque de condicionamento de reagentes por Mecânica dos Fluidos Computacional**. 2009. 67p. M.S. Thesis; Department of Chemistry, Federal University of Minas Gerais, Belo Horizonte.

MITCHELL, C. D.; ROSS, P. A. Model study of air flow in two calf houses. **Farm Building Progress**, p. 19-22, 1977.

MOHSENIN, N. N. **Thermal Properties of Foods and Agricultural Materials**. Gordon and Breasch, New York, 1980.

MOZAMMEL, H; SHAHAB, S; TONY, B; SUDHAGAR, M; LADAN, J; LIM, J. Interaction of Particle size, Moisture content and Compression Pressure on the Bulk density of Wood chip and Straw. In: **Proceedings…** CSBE/SCGAB Annual Conference. The Canadian Society for Bioengineering, 2006.

MUELLER, H. J.; KRAUSE, K. H. Flow simulation for design of ventilation systems in animal houses. **Building Simulation**, New York, p.932-936, 2007.

MUELLER, T. J. **Handbook of Flow Visualization**. Yang, W. J.(Ed.): Hemisphere, New York, 1989.

MUKHTAR, S.; KALBASI, A.; AHMED, A. Carcass Disposal: A Comprehensive Review. **National Agricultural Biosecurity Center**, Kansas State University, p.85, 2004.

MURPHY, G. C. E. **Similitude in engineering**. New York: Ronald Press, 1950.

NÄÄS, I. A.; MOURA, D. J. BUCKLIN, R. A. FIALHO, F. B. An algorithm for determining opening effectiveness in natural ventilation by wind. **Transactions of the ASAE**, v. 41, n. 3, p. 767-771, 1998.

NAKASAKI, K.; SHODA, M.; KUBOTA, H. Effect of temperature on composting of sewage sludge. **Applied and Environmental Microbiology**, v. 500, p. 1526–1530, 1985.

NAPPI, P.; BARBERIS, R. Compost as growing medium: chemical, physical and biological aspects. **Acta Horticulturae**, v. 342, p. 249–256, 1993.

NATURAL RESOURCES CONSERVATION SERVICES (NRCS), 2010. Part 637 Environmental Engineering, National Engineering Handbook, U.S. Department of Agriculture, Washington, D.C.

NORTHEAST REGIONAL AGRICULTURAL ENGINEERING SERVICE (NRAES-76). Guideline for Planning Dairy Freestall Barns. Ithaca, N.Y.: Northeast Regional Agricultural Engineering Service. 1995.

NORTHEAST REGIONAL AGRICULTURAL ENGINEERING SERVICE (NRAES-54). On-Farm Composting Handbook. Waste Management Publications. 1992.

NORTON, T.; GRANT, J.; FALLON, R.; SUN, D. W. A computational fluid dynamics study of air mixing in a naturally ventilated livestock building with different porous eave opening conditions. **Biosystems Engineering**, v. 106, p. 125-137, 2010a.

NORTON, T.; GRANT, J.; FALLON, R.; SUN, D. W. Optimizing the ventilation configuration of naturally ventilated livestock buildings for improved indoor environmental homogeneity. **Building and Environment**, v. 45, p. 983–995, 2010b.

NORTON, T.; SUN, D.; GRANT, J., FALLON, R.; DODD, V. Applications of computational fluid dynamics (CFD) in the modelling and design of ventilation systems in the agricultural industry: A review. **Bioresource Technology**, v. 98, p. 2386–2414, 2007.

OGILVIE, J. R.; BOYD, K. G. Air-movement in modified open front monoslope swine barns. In: **Proceedings…** CSAE, Can. Soc. Agric. Eng., Ottawa, Ont., 1984.

PATANKAR, S.V.; SPALDING, D.V. A calculation procedure for heat, mass and momentum transfer in three-dimensional parabolic flows. **International Journal for Heat and Mass Transfer**, v. 15, p. 1787–1806, 1972.

PAWAR, S. R.; CIMBALA, J. M.; WHEELER, E. F.; LINDBERG, D. V. Analysis of poultry house ventilation using computational fluid dynamics. **Transactions of the ASABE**, v. 50, n. 4, p. 1373-1382, 2007.

PEIGNE, J.; GIRARDIN, P. Environmental impacts of farm-scale composting practices. **Water, Air, and Soil Pollution**, v. 153, p. 45-68, 2004.

PEREIRA, A. R.; MACHADO, E. C. **Análise quantitativa do crescimento de comunidade vegetal**. Campinas: Instituto Agronômico, (Boletim Técnico), 114. 33p. 1987.

PETZEN, J.; WOLFANGER, C.; BONHOTAL, J.; SCHWARZ, M.; TIMOTHY, T.; YOUNGERS, N. **Eagleview compost dairy barn - case study**. Farm viability institute. 2009.

RAE, W. H.; POPE, A. **Low-speed wind tunnel testing.** 2nd ed. John Wiley & sons, 1984.

RAGHOEBARSING, A. A.; POL. A.; VAN DE PAS-SCHOONEN, K. T.; SMOLDERS, A. J. P.; ETTWIG, K. F.; RIJPSTRA, W. I. C; SCHOUTEN, S.; DAMSTE, J. S. S.; OP DEN CAMP, H. J. M.; JETTEN, M. S. M; STROUS, M. A microbial consortium couples anaerobic methane oxidation to denitrification. **Nature**, v. 440, p. 918-921, 2006.

REECE, F. N.; LOTT, B. D.; DEATON, J. W. Ammonia in the atmosphere during brooding affect performance of broiler chikens. **Poultry Science**, v. 59, n. 1, p. 486-488, 1980.

ROBERTS, L. Technology concepts: Power hydrodynamics. **Tech Directions**, v. 60, n. 7, p. 10, 2001.

ROBERTSON, L. A.; CORNELISSE, R.; DE VOS, P.; HADIOETOMO, R.; KUENEN, J. G. Aerobic denitrification in various heterotrophic nitrifiers. **Antonie van Leeuwenhoek**, v. 56, p. 289-299, 1989.

ROCHA, K. S. O. **Modelagem e simulação do processo de resfriamento de grãos armazenados em silos graneleiros por meio das leis de conservação de energia e massa**. 2012; 150p. PhD. Dissertation. Department of Agricultural Engineer, Federal University of Viçosa, Viçosa.

ROSEN, C.; HALBACK, T. R.; MUGAAS, R. **Composting and mulching: A guide to managing organic yard waste**. University of Minnesota Extension Publication. St. Paul, Minnesota. 2000.

ROY, J. C.; BOULARD, T.; KITTAS, C.; WANG, S. Convective and ventilation transfers in greenhouses, part 1: the greenhouse considered as a perfectly stirred tank. **Biosystems Engineering**, v. 83, p. 1–20, 2002.

RUSSELLE, M. P.; BLANCHET, K. M.; RANDALL, G. W.; EVERETT, L. A. 2009. Characteristics and nitrogen value of stratified bedded pack dairy manure. Online. Crop Management. Available at: http://naldc.nal.usda.gov. Accessed 26 Feb 2012.

RYNK, R. **On Farm Composting Handbook. Northeast regional agricultural engineering service**. Cooperative Extension, Ithaca, NY. 1992.

SAINSBURY, D.W.B. Health problems in intensive animal production. In: CLARK, J.A. **Environmental aspects of housing for animal production**. Butterworths: England, p. 439-54, 1981.

SALES, G. T. **Assessment of Biofilter Media particle Sizes for Removing Ammonia**. 2008. 143p. M.S. Thesis; Biosystems and Agricultural Engineering, University of Kentucky.

SANTOS, A. A. C. **Modelagem numérica com validação experimental de escoamento através do bocal inferior de um elemento combustível nuclear**. 2008. 164p. PhD. Dissertation. Department of Mechanical Engineering, Federal University of Minas Gerais, Belo Horizonte.

SCHAUBERGER, G., PIRINGER, M., PETZ, E. Steady state balance model to calculate the indoor climate of livestock buildings, demonstrated for finishing pigs. **International Journal of Biometeorology**, v. 43, p. 154–162, 2000.

SCHLOSS, P. D.; HAY, A. G.; WILSON, D. B.; WALKER, L. P. Molecular assessment of inoculums efficacy and process reproducibility in composting using ARISA. **Transactions of the ASAE**, v. 46, p. 919–927, 2003.

SCHULZE, K.L. Continuous thermophilic composting. **Compost Science**, v. 3, p.22–34, 1962.

SCHURING, D. J. **Scale models in engineering – fundamentals and applications.** New York: Calspan Corporation, 1977.

SEEDORF, J.; HARTUNG, J.; SCHRODER, M.; LINKERT, K. H.; PEDERSEN, S.; TAKAI, H.; JOHNSEN, J. O.; METZ, J. H. M.; GROOT KOERKAMP, P. W. G.; UENK, G. H.; PHILLIPS, V. R.; HOLDEN, M. R.; SNEATH, R. W.; SHORT, J. L. L.; WHITE, R. P.; WATHES, C. M. Survey of Ventilation Rates in Livestock Buildings in Northern Europe. **Journal of Agricultural Engineering Research,** v. 70, p. 39-47, 1998.

SENGA, Y.; MOCHIDA, K.; OKAMOTO, N. Nitrous oxide in brackish Lake Nakaumi, Japan II: The role of nitrification and denitrification in N_2O accumulation. **Liminology**, v. 3, p. 21-27, 2002.

SHANE, E. M.; ENDRES, M. I.; JANNI, K. A. Alternative bedding materials for compost bedded pack barns in Minnesota: a descriptive study. **Applied Engineering in Agriculture**, v. 26, n. 3, p. 465-473, 2010.

SHINDO, S.; BRASK, O. **A smoke generator for low speed wind tunnels**. Technical Note No. 69-1, University of Washington, Department of Aeronautics & Astronautics. 1969.

SIMANGO, D. G.; SCHULTE, D. D. Effect of roof slope on ventilation of non-mechanically ventilated, single-slope MOF swine buildings. **Transactions of the ASAE**, Amer. Soc. Agric. Eng., St. Joseph, Mich, Paper no. 83-4025, 1983.

SINGH, T. N.; SINHA, S.; SINGH V. K. Prediction of thermal conductivity of rock through physico-mechanical properties. **Building and Environment**, v. 42, p. 146–155, 2007.

SMITH, J. F.; HARNER, J. P. **Fan Placement and Heat Stress Abatement in Four-row Freestall Barns.** Kansas State University Agricultural Experiment Station and Cooperative Extension Service. 2001.

STROM, P. F. Effect of temperature on bacterial species diversity in thermophilic solid waste composting. **Applied and Environmental Microbiology**, v. 50, p. 899–905, 1985.

STROUS, M.; JETTEN, M. S. M. Anaerobic oxidation of methane and ammonium. **Annual Review of Microbiology**, v. 58, p. 99–117, 2004.

SUN, H. **Theoretical and experimental study of a High Rise-Hog Building for improved utilization and environmental quality protection**. 2004. 200p. PhD. Dissertation. Department of Agriculture Enginner and Food, University of Ohio.

SUN, S. H.; KEENER, R.; STOWELL, R.; MICHEL, F. C. Two-dimensional computational fluid dynamics (CFD) modeling of air and ammonia distribution in a High-RiseTM Hog Building. **Transactions of the ASAE**, v. 45, n. 5, p. 1559-1568, 2002.

SURFACE WATER INTEGRATED MANAGEMENT (SWIM), 2011. Characterizing dairy manures and slurries. Available at: www.envirolink.govt.nz. Accessed 12 May 2012.

TAKAI, H.; MÖLLER, F.; IVERSEN, M.; JORSAL, S.E.; BILLE-HANSEN, V. Dust control in swine buildings by spraying of rapeseed oil. In: **Proceedings…** Livestock Environment Symposium, 4., 1993, St. Joseph: American Society of Agricultural Engineering, p.726-33, 1993.

TARABA, J.; BEWLEY, J. **Winter Management of Dairy Compost Bedded Pack Barns**. Extension Fact Sheet, 2010.

TATMAN, N. **Wind Tunnel Design and Operation.** 2006. 26p. PhD. Dissertation. Department of Physic. Aerospace Engineering Virginia Tech, Virginia.

TEYE, F. K.; HAUTALA, M. Adaptation of an ammonia volatilization model for a naturally ventilated dairy building. **Atmospheric Environment**, v.42, p.4345–4354, 2008.

TEYE, F. K. **Microclimate and gas emissions in dairy buildings: Instrumentation, theory and measurements**. 2008. 65p. PhD. Dissertation. Department of Agrotechnology, University of Helsinki.

TINÔCO, I. F. F.; SARAZ, J. A. O.; GATES, R. S.; DAMASCENO, F. A.; MARIN, O. L. Z. 3D-CFD modeling of a typical uninsulated and internal misting tunnel ventilated Brazilian poultry house. **Transactions of the ASAE**, St. Joseph, Pittsburgh: ASAE. paper No 1009150, p. 35-42, 2010.

TUCKER, C. B.; WEARY, D. M.; FRASER, D. Free-Stall Dimensions: Effects on preference and stall usage. **Journal of Dairy Science**, v. 87, p. 1208-1216, 2004.

VAN DER TOL, P. P. J.; METZ, J. H. M.; NOORDHUIZEN-STASSEN, E. N.; BACK, W.; BRAAM, C. R.; WEIJS, W. A. The vertical ground reaction force and the pressure distribution on the claws of dairy cows while walking on a flat substrate. **Journal of Dairy Science**, v. 86, p. 2875–2883, 2003.

VAN DER TOL, P. P. J.; METZ, J. H. M.; NOORDHUIZEN-STASSEN, E. N.; BACK, W.; BRAAM, C. R.; WEIJS, W. A. The pressure distribution under the bovine claw during square standing on a flat substrate. **Journal of Dairy Science**, v. 85, p. 1476–1481, 2002.

VAN GINKEL, C. T.; RAATS, P. A. C.; VAN HANEGHEM, I. A. Bulk density and porosity distributions in a compost pile. **Netherlands Journal of Agricultural Science**, v. 47, p. 105–121, 1999.

VAN OUWERKERK, E. N. J.; PEDERSEN, S. Application of the carbon dioxide mass balance method to evaluate ventilation rates in livestock buildings. In: **Proceedings...** XII World Congress on Agricultural Engineering, Milano, Italy, p. 516–529, 1994.

VAN WAGENBERG, A. V.; BJERG, B.; BOT, G. P. A. Measurements and simulation of climatic conditions in the animal occupied zone in a door ventilated room for piglets. In: **Proceedings…** Agricultural Engineering International: The CIGR Journal of Scientific Research and Development, v.4, p.20, 2004.

VEKARIYA, P.; SUBBAIAH, R.; MASHRU, H. Hydraulics of microtube emitters: a dimensional analysis approach. **Irrigation Science**, v. 29, n. 4, p. 341-350, 2011.

VOKEY, F. **Bedding key to compost dairy barn success**. PRO-DAIRY, Northeast DairyBusiness, p. 37-42, 2008.

WAGNER, P. E. 2002. Bedded pack shelters. http://capitaldairy.cas.psu.edu. Accessed 02 May 2012.

WALLIS, R. A. **Axial Flow Fans and Ducts**. Wiley, New York. 1983.

WARNER, R. C. The kinetics of the hydrolysis of urea and of arginine. **The Journal of Biological Chemistry**, v. 142, p. 705-723, 1942.

WASS, J. A. **SigmaPlot 11: Now with total sigmaStat integration. Scientific Computing**, v. 26, n. 1, p. 21-23, 2009.

WEARY, D. M.; TASZKUN, I. Hock lesions and free-stall design. **Journal of Dairy Science**, v. 83, p. 697-702, 2000.

WEINDORF, D. C.; WITTIE, R. Determining Particle Density in Dairy Manure Compost. **The Texas Journal of Agriculture and Natural Resource**, v. 16, p. 60-63, 2003.
WELLER, S. A.; HELDMAN, D. R.; ESMAY, M. L. Air-flow characteristics of a scale Model chamber. **Transactions of the ASAE,** St. Joseph, Mich, Paper No. 67-438, 1970.

WELLS, G. D. 2004. Dairy Barn Ventilation - Exhaust Fan Systems. University of Vermont Extension. Available at: www.uvm.edu/extension. Accessed 12 May 2012.

WILSON, J. D.; BISHOP, R. G. A model study of alternative ventilation systems for a broiler house. **Transactions of the ASAE,** St. Joseph, Mich, Paper No. 71-914, 1974.

WINCHELL, W.; DARBY, D.; BORG, R. Alberta feedlot management guide. 1st edition, Engstrom, D. F. (edit.). **Feeding pen design**. Alberta Agriculture Food and Rural Development. Edmonton, AB, 1996.

WORLEY, M. S.; MANBECK, H. B. Modelling particle transport and air flow in ceiling inlet ventilation systems. **Transactions of the ASAE**, v. 38, n.1, p.231–239, 1995.

WRIGHT, P.; INGLIS, S. Biodrying Dairy Manure. In: **Proceedings...** International Symposium on Composting and Compost Utilization. Emmaus, PA, p. 996-1007, 2002.

XIA, B.; SUN, D. W. Applications of computational fluid dynamics (CFD) in the food industry: a review. **Computers and Electronics in Agriculture**, v. 34, n. 1, p. 5-24, 2002.

YUN, T. S.; SANTAMARINA, J. C. Fundamental study of thermal conduction in dry soils. **Granular Matter**, v. 10, p. 197–207, 2008.

ZDANOWICZ, M.; SHELFORD, A.; TUCKER, C. B.; WEARY, D. M.; VON KEYSERLINGK, M. A. G. Bacterial populations on teat ends of dairy cows housed in free stalls and bedded with either sand or sawdust. **Journal of Dairy Science**, v. 87, n. 6, p. 1694-1701, 2004.

ZHANG, G; STROM, J. S.; LI, B.; ROM, H. B.; MORSING, S.; DAHL, P.; WANG, C. Emission of Ammonia and Other Contaminant Gases from Naturally Ventilated Dairy Cattle Buildings. **Biosystems Engineering**, v. 92, p. 355-364, 2005.

ZHANG, G.; MORSING, S.; BJERG, B.; SVIDT, K.; STROM, J.S. Test room for validation of airflow patterns estimated by computational fluid dynamics. **Journal of Agricultural Engineering Research**, v. 76, p. 141–148, 2000.

ZOES, V.; DINEL, H.; PARÉ, T.; JAOUICH, A. Growth substrates made from duck excreta enriched wood shavings and source-separated municipal solid waste compost and separates: physical and chemical characteristics. **Bioresource Technology**, v.78, p.21-30, 2001.

7 - APPENDICES

Appendix A:

Appendix B:

Appendix C:

Appendix D:

Appendix E:

Appendix F:

APPENDIX A

Table A.1 - Barn characteristics of 42 CBP barns in Kentucky.

Barn	Barn dimension		Pack dimensions		Waterers		Feed Alley	Stock density	Cost	Occupied
	L (m)	W (m)	L (m)	W (m)	L (m)	W (m)	L (m)	(m^2 / cow)	(Dollars)	
1	41.5	15.3	41.5	15.3	1.8	0.6	-	10.0	$60,000	Oct. 2010
2	76.3	30.3	53.4	30.3	-	-	-	9.3	$80,000 and $110,000 including fans	Mar. 2008
3	87.8	16.8	87.8	12.2	3.7	0.6	87.8	7.4	$175,000	-
4	51.5	9.2	51.5	9.2	1.8	0.6	-	5.1	$10,900	Oct. 2010
5	48.8	15.3	42.7	10.7	-	-	-	5.3	-	2003
6	30.5	16.5	24.4	12.2	-	-	30.5	12.4	-	Jun. 2010
7	36.6	16.3	36.6	12.5	2.0	0.7	36.6	11.7	$50,000	Nov. 2009
8	65.9	29.3	65.9	7.9	1.2	0.9	65.9	3.7	$60,000 without concrete	Jan. 2011
9	76.3	27.6	76.3	18.5	3.1	0.6	76.3	13.5	$120,000	Sep. 2010
10	61.0	30.5	61.0	30.5	-	-	-	10.7	$120,000 including fans and lamps	Fall 2009
11	91.5	39.0	91.5	15.3	1.8	0.6	91.5	9.3	$150,000 each with fans and labor	Feb. 2011
12	91.5	39.0	91.5	15.3	1.8	0.6	91.5	9.3		Feb. 2011
13	61.0	37.8	61.0	13.7	1.8	0.6	61.0	8.8	$85,000 each, over $140,000 for concrete, total $400,000 without fans.	Oct. 2010
14	61.0	37.8	61.0	13.7	1.8	0.6	61.0	8.8		Oct. 2010
15	18.3	18.3	18.3	18.3	3.7	0.6	-	2.9	-	Apr. 2010
16	14.6	13.9	14.6	10.1	2.4	0.6	14.6	0.8	-	-
17	37.8	13.7	37.8	13.7	1.5	1.5	21.4	4.3	$55,000 without fans	2008
18	61.0	28.4	61.0	24.4	3.7	0.6	91.5	12.9	$90,000	Nov. 2008
19	21.4	14.0	11.6	14.0	-	-	-	1.7	$8,000	Oct. 2006
20	22.0	18.0	22.0	12.0	0.7	0.7	22.0	0.9	-	7 years
21	36.6	15.3	36.6	15.3	-	-	-	7.9	$30,000 with fans	June 2007
22	61.0	18.9	61.0	15.3	1.8	0.6	61.0	10.2	$40,000	2002

Continue...

Table A.1 - Barn characteristics of 42 CBP barns in Kentucky.

Barn	Barn dimension		Pack dimensions		Waterers		Feed Alley	Stock density	Cost	Occupied
	L (m)	W (m)	L (m)	W (m)	L (m)	W (m)	L (m)	(m^2 / cow)	(Dollars)	
23	61.0	15.3	61.0	15.3	-	-	-	25.8	$85,000	2007
24	30.5	18.9	30.5	15.3	-	-	30.5	12.9	$35,000	2010
25	51.2	38.4	51.2	29.9	2.4	0.8	102.5	9.3	$204,000	Fev. 2010
26	61.0	24.1	61.0	15.6	26.8	0.4	61.0	7.0	$85,000	Jun. 2009
27	36.6	18.0	36.6	12.2	2.4	0.4	36.6	8.6	$65,000 without labor	Sep. 2011
28	36.6	15.3	36.6	15.3	2.4	1.2	-	12.1	$50,000	Aug. 2008
29	61.0	23.8	61.0	14.6	3.7	0.6	45.8	10.0	$105,000 with concrete	Feb. 2007
30	45.8	23.4	45.8	18.8	3.1	0.6	33.6	8.8	$35,000 for building alone	Dec. 2010
31	42.1	45.8	45.8	31.7	3.7	0.6	91.5	11.0	$207,000	Nov. 2010
32	30.5	18.3	30.5	18.3	3.7	0.6	-	11.9	$30,000	Dec. 2008
33	61.0	24.1	61.0	15.6	3.7	0.6	61.0	10.8	$86,000	Nov. 2010
34	51.2	19.1	0.0	0.0	-	-	51.2	3.0	$20,000	Oct. 2010
35	36.6	12.1	36.6	8.5	3.1	0.4	36.6	10.4	$60,000	Fall 2007
36	43.9	14.6	43.9	11.0	-	-	58.6	6,9	-	May 2004
37	45.8	10.7	45.8	10.7	0.3	0.7	-	10.0	$17,000 (Hoop); $25,000 (Metal barn); and $30,000 with feed alley.	2007
38	36.6	21.7	36.6	16.8	-	-	26.8	12.3	$17,000 (Hoop); $25,000 (Metal barn); and $30,000 with feed alley.	2007
39	48.8	22.0	48.8	18.2	1.8	0.6	48.8	12.2	$80,000 for both, including fans and concrete.	Jul. 2010
40	48.8	22.0	48.8	18.2	1.8	0.6	48.8	12.6	$80,000 for both, including fans and concrete.	2002
41	30.5	15.3	30.5	15.3	1.5	1.5	61.0	5.2	$14,000	Jun. 2010
42	53.7	14.9	53.7	14.9	-	-	-	8.0	$25,000	Jun. 2010

Table A.2 - Characteristics of roof and ridge in 42 CBP barns in Kentucky.

Barn	Ridge	Orientation		Roof		Roof Pitch
		Direction	Angle	Structure	Type	V:H
1	Open ridge with cover	E	249°	Wood	Metal	4:12
2	Open ridge with cover	SW	241°	Metal	Metal	4:12
3	Overshot	SW	36°	Metal	Metal	4:12
4	Hoop structure	SW	80°	Hoop	Vinyl	Hoop
5	Overshot	SW	31°	Wood	Metal	4:12
6	Capped ridge	NW	145°	Wood	Metal	4:12
7	Overshot	SW	40°	Wood	Metal	4:12
8	Open ridge with cover	NW	210°	Metal	metal	4:12
9	Overshot	NW	75°	Metal	Metal	4:12
10	Overshot	SE	349°	Wood	Metal	3:12 2 1/2 :12
11	Overshot	SW	23°	Wood	Metal	3:12
12	Overshot	SW	23°	Wood	Metal	2 1/2 :12
13	Open ridge without cover	SE	329°	Wood	Metal	3:12
14	Open ridge without cover	SE	329°	Wood	Metal	3:12
15	Capped ridge	SW	334°	Wood	Metal	4:12
16	Capped ridge	NE	243°	Wood	Metal	5:28
17	Overshot	S	240°	Wood	Metal	4:12
18	Overshot	SW	90°	Wood	Metal	3 1/2 :12
19	Capped ridge	NW	28°	Wood	Metal	3 1/2 :12
20	Overshot	SW	15°	Metal	Metal	1 1/2 : 12 2:12
21	Overshot	NE	233°	Wood	Metal	4:12
22	Capped ridge	SE	35°	Wood	Metal	4:12
23	Capped ridge	SE	305°	Wood	Metal	4:12
24	Capped ridge	SE	286°	Wood	Metal	4:12
25	Open ridge with cover	SE	291°	Wood	Metal	3:12
26	Overshot	SE	265°	Wood	Metal	3 1/2 :12
27	Overshot	SE	330°	Wood	Metal	4:12
28	Overshot	SW	37°	Wood	Metal	4:12
29	Overshot	SE	284°	Wood	Metal	3:12
30	Overshot	NE	253°	Wood	Metal	3 1/2 :12

Continue...

Table A.2 - Characteristics of roof and ridge in 42 CBP barns in Kentucky.

Barn	Ridge	Orientation		Roof		Roof Pitch
		Direction	Angle	Structure	Type	V:H
31	Open ridge with cover	SE	345°	Metal	Metal	4:12
32	Overshot	SW	90°	Wood	Metal	4:12
33	Overshot	SW	74°	Wood	Metal	3 1/2 :12
34	Overshot	NW	112°	Wood	Metal	3.2:12
35	Open ridge with cover	NW	117°	Metal	Metal	4:12
36	Open ridge with cover	SW	335°	Wood	Metal	4:12
37	Hoop structure	NE	224°	Vinyl	Metal	Hoop
38	Overshot	NW	162°	Wood	Metal	4:12
39	Overshot	SW	17°	Wood	Metal	5:12
40	Overshot	SW	17°	Wood	Metal	5:12
41	Open ridge with cover	NW	102°	Wood	Metal	4:12
42	Overshot	NE	204°	Wood	Metal	4:12

Table A.3 - Description of barn ventilation system and lights in CBP barns in Kentucky.

Barn	Type	Ventilation system			Light		
		Amount	Power (W)	Size (m)	Type	Amount	Power (W)
1	Box fans	8	745.7	1.3	-	-	-
2	HVLS Fans	3	1491.4	7.3	HID	3	175
3	Box fans	17	745.7	1.3	HID	2	175
4	Tunnel Ventilation	-	-	-	-	-	-
5	Natural ventilation	-	-	-	-	-	-
6	Box fans	10	494.6	0.5	Incandescent	10	100
	Box fans	8	745.7	0.9	Incandescent	5	
	Box fans	2	745.7	1.2	Incandescent	5	100
7	HVLS Fans	2	1491.4	7.3	HID	6	175
8	Box fans	4	745.7	1.3	-	-	-
9	Box fans	4	745.7	1.3	HID	30	175
10	Box fans	15	745.7	1.3	HID	5	70
11	HVLS Fans	3	1491.4	6.1	Fluorescent	6	192
	HVLS Fans	2	1491.4	7.3	-	-	-
12	HVLS Fans	3	1491.4	6.1	Fluorescent	6	192
	HVLS Fans	2	1491.4	7.3	-	-	-
13	Natural ventilation	-	-	-	Compact Fluorescent	5	32
14	Natural ventilation	-	-	-	Compact Fluorescent	5	32
15	HVLS Fans	1	1491.4	7.3	-	-	-
16	Box fans	4	372.8	0.9	Incandescent	6	100
17	Box fans	6	372.8	0.9	Incandescent	9	100
18	Box fans	20	745.7	1.3	Fluorescent	8	192
19	Box fans	4	372.8	0.9	Compact Fluorescent	2	32
20	Box fans	6	372.8	0.9	-	-	-
	Box fans	4	559.3	1.2	-	-	-
21	Box fans	6	372.8	0.9	HID	3	175
	Box fans	2	745.7	1.2	-	-	-
22	Natural ventilation	-	-	-	HID	12	150
23	Natural ventilation	-	-	-	HID	6	150
24	Natural ventilation	-	-	-	-	-	-

Continue...

Table A.3 - Description of barn ventilation system and lights in CBP barns in Kentucky.

Barn	Type	Ventilation system			Light		
		Amount	Power (W)	Size (m)	Type	Amount	Power (W)
25	HVLS Fans	6	1491.4	7.3	HID	24	150
26	HVLS Fans	3	1491.4	7.3	HID	2	150
27	Natural ventilation	-	-	-	Compact Fluorescent	11	13
28	Box fans	6	1118.5	1.2	Compact Fluorescent	14	13
29	HVLS Fans	3	1491.4	7.3	-	-	-
30	HVLS Fans	2	1491.4	7.3	-	-	-
31	Natural ventilation	-	-	-	-	-	-
32	HVLS Fans	2	1491.4	7.3	Fluorescent	3	96
33	Natural ventilation	-	-	-	-	-	-
34	Natural ventilation	-	-	-	Incandescent	4	100
35	HVLS Fans	2	1491.4	7.3	-	-	-
	Box fans	2	186.4	0.6	-	-	-
36	Box fans	1	372.8	0.9	-	-	-
	Box fans	6	745.7	1.1	-	-	-
37	Natural ventilation	-	-	-	-	-	-
38	Natural ventilation	-	-	-	-	-	-
39	Box fans	8	745.7	1.3	Fluorescent	5	192
40	Box fans	8	745.7	1.3	Fluorescent	5	192
41	Box fans	8	246.1	0.6	-	-	-
42	Box fans	8	745.7	1.3	Incandescent	6	100

Table A.4 - Average bedding temperature (°C) at surface and two depths in nine different locations of CBP barns. Bedding material: A (green sawdust). B (kiln-dried shavings or sawdust), and C (mix).

Barn	Bedding material	Surface temperature			Pack Temperature					
					0.1 m depth			0.2 m depth		
		Average		Std Dev	Average		Std Dev	Average		Std Dev
1	A	17.1	±	1.3	31.9	±	10.2	35.2	±	9.4
2	A	16.5	±	3.6	41.5	±	10.6	53.4	±	4.6
3	B	16.3	±	3.8	36.2	±	9.5	52.1	±	4.6
4	C	15.5	±	3.5	41.1	±	18.7	52.4	±	7.6
5	B	22.2	±	1.3	26.0	±	6.1	27.2	±	6.6
6	B	16.2	±	3.1	34.5	±	15.0	34.0	±	10.1
7	B	13.3	±	4.7	38.3	±	6.0	42.2	±	8.6
8	B	17.8	±	4.1	24.1	±	4.8	24.4	±	3.5
9	C	22.3	±	11.7	38.6	±	13.2	42.5	±	14.8
10	B	17.3	±	5.6	35.6	±	8.6	41.4	±	11.4
11	C	15.2	±	2.5	30.5	±	12.0	34.4	±	6.1
12	C	18.5	±	12.5	31.5	±	7.7	36.4	±	6.9
13	B	11.7	±	5.3	42.0	±	10.7	43.6	±	9.4
14	B	8.9	±	1.6	40.3	±	14.2	38.4	±	14.9
15	B	17.2	±	10.2	52.3	±	7.5	58.0	±	10.3
16	A	8.9	±	2.9	23.5	±	12.6	32.1	±	7.2
17	B	11.7	±	5.0	37.4	±	16.6	36.6	±	17.0
18	B	-5.1	±	3.5	12.3	±	9.7	20.9	±	10.9
19	B	-0.9	±	3.8	39.7	±	5.6	52.8	±	3.2
20	B	23.7	±	1.2	44.0	±	12.4	45.0	±	11.6
21	B	4.5	±	2.4	46.1	±	32.5	50.2	±	14.7
22	A	6.9	±	2.7	28.8	±	5.4	31.6	±	3.2
23	A	6.0	±	2.6	15.3	±	6.0	18.9	±	6.7
24	A	7.2	±	2.5	15.3	±	5.5	19.8	±	4.9
25	B	7.0	±	4.2	17.1	±	3.5	20.2	±	2.3
26	A	6.8	±	4.5	39.5	±	11.2	39.5	±	9.8
27	B	18.2	±	9.1	39.4	±	23.3	43.3	±	14.7
28	A	9.0	±	4.2	45.8	±	11.2	53.0	±	7.0
29	A	5.4	±	3.4	15.5	±	6.7	18.0	±	5.6
30	A	14.2	±	9.8	49.2	±	7.8	52.9	±	4.5

Continue...

Table A.4 - Average bedding temperature (°C) at surface and two depths in nine different locations of CBP barns. Bedding material: A (green sawdust), B (kiln-dried shavings or sawdust), and C (mix).

Barn	Bedding material	Surface temperature			Pack Temperature					
					0.1 m depth			0.2 m depth		
		Average		Std Dev	Average		Std Dev	Average		Std Dev
31	A	11.8	±	8.4	32.8	±	17.2	35.1	±	13.3
32	A	6.7	±	4.4	42.0	±	6.7	44.2	±	6.3
33	B	-1.5	±	16.1	33.0	±	27.0	37.4	±	25.2
34	B	-0.8	±	3.7	27.6	±	29.3	23.3	±	3.9
35	A	-3.5	±	2.6	8.8	±	5.2	13.2	±	4.9
36	A	3.3	±	2.5	15.7	±	6.4	18.2	±	5.8
37	A	4.7	±	2.9	20.2	±	15.3	25.3	±	16.6
38	A	3.8	±	2.3	13.5	±	8.8	17.2	±	9.8
39	A	-1.7	±	4.5	22.8	±	9.0	28.6	±	8.7
40	A	0.0	±	8.3	23.3	±	15.0	27.7	±	11.1
41	B	-4.0	±	2.3	25.2	±	15.1	30.0	±	5.9
42	C	0.9	±	3.5	18.2	±	25.1	24.8	±	5.1

Table A.5 - Moisture content (%) of bedding in CBP barns in Kentucky.

Barn	1	2	3	4	5	6	7	8	9	Average	Std Dev	Min.	Max.	1st Quartile	3rd Quartile
1	49.8	53.8	43.2	44.1	38.2	40.4	30.7	56.4	43.7	44.5	8.0	30.7	56.4	40.4	49.8
2	52.0	56.0	61.5	45.7	49.7	49.0	38.3	39.7	49.2	49.0	7.3	38.3	61.5	45.7	52.0
3	46.3	46.5	46.1	56.8	43.4	54.1	58.7	46.1	44.3	49.1	5.8	43.4	58.7	46.1	54.1
4	37.9	30.5	27.8	34.8	44.3	29.0	36.4	44.9	40.0	36.2	6.3	27.8	44.9	30.5	40.0
5	61.7	56.6	46.9	55.0	52.2	47.5	55.2	43.7	51.3	52.2	5.6	43.7	61.7	47.5	55.2
6	42.9	36.9	41.0	32.0	22.9	31.3	50.1	51.8	47.1	39.6	9.6	22.9	51.8	32.0	47.1
7	49.7	49.4	44.4	45.1	45.1	40.8	48.9	48.1	42.7	46.0	3.2	40.8	49.7	44.4	48.9
8	63.5	61.4	59.5	58.2	65.9	61.0	63.8	61.7	59.3	61.6	2.5	58.2	65.9	59.5	63.5
9	38.8	37.5	34.4	33.6	43.7	53.9	45.7	41.3	47.7	41.9	6.6	33.6	53.9	37.5	45.7
10	51.8	45.4	51.4	38.3	64.0	48.7	57.5	53.6	54.5	51.7	7.3	38.3	64.0	48.7	54.5
11	64.9	62.4	60.9	61.8	56.2	62.4	62.3	59.5	60.7	61.2	2.4	56.2	64.9	60.7	62.4
12	65.6	60.2	59.5	62.4	60.5	55.9	60.1	61.7	57.5	60.4	2.8	55.9	65.6	59.5	61.7
13	62.4	54.7	55.7	59.8	63.4	50.6	60.0	57.5	53.7	57.5	4.2	50.6	63.4	54.7	60.0
14	58.7	57.5	60.1	64.0	55.8	58.9	49.8	51.9	58.7	57.3	4.3	49.8	64.0	55.8	58.9
15	56.2	56.0	53.6	55.4	51.0	51.0	57.2	52.9	58.5	54.7	2.7	51.0	58.6	53.0	56.2
16	69.2	70.6	67.1	66.2	66.4	64.6	64.3	65.9	64.4	66.5	2.2	64.3	70.6	64.6	67.1
17	61.6	62.4	52.7	55.7	50.2	59.1	52.6	56.5	53.7	56.0	4.3	50.2	62.4	52.7	59.1
18	65.1	64.6	64.2	64.0	65.6	65.6	66.0	63.5	65.1	64.8	0.8	63.5	66.0	64.2	65.6
19	69.2	69.5	70.2	68.0	71.0	67.3	68.3	68.0	64.5	68.4	1.9	64.5	71.0	68.0	69.5
20	57.0	62.7	53.6	60.9	62.7	62.0	58.3	63.0	63.0	60.3	3.3	53.6	63.0	58.3	62.7
21	63.4	64.5	55.0	56.7	59.1	56.9	58.8	59.2	55.4	58.8	3.3	55.0	64.5	56.8	59.2
22	58.3	56.5	43.9	53.9	48.3	52.6	50.5	49.9	53.4	52.0	4.4	43.9	58.3	50.0	53.9
23	67.0	68.8	69.7	66.7	68.1	65.9	67.2	66.2	66.1	67.3	1.3	65.9	69.7	66.3	68.1
24	62.9	62.9	67.3	63.6	64.2	62.5	63.8	62.9	65.6	64.0	1.6	62.5	67.3	62.9	64.2
25	64.5	63.7	61.1	64.0	59.2	58.9	60.1	59.4	59.5	61.2	2.3	58.9	64.5	59.4	63.8

Continue...

Table A.5 - Moisture content (%) of bedding in CBP barns in Kentucky.

Barn	1	2	3	4	5	6	7	8	9	Average	Std Dev	Min.	Max.	1st Quartile	3rd Quartile
26	56.6	58.8	54.9	57.9	56.1	54.1	54.9	63.3	58.5	57.3	2.8	54.1	63.3	55.0	58.5
27	68.3	67.9	68.1	66.8	67.0	67.1	67.6	66.1	70.6	67.8	1.3	66.2	70.7	67.0	68.2
28	66.3	65.1	63.3	66.2	62.1	59.6	64.3	65.2	69.3	64.6	2.8	59.7	69.4	63.3	66.2
29	64.5	60.0	62.4	60.9	58.2	59.2	63.4	59.2	61.7	61.1	2.1	58.2	64.5	59.2	62.4
30	46.5	50.0	51.2	43.4	46.2	47.7	44.2	48.2	49.0	47.4	2.6	43.4	51.2	46.2	49.0
31	56.8	61.7	61.9	56.9	60.6	61.0	62.2	65.2	68.6	61.7	3.7	56.8	68.7	60.6	62.3
32	67.7	65.8	65.5	68.3	64.8	66.8	67.2	64.8	66.6	66.4	1.3	64.8	68.3	65.6	67.3
33	69.9	68.9	69.9	68.3	68.7	70.4	70.3	70.4	68.1	69.5	0.9	68.2	70.5	68.7	70.4
34	68.2	71.7	69.1	67.3	66.1	71.9	70.3	67.1	68.0	68.9	2.0	66.2	71.9	67.3	70.3
35	48.6	63.2	69.4	63.3	64.1	62.5	64.6	65.0	62.4	62.6	5.6	48.7	69.4	62.5	64.6
36	71.8	71.9	70.8	71.5	73.2	71.6	71.3	72.8	70.9	71.8	0.8	70.8	73.3	71.3	71.9
39	64.7	66.1	68.2	66.9	65.8	67.0	66.5	66.2	66.9	66.5	1.0	64.8	68.2	66.1	67.0
40	66.6	65.1	62.8	66.7	65.1	61.8	66.1	63.3	64.0	64.6	1.7	61.8	66.7	63.3	66.1
41	72.3	70.3	69.1	73.6	71.6	66.7	71.4	70.9	65.2	70.1	2.7	65.2	73.6	69.1	71.7
42	68.2	68.6	70.2	67.7	68.4	70.2	70.7	67.6	69.9	69.1	1.2	67.6	70.7	68.3	70.2

Table A.6 - Bedding chemical characteristics in 42 bedding compost materials.

Barn	P (g/kg)	K (g kg)	Ca (g/kg)	Mg (g/kg)	Zn (ppm)	Cu (ppm)	Mn (ppm)	Fe (ppm)
1	0.5	1.6	2.3	0.7	168.0	30.0	436.9	7271.2
2	0.5	1.6	1.4	0.5	175.0	39.9	189.2	768.3
3	0.2	0.8	0.8	0.2	66.2	9.2	113.1	3624.0
4	0.2	0.4	0.6	0.2	40.7	8.1	121.0	764.9
5	0.4	1.1	1.5	0.5	137.3	32.4	150.3	1304.6
6	0.8	2.0	2.0	0.8	209.5	46.5	297.8	2143.4
7	0.5	2.2	3.6	0.7	202.7	55.8	238.7	1968.7
8	0.5	1.8	1.6	0.4	147.3	38.6	241.8	7281.7
9	0.6	1.7	2.0	0.7	161.7	35.0	818.9	9077.7
10	0.6	1.6	1.5	0.6	142.2	60.9	207.9	1647.1
11	0.3	0.9	4.1	0.5	87.0	16.6	183.2	1744.9
12	0.2	0.7	1.8	0.3	77.0	14.7	167.5	1870.8
13	0.3	1.0	1.5	0.4	94.2	15.0	129.7	3792.4
14	0.4	0.9	1.4	0.4	112.9	28.1	153.9	2935.6
15	0.4	1.4	1.4	0.4	96.1	44.4	165.3	938.8
16	0.5	1.6	1.6	0.5	152.2	55.4	208.0	966.6
17	0.4	1.3	2.7	0.7	123.8	30.2	163.6	1760.7
18	0.6	1.8	2.6	0.7	137.4	39.8	215.1	2756.7
19	0.4	0.9	1.2	0.4	99.8	44.4	166.0	480.8
20	0.2	0.6	0.7	0.2	32.7	13.1	241.2	4960.6
21	0.4	1.0	1.1	0.3	102.8	28.1	129.7	493.3
22	0.3	0.9	0.9	0.3	90.2	17.5	159.0	1428.9
23	0.3	1.0	0.8	0.3	85.3	17.6	140.1	733.2
24	0.4	1.9	1.0	0.4	75.8	12.1	277.1	980.7
25	0.5	1.8	1.4	0.5	139.3	37.3	192.3	922.4
26	0.4	1.0	0.9	0.4	71.9	17.7	210.8	5032.2
27	0.3	0.8	1.0	0.3	52.1	9.6	154.4	3434.2
28	0.4	1.4	1.1	0.4	92.4	19.5	571.6	7582.3
29	0.5	1.7	1.4	0.4	136.0	27.7	224.5	1661.6
30	0.3	1.2	1.1	0.3	140.0	39.3	188.3	471.4
31	0.2	0.7	1.2	0.3	36.5	11.2	196.0	1379.8
32	0.4	1.6	4.3	0.7	138.6	43.3	241.7	5812.8
33	0.3	0.9	0.9	0.3	65.8	9.6	155.5	7487.0
34	0.2	0.6	0.9	0.3	57.2	14.2	115.5	696.6
35	0.4	1.5	1.2	0.5	118.1	38.2	170.8	597.0

Continue...

Table A.6 - Bedding chemical characteristics in 42 compost dairy barns in Kentucky.

Barn	P (g/kg)	K (g kg)	Ca (g/kg)	Mg (g/kg)	Zn (ppm)	Cu (ppm)	Mn (ppm)	Fe (ppm)
36	0.4	1.0	1.2	0.3	155.8	29.8	212.1	902.7
37	0.4	1.4	1.3	0.4	79.3	18.4	170.3	2646.6
38	0.3	0.9	1.0	0.3	66.4	12.1	159.0	4738.5
39	0.4	0.9	0.9	0.3	50.0	7.7	158.8	1963.1
40	0.3	0.9	0.9	0.3	67.3	10.0	168.1	1726.6
41	0.4	1.1	0.9	0.3	110.6	19.2	147.8	981.4
42	0.5	1.4	0.8	0.3	70.9	8.0	163.9	1831.2
Average	0.4	1.2	1.5	0.4	106.0	26.3	209.9	2606.2
Std dev.	0.1	0.4	0.9	0.2	44.2	14.8	125.8	2323.9

APPENDIX B

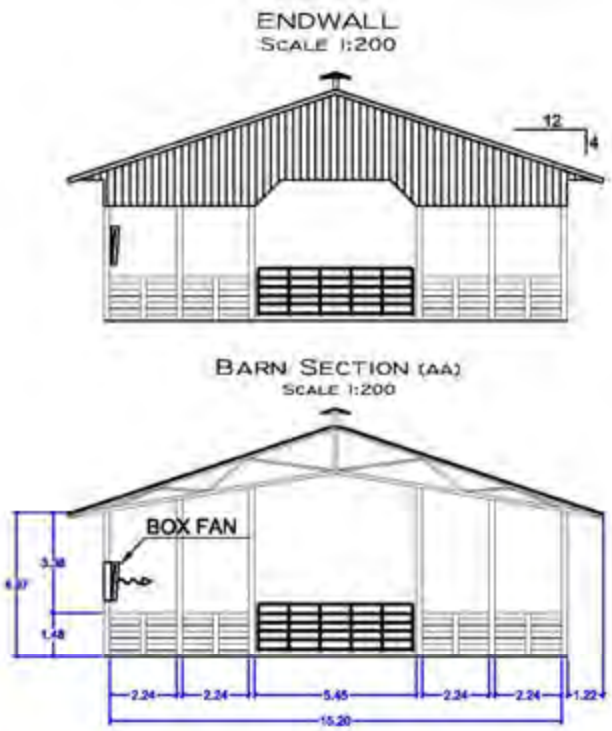

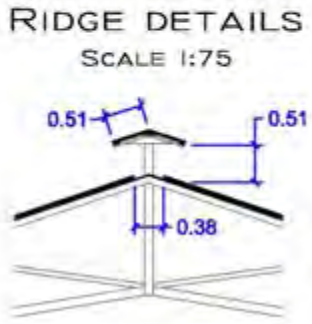

DEPARTMENT OF AGRICULTURAL ENGINEERING							
DESIGN: DAMASCENO	☐ INFORMATION	SHEET: 1/2	REVISIONS	DATE	CHK	CBP BARN 1	
UNITS: METERS	☐ SUBMITTAL					DESCRIPTION: PLAN,ELEV., SECTION, RIDGE	
SCALE: 1:200 AND 1:75	☐ APPROVAL						
DATE: FEB./2012	☐ CONSTRUCTION	FILE: BARN1.DWG				FACILITY: 53406	
	☐ OTHER						

Figure B.1 - Details about end wall, barn section, and ridge of CBP Barn 1.

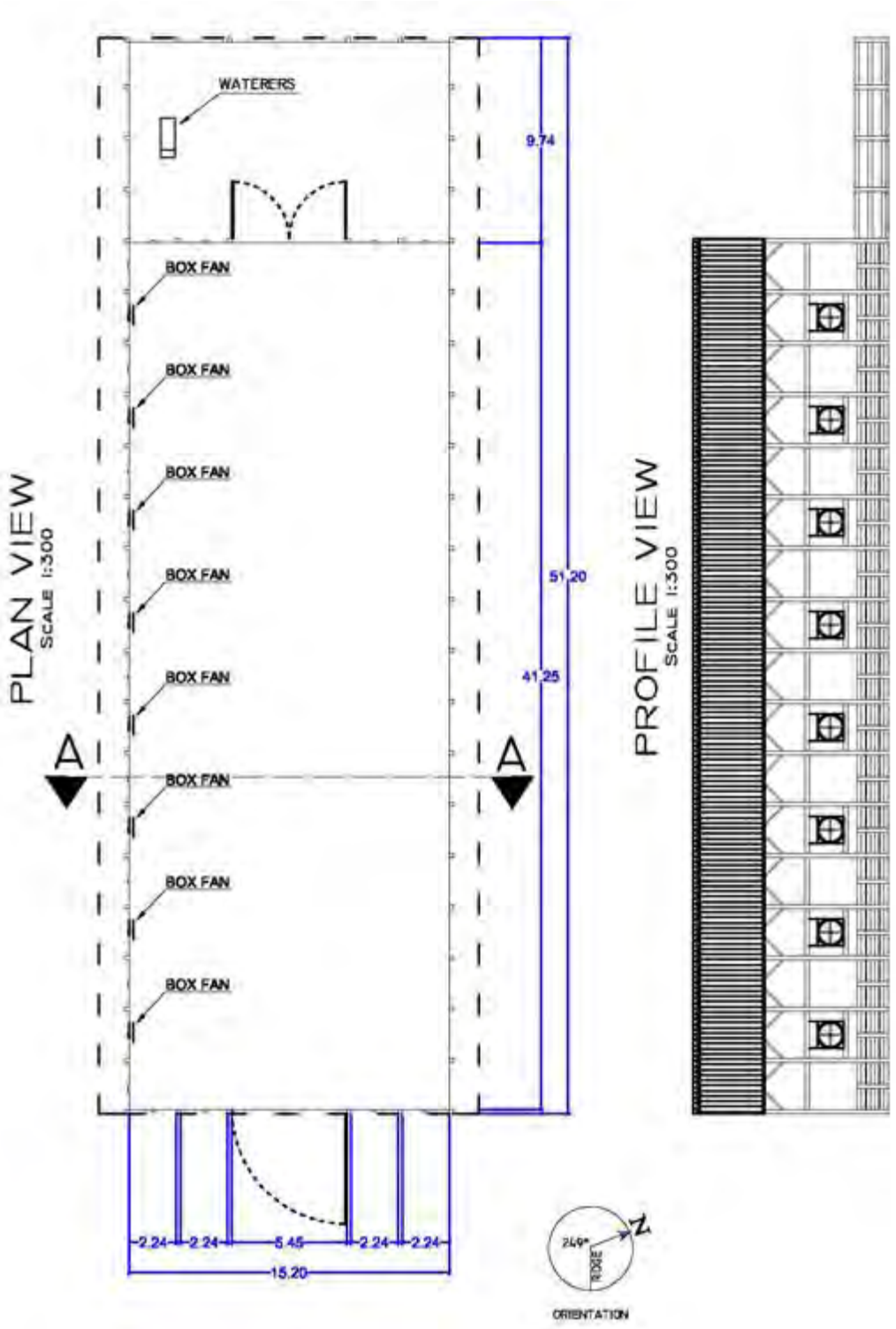

DEPARTMENT OF AGRICULTURAL ENGINEERING							
DESIGN: DAMASCENO	☐ INFORMATION	SHEET: 2/2	REVISIONS	DATE	CHK	CBP BARN 1	
UNITS: METERS	☐ SUBMITTAL					DESCRIPTION: PLAN,ELEV., SECTION, RIDGE	
SCALE: 1:300	☐ APPROVAL						
DATE: FEB./2012	☐ CONSTRUCTION	FILE: BARN 1.DWG				FACILITY: 53406	
	☐ OTHER						

Figure B.2 - Details about plan view and profile of CBP Barn 1.

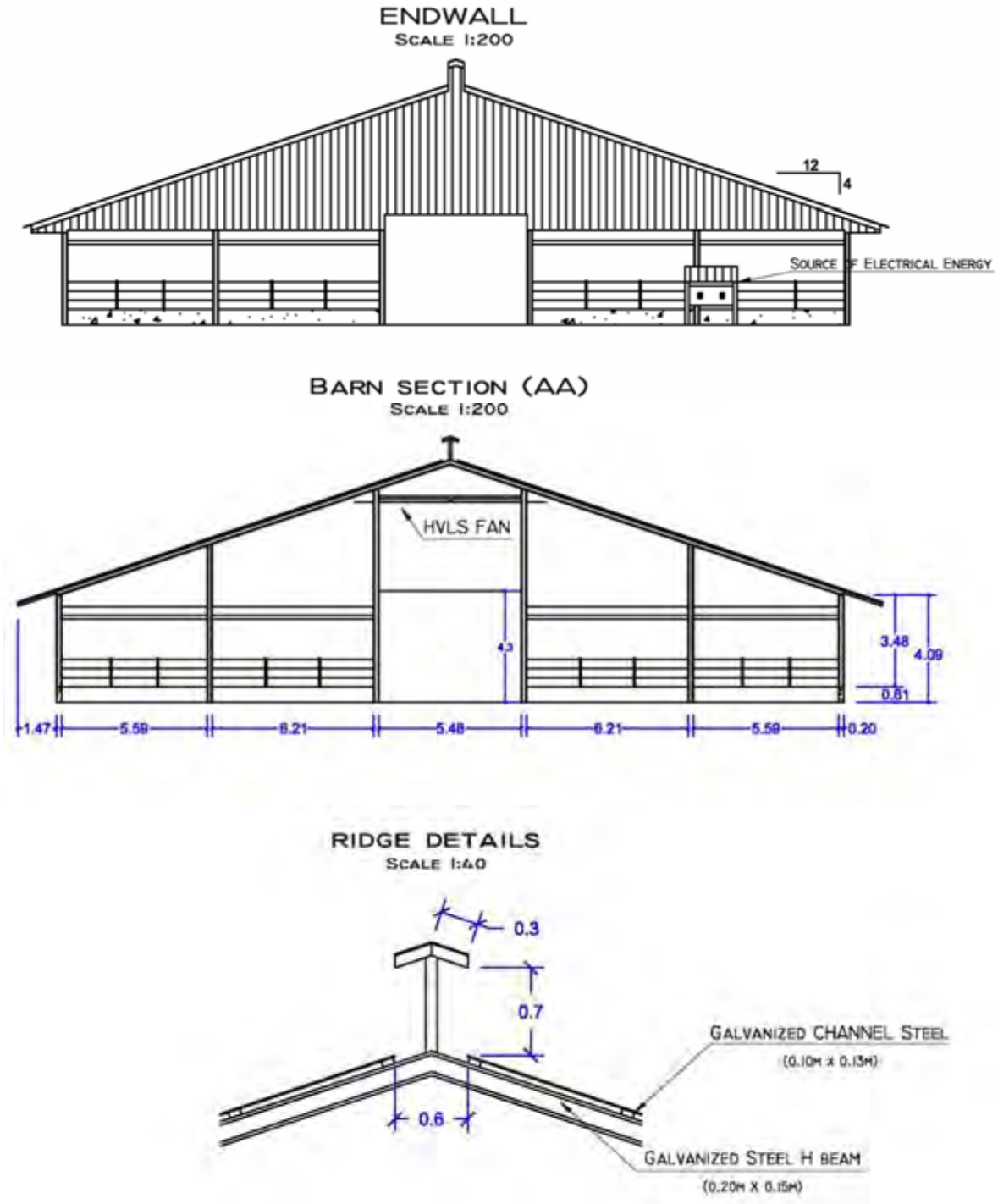

Figure B.3 - Details about end wall, barn section, and ridge of CBP Barn 2.

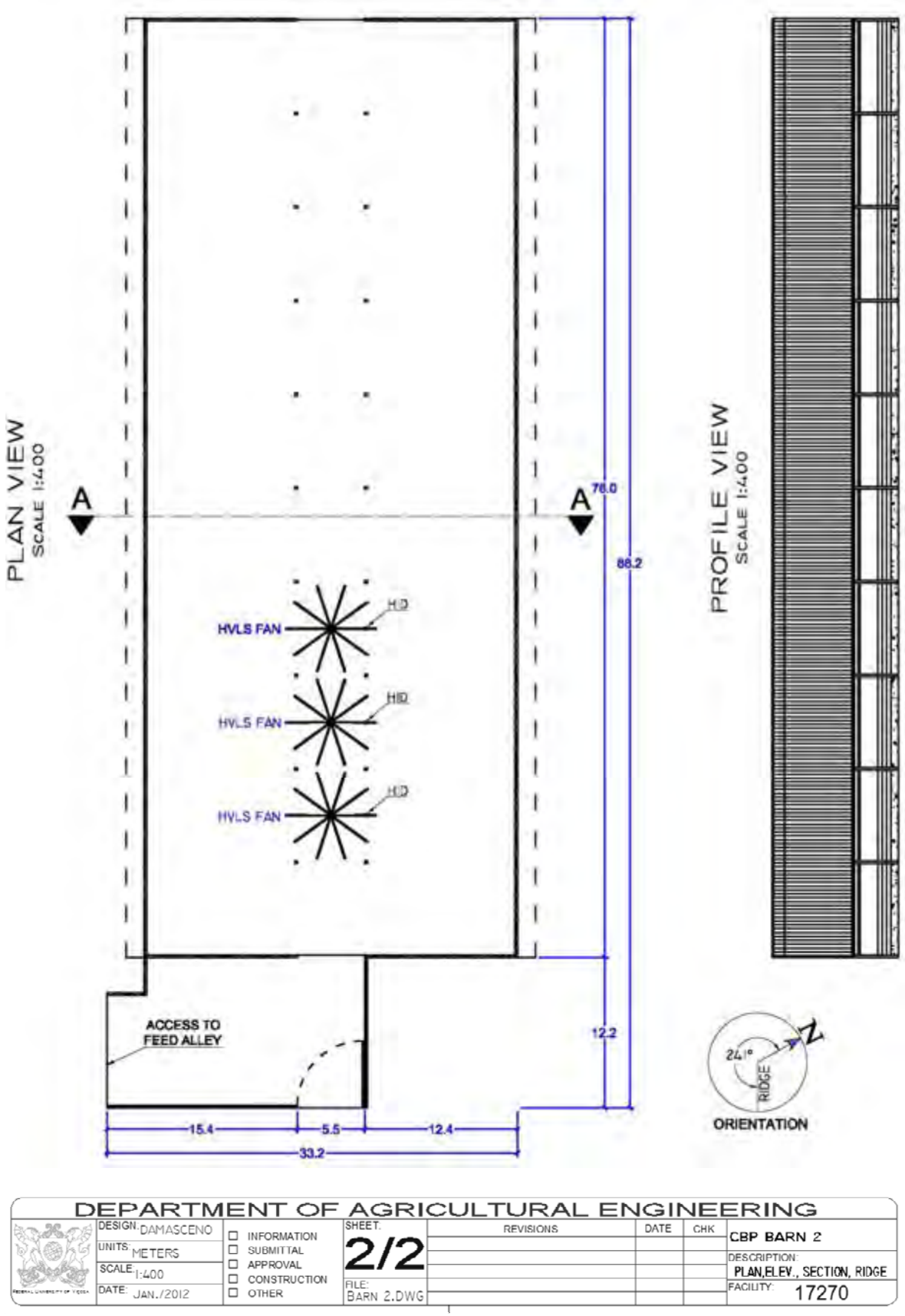

Figure B.4 - Details about plan view and profile of CBP Barn 2.

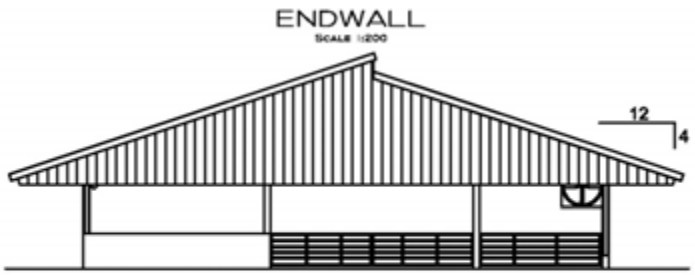

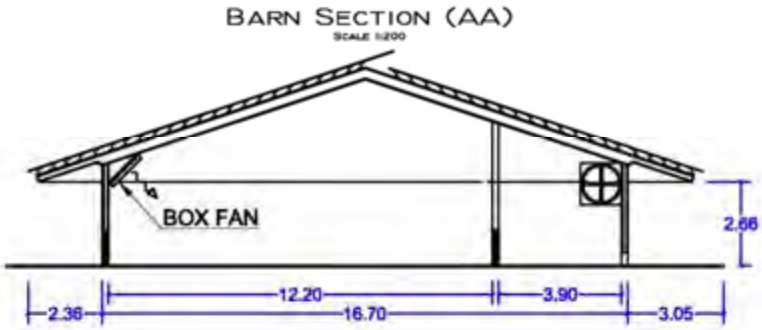

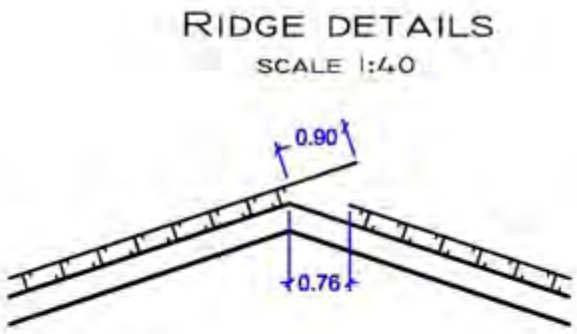

DEPARTMENT OF AGRICULTURAL ENGINEERING

DESIGN: DAMASCENO	☐ INFORMATION	SHEET: 1/2	REVISIONS	DATE	CHK	CBP BARN 3
UNITS: METERS	☐ SUBMITTAL					DESCRIPTION: PLAN,ELEV., SECTION, RIDGE
SCALE: 1:40 AND 1:200	☐ APPROVAL					FACILITY: 53622
DATE: FEB./2012	☐ CONSTRUCTION	FILE: BARN 3.DWG				
	☐ OTHER					

Figure B.5 - Details about end wall, barn section, and ridge of CBP Barn 3.

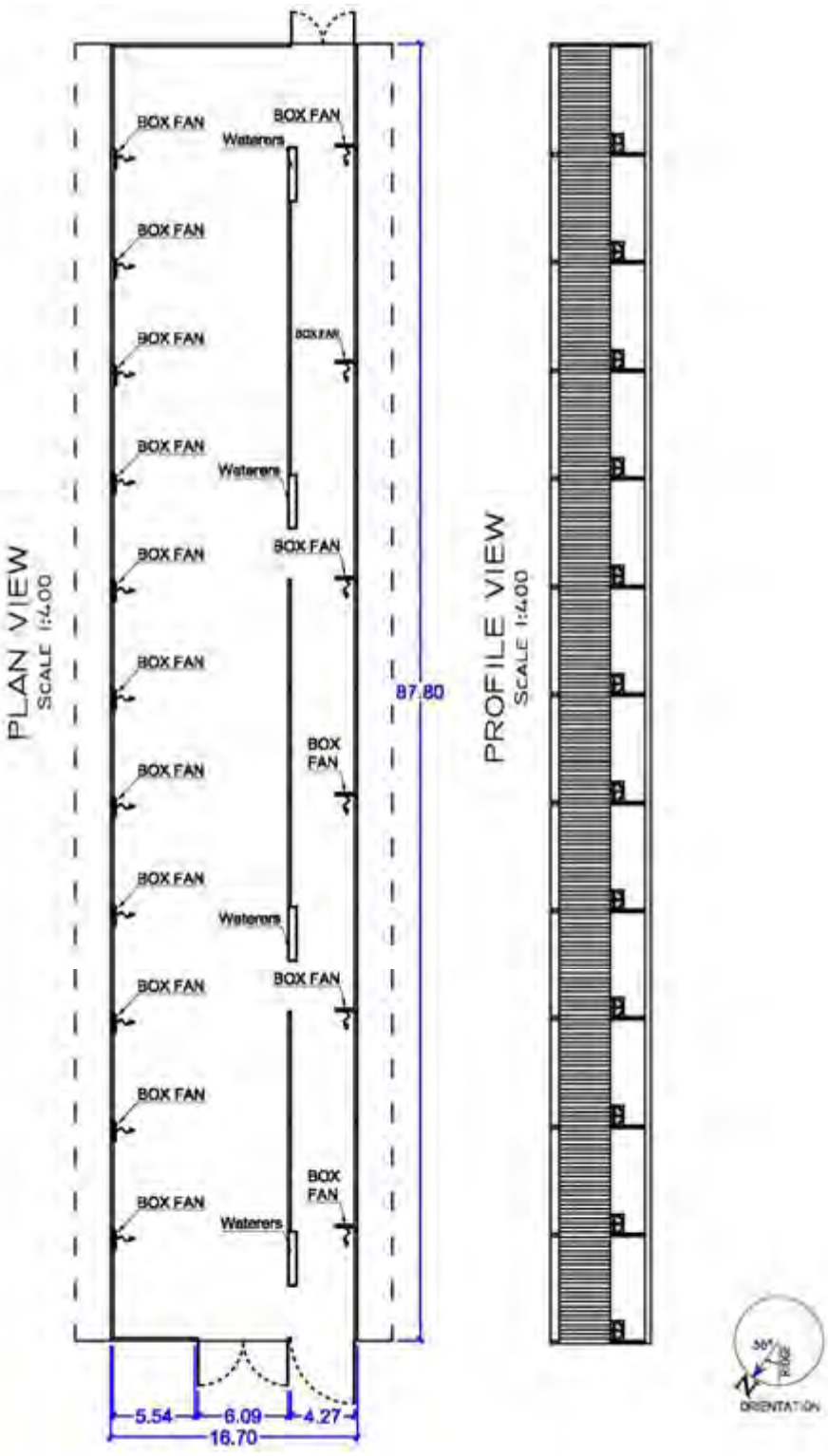

Figure B.6 - Details about plan view and profile of CBP Barn 3.

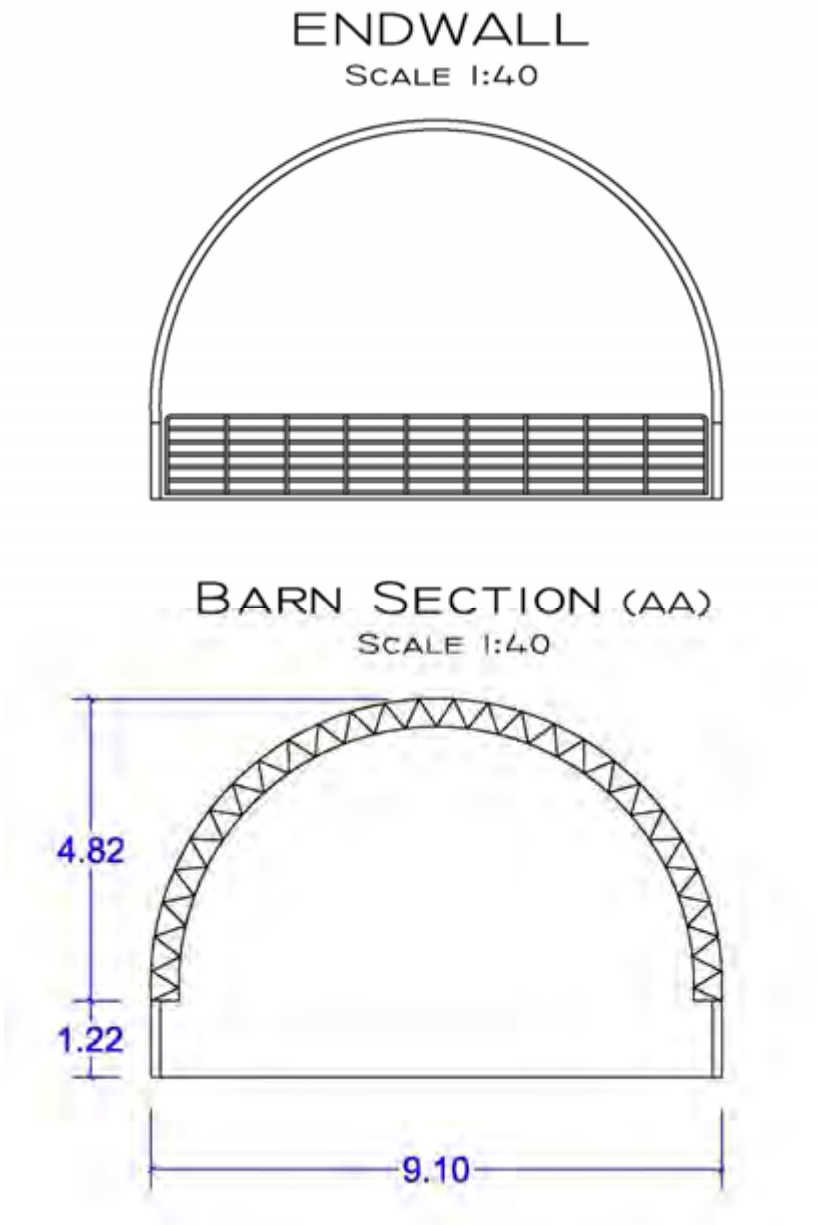

Figure B.7 - Details about end wall, barn section, and ridge of CBP Barn 4.

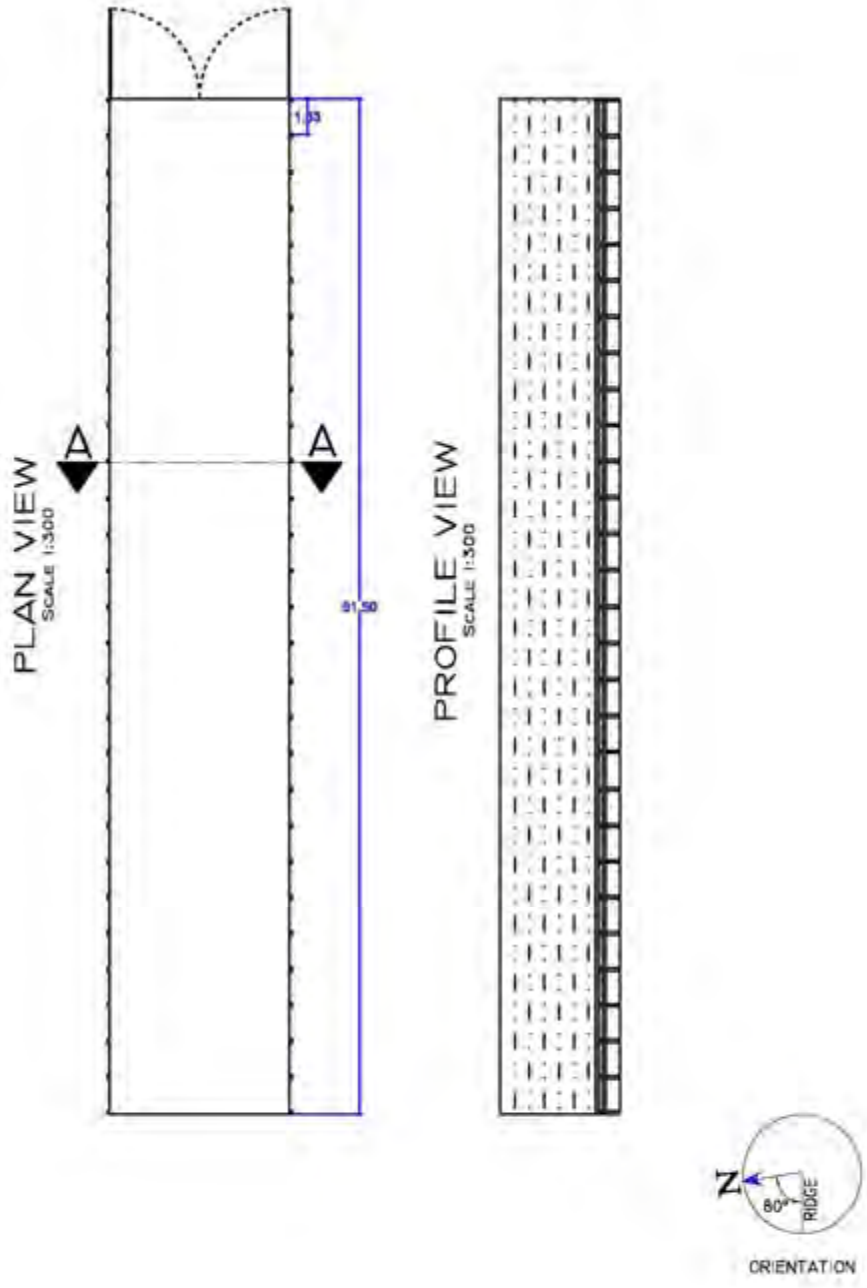

DEPARTMENT OF AGRICULTURAL ENGINEERING							
DESIGN: DAMASCENO	☐ INFORMATION	SHEET: 2/2	REVISIONS	DATE	CHK	CBP BARN 4
UNITS: METERS	☐ SUBMITTAL					DESCRIPTION: PLAN,ELEV., SECTION, RIDGE
SCALE: 1:300	☐ APPROVAL					FACILITY: 26872
DATE: FEB./2012	☐ CONSTRUCTION	FILE: BARN 4.DWG				
	☐ OTHER					

Figure B.8 - Details about plan view and profile of CBP Barn 4.

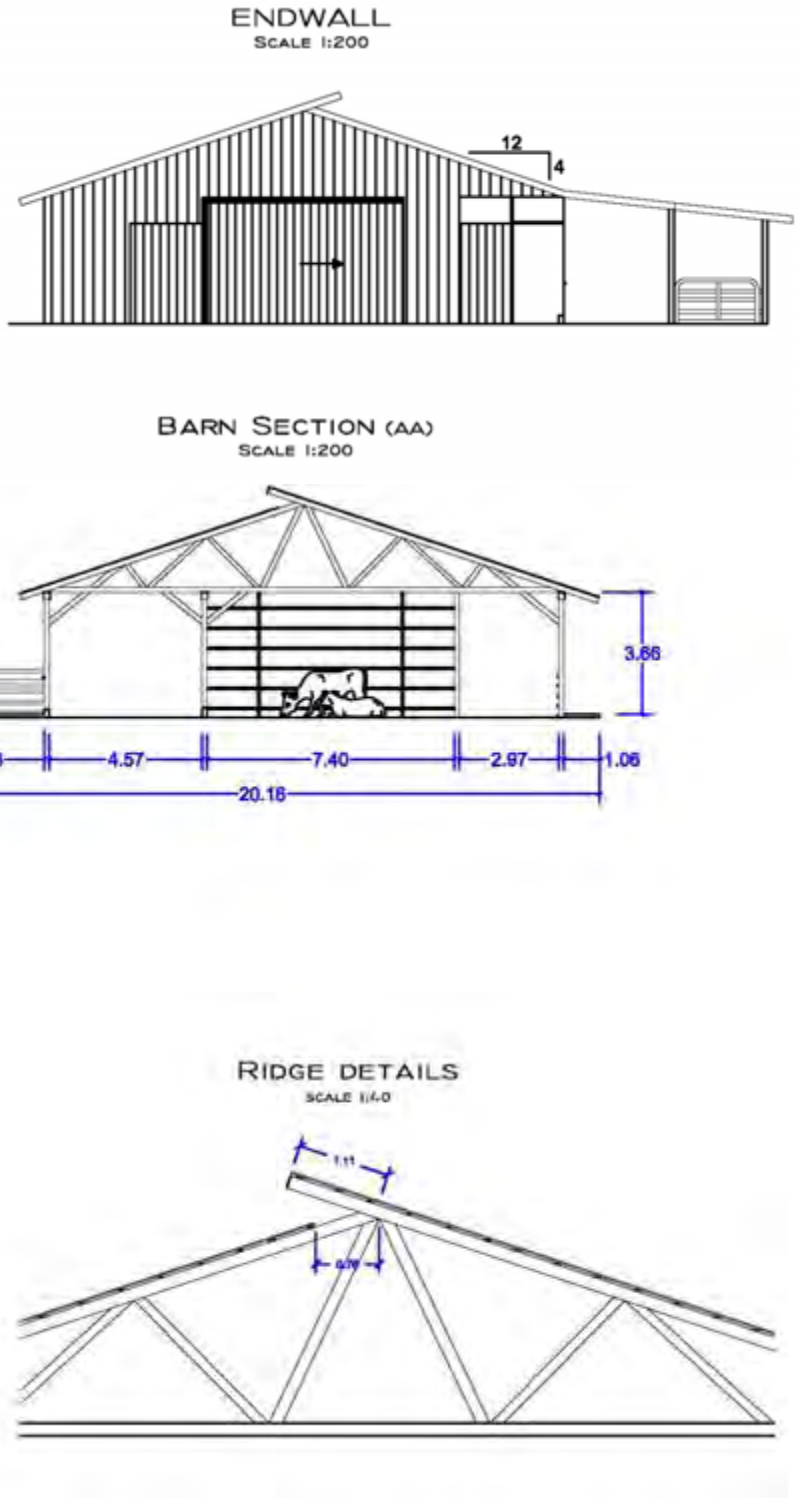

Figure B.9 - Details about end wall, barn section, and ridge of CBP Barn 5.

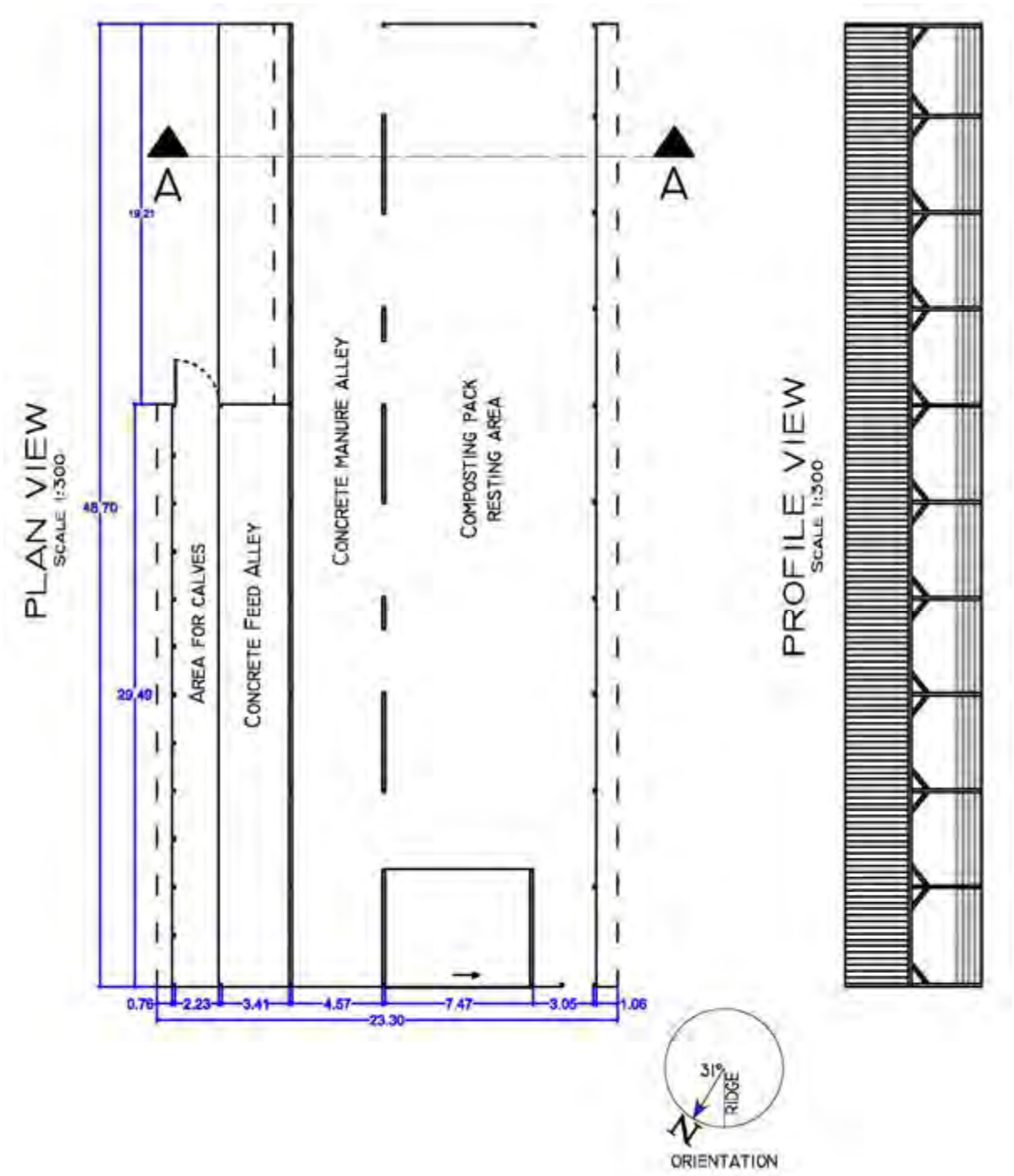

DEPARTMENT OF AGRICULTURAL ENGINEERING							
DESIGN: DAMASCENO	☐ INFORMATION	SHEET: 2/2	REVISIONS	DATE	CHK	CBP BARN 5
UNITS: METERS	☐ SUBMITTAL					DESCRIPTION: PLAN,ELEV., SECTION, RIDGE
SCALE: 1:300	☐ APPROVAL					
DATE: FEB./2012	☐ CONSTRUCTION	FILE: BARN 5.DWG				FACILITY: 44991
	☐ OTHER					

Figure B.10 - Details about plan view and profile of CBP Barn 5.

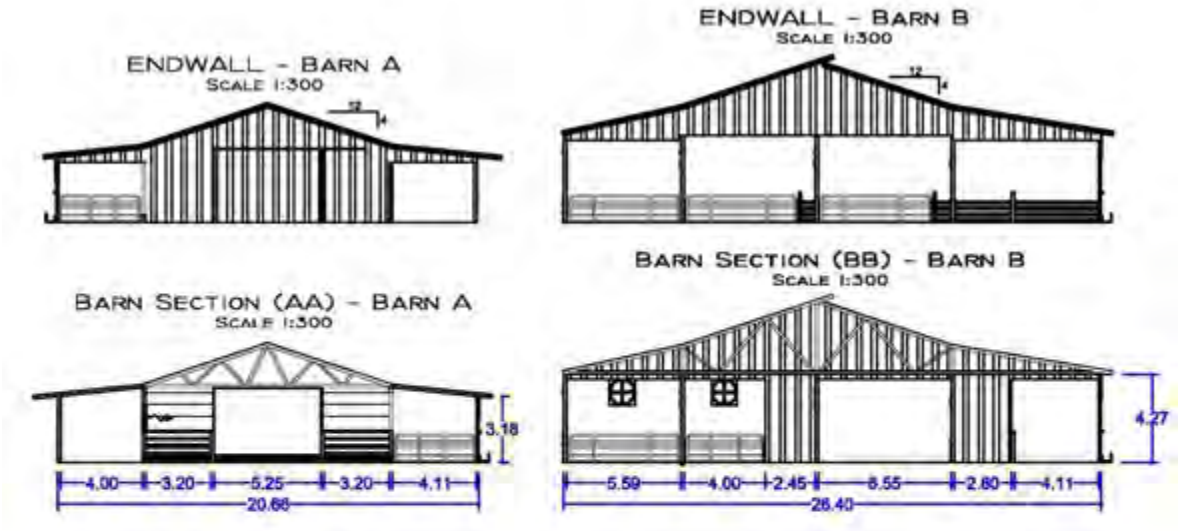

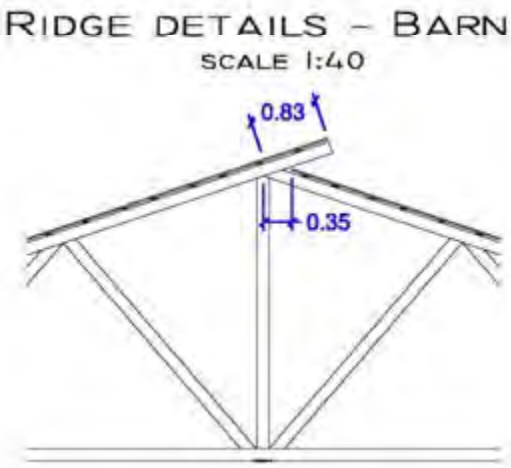

DEPARTMENT OF AGRICULTURAL ENGINEERING							
DESIGN: DAMASCENO	☐ INFORMATION	SHEET: 1/2	REVISIONS	DATE	CHK	CBP BARN 6	
UNITS: METERS	☐ SUBMITTAL						
SCALE: 1:300 AND 1:40	☐ APPROVAL					DESCRIPTION: PLAN,ELEV., SECTION, RIDGE	
DATE: FEB./2012	☐ CONSTRUCTION	FILE: BARN 6.DWG				FACILITY: 91235	
	☐ OTHER						

Figure B.11 - Details about end wall, barn section, and ridge of CBP Barn 6.

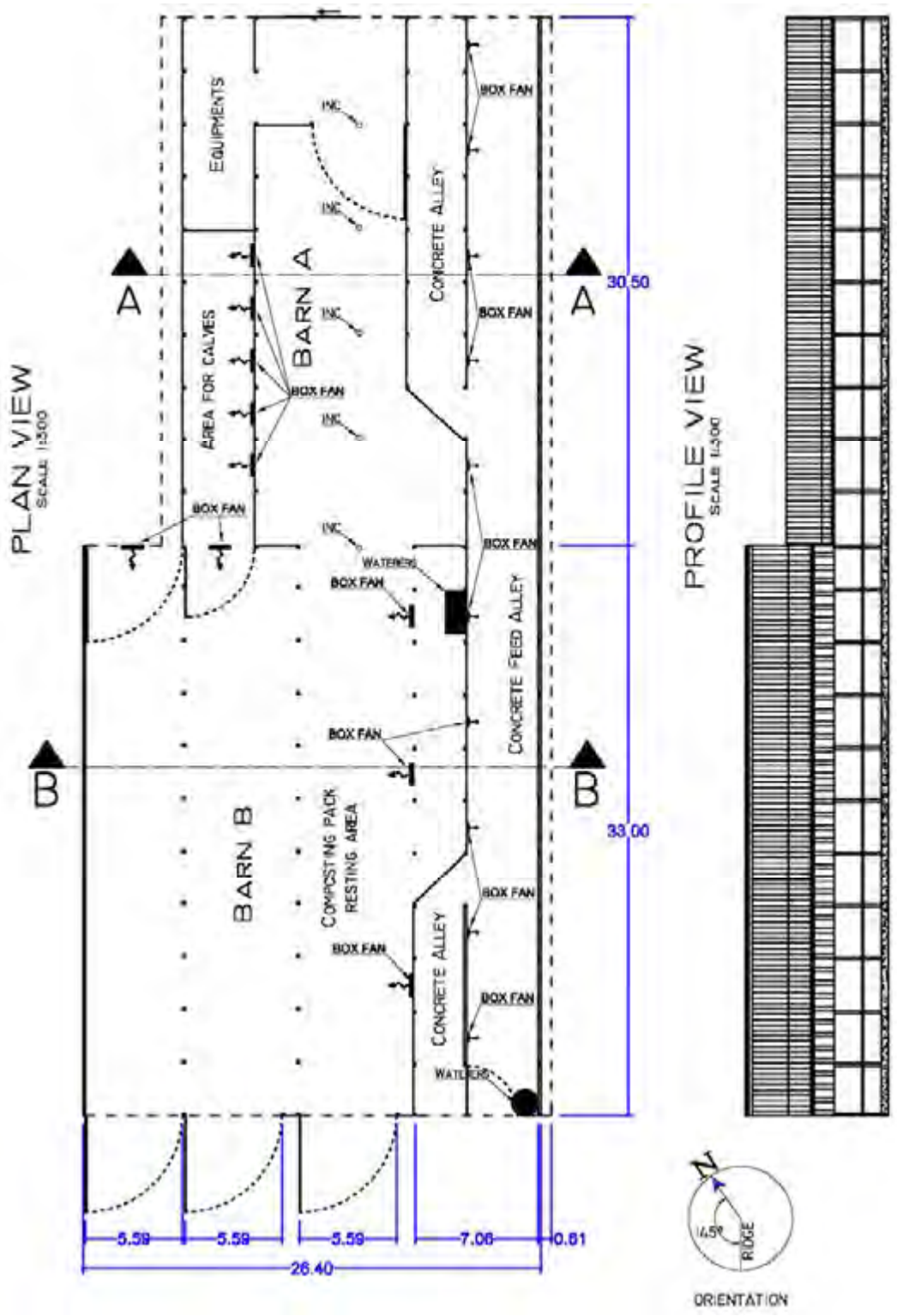

DEPARTMENT OF AGRICULTURAL ENGINEERING							
DESIGN: DAMASCENO	☐ INFORMATION	SHEET: 2/2	REVISIONS	DATE	CHK	CBP BARN 6	
UNITS: METERS	☐ SUBMITTAL					DESCRIPTION: PLAN,ELEV., SECTION, RIDGE	
SCALE: 1:300	☐ APPROVAL					FACILITY: 91235	
DATE: FEB./2012	☐ CONSTRUCTION	FILE: BARN 6.DWG					
	☐ OTHER						

Figure B.12 - Details about plan view and profile of CBP Barn 6.

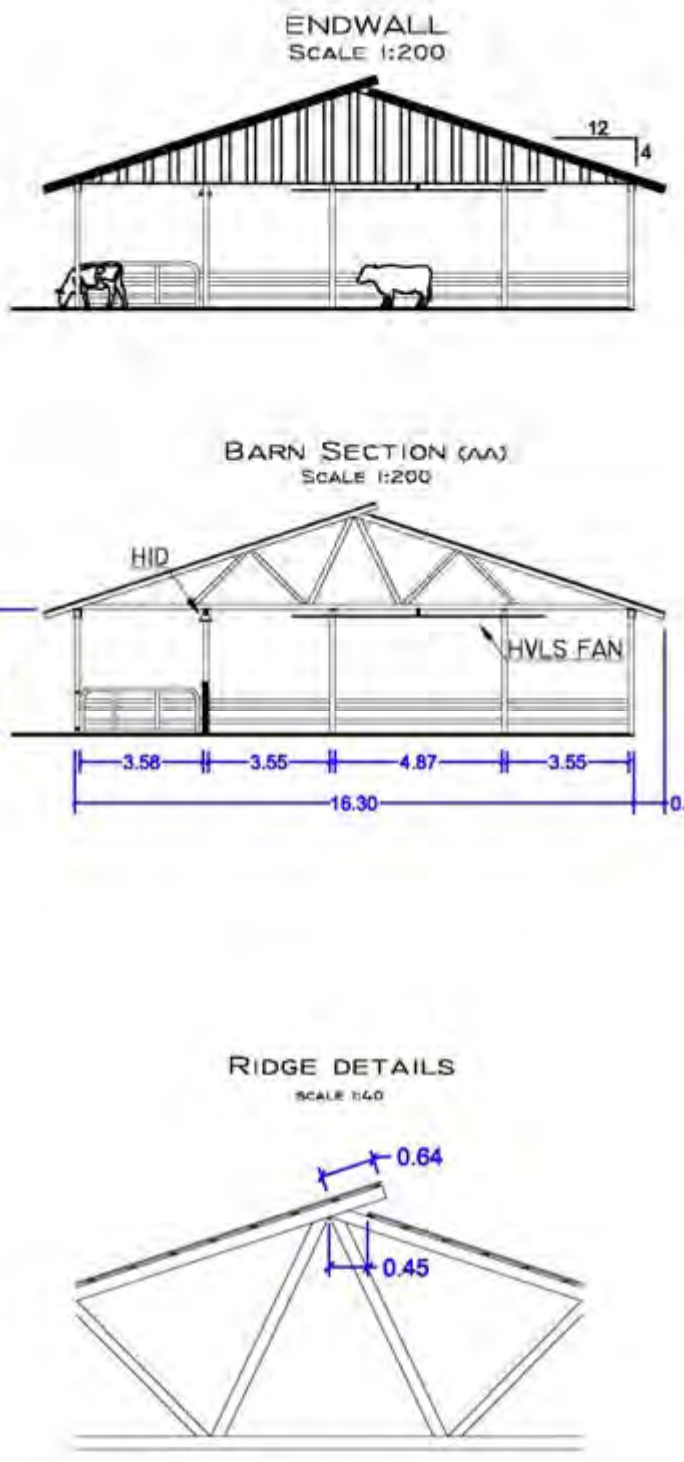

Figure B.13 - Details about end wall, barn section, and ridge of CBP Barn 7.

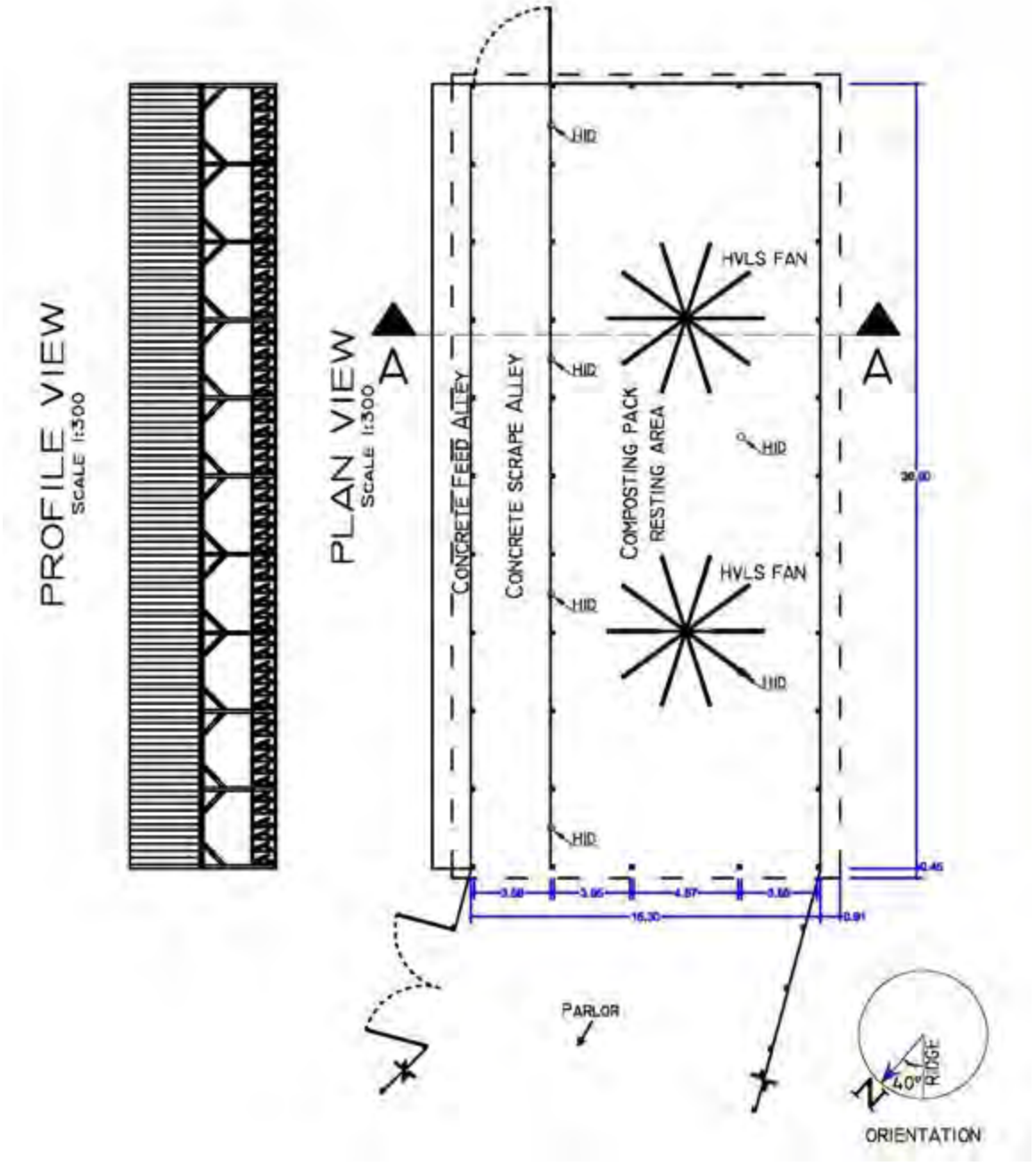

DEPARTMENT OF AGRICULTURAL ENGINEERING							
DESIGN: DAMASCENO	☐ INFORMATION	SHEET: 2/2	REVISIONS	DATE	CHK	CBP BARN 7
UNITS: METERS	☐ SUBMITTAL					DESCRIPTION: PLAN,ELEV., SECTION, RIDGE
SCALE: 1:300	☐ APPROVAL					FACILITY: 29392
DATE: FEB./2012	☐ CONSTRUCTION	FILE: BARN 7.DWG				
	☐ OTHER					

Figure B.14 - Details about plan view and profile of CBP Barn 7.

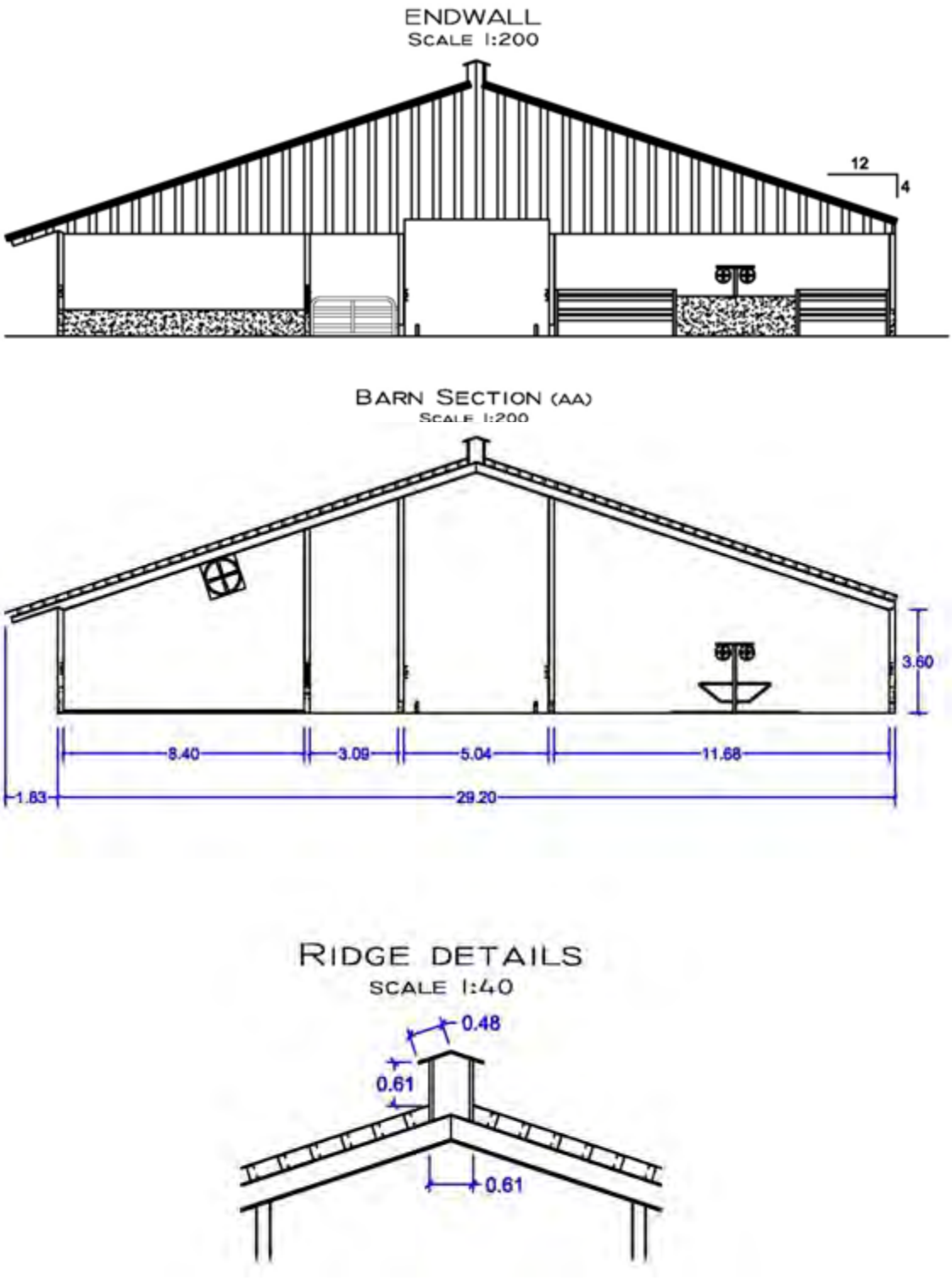

Figure B.15 - Details about end wall, barn section, and ridge of CBP Barn 8.

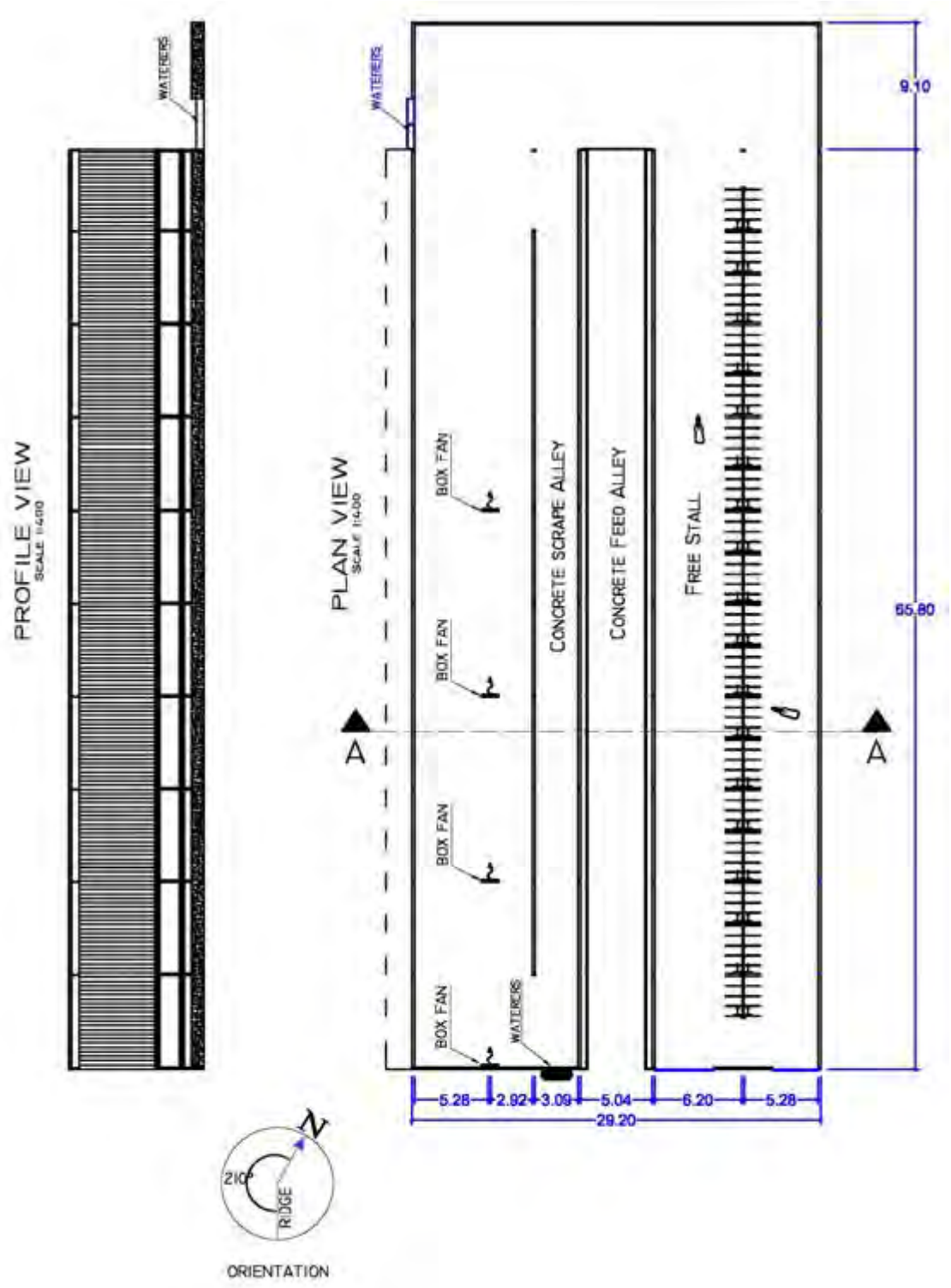

DEPARTMENT OF AGRICULTURAL ENGINEERING							
DESIGN: DAMASCENO	☐ INFORMATION	SHEET: 2/2	REVISIONS	DATE	CHK	CBP BARN 8	
UNITS: METERS	☐ SUBMITTAL					DESCRIPTION: PLAN,ELEV., SECTION, RIDGE	
SCALE: 1:400	☐ APPROVAL					FACILITY: 59613	
DATE: Feb./2012	☐ CONSTRUCTION	FILE: Barn 8.DWG					
	☐ OTHER						

Figure B.16 - Details about plan view and profile of CBP Barn 8.

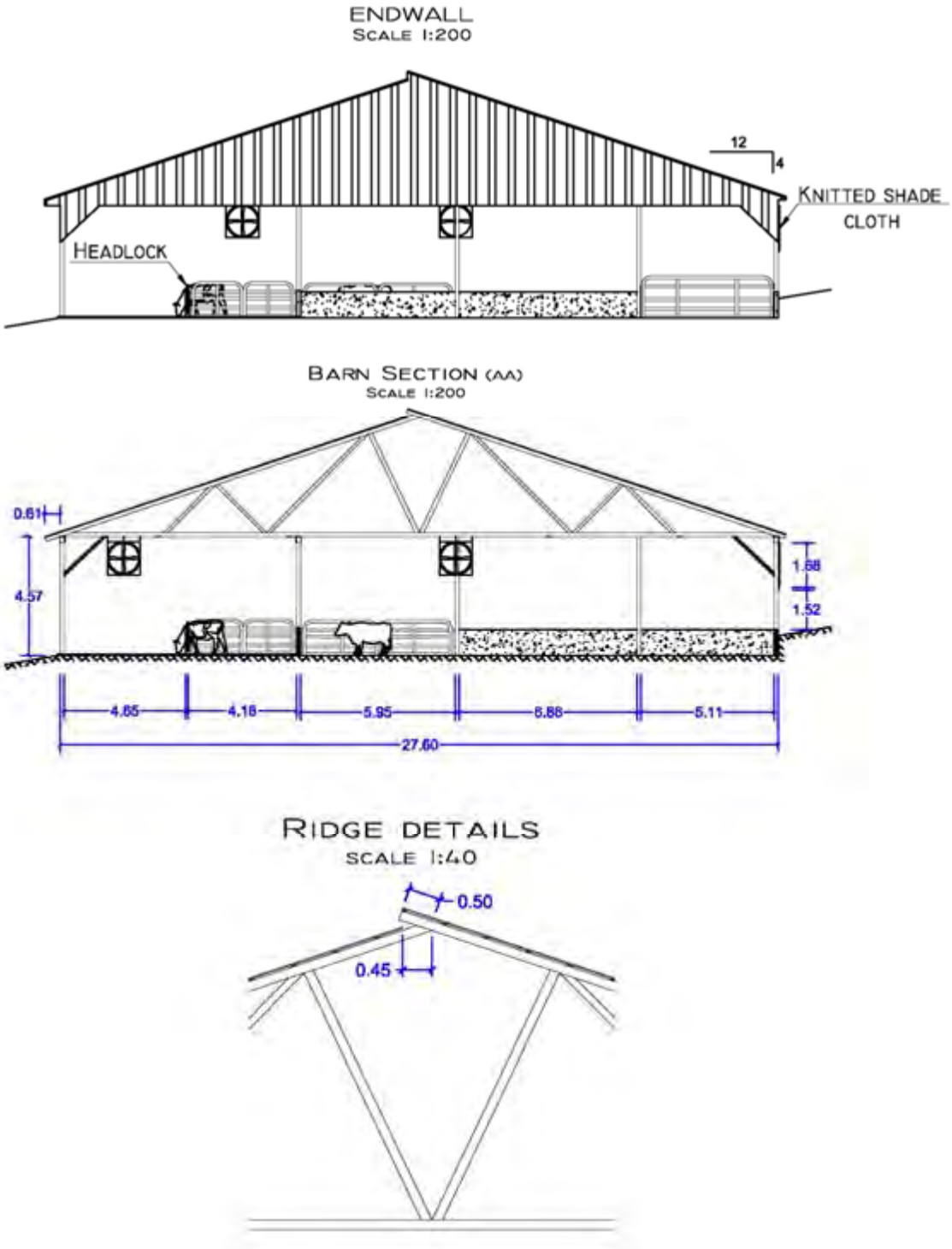

Figure B.17 - Details about end wall, barn section, and ridge of CBP Barn 9.

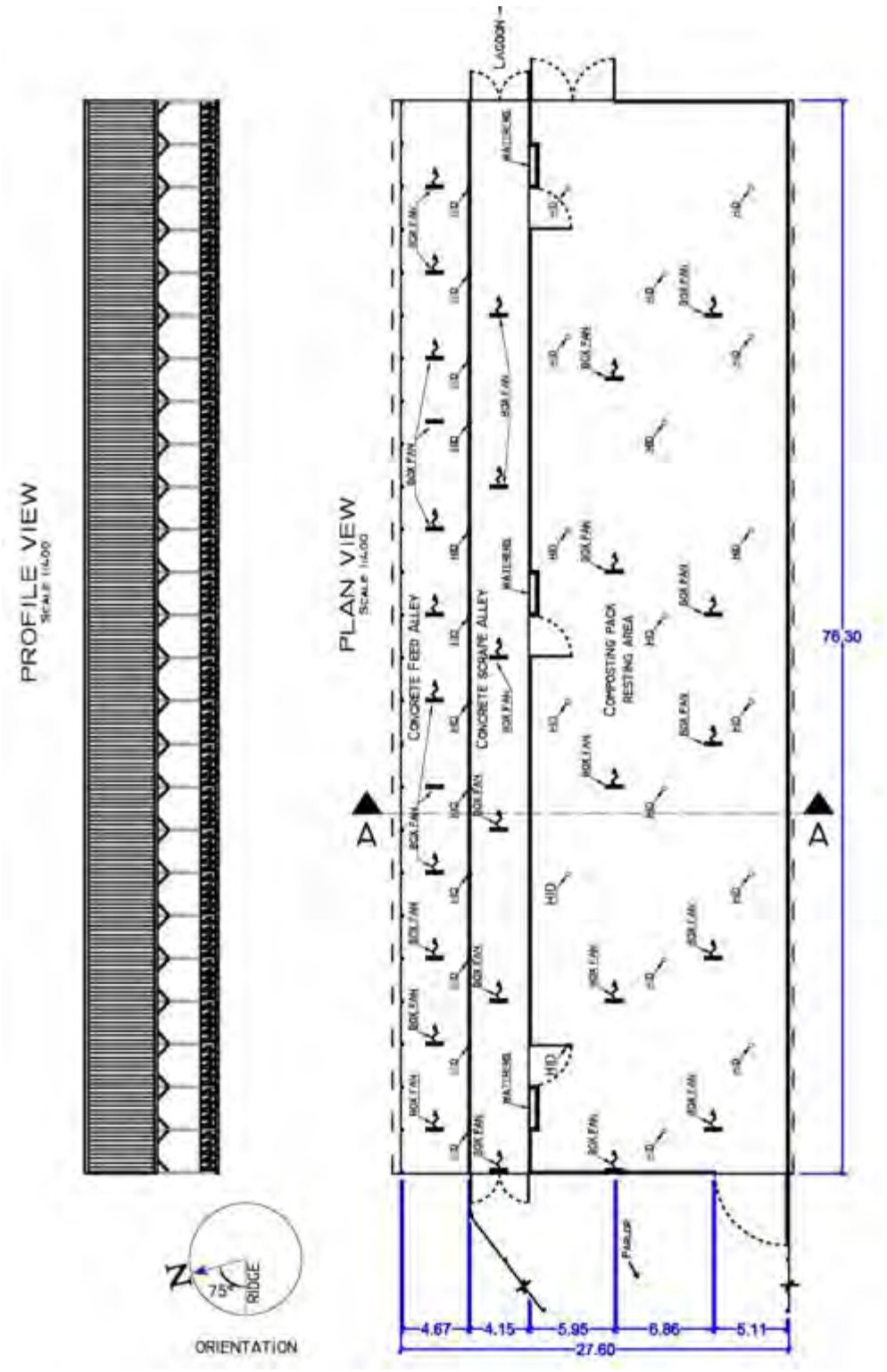

DEPARTMENT OF AGRICULTURAL ENGINEERING								
	DESIGN: DAMASCENO	☐ INFORMATION	SHEET: 2/2	REVISIONS	DATE	CHK	CBP BARN 9	
	UNITS: METERS	☐ SUBMITTAL					DESCRIPTION:	
	SCALE: 1:400	☐ APPROVAL					PLAN,ELEV., SECTION, RIDGE	
	DATE: FEB./2012	☐ CONSTRUCTION	FILE: BARN 9.DWG				FACILITY: 59613	
		☐ OTHER						

Figure B.18 - Details about plan view and profile of CBP Barn 9.

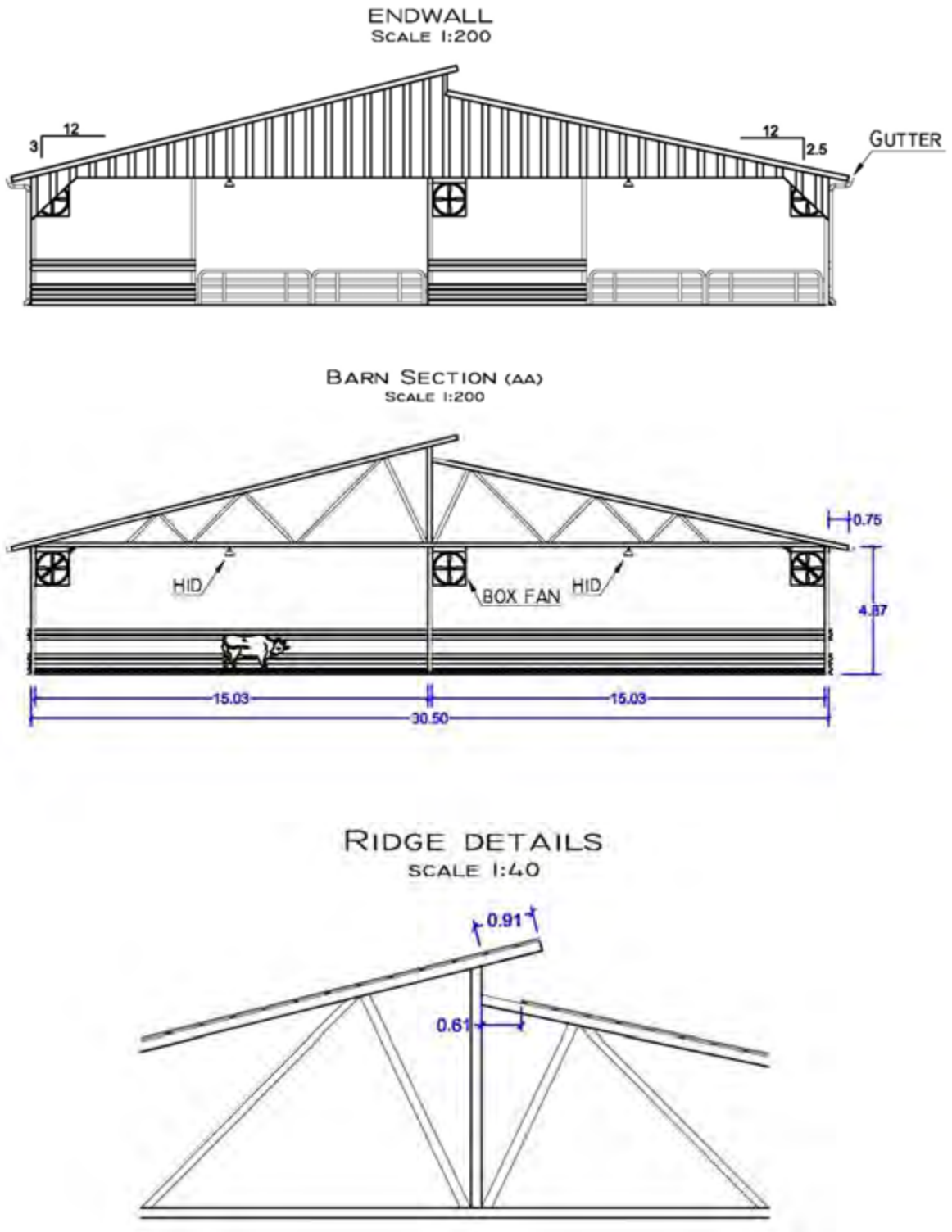

Figure B.19 - Details about end wall, barn section, and ridge of CBP Barn 10.

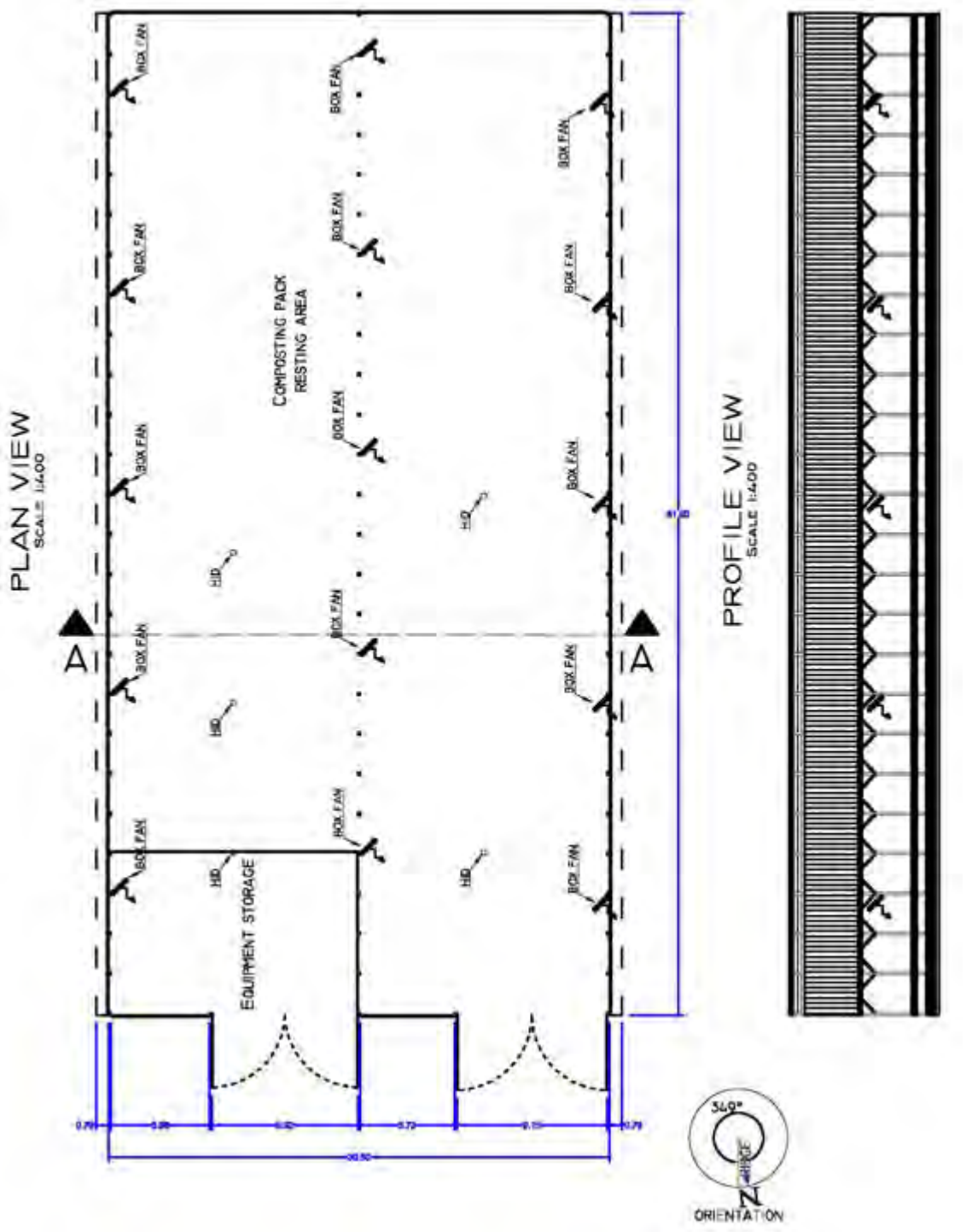

DEPARTMENT OF AGRICULTURAL ENGINEERING							
	DESIGN: DAMASCENO	☐ INFORMATION	SHEET: 2/2	REVISIONS	DATE	CHK	CBP BARN 10
	UNITS: METERS	☐ SUBMITTAL					DESCRIPTION: PLAN,ELEV., SECTION, RIDGE
	SCALE: 1:400	☐ APPROVAL					
	DATE: FEB./2012	☐ CONSTRUCTION	FILE: BARN 10.DWG				FACILITY: 24262
		☐ OTHER					

Figure B.20 - Details about plan view and profile of CBP Barn 10.

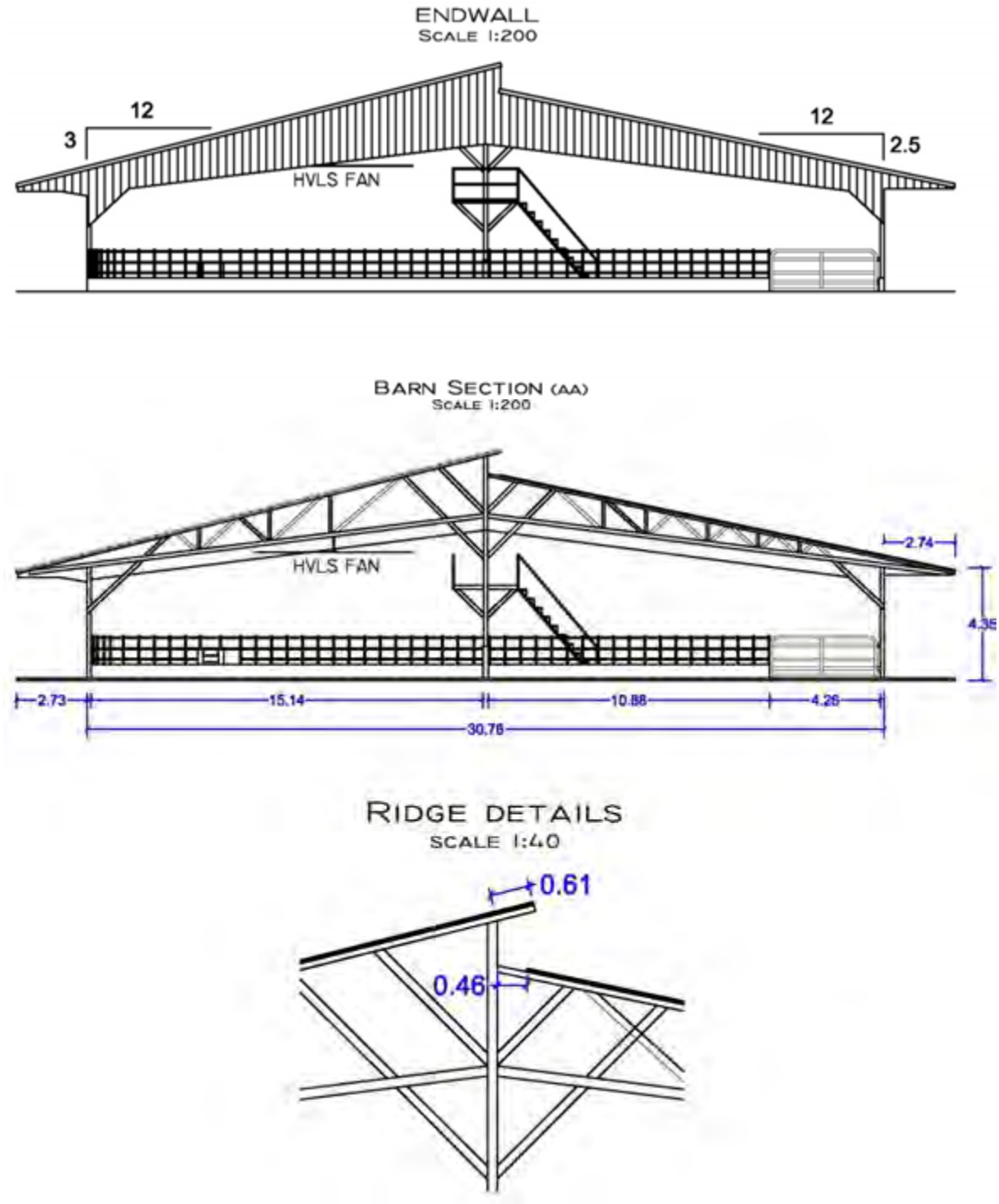

Figure B.21 - Details about end wall, barn section, and ridge of CBP Barns 11 and 12.

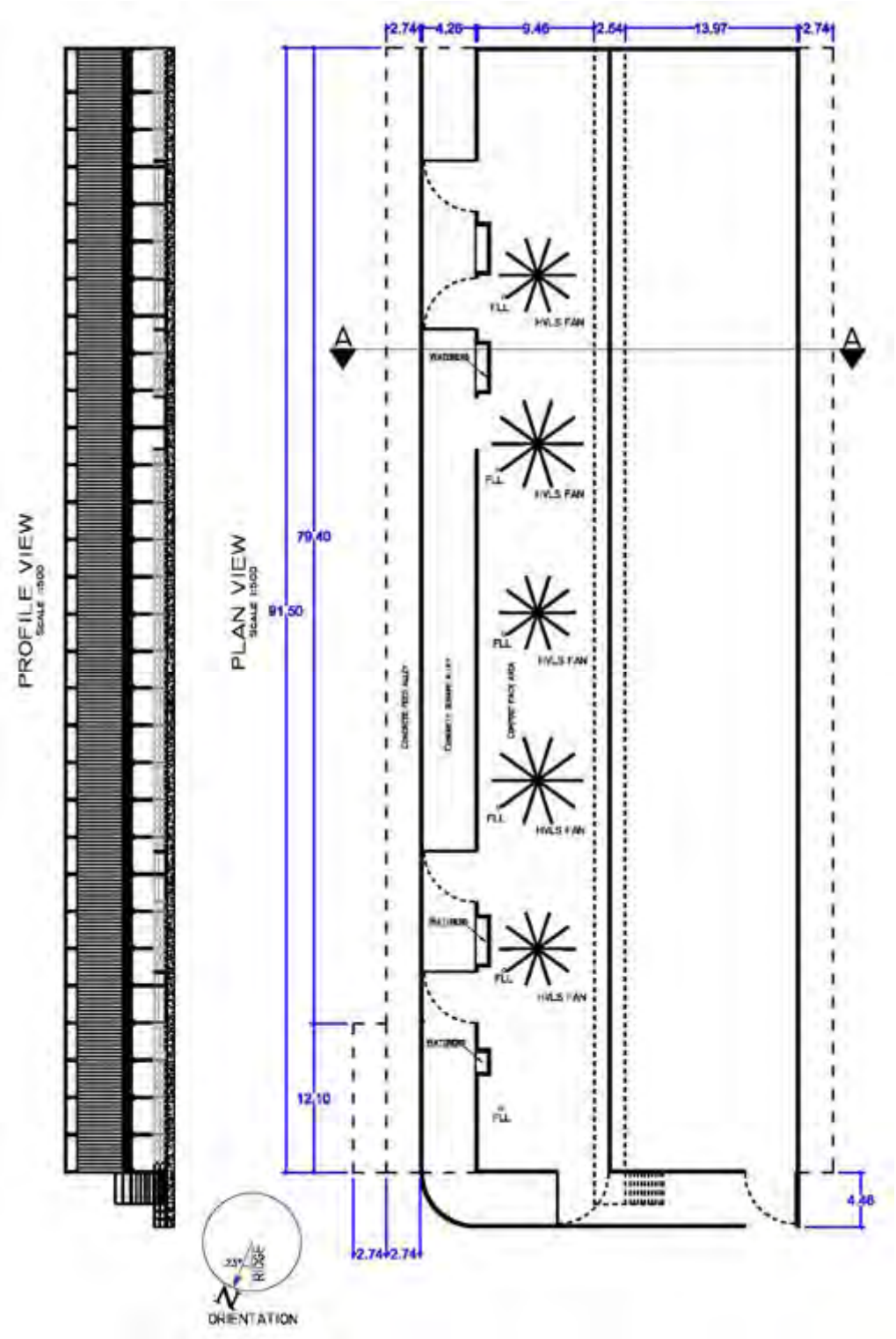

DEPARTMENT OF AGRICULTURAL ENGINEERING							
DESIGN: DAMASCENO	☐ INFORMATION	SHEET: 2/2	REVISIONS	DATE	CHK	CBP BARN 11 AND 12	
UNITS: METERS	☐ SUBMITTAL					DESCRIPTION: PLAN,ELEV., SECTION, RIDGE	
SCALE: 1:500	☐ APPROVAL						
DATE: FEB./2012	☐ CONSTRUCTION	FILE: BARN 11 AND 12.DWG				FACILITY: 87641	
	☐ OTHER						

Figure B.22 - Details about plan view and profile of CBP Barns 11 and 12.

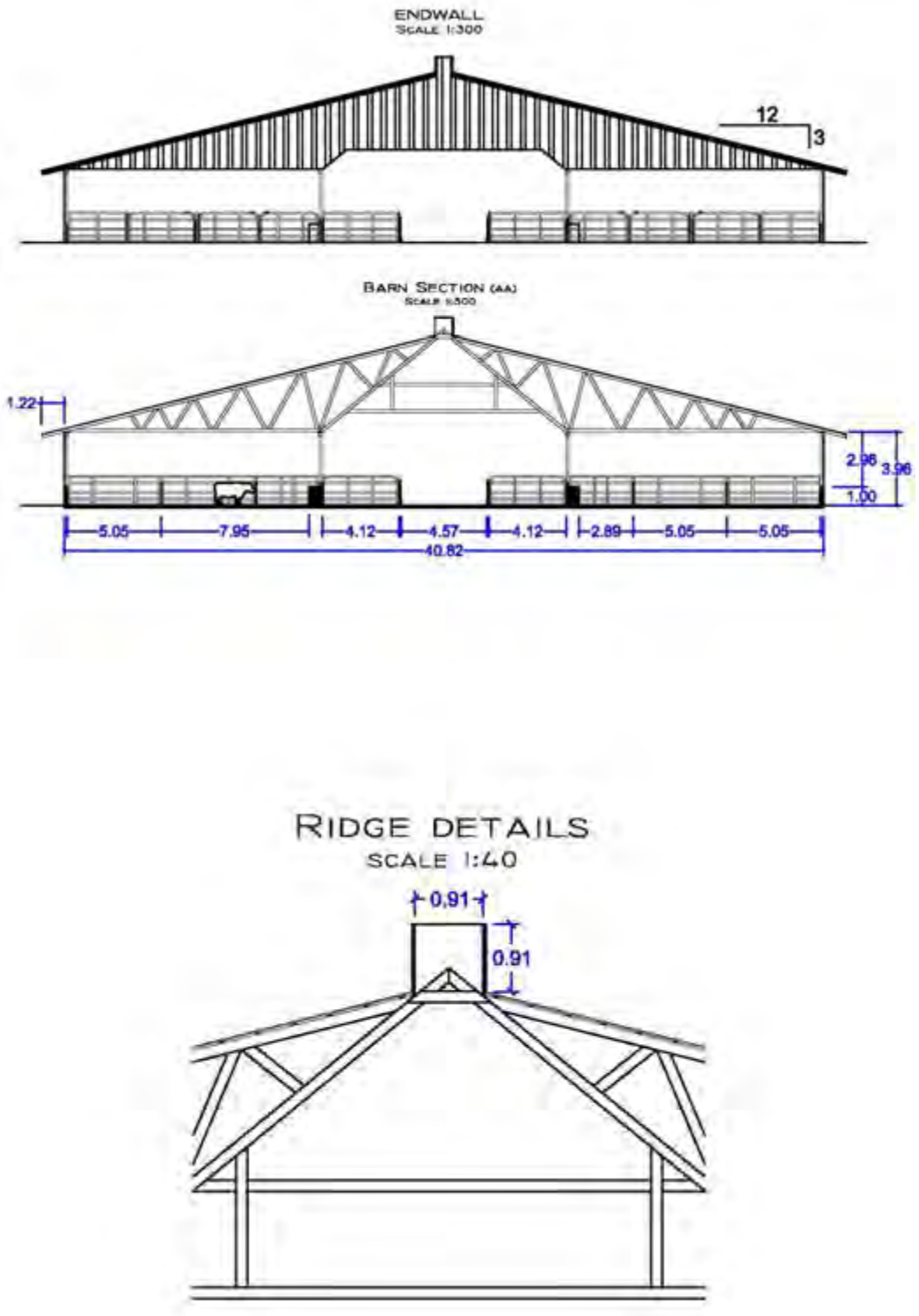

Figure B.23 - Details about end wall, barn section, and ridge of CBP Barns 13 and 14.

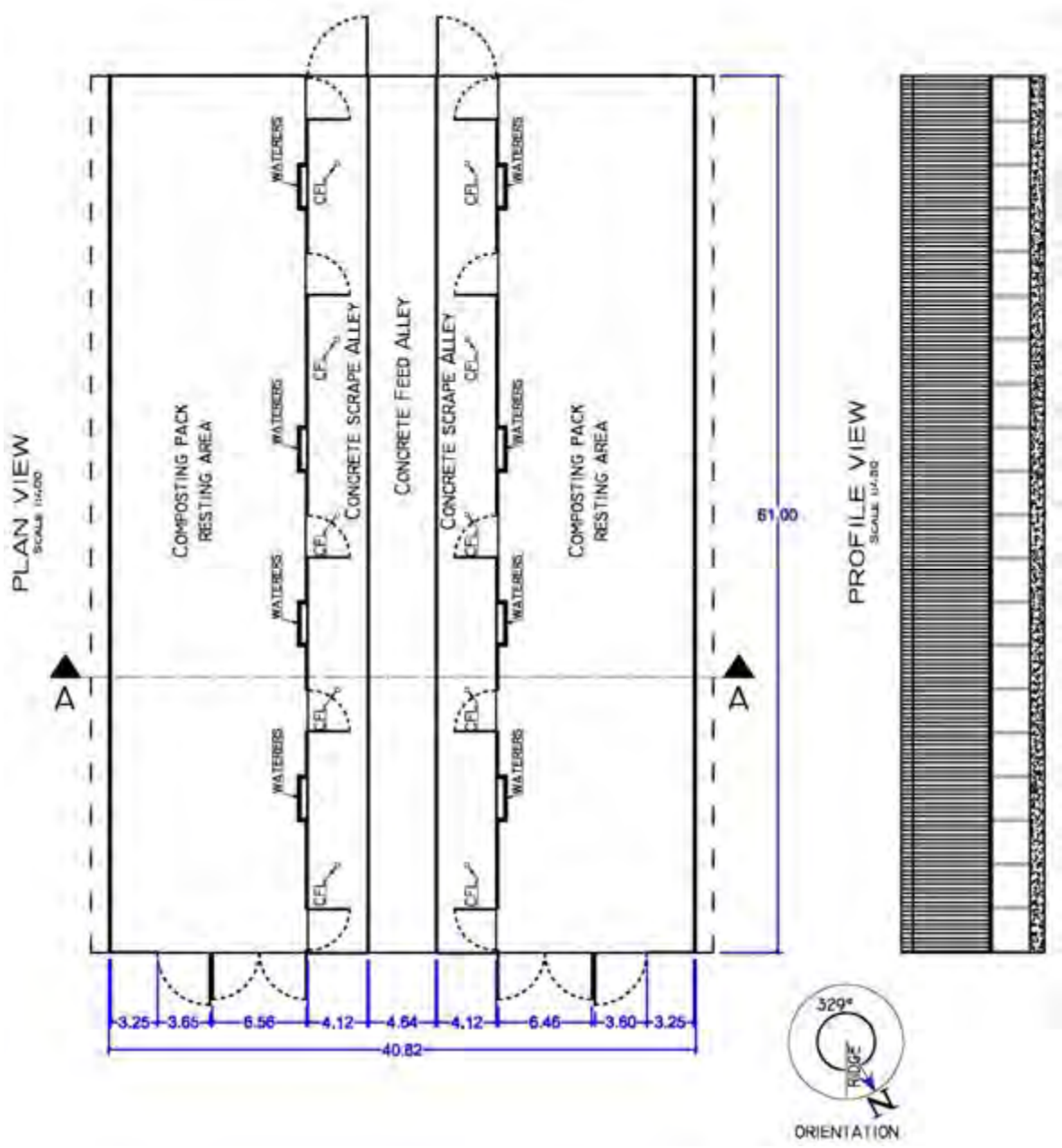

DEPARTMENT OF AGRICULTURAL ENGINEERING							
DESIGN: DAMASCENO	☐ INFORMATION	SHEET: 2/2	REVISIONS	DATE	CHK	CBP BARN 13 AND 14	
UNITS: METERS	☐ SUBMITTAL					DESCRIPTION: PLAN,ELEV., SECTION, RIDGE	
SCALE: 1:400	☐ APPROVAL						
DATE: FEB./2012	☐ CONSTRUCTION	FILE: BARN 13 AND 14.DWG				FACILITY: 58678	
	☐ OTHER						

Figure B.24 - Details about plan view and profile of CBP Barns 13 and 14.

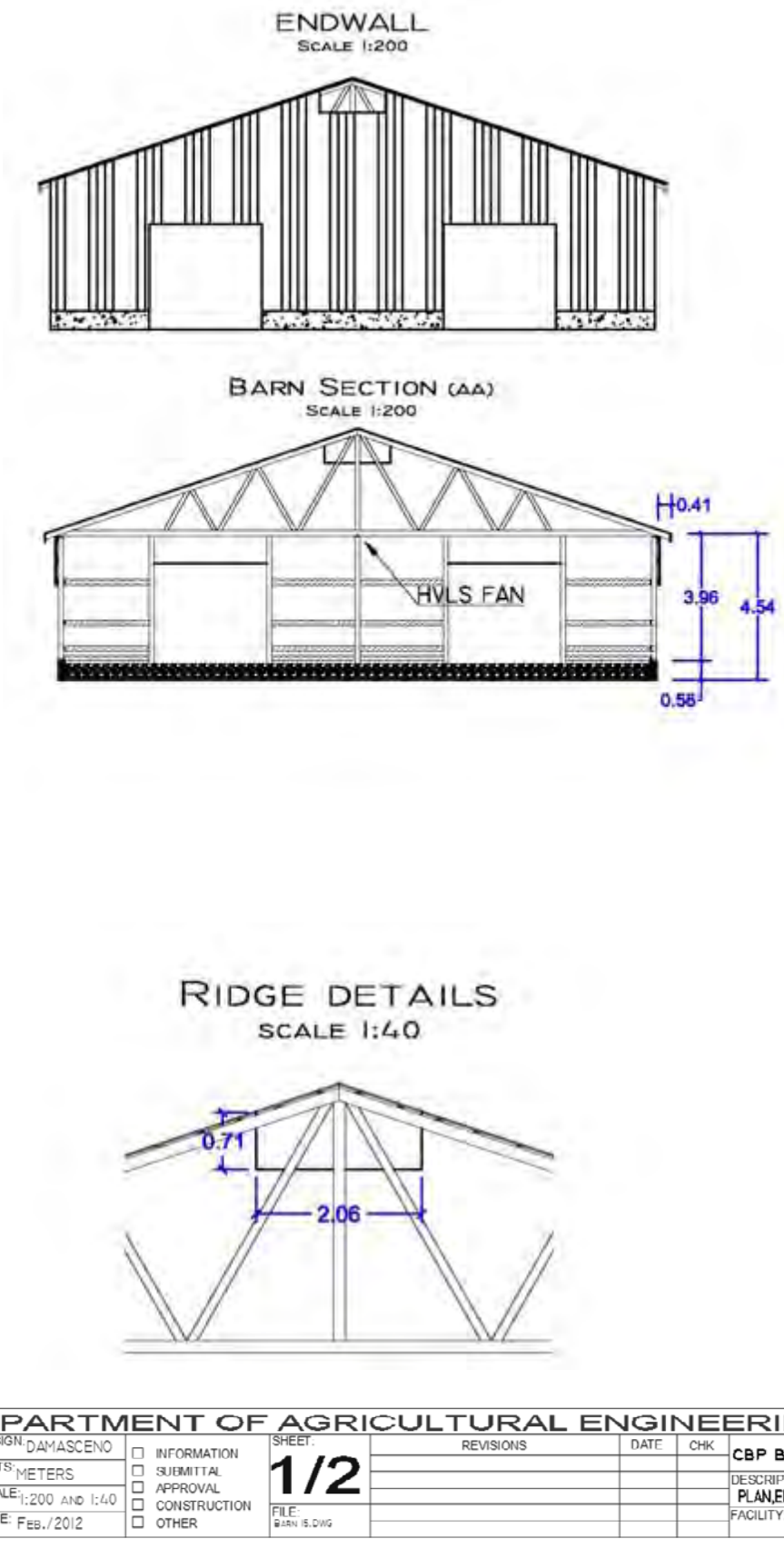

Figure B.25 - Details about end wall, barn section, and ridge of CBP Barn 15.

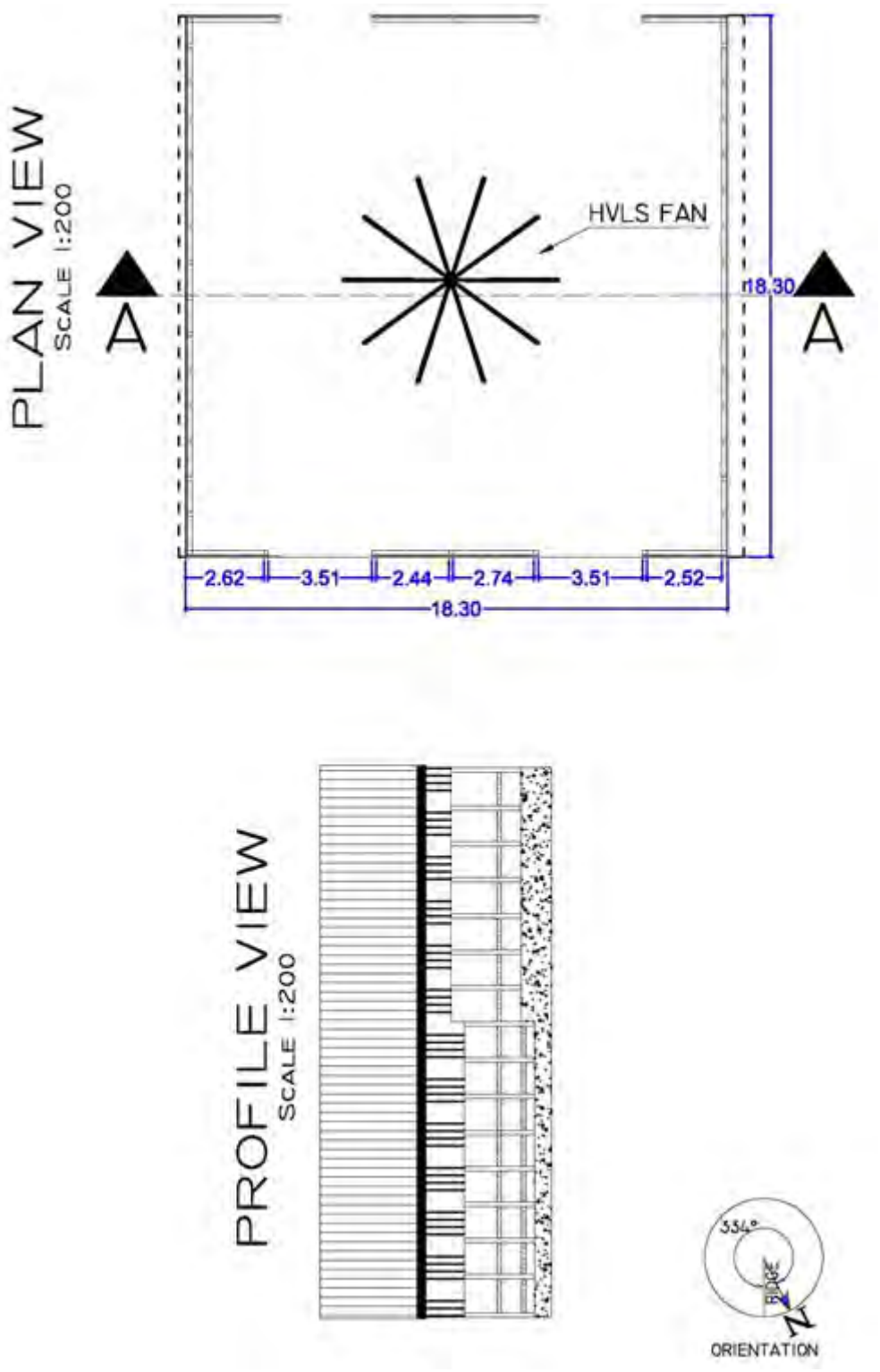

Figure B.26 - Details about plan view and profile of CBP Barn 15.

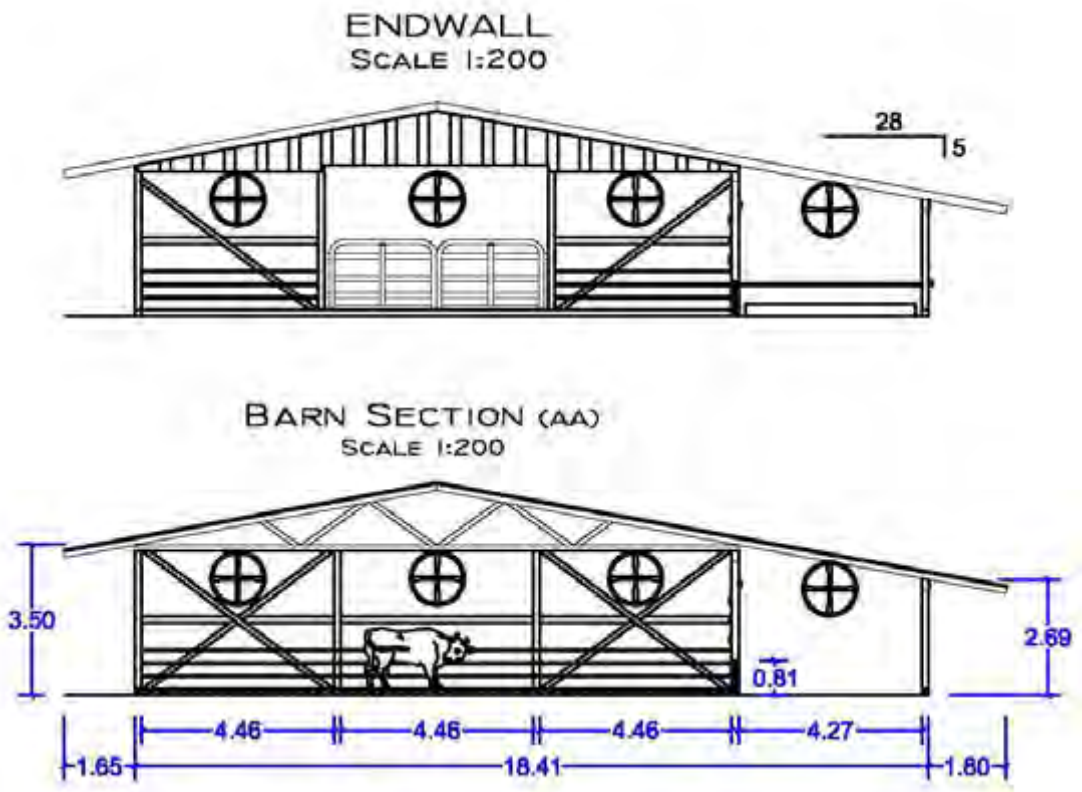

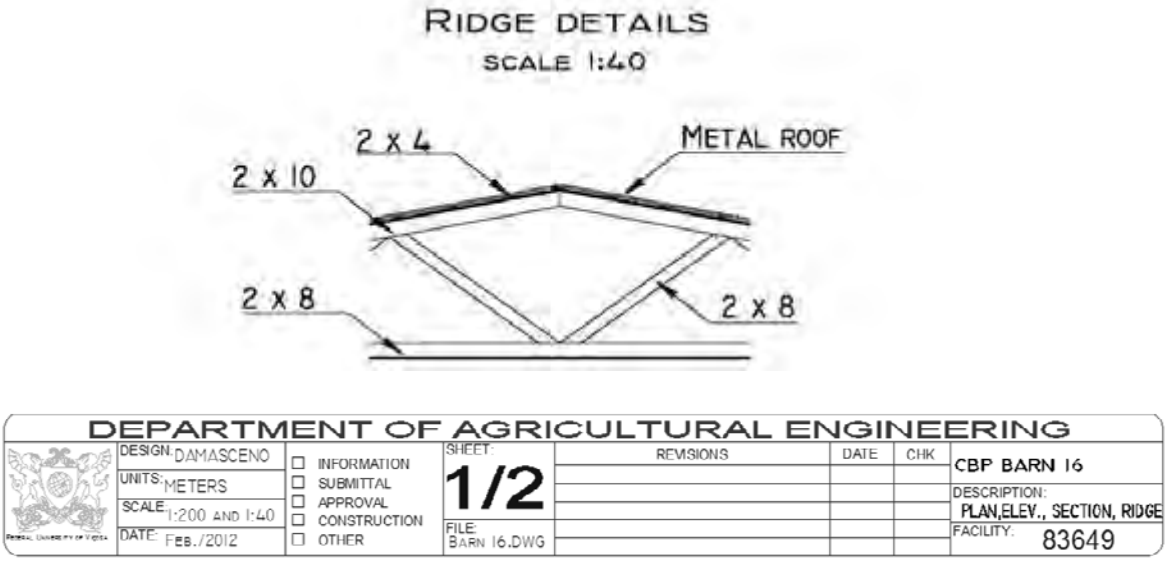

Figure B.27 - Details about end wall, barn section, and ridge of CBP Barn 16.

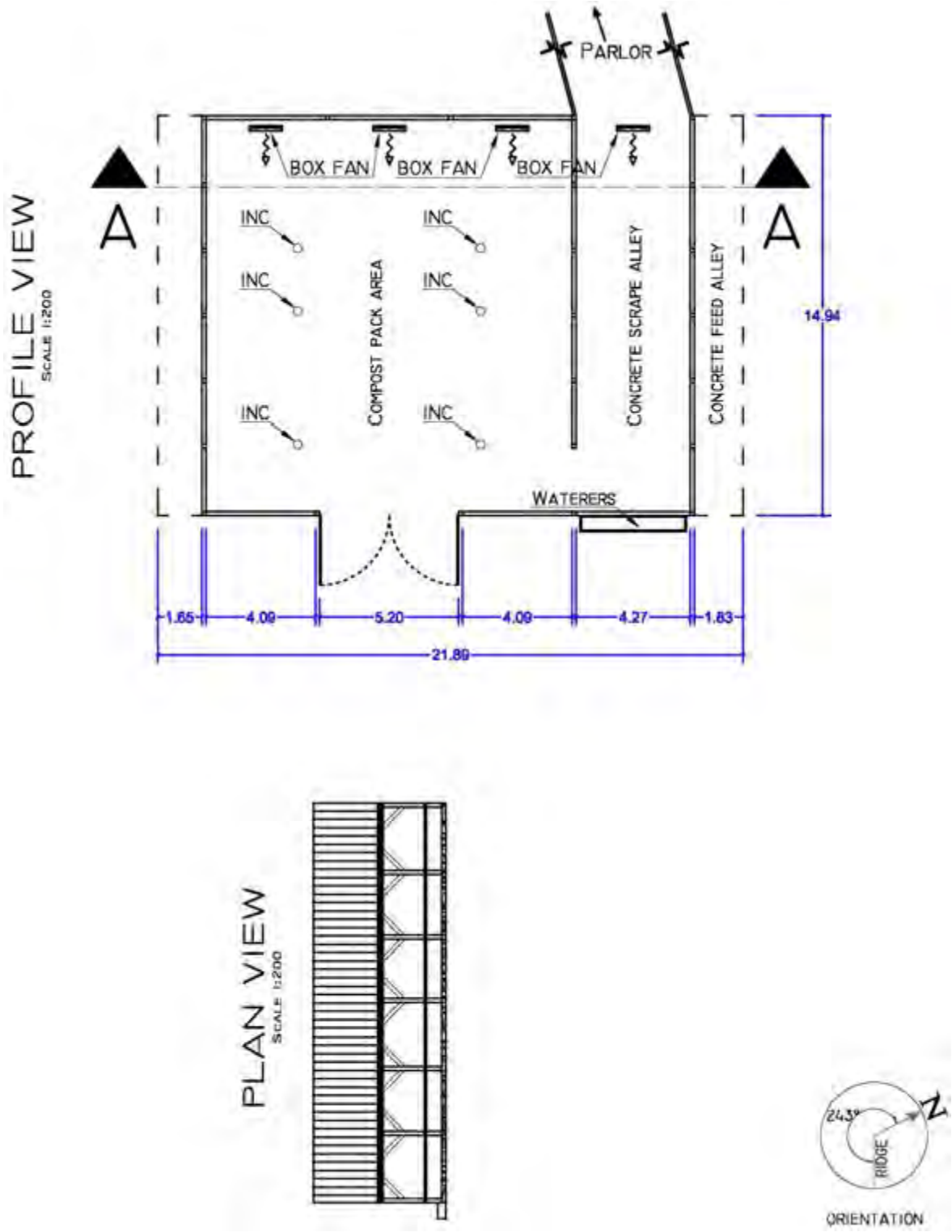

Figure B.28 - Details about plan view and profile of CBP Barn 16.

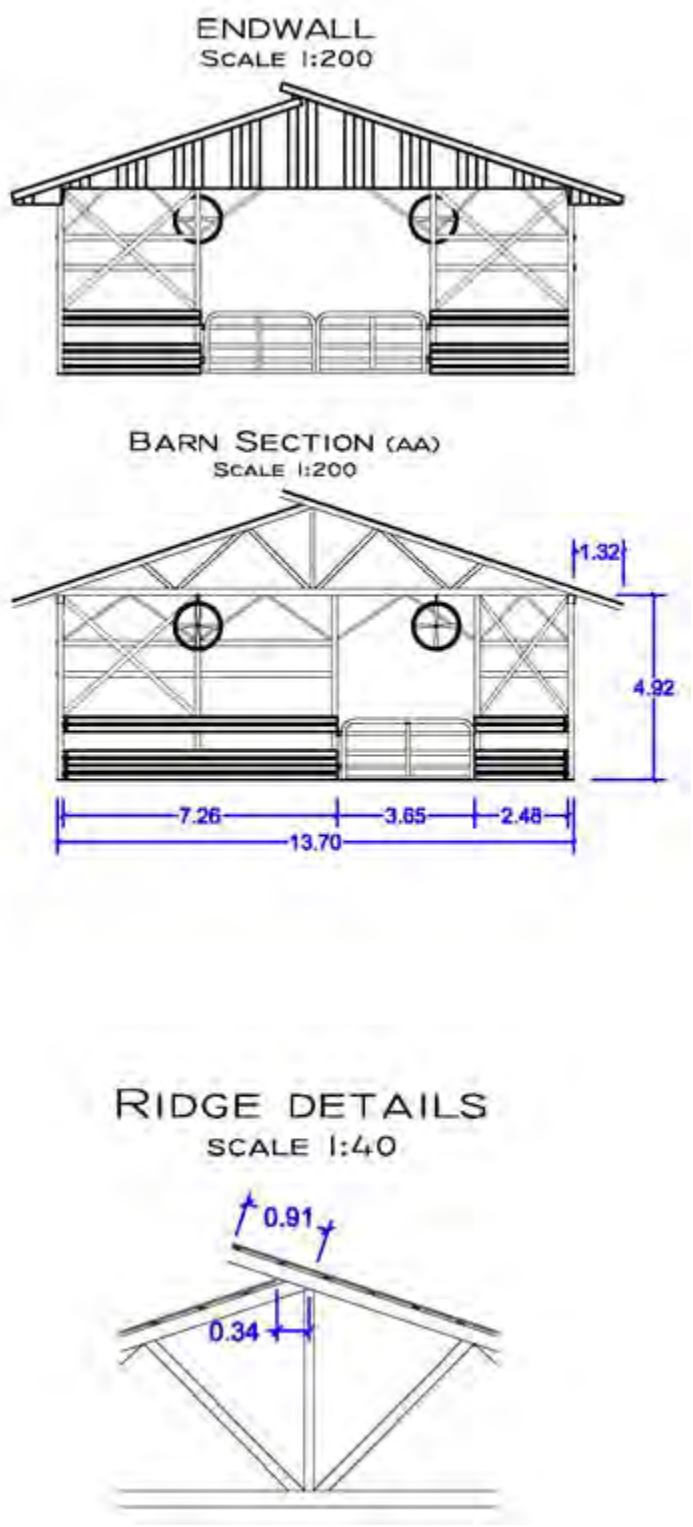

Figure B.29 - Details about end wall, barn section, and ridge of CBP Barn 17.

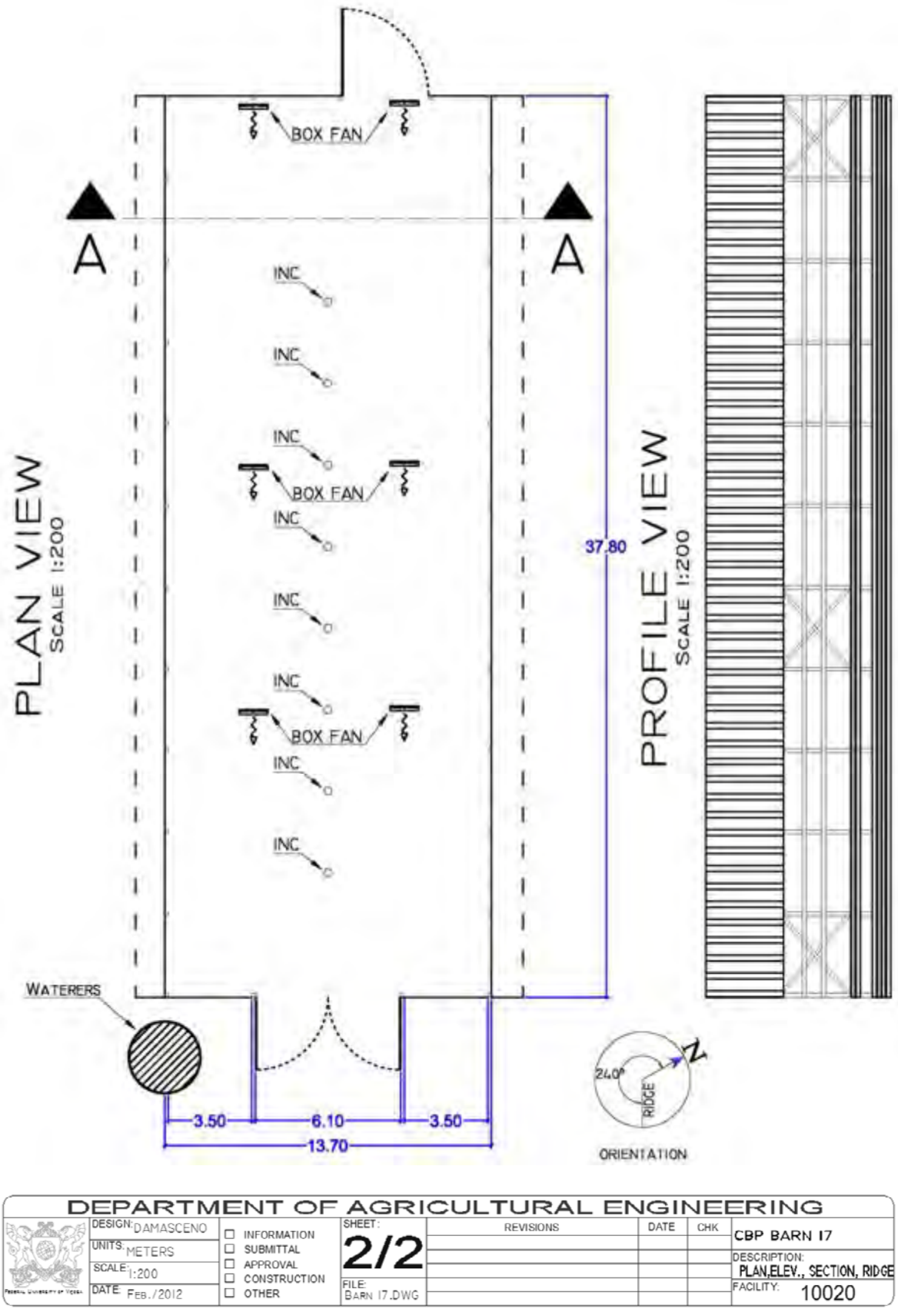

Figure B.30 - Details about plan view and profile of CBP Barn 17.

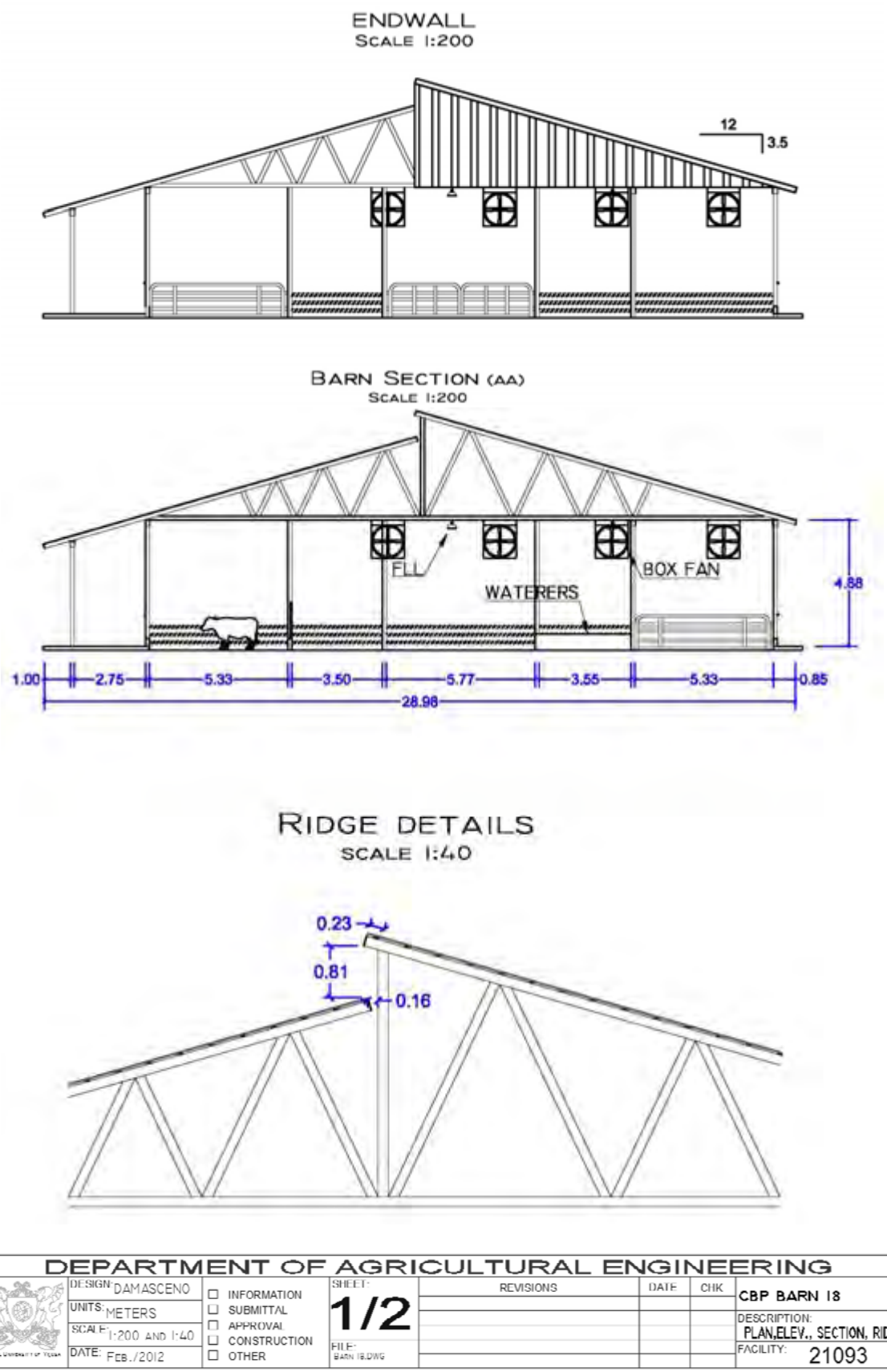

Figure B.31 - Details about end wall, barn section, and ridge of CBP Barn 18.

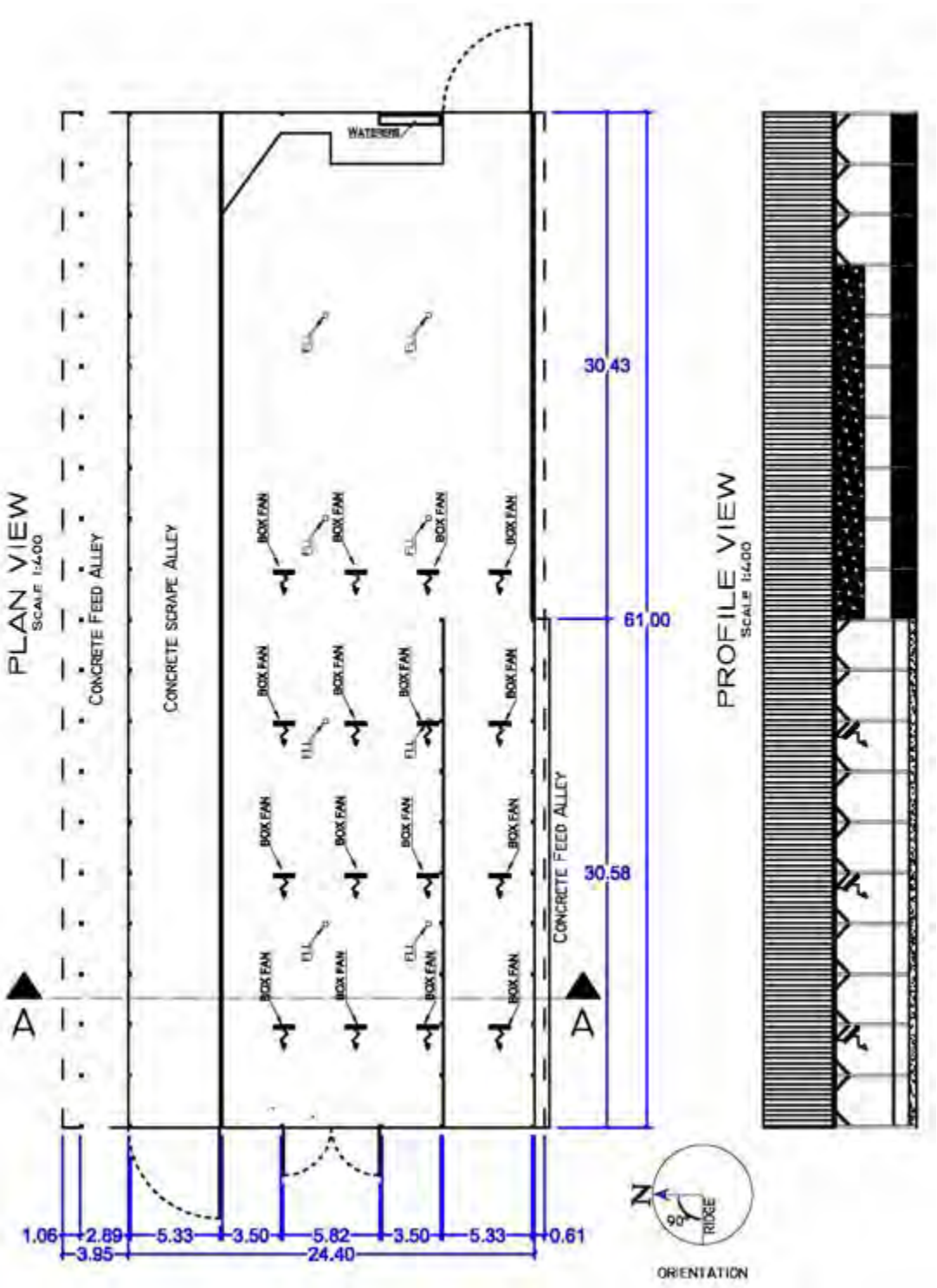

Figure B.32 - Details about plan view and profile of CBP Barn 18.

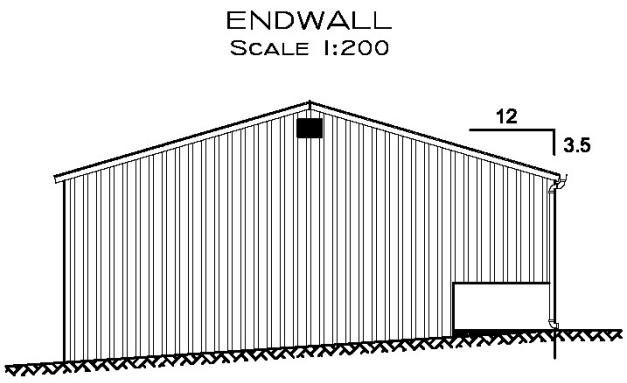

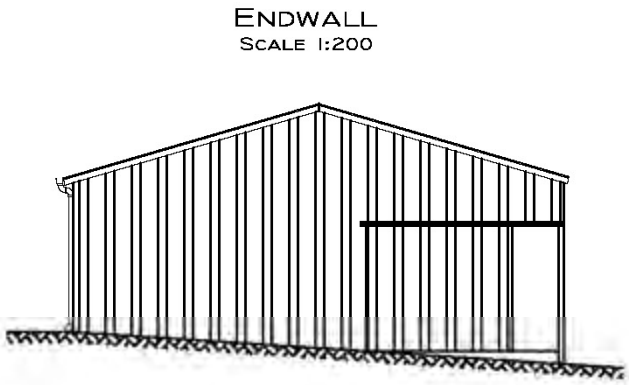

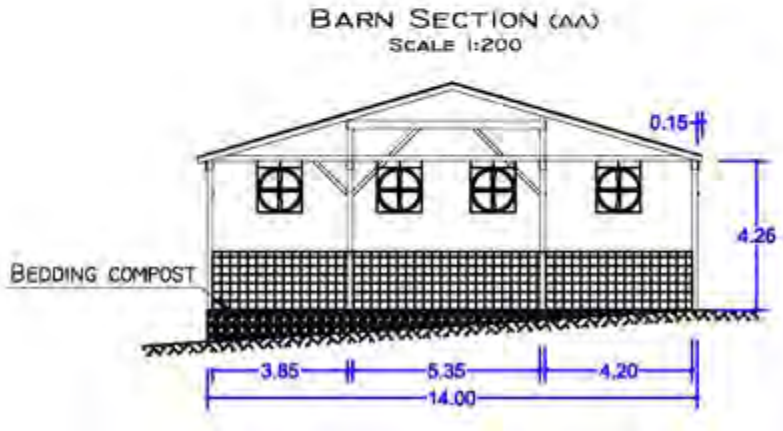

DEPARTMENT OF AGRICULTURAL ENGINEERING							
DESIGN: DAMASCENO	☐ INFORMATION	SHEET: 1/2	REVISIONS	DATE	CHK	CBP BARN 19	
UNITS: METERS	☐ SUBMITTAL					DESCRIPTION: PLAN,ELEV., SECTION, RIDGE	
SCALE 1:200	☐ APPROVAL						
DATE FEB./2012	☐ CONSTRUCTION	FILE: BARN 19.DWG				FACILITY: 64529	
	☐ OTHER						

Figure B.33 - Details about end wall, barn section, and ridge of CBP Barn 19.

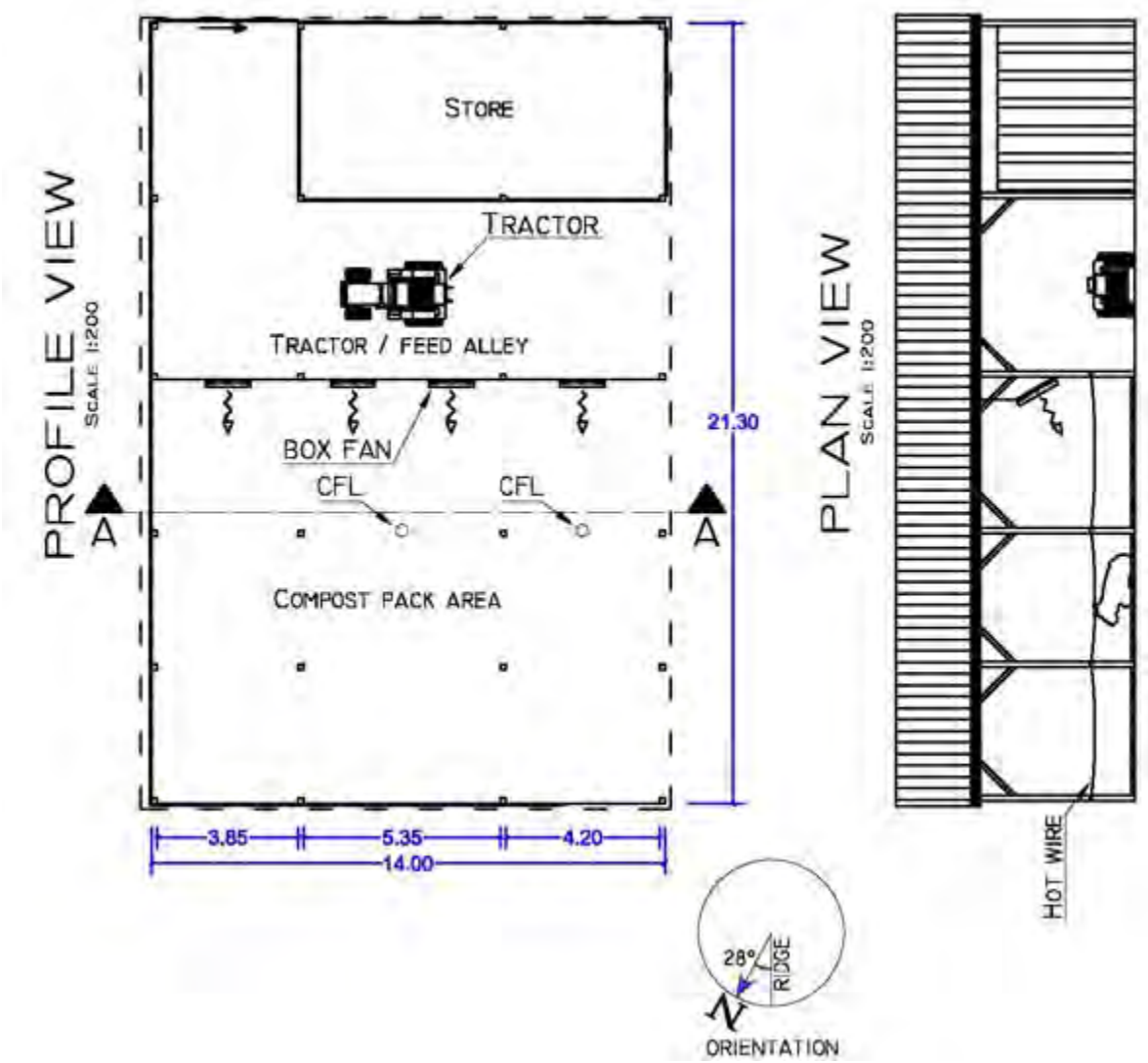

DEPARTMENT OF AGRICULTURAL ENGINEERING							
DESIGN: DAMASCENO	☐ INFORMATION	SHEET: 2/2	REVISIONS	DATE	CHK	CBP BARN 19
UNITS: METERS	☐ SUBMITTAL					DESCRIPTION: PLAN,ELEV., SECTION, RIDGE
SCALE: 1:200	☐ APPROVAL					FACILITY: 64529
DATE: FEB./2012	☐ CONSTRUCTION	FILE: BARN 19.DWG				
	☐ OTHER					

Figure B.34 - Details about plan view and profile of CBP Barn 19.

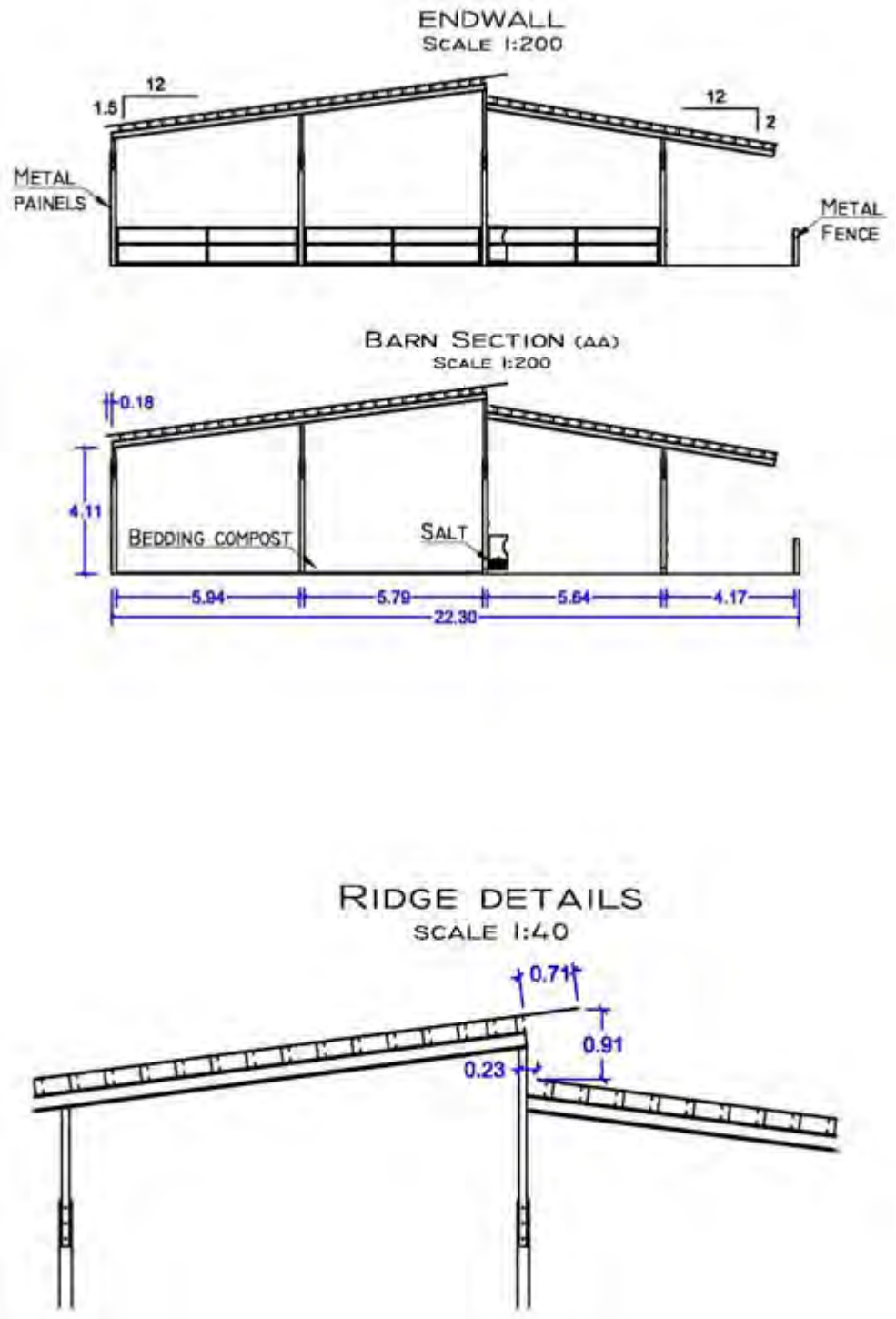

DEPARTMENT OF AGRICULTURAL ENGINEERING							
	DESIGN: DAMASCENO	☐ INFORMATION	SHEET: 1/2	REVISIONS	DATE	CHK	CBP BARN 20
	UNITS: METERS	☐ SUBMITTAL					DESCRIPTION: PLAN,ELEV., SECTION, RIDGE
	SCALE: 1:200 AND 1:40	☐ APPROVAL					
	DATE: FEB./2012	☐ CONSTRUCTION	FILE: BARN 20.DWG				FACILITY: 12673
		☐ OTHER					

Figure B.35 - Details about end wall, barn section, and ridge of CBP Barn 20.

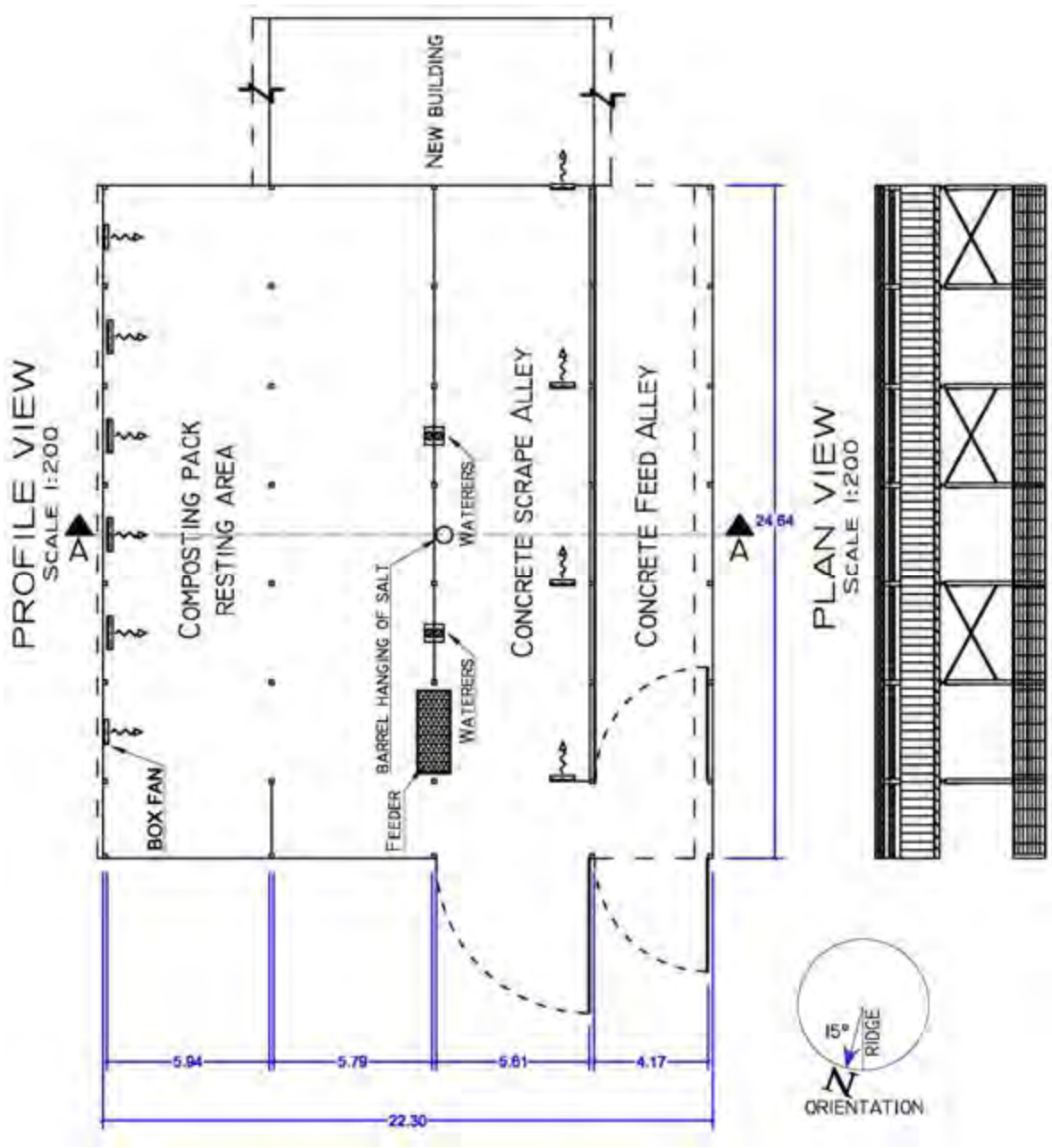

DEPARTMENT OF AGRICULTURAL ENGINEERING							
DESIGN: DAMASCENO	☐ INFORMATION	SHEET: 2/2	REVISIONS	DATE	CHK	CBP BARN 20	
UNITS: METERS	☐ SUBMITTAL					DESCRIPTION: PLAN,ELEV., SECTION, RIDGE	
SCALE: 1:200	☐ APPROVAL					FACILITY: 12673	
DATE: FEB./2012	☐ CONSTRUCTION	FILE: BARN 20.DWG					
	☐ OTHER						

Figure B.36 - Details about plan view and profile of CBP Barn 20.

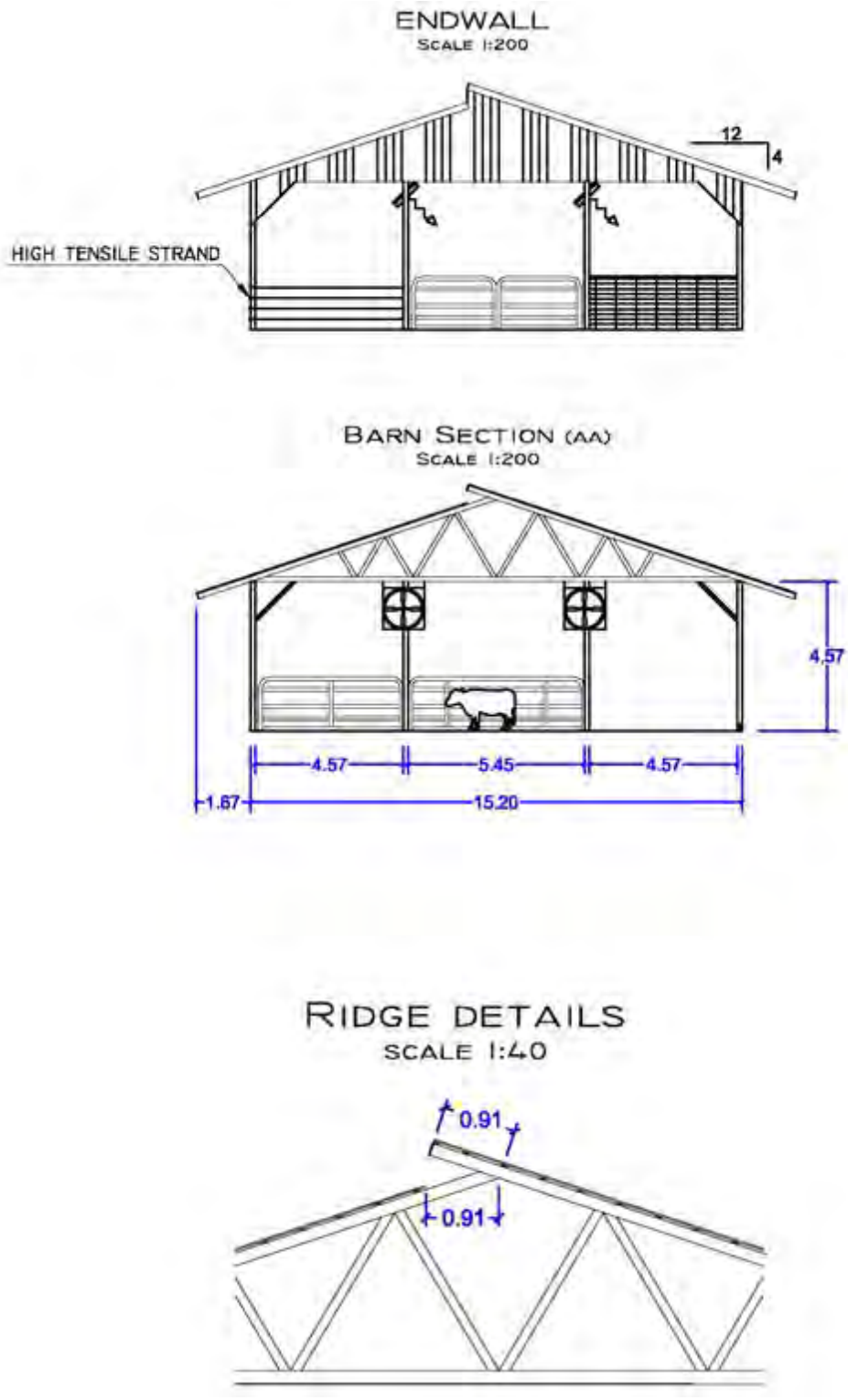

Figure B.37 - Details about end wall, barn section, and ridge of CBP Barn 21.

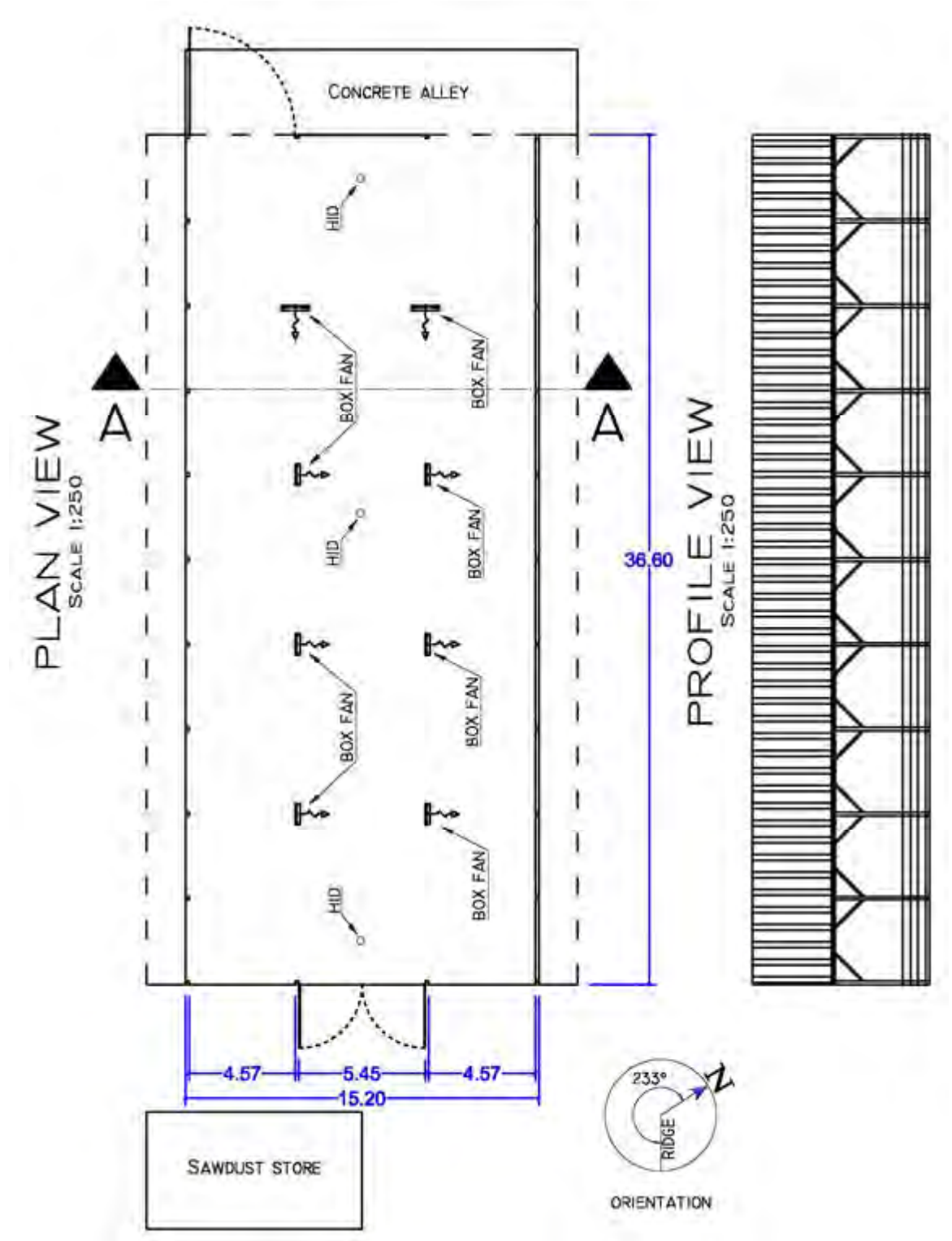

DEPARTMENT OF AGRICULTURAL ENGINEERING							
DESIGN: DAMASCENO	☐ INFORMATION	SHEET: 2/2	REVISIONS	DATE	CHK	CBP BARN 21	
UNITS: METERS	☐ SUBMITTAL					DESCRIPTION: PLAN,ELEV., SECTION, RIDGE	
SCALE: 1:250	☐ APPROVAL						
DATE: FEB./2012	☐ CONSTRUCTION	FILE: BARN 21.DWG				FACILITY: 13146	
	☐ OTHER						

Figure B.38 - Details about plan view and profile of CBP Barn 21.

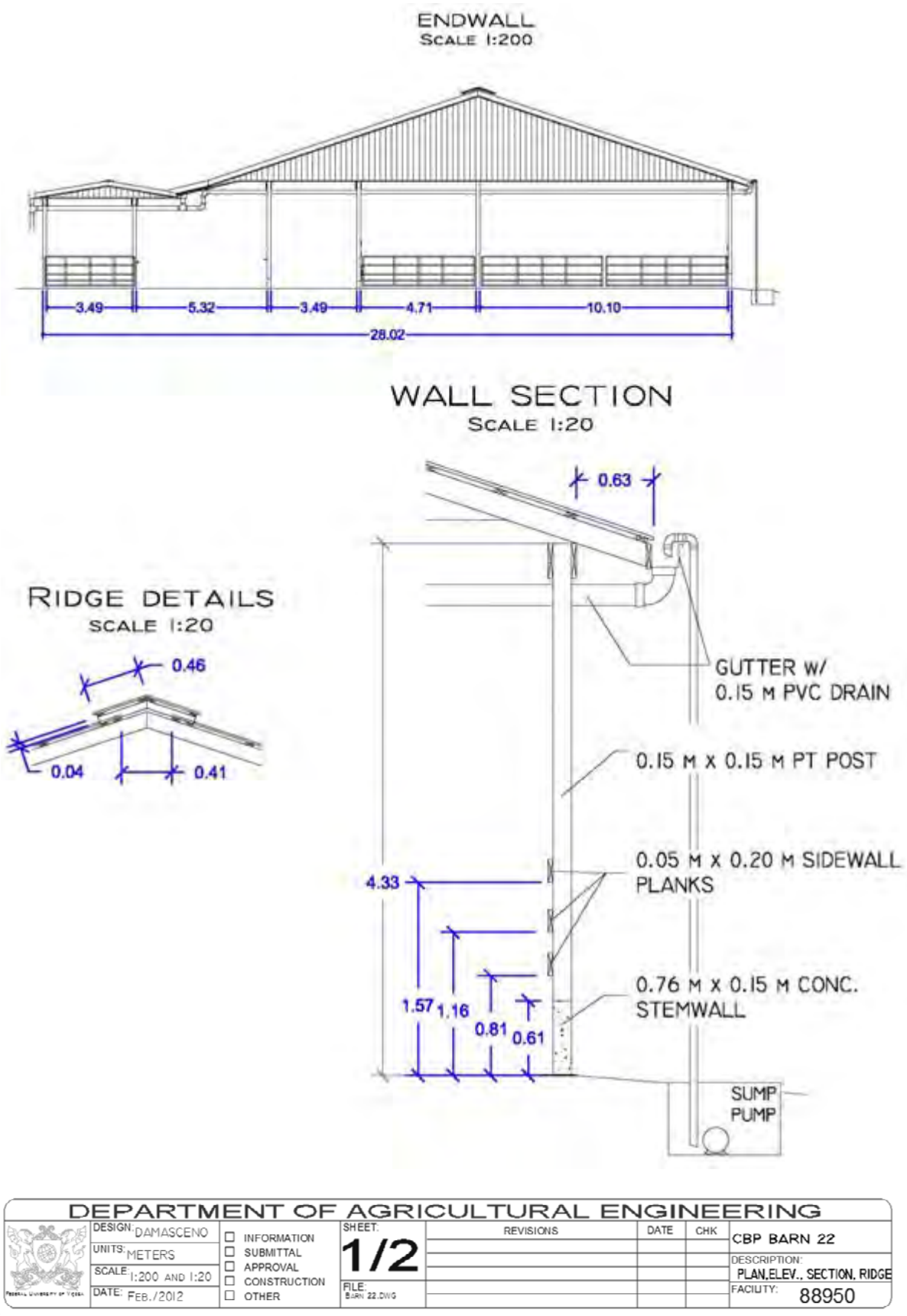

Figure B.39 - Details about end wall, barn section, and ridge of CBP Barn 22.

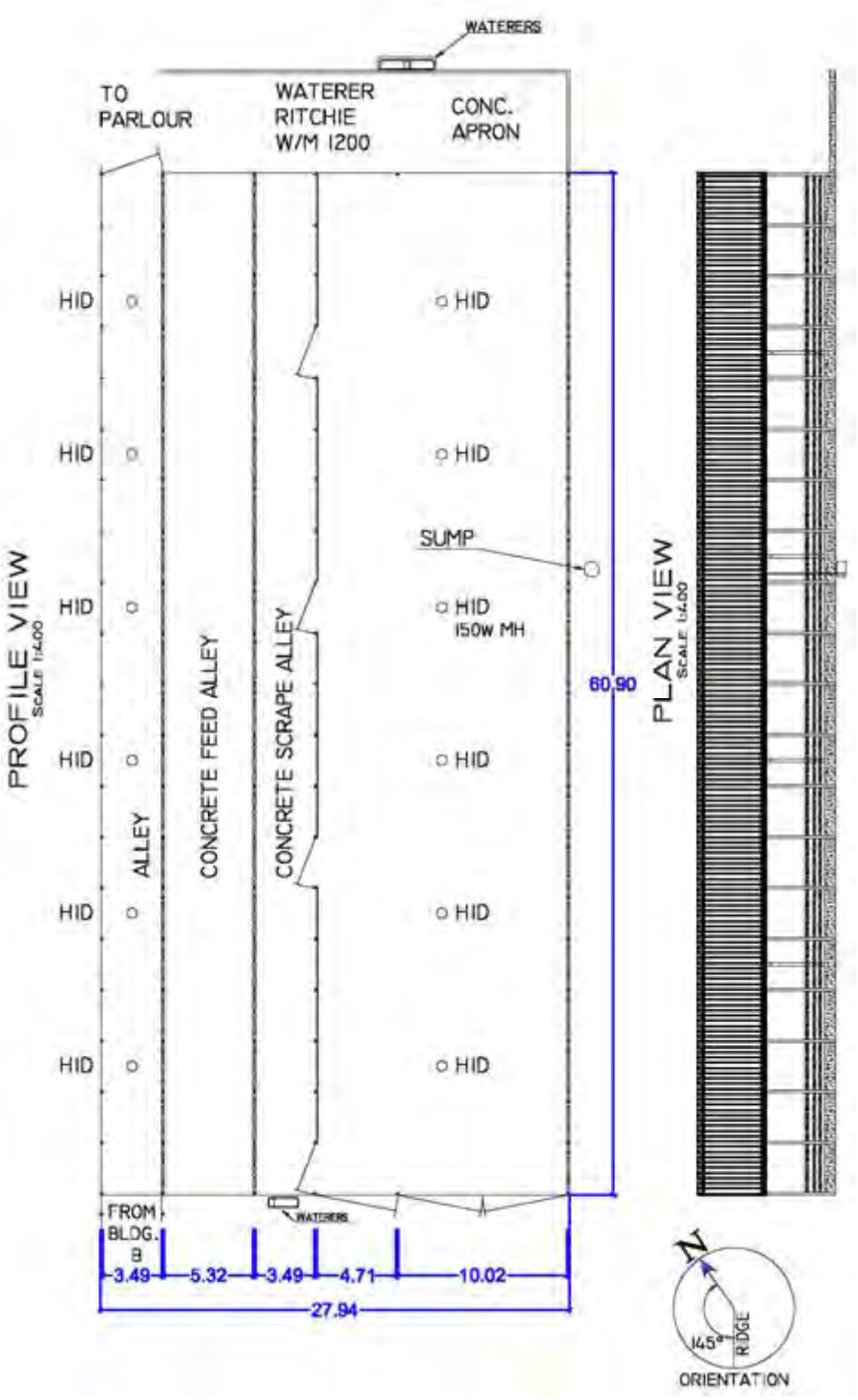

DEPARTMENT OF AGRICULTURAL ENGINEERING

DESIGN: DAMASCENO	☐ INFORMATION	SHEET: 2/2	REVISIONS	DATE	CHK	CBP BARN 22
UNITS: METERS	☐ SUBMITTAL					DESCRIPTION: PLAN,ELEV., SECTION, RIDGE
SCALE: 1:400	☐ APPROVAL					
DATE: FEB./2012	☐ CONSTRUCTION	FILE: BARN 22.DWG				FACILITY: 88950
	☐ OTHER					

Figure B.40 - Details about plan view and profile of CBP Barn 22.

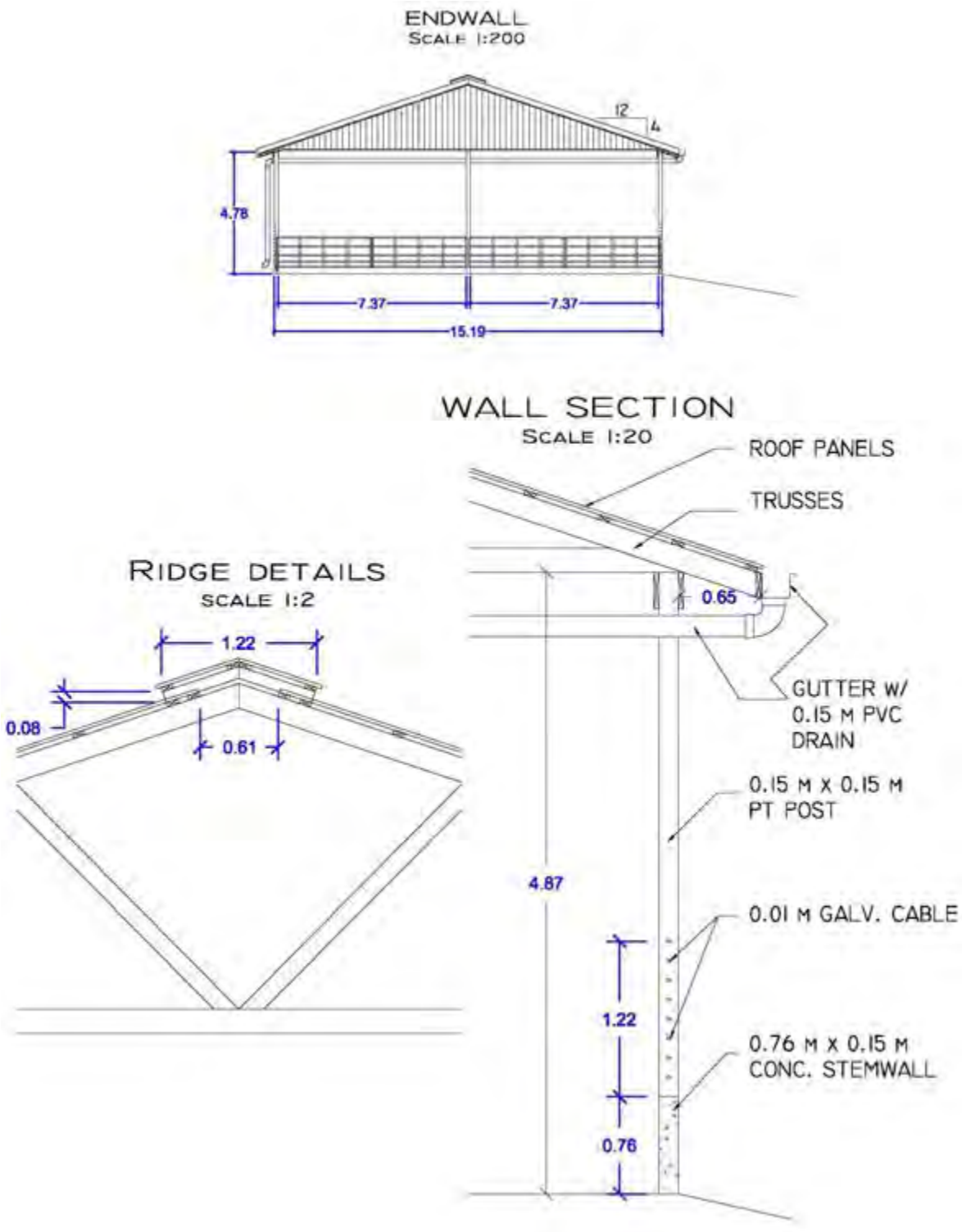

Figure B.41 - Details about end wall, barn section, and ridge of CBP Barn 23.

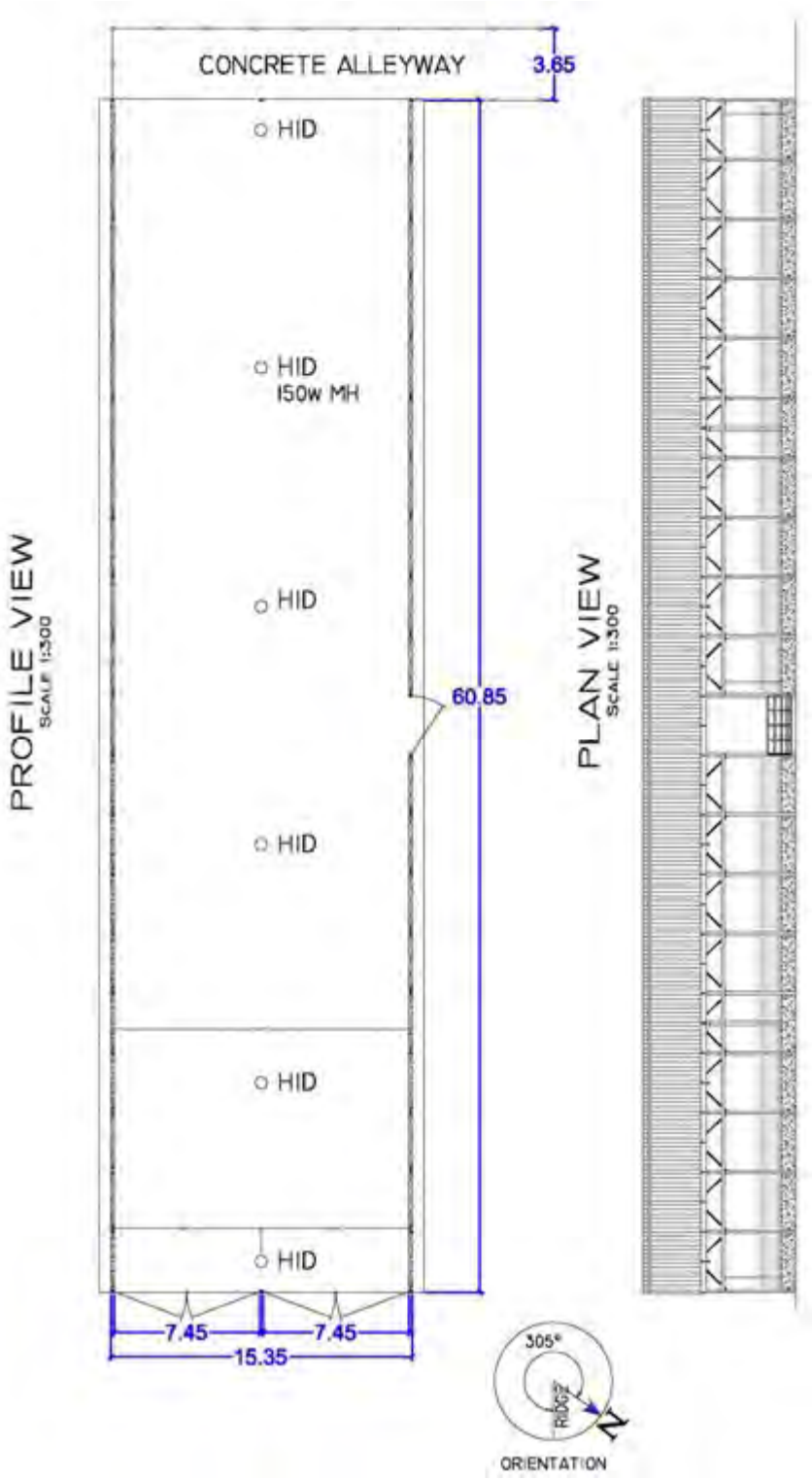

DEPARTMENT OF AGRICULTURAL ENGINEERING

DESIGN: DAMASCENO	☐ INFORMATION	SHEET: 2/2	REVISIONS	DATE	CHK	CBP BARN 23
UNITS: METERS	☐ SUBMITTAL					DESCRIPTION: PLAN,ELEV., SECTION, RIDGE
SCALE: 1:300	☐ APPROVAL					
DATE: FEB./2012	☐ CONSTRUCTION	FILE: BARN 23.DWG				FACILITY: 74783
	☐ OTHER					

Figure B.42 - Details about plan view and profile of CBP Barn 23.

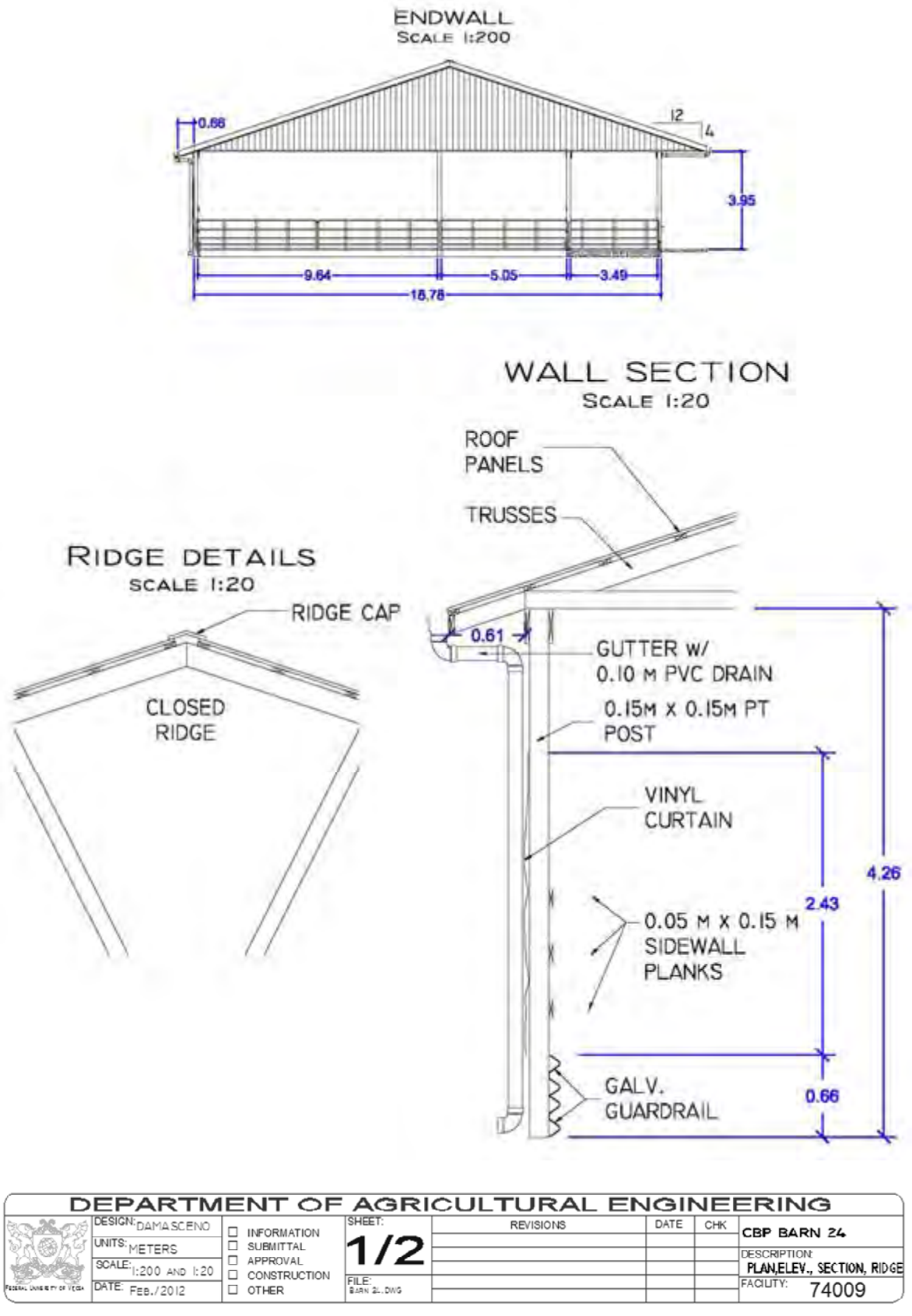

Figure B.43 - Details about end wall, barn section, and ridge of CBP Barn 24.

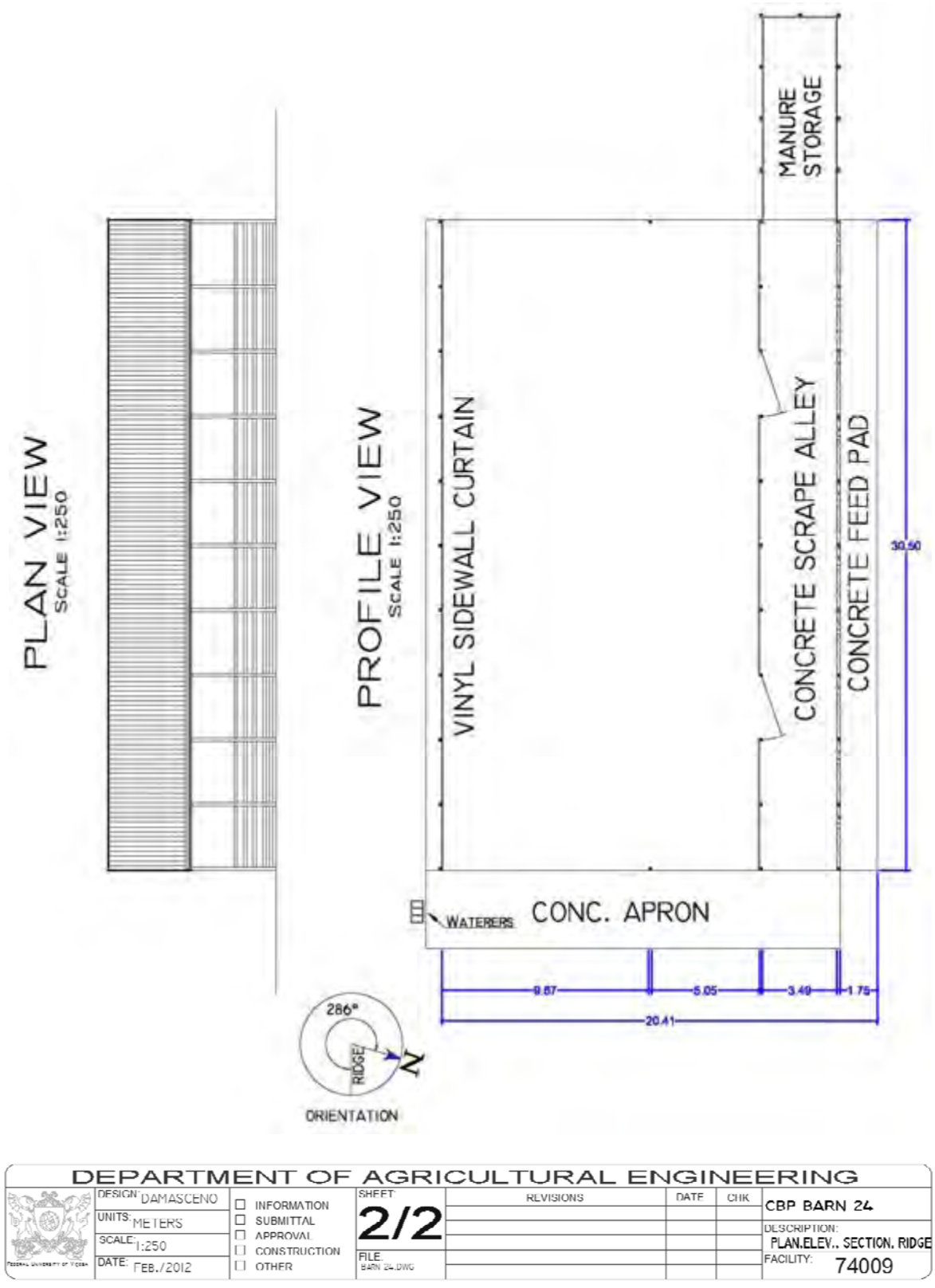

Figure B.44 - Details about plan view and profile of CBP Barn 24.

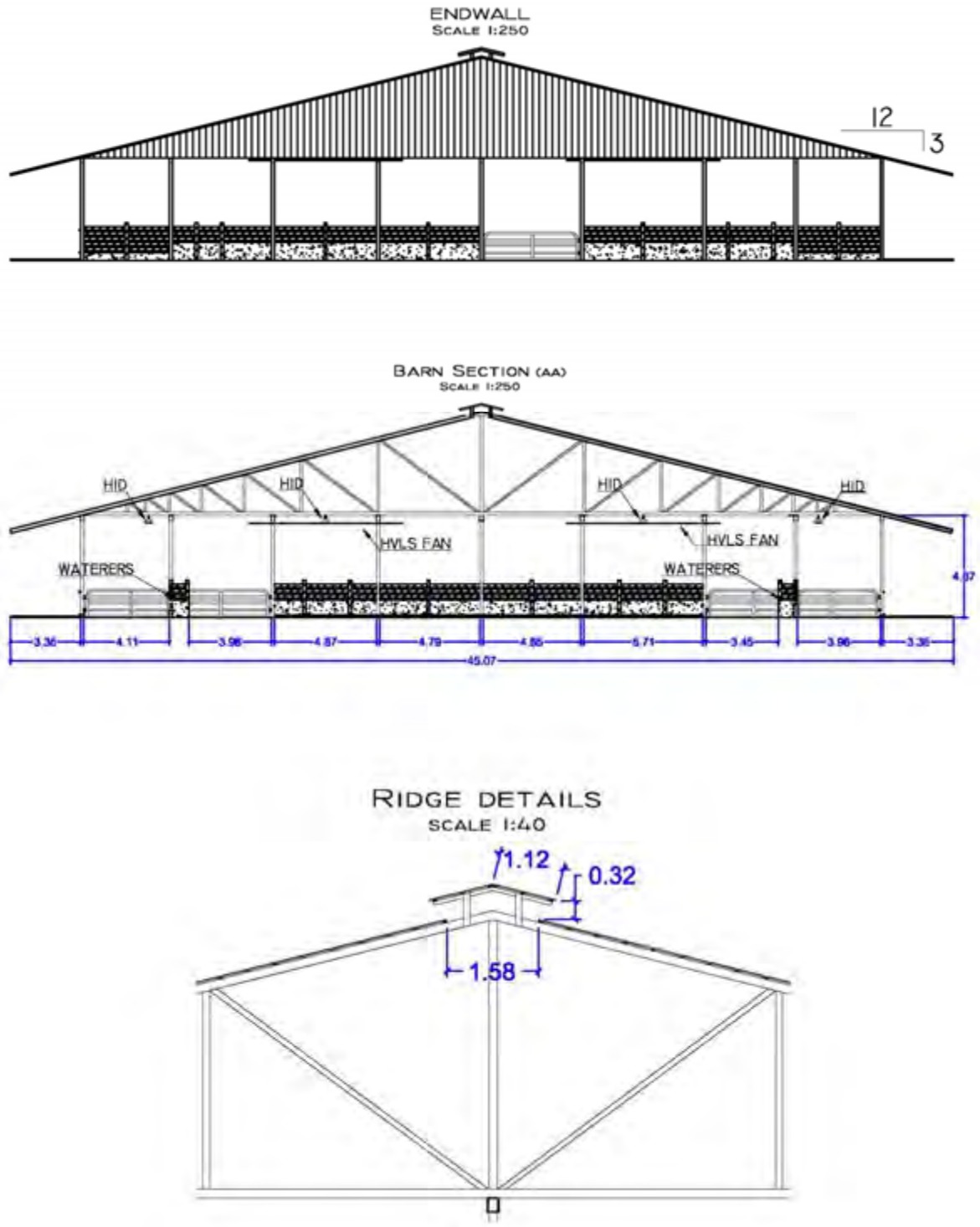

Figure B.45 - Details about end wall, barn section, and ridge of CBP Barn 25.

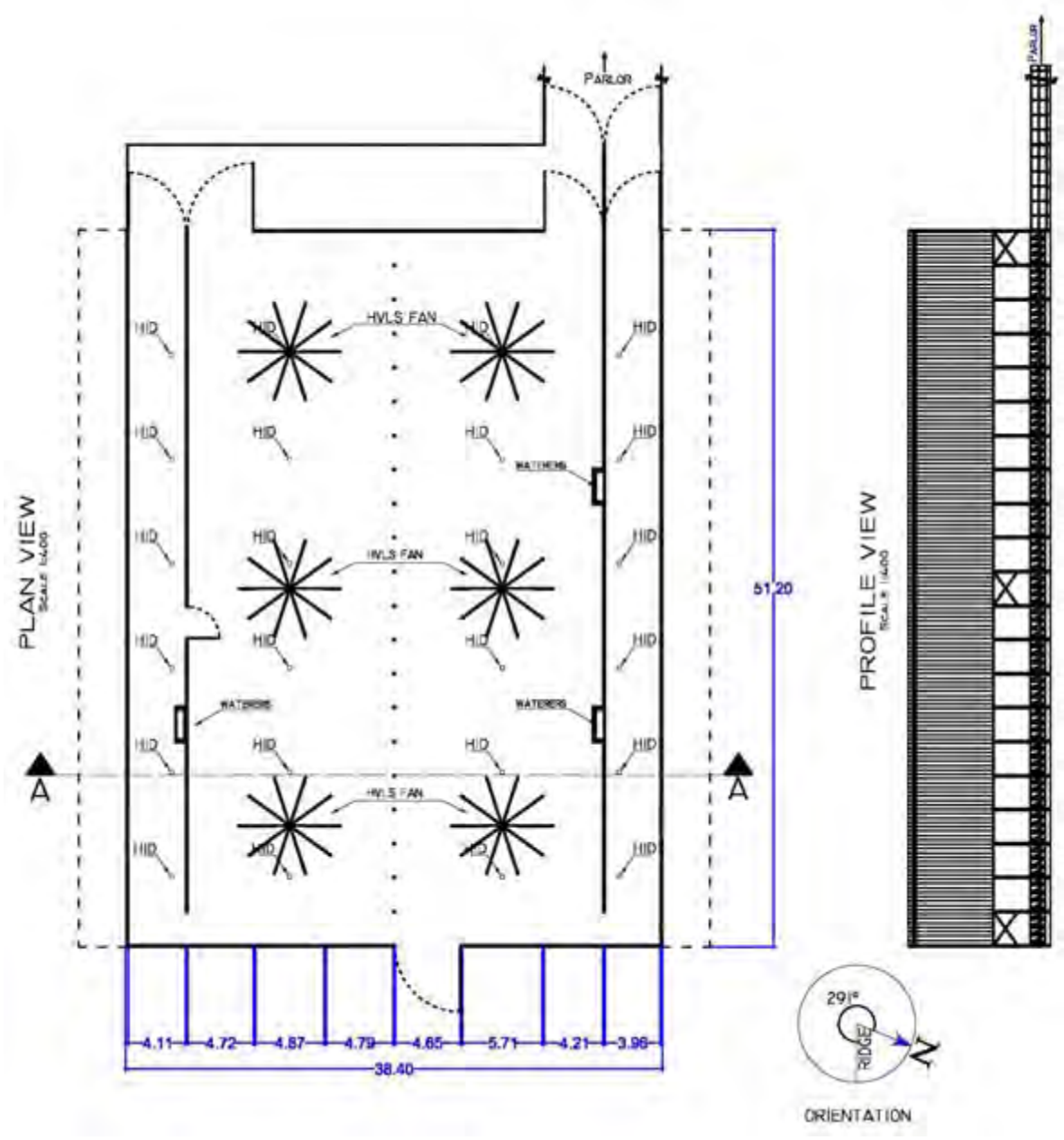

DEPARTMENT OF AGRICULTURAL ENGINEERING							
DESIGN: DAMASCENO	☐ INFORMATION	SHEET: 2/2	REVISIONS	DATE	CHK	CBP BARN 25	
UNITS: METERS	☐ SUBMITTAL					DESCRIPTION: PLAN,ELEV., SECTION, RIDGE	
SCALE: 1:400	☐ APPROVAL						
DATE: Feb./2012	☐ CONSTRUCTION	FILE: Barn 25.DWG				FACILITY: 57936	
	☐ OTHER						

Figure B.46 - Details about plan view and profile of CBP Barn 25.

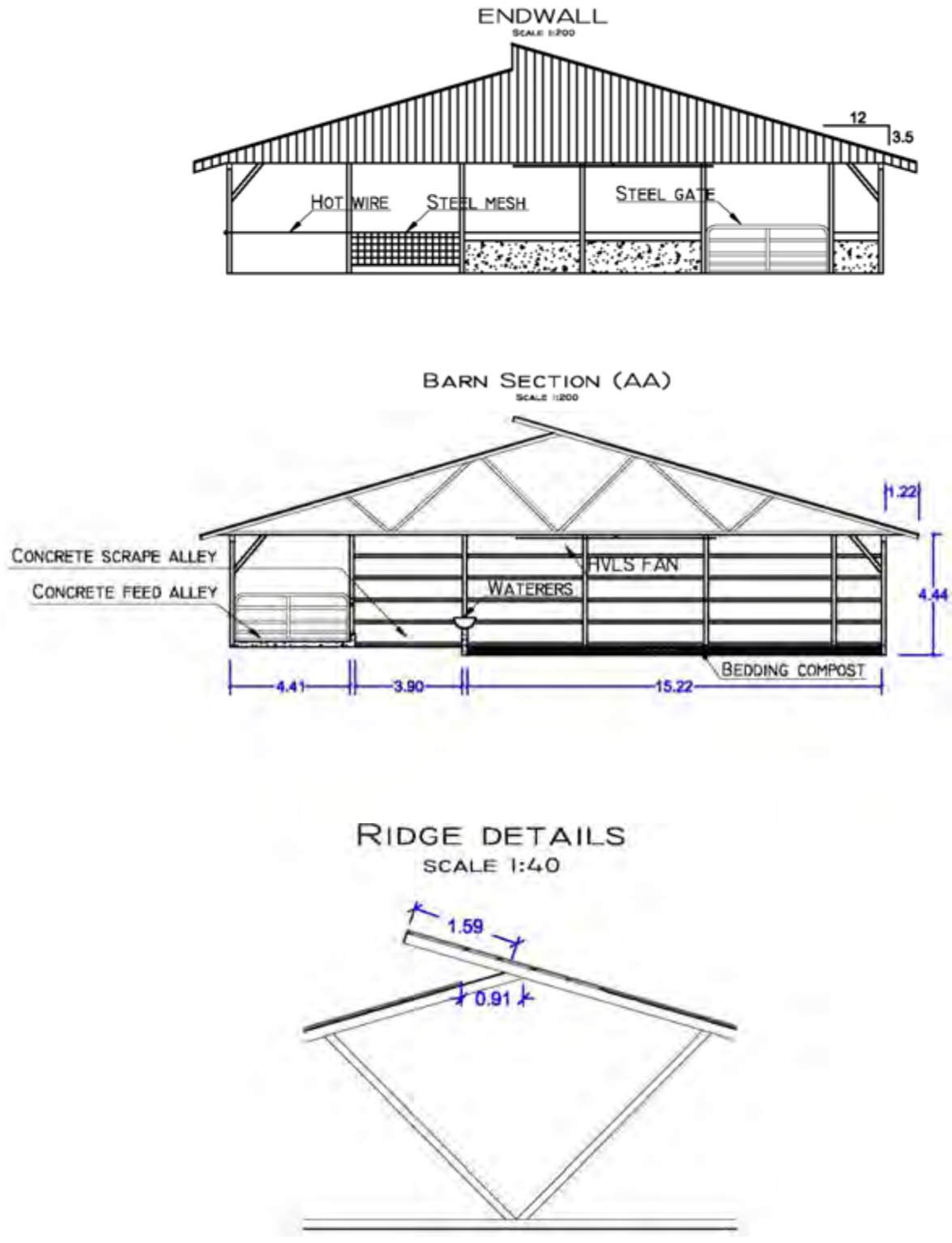

Figure B.47 - Details about end wall, barn section, and ridge of CBP Barn 26.

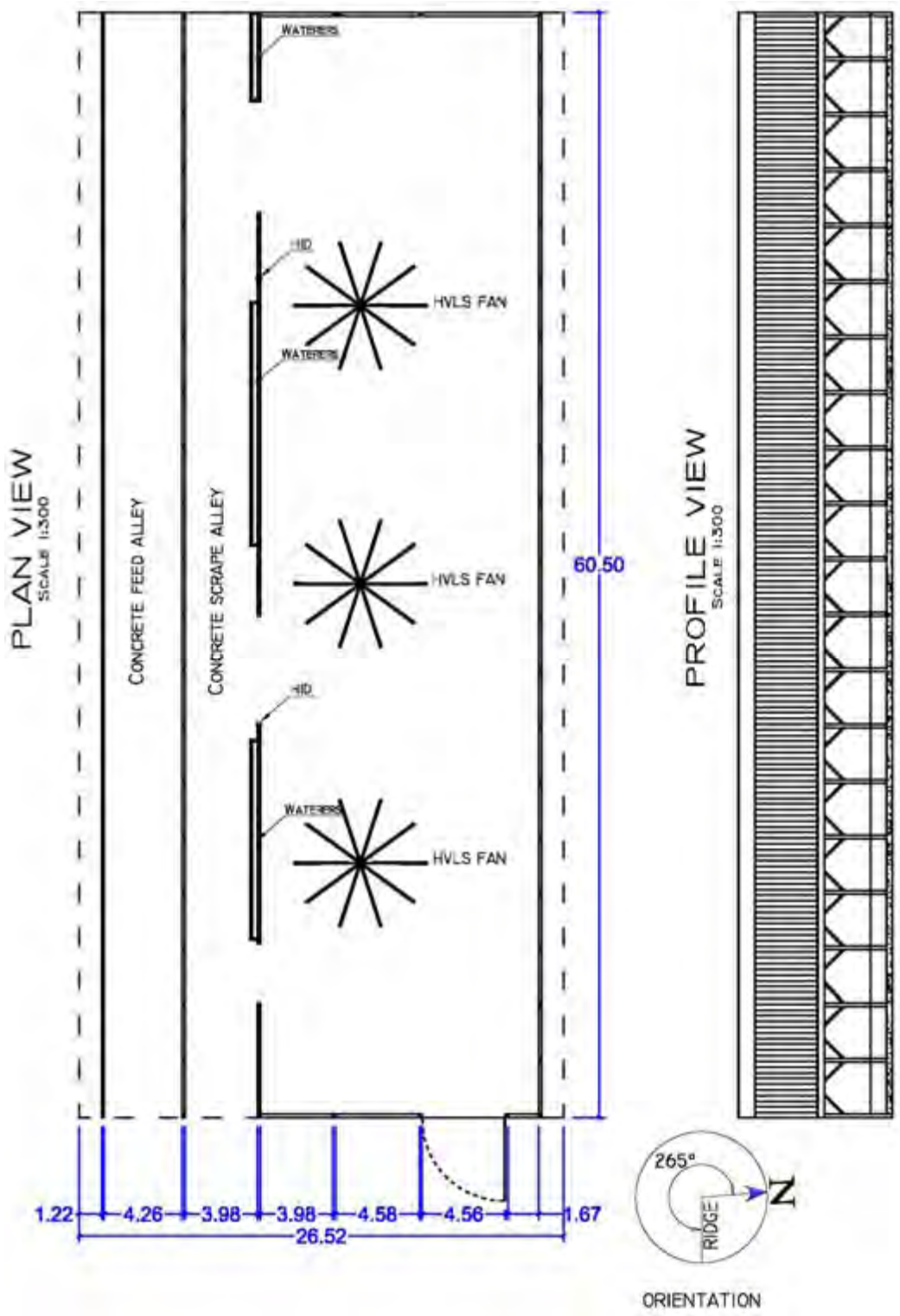

DEPARTMENT OF AGRICULTURAL ENGINEERING							
	DESIGN: DAMASCENO	☐ INFORMATION	SHEET: 2/2	REVISIONS	DATE	CHK	CBP BARN 26
	UNITS: METERS	☐ SUBMITTAL					DESCRIPTION: PLAN,ELEV., SECTION, RIDGE
	SCALE: 1:300	☐ APPROVAL					
	DATE: FEV./2012	☐ CONSTRUCTION	FILE: BARN 26.DWG				FACILITY: 72471
		☐ OTHER					

Figure B.48 - Details about plan view and profile of CBP Barn 26.

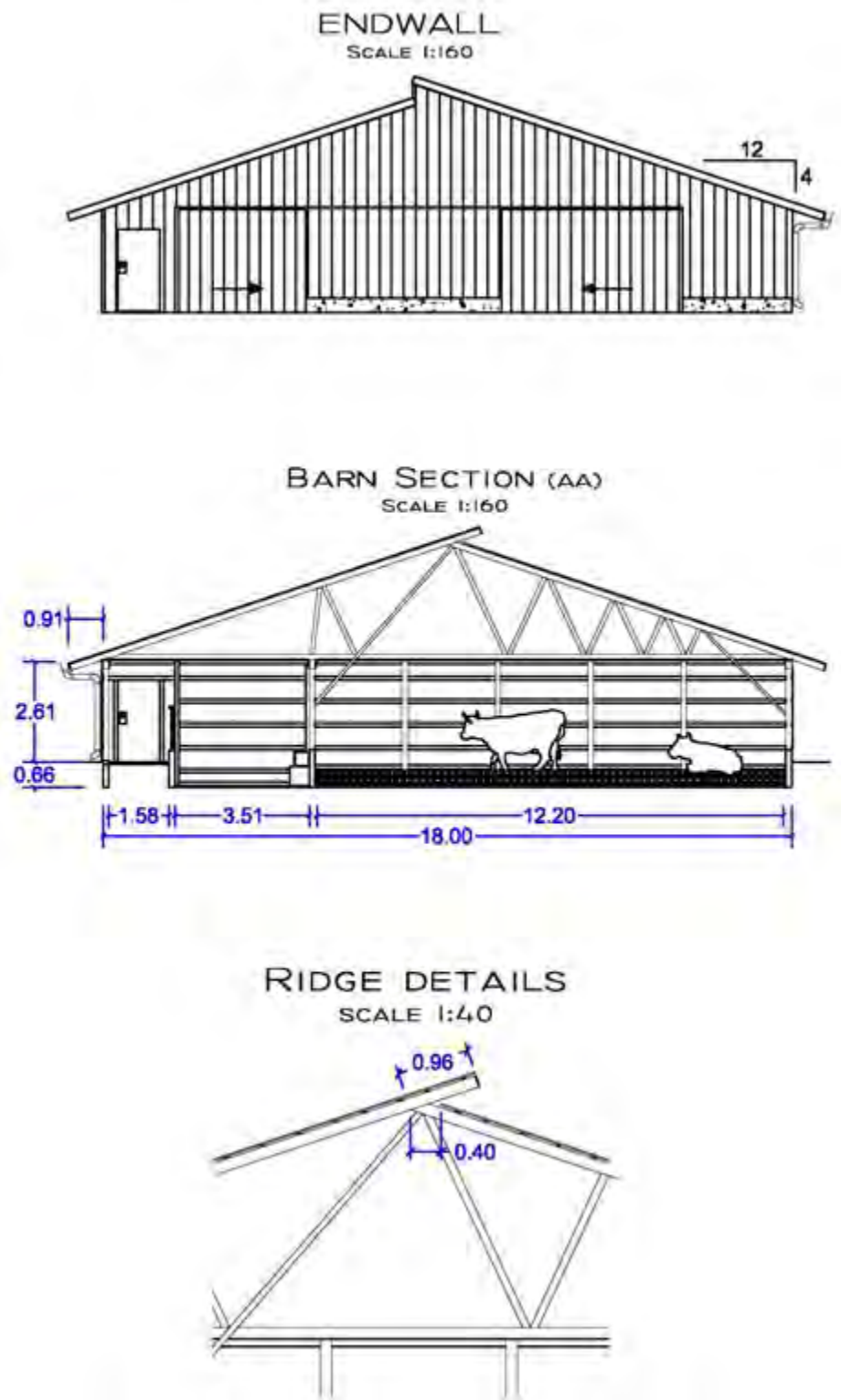

Figure B.49 - Details about end wall, barn section, and ridge of CBP Barn 27.

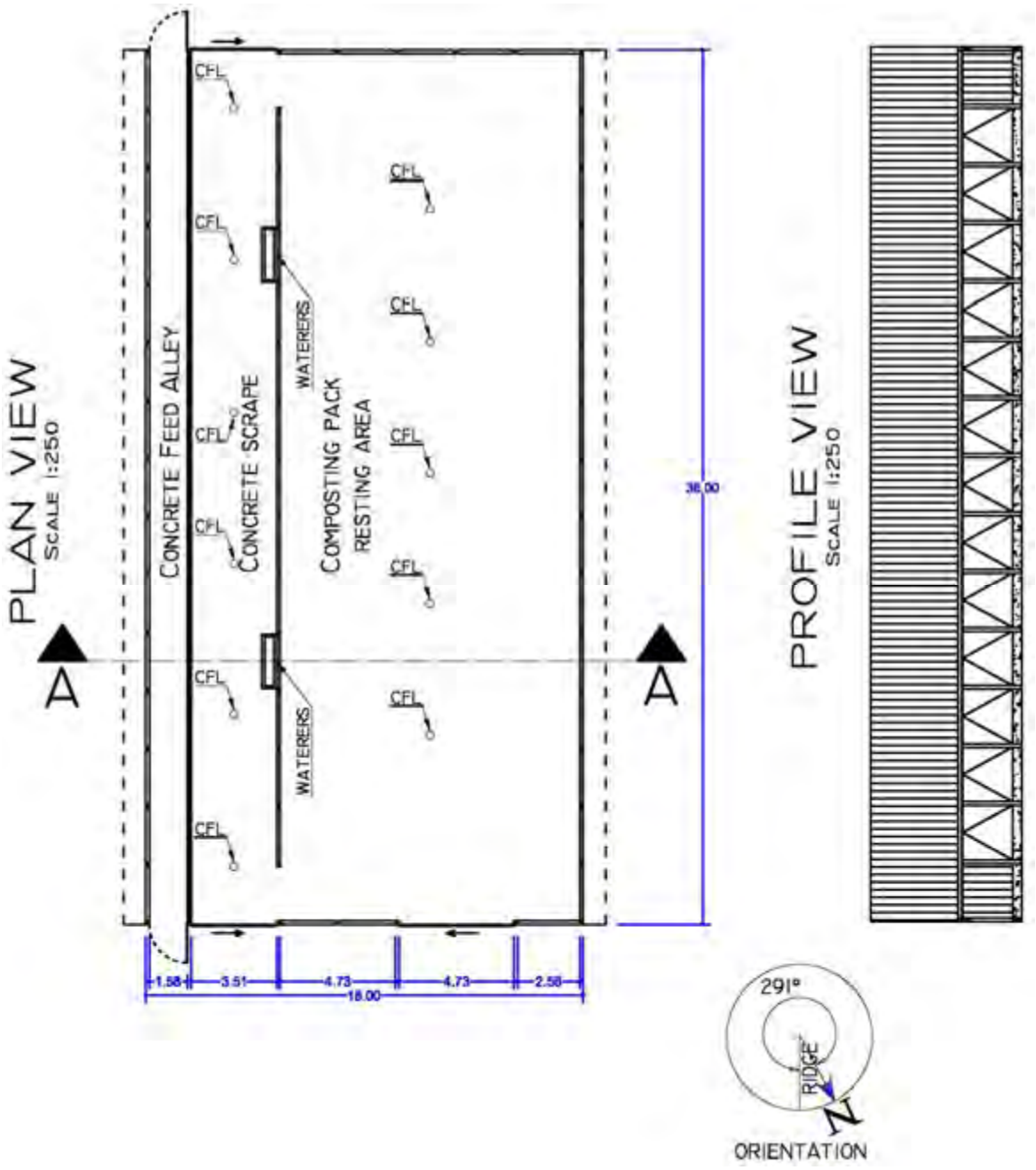

DEPARTMENT OF AGRICULTURAL ENGINEERING

DESIGN: DAMASCENO	☐ INFORMATION	SHEET: 2/2	REVISIONS	DATE	CHK	CBP BARN 27
UNITS: METERS	☐ SUBMITTAL					DESCRIPTION: PLAN,ELEV., SECTION, RIDGE
SCALE: 1:250	☐ APPROVAL					FACILITY: 94521
DATE: FEB./2012	☐ CONSTRUCTION	FILE: BARN 27.DWG				
	☐ OTHER					

Figure B.50 - Details about plan view and profile of CBP Barn 27.

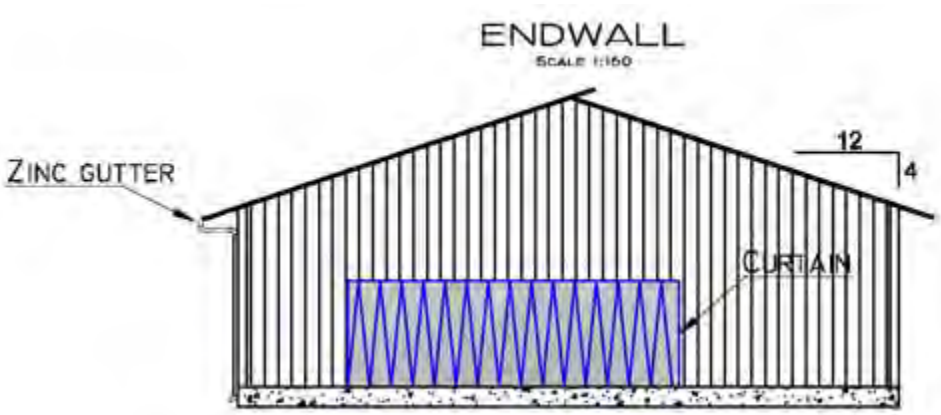

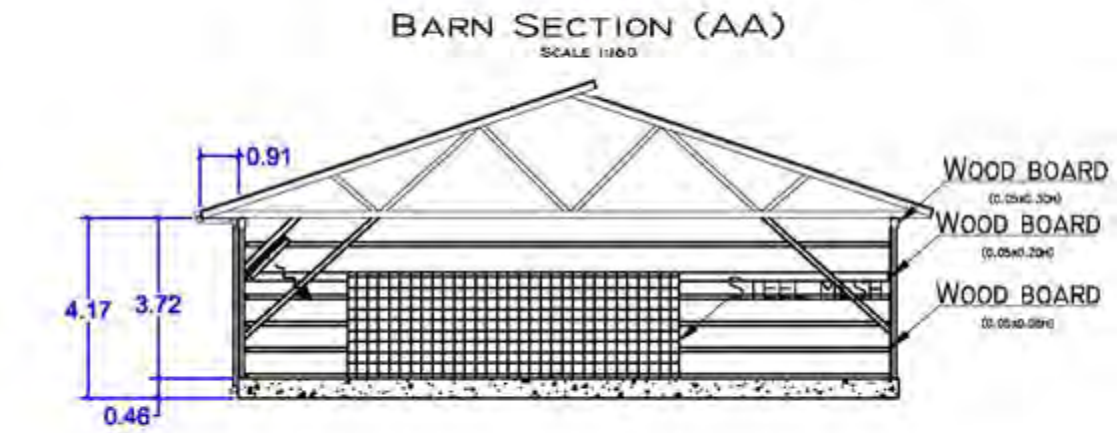

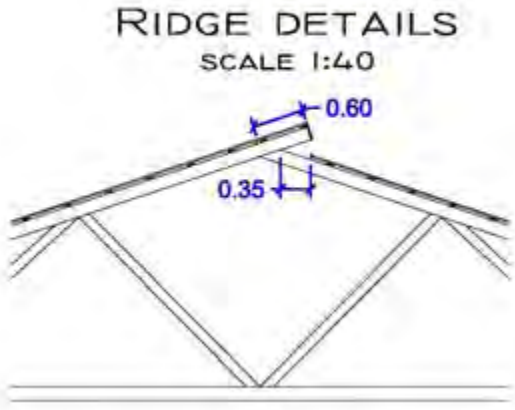

DEPARTMENT OF AGRICULTURAL ENGINEERING							
DESIGN: DAMASCENO	☐ INFORMATION	SHEET: 1/2	REVISIONS	DATE	CHK	CBP BARN 28	
UNITS: METERS	☐ SUBMITTAL					DESCRIPTION: PLAN,ELEV., SECTION, RIDGE	
SCALE: 1:160 AND 1:40	☐ APPROVAL						
DATE: FEB./2012	☐ CONSTRUCTION	FILE: BARN 28.DWG				FACILITY: 94521	
	☐ OTHER						

Figure B.51 - Details about end wall, barn section, and ridge of CBP Barn 28.

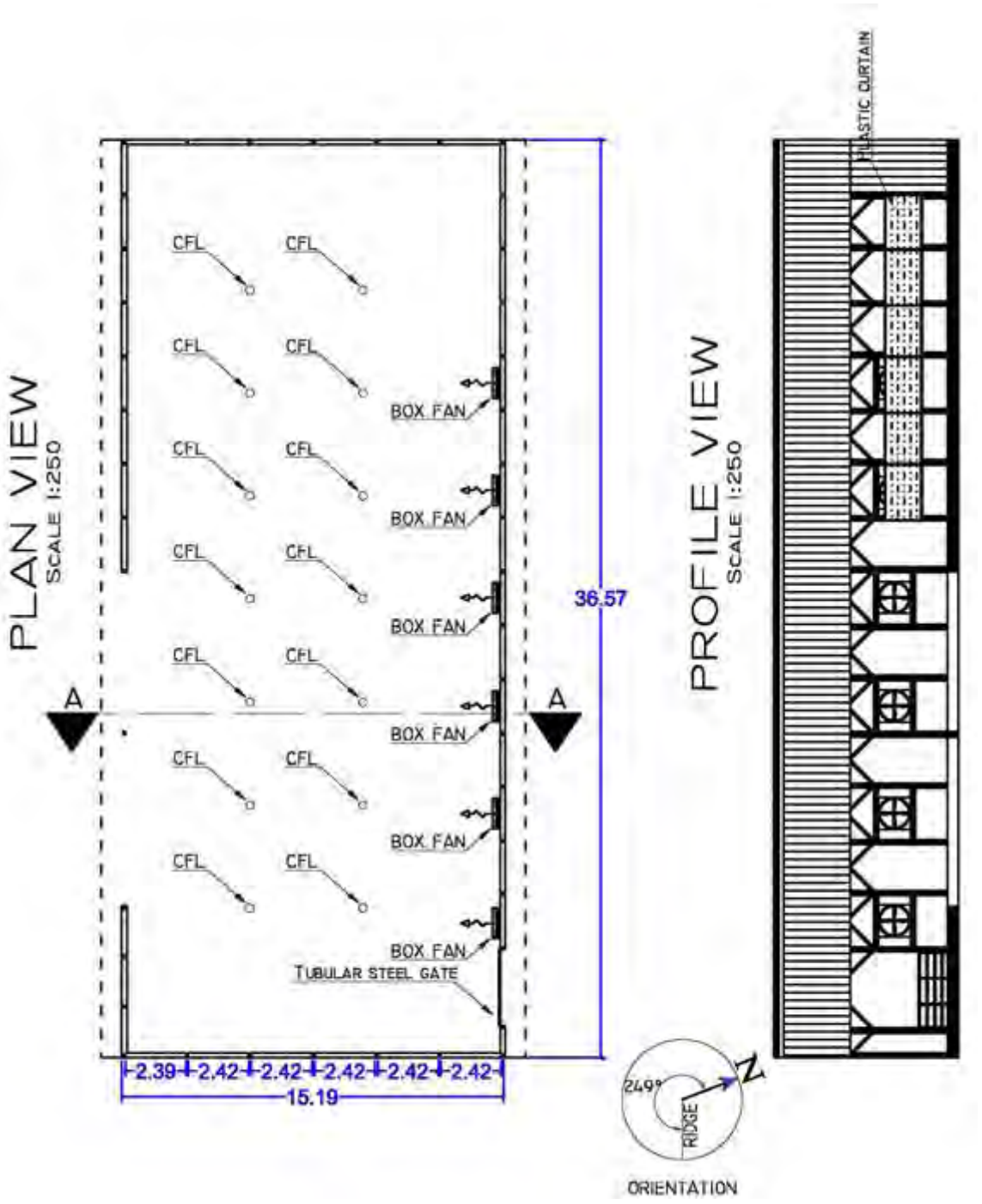

DEPARTMENT OF AGRICULTURAL ENGINEERING							
DESIGN: DAMASCENO	☐ INFORMATION	SHEET: 2/2	REVISIONS	DATE	CHK	CBP BARN 28
UNITS: METERS	☐ SUBMITTAL					DESCRIPTION: PLAN,ELEV., SECTION, RIDGE
SCALE: 1:250	☐ APPROVAL					
DATE: FEB./2012	☐ CONSTRUCTION	FILE: BARN 28.DWG				FACILITY: 94521
	☐ OTHER					

Figure B.52 - Details about plan view and profile of CBP Barn 28.

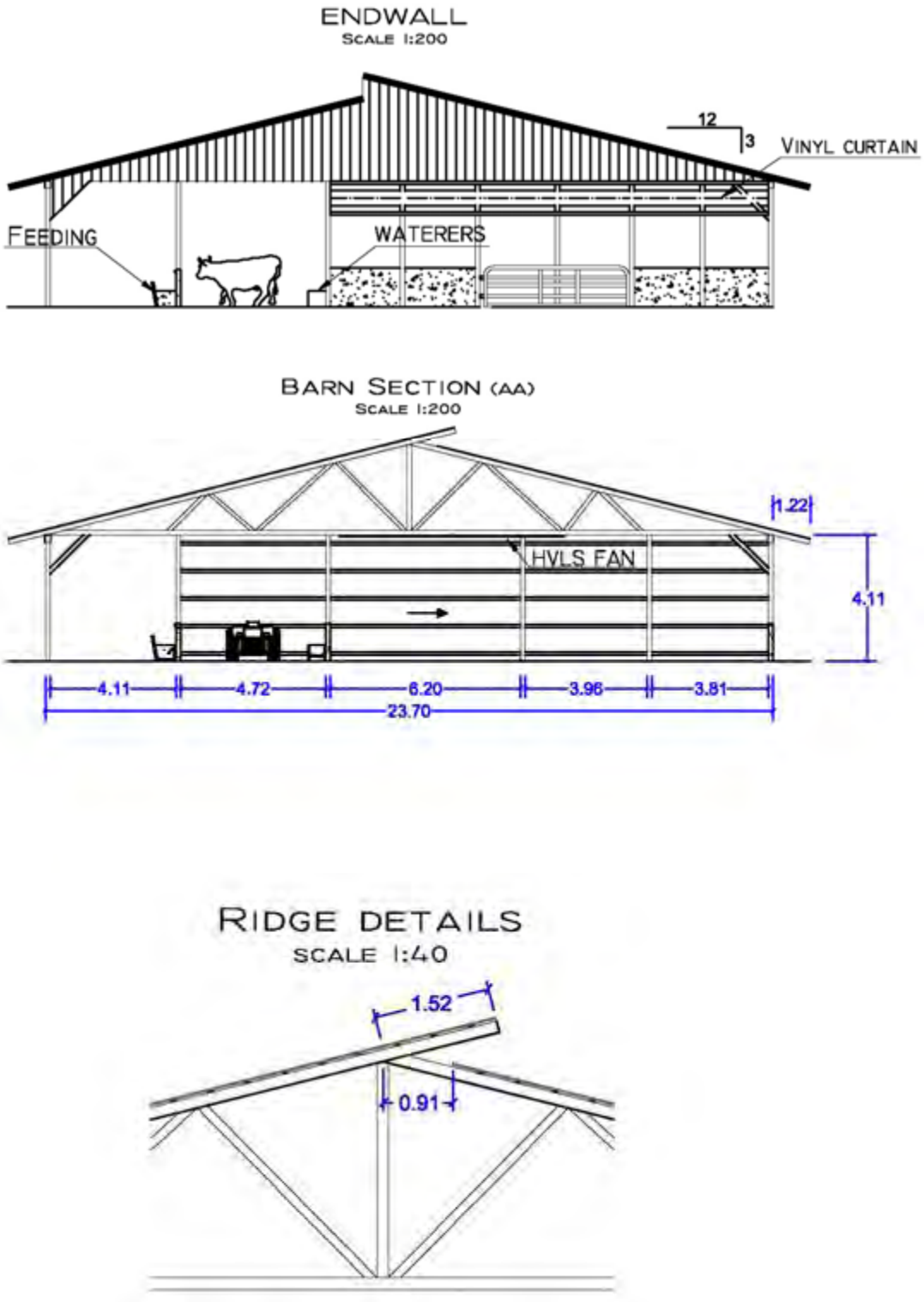

Figure B.53 - Details about end wall, barn section, and ridge of CBP Barn 29.

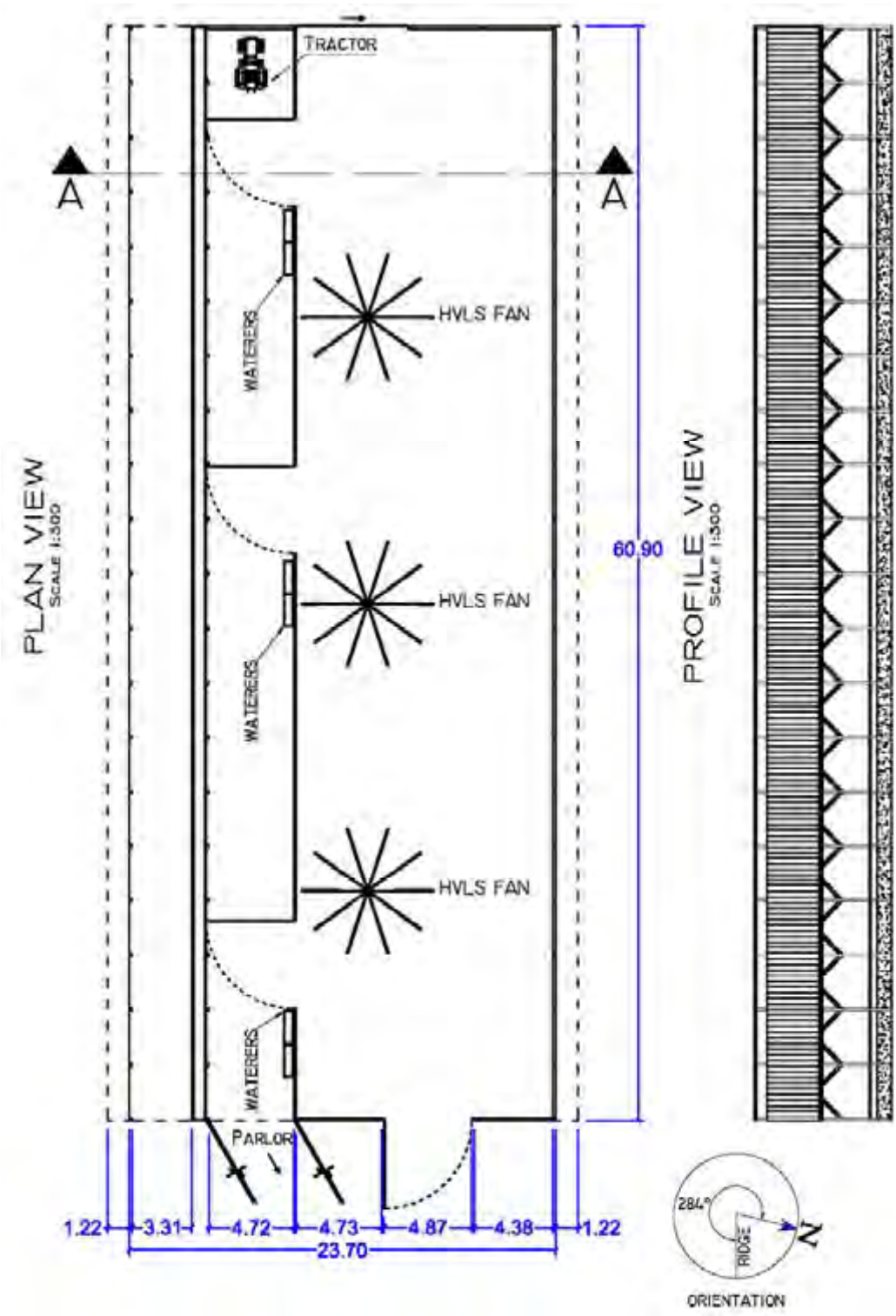

DEPARTMENT OF AGRICULTURAL ENGINEERING							
DESIGN: DAMASCENO	☐ INFORMATION	SHEET: 2/2	REVISIONS	DATE	CHK	CBP BARN 29	
UNITS: METERS	☐ SUBMITTAL					DESCRIPTION: PLAN,ELEV., SECTION, RIDGE	
SCALE: 1:300	☐ APPROVAL						
DATE: FEB./2012	☐ CONSTRUCTION	FILE: BARN 29.DWG				FACILITY: 81572	
	☐ OTHER						

Figure B.54 - Details about plan view and profile of CBP Barn 29.

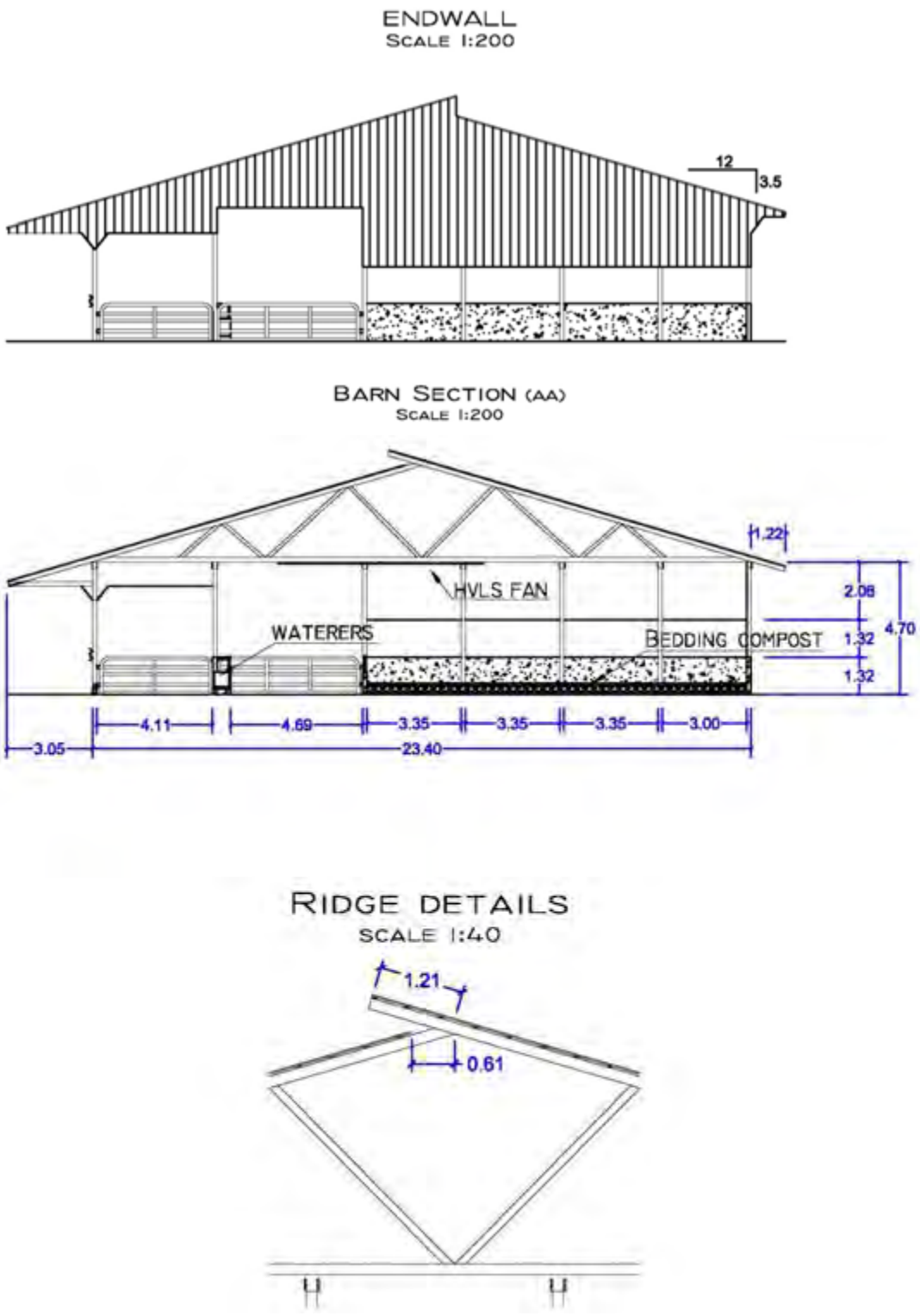

Figure B.55 - Details about end wall, barn section, and ridge of CBP Barn 30.

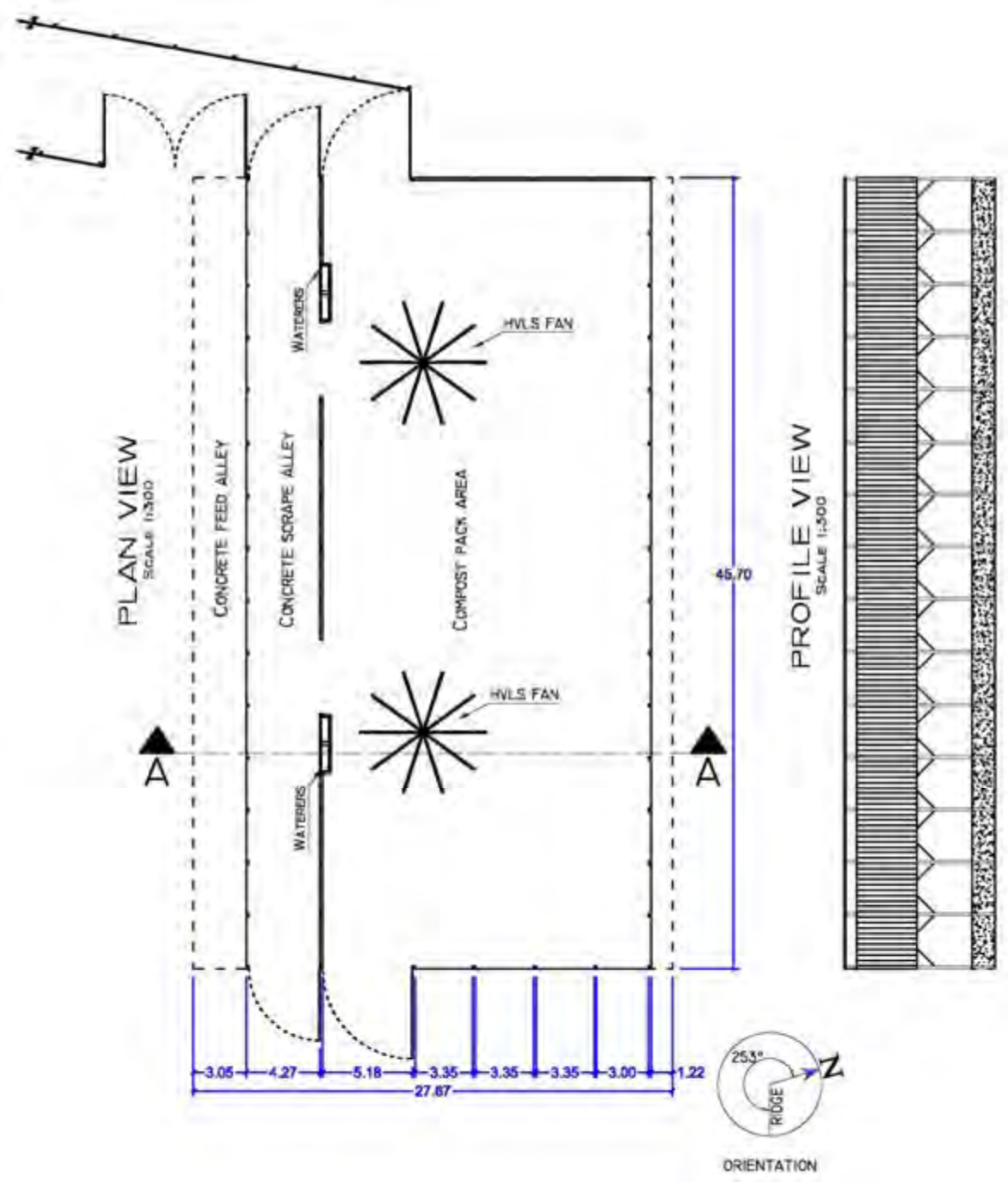

DEPARTMENT OF AGRICULTURAL ENGINEERING							
DESIGN: DAMASCENO	☐ INFORMATION	SHEET: 2/2	REVISIONS	DATE	CHK	CBP BARN 30	
UNITS: METERS	☐ SUBMITTAL					DESCRIPTION: PLAN,ELEV., SECTION, RIDGE	
SCALE: 1:300	☐ APPROVAL						
DATE: FEB./2012	☐ CONSTRUCTION	FILE: BARN 30.DWG				FACILITY: 82265	
	☐ OTHER						

Figure B.56 - Details about plan view and profile of CBP Barn 30.

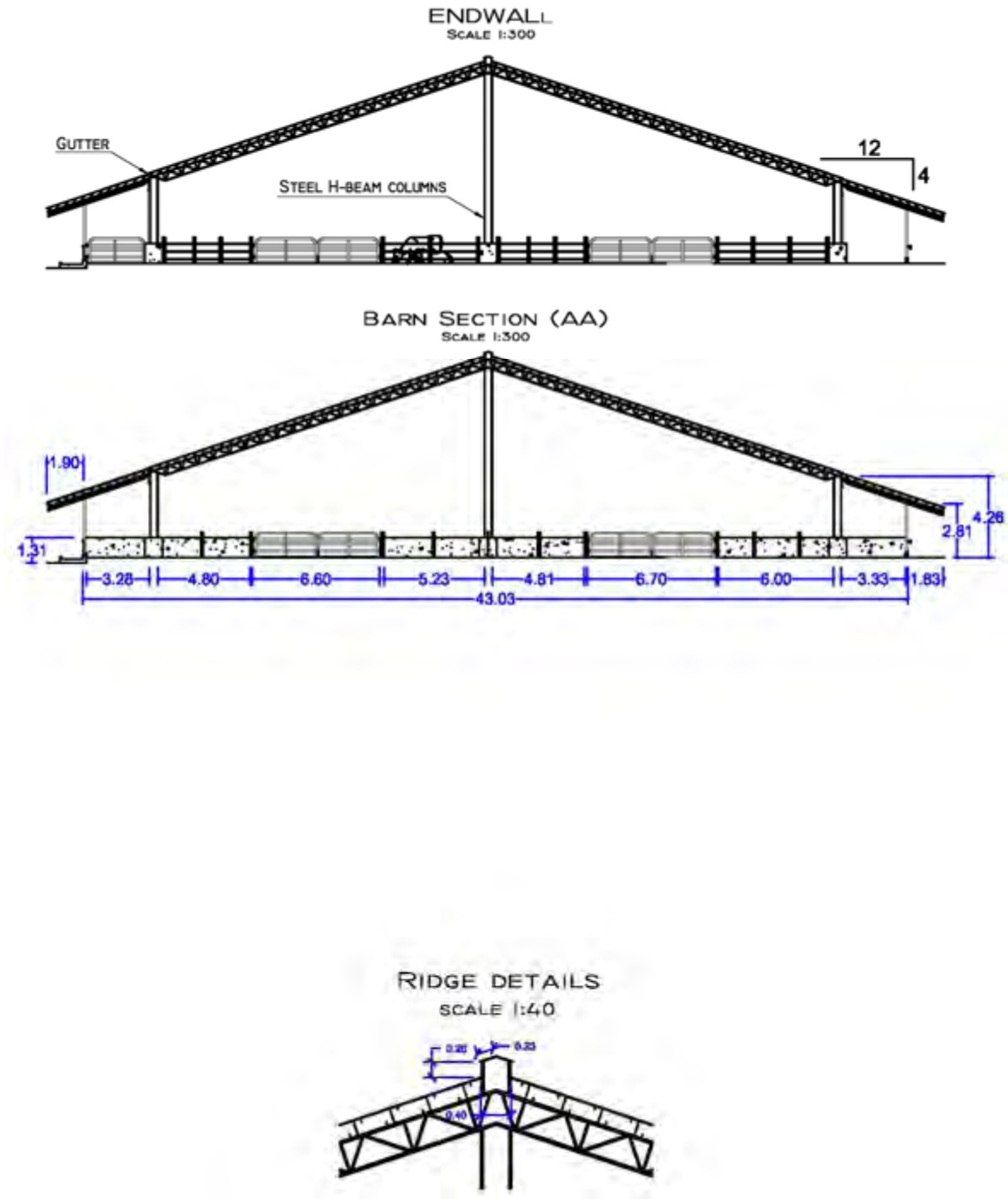

Figure B.57 - Details about end wall, barn section, and ridge of CBP Barn 31.

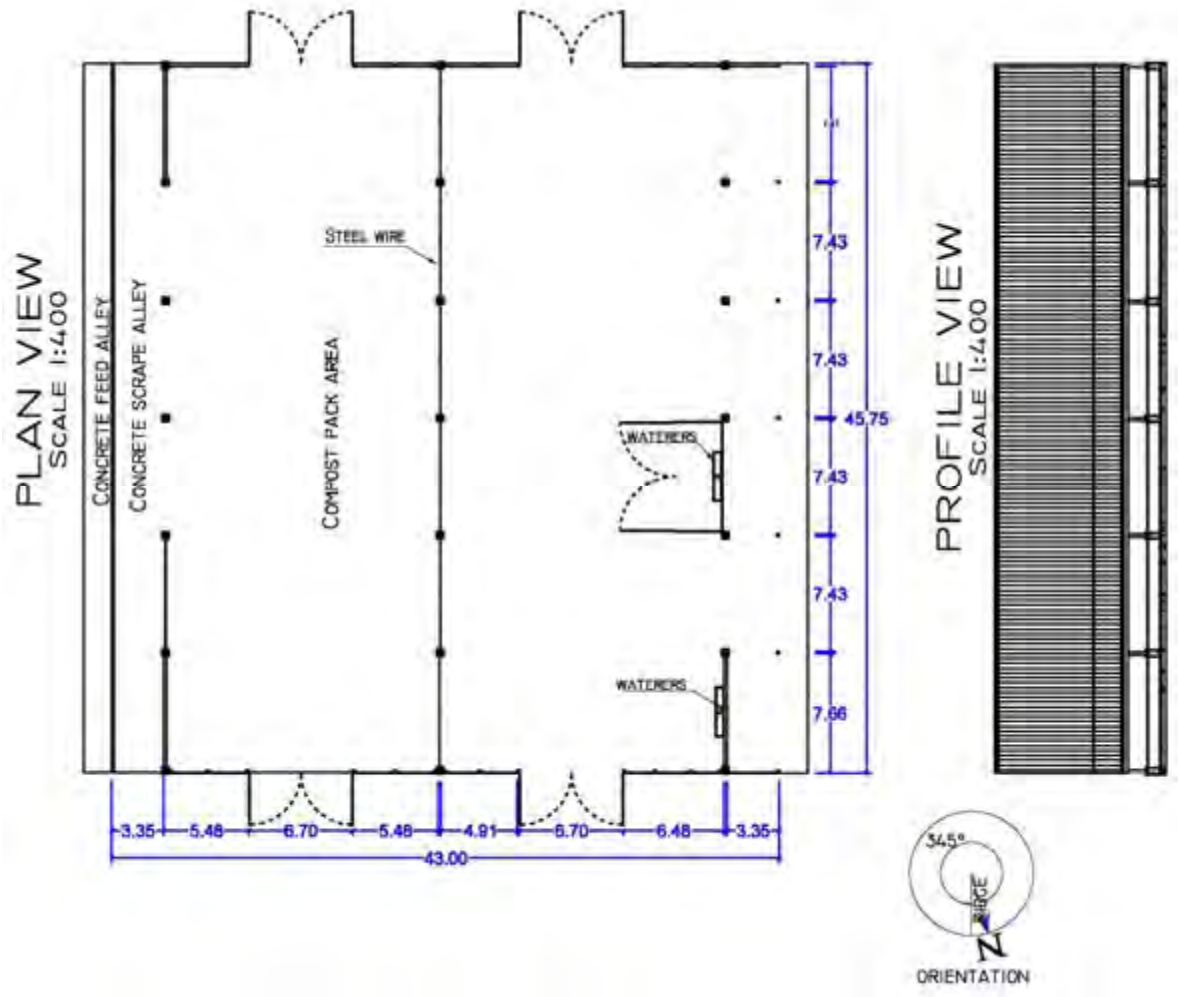

DEPARTMENT OF AGRICULTURAL ENGINEERING							
DESIGN: DAMASCENO	☐ INFORMATION	SHEET: 2/2	REVISIONS	DATE	CHK	CBP BARN 31	
UNITS: METERS	☐ SUBMITTAL					DESCRIPTION: PLAN,ELEV., SECTION, RIDGE	
SCALE: 1:400	☐ APPROVAL						
DATE: FEB./2012	☐ CONSTRUCTION	FILE: BARN 31.DWG				FACILITY: 99923	
	☐ OTHER						

Figure B.58 - Details about plan view and profile of CBP Barn 31.

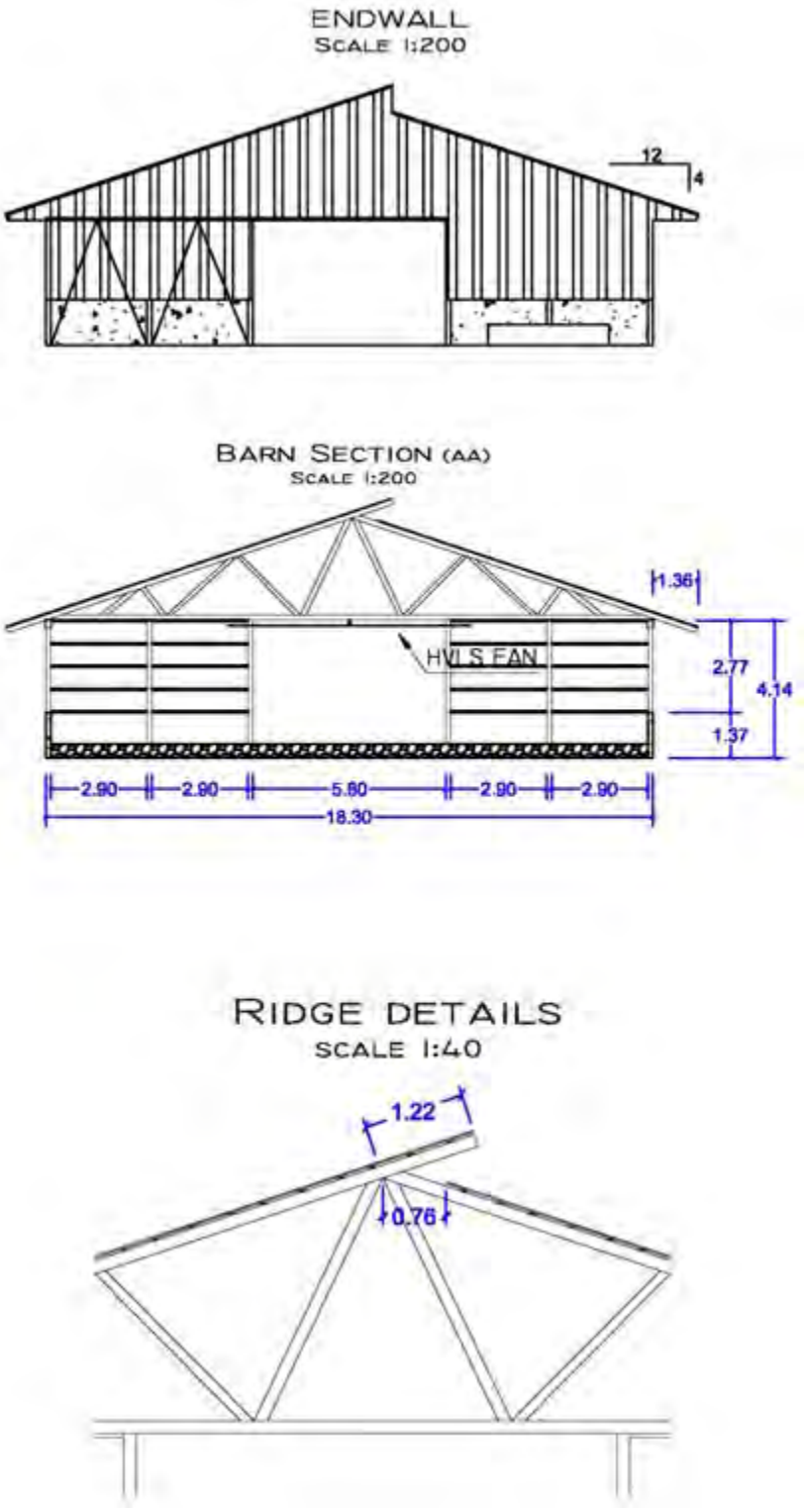

Figure B.59 - Details about end wall, barn section, and ridge of CBP Barn 32.

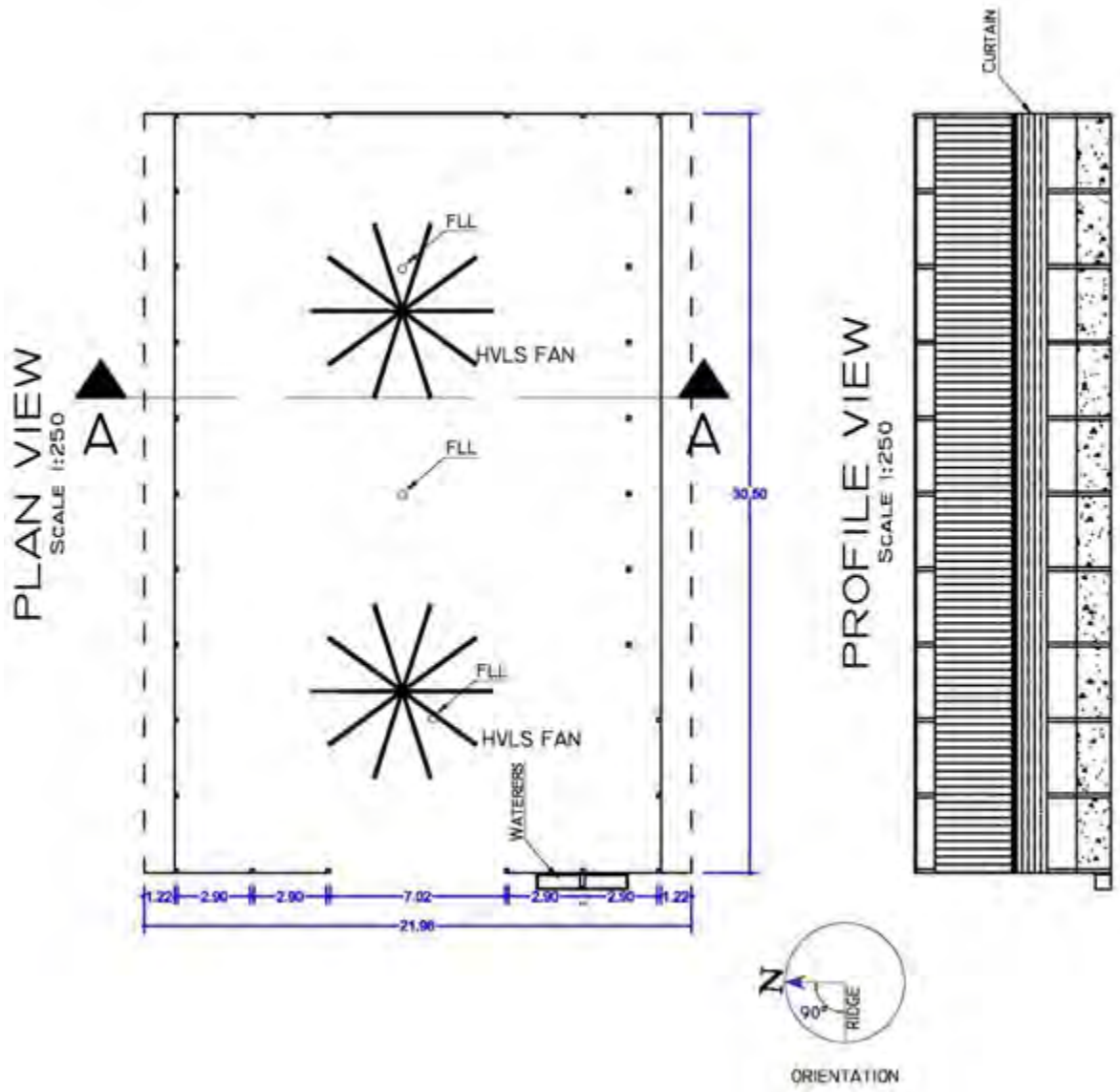

DEPARTMENT OF AGRICULTURAL ENGINEERING							
DESIGN: DAMASCENO	☐ INFORMATION	SHEET: 2/2	REVISIONS	DATE	CHK	CBP BARN 32	
UNITS: METERS	☐ SUBMITTAL					DESCRIPTION: PLAN,ELEV., SECTION, RIDGE	
SCALE: 1:250	☐ APPROVAL						
DATE: FEB./2012	☐ CONSTRUCTION	FILE: BARN 32.DWG				FACILITY: 25745	
	☐ OTHER						

Figure B.60 - Details about plan view and profile of CBP Barn 32.

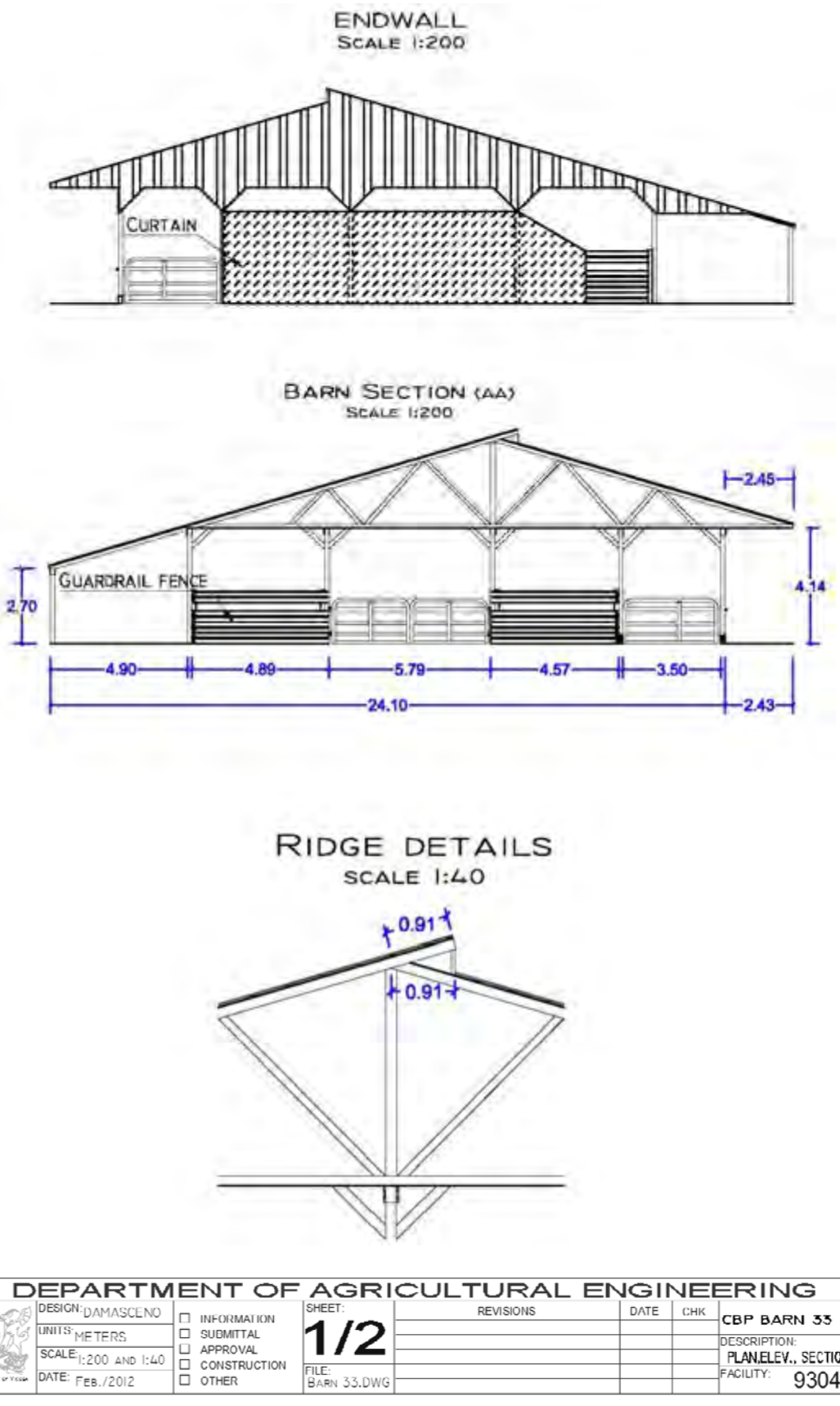

Figure B.61 - Details about end wall, barn section, and ridge of CBP Barn 33.

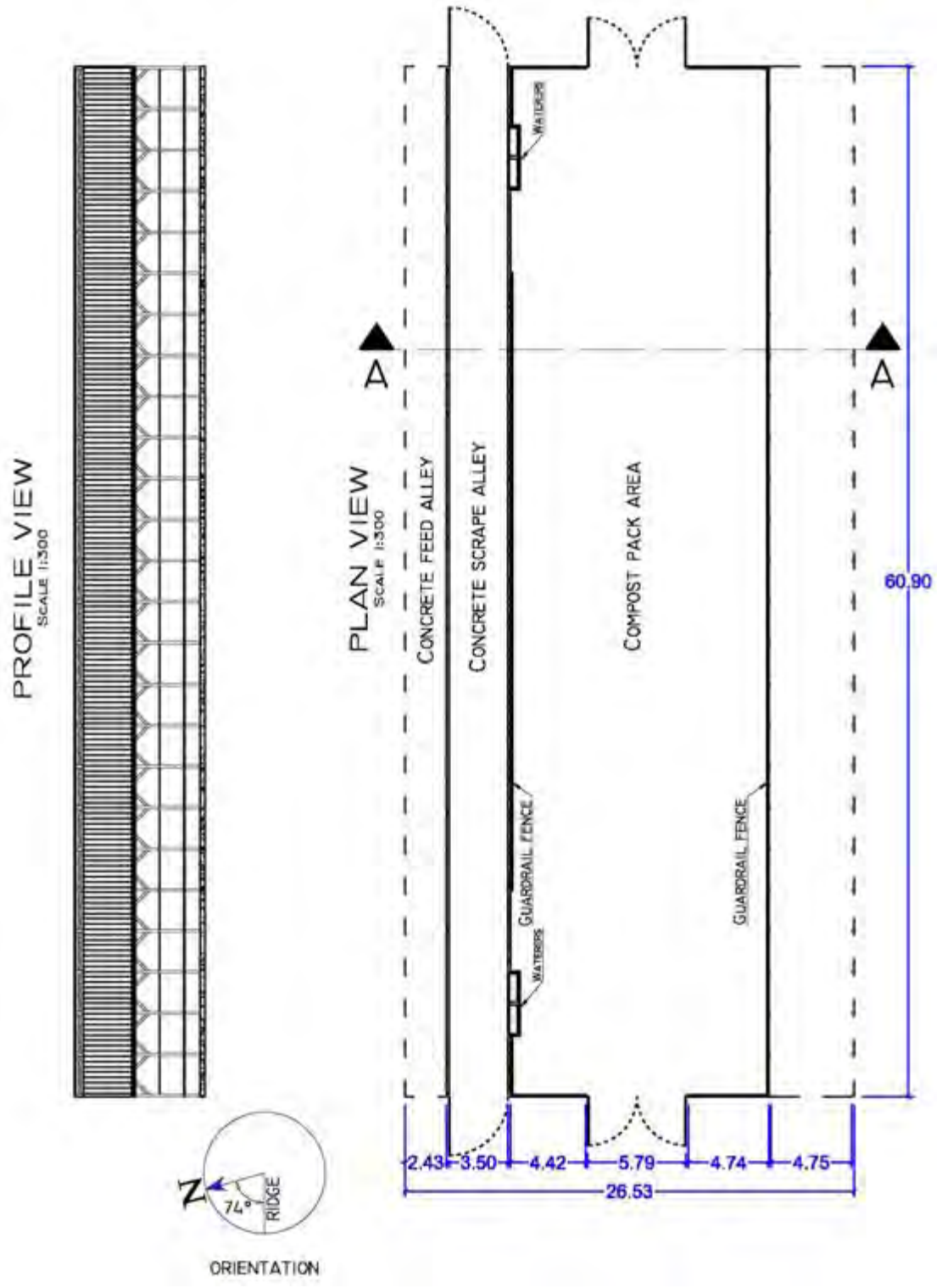

DEPARTMENT OF AGRICULTURAL ENGINEERING							
DESIGN: DAMASCENO	☐ INFORMATION	SHEET: 2/2	REVISIONS	DATE	CHK	CBP BARN 33
UNITS: METERS	☐ SUBMITTAL					DESCRIPTION: PLAN,ELEV., SECTION, RIDGE
SCALE: 1:300	☐ APPROVAL					
DATE: FEB./2012	☐ CONSTRUCTION	FILE: BARN 55.DWG				FACILITY: 93048
	☐ OTHER					

Figure B.62 - Details about plan view and profile of CBP Barn 33.

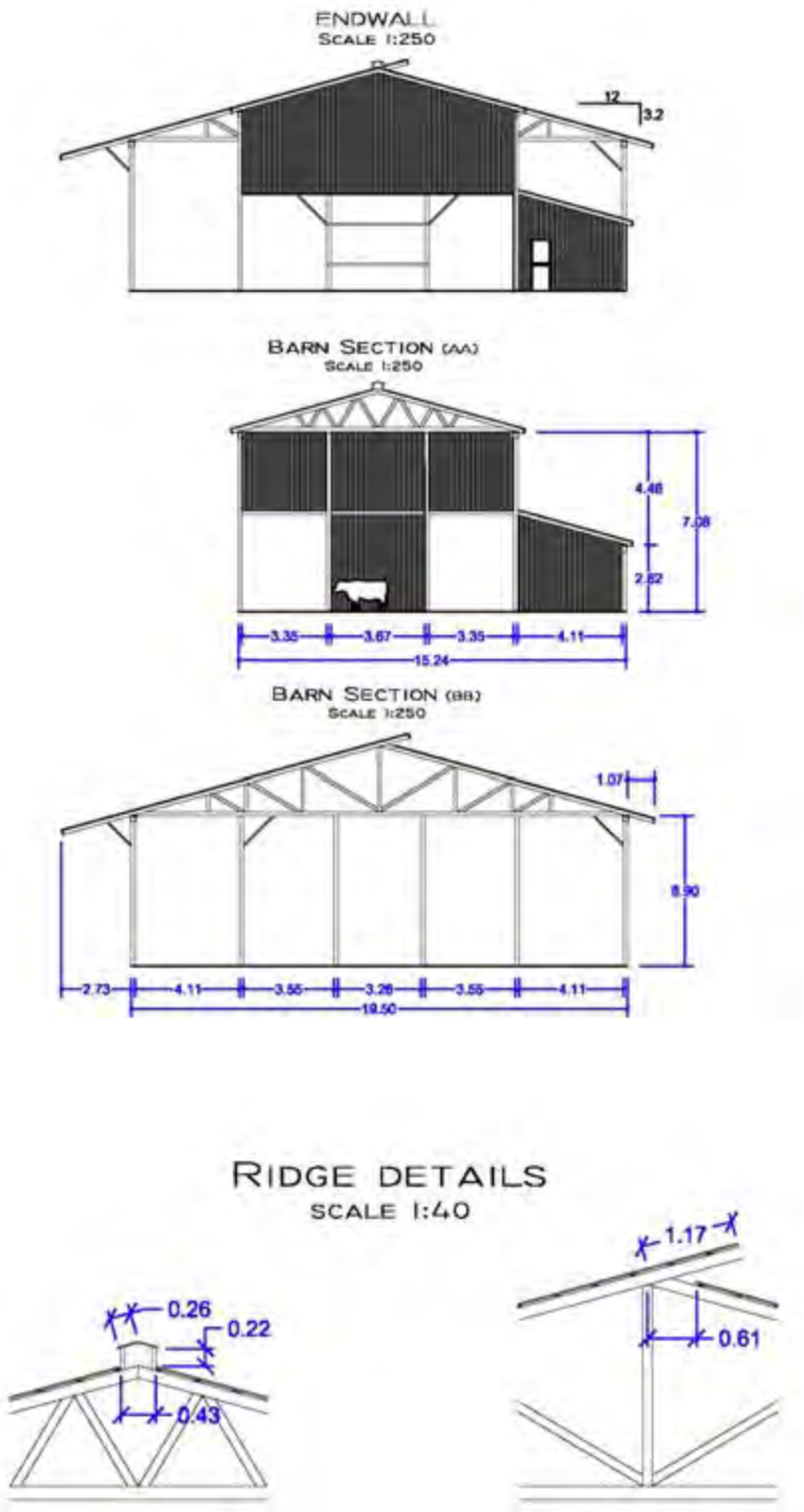

Figure B.63 - Details about end wall, barn section, and ridge of CBP Barn 34.

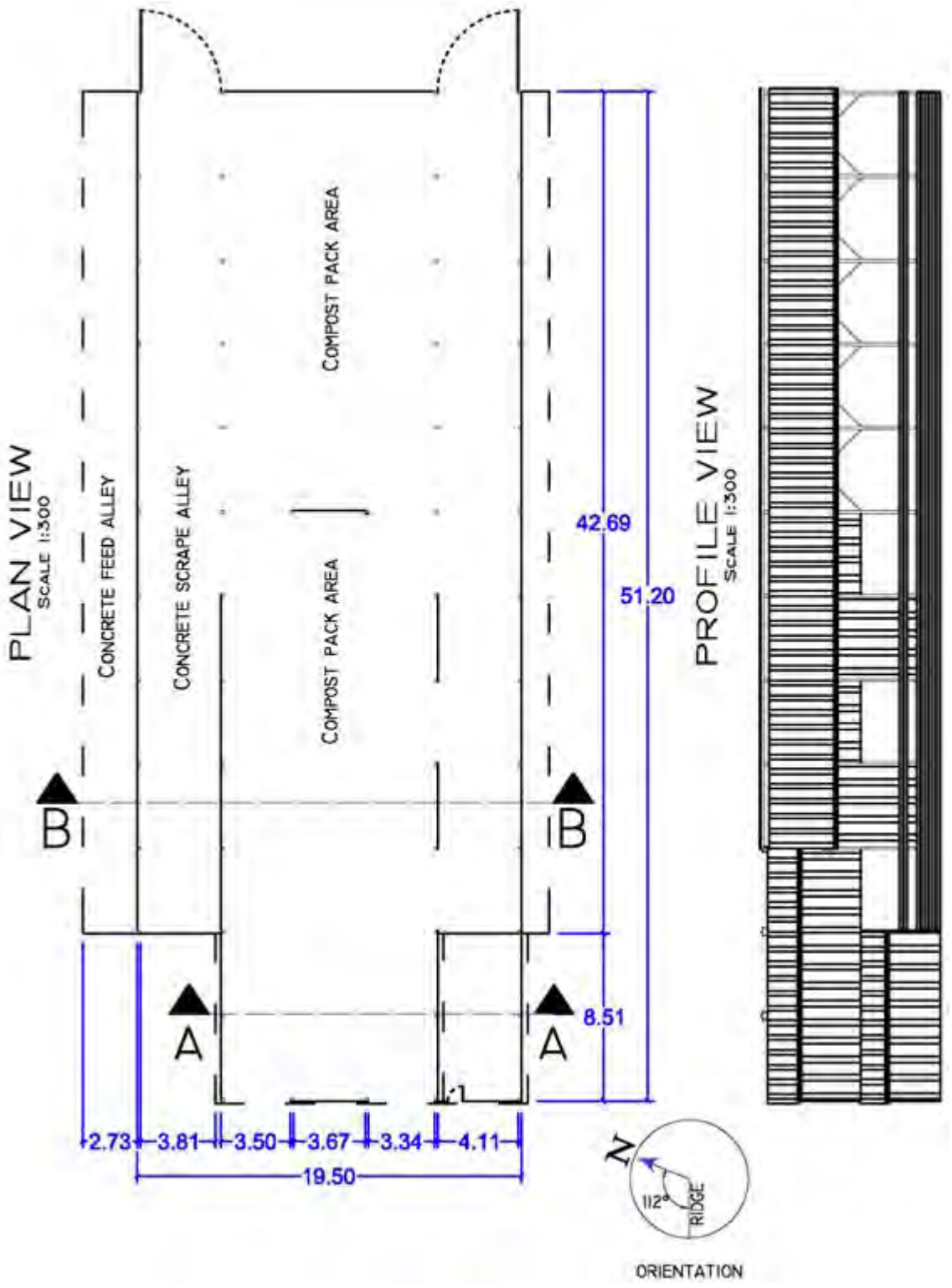

DEPARTMENT OF AGRICULTURAL ENGINEERING							
DESIGN: DAMASCENO	☐ INFORMATION	SHEET: 2/2	REVISIONS	DATE	CHK	CBP BARN 34	
UNITS: METERS	☐ SUBMITTAL					DESCRIPTION: PLAN,ELEV., SECTION, RIDGE	
SCALE: 1:300	☐ APPROVAL					FACILITY: 82414	
DATE: FEB./2012	☐ CONSTRUCTION	FILE: BARN 34.DWG					
	☐ OTHER						

Figure B.64 - Details about plan view and profile of CBP Barn 34.

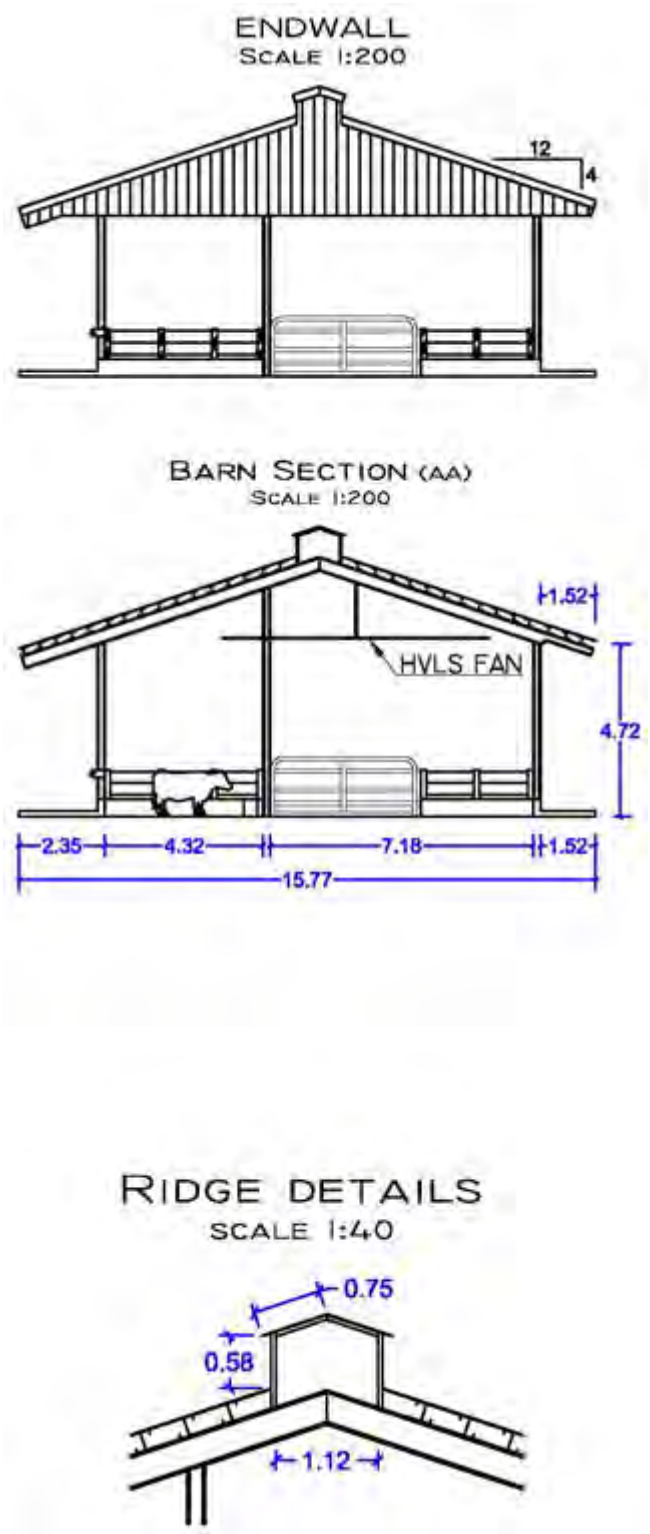

Figure B.65 - Details about end wall, barn section, and ridge of CBP Barn 35.

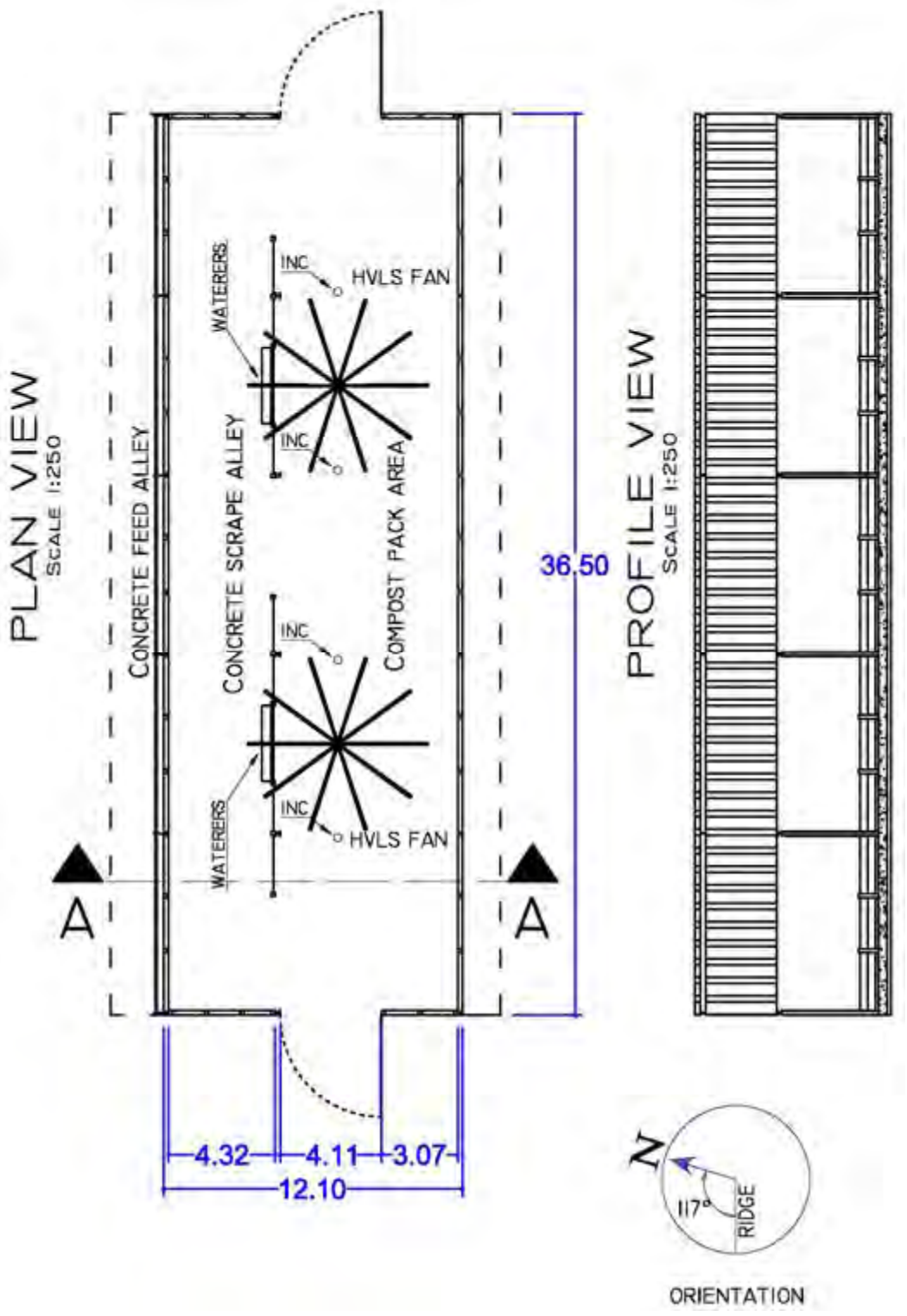

DEPARTMENT OF AGRICULTURAL ENGINEERING

DESIGN: DAMASCENO	☐ INFORMATION	SHEET: 2/2	REVISIONS	DATE	CHK	CBP BARN 35
UNITS: METERS	☐ SUBMITTAL					DESCRIPTION: PLAN,ELEV., SECTION, RIDGE
SCALE: 1:250	☐ APPROVAL					
DATE: FEB./2012	☐ CONSTRUCTION	FILE: BARN 35.DWG				FACILITY: 98271
	☐ OTHER					

Figure B.66 - Details about plan view and profile of CBP Barn 35.

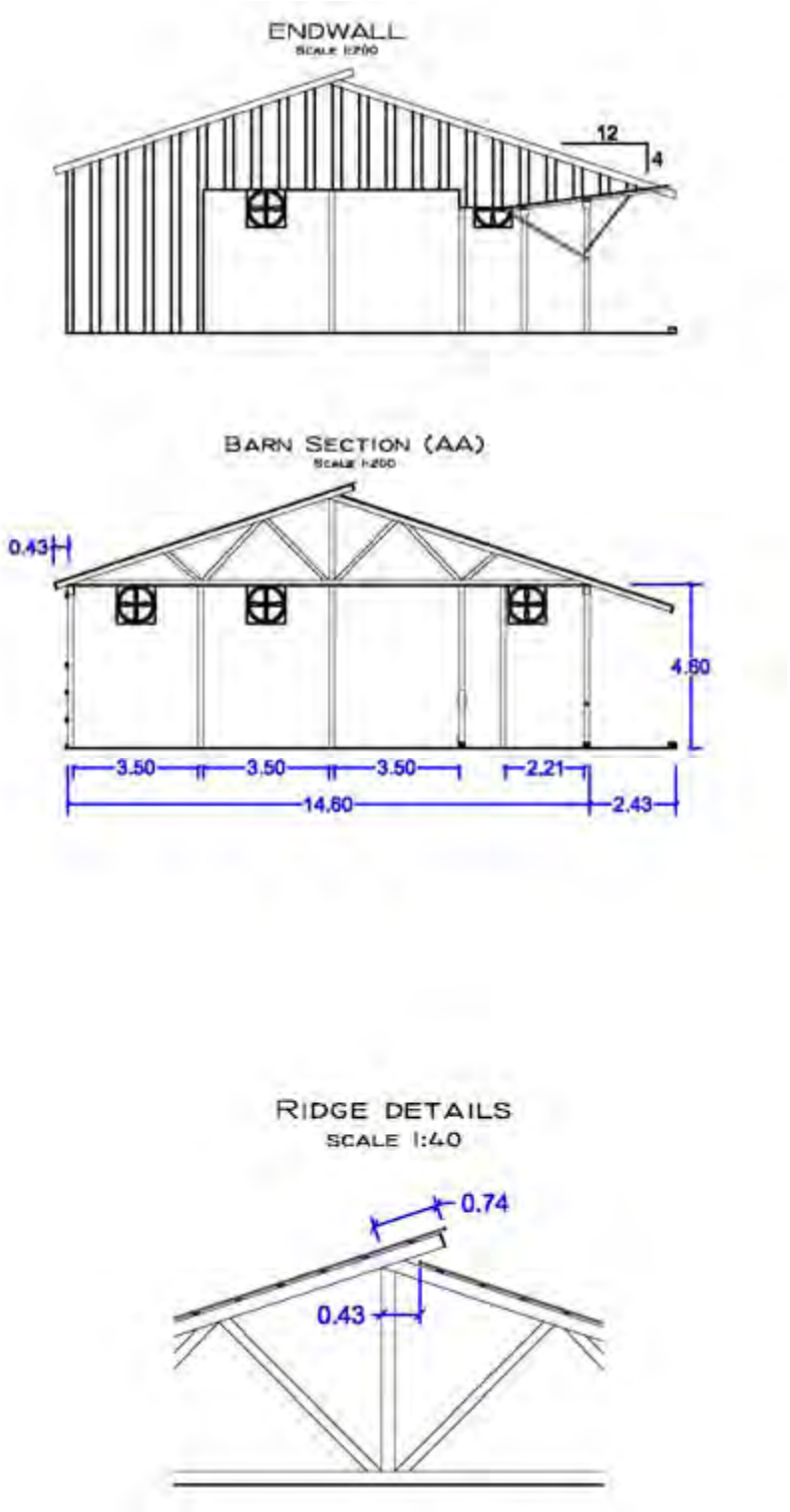

Figure B.67 - Details about end wall, barn section, and ridge of CBP Barn 36.

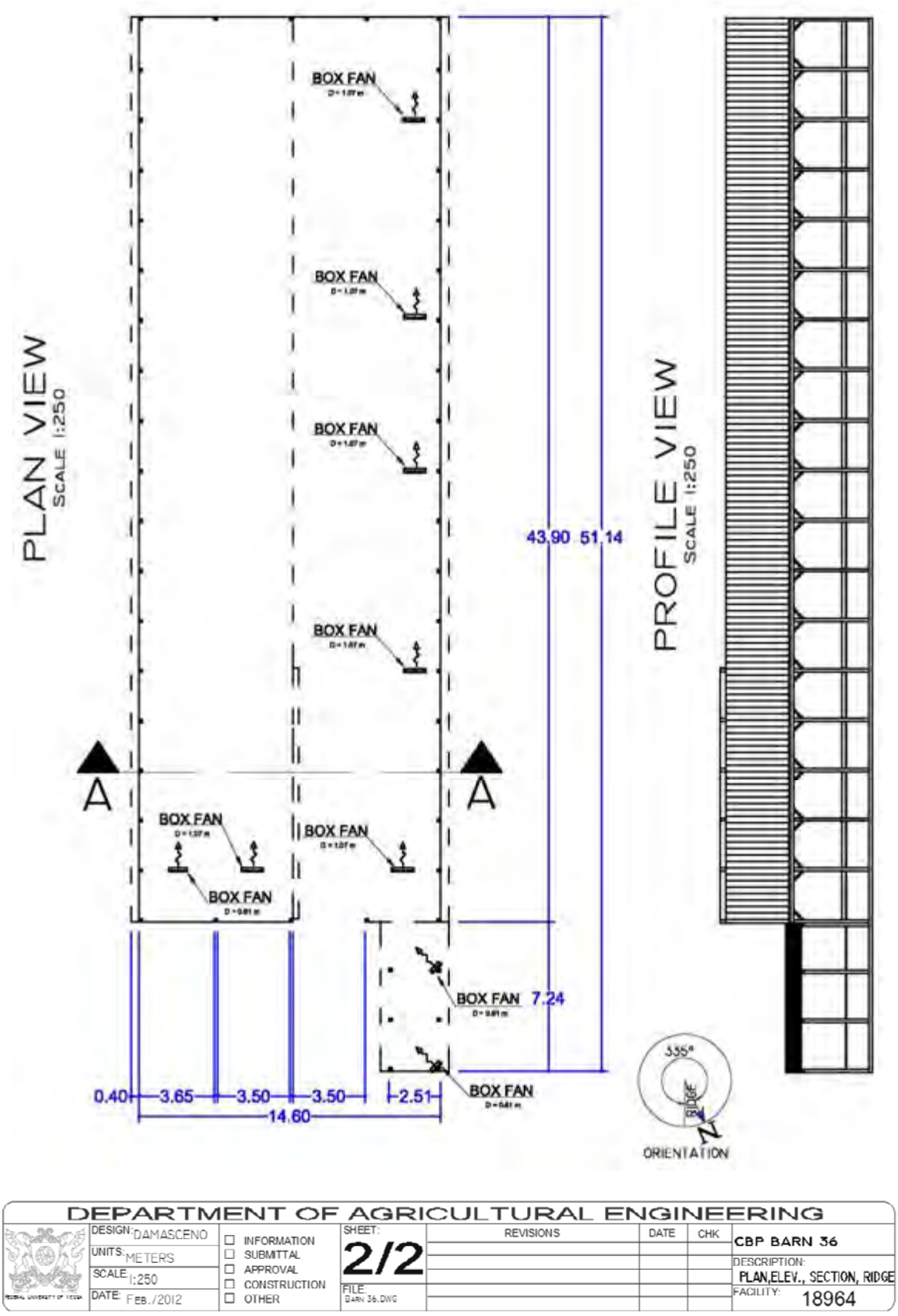

DEPARTMENT OF AGRICULTURAL ENGINEERING							
DESIGN: DAMASCENO	☐ INFORMATION	SHEET: 2/2	REVISIONS	DATE	CHK	CBP BARN 36	
UNITS: METERS	☐ SUBMITTAL					DESCRIPTION: PLAN,ELEV., SECTION, RIDGE	
SCALE: 1:250	☐ APPROVAL					FACILITY: 18964	
DATE: FEB./2012	☐ CONSTRUCTION	FILE: BARN 36.DWG					
	☐ OTHER						

Figure B.68 - Details about plan view and profile of CBP Barn 36.

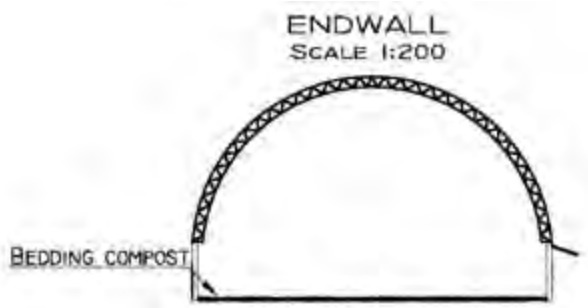

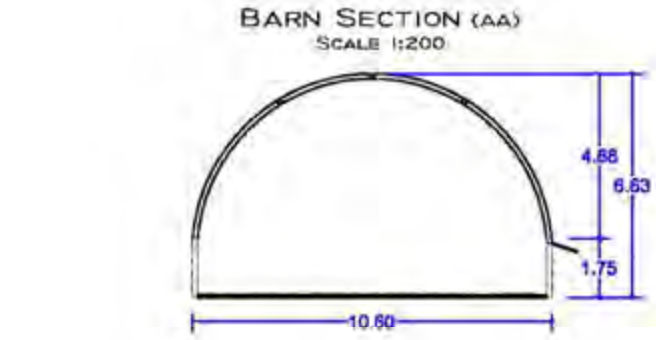

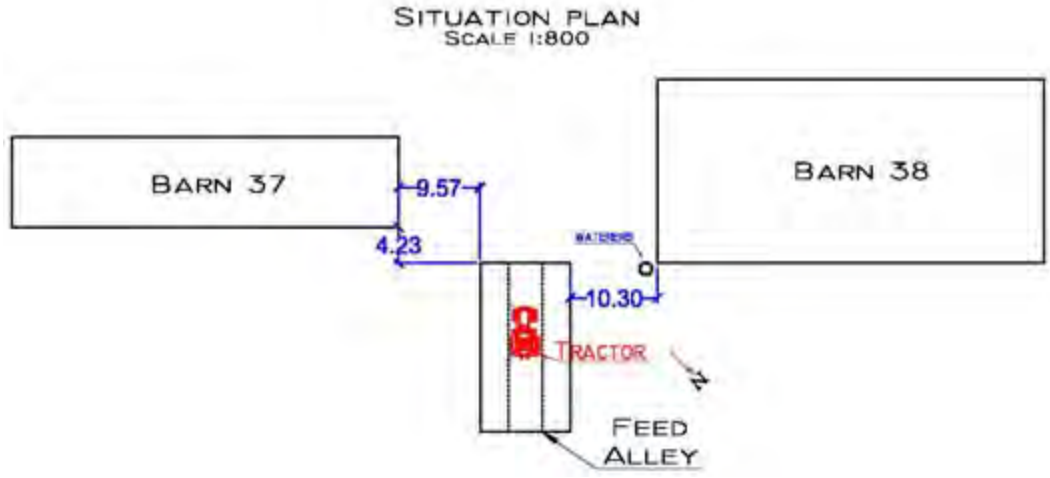

DEPARTMENT OF AGRICULTURAL ENGINEERING

DESIGN: DAMASCENO	☐ INFORMATION	SHEET: 1/2	REVISIONS	DATE	CHK	CBP BARN 37
UNITS: METERS	☐ SUBMITTAL					DESCRIPTION: PLAN,ELEV., SECTION, RIDGE
SCALE: 1:200 AND 1:800	☐ APPROVAL					FACILITY: 24423
DATE: FEB./2012	☐ CONSTRUCTION	FILE: BARN 37.DWG				
	☐ OTHER					

Figure B.69 - Details about end wall, barn section, and ridge of CBP Barn 37.

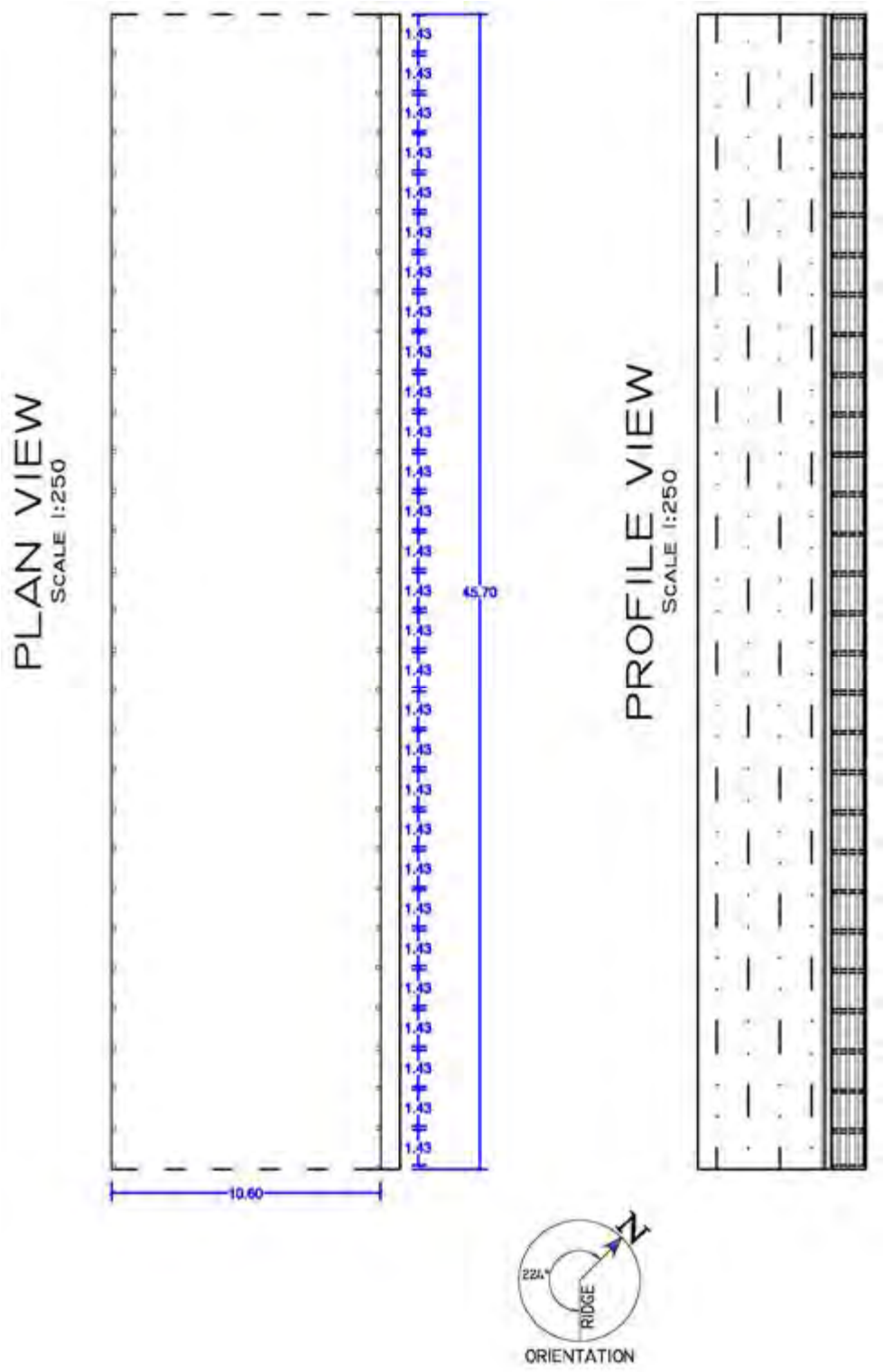

DEPARTMENT OF AGRICULTURAL ENGINEERING

DESIGN: DAMASCENO	☐ INFORMATION	SHEET: 2/2	REVISIONS	DATE	CHK	CBP BARN 37
UNITS: METERS	☐ SUBMITTAL					DESCRIPTION: PLAN,ELEV., SECTION, RIDGE
SCALE: 1:250	☐ APPROVAL					
DATE: FEB./2012	☐ CONSTRUCTION	FILE: BARN 37.DWG				FACILITY: 24423
	☐ OTHER					

Figure B.70 - Details about plan view and profile of CBP Barn 37.

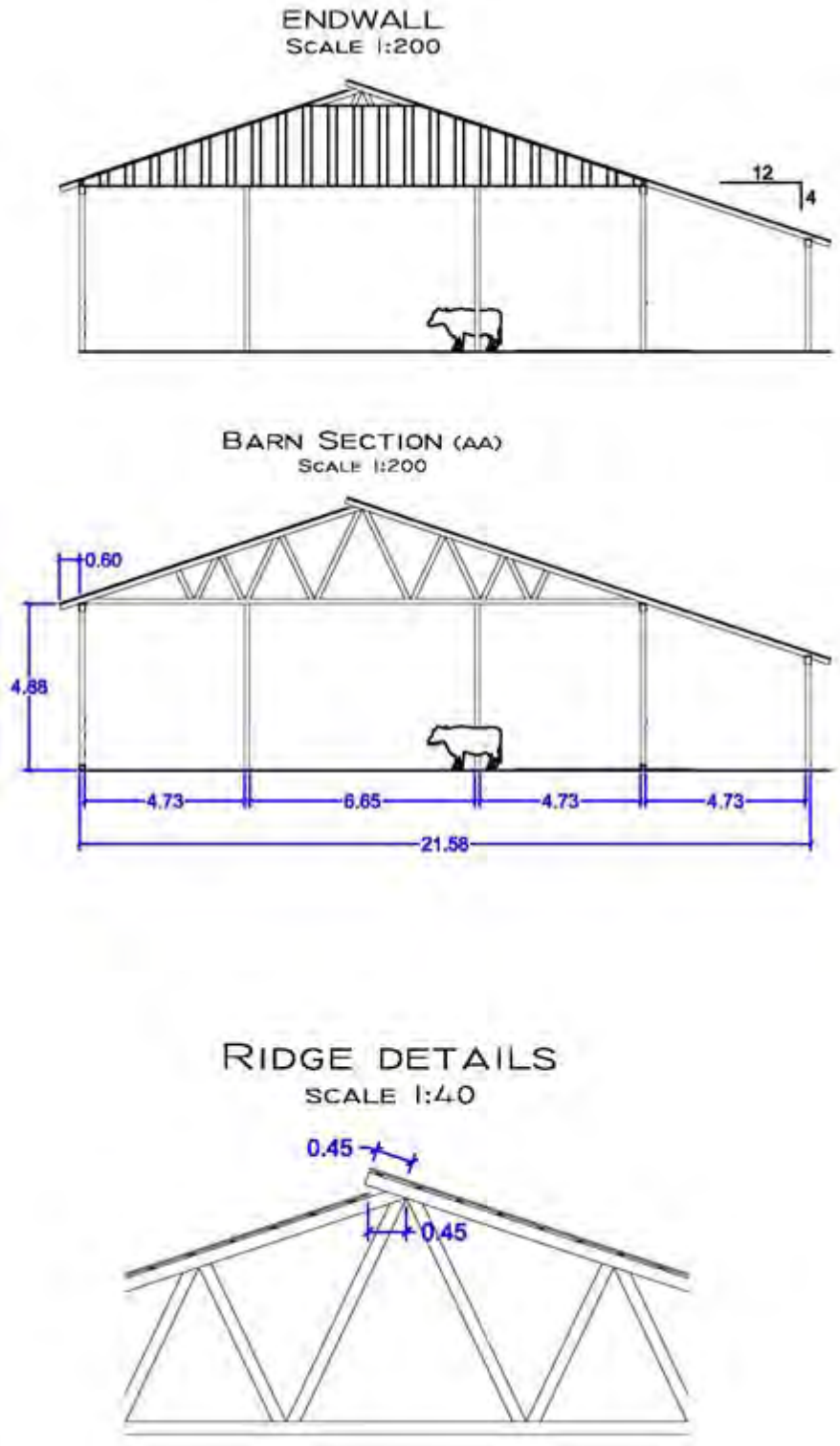

Figure B.71 - Details about end wall, barn section, and ridge of CBP Barn 38.

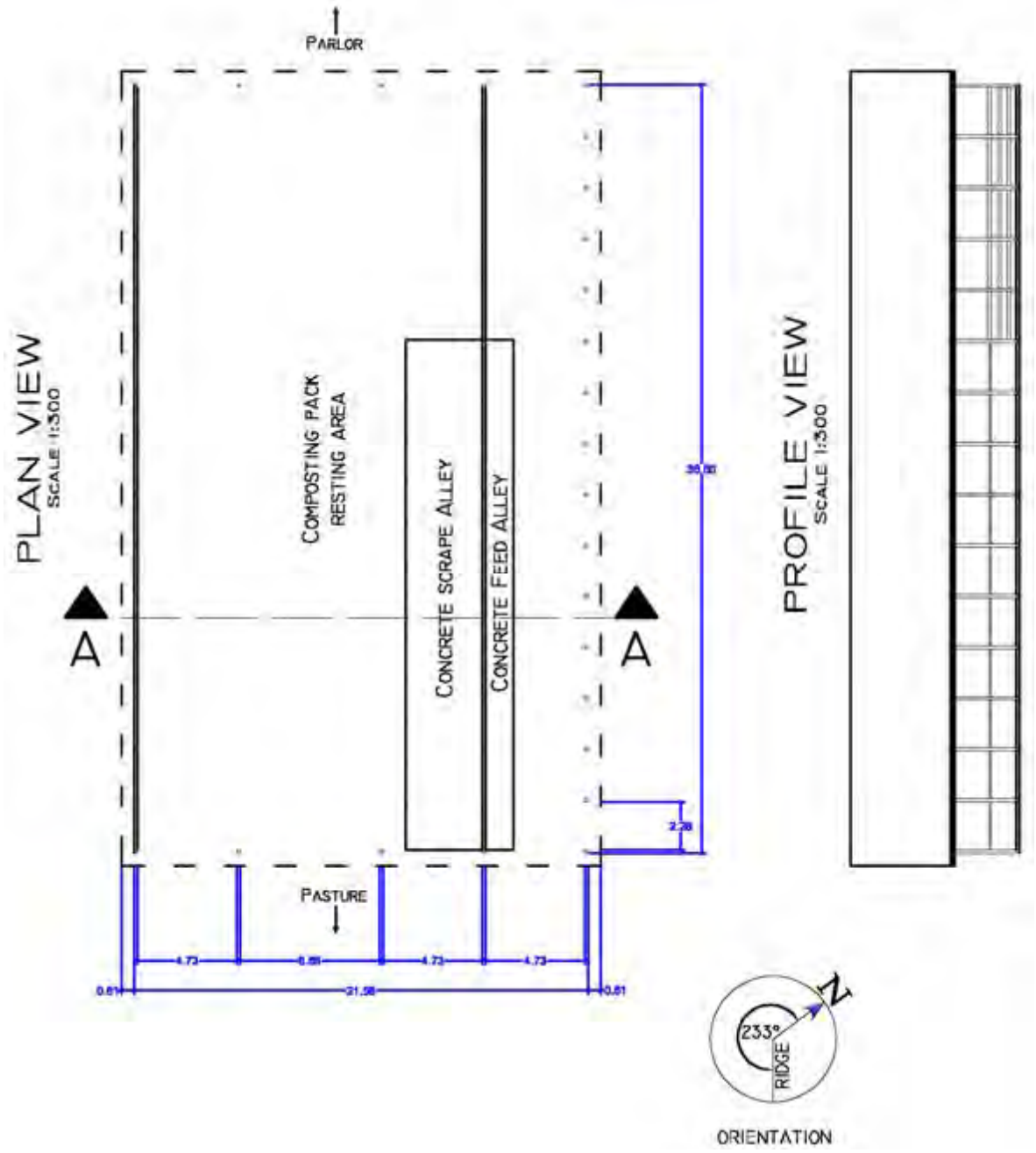

Figure B.72 - Details about plan view and profile of CBP Barn 38.

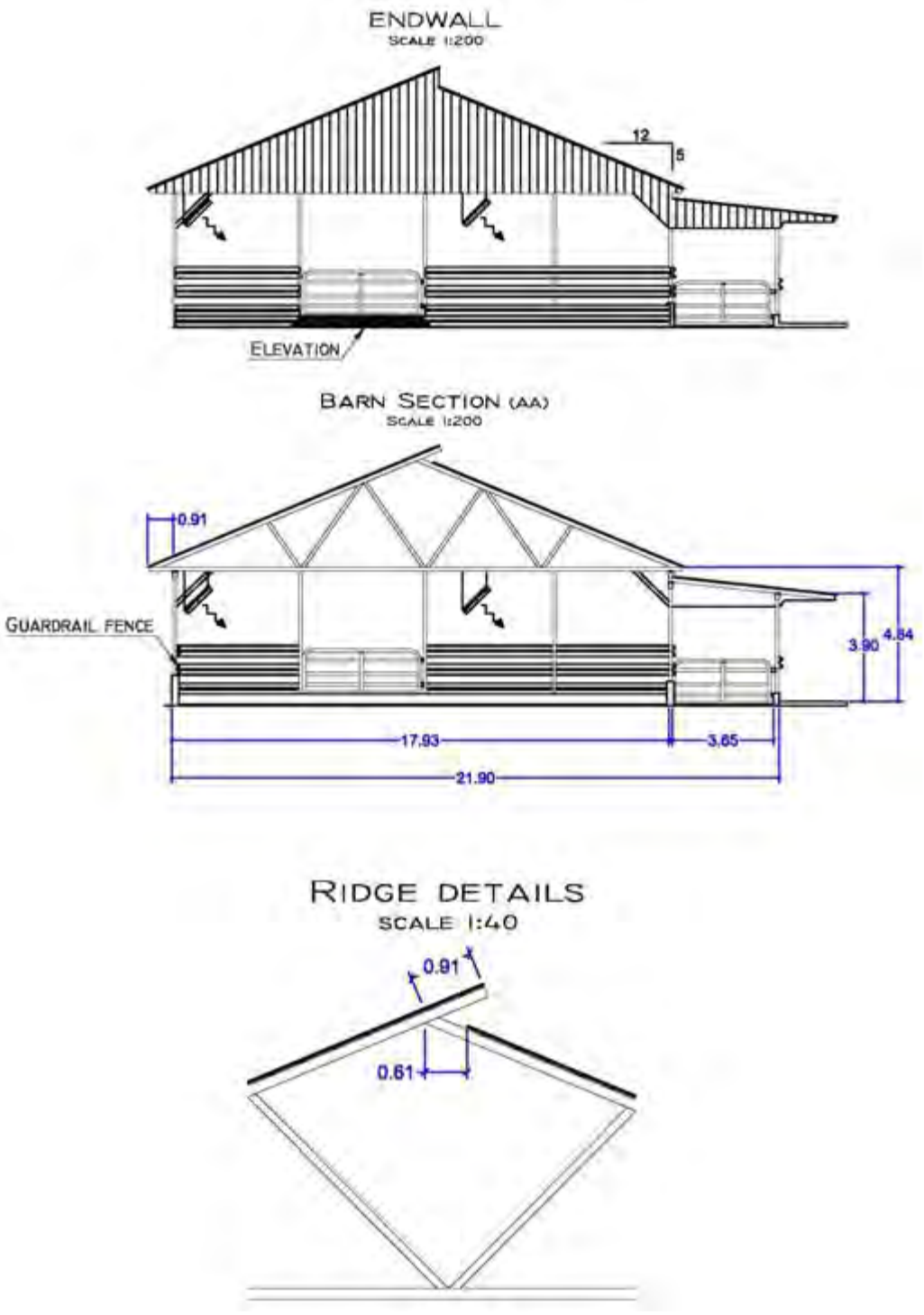

Figure B.73 - Details about end wall, barn section, and ridge of CBP Barn 39 and 40.

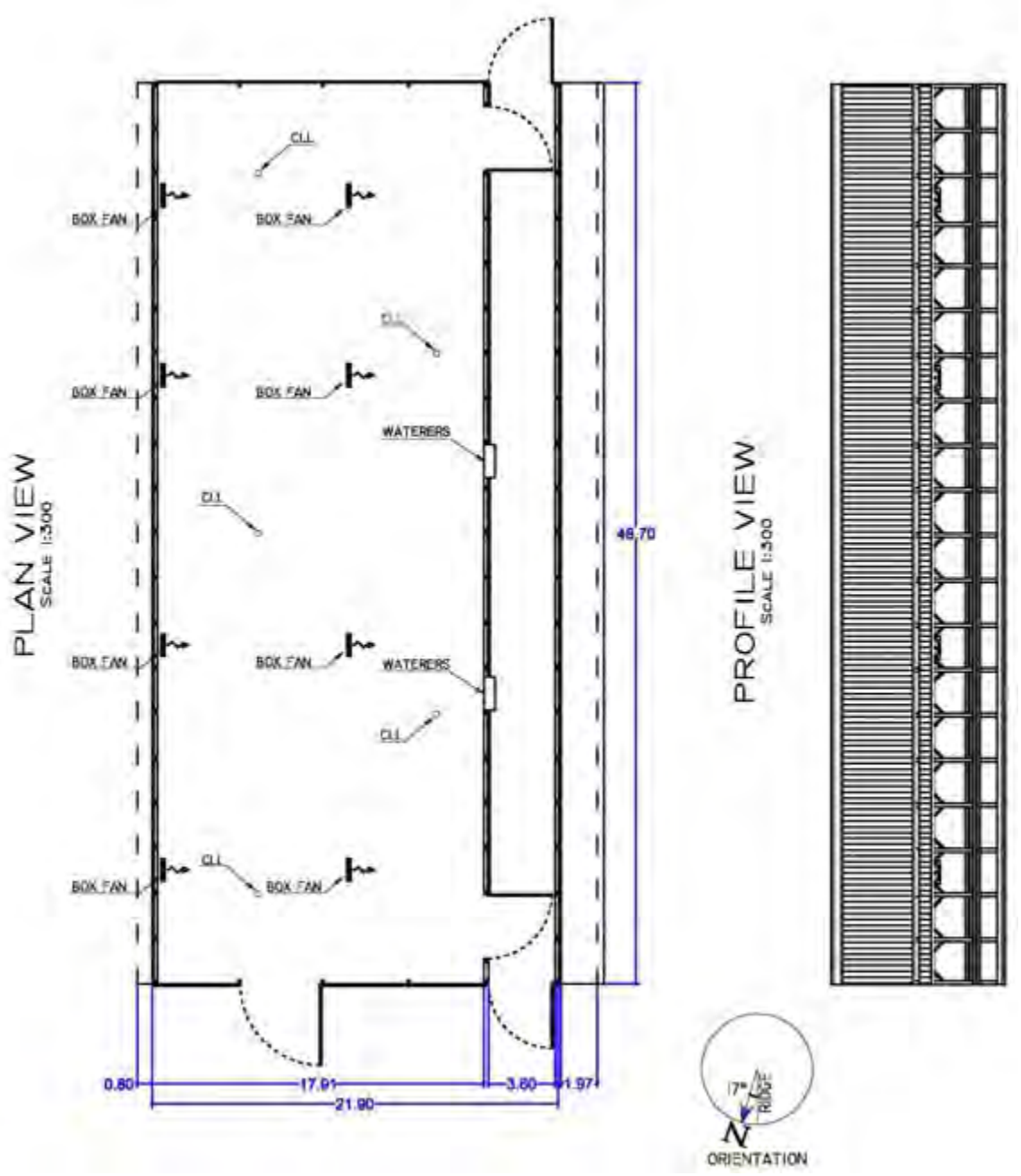

DEPARTMENT OF AGRICULTURAL ENGINEERING							
	DESIGN: DAMASCENO	☐ INFORMATION	SHEET: 2/2	REVISIONS	DATE	CHK	CBP BARN 39 AND 40
	UNITS: METERS	☐ SUBMITTAL					DESCRIPTION: PLAN,ELEV., SECTION, RIDGE
	SCALE: 1:200 AND 1:40	☐ APPROVAL					FACILITY: 97082 and 16781
	DATE: FEB./2012	☐ CONSTRUCTION	FILE: BARN 39.DWG				
		☐ OTHER					

Figure B.74 - Details about plan view and profile of CBP Barn 39 and 40.

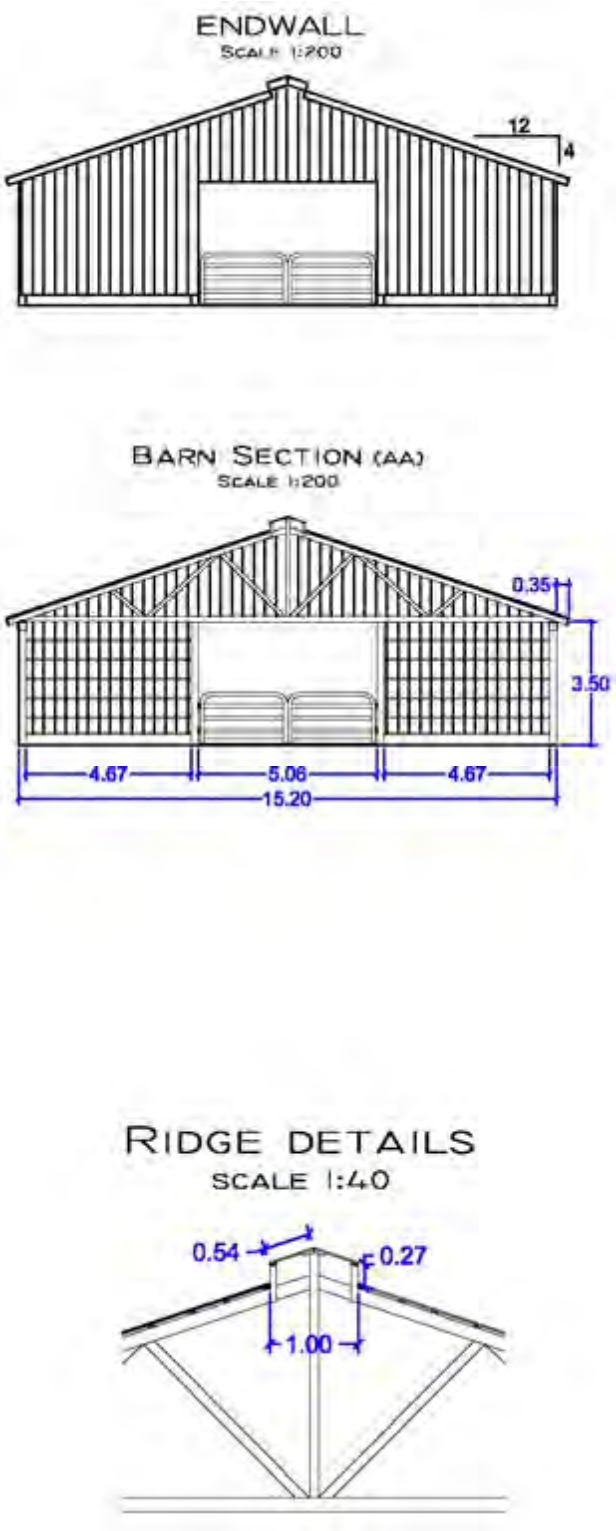

Figure B.75 - Details about end wall, barn section, and ridge of CBP Barn 41.

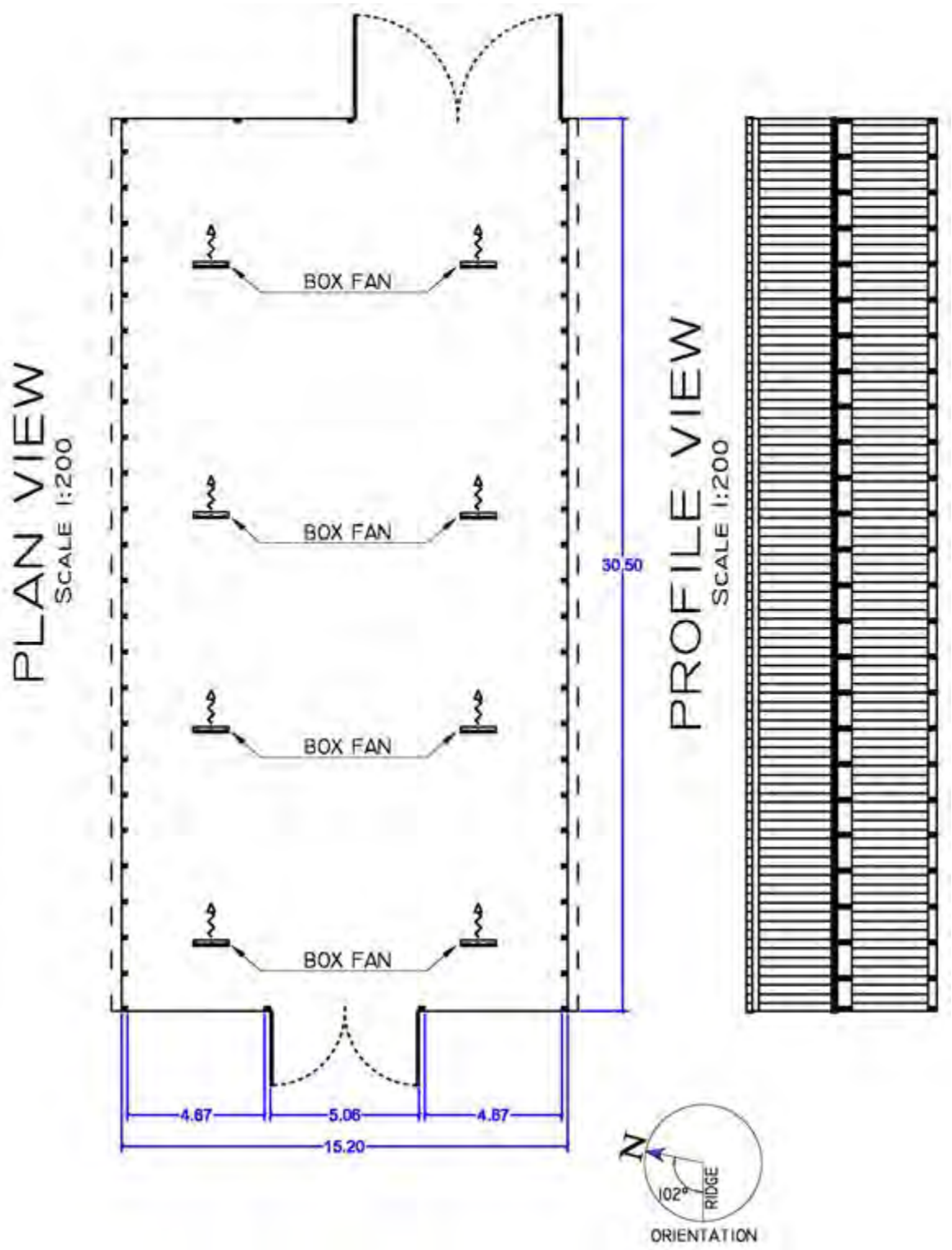

DEPARTMENT OF AGRICULTURAL ENGINEERING							
DESIGN: DAMASCENO	☐ INFORMATION	SHEET: 2/2	REVISIONS	DATE	CHK	CBP BARN 41	
UNITS: METERS	☐ SUBMITTAL					DESCRIPTION: PLAN,ELEV., SECTION, RIDGE	
SCALE: 1:200	☐ APPROVAL						
DATE: Feb./2012	☐ CONSTRUCTION	FILE: BARN 41.DWG				FACILITY: 93171	
	☐ OTHER						

Figure B.76 - Details about plan view and profile of CBP Barn 41.

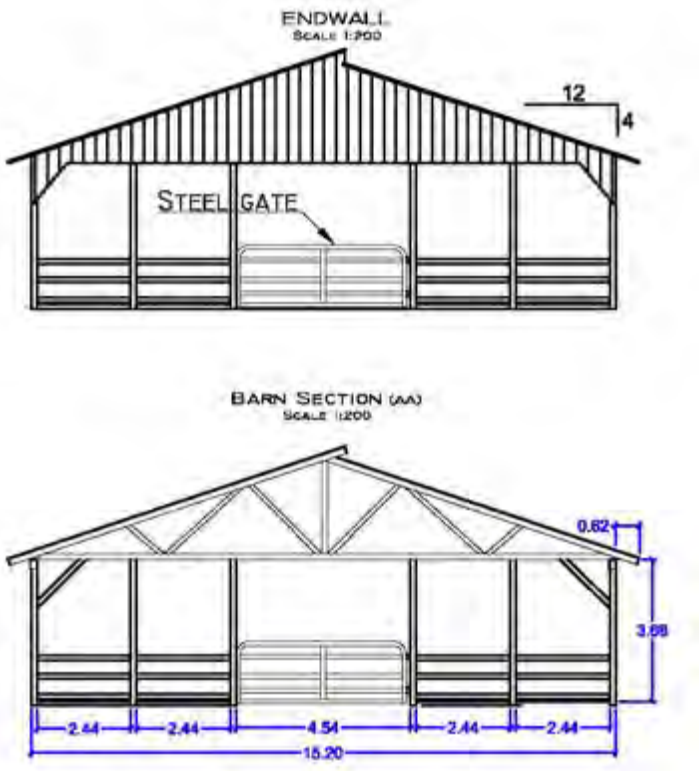

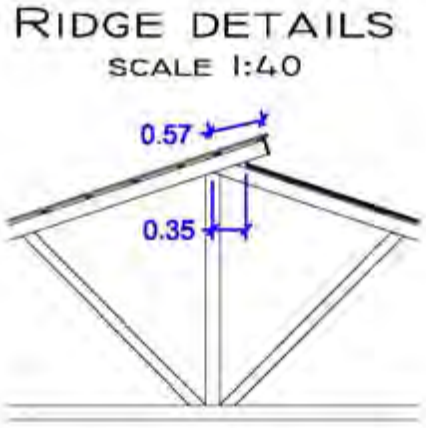

DEPARTMENT OF AGRICULTURAL ENGINEERING							
DESIGN: DAMASCENO	☐ INFORMATION	SHEET: 1/2	REVISIONS	DATE	CHK	CBP BARN 42	
UNITS: METERS	☐ SUBMITTAL					DESCRIPTION: PLAN,ELEV., SECTION, RIDGE	
SCALE: 1:200 AND 1:40	☐ APPROVAL						
DATE: FEB./2012	☐ CONSTRUCTION	FILE: BARN 42.DWG				FACILITY: 66447	
	☐ OTHER						

Figure B.77 - Details about end wall, barn section, and ridge of CBP Barn 42.

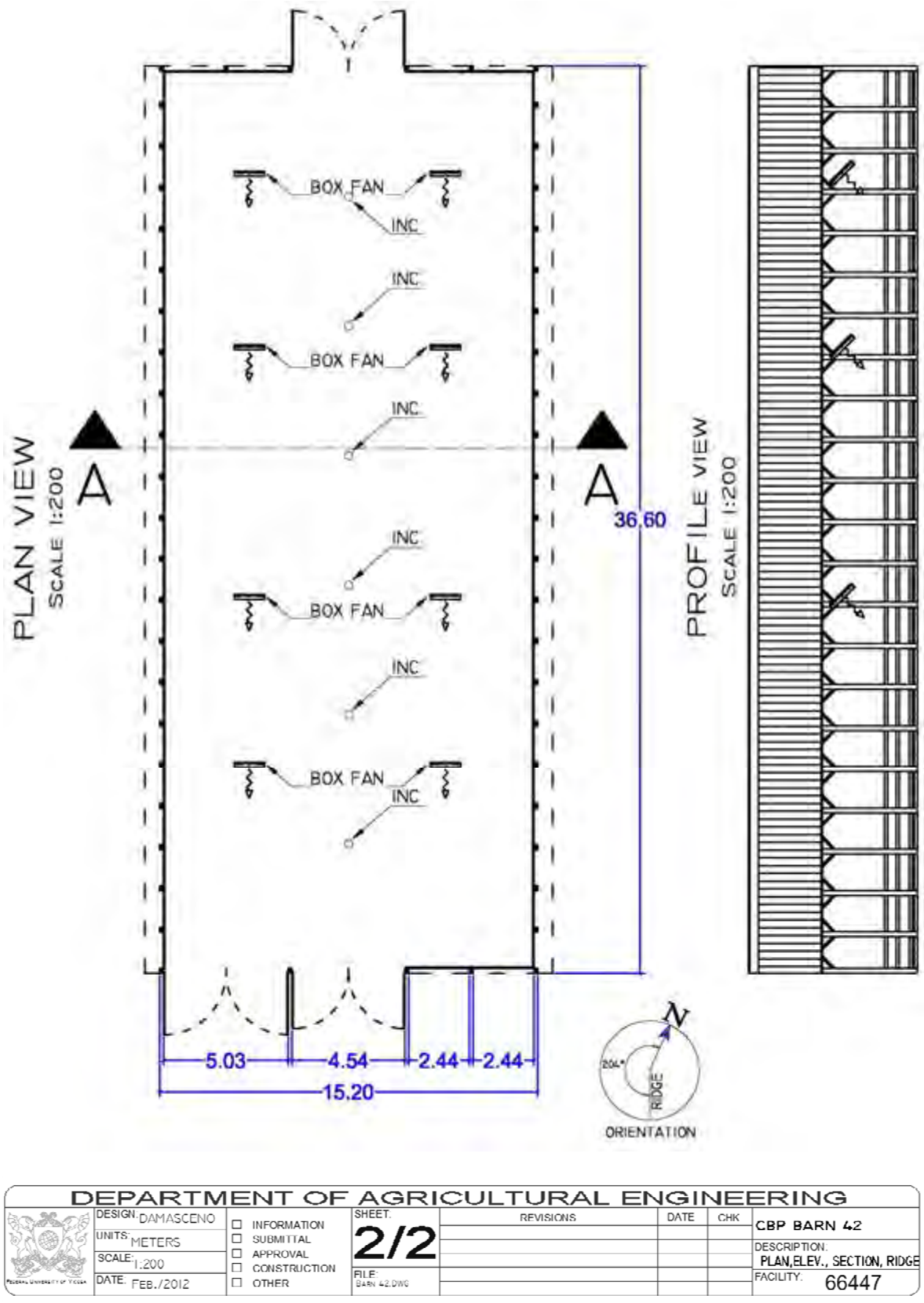

Figure B.78 - Details about plan view and profile of CBP Barn 42.

APPENDIX C

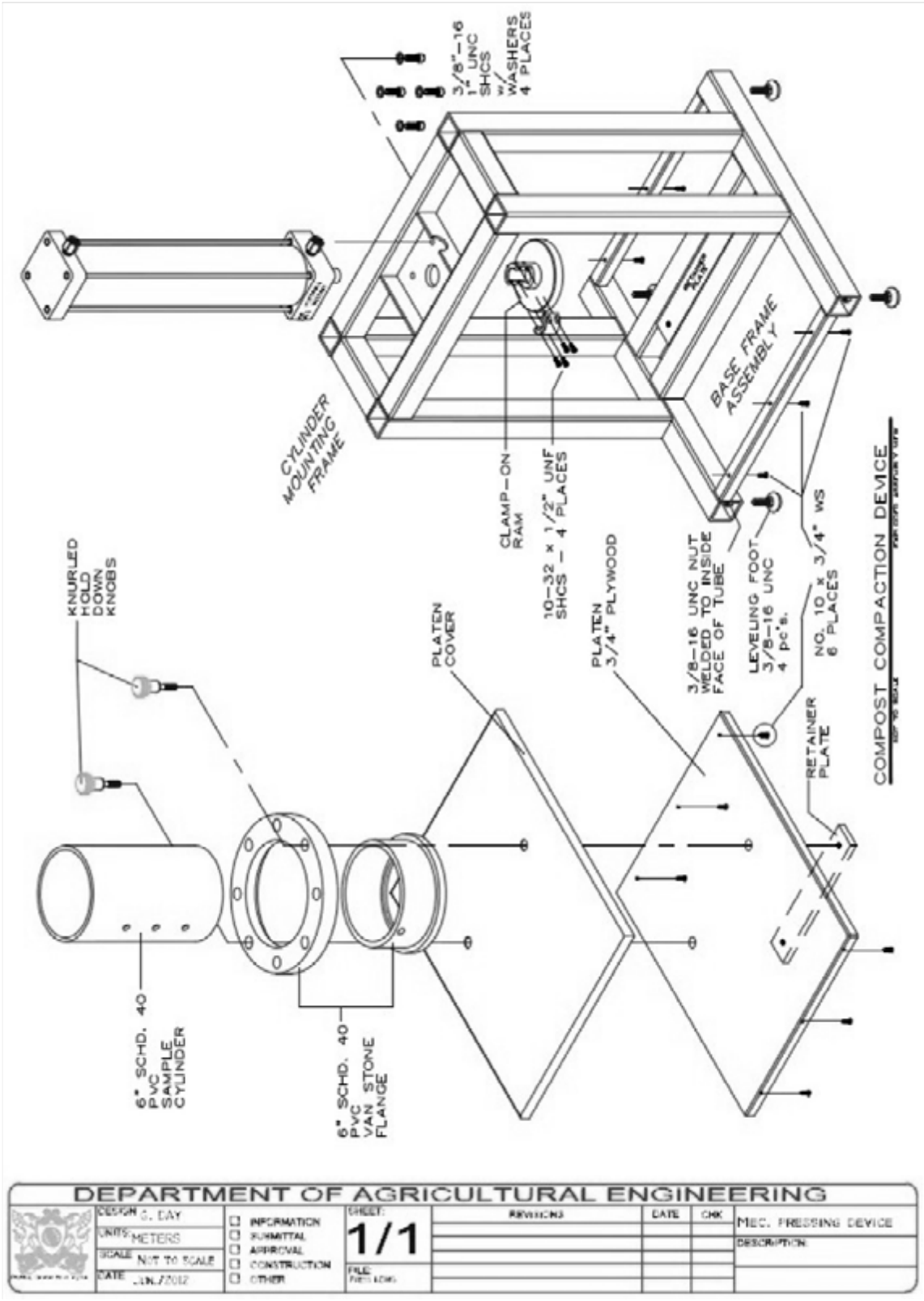

Figure C.1 - Compost compact device designed used in this study.

APPENDIX D

D.1 - Determination of groups π Buckingham.

Table D.1 is showing the dimensional parameters that affect the ventilation characteristics inside of CBP barn.

Table D.1 - Variables affecting ventilation characteristics in CBP barn.

Variable n◦	Description	Units (S.I)	Symbols	Dimensional symbol
1	Building length	m	l	L
2	Building width	m	w	L
3	Building height	m	h	L
4	Gravitational acceleration	$m\ s^{-2}$	g	$L\ T^{-2}$
5	Coefficient of heat transfer	$kg\ s^{-3}\ K^{-1}$	h_c	$M\ T^{-3}\ \theta^{-1}$
6	Heat	$kg\ m^2\ s^{-2}$	Q	$M\ L^2\ T^{-2}$
7	Wind velocity	$m\ s^{-1}$	v_w	$L\ T^{-1}$
8	Temperature of air	K	T_a	θ
9	Density of air	$kg\ m^{-3}$	ρ	$M\ L^{-3}$
10	Specific heat of air	$m^2\ s^{-2}\ K^{-1}$	c_p	$L^2\ T^{-2}\ \theta^{-1}$
11	Heat transfer coefficient	$kg\ s^{-3}\ K^{-1}$	U	$M\ T^{-3}\ \theta^{-1}$
12	Dynamic viscosity of air	$kg\ m^{-1}\ s^{-1}$	μ	$M\ L^{-1}\ T^{-1}$
13	Thermal conductivity of air	$kg\ m\ s^{-3}\ K^{-1}$	k	$M\ L\ T^{-3}\ \theta^{-1}$
14	Coefficient of thermal expansion	βe	k^{-1}	θ^{-1}

Determination of π groups

The number of dimensional parameter is *n* and *r* is the number of primary dimensions. So, dimensional parameter is n = 14 and primary dimensions is k = 4. Using four selected repeating variable (l^x, $v_w{}^y$, $T_a{}^z$, and ρ^k) which together must contain L, M, T, and θ. Therefore, n - k = 10 π groups, forming the dimensionless groups are obtained:

Number of physical quantities: n = 14

Number of basic dimensions: k = 4

Pi term number: n – k = 10

Physics quantities

Building length:	l	L
Wind velocity:	v_w	$L^2 T^{-1}$
Temperature of air:	T_a	θ
Density of air:	ρ	$M L^{-3}$

Determination of π terms

$\pi_1 \rightarrow$ Variable 2: Building width, w

$$\pi_1 = l^x \cdot {v_w}^y \cdot {T_a}^z \cdot \rho^k \cdot w^1$$

$$\pi_1 = (L)^x \cdot (L\,T^{-1})^y \cdot (\theta)^z \cdot (M\,L^{-3})^k \cdot L^1$$

$$\pi_1 = (L)^{x+2y-3k+1} \cdot (T)^{-y} \cdot (M)^k \cdot (\theta)^z = L^0 \cdot T^0 \cdot M^0 \cdot \theta^0$$

$$\begin{cases} x + 2y - 3k + 1 = 0 & \rightarrow x = -1 \\ -y = 0 & \rightarrow y = 0 \\ k = 0 & \rightarrow k = 0 \\ z = 0 & \rightarrow z = 0 \end{cases}$$

$$\pi_1 = l^{-1} \cdot {v_w}^0 \cdot {T_a}^0 \cdot \rho^0 \cdot w^1$$

$$\pi_1 = w \cdot l^{-1}$$

$\pi_2 \rightarrow$ Variable 3: Building height, h

$$\pi_2 = l^x \cdot {v_w}^y \cdot {T_a}^z \cdot \rho^k \cdot h^1$$

$$\pi_2 = (L)^x \cdot (L\,T^{-1})^y \cdot (\theta)^z \cdot (M\,L^{-3})^k \cdot L^1$$

$$\pi_2 = (L)^{x+2y-3k+1} \cdot (T)^{-y} \cdot (M)^k \cdot (\theta)^z = L^0 \cdot T^0 \cdot M^0 \cdot \theta^0$$

$$\begin{cases} x + 2y - 3k + 1 = 0 & \rightarrow x = -1 \\ -y = 0 & \rightarrow y = 0 \\ k = 0 & \rightarrow k = 0 \\ z = 0 & \rightarrow z = 0 \end{cases}$$

$$\pi_2 = l^{-1} \cdot {v_w}^0 \cdot {T_a}^0 \cdot \rho^0 \cdot h^1$$

$$\pi_2 = h \cdot l^{-1}$$

$\pi_3 \rightarrow$ Variable 4: gravitational acceleration, g

$$\pi_3 = l^x \cdot {v_w}^y \cdot {T_a}^z \cdot \rho^k \cdot g^1$$

$$\pi_3 = (L)^x \cdot (L\,T^{-1})^y \cdot (\theta)^z \cdot (M\,L^{-3})^k \cdot (M\,L^{-2})^1$$

$$\pi_3 = (L)^{x+y-3k-2} \cdot (T)^{-y} \cdot (M)^{k+1} \cdot (\theta)^z = L^0 \cdot T^0 \cdot M^0 \cdot \theta^0$$

$$\begin{cases} x + y - 3k - 2 = 0 \\ -y = 0 \\ z = 0 \\ k + 1 = 0 \end{cases} \quad \begin{matrix} \rightarrow x = -1 \\ \rightarrow y = 0 \\ \rightarrow z = 0 \\ \rightarrow k = -1 \end{matrix}$$

$$\pi_3 = l^{-1} \cdot {v_w}^0 \cdot {T_a}^0 \cdot \rho^{-1} \cdot g^1$$

$$\pi_3 = g \cdot l^{-1} \cdot \rho^{-1}$$

$\pi_4 \rightarrow$ Variable 5: Coefficient of heat transfer, h_c

$$\pi_4 = l^x \cdot {v_w}^y \cdot {T_a}^z \cdot \rho^k \cdot {h_c}^1$$

$$\pi_4 = (L)^x \cdot (L\,T^{-1})^y \cdot (\theta)^z \cdot (M\,L^{-3})^k \cdot (M\,T^{-3}\,\theta^{-1})^1$$

$$\pi_4 = (L)^{x+y-3k} \cdot (T)^{-y-3} \cdot (M)^{k+1} \cdot (\theta)^{z-1} = L^0 \cdot T^0 \cdot M^0 \cdot \theta^0$$

$$\begin{cases} x + y - 3k = 0 \\ -y - 3 = 0 \\ k + 1 = 0 \\ z - 1 = 0 \end{cases} \quad \begin{matrix} \rightarrow x = 0 \\ \rightarrow y = -3 \\ \rightarrow k = -1 \\ \rightarrow z = 1 \end{matrix}$$

$$\pi_4 = l^0 \cdot {v_w}^{-3} \cdot {T_a}^1 \cdot \rho^{-1} \cdot {h_c}^1$$

$$\pi_4 = {v_w}^{-3} \cdot {T_a}^1 \cdot \rho^{-1} \cdot {h_c}^1$$

$\pi_5 \rightarrow$ Variable 6: Heat, Q

$$\pi_5 = l^x \cdot {v_w}^y \cdot {T_a}^z \cdot \rho^k \cdot Q^1$$

$$\pi_5 = (L)^x \cdot (L\,T^{-1})^y \cdot (\theta)^z \cdot (M\,L^{-3})^k \cdot (M\,L^2T^{-2})^1$$

$$\pi_5 = (L)^{x+y-3k+2} \cdot (T)^{-y-2} \cdot (M)^{k+1} \cdot (\theta)^z = L^0 \cdot T^0 \cdot M^0 \cdot \theta^0$$

$$\begin{cases} x + y - 3k + 2 = 0 \\ -y - 2 = 0 \\ z = 0 \\ k + 1 = 0 \end{cases} \quad \begin{matrix} \rightarrow x = -3 \\ \rightarrow y = -2 \\ \rightarrow z = 0 \\ \rightarrow k = -1 \end{matrix}$$

$$\pi_5 = l^{-3} \cdot {v_w}^{-2} \cdot {T_a}^0 \cdot \rho^{-1} \cdot Q^1$$

$$\pi_5 = Q \cdot l^{-3} \cdot {v_w}^{-2} \cdot \rho^{-1}$$

$\pi_6 \rightarrow$ Variable 10: Specific heat of air, c_p

$$\pi_6 = l^x \cdot {v_w}^y \cdot {T_a}^z \cdot \rho^k \cdot {c_p}^1$$

$$\pi_6 = (L)^x \cdot (L\,T^{-1})^y \cdot (\theta)^z \cdot (M\,L^{-3})^k \cdot (L^2\,T^{-2}\,\theta^{-1})^1$$

$$\pi_6 = (L)^{x+y-3k+2} \cdot (T)^{-y-2} \cdot (M)^k \cdot (\theta)^{z-1} = L^0 \cdot T^0 \cdot M^0 \cdot \theta^0$$

$$\begin{cases} x + y - 3k + 2 = 0 \\ -y - 2 = 0 \\ z - 1 = 0 \\ k = 0 \end{cases} \quad \begin{array}{l} \rightarrow x = 0 \\ \rightarrow y = -2 \\ \rightarrow z = 1 \\ \rightarrow k = 0 \end{array}$$

$$\pi_6 = l^0 \cdot {v_w}^{-2} \cdot {T_a}^1 \cdot \rho^0 \cdot {c_p}^1$$

$$\pi_6 = c_p \cdot {v_w}^{-2} \cdot T_a$$

$\pi_7 \rightarrow$ Variable 11: Heat transfer coefficient, U

$$\pi_7 = l^x \cdot {v_w}^y \cdot {T_a}^z \cdot \rho^k \cdot U^1$$

$$\pi_7 = (L)^x \cdot (L\,T^{-1})^y \cdot (\theta)^z \cdot (M\,L^{-3})^k \cdot (M\,T^{-3}\,\theta^{-1})^1$$

$$\pi_7 = (L)^{x+y-3k} \cdot (T)^{-y-3} \cdot (M)^{k+1} \cdot (\theta)^{z-1} = L^0 \cdot T^0 \cdot M^0 \cdot \theta^0$$

$$\begin{cases} x + y - 3k = 0 \\ -y - 3 = 0 \\ z - 1 = 0 \\ k + 1 = 0 \end{cases} \quad \begin{array}{l} \rightarrow x = 0 \\ \rightarrow y = -3 \\ \rightarrow z = 1 \\ \rightarrow k = -1 \end{array}$$

$$\pi_7 = l^0 \cdot {v_w}^{-3} \cdot {T_a}^1 \cdot \rho^{-1} \cdot U^1$$

$$\pi_7 = U \cdot {v_w}^{-3} \cdot {T_a}^1 \cdot \rho^{-1}$$

$\pi_8 \rightarrow$ Variable 12: Dynamic viscosity of air, μ

$$\pi_8 = l^x \cdot {v_w}^y \cdot {T_a}^z \cdot \rho^k \cdot \mu^1$$

$$\pi_8 = (L)^x \cdot (L\,T^{-1})^y \cdot (\theta)^z \cdot (M\,L^{-3})^k \cdot (M\,L^{-1}\,T^{-1})^1$$

$$\pi_8 = (L)^{x+2y-3k-1} \cdot (T)^{-y-1} \cdot (M)^{k+1} \cdot (\theta)^z = L^0 \cdot T^0 \cdot M^0 \cdot \theta^0$$

$$\begin{cases} x + 2y - 3k - 1 = 0 \\ -y - 1 = 0 \\ z = 0 \\ k + 1 = 0 \end{cases} \quad \begin{array}{l} \rightarrow x = -1 \\ \rightarrow y = -1 \\ \rightarrow z = 0 \\ \rightarrow k = -1 \end{array}$$

$$\pi_8 = l^{-1} \cdot {v_w}^{-1} \cdot {T_a}^0 \cdot \rho^{-1} \cdot \mu^1$$

$$\pi_8 = \mu \cdot l^{-1} \cdot {v_w}^{-1} \cdot \rho^{-1}$$

$\pi_9 \rightarrow$ Variable 13: Thermal conductivity of air, k

$$\pi_9 = l^x \cdot {v_w}^y \cdot {T_a}^z \cdot \rho^k \cdot k^1$$

$$\pi_9 = (L)^x \cdot (L\,T^{-1})^y \cdot (\theta)^z \cdot (M\,L^{-3})^k \cdot (M\,L\,T^{-3}\theta^{-1})^1$$

$$\pi_9 = (L)^{x+2y-3k+1} \cdot (T)^{-y-3} \cdot (M)^{k+1} \cdot (\theta)^{z-1} = L^0 \cdot T^0 \cdot M^0 \cdot \theta^0$$

$$\begin{cases} x + y - 3k + 1 = 0 \\ -y - 3 = 0 \\ z - 1 = 0 \\ k + 1 = 0 \end{cases} \begin{matrix} \rightarrow x = -1 \\ \rightarrow y = -3 \\ \rightarrow z = 1 \\ \rightarrow k = -1 \end{matrix}$$

$$\pi_9 = l^{-1} \cdot {v_w}^{-3} \cdot {T_a}^{1} \cdot \rho^{-1} \cdot k^{1}$$

$$\pi_9 = k \cdot l^{-1} \cdot {v_w}^{-3} \cdot {T_a}^{1} \cdot \rho^{-1}$$

$\pi_{10} \rightarrow$ Variable 14: Coefficient of thermal expansion, β_e

$$\pi_{10} = l^{x} \cdot {v_w}^{y} \cdot {T_a}^{z} \cdot \rho^{k} \cdot {\beta_e}^{1}$$

$$\pi_{10} = (L)^{x} \cdot (L\,T^{-1})^{y} \cdot (\theta)^{z} \cdot (M\,L^{-3})^{k} \cdot (\theta^{-1})^{1}$$

$$\pi_{10} = (L)^{x+y-3k} \cdot (T)^{-y} \cdot (M)^{k} \cdot (\theta)^{z-1} = L^{0} \cdot T^{0} \cdot M^{0} \cdot \theta^{0}$$

$$\begin{cases} x + y - 3k = 0 \\ -y = 0 \\ z - 1 = 0 \\ k = 0 \end{cases} \begin{matrix} \rightarrow x = 0 \\ \rightarrow y = 0 \\ \rightarrow z = 1 \\ \rightarrow k = 0 \end{matrix}$$

$$\pi_{10} = l^{0} \cdot {v_w}^{0} \cdot {T_a}^{1} \cdot \rho^{0} \cdot {\beta_e}^{1}$$

$$\pi_{10} = \beta_e \cdot T_a$$

Table D.2 - Pi terms and independent dimensionless found.

Term nº	Pi term
1	$\pi_1 = w \cdot l^{-1}$
2	$\pi_2 = h \cdot l^{-1}$
3	$\pi_3 = g \cdot l^{-1} \cdot \rho^{-1}$
4	$\pi_4 = {v_w}^{-3} \cdot {T_a}^{1} \cdot \rho^{-1} \cdot {h_c}^{1}$
5	$\pi_5 = Q \cdot l^{-3} \cdot {v_w}^{-2} \cdot \rho^{-1}$
6	$\pi_6 = c_p \cdot {v_w}^{-2} \cdot T_a$
7	$\pi_7 = U \cdot {v_w}^{-3} \cdot {T_a}^{1} \cdot \rho^{-1}$
8	$\pi_8 = \mu \cdot l^{-1} \cdot {v_w}^{-1} \cdot \rho^{-1}$
9	$\pi_9 = k \cdot l^{-1} \cdot {v_w}^{-3} \cdot {T_a}^{1} \cdot \rho^{-1}$
10	$\pi_{10} = \beta_e \cdot T_a$

However, the group calculated was certificated using the dimensions (LTMθ).

According Newton's Second Law, $F = m \cdot a$, the mass can be written as $m = \rho \cdot \forall$ and if the volume had dimension of L^3, $m \propto \rho \cdot L^3$. The acceleration can be rewritten as $a = dv/ds = v \cdot dv/ds$. So, $F \propto \rho \cdot V^2 \cdot L^2$ (Fox and McDonald, 1998).

$$F = m \cdot a \ \therefore F = kg \cdot m \cdot s^{-2} \therefore F = M \cdot L \cdot T^{-2} \ \therefore M = F \cdot L^{-1} \cdot T^{2}$$

Thus we get,

$$[\pi_1] = [l]^x \cdot [v_w]^y \cdot [T_a]^z \cdot [\rho]^k \cdot [w]^1$$
$$[\pi_1] = [L]^{-1} \cdot [L\ T^{-1}]^0 \cdot [\theta]^0 \cdot [M\ L^{-3}]^0 \cdot [L]^1$$
$$[\pi_1] = [L^{-1}] \cdot [L^0\ T^0] \cdot [\theta^0] \cdot [M^0\ L^0] \cdot [L^1]$$
$$[\pi_1] = 1$$

$$[\pi_2] = [l]^x \cdot [v_w]^y \cdot [T_a]^z \cdot [\rho]^k \cdot [h]^1$$
$$[\pi_2] = [L]^{-1} \cdot [L\ T^{-1}]^0 \cdot [\theta]^0 \cdot [M\ L^{-3}]^0 \cdot [L]^1$$
$$[\pi_2] = [L^{-1}] \cdot [L^0\ T^0] \cdot [\theta^0] \cdot [M^0\ L^0] \cdot [L^1]$$
$$[\pi_2] = 1$$

$$[\pi_3] = [l]^x \cdot [v_w]^y \cdot [T_a]^z \cdot [\rho]^k \cdot [g]^1$$
$$[\pi_3] = [L]^{-1} \cdot [L\ T^{-1}]^0 \cdot [\theta]^0 \cdot [M\ L^{-3}]^{-1} \cdot [M\ L^{-2}]^1$$
$$[\pi_3] = [L^{-1}] \cdot [L^0\ T^0] \cdot [\theta^0] \cdot [M^{-1}\ L^3] \cdot [M\ L^{-2}]$$
$$[\pi_3] = 1$$

$$[\pi_4] = [l]^x \cdot [v_w]^y \cdot [T_a]^z \cdot [\rho]^k \cdot [h_c]^1$$
$$[\pi_4] = [L]^0 \cdot [L\ T^{-1}]^{-3} \cdot [\theta]^1 \cdot [M\ L^{-3}]^{-1} \cdot [M\ T^{-3}\ \theta^{-1}]^1$$
$$[\pi_4] = [L^0] \cdot [L^{-3}\ T^3] \cdot [\theta^1] \cdot [M^{-1}\ L^3] \cdot [M\ T^{-3}\ \theta^{-1}]$$
$$[\pi_4] = 1$$

$$[\pi_5] = [l]^x \cdot [v_w]^y \cdot [T_a]^z \cdot [\rho]^k \cdot [Q]^1$$
$$[\pi_5] = [L]^{-3} \cdot [L\ T^{-1}]^{-2} \cdot [\theta]^0 \cdot [M\ L^{-3}]^{-1} \cdot [M\ L^2\ T^{-2}]^1$$
$$[\pi_5] = [L^{-3}] \cdot [L^{-2}\ T^2] \cdot [\theta^0] \cdot [M^{-1}\ L^3] \cdot [M^1\ L^2\ T^{-2}]$$
$$[\pi_5] = 1$$

$$[\pi_6] = [l]^x \cdot [v_w]^y \cdot [T_a]^z \cdot [\rho]^k \cdot [c_p]^1$$
$$[\pi_6] = [L]^0 \cdot [L\ T^{-1}]^{-2} \cdot [\theta]^1 \cdot [M\ L^{-3}]^0 \cdot [L^2\ T^{-2}\ \theta^{-1}]^1$$
$$[\pi_6] = [L^0] \cdot [L^{-2}\ T^2] \cdot [\theta^1] \cdot [M^0\ L^0] \cdot [L^2\ T^{-2}\ \theta^{-1}]$$
$$[\pi_6] = 1$$

$$[\pi_7] = [l]^x \cdot [v_w]^y \cdot [T_a]^z \cdot [\rho]^k \cdot [U]^1$$
$$[\pi_7] = [L]^0 \cdot [L\ T^{-1}]^{-3} \cdot [\theta]^1 \cdot [M\ L^{-3}]^{-1} \cdot [M\ T^{-3}\ \theta^{-1}]^1$$
$$[\pi_7] = [L^0] \cdot [L^{-3}\ T^3] \cdot [\theta^1] \cdot [M^{-1}\ L^3] \cdot [M\ T^{-3}\ \theta^{-1}]$$
$$[\pi_7] = 1$$

$$[\pi_8] = [l]^x \cdot [v_w]^y \cdot [T_a]^z \cdot [\rho]^k \cdot [\mu]^1$$
$$[\pi_8] = [L]^{-1} \cdot [L\ T^{-1}]^{-1} \cdot [\theta]^0 \cdot [M\ L^{-3}]^{-1} \cdot [M\ L^{-1}\ T^{-1}]^1$$
$$[\pi_8] = [L^{-1}] \cdot [L^{-1}\ T^1] \cdot [\theta^0] \cdot [M^{-1}\ L^3] \cdot [M\ L^{-1}\ T^{-1}]$$
$$[\pi_8] = 1$$

$$[\pi_9] = [l]^x \cdot [v_w]^y \cdot [T_a]^z \cdot [\rho]^k \cdot [k]^1$$
$$[\pi_9] = [L]^{-1} \cdot [L\ T^{-1}]^{-3} \cdot [\theta]^1 \cdot [M\ L^{-3}]^{-1} \cdot [M\ L\ T^{-3}\theta^{-1}]^1$$
$$[\pi_9] = [L^{-1}] \cdot [L^{-3}\ T^3] \cdot [\theta^1] \cdot [M^{-1}\ L^3] \cdot [M\ L\ T^{-3}\theta^{-1}]$$
$$[\pi_9] = 1$$

$$[\pi_{10}] = [l]^x \cdot [v_w]^y \cdot [T_a]^z \cdot [\rho]^k \cdot [\beta_e]^1$$
$$[\pi_{10}] = [L]^0 \cdot [L\ T^{-1}]^0 \cdot [\theta]^1 \cdot [M\ L^{-3}]^0 \cdot [\theta^{-1}]^1$$
$$[\pi_{10}] = [L^0] \cdot [L^0\ T^0] \cdot [\theta^1] \cdot [M^0\ L^0] \cdot [\theta^{-1}]$$
$$[\pi_{10}] = 1$$

D.2 - The dimensionless groups found

D.2.1 - Reynolds number (R_e):

$$\pi_8 = \mu \cdot l^{-1} \cdot {v_w}^{-1} \cdot \rho^{-1} = 1/R_e$$

The Reynolds number (R_e) expresses the ratio of inertial forces to viscous forces, defined by $R_e = V\ L\ \nu^{-1} = V\ L\ \mu\ \rho^{-1}$.

Where, V: velocity of the fluid, (m s^{-1}); L: dimension, (m); ν: kinematic viscosity, (m^2 s^{-1}); μ: dynamic viscosity, (kg m^{-1} s^{-1}); and ρ: density of the fluid, (kg m^{-3}).

D.2.2 - Eckert number (E_c):

$$\pi_6 = c_p \cdot {v_w}^{-2} \cdot T_a = 1/E_c$$

The Eckert number (E_c) is used to calculate flow. It is expresses the relationship between a flow`s kinetic energy and enthalpy, thus is used to characterize dissipation. It is defined as $E_c = \frac{V^2}{c_p \cdot \Delta t}$ =kinect energy/enthalpy.

where, C_p: specific heat of the fluid, (J kg^{-1} K^{-1}); and Δt: temperature difference of the flow, (K).

D.2.3 - Prandtl number (P_r):

$$\frac{\pi_6 \cdot \pi_8}{\pi_9} = \mu \cdot c_p \cdot k^{-1} = P_r$$

Prandtl number (P_r) is the ratio of momentum diffusivity (kinematic viscosity) to thermal diffusivity. The P_r is defined as:

$$P_r = \frac{\nu}{\alpha} = \frac{\text{Viscous diffusion rate}}{\text{Thermal diffusion rate}} = \frac{C_p \cdot \mu}{k}$$

where, α: thermal diffusivity, (m^2 s^{-1}); and k: thermal conductivity, (W m^{-1} K^{-1}).

D.2.4 - Peclet number (P_e):

$$\frac{\pi_6}{\pi_9} = \rho \cdot c_p \cdot v_w \cdot l \cdot k^{-1} = R_e \cdot P_r$$

Peclet number (P_e) is the ratio between the rates of heat transfer by conduction and advection, defined by $V \cdot L \cdot \alpha^{-1} = (R_e \cdot P_r)$.

D.2.5 - Grashof number (G_r):

$$\frac{\pi_3 \cdot \pi_{10}}{(\pi_8)^2} = \frac{g \cdot \beta_e \cdot (T_s - T_\infty) \cdot L^3}{\nu^2} = \frac{\text{Buoyant force}}{\text{Viscous force}} = G_r \therefore \nu = \frac{\mu}{\rho}$$

The Grashof number is a dimensionless quantity used in analyzing the velocity distribution in free convection systems. In the systems encountered most commonly in CBP barns, free convection is the natural tendency of the wind (air movement) to migrate due to some driving force. In free convection, the driving force is a buoyancy force caused by a temperature gradient, as the fluid would be at rest in the absence of temperature variations. The Grashof number is analogous to the Reynolds number in forced convection.

D.2.6 - Nusselt number (N_u):

$$\frac{\pi_4}{\pi_9} = h_c \cdot l \cdot k^{-1} = N_u$$

A dimensionless number used in the study of forced convection which gives a measure of the ratio of the total heat transfer to conductive heat transfer, and is equal to the heat transfer coefficient times a characteristic length divided by the thermal conductivity.

D.3 - Calculate of air speed and floor surface temperature to the full model

a) Air speed in the full model:

$$[\mathrm{Re}]_{\mathrm{Model}} = [\mathrm{Re}]_{\mathrm{Full}}$$

$$\left(\frac{\rho \cdot v \cdot L}{\mu}\right)_{\mathrm{Model}} = \left(\frac{\rho \cdot v \cdot L}{\mu}\right)_{\mathrm{Full}}$$

$$\left(\frac{\rho}{\mu}\right)_{\mathrm{Model}} = \left(\frac{\rho}{\mu}\right)_{\mathrm{Full}}$$

Then,

$$(v \cdot L)_{\mathrm{Model}} = (v \cdot L)_{\mathrm{Full}}$$

So, scale used in this reduce model was 1:16,

$$V_{\mathrm{model}} = \frac{V_{\mathrm{Full}}}{16}$$

According Table 4.1, the air speed found in the Barn 24, which was used as a base to build the reduced model, was 0.7 m s^{-1}. Then,

$$V_{\mathrm{model}} = 0.7 \text{ m s}^{-1} / 16$$

$$V_{\mathrm{model}} = 0.04 \text{ m s}^{-1}$$

b) Temperature of the floor in the full model:

Using the Pi terms found in Appendix - Table C.2:

$$\pi_6 = Q \cdot l^{-3} \cdot {v_w}^{-2} \cdot \rho^{-1}$$

$$(Q \cdot l^{-3} \cdot v_w{}^{-2} \cdot \rho^{-1})_{Model} = (Q \cdot l^{-3} \cdot v_w{}^{-2} \cdot \rho^{-1})_{Full}$$

$$(\rho^{-1})_{Model} = (\rho^{-1})_{Full}$$

Then,

$$(Q \cdot l^{-3} \cdot v_w{}^{-2})_{Model} = (Q \cdot l^{-3} \cdot v_w{}^{-2})_{Full}$$

l_{model} = 1.35 m (Figure 3.22);

$v_{w\ model}$ = 0.04 m s^{-1}

l_{full} = 21.6 m

$v_{w\ model}$ = 0.7 m s^{-1} (Table 4.1)

So, using these values in the equation above:

$$(Q \cdot 1.35^{-3} \cdot 0.04^{-2})_{Model} = (Q \cdot 21.6^{-3} \cdot 0.7^{-2})_{Full}$$

$$(Q)_{Model} = 7.97 \cdot 10^{-5} \cdot (Q)_{Full}$$

Calculating the heat flux in the compost area:

i) Average temperatures: floor surface (T_s), compost at 0.2 m deep (T_c), and the environment (T_{air}):

T_s = 7.2°C = 280.35 K → Appendix - Table A.4 → Barn 24;

T_{air} = 6.9°C = 280.05 K → Table 4.1→ Barn 24;

ii) Properties of the mean air temperature (Values in Appendix - Table D.3):

Variable	Value	Unit (S.I)
ρ	1.2613	kg m^{-3}
ν	1.39 ·10^{-5}	m^2 s^{-1}
k	0.024626	W m^{-1} K^{-1}
β	0.0035708	K^{-1}
L	21.6	m
Pr	0.718	

$$G_r = g \cdot \beta \cdot (T_s - T_\infty) \cdot L^3 \cdot \nu^{-2}$$

$$G_r = 5.46 \cdot 10^{11}$$

For calculating the Nusselt number (N_u) of equation (D.2.6), is recommended by McAdams (1954) using the equation (D.2.7) for Gr > 10^9 where the heat transfer coefficient is independent of the length (L).

$$N_u = 0.13 \cdot (Gr \cdot Pr)^{1/3} = 951.4 \quad \text{(E.1)}$$

Then, the coefficients of heat transfer is:

$$h = \frac{k \cdot N_u}{L} = 1.08 \text{ W m}^{-2} \text{ K}^{-1}$$

The heat transfer in the full scale CBP barn is:

$$Q_{full} = h \cdot A \cdot \Delta T$$

$$Q_{full} = 106.8 \text{ W}$$

So,

$$(Q)_{Model} = 7.97 \cdot 10^{-7} \cdot (Q)_{Full}$$

The value of heat flux (q''_{model}) is:

$$q''_{model} \approx 1 \cdot 10^{-1} \text{ W m}^{-2}$$

Table D.3 - Thermal properties of the air at atmospheric pressure.

T (K)	ρ (kg m^{-3})	c_p (kJ kg^{-1} K^{-1})	$\mu \cdot 10^7$ (kJ kg^{-1} K^{-1})	$\nu \cdot 10^7$ (m^2 s^{-1})	$k \cdot 10^7$ (W m^{-1} K^{-1})	$\alpha \cdot 10^7$ (m^2 s^{-1})	Pr
200	1.7458	1.007	132.5	7.590	18.1	10.3	0.737
250	1.3947	1.006	159.6	11.44	22.3	15.9	0.720
300	1.1614	1.007	184.6	15.89	26.3	22.5	0.707
350	0.9950	1.009	208.2	20.92	30.0	29.9	0.700

Source: Incropera and DeWitt (2001).

APPENDIX E

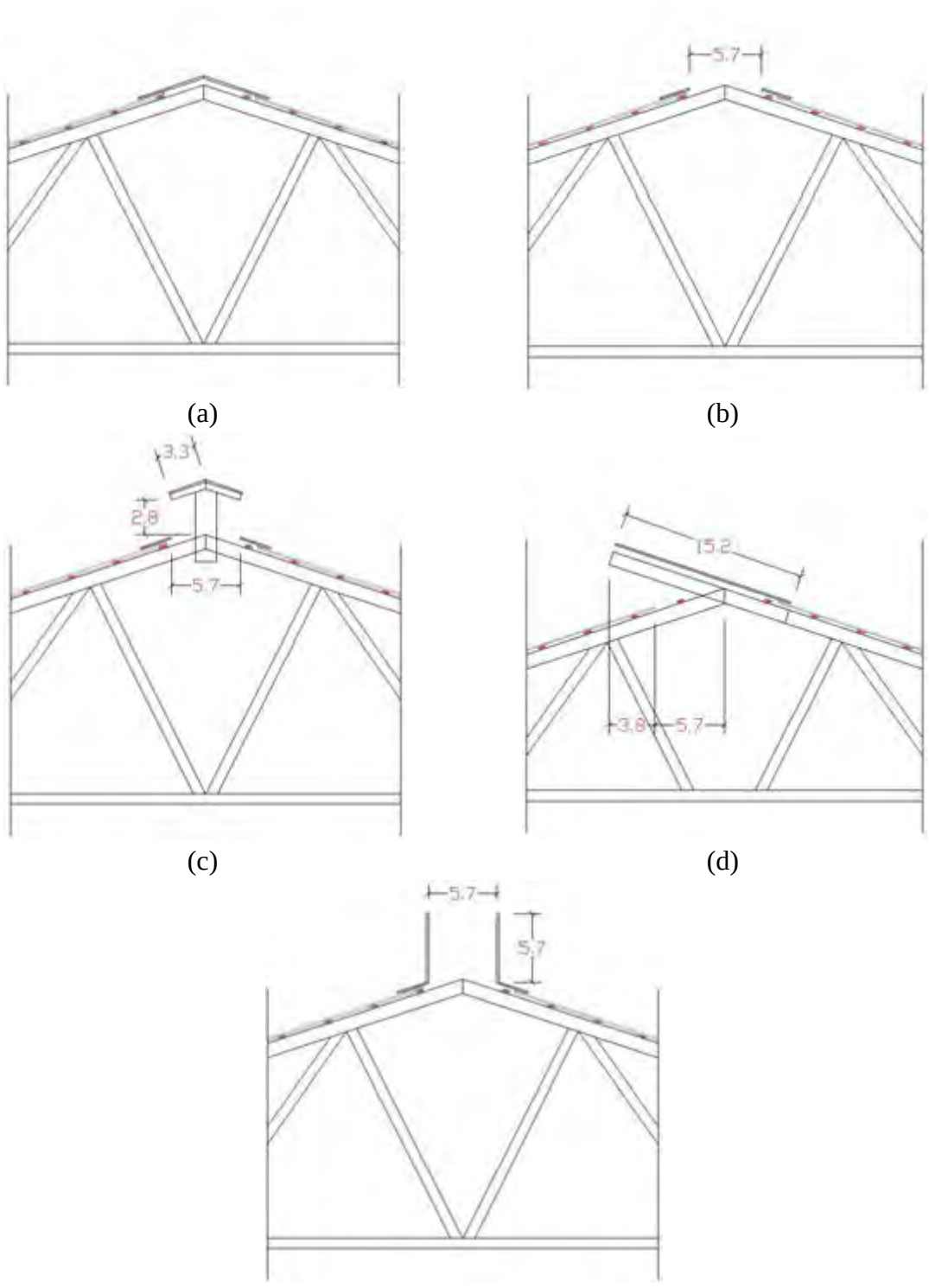

(a) (b) (c) (d) (e)

Figure E.1 - Types of ridge vents: (a) closed ridge - CLR, (b) open ridge - OPR, (c) elevated ridge - ELR, (d) overshot ridge - OVR, and (e) open ridge with chimney - ORC, used in presented study. Dimensions in centimeters (cm).

APPENDIX F

Table F.1 - Analysis of variance to particle weight fractions for all compost material.

TABELA DE ANÁLISE DE VARIÂNCIA

FV	GL	SQ	QM	Fc	Pr>Fc
trat	5	28289.661189	5657.932238	81.537	0.0000
erro	246	17070.190471	69.391018		
Total corrigido	251	45359.851660			

CV (%) = 49.98
Média geral: 16.6668254 Número de observações: 252

Teste Tukey para a FV trat

DMS: 5.22235316385467 NMS: 0.05

Média harmonica do número de repetições (r): 42
Erro padrão: 1.285366523386

Tratamentos	Médias	Resultados do teste
Finer	30.104286	a
PS2	26.051429	a b
PS5	24.710714	b
PS4	10.243095	c
Coarser	4.797619	d
PS3	4.093810	d

Table F.2 - Analysis of variance to thermal conductivity in different particle weight fractions for all compost materials.

Variável analisada: Thermal conductivity

Opção de transformação: Variável sem transformação (Y)

TABELA DE ANÁLISE DE VARIÂNCIA

FV	GL	SQ	QM	Fc	Pr>Fc
TRAT	4	0.747026	0.186757	47.816	0.0000
erro	205	0.800678	0.003906		
Total corrigido	209	1.547704			

CV (%) = 31.58
Média geral: 0.1978810 Número de observações: 210

Teste Tukey para a FV TRAT

DMS: 0.0375439678889858 NMS: 0.05

Média harmonica do número de repetições (r): 42
Erro padrão: 0.00964333747961254

Tratamentos	Médias	Resultados do teste
PS5	0.310738	a
PS4	0.200286	b
PS3	0.179524	b c
PS2	0.151833	c
Finer	0.147024	c

Table F.3 - Analysis of variance to thermal resistivity in different particle weight fractions for all compost materials.

```
------------------------------------------------------------------------------
                    TABELA DE ANÁLISE DE VARIÂNCIA
------------------------------------------------------------------------------
FV                     GL                 SQ               QM         Fc  Pr>Fc
------------------------------------------------------------------------------
TRAT                    4     2682694.497429     670673.624357     46.878 0.0000
erro                  205     2932874.110238      14306.702977
------------------------------------------------------------------------------
Total corrigido       209     5615568.607667
------------------------------------------------------------------------------
CV  (%) =              20.25
Média geral:        590.6966667      Número de observações:          210
------------------------------------------------------------------------------
   Teste Tukey para a FV TRAT
------------------------------------------------------------------------------
DMS: 71.8551564486023  NMS: 0.05
------------------------------------------------------------------------------
Média harmonica do número de repetições (r): 42
Erro padrão: 18.4563210082947
------------------------------------------------------------------------------
Tratamentos                          Médias      Resultados do teste
------------------------------------------------------------------------------
Finer                               722.588095   a
PS2                                 682.300000   a
PS3                                 599.785714     b
PS4                                 548.421429     b
PS5                                 400.388095       c
------------------------------------------------------------------------------
```

Table F.4 - Multiple linear regression to thermal conductivity in function moisture content and static compaction degree for Green sawdust.

Multiple Linear Regression

Data source: Data 1 in Notebook2

Col 3 = -0.0619 + (0.311 * Col 1) + (0.478 * Col 2)

N = 18

R = 0.916 Rsqr = 0.838 Adj Rsqr = 0.817

Standard Error of Estimate = 0.038

	Coefficient	**Std. Error**	**t**	**P**	**VIF**
Constant	-0.0619	0.0350	-1.767	0.098	
Col 1	0.311	0.0525	5.924	<0.001	1.000
Col 2	0.478	0.0732	6.529	<0.001	1.000

Analysis of Variance:

	DF	**SS**	**MS**	**F**	**P**
Regression	2	0.113	0.0563	38.863	<0.001
Residual	15	0.0217	0.00145		
Total	17	0.134	0.00790		

Column	**SSIncr**	**SSMarg**
Col 1	0.0508	0.0508
Col 2	0.0617	0.0617

The dependent variable Col 3 can be predicted from a linear combination of the independent variables:

	P		
Col 1	<0.001	Col 2	<0.001

Table F.5 - Multiple linear regression to thermal conductivity in function moisture content and static compaction degree for Kiln-dried shavings or sawdust.

Multiple Linear Regression
Data source: Data 1 in Notebook2

Col 3 = -0.0679 + (0.342 * Col 1) + (0.487 * Col 2)

N = 18

R = 0.937 Rsqr = 0.877 Adj Rsqr = 0.861

Standard Error of Estimate = 0.034

	Coefficient	Std. Error	t	P	VIF
Constant	-0.0679	0.0315	-2.154	0.048	
Col 1	0.342	0.0472	7.233	<0.001	1.000
Col 2	0.487	0.0658	7.404	<0.001	1.000

Analysis of Variance:

	DF	SS	MS	F	P
Regression	2	0.125	0.0627	53.561	<0.001
Residual	15	0.0176	0.00117		
Total	17	0.143	0.00841		

Column	SSIncr	SSMarg
Col 1	0.0612	0.0612
Col 2	0.0642	0.0642

The dependent variable Col 3 can be predicted from a linear combination of the independent variables:

	P
Col 1	<0.001
Col 2	<0.001

Table F.6 - Multiple linear regression to thermal conductivity in function moisture content and static compaction degree for Mix.

Multiple Linear Regression
Data source: Data 1 in Notebook2

Col 3 = -0.0537 + (0.360 * Col 1) + (0.434 * Col 2)
N = 18

R = 0.911 Rsqr = 0.829 Adj Rsqr = 0.806

Standard Error of Estimate = 0.040

	Coefficient	Std. Error	t	P	VIF
Constant	-0.0537	0.0373	-1.441	0.170	
Col 1	0.360	0.0558	6.453	<0.001	1.000
Col 2	0.434	0.0779	5.578	<0.001	1.000

Analysis of Variance:

	DF	SS	MS	F	P
Regression	2	0.119	0.0595	36.375	<0.001
Residual	15	0.0246	0.00164		
Total	17	0.144	0.00845		

Column	SSIncr	SSMarg
Col 1	0.0681	0.0681
Col 2	0.0509	0.0509

The dependent variable Col 3 can be predicted from a linear combination of the independent variables:

	P
Col 1	<0.001
Col 2	<0.001

Table F.7 - Multiple linear regression to thermal conductivity in function moisture content and dynamic compaction degree for Green sawdust.

Multiple Linear Regression
Data source: Data 1 in Notebook5

Col 3 = -0.131 + (0.269 * Col 1) + (0.689 * Col 2)

N = 12

R = 0.962 Rsqr = 0.925 Adj Rsqr = 0.908

Standard Error of Estimate = 0.030

	Coefficient	Std. Error	t	P	VIF
Constant	-0.131	0.0376	-3.481	0.007	
Col 1	0.269	0.0762	3.535	0.006	1.000
Col 2	0.689	0.0696	9.907	<0.001	1.000

Analysis of Variance:

	DF	SS	MS	F	P
Regression	2	0.0965	0.0482	55.323	<0.001
Residual	9	0.00785	0.000872		
Total	11	0.104	0.00948		

Column	SSIncr	SSMarg
Col 1	0.0109	0.0109
Col 2	0.0856	0.0856

The dependent variable Col 3 can be predicted from a linear combination of the independent variables:

	P
Col 1	0.006
Col 2	<0.001

Table F.8 - Multiple linear regression to thermal conductivity in function moisture content and dynamic compaction degree for Kiln-dried shavings or sawdust.

Multiple Linear Regression
Data source: Data 1 in Notebook5

Col 3 = -0.127 + (0.271 * Col 1) + (0.680 * Col 2)

N = 12

R = 0.978 Rsqr = 0.956 Adj Rsqr = 0.947

Standard Error of Estimate = 0.022

	Coefficient	Std. Error	t	P	VIF
Constant	-0.127	0.0278	-4.556	0.001	
Col 1	0.271	0.0564	4.803	<0.001	1.000
Col 2	0.680	0.0515	13.218	<0.001	1.000

Analysis of Variance:

	DF	SS	MS	F	P
Regression	2	0.0943	0.0471	98.891	<0.001
Residual	9	0.00429	0.000477		
Total	11	0.0986	0.00896		

Column	SSIncr	SSMarg
Col 1	0.0110	0.0110
Col 2	0.0833	0.0833

The dependent variable Col 3 can be predicted from a linear combination of the independent variables:

	P
Col 1	<0.001
Col 2	<0.001

Table F.9 - Multiple linear regression to thermal conductivity in function moisture content and dynamic compaction degree for Mix.

Multiple Linear Regression
Data source: Data 1 in Notebook5

Col 3 = -0.112 + (0.00193 * Col 1) + (0.623 * Col 2)
N = 12

R = 0.966 Rsqr = 0.934 Adj Rsqr = 0.919

Standard Error of Estimate = 0.025

	Coefficient	Std. Error	t	P	VIF
Constant	-0.112	0.0322	-3.484	0.007	
Col 1	0.00193	0.000450	4.294	0.002	1.000
Col 2	0.623	0.0596	10.442	<0.001	1.000

Analysis of Variance:

	DF	SS	MS	F	P
Regression	2	0.0816	0.0408	63.737	<0.001
Residual	9	0.00576	0.000640		
Total	11	0.0873	0.00794		

Column	SSIncr	SSMarg
Col 1	0.0118	0.0118
Col 2	0.0698	0.0698

The dependent variable Col 3 can be predicted from a linear combination of the independent variables:

	P
Col 1	0.002
Col 2	<0.001

Table F.10 - Multiple linear regression to thermal resistivity in function moisture content and static compaction degree for Green sawdust.

Multiple Linear Regression
Data source: Data 1 in Notebook6

Col 3 = 1229.382 - (825.693 * Col 1) - (1099.412 * Col 2)

N = 18

R = 0.968 Rsqr = 0.938 Adj Rsqr = 0.930

Standard Error of Estimate = 54.938

	Coefficient	Std. Error	t	P	VIF
Constant	1229.382	50.603	24.295	<0.001	
Col 1	-825.693	75.821	-10.890	<0.001	1.000
Col 2	-1099.412	105.728	-10.399	<0.001	1.000

Analysis of Variance:

	DF	SS	MS	F	P
Regression	2	684279.297	342139.648	113.361	<0.001
Residual	15	45272.289	3018.153		
Total	17	729551.586	42914.799		

Column	SSIncr	SSMarg
Col 1	357928.582	357928.582
Col 2	326350.715	326350.715

The dependent variable Col 3 can be predicted from a linear combination of the independent variables:

	P
Col 1	<0.001
Col 2	<0.001

Table F.11 - Multiple linear regression to thermal resistivity in function moisture content and static compaction degree for Kiln-dried shavings or sawdust.

Multiple Linear Regression
Data source: Data 1 in Notebook6

Col 3 = 1282.485 - (972.177 * Col 1) - (1164.851 * Col 2)

N = 18

R = 0.964 Rsqr = 0.929 Adj Rsqr = 0.920

Standard Error of Estimate = 66.245

	Coefficient	Std. Error	t	P	VIF
Constant	1282.485	61.018	21.018	<0.001	
Col 1	-972.177	91.427	-10.633	<0.001	1.000
Col 2	-1164.851	127.489	-9.137	<0.001	1.000

Analysis of Variance:

	DF	SS	MS	F	P
Regression	2	862548.929	431274.464	98.276	<0.001
Residual	15	65826.234	4388.416		
Total	17	928375.163	54610.304		

Column	SSIncr	SSMarg
Col 1	496191.886	496191.886
Col 2	366357.043	366357.043

The dependent variable Col 3 can be predicted from a linear combination of the independent variables:

	P
Col 1	<0.001
Col 2	<0.001

Table F.12 - Multiple linear regression to thermal resistivity in function moisture content and static compaction degree for Mix.

Multiple Linear Regression
Data source: Data 1 in Notebook6

Col 3 = 1229.610 - (987.615 * Col 1) - (948.268 * Col 2)

N = 18

R = 0.957 Rsqr = 0.916 Adj Rsqr = 0.905

Standard Error of Estimate = 67.764

	Coefficient	Std. Error	t	P	VIF
Constant	1229.610	62.417	19.700	<0.001	
Col 1	-987.615	93.523	-10.560	<0.001	1.000
Col 2	-948.268	130.411	-7.271	<0.001	1.000

Analysis of Variance:

	DF	SS	MS	F	P
Regression	2	754863.347	377431.674	82.195	<0.001
Residual	15	68878.560	4591.904		
Total	17	823741.907	48455.406		

Column	SSIncr	SSMarg
Col 1	512075.963	512075.963
Col 2	242787.384	242787.384

The dependent variable Col 3 can be predicted from a linear combination of the independent variables:

	P
Col 1	<0.001
Col 2	<0.001

Table F.13 - Multiple linear regression to thermal resistivity in function moisture content and dynamic compaction degree for Green sawdust.

Multiple Linear Regression
Data source: Data 1 in Notebook2

Col 3 = 1187.716 - (497.389 * Col 1) - (12.442 * Col 2)

N = 12

R = 0.993 Rsqr = 0.987 Adj Rsqr = 0.984

Standard Error of Estimate = 21.741

	Coefficient	Std. Error	t	P	VIF
Constant	1187.716	27.715	42.855	<0.001	
Col 1	-497.389	56.135	-8.861	<0.001	1.000
Col 2	-12.442	0.512	-24.279	<0.001	1.000

Analysis of Variance:

	DF	SS	MS	F	P
Regression	2	315739.270	157869.635	333.989	<0.001
Residual	9	4254.112	472.679		
Total	11	319993.382	29090.307		

Column	SSIncr	SSMarg
Col 1	37109.325	37109.325
Col 2	278629.945	278629.945

The dependent variable Col 3 can be predicted from a linear combination of the independent variables:

	P
Col 1	<0.001
Col 2	<0.001

Table F.14 - Multiple linear regression to thermal resistivity in function moisture content and dynamic compaction degree for Kiln-dried shavings or sawdust.

Multiple Linear Regression
Data source: Data 1 in Notebook5

Col 3 = 1211.623 - (532.158 * Col 1) - (12.924 * Col 2)

N = 12
R = 0.983 Rsqr = 0.966 Adj Rsqr = 0.959

Standard Error of Estimate = 36.551

	Coefficient	Std. Error	t	P	VIF
Constant	1211.623	46.593	26.004	<0.001	
Col 1	-532.158	94.373	-5.639	<0.001	1.000
Col 2	-1292.434	86.151	-15.002	<0.001	1.000

Analysis of Variance:

	DF	SS	MS	F	P
Regression	2	343148.017	171574.009	128.428	<0.001
Residual	9	12023.558	1335.951		
Total	11	355171.575	32288.325		

Column	SSIncr	SSMarg
Col 1	42478.822	42478.822
Col 2	300669.195	300669.195

The dependent variable Col 3 can be predicted from a linear combination of the independent variables:

	P
Col 1	<0.001
Col 2	<0.001

Table F.15 - Multiple linear regression to thermal resistivity in function moisture content and dynamic compaction degree for Mix.

Multiple Linear Regression
Data source: Data 1 in Notebook2

Col 3 = 1205.911 - (566.171 * Col 1) - (11.412 * Col 2)

N = 12 Missing Observations = 12

R = 0.992 Rsqr = 0.983 Adj Rsqr = 0.979

Standard Error of Estimate = 23.204

	Coefficient	Std. Error	t	P	VIF
Constant	1205.911	29.580	40.768	<0.001	
Col 1	-566.171	59.913	-9.450	<0.001	1.000
Col 2	-11.412	0.547	-20.866	<0.001	1.000

Analysis of Variance:

	DF	SS	MS	F	P
Regression	2	282514.235	141257.117	262.347	<0.001
Residual	9	4845.929	538.437		
Total	11	287360.164	26123.651		

Column	SSIncr	SSMarg
Col 1	48082.414	48082.414
Col 2	234431.821	234431.821

The dependent variable Col 3 can be predicted from a linear combination of the independent variables:

	P
Col 1	<0.001
Col 2	<0.001

Table F.16 - Analysis of variance to thermal conductivity (k) in different moisture content (MC) and static compaction degree (SC) for all compost materials.

```
Variável analisada: k

Opção de transformação: Variável sem transformação ( Y )

-------------------------------------------------------------------------------
                     TABELA DE ANÁLISE DE VARIÂNCIA
-------------------------------------------------------------------------------
FV                     GL                 SQ               QM         Fc  Pr>Fc
-------------------------------------------------------------------------------
MC                      2          15.878701          7.939351   1597.882 0.0000
SC                      5          15.037659          3.007532    605.299 0.0000
erro                 4528          22.498140          0.004969
-------------------------------------------------------------------------------
Total corrigido      4535          53.414501
-------------------------------------------------------------------------------
CV  (%) =              35.10
Média geral:          0.2008428      Número de observações:         4536
-------------------------------------------------------------------------------
   Teste Tukey para a FV MC
-------------------------------------------------------------------------------
DMS: 0.00601234749076705  NMS: 0.05
-------------------------------------------------------------------------------
Média harmonica do número de repetições (r): 1512
Erro padrão: 0.00181277626663453
-------------------------------------------------------------------------------
Tratamentos                          Médias      Resultados do teste
-------------------------------------------------------------------------------
30                                  0.135912 a1
45                                  0.187604    a2
60                                  0.279013       a3
-------------------------------------------------------------------------------
   Teste Tukey para a FV SC
-------------------------------------------------------------------------------
DMS: 0.0103385638674625  NMS: 0.05
-------------------------------------------------------------------------------
Média harmonica do número de repetições (r): 756
Erro padrão: 0.00256365278182262
-------------------------------------------------------------------------------
Tratamentos                          Médias      Resultados do teste
-------------------------------------------------------------------------------
Fluffy                              0.122601 a1
0                                   0.132481 a1
14.5                                0.192725    a2
29                                  0.229508       a3
43.5                                0.252398          a4
58                                  0.275344             a5
-------------------------------------------------------------------------------
```

Table F.17 - Analysis of variance to thermal resistivity (rho) in different moisture content (MC) and static compaction degree (SC) for all compost materials.

```
Variável analisada: RHO
Opção de transformação: Variável sem transformação ( Y )
--------------------------------------------------------------------------------
                    TABELA DE ANÁLISE DE VARIÂNCIA
--------------------------------------------------------------------------------
FV                     GL                SQ               QM         Fc  Pr>Fc
--------------------------------------------------------------------------------
MC                      2    84768364.414369   42384182.207185   2399.893 0.0000
SC                      5   119427953.545884   23885590.709177   1352.459 0.0000
erro                 4528    79968392.717152      17660.864116
--------------------------------------------------------------------------------
Total corrigido      4535   284164710.677405
--------------------------------------------------------------------------------
CV  (%) =              21.54
Média geral:        616.8897928      Número de observações:         4536
--------------------------------------------------------------------------------
   Teste Tukey para a FV MC
--------------------------------------------------------------------------------
DMS: 11.335219789401  NMS: 0.05
--------------------------------------------------------------------------------
Média harmonica do número de repetições (r): 1512
Erro padrão: 3.41766962785626
--------------------------------------------------------------------------------
Tratamentos                          Médias      Resultados do teste
--------------------------------------------------------------------------------
60                                  451.055423 a1
45                                  613.748347    a2
30                                  785.865608       a3
--------------------------------------------------------------------------------
   Teste Tukey para a FV SC
--------------------------------------------------------------------------------
DMS: 19.4915370284921  NMS: 0.05
--------------------------------------------------------------------------------
Média harmonica do número de repetições (r): 756
Erro padrão: 4.83331473942492
--------------------------------------------------------------------------------
Tratamentos                          Médias      Resultados do teste
--------------------------------------------------------------------------------
58                                  443.349735 a1
43.5                                476.126455    a2
29                                  514.993519       a3
14.5                                596.467460          a4
0                                   804.187037             a5
F                                   866.214550                a6
--------------------------------------------------------------------------------
```

Table F.18 - Analysis of variance to thermal conductivity (k) in different moisture content (MC) and dynamic compaction degree (DC) for all compost materials.

```
Variável analisada: k
Opção de transformação: Variável sem transformação ( Y )
--------------------------------------------------------------------------------
                    TABELA DE ANÁLISE DE VARIÂNCIA
--------------------------------------------------------------------------------
FV                     GL                SQ               QM         Fc  Pr>Fc
--------------------------------------------------------------------------------
MC                      2          20.748868         10.374434   1671.811 0.0000
DC                      3           2.790090          0.930030    149.872 0.0000
erro                 3018          18.728215          0.006206
--------------------------------------------------------------------------------
Total corrigido      3023          42.267173
--------------------------------------------------------------------------------
CV  (%) =             32.57
Média geral:          0.2418687      Número de observações:         3024
--------------------------------------------------------------------------------
   Teste Tukey para a FV MC
--------------------------------------------------------------------------------
DMS: 0.00823049820589862  NMS: 0.05
--------------------------------------------------------------------------------
Média harmonica do número de repetições (r): 1008
Erro padrão: 0.00248118018777819
--------------------------------------------------------------------------------
Tratamentos                          Médias      Resultados do teste
--------------------------------------------------------------------------------
30                                  0.150047 a1
45                                  0.224783    a2
60                                  0.350777       a3
--------------------------------------------------------------------------------
   Teste Tukey para a FV DC
--------------------------------------------------------------------------------
DMS: 0.0104170309506276  NMS: 0.05
--------------------------------------------------------------------------------
Média harmonica do número de repetições (r): 756
Erro padrão: 0.00286502009864341
--------------------------------------------------------------------------------
Tratamentos                          Médias      Resultados do teste
--------------------------------------------------------------------------------
15                                  0.198185 a1
29                                  0.231403    a2
44                                  0.258775       a3
58                                  0.279111          a4
--------------------------------------------------------------------------------
```

Table F.19 - Analysis of variance to thermal resistivity (rho) in different moisture content (MC) and dynamic compaction degree (DC) for all compost materials.

```
 Variável analisada: RHO
 Opção de transformação: Variável sem transformação ( Y )
--------------------------------------------------------------------------------
                     TABELA DE ANÁLISE DE VARIÂNCIA
--------------------------------------------------------------------------------
FV                      GL                 SQ                QM         Fc  Pr>Fc
--------------------------------------------------------------------------------
MC                       2    74382330.284365   37191165.142183   2456.087 0.0000
DC                       3     8338082.144299    2779360.714766    183.548 0.0000
erro                  3018    45699896.688360      15142.444231
--------------------------------------------------------------------------------
Total corrigido       3023   128420309.117024
--------------------------------------------------------------------------------
CV  (%) =               24.50
Média geral:        502.2878968      Número de observações:         3024
--------------------------------------------------------------------------------
   Teste Tukey para a FV MC
--------------------------------------------------------------------------------
DMS: 12.8568786636429  NMS: 0.05
--------------------------------------------------------------------------------
Média harmonica do número de repetições (r): 1008
Erro padrão: 3.87585682164862
--------------------------------------------------------------------------------
Tratamentos                          Médias      Resultados do teste
--------------------------------------------------------------------------------
60                                  320.108135 a1
45                                  483.815476    a2
30                                  702.940079       a3
--------------------------------------------------------------------------------
   Teste Tukey para a FV DC
--------------------------------------------------------------------------------
DMS: 16.2724660910133  NMS: 0.05
--------------------------------------------------------------------------------
Média harmonica do número de repetições (r): 756
Erro padrão: 4.47545395863856
--------------------------------------------------------------------------------
Tratamentos                          Médias      Resultados do teste
--------------------------------------------------------------------------------
58                                  443.390212 a1
44                                  470.972354    a2
29                                  511.965741       a3
15                                  582.823280          a4
--------------------------------------------------------------------------------
```

Table F.20 - Analysis of variance to heated floor area (Area) in different ridge design (Ridge) and wind direction (Direction) for all CFD models tested.

Two Way Analysis of Variance

Data source: Data 1 in Notebook1

General Linear Model (No Interactions)

Dependent Variable: Col 3

Normality Test: Passed (P = 0.373)

Equal Variance Test: Passed (P = 1.000)

Source of Variation	DF	SS	MS	F	P
Col 1	4	1620.038	405.010	0.531	0.716
Col 2	3	526.051	175.350	0.230	0.874
Residual	12	9155.593	762.966		
Total	19	11301.682	594.825		

Power of performed test with alpha = 0.0500: for Col 1 : 0.0500
Power of performed test with alpha = 0.0500: for Col 2 : 0.0500

```
--------------------------------------------------------------------------------
   Teste Tukey para a FV RIDGE
--------------------------------------------------------------------------------


DMS: 0  NMS: 0.05
--------------------------------------------------------------------------------


Média harmonica do número de repetições (r): 4
Erro padrão: 0
--------------------------------------------------------------------------------


Tratamentos                          Médias      Resultados do teste
--------------------------------------------------------------------------------
ELR                                 19.457500 a1
OVR                                 23.497500    a2
CLR                                 24.462500       a3
OPR                                 27.512500          a4
ORC                                 45.292500             a5
--------------------------------------------------------------------------------
--------------------------------------------------------------------------------
   Teste Tukey para a FV DIRECTION
--------------------------------------------------------------------------------


DMS: 0  NMS: 0.05
--------------------------------------------------------------------------------


Média harmonica do número de repetições (r): 5
Erro padrão: 0
--------------------------------------------------------------------------------


Tratamentos                          Médias      Resultados do teste
--------------------------------------------------------------------------------
S to N                              19.712000 a1
N to S                              27.922000    a2
E to W                              32.178000       a3
W to E                              32.366000          a4
--------------------------------------------------------------------------------
```